Changes in climate and palaeoenvironment during the Late Jurassic–Early Cretaceous in southern South America and western Antarctica

INAUGURAL – DISSERTATION

Zur Erlangung der Doktorwürde
der Naturwissenschaftlich-Mathematischen Gesamtfakultät
der Ruprecht-Karls-Universität
Heidelberg

vorgelegt von

Sven Brysch

Heidelberg, 2018

Changes in climate and palaeoenvironment during the Late Jurassic–Early Cretaceous in southern South America and western Antarctica

INAUGURAL – DISSERTATION

Zur Erlangung der Doktorwürde
der Naturwissenschaftlich-Mathematischen Gesamtfakultät
der Ruprecht-Karls-Universität
Heidelberg

vorgelegt von
Sven Brysch, M.Sc.
aus Rastatt, Deutschland

Heidelberg, 2018

Gutachter:
Prof. Dr. Wolfgang Stinnesbeck
PD Dr. André Bahr

Tag der mündlichen Prüfung 26.10.2018

Table of Contents

Abstract

The palaeoenvironmental changes of Upper Jurassic (Middle Tithonian) to Lower Cretaceous (Lower Albian) sediments are here analysed along a North-South transect following the southwestern margin of Gondwana (central Chile, Patagonia, and Antarctica). The focus of this high-resolution multidisciplinary study is paid to climatic perturbations, which are evident in palynofacies and lithofacies records as well as by presence/absence of the cold-water indicative mineral glendonite.

In central Chile two sections corresponding to the Tithonian–Hauterivian Lo Valdés Formation were analysed from the Mendoza-Neuquén backarc basin. An uppermost Tithonian unit was identified which corresponds to a relatively low sea level and deposition in proximal to inner platform environments. This interval is followed by a transgressive interval in the Berriasian, leading to deep shelf to basin depositional settings. The early–Middle Valanginian shows again a relatively low sea level with inner platform to slope deposits, followed by a second transgressive phase in the Upper Valanginian to Hauterivian at the top of the sections, represented by deep shelf to basin deposits. Sedimentary organic matter (OM) in the sections is intensely altered by thermal degradation and mostly consists of terrestrial OM with only very minor amounts of marine OM. Calpionellids are found in the Berriasian interval, indicating warm, oxygen-rich conditions at least for the water column. Corresponding to both intervals of low sea level (uppermost Tithonian, early–Middle Valanginian) microscopic glendonite was identified in the insoluble sample residue. The occurrence of glendonites in these shallow marine shelf environments indicates cold water temperatures and thus provides evidence for significant climatic cooling in the latest Tithonian and early–Middle Valanginian.

In Patagonia (Región de Magallanes y de la Antártica Chilena) drilled core cuttings of two wells were analysed reaching from the Tithonian to Berriasian and Hauterivian to Aptian (Sofia 1 core – Tobífera Formation, lower and middle Zapata Formation, Austral Basin, backarc) and from the Upper Barremian to Lower Aptian (Nevenka 1 core – Springhill/Río Mayer Formation, Austral Basin, backarc). Samples of the Sofia 1 core show highly altered organic matter but information about the depositional setting could still be obtained by using the opaque:translucent ratio of phytoclasts and the shape and size of organic particles. Organic matter is better preserved in the Nevenka 1 core and the AOM-Phytoclast-Palynomorph relationship was used to identify depositional environments. Both Patagonian sections present a predominance of siliciclastic sedimentation while increased carbonate content was confined to short intervals. Microscopic glendonites were detected in the Upper Barremian and Lower Aptian section and are accompanied by proximal depositional environments, thus pointing to low sea level reflecting glacioeustasy.

In Antarctica, the sampled interval ranges from the Middle Tithonian to the Lower Albian. Analysed sections include the Anchorage-, President Beaches- and Chester Cone Formation of the Byers Group (Byers Peninsula, intra-arc), the Himalia Ridge-, Spartan Glacier- and Pluto Glacier Formation of the Fossil Bluff Group (Alexander Island, forearc), the Nordenskjöld Formation and the Kotick Point Formation of the Gustav Group (James Ross Island, backarc). In the Byers- and Fossil Bluff Groups, a few samples show increased carbonate contents while most are composed of siliciclastic material. In contrast, carbonate content in the Nordenskjöld- and Kotick Point Formation is generally higher reaching up to 44 %. Again, occurrences of microscopic glendonite are majorly observed in intervals of proximal deposition in the Upper Tithonian, lowermost and uppermost Berriasian, lower and Upper

Valanginian, Lower Barremian and throughout the Aptian. Presence of micro-glendonite and majorly concurrent proximal deposition points to intervals of low sea level, which is interpreted as a result of glacioeustasy. Scarce occurrences of micro-glendonite in intervals with distal depositional settings are considered to reflect cool bottom water conditions in times of higher sea level.
Micrometre-sized glendonite pseudomorphs after ikaite are therefore recorded from all studied areas along the North-South transect (central Chile, Patagonia, Antarctica), but their restriction to specific levels of the Tithonian to Aptian sediment succession provides strong evidence for episodic cooling. Until now glendonites of Late Jurassic–Early Cretaceous ages have only been known from northern high latitudes. The new data from Chile and Antarctica provide strong evidence for repeated small scale glaciations in the southern hemisphere. These cold episodes in the Upper Tithonian, lowermost Berriasian, Valanginian, lowermost Hauterivian, Lower Barremian, Aptian and Lower Albian punctuated the Early Cretaceous greenhouse climate in both the northern and southern hemispheres and must thus have been global events.

Kurzfassung

Im Rahmen der vorliegenden Arbeit wurden entlang eines Nord-Süd-Transekts, der dem südwestlichen Rand Gondwanas (Zentralchile, Patagonien, Antarktis) folgt, anhand mehrerer Sedimentabfolgen die Paläoumweltveränderungen während des späten Jura (mittleres Tithonium) bis zur frühen Kreide (unteres Albium) analysiert Der Fokus dieser hochaufgelösten multidisziplinären Studie liegt auf klimatischen Störungen, die in Palynofazies- und Lithofazies-Aufzeichnungen sowie in der An- beziehungsweise Abwesenheit des Kaltwasser-anzeigenden Minerals Glendonit sichtbar werden.
In Zentralchile wurden zwei Profile aus dem Mendoza-Neuquén backarc-basin analysiert, die der Lo Valdés Formation (Tithonium–Hauterivium) entsprechen. Das Intervall aus dem oberen Tithonium zeigt einen relativ niedrigen Meeresspiegel und Ablagerungen der proximalen bis inneren Plattform. Diesem Intervall folgt eine transgressive Phase im Berriasium, welche zu einem Ablagerungsmilieu des tiefen Schelfs führte. Das frühe–mittlere Valanginium ist erneut von einem niedrigen Meeresspiegel und Ablagerungen der inneren Plattform bis zum Kontinentalhang geprägt. Während des späten Valanginiums und des Hauteriviums am Top der untersuchten Profile, folgte eine zweite transgressive Phase, die durch Ablagerungen des tiefen Schelfs und des Beckens gekennzeichnet ist. Die sedimentäre organische Materie (OM) in diesen Profilen ist stark alteriert und besteht überwiegend aus terrestrischer OM, wohingegen marine OM nur geringfügig vertreten ist. Das Auftreten von Calpionellen im Intervall des Berriasiums deutet auf warme, sauerstoffreiche Bedingungen hin, die zumindest in den oberen Wasserschichten vorherrschte. Zeitgleich zu beiden Intervallen mit reduziertem Meeresspiegel (oberstes Tithonium, frühes–mittleres Valanginium) wurde das Auftreten von mikroskopischen Glendoniten in den Probenrückständen festgestellt. Das Auftreten von Glendoniten in den Ablagerungsräumen des flachmarinen Schelfs, deutet auf kalte Wassertemperaturen hin und liefert Belege für signifikante klimatische Abkühlung während des spätesten Tithoniums und des frühen–mittleren Valanginiums.
In Patagonien (Región de Magallanes y de la Antártica Chilena) wurde das Bohrklein zweier Bohrkerne untersucht, die vom Tithonium bis Berriasium und Hauterivium bis Aptium (Bohrung

Sofia 1 – Tobífera Formation, untere und mittlere Zapata Formation, Austral Becken, backarc) beziehungsweise vom oberen Barremium bis unteren Aptium (Bohrung Nevenka 1 – Springhill/Río Mayer Formation, Austral Becken, backarc) reichen. Die Proben aus dem Sofia 1 Bohrkern sind von stark alterierter organischer Materie geprägt. Anhand des Verhältnisses von opaken zu durchsichtigen Phytoklasten und der Verteilung von Form und Größe organischer Partikel konnten dennoch Informationen über das Ablagerungsmilieu gewonnen werden. Die organische Materie des Nevenka 1 Bohrkerns ist besser erhalten, weshalb zusätzlich das Verhältnis von AOM-Phytoklasten-Palynomorphen verwendet wurde, um die Paläo-Umwelt zu identifizieren. Beide Profile aus Patagonien bestehen überwiegend aus siliziklastischen Sedimenten, erhöhter Gehalt an Karbonat ist auf kurze Intervalle beschränkt. Begleitet von proximalen Ablagerungsbedingungen wurde das Auftreten von Mikroglendoniten im oberen Barremium und unteren Aptium beobachtet, was auf einen glazioeustatischen Einfluss auf den Meeresspiegel hindeutet.

Aus dem Untersuchungsgebiet in der Antarktis reicht das beprobte Intervall vom mittleren Tithonium bis zum unteren Albium. Die analysierten Profile umfassen die Anchorage-, President Beaches- und Chester Cone Formationen der Byers Gruppe (Byers Peninsula, intra-arc), die Himalia Ridge-, Spartan Glacier- und Pluto Glacier Formationen der Fossil Bluff Gruppe (Alexander Island, forearc) sowie die Nordenskjöld- und Kotick Point Formationen (James Ross Island, backarc). Die Proben der Byers- und Fossil Bluff Gruppen bestehen überwiegend aus siliziklastischem Material wobei vereinzelt erhöhte Gehalte an Karbonat auftreten. Die Proben aus den Nordenskjöld- und Kotick Point Formationen zeigen hingegen durchgehend höhere Gehalte an Karbonat, die Anteile von bis zu 44 % erreichen. Auch hier wurden Vorkommen von Mikroglendoniten hauptsächlich in den Intervallen festgestellt, die von proximalen Ablagerungsmilieus gekennzeichnet sind: oberes Tithonium, unterstes und oberstes Berriasium, unteres und oberes Valanginium, unteres Barremium und durchgehend innerhalb des Aptium. Die Beschränkung von Mikroglendonit-Vorkommen auf Einheiten mit proximalen Ablagerungsbedingungen und folglich niedrigem Meeresspiegel, deutet auf glazioeustatischen Einfluss hin. Vereinzeltes Auftreten von Mikroglendoniten wurde auch in Intervallen mit distalen Ablagerungsbedingungen beobachtet, wo sie auf kalte Tiefenwässer in Zeiten erhöhten Meeresspiegels hindeuten.

Somit wurde aus allen untersuchten Gebieten entlang des Nord-Süd-Transekts (Zentralchile, Patagonien, Antarktis) das Auftreten von Mikrometer-großen Glendonit-Pseudomorphen nach Ikait beobachtet. Die Beschränkung auf spezielle Niveaus des Oberjura und der Unterkreide (Tithonium bis Aptium) liefert deutliche Hinweise auf episodische Abkühlperioden. Bislang sind Glendonite von spätjurassisch-frühkretazischem Alter nur aus den nördlichen hohen Breiten bekannt. Die neuen Daten aus Chile und der Antarktis liefern nun starke Belege für wiederholte Vereisungen auf der südlichen Hemisphäre. Diese kalten Episoden im oberen Tithonium, untersten Berriasium, Valanginium, untersten Hauterivium, unteren Barremium, Aptium und unteren Albium unterbrachen das frühkretazische Treibhausklima sowohl in der nördlichen als auch in der südlichen Hemisphäre und müssen daher Ereignisse von globaler Reichweite gewesen sein.

List of Abbreviations

AF	Anchorage Formation
AOM	Amorphous Organic Matter
AOMT	Amorphous Organic Matter (terrestrial)
AOMA	Amorphous Organic Matter (aquatic)
CCF	Chester Cone Formation
C/N	C_{org}/Nitrogen Ratio
CNS	Carbon, Nitrogen, Sulphur
CM	Cajón del Morado
DPM	Devils Point Member
EDX	Energy Dispersive X-Ray Analysis
FBG	Fossil Bluff Group
HRF	Himalia Ridge Formation
KPF	Kotick Point Formation
LMG	LeMay Group
LV	Lo Valdés
LVF	Lo Valdés Formation
LZF	Lower Zapata Formation
MS	Magnetic Susceptibility
MZF	Middle Zapata Formation
NF	Nordenskjöld Formation
OM	Organic Matter
OP/TR	Opaque/translucent ratio
PBF	President Beaches Formation
PGF	Pluto Glacier Formation
RMF	Ramp Microfacies Type
S/RMF	Springhill/Río Mayer Formation
SD	Standard Deviation
SEM	Scanning Electron Microscopy
SGF	Spartan Glacier Formation
SHM	Sealer Hill Member
SMF	Standard Microfacies Type
SOM	Sedimentary Organic Matter
TAI	Thermal Alteration Index
TF	Tobífera Formation
TIC	Total Inorganic Carbon
TOC	Total Organic Carbon

1. INTRODUCTION

1.1. Climatic oscillations during the Late Mesozoic

Although there is little doubt that the Mesozoic represented an exceedingly long period of extreme warmth, it was also punctuated by climatic oscillations (e.g. Price, 1999; Dromart et al., 2003a, 2003b; Bornemann et al., 2008; Geleotti et al., 2009; Donnadieu et al., 2011; Hu et al., 2012; Bodin et al., 2015). It is a widely debated issue, however, whether these oscillations in global temperatures were sufficient to lead to significant cooling and the formation of polar ice (e.g. Barron, 1983; Kemper, 1987; Crowley & North, 1991; Frakes et al., 1992; Hallam, 1993; Chumakov, 1995; Bennett et al., 1996; Frakes, 1999; Oyarzun et al., 1999; Dromart et al., 2003a, b; Steuber et al., 2005; McArthur et al., 2007). Kemper (1987) and Donnadieu et al. (2011) suggest that within the Mesozoic the periods of climatic oscillations and cold climate lasted from a few thousand to >2 Ma and were separated by intervals of warm steadied climate.

Cretaceous icehouse interludes are indicated by carbon isotope fluctuations (Weissert, 1989; Weissert & Lini, 1991; Barclay et al., 2010; Jarvis et al., 2011; McAnena et al., 2013; Hollis et al., 2014). Although Barral et al. (2017) recognise pCO_2 in the Cretaceous to be decoupled from temperature at the Ma scale, the authors still consider CO_2 as the main driver of temperature. Negative carbon excursions during the Early Valanginian, the mid- Hauterivian–Barremian and the Aptian–Early Albian boundary, are explained by decelerated carbon cycling and to represent cool or icehouse climates (Weissert & Lini, 1991; Bodin et al., 2015). The reasons proposed for decreased atmospheric CO_2 include (1) increased primary productivity and hence increased organic carbon burial (Dromart et al., 2003a; McAnena et al., 2013; Bodin et al., 2015), (2) a general demise of carbonate platforms (Donnadieu et a., 2011), (3) enhanced sequestration of organic carbon in sediments (Dromart et al., 2003a), or (4) storage of organic carbon in coastal areas and/or enhanced preservation within stratified waters in high-latitude basins (Price & Mutterlose, 2004). Donnadieu et al. (2011) showed that the general demise of carbonate platforms which accompanied short-lived cold interludes ("cold snaps") is capable of creating fast atmospheric CO_2 decrease and a moderate sea level drop caused by ice sheet build-up. Carbonate production decline was temporary and therefore cold phases were relative short-lived events, possibly resulting from ice sheet waxing and waning (Donnadieu et al., 2011). All of the occurrences of decreased CO_2 contents have been associated with potentially ice-rafted clasts (Francis & Frakes, 1993). For example, breccia and claystone with granitic pebbles within the late Jurassic Flamenco Formation in Tierra del Fuego are suggested to be deposits formed by mountain glaciers (Cecioni, 1981).

Eustatic sea level changes are an important criterion indicating glacial periods (e.g. Bjørlykke, 1985; Kemper, 1987; Gale et al., 2002; Dromart et al., 2003a, 2003b; Donnadieu et al., 2011; Husinec et al., 2012). Sea level curves based on sequence stratigraphy imply that during the late Mesozoic sea level repeatedly rose and fell by about 100 m in less than 1 million years (Haq et al., 1987, Haq., 2014). Goldhammer et al. (1987) and Masetti et al. (1991) note that tectonic movements cannot operate on a sufficiently rapid timescale to account for the observed short-termed sea level changes. The synchronous changes of the eustatic sea level curve (e.g. Haq et al., 1987; Haq, 2014) require significant amounts of ice, not just small isolated mountain ice sheets (Rowley & Markwick, 1992) as

was suggested by several authors (e.g. Dromart et al., 2003a; Miller et al., 2005a, 2005b; Steuber et al., 2005; Donnadieu et al., 2011; Hut et al., 2012). Rapid (<1 My) global sea-level fluctuations of up to 50 m have been reported by Immenhauser and Scott (2002) Gréselle and Pittet (2005, 2010), Bover-Arnal et al. (2009, 2014), Rameil et al. (2012) Maurer et al. (2013) and other authors for the Late Valanginian, the late Early Aptian and the latest Aptian-earliest Albian, suggesting glacio-eustasy as the driving mechanism. These sea level changes may have resulted from an Antarctic ice sheet (Stoll & Schrag, 1996, 2000) and may have been controlled by orbital variations (Matthews & Frohlich, 1991). Using Strontium data, Stoll and Schrag (1996) suggest that Berriasian-Valanginian sea level varied by about 50 m over time scales of 200-500 ka.

By the use of general circulation models (GCM), Moore et al. (1992), Valdes et al. (1995) and Sellwood et al. (2000) simulated significant amounts of sea-ice in Antarctica during the late Jurassic (Kimmeridgian–Tithonian) as a result of Milankovitch (eccentricity-forced) orbital perturbations. In their simulations, the sea-ice front extended to 45° north and 50° south. Price and Nunn (2010) also suggest cool polar temperatures during the Cretaceous by simulation with a GCM. In their interpretation, episodes with ice-covered poles correspond to phases with aridity in Europe, which would support the idea of cool or glacial events (Price, 1999). Prentice and Matthews (1991) suggest that high sea surface temperatures enhanced vapour transport to the centre of Antarctica, where temperatures remained low and led to the formation of an ice cap.

Changes in the Mesozoic faunal and floral assemblages in both the marine and terrestrial realms are associated to temperature variations (e.g. Vakhrameyev, 1982; Kemper, 1987; Price, 1999; Zakharov & Rogov, 2003). The potential existence of Boreal and Austral realms during parts of the Mesozoic supports the idea of cold or even sub-freezing high-latitude conditions. These regions are generally low in diversity, but temperature is an important controlling factor of the faunal distribution (Middlemiss, 1984; Rawson, 1973; Stevens, 1973). At the end of the Jurassic, provinciality amongst faunas became most remarkable (Casey & Rawson, 1973). A distinct bipolarity exists in the distribution of Pliensbachian and Tithonian (Early and Late Jurassic) and Aptian–Albian (Early Cretaceous) bivalves (Crame, 1986, 1993) and thus corresponds to episodes from which glacial sediments and glendonites have been reported (Price, 1999 and references therein). A tendency towards bipolar taxa occurs when the Earth's pole–equator temperature profile increases, leading to the expulsion of taxon from equatorial regions (Crame, 1993). Extensive floral evidence (Parrish et al., 1998; Philippe & Thevenard, 1996; Spicer & Parrish, 1986) also implies that permanent ice at high latitudes may have repeatedly existed during the Jurassic and Cretaceous (Price, 1999 and references therein).

Several authors report on significant perturbations of the Early Cretaceous northern hemisphere climate, with repeated cool excursions punctuating otherwise warm conditions (e.g. Galloway et al., 2015; Kemper, 1987; Kessels et al., 2006; Price & Mutterlose, 2004; Price & Nunn, 2010). Early Cretaceous occurrences of glendonites are known from high northern palaeolatitudes, e.g. the Valanginian and Early Hauterivian of eastern Siberia, the Valanginian of Spitsbergen in Svalbard (Kemper, 1987; Price & Nunn, 2010), and the Valanginian of the Sverdrup Basin in the Canadian Arctic (Kemper & Schmitz, 1975, 1981) (Fig. 1). Ice-rafted deposits were documented in lower Cretaceous sediments confirming the presence of polar ice (Frakes & Francis, 1988). For the southern hemisphere, on the other hand, evidence for major cooling events is rare and majorly restricted to Australia. In this southern continent, boulder-sized clasts considered to be glacial dropstones, as well

as glendonite nodules and cryoturbational structures, were found in the Bulldog Shale (Woolnough & David, 1926; Frakes & Francis, 1988; Sheard, 1990; Francis & Frakes, 1993), while isotopic evidence suggests the presence of glacial meltwaters (Price, 1999).

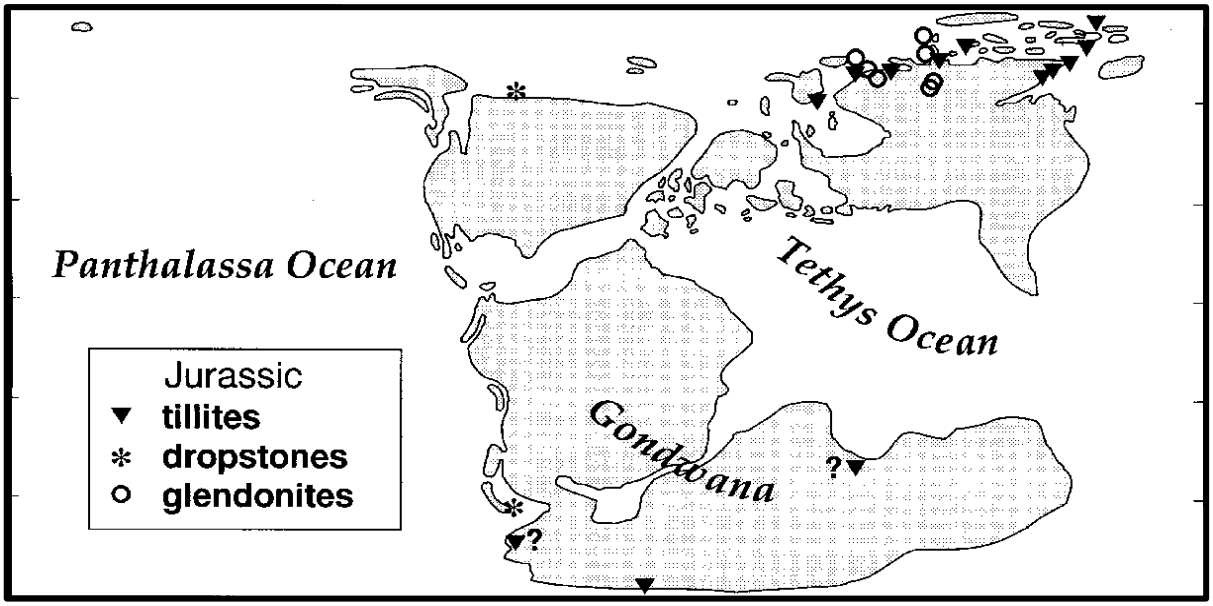

Figure 1: Distribution of potentially glacially derived sediments and glendonites during the Late Jurassic (Price, 1999).

1.2 Ikaite – the Glendonite precursor

Pauly (1963) identified ikaite in 1963 after discovering the mineral in the Ikka Fjord in Greenland. Ikaite is a metastable low-temperature polymorph of calcium carbonate which crystallises at about freezing temperatures but easily decomposes to a loose mush of calcite and water at higher temperatures (De Lurio & Frakes, 1999). Naturally occurring ikaite has been observed only at temperatures between -1.9° C and 7° C; it is present in both marine and non-marine water that is alkaline and/or rich in orthophosphate (Huggett et al., 2005). Typically, ikaite is formed through precipitation from supersaturated aqueous solutions (Boch et al., 2015). Its widespread occurrence in modern sediments of cold climate shelves and estuaries as well as in deeper ocean basins indicates that its formation is a relatively common process controlled mainly by temperature and alkalinity (Selleck et al., 2007). Ikaite has likewise been found in (cold) shelf sediments (Schultz, 1998) and also occurs at temperate and tropical latitudes, but only in deep (4 km) waters (Stein & Smith, 1986; Markwick & Rowley, 1998). Modern ikaite was found more recently also in Antarctic and Arctic sea ice (Dieckmann et al., 2008; Dieckmann et al., 2010).

Sherman and Smith (1985) suggested that sodium hexametaphosphate and magnesium ions together with other inhibitors would be needed to favour (metastable) ikaite precipitation and block calcite precipitation in seawater at ‘normal’ pressures and low temperatures. In contrast, Hu et al. (2014), argue that phosphate concentrations do not influence the precipitation of ikaite and state that in their

study the controlling factor of ikaite precipitation was pH (due to its strong influence on CO_3^{2-} concentrations). The crystal lattice of the monoclinic ikaite is hydrated with water molecules ($CaCO_3$ x $6H_2O$) (Hu et al., 2014). As pseudomorphs after ikaite are usually composed of calcite, it is suggested that they formed by in situ redistribution of the calcium and carbonate ions of the precursor ikaite crystals (Huggett et al., 2005). The reaction of transformation ($CaCO_3$ x $6H_2O$ → $CaCO_3$ + $6H_2O$) results in a 68.6% volume loss as the structural waters are released from the ikaite crystal (Larsen, 1994). Several authors (e.g. Marland, 1975; and Swainson & Hammond, 2001; Boch et al., 2015; Brooks, 2016; Fairchild et al., 2016; Oehlerich et al., 2013) suggest a rapid conversion of ikaite to calcite when temperature rises above ~4 °C at atmospheric pressures. The exact temperature however, depends on water chemistry (Jansen et al., 1987; Larsen, 1994; Pauly, 1963; Stein & Smith, 1986; Suess et al., 1982). Chemical analysis shows that minor amounts of Mg, Fe and Mn are substituted for Ca. Transformation can also lead to extensive replacement of $CaCO_3$ by ferroan dolomite (ankerite) (Huggett et al., 2005). The transformation of ikaite to stellate glendonite clusters takes place in situ and therefore also within the sediment pile rather than at the sediment–water interface. This is indicated by the random orientation of long axes, coupled with the partial or complete enclosure of fossils or pebbles in larger clusters (Selleck et al., 2007).

The relatively strict temperature limits on its stability make ikaite a suitable indicator of cold water conditions and thus of great palaeoclimatic significance when its former presence can be verified in ancient sediments. Meanwhile, ikaite has received widespread acceptance as the precursor mineral for glendonite and related pseudomorphs (Carr et al., 1989; Suess et al., 1982; Swainson & Hammond, 2001).

1.3 Glendonite

With time, metastable ikaite transforms to one of its pseudomorphs, glendonite. Single crystals are mostly elongate in c-direction, with multiple 'scalenohedral' terminations and imperfect development of the hexagonal prism (plate 1) (Kemper, 1987; Huggett et al., 2005). Glendonite is known from many localities and strata since the Precambrian (Johnston, 1995; James et al., 2005) to Recent. The pseudomorphs have been reported from diverse sedimentary facies ranging from lacustrine through estuarine, tidal flat and shallow to deep marine. However, they are not omnipresent in any of these facies and only occur over limited stratigraphic intervals (Huggett et al., 2005). Glendonite findings were repeatedly reported from marine sediments associated with dropstones, and the mineral is abundantly present in Quaternary sediments from periglacial regions. As a successor of ikaite, glendonite is thus an important climate proxy used to determine cold-water sedimentary facies and glaciomarine settings of the environments in which they occur (e.g. Kemper & Schmitz, 1975, 1981; Kaplan, 1978, 1979; Markwick & Rowley, 1998; De Lurio & Frakes, 1999; Price, 1999; Lippert, 2004; Selleck et al., 2007; Price & Nunn, 2010; Rogov & Zakharov, 2010; Herrle et al., 2015; Vickers et al., 2016; Rogov et al., 2017). Glendonites are important archives for palaeoenvironmental reconstructions (Bradshaw et al., 1995; Brandley & Krause, 1994; Brandt, 1986; Frakes & Francis, 1988; Johnston, 1995; Sheard, 1990; Shi, 2001; Yan, 1996). In particular, it is clear that the presence of ikaite pseudomorphs, such as glendonite, provides a qualitative indication of low water temperature during the period of ikaite growth (Alley & Frakes, 2003; De Lurio & Frakes, 1999; Marland, 1975;

Selleck et al., 2007; Spielhagen & Tripati, 2009). Rogov et al. (2017) reviewed all known occurrences of Early Cretaceous glendonites in both the northern and southern hemispheres (Fig. 2). Glendonite distribution correlates with episodes of global climatic cooling, the most prominent being cooling events during the Valanginian and Late Aptian (Rogov et al., 2017).

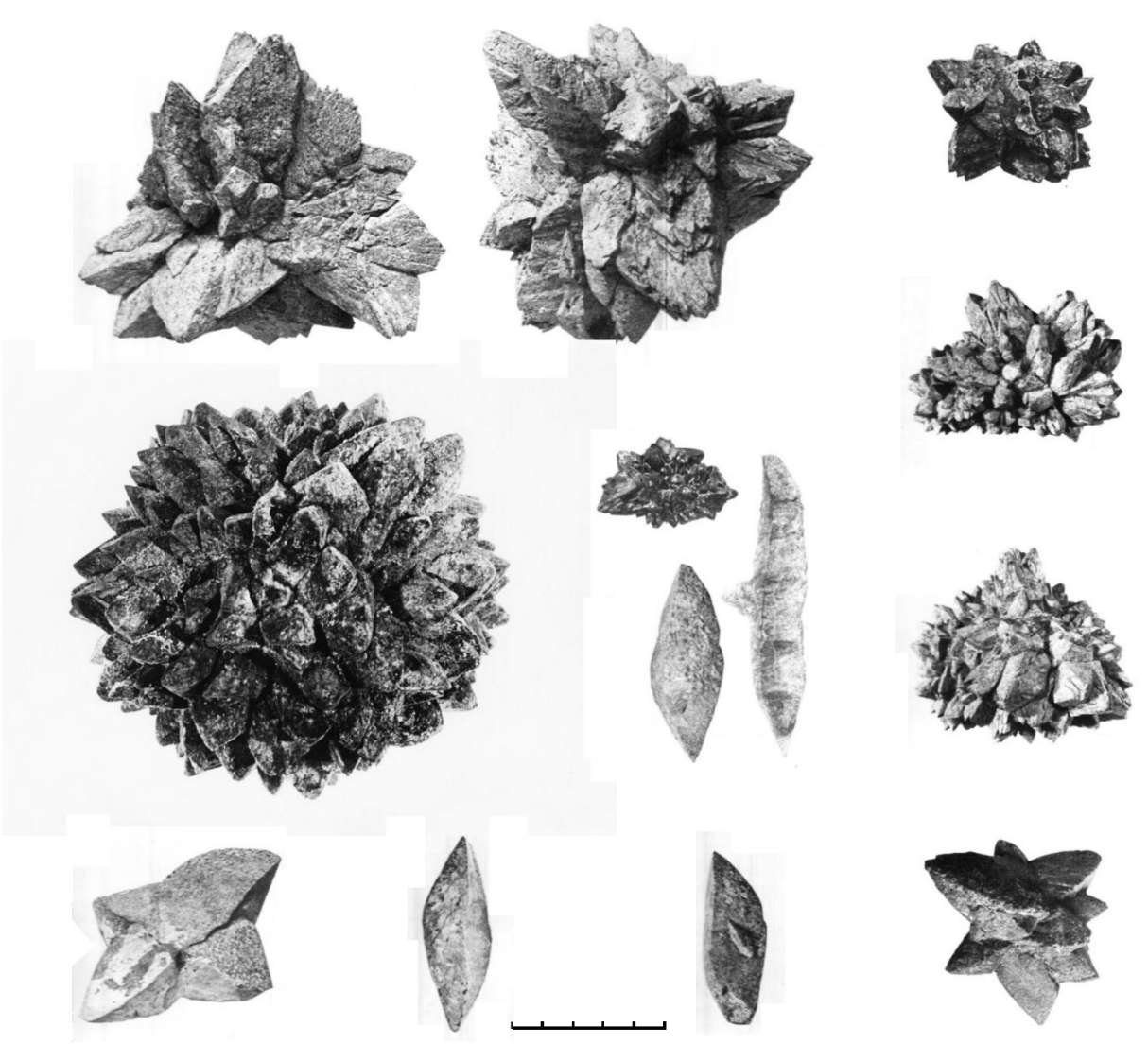

Plate 1: Glendonite aggregates in various forms and sizes, scale bar in cm; compiled and modified from Kemper (1987) and De Lurio and Frakes (1999).

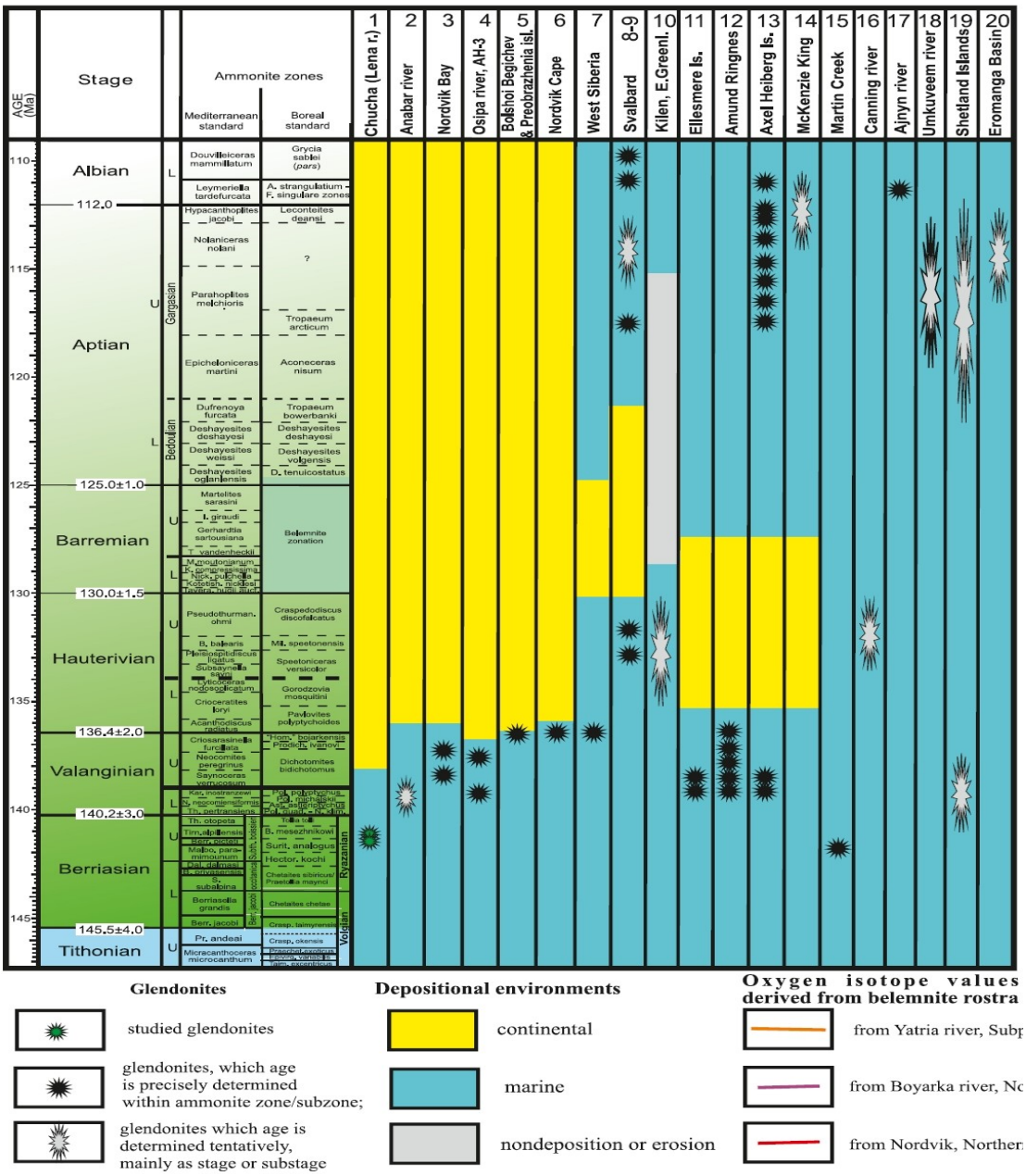

Figure 2: Correlation chart of Early Cretaceous glendonite occurrences across the Northern Hemisphere. Modified after Rogov et al. (2017).

1.4 Calpionellids

Calpionellids represent one of the most important groups of tropical calcareous microplankton in the Late Jurassic–Early Cretaceous Tethyan realm and are usually present in abundance in pelagic carbonates (Rehakova & Michalik, 1997). They represent a key role in biostratigraphic correlation of these deposits (Michalik, 1995). While Remane (1964, 1965) was the first to use calpionellids in stratigraphy, Allemann et al. (1971) introduced the standard calpionellid zonation which is still used today. In recent years findings of calpionellids in western Cuba (López-Martinez et al., 2013) and

Mexico (Adatte et al., 1994, 1996; López-Martinez et al., 2015; Zell et al., 2015) extended the area of application westwards to the ancient Gulf of Mexico and the Pacific. Adatte et al. (1994, 1996) assume a sporadic influence of the Tethys on central-east Mexico during the Tithonian and no permanent connection. Stinnesbeck et al. (2014) suggest two corridors that connected central Chile to the Tethyan realm. The equatorial Hispanic corridor linked the eastern Pacific with the western Tethys Ocean. During the Berriasian, new pathways between Antarctica and South America–Africa are suggested by the dominance of cosmopolitans and by the abundance of Indo-Pacific taxa (Salazar, 2012). Stinnesbeck et al. (2014) conclude that the Indo-Austral Seaway was linked to the eastern Tethys during the Early Cretaceous. The second corridor that connected the eastern Tethys with central Chile is the Indo-Austral Seaway (Stinnesbeck et al. 2014). The same path might have brought calpionellids to West Central Argentina (Riccardi 2015) and from there on to central Chile. López-Martinez et al. (2015) suggest a constant arrival of calpionellids to Mexican regions through a permanent connection with the main part of the Tethys. Kietzmann (2017) reports occurrences of calpionellids from the Argentinian Neuquén Basin which show some differences with the Tethys but are more similar to the Tithonian–Berriasian occurrences in Mexico and Cuba. In the study of Kietzmann (2017) no potential migratory pathways are discussed. Calpionellids characterise the Tithonian–Hauterivian interval in the Tethyan realm, with a potential biostratigraphic application from the Upper Tithonian into the Upper Valanginian (e.g. Reháková & Michalík 1997, Andreini et al. 2007, Wimbledon et al. 2013). However, even for the Tethyan realm long-distance bio-chronostratigraphic correlations are still unclear (Andreini et al. 2007).

1.5 Carbonate Microfacies

The study of microfacies serves the purpose of the recognition of overall patterns that reflect the history of carbonate rocks. Occurrence of identical biota and comparable depositional environments results in time-specific microfacies types. Similar properties in individual microfacies types from limestones which are not restricted to specific time intervals are used to define standard microfacies types (SMF types) (Flügel, 2004). SMF types define major depositional and biological controls and indicate major depositional settings (Wilson, 1975).

Inner ramp

In the inner ramp the sea floor is continuously affected by wave agitation (Flügel, 2004). This setting includes the euphotic zone between the upper shoreface and the fair-weather wave base (Fig. 3). The inner ramp zone is characterised by sand shoals or organic barriers and shoreface deposits. Frequently occurring ooids or various skeletal grains, usually foraminifera, calcareous algae, or molluscs and some peloids make up the sands. Frequent limestone types are grainstones and packstones. The inner ramp facies zone comprises open-marine environments with good water circulation. However, it also includes protected environments with restricted water circulation. Therefore sand shoal environments with oolitic and bioclastic grainstones and packstones as well as lagoonal environments behind shoals or islands and peritidal environments are common. Open and protected inner ramps are commonly represented by bioclastic packstones and wackestones. Abundant echinoderm fragments are common

in protected and low-energy inner ramps. Skeletal grains such as bivalve shells, gastropods, bryozoans, and benthic foraminifera may be associated.

Mid-ramp

This microfacies type reflects the zone between fair-weather wave base and the storm wave base where water depths reach some tens of metres (Fig. 3). Thick oolitic and bioclastic sand shoals as well as intraclast and breccia beds may be common (Flügel, 2004). Sedimentary features related to storms are grading in packstone and grainstone beds, hummocky cross-stratification and tempestite units. Usually skeletal grains show signs of transport. Burrowed bioclastic lime mudstones and marls are common in fair-weather phases of mid-ramp settings. Lateral sediment transport in offshore zones may contribute large amounts of fine-grained sediment in this ramp setting. Mudstone, wackestone, packstone and some grainstones are common lithologies in mid-ramp environments. Skeletal grains are often worn and echinoderms are present.

Outer ramp

The outer ramp zone is located below normal storm wave base (Fig. 3) where water depths reach tens of meters to several hundreds of metres. Characteristically the zone comprises low energy allochthonous and autochthonous carbonates as well as hemipelagic sediments. Evidence of direct storm reworking is scarce, but storm-related deposits might occur. Bedded (or laminated) argillaceous lime mudstones and wackestones associated and/or interbedded with marl or shale beds are common. Calcisiltite matrix is abundant and biota comprise foraminifera, sponges, bryozoans, brachiopods, molluscs, and echinoderms. Burrows are common. Restricted bottom conditions may develop in deeper outer ramp settings. In the outer ramp environment skeletal grains are usually well preserved. Mudstones, wackestones, packstones and some tempestite beds (grainstones) occur.

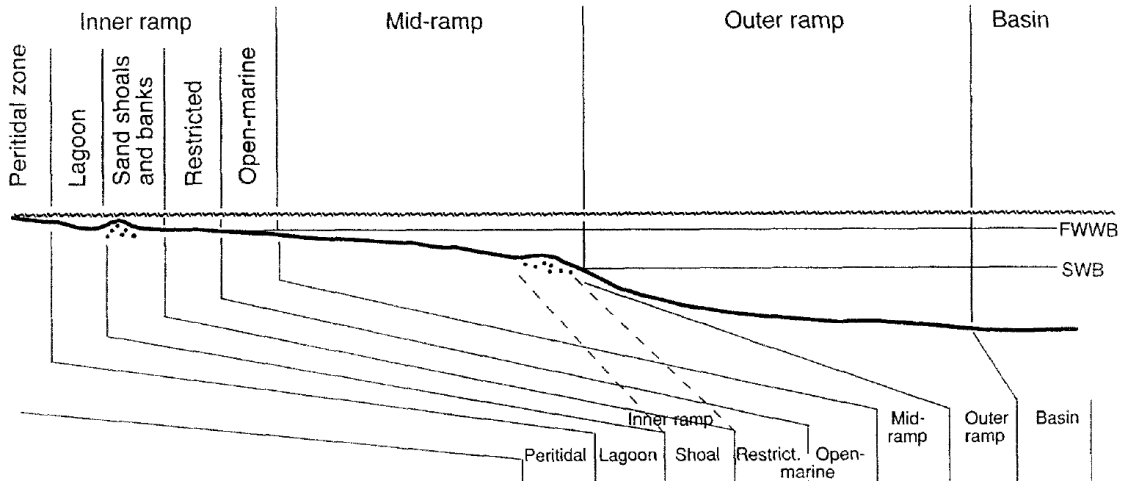

Figure 3: Distribution of microfacies types in different parts of a homoclinal carbonate ramp (generalised) (Flügel, 2004).

1.6 Palynofacies

The term palynofacies was coined by Combaz (1964) to encompass the total complement of acid-resistant organic matter recovered from a sediment or sedimentary rock by palynological processing techniques using HCl and HF. Powell et al. (1990) redefined it as "a distinctive assemblage of palynoclasts whose composition reflects a particular sedimentary environment". Therefore all sedimentary deposits containing organic matter have an associated palynofacies (e.g. consisting of varying amounts of phytoclasts and/or sporomorphs). Ideally, it is an association of organic components that is distinctive of a sedimentary deposit reflecting a particular depositional environment. In practice, however, many palynofacies are biostratigraphical or palaeoenvironmental indistinctive and therefore vary in their interpretative value. Palaeoenvironmental interpretation should hence not be accomplished on palynofacies alone but be considered with reference to other characteristics of a deposit (Tyson, 1995; Traverse, 2007).

Other terms which are commonly used to describe the organic components within a sedimentary rock are “organic matter” (OM) or “sedimentary organic matter” (SOM). Because palynofacies describes the composition of organic matter of sedimentary rocks of distinct depositional environments, the palynofacies analysis represents a suitable approach of characterising certain depositional environments (cf. Tyson 1995). Factors affecting the character of Sedimentary Organic Matter (SOM) on a global scale are time, climate, tectonics and changes in sea level. The kind of sediment and its availability as well as accumulation rate, proximity and composition of the terrestrial vegetation (if present), water chemistry and the biological activity within it are all regionally important. Climate affects the whole range from terrestrial through estuarine to shallow marine environments whereas deeper marine realms are affected only indirectly (Batten et al., 1996).

Sedimentary organic matter derives from various kinds of sources including land plants, associated life forms (e.g. fungi and beetle carapaces), aquatic plants and algae, and a wide variety of resistant bodies, such as the cysts of phytoplankton (Batten & Stead, 2005). Some of these will have been eaten and excreted and therefore also faecal pellets occur in sediments. Most organic material is rapidly degraded by multiple processes (e.g. microbial activity or diagenetic processes), both on its way of transportation and after it has been buried in sediment (Batten et al., 1996). The physical and chemical alterations which occur both before and after deposition, result in the preservation of organic matter in almost all but the most thermally stressed sedimentary rocks (Batten et al., 1996). Thermal alteration of organic matter occurs with increasing depth of burial (catagenesis and metamorphism; e.g. see Bostick, 1979) resulting in a change of colour (e.g. Raynaud & Robert 1976; Suárez-Ruiz et al., 2012), but also chemical reactions take place. Higher temperatures lead to cracking of larger molecules, redistribution of hydrogen atoms and the breaking of some carbon-carbon bonds which results in compounds of increasing hydrogen content. At temperatures above 150°C maturation leads to the production of methane before at even higher temperatures this too ceases and graphite carbon is generated as the end product (Tyson, 1995).

1.6.1 Palynomorphs

The term palynomorph was created by Tschudy (1961) and refers to all discrete acid-resistant, organic-walled microfossils that can be found in a palynological preparation. These palynomorphs are all microfossils.

Since the onset of acritarch occurrences 1.4 billion years ago, palynomorphs consisting of chitinous, sporopolleninous and some other very robust organic compounds occur in sedimentary rocks of all ages and numerous environments (Traverse, 2007). Palynomorphs originate both on land (sporomorphs) and in aquatic environments (fresh water: some algae, some dinoflagellates and a few sporomorphs; salt water: most dinoflagellates, acritarchs, and other algal microscopic remains, foraminiferal test linings and a few sporomorphs). Palynomorphs, particularly sporomorphs and dinoflagellates, tend to be much more abundant than most other fossils. This increased abundance in sediments can be partly explained by the small size of palynomorphs (cf. Jaenicke, 2005). Additionally, sporopollenin, dinosporin (of dinocysts) and chitin which are the basic components of the walls of palynomorphs show substantial resistance against chemically alterations. Due to their small size which is equivalent to silt particles, palynomorphs are sparse or absent in well-sorted, coarse-grained sandstones and fine-grained claystones (Traverse, 2007). Palynomorphs are sensitive to oxidation and high alkalinity but also to high temperatures and pressures and are therefore of limited use when recovered from rocks in which the organic matter has been altered by heat and/or pressure (Traverse, 2007). Only a small fraction of what was produced and is theoretically available for deposition ends up buried in sediment. And even then the majority is at least partly decayed. The degree of reworking of the sediment by currents and storm-wave action and the amount of bioturbation and oxygen levels, all play a major role in the preservation of organic matter. The morphology of grains also has an impact on occurrence and distribution in sediments, since some are more easily transported by wind and water than others (Tyson, 1995; Traverse, 2007). Bacterial decomposition is one of the first reasons for component breakdown, and it is commonly accompanied by fungal attack and physical degradation. Fulvic and humic acids are products of these decomposition processes (Huc, 1980; Tissot & Welte, 1984). In organic matter compositions, the most readily identifiable palynological particles are usually dinoflagellate cysts, acritarchs and other palynomorphs. The amorphous component of many residues may be derived from plant debris, algae and bacteria (Batten et al., 1996). Some amorphous masses may be partly derived from dissolved organic matter that has re-precipitated (Gordon, 1970; Rice et al., 1986; Tyson, 1995). The scarcity of structured marine organic material (marine palynomorphs) in many sediments is caused by the lack of resistant tissues comparable to those of vascular plants – both degradation and maturation destroy morphological characters (Batten et al., 1996).

Sporomorphs

As there is no such thing as an all-encompassing term for those palynomorphs that are spores/pollen of embryophytic plants, Traverse (2007) suggested the term “sporomorphs” which includes various “things with sporopolleninous exines that occur as fossils” including miospores, megaspores, prepollen and pollen. Sporomorphs are palynomorphs which are produced by terrestrial macrophytes (Tyson 1995). During the life cycle of plants, bryophytes and ferns produce spores, whereas pollen are produced by conifers and angiosperms (Armstrong & Brasier, 2005). These microscopic grains can be transported over long distances by wind or water, ultimately settling on the ground of ponds, lakes, rivers and oceans. Generally, transport of small spores and pollen grains by water is seen as more significant than wind dispersal (Batten et al., 1996). Settling rates of small palynomorphs (including miospores) are comparable to those of fine silt. Spores and pollen grains can be especially abundant in

fine grained facies of both marine and non-marine environments (Cross et al. 1966; Bradshaw & Webb, 1985; Batten et al., 1996).
According to Tyson (1995) the fossil spore/pollen can be described basically as a tough, hollow, variously ornamented and grooved bag, ball, or case, from which the inner wall layers and the protoplasm have been removed through biodegradation by bacteria, by fungi and perhaps also by non-biological lysis. In the fossil record, the bag or ball is generally found variously distorted and squashed flat which means that these fossils are not always spheres as idealistically drawn, but disk-like objects that twist and turn.

Fungi

Most probably the fungi that are present in palynological preparations represent terrestrial organisms that attacked wood and leaf detritus (Batten et al., 1996). Fungi can be relatively numerous in Jurassic and younger deposits (cf. Robinson 1990; Taylor 1990; Elsik 1992). However, documentation on the facies distribution of fungal spores in sediments is scarce (Batten et al., 1996). Apparently their presence correlates, at least in part, with abundances of land plant debris and, therefore, can be linked to swamp, fluvial-lacustrine, lagoonal, delta-top and near-shore marine facies (Muller 1959; Cross et al. 1966; Dickinson et al. 1974; Given et al. 1983; Traverse 1992; Oboh 1992a, b; van Waveren 1993). In palynological samples most fungi are preserved as remains of filaments, (structured organic matter) or sclerotia and spores (classified as palynomorphs). If their occurrence is uncommon, they can be grouped as “fungal remains” (Batten et al., 1996).

Dinoflagellates (Phylum Dinoflagellata)

There are various factors that influence the distribution and productivity of dinoflagellates (sunlight, water temperature, salinity, nutrient levels, currents and circulation). Comparable factors and life cycles are thought to apply also to most acritarchs (Tappan, 1980). As part of their life cycle, some dinoflagellates encyst within a resistant sporopolleninous organic wall which may be preserved in the palynological record. Dinoflagellate remains are common in Late Triassic to Recent deposits of fresh water and brackish settings, but most frequently of marine environments (Traverse, 2007). The ratio of cysts to miospores is frequently used as an indicator of proximity to shore and indicates transgressive and regressive phases (Davies et al., 1982; Mutterlose & Harding, 1987; Habib & Miller, 1989).

Acritarchs (Group Acritarcha)

The term “acritarch” means “of uncertain origin” making the acritarchs a polyphyletic group of palynomorphs (Tyson 1995). According to Traverse (2007) most, if not all acritarchs belong to the marine phytoplankton but also many brackish-water or freshwater forms exist. The wall of acritarchs contains sporopollenin or a very similar compound, and with 15–80 μm they range well within palynomorph size. Apparently, acritarch abundance seems to be linked to major variations in global sea-level and a greater potential for speciation in stable shelf environments (Tyson, 1995). In Mesozoic to Cenozoic marine strata they mostly show low diversity and are mostly only a minor component of normal marine microplankton assemblages.

Prasinophyte algae (Division Prasinophyta or Chlorophyta)

Modern forms of the prasinophyte algae are usually placed in the Class Prasinophyceae (division Chlorophyta) (Tyson, 1995, Lewis et al., 2004). The affinity of fossil 'leiosphere' prasinophytes is more difficult because, by definition, they principally lack characteristic morphological features. In contrast to the meroplanktonic cyst-forming dinoflagellates, the prasinophytes have holo- planktonic life cycles and therefore show more pelagic distribution patterns. They tend to be most common in finely laminated organic-rich and oxygen depleted deposits (Wall & Dale, 1974; Tappan, 1980). Even if prasinophytes are abundant in organic-rich deposits the palynofacies are usually dominated by AOM (Batten et al., 1996). Their presence in basin margin successions generally indicates marine or brackish-marine conditions but can also point to short-lived marine incursions (Guy-Ohlson & Norling, 1988; Lister & Satten, 1988). Sometimes they have also been reported from deposits of hypersaline and partly anoxic lagoonal environments (Hunt, 1987).

Foraminiferal Inner Tests (= "Foraminifera")

The "chitinous" linings of benthonic and possibly also some planktonic foraminifers have a lipid or polysaccharide composition, nearly always occur in planispiral forms and indicate marine depositional environments (Ercegovac & Kostić, 2006), although they can also be abundant in estuarine marshes with varying salinities (Farr, 1989). They have been widely used as marine indicators in ancient successions (Lister & Batten, 1988; Courtinat, 1989; Stancliffe, 1989; Courtinat & Méon, 1991; Oboh, et al., 1992), whether occurring in abundance or as isolated specimens (Batten et al., 1996). They can be common in carbonates (Traverse & Ginsburg, 1966), in warm, shallow waters of clastic shelfs that are only marginally affected by terrestrial input and in deposits beneath areas of upwelling (Cross et al., 1966; Powell et al., 1990; van Waveren, 1993). They have also been associated with restricted marine settings that were prone to the accumulation of AOM (e.g. Powell et al., 1990; Courtinat & Méon, 1991) and, as redeposited elements, with deep water turbidites (Tyson, 1984).

1.6.2 Phytoclast Group

Both macroscopic and microscopic remains of land plants may be abundant in sediments ranging in grain size from muds to fine sands. Most terrestrial organic matter accumulates within fluvial-lacustrine systems, in estuaries and in near shore marine environments (Tyson, 1995). Once in the sea, it tends to be deposited on the inner shelf where it is often altered by reworking and biological degradation. Particulate organic matter may, however, also be concentrated in turbidites (Habib, 1983; Tyson, 1984).

The majority of dispersed fossilising phytoclasts are derived from the ligno-cellulosic tissues of terrestrial macrophytes (Tyson, 1995). Many phytoclasts are, therefore, modified lignocellulosic matter that has its origins in vascular and mechanical support tissues (xylem) of plants exhibiting secondary growth. It is only slowly degraded by bacteria and fungi. Most of the wood in Mesozoic deposits is gymnospermous (Batten et al., 1996).

Opaque and semi-opaque phytoclasts

Opaque material is formed during desiccation, oxidation and fungal mouldering of woody material which was exposed to atmospheric oxygen of peats and soils (Tyson, 1995). It seems likely that a gradually degradation of phytoclasts takes place during the ways of transportation. Highest values of degradation occur, where the wood is at least periodically exposed to the atmosphere in alternating wet-dry cycles. Coupled with this, there are also the effects of thermal alteration to be taken into account; the higher the maturation level, the lower the chances of encountering any particles that are not black (cf. Batten, 1982).

Cuticles

Cuticles are the outermost cover of epidermal cells of leaves and stems of most higher plants (Batten et al., 1996). Especially when the overlying wax layer is missing or damaged, cutin is more vulnerable to degradation than lignin. Due to their susceptibility to degradation, their abundance in the sediment decreases rapidly away from delta distributaries (Muller, 1959; Gastaldo & Huc, 1992). Therefore cuticles become reduced to small pieces and uncommon in the marine realm (Batten et al., 1996).

Frequency distribution of phytoclasts

Proportion and texture of the remains of higher plant material are good indicators for the characterisation of the depositional environment concerning its distance to the mainland and temporal change of facies (Cassens, 1999). Abundance and preservation state of phytoclasts, for example, point to the relative distance to terrigenous provenance of the fluviatile or turbiditic transport systems. In the stratigraphic and lithofacies context changes of the proportions of phytoclasts can also be used to delineate shallowing upward cycles. In the ideal case a shallowing upward cycle is connected to an increase in input of phytoclasts by concurrently decreasing abundances of the relatively autochthonous palynofacies-fraction of marine plankton (Cassens, 1999).

The ratio of oxidised (opaque) to non- or barely oxidised (translucent) phytoclasts gives information about the depositional environment (Tyson, 1995). The proportion of opaque to translucent phytoclasts is both influenced by the length of the route of transport and by the redox-conditions within the uppermost sediment-layers (Tyson, 1995; Bombardiere & Gorin, 1998). Distal depositional environments are characterised by long routes of transport increasing the OP/TR-values (opaque phytoclasts dominate) due to oxidation at the water surface. Typical phytoclast-associations for those scenarios are composed of mainly small and spherical particles. Post-sedimentary oxidation of the phytoclasts is indicated by concurrent sandy, subaeric lithofacies or highly reworked and redeposited sediments (Tyson, 1995). Both the effects of resedimentation and extreme low rates of sedimentation may lead to nearly complete oxidation of the phytoclasts (Bombardiere & Gorin, 1998).

1.6.3 Zooclasts

In palynological preparations organic particles derived from animals are not common and are often only present in trace amounts (Tyson, 1995). Zooclasts may be differentiated from plant cuticles due to their stronger fluorescence (Goodarzi, 1984). Fragments of arthropod exoskeletons occur in Silurian and younger deposits. Organic linings of ostracod (Goodall et al., 1992) and bivalve shells might also be found.

1.6.4 Amorphous Organic Matter

The term amorphous organic matter (AOM) implies the lack of a distinct shape or outline. Most commonly a combination of grazing, bacterial, fungal and other degradation processes leads to the loss of structured outlines (Tyson, 1995; Batten et al., 1996). The physical appearance and chemical composition of all AOM is not invariably the same (Batten et al., 1996) but rather depends on origin, environment of deposition and degree of thermal alteration (Batten, 1983). Pacton et al. (2011) suggest that AOM can have different origins in a similar environment, and can be composed of autochthonous and more or less degraded allochthonous particles. Among all constituents of sedimentary organic matter, AOM is very problematic in terms of palaeoenvironmental interpretation. According to Tyson (1995), AOM is the dominant organic component in dysoxic to anoxic depositional environments and its abundance increases with growing nutrient availability and decreasing oxygen in the water.

AOM of terrestrial origin

AOM of terrestrial origin (AOMT) comprises biodegraded remains of land plant tissues (Stach 1982; Teichmüller 1982; cf. Styan & Bustin 1983). What remains of this process are featureless degraded tissues in which (almost) all signs of the original composition have been destroyed. According to Batten (1973, 1983) such organic matter may dominate palynofacies assemblages associated with shallow fresh to brackish water lagoonal and swamp-marsh conditions. Palynomorph and phytoclast composition of the rest of the sample is another indicator towards a possible terrestrial origin of the AOM (Batten, 1981).

AOM of aquatic origin

There is often a continuous gradation from particles suggesting derivation from higher plants to entirely unstructured masses (Tyson, 1995). In transmitted light it is therefore often difficult to distinguish between AOM of structureless terrestrial and marine origin. Organic matter of amorphous shape of aliphatic (algal) structure shows stronger fluorescence than that of mainly aromatic (woody) structure (Bertrand et al., 1986). Most easily, AOM of marine origin (AOMA) is thus determined in fluorescent light, provided that it is thermally immature (biochemical fluorescence) or mature to the state of liquid hydrocarbon generation (thermochemical fluorescence; e.g. Bujak & Davies, 1983). Unfortunately, organic matter loses its ability to fluorescence with stronger degradation (e.g. Tyson, 1995; Batten et al., 1996). Some marine palynomorphs may be transformed to AOMA and deposited as faecal pellets (Bradley, 1966; Honjo & Roman, 1978; Turner & Ferrante, 1979; Pilskaln & Honjo, 1987) and these may be preserved in ancient sediments (Porter & Robbins, 1981; Batten, 1983).

1.6.5 Reworked Organic Matter

Reworked palynomorphs are usually less common in palynological samples than particles that are in situ; the two can be distinguished if they differ significantly in colour, and/or preservation state. Gregory and Hart (1992) link reworking to parts of lowstand and highstand systems tracts in sequence stratigraphic interpretations. Recycling might also be implied by the presence and ratio of rounded to angular phytoclasts, varying degrees of degradation of those particles and colour differences in the amorphous debris.

1.6.6 Importance of Anoxia

The lower the energy of a depositional environment, the closer it gets to the state of stagnation. This condition is characterised by very little disturbance and lowered oxygen levels in which the accumulating organic matter is only partially consumed by bacteria or other organisms (Tyson, 1995). In such low-energy settings the bottom-water and possibly also (some of) the overlying water column are dysoxic or anoxic. As several authors (e.g. Calvert & Pedersen, 1992; Jewell, 1992; Bertrand & Lallier-Verges, 1993) showed, anoxia seems to be a key to preservation of sedimentary organic matter. Anoxia is favoured by accompanying marine transgressions, especially in restricted (silled) basins (Rhoads & Morse, 1971; Demaison & Moore, 1980; Marshall & Batten, 1988; Arthur & Sageman, 1994). High productivity increases the probability of anoxia but is not inevitably the determining factor (Tyson & Pearson, 1991). The exceeding demand for oxygen by bacteria and other organisms may occur only in the upper few centimetres of sediments and at the sediment/water interface, but in some cases it may also extend upwards into the water column (Tyson et al,. 1979; Waples, 1983).

1.7 Geological Framework and Sections

Spreading of the Central Atlantic took place between 160 and 140 Ma and after its cessation the mid-ocean ridge jumped southward initiating the opening of the proto-Caribbean Basin (Seton et al., 2012). At around 145 Ma spreading formed a triple junction to the east between the mid-ocean ridge of the Central Atlantic and rift axis of the Equatorial/South Atlantic. To the west, the spreading ridge of the proto-Caribbean Basin formed a ridge–ridge–transform triple junction with the spreading ridge of the Andean back-arc basin and the trans-American subduction zone. The Agulhas-Falkland transform extended eastward connecting to the mid-ocean ridge in the Weddell Sea, which was established at 160 Ma. The Weddell Sea ridge joined with mid-ocean ridges along East Africa, including between Africa and Antarctica (Fig. 4).

Figure 4 (Page 22): Global plate reconstructions at 160 Ma (Seton et al., 2012); abbreviations include: ALA = Alaska, CA = Central Atlantic, CAP = Capricorn, CAR = Caribbean, CAT = Catequil, CCO = Cache Creek Ocean, COL = Colorado, CS = Caroline Sea, JUN = Junction, MOO = Mongol–Okhotsk Ocean, NL = North Loyalty Basin, NMT = North Meso-Tethys, NNT = North Neo-Tethys, PAR = Parana, PAT = Patagonia, PS = Philippine Sea, PSC = Proto-South China Sea, SCO = Scotia Sea, SLB = South Loyalty Basin, SMT = South Meso-Tethys, TS = Tasman Sea.

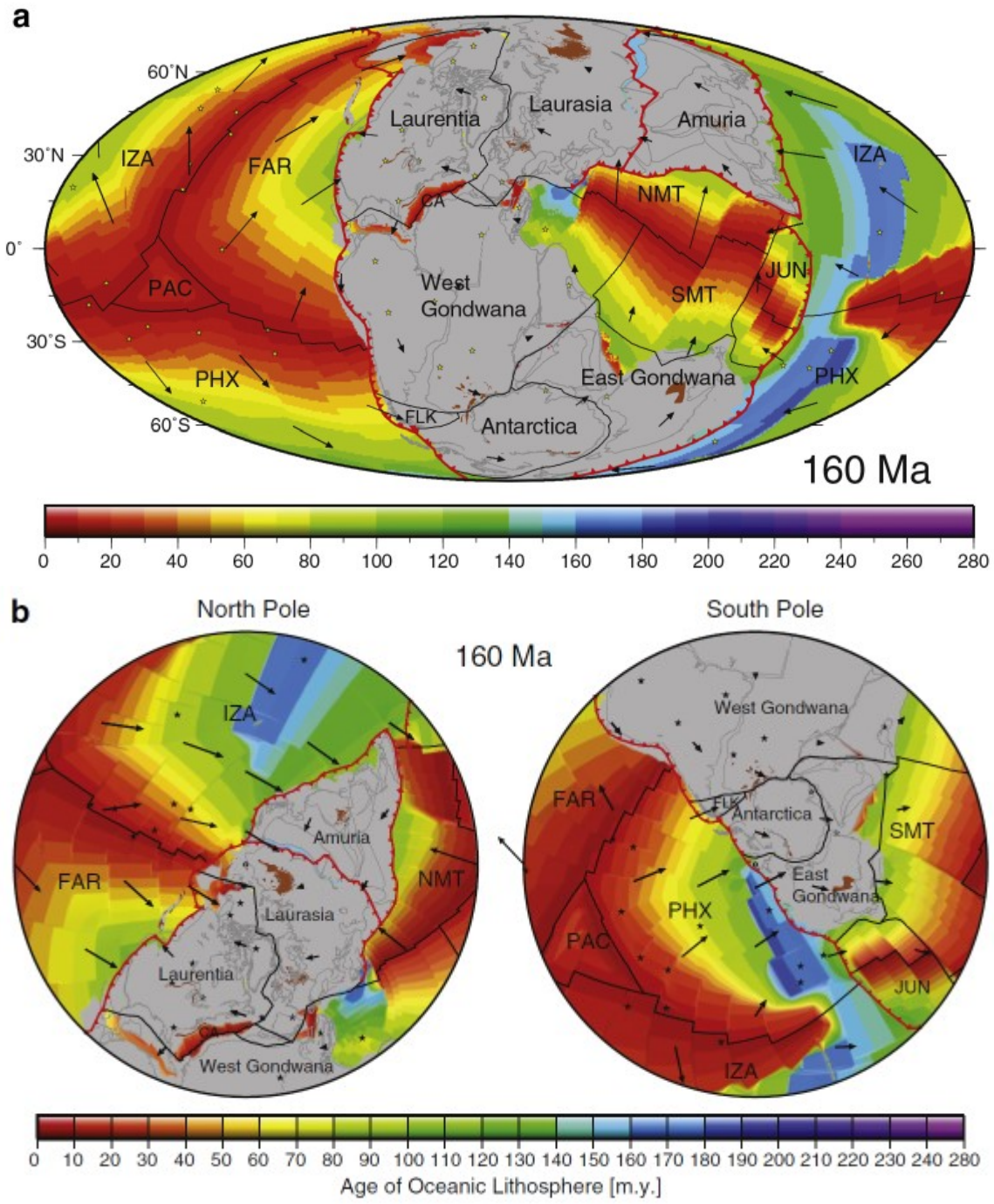

The E–W trending Phoenix lineations form the southern arm of the Pacific triangle (PAC) (Fig. 4a) with magnetic anomalies ranging from ~156–123 Ma (Larson, 1976; Cande et al., 1978; Atwater, 1990). The lineations disappear under the Ontong Java Plateau to the west and abut against a complex set of fan-shaped lineations (Magellan lineations) and NE–SW directed lineations (~147–136 Ma) south of the Mid-Pacific Mountains (Nakanishi & Winterer, 1998) to the east (Fig. 4). The complex Magellan and Mid-Pacific lineations suggest the existence of several microplates (e.g. Trinidad and Magellan) at the Phoenix (PHX)–Pacific (PAC)–Farallon (FAR) triple junction (Atwater, 1990) (Fig. 4b).

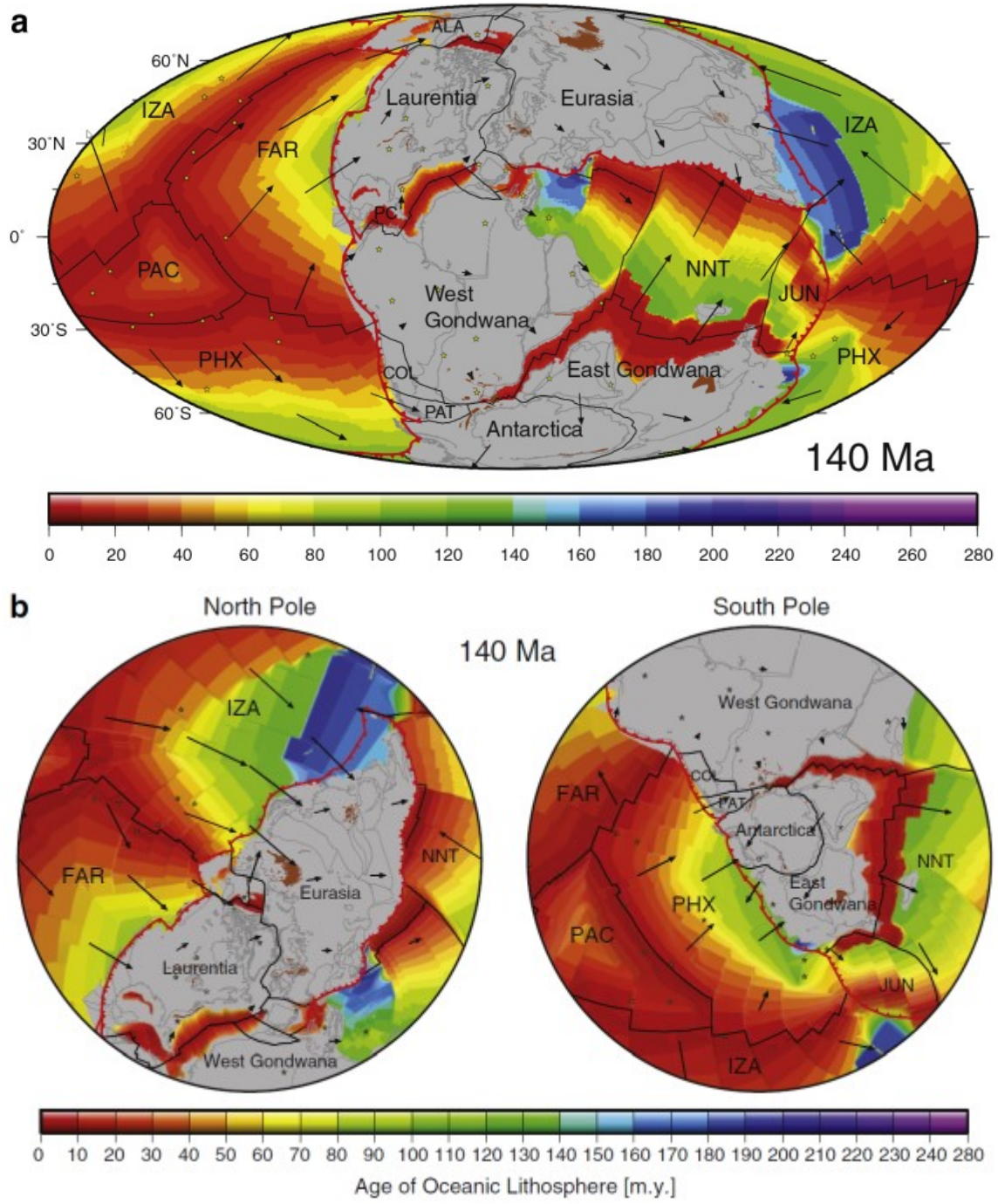

Figure 5: Global plate reconstructions at 140 Ma (Seton et al., 2012); abbreviations as in Fig. 4.

The early–mid Cretaceous (140–120 Ma) marks a significant increase in seafloor spreading rates in Panthalassa corresponding to the mid-Cretaceous seafloor spreading pulse (Seton et al., 2012). Spreading occurred between the Pacific (PAC), Farallon (FAR), Izanagi (IZA) and Phoenix (PHX) plates (Figs. 5a, 5b). The East African and Weddell Sea spreading ridges were active during this time period and connected to the South Atlantic via the Agulhas-Falkland transform (Fig. 6) (Seton et al., 2012).

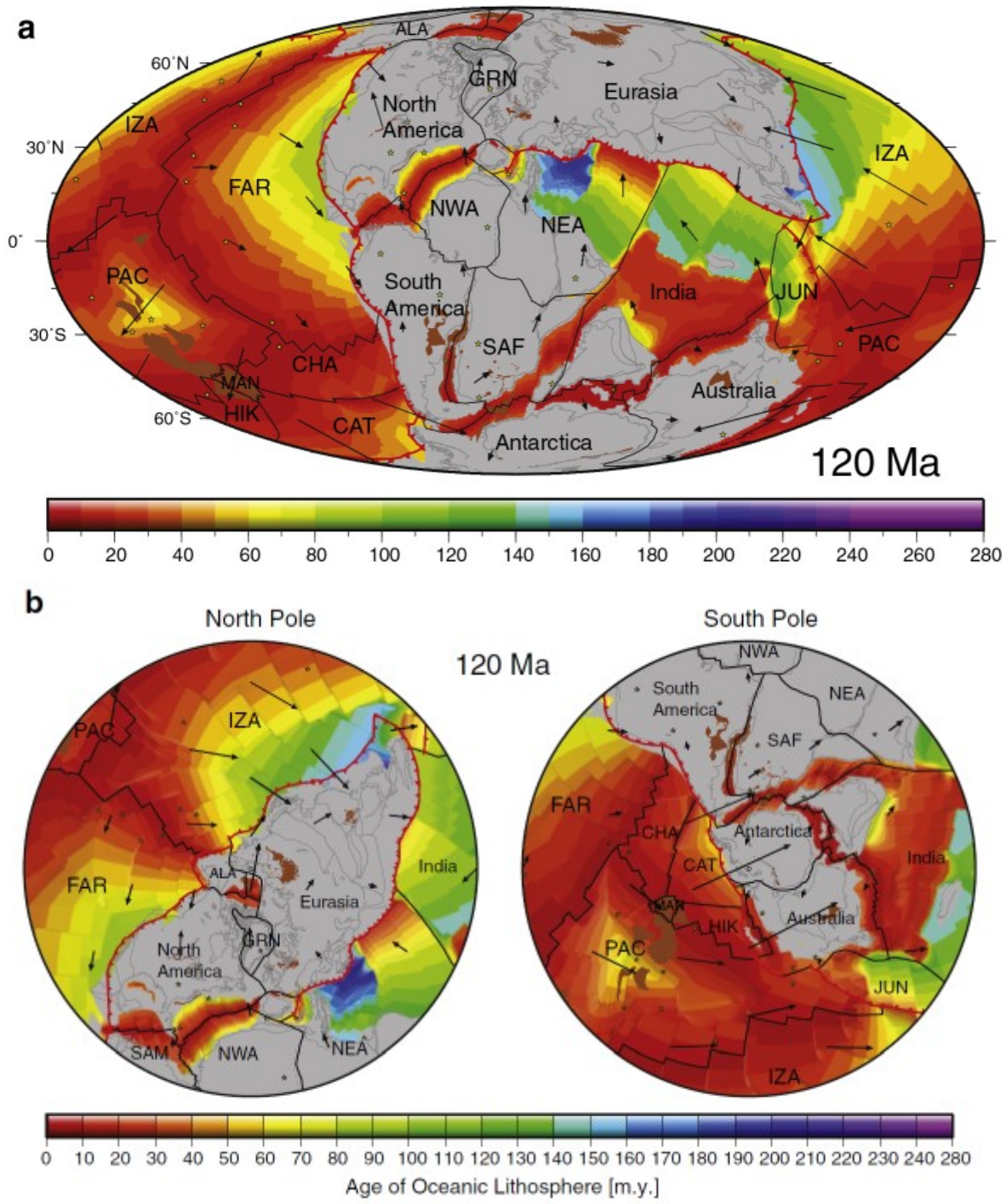

Figure 6: Global plate reconstructions at 120 Ma (Seton et al., 2012); abbreviations as in Fig. 4.

1.7.1 Central Chile

In central Chile, the Late Jurassic–Early Cretaceous subduction of the Farallon and Pheonix plates under the continental South American plate (Seton et al., 2012) resulted in the separation of the region in a dynamic volcanic arc with fore-arc, intra-arc and back-arc basins (Mpodozis & Ramos, 1989) (Figs. 7, 8). Two separate depositional areas accumulated marine deposits during the Late Jurassic to Early Cretaceous due to morphological changes caused by the flat-slab subduction zone. In the two segments which are located today between 18°–27°S and 33°–46°S, the Central Depression (the morphological unit that separates the Coastal Cordillera from the Principal or Main Cordillera) is well developed (Charrier et al., 2007; Charrier et al., 2014). A volcanic arc separates the two basins and allows for the identification of three palaeogeographic domains (Fig. 8).

Sedimentary Basin

From west to east, these are the Lo Prado fore-arc Basin and the Mendoza-Neuquén back-arc Basin, separated by the Lo Prado-Pelambres Volcanic arc (Figs. 7, 8) (Charrier et al., 2007). In the region of central Chile (today at 30°S to 39°S) the back-arc basin is considerably wider in E-W direction than to the north, and is known as the Mendoza–Neuquén Basin (Fig. 7). This depocentre represents the southernmost part of the Jurassic–Early Cretaceous back-arc basin that gradually bends south and extends eastwards into Argentina (Fig. 7). It extends, without interruption, along the eastern side of the magmatic arc from southern Peru to southern Chile (Charrier et al., 2007). The studied area (Figs. 7, 8) forms part of the central Chilean subduction system (Charrier et al. 2007) and represents a succession of volcanic rocks and intercalated sediments reaching from the Jurassic to present (Salazar, 2012). As it forms part of the Andean orogeny, the succession was repeatedly compressed and folded since the late Cretaceous. Tectonic orientations follow the regional trend and are directed North-South. In the western part of the Mendoza–Neuquén Basin, in central Chile at the latitude of Santiago, the Upper Jurassic–Lower Cretaceous transgression–regression cycle is conformed by a thick succession of neritic to shallow marine sediments of the San José (Aguirre, 1960), Lo Valdés (González, 1963; Hallam et al., 1986) and Baños del Flaco (Klohn, 1960; González & Vergara, 1962; Covacevich et al., 1976; Arcos, 1987) formations. In the segment of Santiago-Curicó, the Upper Jurassic and Lower Cretaceous sediment succession is differentiated in the Río Colina, Nacientes del Teno, Rio Damas, Leñas Espinoza, Baños del Flaco and Lo Valdés formations.

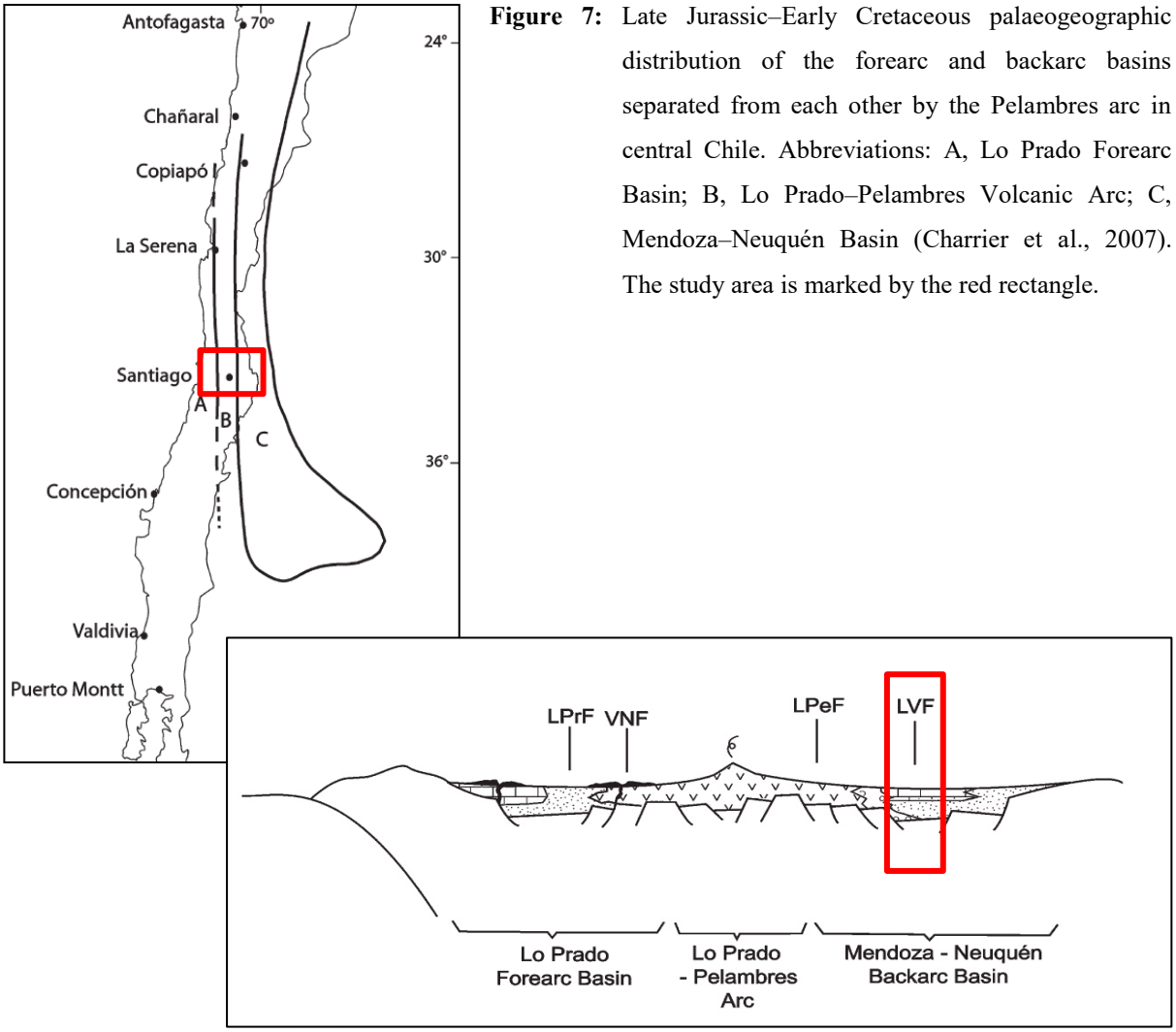

Figure 7: Late Jurassic–Early Cretaceous palaeogeographic distribution of the forearc and backarc basins separated from each other by the Pelambres arc in central Chile. Abbreviations: A, Lo Prado Forearc Basin; B, Lo Prado–Pelambres Volcanic Arc; C, Mendoza–Neuquén Basin (Charrier et al., 2007). The study area is marked by the red rectangle.

Figure 8: Schematic palaeogeographic cross-section for the first substage (late Early Jurassic–late Early Cretaceous) of the Andean evolution in central Chile between 32ºS and 33ºS (after Charrier et al., 2007). Abbreviations: LPeF, Los Pelambres Formation; LPrF, Lo Prado Formation; LVF, Lo Valdés Formation; VNF, Veta Negra Formation. The study area is marked by the red rectangle.

Lo Valdés Formation

In the central Chilean study area, two sections of the Lo Valdés Formation (Lo Valdés and Cajón del Morado) were analysed, which were previously described lithostratigraphically by Salazar and Stinnesbeck (2015a), resumed here:

Lithostratigraphy

The Lo Valdés Formation is exposed in the high Andes of central Chile, east and southeast of Santiago, and was deposited as part of the northwestern Neuquén basin, which is majorly defined on the eastern side of the Andes in Argentina (Fig. 8, 9) (Charrier et al., 2007). The Lo Valdés Formation

was originally defined by González (1963) and Biro (1964) divided the unit into three lithostratigraphic members (from bottom to top): (1) "Spilitas", member, dominated by porphyric andesite ("spilite") and volcanic breccia, lower-middle and lower part of the Late Tithonian, (2) "Arenáceo", member, composed mainly of sandstone and minor conglomerate and breccia, middle part of the Late Tithonian, (3) "Calcáreo", upper member, consisting of limestone, siltstone and calcareous sandstone, latest Tithonian to Hauterivian, or possibly Barremian (Biro, 1964).
Salazar and Stinnesbeck (2015a) emended the formation and proposed a formal separation of the volcanic "Spilitas" member from the overlying sedimentary rocks of the Lo Valdés Formation. The Lo Valdés Formation therefore comprises the former "Arenáceo" and "Calcáreo" members and consists of siliciclastic and carbonaceous sedimentary rocks. The formation was formally divided by Salazar and Stinnesbeck (2015a) into three members (from base to top), the Escalador, Placa Roja and Cantera Members. The formation conformably overlies continental "red-bed" deposits of the Río Damas Formation, assigned to a delta system of the Kimmeridgian. It conformably underlies continental deposits of the Colimapu Formation of Aptian-Albian age (Klohn, 1960; Thiele and Cubillos, 1980).
The thickness of the Lo Valdés Formation reaches 1173 m at Cajón del Morado and 1635 m at the type locality at Lo Valdés (Salazar and Stinnesbeck, 2015a). In both localities the sections consist of andesite, conglomerate, sandstone, siltstone, limestone and volcanoclastic rocks. De Lurio and Frakes (1999), Biro-Bagóczky (1964), Hallam et al. (1986) and Salazar (2012) assigned a Lower-Middle Tithonian to Hauterivian-?Barremian age to the succession. At the type locality, Salazar and Stinnesbeck (2015a) divided the unit into three members, from bottom to top: (1) Spilite Member, 762 m thick, dominated by porphyric andesite and volcanic breccia, and infrequent layers of sandstone, limestone and siltstone. They assigned this member to the lower-middle and lower part of the Upper Tithonian. (2) Sandstone Member, 72 m thick, mainly composed of sandstone and minor conglomerate and breccia. Salazar and Stinnesbeck (2015a) assigned this member to the middle part of the Upper Tithonian. (3) Calcareous member, 622 m thick, consisting of limestone, siltstone and calcareous sandstone; this unit also contains a 20 m thick andesite. The two sections analysed in the present study are located within this upper member, which was assigned to the uppermost Tithonian to Hauterivian-?Barremian. A detailed description of the fossil assemblage of the Lo Valdés Formation was given by Salazar (2012).

Tectonic background and paleogeography

Stratigraphic and geochronological data indicate that during the Late Jurassic to Early Cretaceous (~160-140 Ma), the progressive emersion of the Andean arc and fore-arc domains disconnected the Neuquén back-arc region from the Pacific Ocean (Rossel et al., 2014). Back-arc volcanic intercalations are intermittently present within the Tithonian of the Lo Valdés Formation (Biro-Bagóczky, 1964). During the Tithonian, the northwestern Neuquén basin may not have been well connected with the Tethyan region, as is suggested by the dominance of endemic taxa (Salazar, 2012; Salazar & Stinnesbeck, 2015b). During the Berriasian, new pathways between Antarctica and South America–Africa are suggested by the dominance of Cosmopolitans and abundance of Indo-Pacific taxa (Salazar, 2012). It is suggested that the Indo-Austral Seaway was linked to the eastern Tethys since the Early Cretaceous (Stinnesbeck et al., 2014).

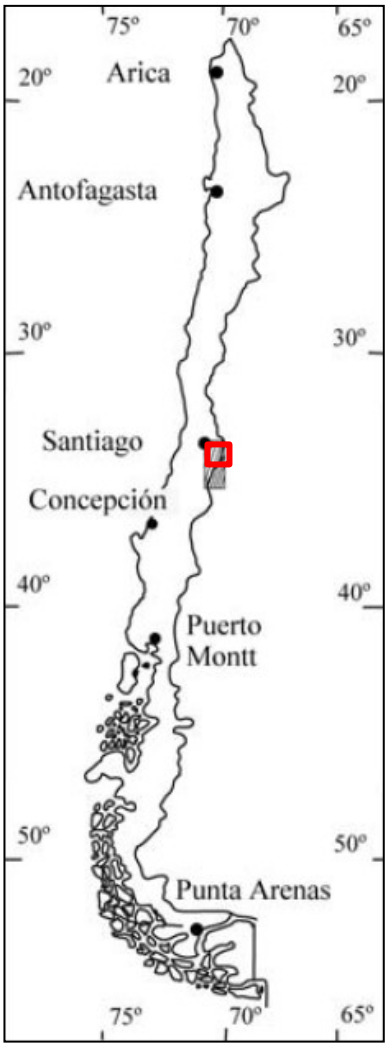

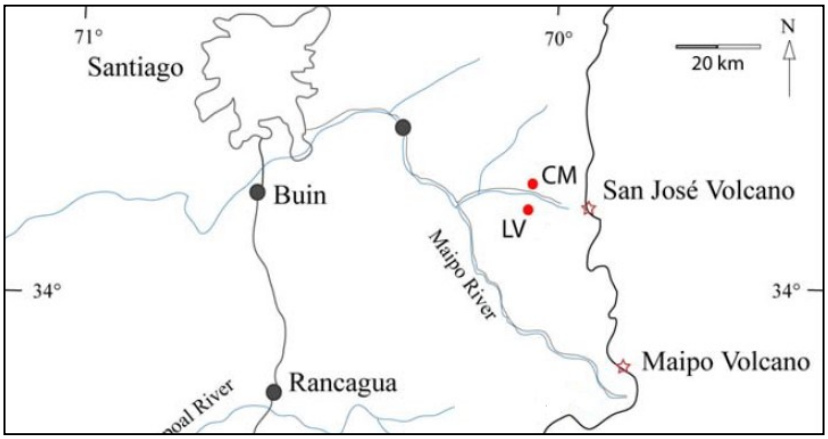

Figure 9 (top)**:** Indication of the localities east of Santiago; Salazar and Stinnesbeck (2015a). The studied sections are marked by red dots.

Figure 10 (left)**:** Map of Chile with indication of the study area (red rectangle).

Cajón del Morado Section

The Lo Valdés Formation is exposed on the eastern hillside of the Cajón del Morado valley, at approximately 6 km north of the Baños Morales village (Figs. 9, 10). At Cajón del Morado (GPS: -33.777500, -70.030556) the Tithonian to Hauterivian interval of the Lo Valdés Formation is 582 m thick (Salazar, 2012).

Escalador Member: The sandstone member is 160 m thick and overlies the Andesite with a sharp and possibly non-conformable contact. The lowermost unit consists of cross-laminated calcareous sandstone with fragments of bivalves and gastropods. Upsection, a combination of alternating sandy limestone and calcareous sandstone is present. These sediments are occasionally laminated, while ooids were identified in other units. Fossils are abundant and comprise bivalves (e.g. inoceramids, oysters and trigoniids), gastropods, ammonoids, scarce algae, bryozoans, sponges and corals (Placocoeniidae) (Salazar, 2012).

Placa Roja Member: The siltstone member is 217 m thick and consists of siltstone, calcareous siltstone and silty limestone (biomicrite, wackestone and packstone) with abundant organic matter and occasional disseminated pyrite. The fossil assemblage consists of ammonoids, oysters and other bivalves, algae, benthic foraminifers, rare fragments of gastropods and echinoderms. The top of the

member is characterised by a 5 m thick horizontally laminated silty limestone (biomicrite, wackestone) with disseminated pyrite, organic matter and abundant fossil remains. The contact between the Siltstone Member and overlying Limestone Member is gradual and characterised by an increase in carbonate content (Salazar, 2012).

Cantera Member: Between 376 m and 582 m, the section is predominantly composed of limestone (calci-mudstone, wackestone) interlayered with silty limestone and calcareous siltstone. The base of the unit is characterised by a rhythmically bedded succession of silty limestone (biomicrite, calci-mudstone). The faunal assemblage consists of ammonoids, common fragments of oysters, other bivalves, rare annelids, echinoderms, bryozoans and pentacrinoids. Disseminated pyrite is common. Faunal abundance decreases in the middle part of the unit (454 m to 483 m) but increases again in the upper part. The lower 20 m, from 513 m to 533 m, are characterised by calcareous siltstone.

Lo Valdés Section

The type locality of the Lo Valdés Formation is situated on the southern side of the Rio Volcán valley, located between Cerro Catedral and Quebrada Lo Valdés (GPS: -33.830556, -70.047778) (Figs. 9, 10). In the type Locality at Lo Valdés the total thickness of the Tithonian–Hauterivian deposits is 539 m (Salazar, 2012).

Escalador Member: The sandstone member is approximately 73 m thick and forms the base of the Lo Valdés Formation. It consists of well-sorted and fine-grained calcareous sandstone with occasional horizontal and cross-lamination. Fossil content includes ammonoids, inoceramids, oysters, trigoniids and other bivalves, rare gastropods and corals. The uppermost part of the Sandstone Member is devoid of fossils (Salazar, 2012).

Placa Roja Member: The siltstone member is 193 m thick and consists of siltstone, calcareous siltstone and silty limestone. A unit of rhythmically bedded siltstone and calcareous siltstone forms the base of the Member. Its fossil content is restricted to ammonoids, oysters, inoceramids and other bivalves, rare gastropods, radiolarians, benthic foraminifera as well as calcispheres. The member contains high concentrations of organic matter. Between 193 m and 242 m the calcareous siltstone and silty limestone show horizontal lamination and disseminated pyrite. Up section, the unit consists of rhythmically bedded calcareous siltstone and silty mudstone to wackestone with horizontal lamination. The uppermost unit of the Member is conformed by silty limestone and calcareous siltstone (Salazar, 2012).

Cantera Member: The limestone member is 252 m thick and consists of sandy and silty limestone and calcareous siltstone. The base of the member, from 287 m to 390 m, is a 103 m thick unit of sandy wackestone. Infrequent layers with increased amount of disseminated pyrite occur. Faunal content consists of ammonoids, oysters, inoceramids, other bivalves, foraminifers, gastropods, bryozoans and echinoderms. From 390 m to 446 m, a unit of sandy wackestone is highly fossiliferous. Between 446 m and 539 m, sandy wackestone is intercalated with calcareous siltstone. A fossil-free volcanoclastic breccia with angular clasts of silty limestone overlies the Lo Valdés Formation with a conformable contact (Salazar, 2012).

1.7.2 Patagonia

Sedimentary Basin

The Austral Basin (Rocas Verdes Marginal Basin/Magallanes Basin) (Fig. 11) comprises an approximately 8.000 m thick sedimentary succession which dates from the Late Jurassic to Cenozoic and is almost exclusively composed of siliciclastic rocks (Valera et al., 2012). Towards the south it overlies the Tierra del Fuego igneous and metamorphic basement complex (Hervé et al., 2010). Carbonate sediments are of limited thickness and are restricted to a few locations within the basin (Peroni et al., 2002). The Austral Basin is a back-arc basin of Late Jurassic–Early Cretaceous age that is characterised by rifting and sea-floor spreading along the western margin of the Patagonian-Fuegian Andes (Katz, 1963; Dalziel et al., 1974; Dalziel, 1981; Biddle et al., 1986; Calderón et al., 2007a). Today, the Magallanes/Austral Basin is located on- and offshore in the southernmost region of South America in Argentina and Chile (Fig. 11) and lies south of the Aysen triple junction (46°30'S) of the South American, Nazca and Antarctic plates (Ramos, 1989; González et al., 1998). The Río Chico High represents its continuation to the south, separating this basin from the neighbouring offshore Malvinas Basin to the east (Schwarz et al., 2011; Sachse et al., 2016). The Magallanes/Austral Basin covers an area of about 230.000 km^2, with ~85% of its expanse located in Argentina (Schwarz et al., 2011). To the northeast, it bounds to the Deseado Massif, an old basement high, while its western limit is the Patagonian batholith (Upper Proterozoic–Lower Cambrian) and the deformed belt of the Southern Andes (Biddle et al., 1986; González et al., 1998). The geologic evolution of the basin is closely linked to volcanic activity and subsidence during the breakup of Gondwana, which is evident since the Late Triassic and Early Jurassic (González et al., 1998). The evolution and development of the basin accomplished within three stages (Biddle et al. 1986, Schwarz et al., 2011; Varela et al., 2012).

Rift/Syn-rift stage: This stage is dated to the Middle-Late Jurassic and led to the development of the Rocas Verdes Basin, reflecting the opening of the Weddell Sea. It is characterised by extensional asymmetric hemigraben tectonics and basins filled by lacustrine, volcaniclastic and alluvial sediments of the **"**Serie Tobífera**"**. To the west, in the Chilean region of the basin, marine sediments are assigned to the Oxfordian–Kimmeridgian. The rift and thermal subsidence stages of the Austral Basin mainly coincide with the deposition of the Rocas Verdes Marginal Basin, whereas the foreland stage of the Austral Basin is simultaneous with the evolution of the Magallanes Basin (Varela et al., 2012).

Thermal subsidence stage: During the Late Jurassic–Lower Cretaceous (?Tithonian, Berriasian–Barremian) sag/thermal subsidence phase, the basin was located inside a magmatic arc with active subduction, and represented a back-arc setting with relatively constant subsidence. Deposition of the Springhill-Río Mayer/Zapata Formation took place during the sag phase that represents a long-term (>25 Ma) transgressive cycle characterised by low-frequency sea-level fluctuations (Schwarz et al., 2011; Varela et al., 2012).

Foreland stage: Several pulses of deformation occurred during the foreland phase of the basin, dated to late Early Cretaceous (Aptian) to Cenozoic. During this interval, deformation and depocentres migrated south- and eastwards. Several transgressive-regressive megasuccessions are identified for the Cretaceous, which were controlled by both regional tectonics and global eustasy (Schwarz et al., 2011). During the Cretaceous, the Tierra de Fuego region persisted in an offshore setting.

As extension decreased, fine-grained sediments of the Lower Cretaceous marine Zapata Formation accumulated in the Rocas Verdes Basin, with sediment input derived from local basement uplifts (Fildani & Hessler, 2005; Varela et al., 2012). Early Cretaceous subsidence and sedimentation continued for almost 20 Ma to the onset of foreland basin sedimentation at around 100 Ma (Fildani et al., 2003; Fildani & Hessler, 2005; Calderón et al., 2007a; Fosdick et al., 2011). The presence of a well-developed subaerial fold-and-thrust belt is indicated by deep-marine sedimentation of the Punta Barrosa Formation overlying shelf-marine sediments of the Zapata Formation (Wilson, 1991; Fildani et al., 2003; Fildani & Hessler, 2005; Romans et al., 2010, 2011; Fosdick et al., 2011).

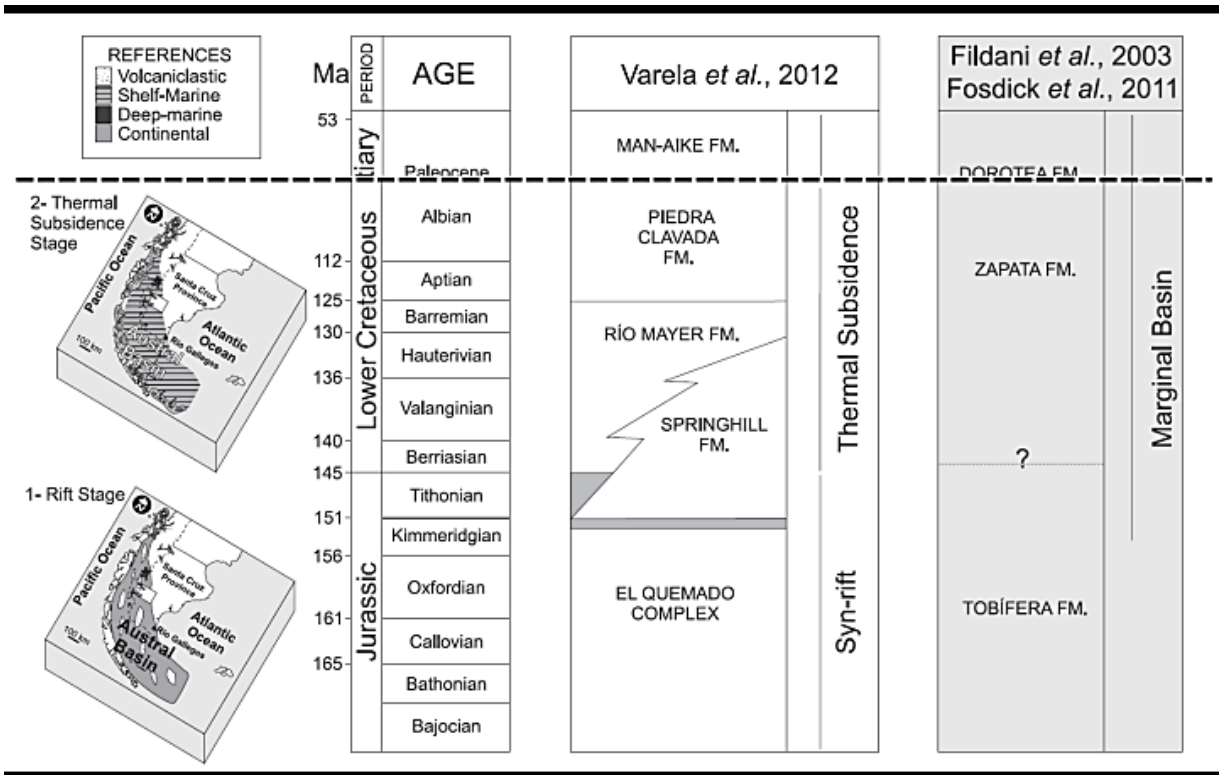

Fig. 11: Stratigraphic summary and geological history of the Austral Basin from the Jurassic to Lower Cretaceous (excluding the foreland stage) compared to the Rocas Verdes Marginal Basin-Magallanes Basin. Middle to Upper Jurassic "Rift/Syn-rift Stage"; Upper Jurassic to Lower Cretaceous "Thermal Subsidence Stage"; modified from Varela et al. (2012).

Springhill/Río Mayer Formation

Lithostratigraphy

The sampled interval of the Springhill/Río Mayer Formation of the Nevenka 1 core (GPS: -52.588539, -69.333403) was deposited mostly during the Late Barremian–Early Aptian. The sampled interval is located in the southern Austral Basin (Magallanes Basin) (Fig. 12), where the Aptian part of the sedimentary succession belongs to the Río Mayer Formation (Archangelsky et al., 2009). The

succession is composed of fluvial, marginal-marine, coastal and shallow-marine siliciclastic rock deposits with a general retrogradational stacking pattern (Kielbowicz et al., 1984; Biddle et al., 1986; Arbe & Fernández Bell Fano, 2002; Schwarz et al., 2011).

Tectonic background and paleogeography

The Austral Basin (Magallanes Basin) was characterised by rifting and sea-floor spreading along the western margin of the Patagonian-Fuegian Andes (Biddle et al., 1986; Calderón et al., 2007a; Fosdick et al., 2011). The Early Cretaceous sediment succession represents a homogenous seismic unit resembling a (Jurassic) graben and half graben infill, while its top reflection line is almost continuous across the entire study area (Sachse et al., 2016). Backstepping continued through the Hauterivian and Barremian, with progressive onlap of siliciclastic marine deposits onto the Río Chico or Dungeness High (Biddle et al., 1986; Galeazzi, 1998). A long-term transgressive cycle was noted by Schwarz et al. (2011) which according to these authors ended in the Barremian.

Tobífera & Zapata Formations

Lithostratigraphy

Sediments of the Sofia 1 core (GPS: -51.540325, -72.595639) were deposited more proximal to the Andean orogen, a position that is now at the foot of the fold-thrust belt (Fildani & Hessler, 2005) (Fig. 12). The lithostratigraphic succession has been referred to as the Late Jurassic Tobífera Formation (Tithonian) and the Early Cretaceous lower to middle Zapata Formation (Berriasian–Aptian/Albian) (cf. Fildani et al., 2003; Fosdick et al., 2011; Varela et al., 2012). The Tobífera Formation mainly consists of volcaniclastic deposits with intercalated continental/sandstone deposits (Rosello et al., 2008; Schwarz et al., 2011).

Tectonic background and paleogeography

The Zapata Formation was deposited in an irregular basin bordered by an Early Cretaceous arc to the west (Fildani et al., 2008). The organic-rich shales of Late Jurassic and Early Cretaceous age formed under anoxic marine conditions within a Neocomian sag on the edge of the Andes margin (Stinnesbeck et al., 2014; EIA, 2015). Interbedded shale and siltstone were mostly deposited in shallow water and in areas of oceanic crust emplacement, also as deeper hemipelagic deposits (Fildani & Hessler, 2005). A highly irregular basin partitioned by horsts is indicated by sand deposition confined to sub-basins closer to the arc (Fildani & Hessler, 2005). Changes in depositional regimes and sediment dispersal of the Late Jurassic-Early Cretaceous extensional Rocas Verdes back-arc basin (Tobífera and Zapata formations) are related to the onset of Andean contraction and transition to the Magallanes retroarc foreland basin (Rabinowitz & La Brecque, 1979; Dalziel, 1986; Ramos, 1988; Fildani & Hessler, 2005).

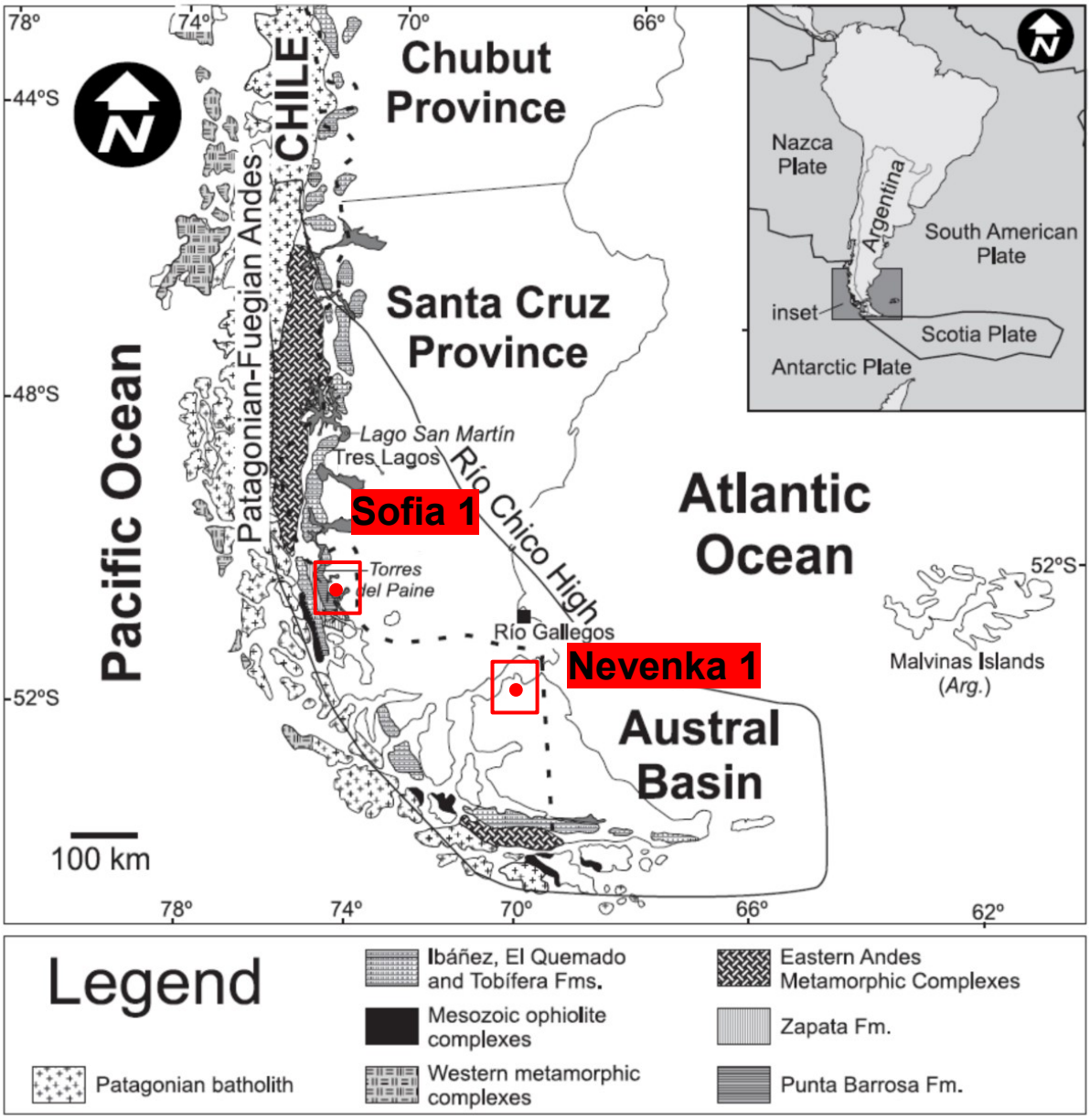

Figure 12: Location of the Magallanes/Austral Basin and indication of the localities of the wells (red rectangles), Varela et al. (2012).

1.7.3 Antarctica

During early Mesozoic–late Cenozoic times the Antarctic Peninsula region was characterised by the easterly subduction of Pacific Ocean lithosphere (Phoenix plate) beneath Gondwana (e.g. Barker et al., 1991; Seton et al., 2012). The magmatic and associated subduction zone (Antarctic Peninsula Volcanic Group) are expressed by a thick extrusive volcanic succession as well as a predominantly calcalkaline batholith. Magmatic activity was basically continuous, with marked intervals during the Early Jurassic, Early Cretaceous, Late Cretaceous and Eocene times (Pankhurst, 1982). The analysed sections of the Antarctic study area (Fig. 13) are mostly combined sections.

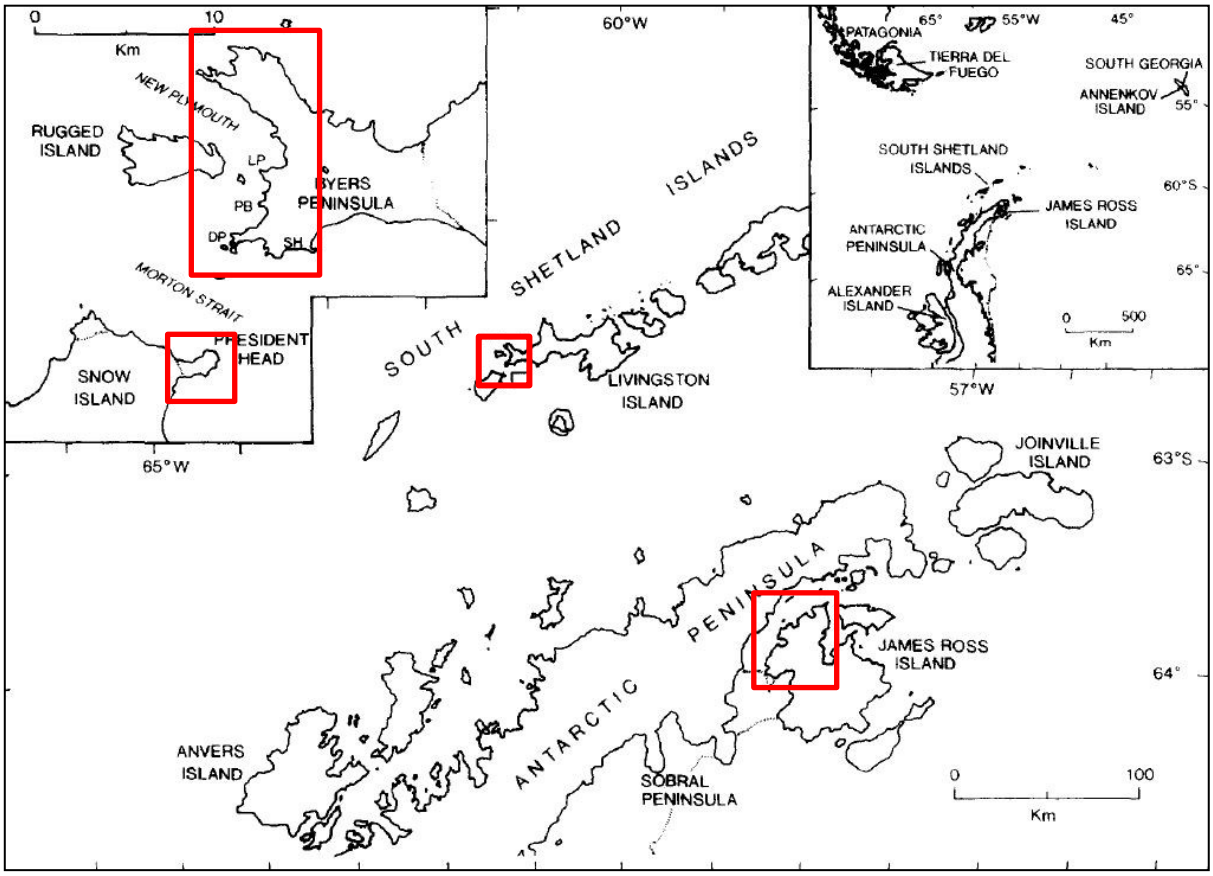

Figure 13: Location map for the Antarctic Peninsula region. Left inset shows the position of the Byers Peninsula. *DP*=Devils Point, *LP*=Laager Point, *PB*=President Beaches, *SH*= Sealer Hill. Right inset is a map of the Antarctic Peninsula, Scotia Arc and southernmost South America; Duane (1994). Study areas marked by red rectangles.

Byers Group – Livingston and Snow Island

Tectonic background and paleogeography

Byers Peninsula is located at the western end of Livingston Island, and forms part of the South Shetland Islands, western Antarctica (Fig. 13). The peninsula likely represents a narrow arc terrain which broke off from the Pacific margin of Gondwana during the Late Jurassic (Crame et al., 1993). The arc was characterised by a subdued relief at its northern end and fine-grained marine sediments which accumulated over a wide area. From approximately the Oxfordian to Aptian, dark-coloured organic-rich mudstones with thin interbedded air-fall tuffs were deposited in a quiet-water euxinic environment throughout the South Atlantic region including the South Shetland Islands (Crame et al., 1993). The authors suggested that the Byers Peninsula sediment succession reflects a marginal fore-arc position. Late Jurassic–Early Cretaceous ammonites and palynomorphs as well as Early Cretaceous plant macrofossils have been reported from Byers Peninsula and indicate that the lower, marine part of the group is Kimmeridgian–Valanginian in age (e.g., Crame et al**.,** 1993; Duane, 1996; Hathway & Lomas, 1998).

The Byers Group, exposed in the western South Shetland Islands, is a 2.7 km thick succession of which the lower 1.3 km are marine clastic rocks, representing Late Jurassic–Early Cretaceous sedimentation and volcanism on the Pacific flank of the Antarctic Peninsula magmatic arc (Hathway & Lomas, 1998). The base of the Byers Group consists of radiolarian-rich, hemipelagic mudstone of the Kimmeridgian–Tithonian Anchorage Formation, succeeded by terrigenous, slope-apron mudstone and sandstone of the Berriasian President Beaches Formation (Hathway & Lomas, 1998). These deep-marine strata are overlain by the Chester Cone Formation which consists of shallower-marine conglomerate and mudstone of Berriasian–Valanginian age. The type area for the Byers Group is Byers Peninsula, Livingston Island (Fig. 13, 14). The Byers Group is also present on President Head, Snow Island (Fig. 15). Here, the unit consists of sedimentary and igneous rocks with a minimum thickness of 2.7 km, with unexposed base and top.

Sedimentary Basin

On the northern Antarctic Peninsula the Late Jurassic mudstones crop out on both the margins of the Pacific (fore-arc) and the Weddell Sea (back-arc) (Pirrie & Crame, 1995). The Tithonian is characterized by arc uplift and oxygenation in the fore-arc basin (Anchorage Formation), and the contemporaneous development of a restricted basin in the back-arc region (Nordenskjöld Formation). In latest Tithonian–earliest Berriasian times the arc supplied volcaniclastic sediment to the fore-arc basin. During that time the back-arc basin changed from dysaerobic to aerobic conditions (Pirrie & Crame, 1995).

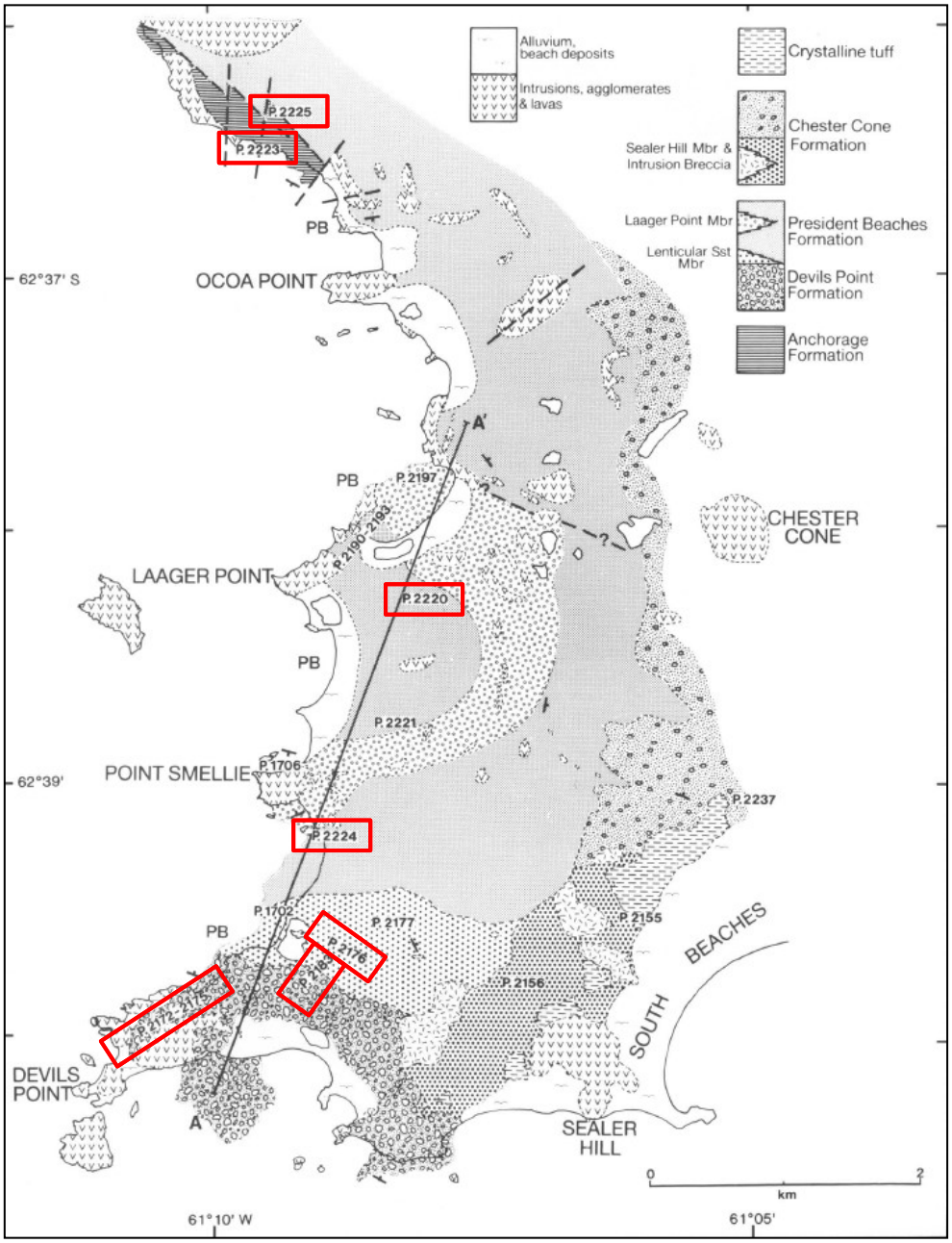

Figure 14: Geological map of western Byers Peninsula. Studied sections are marked by section numbers and red rectangles; Crame et al. (1993).

Anchorage Formation

Lithostratigraphy

The composite type section of the Anchorage Formation (AF) (GPS: -62.611881, -61.141388) (Fig. 14) can be subdivided into three distinct units (Crame et al., 1993). The basal strata, which are not included in the present study, consist of an at least 24 m thick succession of interbedded, dark grey to black unbioturbated, radiolarian-rich mudstone. This basal unit underlies a 30 m thick unit of dark

grey, planar-bedded and unbioturbated radiolarian-rich mudstone, interbedded with layers of normally graded tuff of 1-10 cm thickness, while sandstone is scarce. Upsection, a gradual transition into a mudstone-dominated unit of at least 40 m thickness is identified, in which the radiolarian-rich mudstone is intensely bioturbated. The mudstone is interpreted as a deposit of hemipelagic suspension (Hathway & Lomas, 1998). Sandstone and occasional interbedded tuff layers were interpreted by Pirrie and Crame (1995) as turbidites, even though tuffs may also represent fallout from suspension directly following eruptions. Age control is poor for the AF, but according to Smellie et al. (1980), Crame (1984) and Pirrie and Crame (1995) the molluscan assemblage suggests Kimmeridgian–Tithonian ages. Radiolarians are strongly recrystallized and thus provide no additional biostratigraphical information (Hathway & Lomas, 1998). A Middle Tithonian age is indicated for the sampled interval of the AF based on the revised stratigraphy of the Byers Group by Hathway and Lomas (1998).

Tectonic background and paleogeography

The Anchorage Formation of Livingston Island represents the only known occurrence of Late Jurassic deposits on the Pacific margin of the Antarctic Peninsula (Pirrie & Crame, 1995). According to Smellie et al. (1980) the AF was deposited in a low-energy shelf with anaerobic-dysaerobic bottom conditions and periodic introduction of sand by storms. Pirrie and Crame (1995), on the other hand, favoured a slightly deeper environment below the storm wave base. A transition from anaerobic–dysaerobic to dysaerobic–aerobic conditions was reported by Pirrie and Crame (1995), and is also known from the Nordenskjöld Formation on the Weddell Sea margin of the Antarctic Peninsula (Hathway & Lomas, 1998). The transition from dysaerobic to aerobic conditions was diachronous, in the Anchorage Formation occurring during the late Kimmeridgian–early Tithonian and in the Nordenskjöld Formation during the Late Tithonian or Early Berriasian (Pirrie & Crame, 1995). This diachroneity is linked to the development of the magmatic arc of the Antarctic Peninsula: In the Tithonian arc, uplift resulted in increasing oxygenation of the fore-arc basin, while restricted conditions developed in the back-arc region. The arc supplied volcaniclastic material to the fore-arc basin from the latest Tithonian-earliest Berriasian (Pirrie & Crame, 1995).

President Beaches Formation

Lithostratigraphy

Instead of a type section, a type area was defined about 0.5 to 1.5 km inland from President Beaches on western Byers Peninsula (marked PB in figure 14). Hathway and Lomas (1998) suggest a thickness of at least 600 m for the President Beaches Formation (PBF). Due to poor exposure its precise thickness and internal stratigraphy are difficult to determine. The PBF consists of poorly lithified parallel-laminated mudstone in which radiolarians are rare to absent. Trace fossils are also scarce and pyrite is only present locally. Carbonate concretions of 2–5 cm diameter form laterally persistent horizons. In most sections, sandstone is rare and only occurs as grey-green laminae and forming thin layers of up to 4 cm thickness (Hathway & Lomas, 1998). Thicker bedded (15–100 cm) sandstone is largely confined to lenticular units in which individual sandstone beds are graded and present Bouma

T_{abc} successions. Up to 20 m thick chaotic, structureless sand and granule-rich mudstone containing disrupted sandstone rafts is also common. Fossils consist of dinoflagellate cysts and ammonites. Hathway and Lomas (1998) reported occurrences of *'Spiticeras'* and *Bochianites.* Both forms however, are rather indicative of a Valanginian age (W. Stinnesbeck, pers. commun., 2018). Duane (1996) recognised the *Kalyptea wisemaniae* (latest Early Berriasian) and *Cassiculosphaeridia delicata* (Berriasian) Interval Zones of Helby et al. (1987) and therefore assigned a latest Early Berriasian–Berriasian age to the President Beaches Formation.

Chester Cone Formation

Lithostratigraphy

The lower part of this lithostratigraphic unit consists of conglomerate and sandstone of the Devils Point Member (DPM) whereas the mudstone-dominated Sealer Hill Member (SHM) forms the upper part of the Chester Cone Formation (CCF).

Devils Point Member: The composite type section is 233.5 m thick and was measured NE of Devils Point by Hathway and Lomas (1998) (GPS: -62.664887, -61.159939) (Fig. 14). In this area the Devils Point Member forms a northward-thinning wedge. Pebble conglomerates are abundant in the lower part of the DPM whereas higher portions of the unit are conformed by granule conglomerate, sandstone, and minor mudstone. Except for low-angle planar cross-bedding near Devils Point, most beds are structureless (Crame et al., 1993). The upper part of the member crops out 1.2 km south of Chester Cone; it is 45–50 m thick and conformed by plant-debris-rich coarse-grained sandstone and granule conglomerate (Hathway & Lomas, 1998). The beds are usually amalgamated; in the uppermost levels of the unit, finely laminated mudstone is gradually more abundant. Up to 30 cm thick sandstone beds are sharp-based and normally graded. The conglomerates contain rare transported thick-shelled bivalves which are non-age-diagnostic (Crame et al., 1993). Most palynological samples from mudstone interbedded in the conglomerate are barren (Duane, 1994, 1996), but a latest Berriasian-Early Valanginian age was assigned to the member (Hathway & Lomas, 1998).

Sealer Hill Member: The type section of the Sealer Hill Member is located 1.1 km south of Chester Cone (GPS: -62.662051, -61.140298) (Fig. 14). It is 56 m thick and shows a consistent 30° dip to the northeast (Hathway & Lomas, 1998). The unit is intermittently exposed from the Sealer Hill area NE to the Chester Cone plug (Fig. 14) (Crame et al., 1993). Lithologically similar marine strata on President Head, Snow Island (Fig. 13 left inset, Fig. 15) are also assigned to the SHM. A rapid decrease in the sand-stone/mudstone ratio marks the basal contact of the SHM with the underlying DPM on Byers Peninsula (Hathway & Lomas, 1998). The SHM consists mainly of finely laminated unbioturbated mudstones with intercalated fine grained sandstone. Scarce thicker sandstone beds show sharp, planar bases. Mudstone intraclasts are present within some of the beds of the lower parts. Very rare up to 1 m thick beds of poorly sorted, structureless conglomerate are present. Carbonate concretions up to 1.6 m across are a prominent feature of the member (Hathway & Lomas, 1998). Laterally continuous concretionary horizons and at some levels up to 2.5 cm thick, bedding-parallel fibrous calcite veins are also common (Hathway & Lomas, 1998).

The lower part of the member is characterised by dinoflagellate cysts indicating a latest Berriasian-Early Valanginian age, while those from the upper part suggest a mid-Valanginian age (Duane, 1996).

Duane (1996) correlated the SHM strata on President Head with the lower part of the member on Byers Peninsula. Ammonites in the upper part of the type section are strongly indicative of a Valanginian age (Covacevich, 1976).

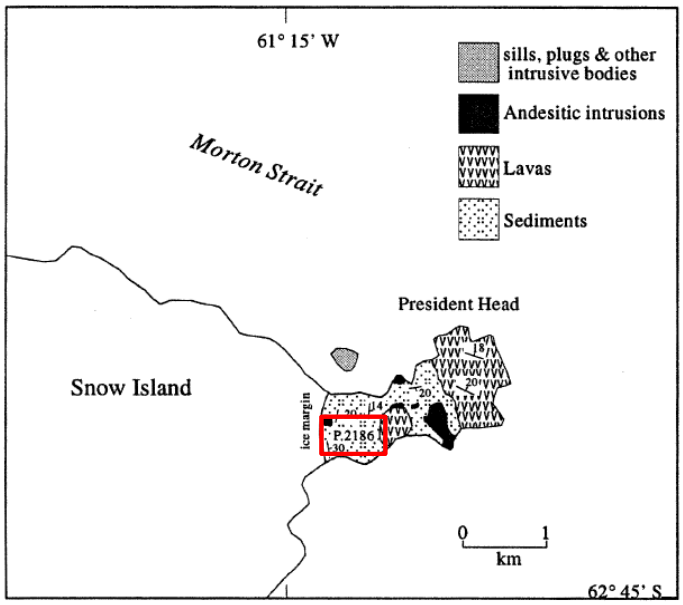

Figure 15: Geological map of President Head, Snow Island showing the location of the studied section P.2186 (red rectangle) (Duane, 1996).
GPS: -62.734496, -61.237338

Fossil Bluff Group – Alexander Island

Tectonic background and paleogeography

A well-exposed, 4000 m thick Upper Jurassic–Lower Cretaceous fore-arc basin succession crops out on the eastern coast of Alexander Island (Fig. 16, upper left inset) (Butterworth et al., 1988). To the east, Alexander Island is separated from the mainland by King George VI Sound (Fig. 16) and to the west by a faulted unconformable contact with the LeMay Group (LMG) (Edwards, 1979; Tranter, 1987; Butterworth et al., 1988; Storey & Nell, 1988). The LMG was deformed prior to deposition of the FBG (Storey & Nell, 1988) resulting in the LeMay Range Fault (Edwards, 1979). The top of the FBG is not exposed. Strata display a low-angle regional dip and become overall younger in southern or southwestern directions. The eastern coast of Alexander Island represents the type area of the Fossil Bluff Group (FBG), with type localities defined from the area between Belemnite Point and Fossil Bluff (Fig. 16, lower left inset) (Butterworth et al., 1988). The authors subdivided the succession into four formations (Ablation Point-, Himalia Ridge-, Spartan Glacier- and Pluto Glacier Formation), and elevated the whole succession to group status (Fossil Bluff Group). The four formations range from the Upper Jurassic (Kimmeridgian) to Lower Cretaceous (Albian) (Crame & Howlett, 1988).

Sedimentary Basin

Marine conglomerate, mudstone and sandstone form a complex, laterally variable succession of submarine fan and deltaic deposits that built out on the fore-arc (Pacific) margin of the Antarctic Peninsula (e.g. Butterworth, 1985; Crame & Howlett, 1988). These deposits accumulated in a fault-bounded basin which developed at least partly on top of the metasedimentary rocks of the extensive LeMay Group (Crame & Howlett, 1988).

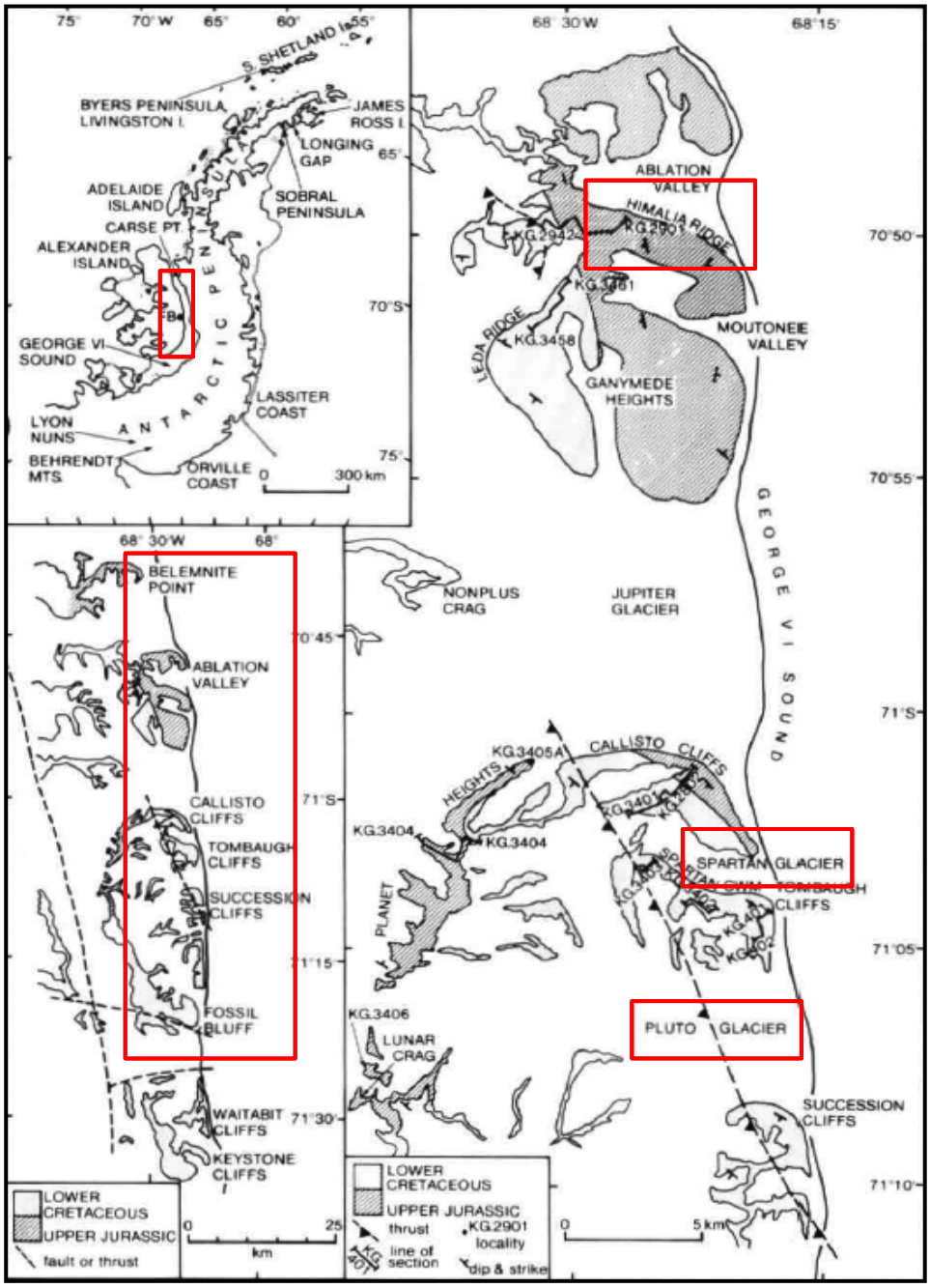

Figure 16: Locality of Alexander Island and sketch map of the Fossil Bluff Group (Crame & Howlett, 1988).

Himalia Ridge Formation

Lithostratigraphy

The Himalia Ridge Formation (HRF) is a submarine fan unit in which inner-fan channel conglomerates are incised into interchannel mudstones and sandstones (Butterworth et al., 1988). The type section reaches a maximum thickness of 2200 m at Himalia Ridge (GPS: -70.833333, -68.450000) (Fig. 16) (Butterworth et al., 1988). There, the type section consists of a lower 1100 m thick mudstone dominated unit of which the lowermost 30 m are characterised by black mudstone and subordinate, channelled mud-flake breccia (Butterworth et al., 1988). This unit underlies 1000 m of dark mudstone with interbedded fine-grained sandstone, and rare coarser-grained volcaniclastic and feldspar-rich channelled sandstone. A conglomeratic unit is represented by a single 100 m thick lenticular channelled complex. The HRF consists of a very variable base that rests unconformably on both the Ablation Point Formation and on the LeMay Group of central Alexander Island (Butterworth et al., 1988). The sandstone-dominated section above the topmost conglomerate complex represents the upper boundary of the formation. The HRF crops out extensively on Ganymede Heights and west of Belemnite Point (Fig. 16). Farther south, the formation occurs at the northern end of Planet Heights, and the basal sections at Tombaugh and Callisto cliffs (Fig. 16).

The lower 1000 m of the HRF contains a diverse and abundant molluscan assemblage (Butterworth et al., 1988). The perisphinctid ammonites (largely species of the genera *Virgatosphinctes* and *Aulacosphinctoides*) of the lower faunal assemblage (basal 400 m) indicate a Tithonian age (Thomson, 1979; Butterworth et al., 1988). The associated belemnites and bivalves confirm this interpretation and suggest an early Tithonian age (Willey, 1973; Crame, 1982, 1983; Crame & Howlett, 1988). The ammonites and accompanying fossils of the fossiliferous interval between 700-1100 m are indicative of a Late Tithonian age (e.g. *Blanfordiceras* aff. *wallichi* Gray and *"Berriasella" subprivasensis* Krantz) (Thomson, 1979; Crame & Howlett, 1988). Apart from ammonites assigned to the genera *Haplophylloceras* and *Raimondiceras* in the very topmost 50 m of the unit, the rest of the upper 1000 m of the formation lacks fossils. The ammonites near the top of the HRF are associated with a variety of bivalves. This assemblage is widely considered as Berriasian in age (Thomson, 1979; Taylor et al., 1979; Crame, 1985; Howlett, 1986; Crame & Howlett, 1988).

Spartan Glacier Formation

Lithostratigraphy

The type section of the Spartan Glacier Formation (SGF) is exposed on the mountain ridges south and southwest of Spartan Glacier (GPS: -71.050000, -68.333333) and reaches a thickness of 1000 m (Butterworth et al., 1988). The SGF crops out over a wide area from Ganymede Heights in the north to Fossil Bluff in the south (Fig. 16). This lithostratigraphic unit is conformed by mud- and siltstone with thin interbedded fine-grained sandstone. The sandstone beds are commonly graded and/or parallel- or ripple cross-laminated and form laterally discontinuous units of 2–20 m thickness. Throughout the formation, calcareous concretions are common and groups of sandstone dykes and sills occur at several localities (Taylor, 1982). The base of the Spartan Glacier Formation is marked by the cessation of coarse-grained sedimentation of the underlying HRF. The mudstone-dominated succession of the

SGF underlies the sandstones of the Pluto Glacier Formation (Butterworth et al., 1988).

The formation contains a variety of fossil molluscs and is broadly divided into three faunas. The lowest 580 m of the SGF contain occurrences of the ammonites *Olcostephanus* and *Bochianites*, and are regarded as Valanginian in age (Howlett, 1986; Crame & Howlett, 1988). At the upper end of this interval further belemnopseids are present which are related to *Belemnopsis* indicating a Late Valanginian or Early Hauterivian age (Besairie & Collignon, 1956). The fauna between 580–950 m is dominated by bivalves, and starts around the last occurrence of the belemnopseid belemnites. No diagnostic ammonites are present (only indeterminate phylloceratids), and consequently only a tentative Late Hauterivian–Barremian age is suggested by Crame & Howlett. (1988). The fauna from 950 m upsection contains abundant aconeceratid ammonites (e.g. *Sanmartinoceras* (*Sanmartinoceras*) and S. (*Theganeceras*) and bivalves and is regarded as Aptian in age (Butterworth et al., 1988).

Pluto Glacier Formation

Lithostratigraphy

The type section for the Pluto Glacier Formation (PGF) is defined at the southwestern margin of Spartan Glacier (GPS: -71.116667, -68.366667) (Fig. 16) (Butterworth et al., 1988). The outcrops do not comprise a complete section through the formation and the uppermost levels are exposed on the Succession Cliffs of the Pluto Glacier (Fig. 16). The outcrops on the ridges south of Spartan Glacier and on Succession Cliffs indicate a minimum thickness of 350 m. In the lowermost part of the formation medium-grained sandstone beds crop out at a 14 m thick scarp overlying siltstone of the Pluto Glacier Formation. This basal unit has been defined by Butterworth et al. (1988) as the Callisto Cliffs Member of the Spartan Glacier Formation. The unit underlies a 238 m thick unit of alternating sandstone and siltstone. The sandstone units are typically fine to medium grained and are usually intensely bioturbated. Herringbone cross-stratification is present in areas where bioturbation is less intense (Butterworth et al., 1988). Large diagenetic carbonate concretions occur in a 68 m thick interval of medium-thick bedded, planar laminated sandstone at the 160 m level of the section. The upper part of the formation is dominated by thick-bedded, parallel-laminated to convoluted sandstone (Butterworth et al., 1988). This sandstone contains large calcareous concretions, commonly aligned along diffuse bedding planes (Horne & Taylor, 1969) which are interbedded with siltstone and tuff (Taylor et al., 1979). Bioturbation is common.

Aconeceratid ammonites and large lytoceratids are common in the lower half of the section (Butterworth et al., 1988). In the upper half ammonites are rare. The assemblage of bivalves and associated dimitobelid belemnites indicates an Aptian age (Crame & Howlett, 1988). At Succession Cliffs dimitobelids occur together with tetragonitid, desmoceratid and silesitid ammonites as well as inoceramid bivalves, an assemblage which is indicative of an Albian age (Thomson, 1983; Doyle, 1987; Crame & Howlett, 1988).

Nordenskjöld Formation and Gustav Group – James Ross Island

Sedimentary Basin

The Larsen Basin is a major sedimentary basin on the eastern side of the Antarctic Peninsula. It developed during Jurassic times in a back-arc setting connected to a volcanic arc that formed by subduction of oceanic crust beneath Gondwana (Macdonald et al., 1988; Hathway, 2000; Carvalho et al., 2013). Its development may have been influenced by the opening of the Weddell Sea during the Late Jurassic to Late Cretaceous (Storey & Nell, 1988; Storey et al., 1996). Increased rates of convergence during the Early Cretaceous resulted in major uplift of the magmatic arc and subsidence of the back-arc region (Elliot, 1988). The sediment fill of the Larsen Basin was completely derived from the emerging volcanic arc (Carvalho et al., 2013). Del Valle and Fourcade (1992) defined the northern part of the Larsen Basin as the James Ross Sub-basin, an ensialic back-arc basin (Elliot, 1988). Most outcrops of this sub-basin are located to the east of the arc terrane in the James Ross Island area (Fig. 17) (Carvalho et al., 2013). 5–6 km of strata ranging from Tithonian to Eocene have been deposited in the James Ross Basin.

Tectonic background and paleogeography

The Kimmeridgian to Berriasian Nordenskjöld Formation represents the oldest sedimentary unit within the James Ross Island area (Whitham & Doyle, 1989). The outcrops of the formation (which have undergone considerable thermal alteration) are basically restricted to several small outcrops at the eastern coastline of the Antarctic Peninsula (Fig. 17) and large glide blocks enclosed within Lower Cretaceous strata (the Gustav Group) (Ditchfield et al., 1994). The glide blocks have undergone less thermal alteration and yield the only palynological data available for the stratigraphic classification of the Nordenskjöld Formation (Pirrie et al., 1992). Doyle and Whitham (1991) suggest that the Nordenskjöld Formation was deposited in a silled basin (a basin in which a submarine sill restricted water exchanges).

The allochthonous material of the glide blocks was originally derived from the faulted and unstable basin margin during the Early Cretaceous (Ineson 1985). Block A crops out in Sharp Valley, James Ross Island (GPS: -63.866614, -58.066696) where it is enclosed within the Cretaceous strata (Snape, 1992). Based on the preservation of organic matter and the absence of current-formed structures and bioturbation Farquharson (1983) suggested deposition in a calm, anoxic marine environment, below wave-base.

Nordenskjöld Formation

Lithostratigraphy

The Nordenskjold Formation (Farquharson, 1983) is dominated by hemipelagic and pelagic sediments (Dyle & Witham, 1991; Witham, 1993) that consist of a uniform succession of finely-laminated, carbonaceous radiolarian bearing mudstone interbedded with thin ash-fall tuffs (Ineson, 1985). The formation is subdivided into the Longing, Ameghino and Larsen members (Whitham & Doyle, 1989). In the present study, the sampled section forms part of the Longing member which is derived from the north-west coast of James Ross Island (GPS: -63.849202, -58.036533) (Fig. 17), where breccia beds,

isolated clasts and large glide blocks of the formation occur in the Lower Cretaceous Gustav Group (Ineson, 1985).

Snape (1992) suggested a Tithonian age for Association A of Block A, based on synthesis of the palynostratigraphical data from Australia (Helby et al., 1987), Papua New Guinea (Davey, 1988) and Madagascar (Chen, 1978). A Middle Tithonian age, equivalent to the middle-upper part of the *Dingodinium jurassicum* Zone (Australia; Helby et al., 1987), upper *Nummus similis* and *Broomea simplex–Rhynchodiniopsis serrata* Zones (Papua New Guinea; Davey, 1988) and the upper part of Zone IV (Madagascar; Chen, 1978) was proposed by Snape (1992).

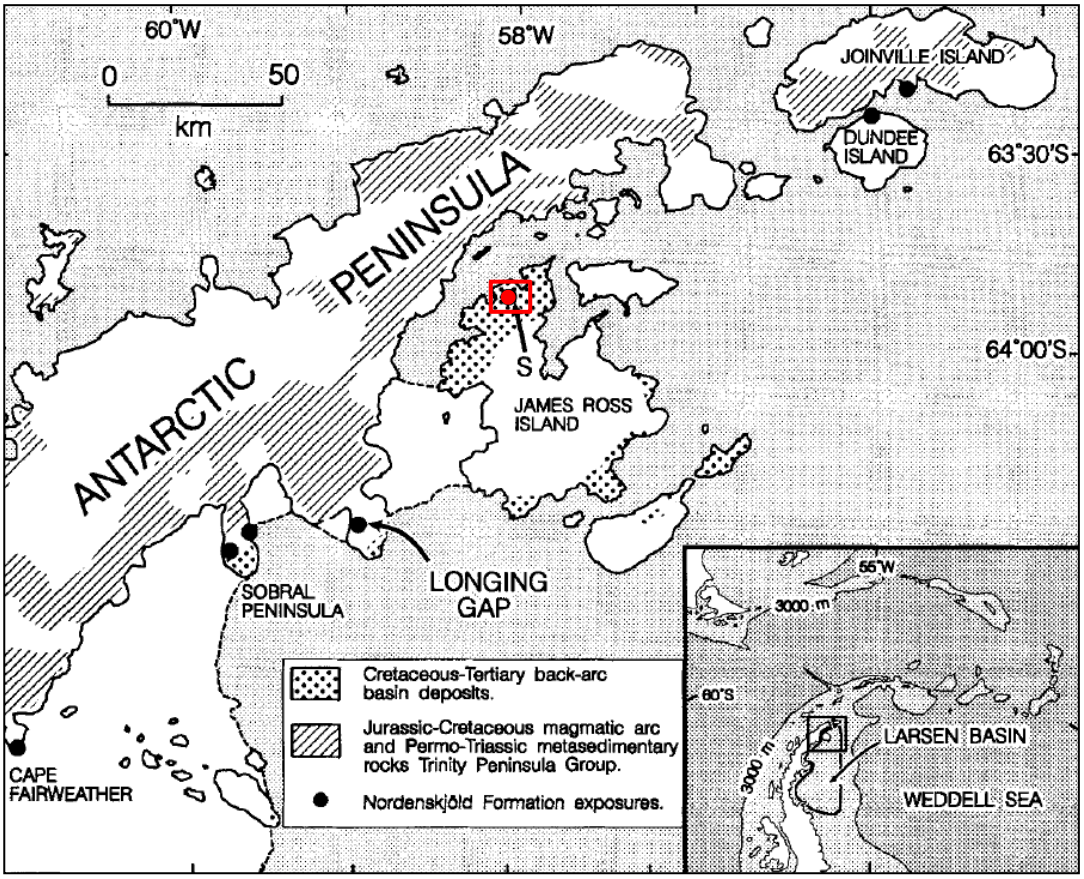

Figure 17: Map of the northern Antarctic Peninsula showing the location of James Ross Island and exposures of the Nordenskjöld Formation (Whitham, 1993). Study area marked by the red rectangle.

Gustav Group – Kotick Point Formation

Lithostratigraphy

Ineson et al. (1986) introduced the Gustav Group for the lowermost Cretaceous strata in the James Ross Island area (Fig. 18) (Keating et al., 1992). The group is divided into four formations – Lagrelius Point, Kotick Point, Whisky Bay and Hidden Lake. The Aptian/Albian Kotick Point Formation

consists of a thick succession of medium to very fine-grained sandstone, silty mudstone as well as coarse grained poorly sorted breccia and conglomerate (Ineson et al., 1986). Ineson (1989) interpreted the Gustav Group as a coarse-grained submarine fan deposit interspersed with finer-grained, deep marine slope sediments.

The palynomorph assemblage from the Kotick Point Formation contains relatively diverse and well-preserved dinoflagellates (Keating et al., 1992). The local first occurrence of *E. turneri* coincides with the base of the *Diconodinium davidii* Zone of Helby et al. (1987) in Australia wherefore Keating et al. (1992) assigned a tentative Late Aptian age to the lowermost part of the sampled interval of the Kotick Point Formation. The assemblage of the middle part of the sampled interval includes *Canninginopsis intermedia, Diconodinium davidii, D. cerviculum, M. australis, M. macwhaei, M. tetracantha and Tanyosphaeridium isocalamus* (Keating et al., 1992). This interval is equivalent to Late Aptian to Early Albian assemblages from Australia (Morgan, 1980; Helby et al., 1987; Keating et al., 1992). Palynomorph assemblages of the upper interval compare well with those described from Early Albian strata in Australia by Morgan (1980) and Helby et al. (1987) (Keating et al., 1992). An important occurrence of *M. tetracantha* in the upper part of the interval was detected by Keating et al. (1992). The last occurrence of *M. tetracantha* in the uppermost interval of the sampled section is indicative of an Early Albian age.

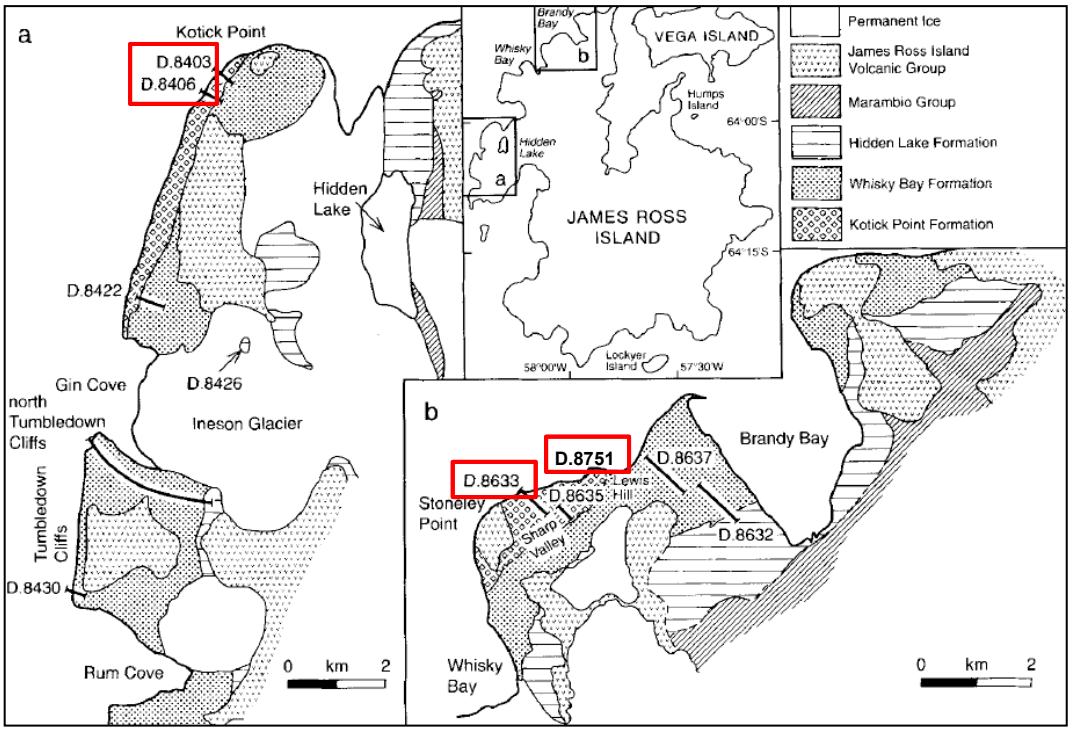

Figure 18: Locality and s ketch maps of a) west and b) north-west James Ross Island showing the location of the sections investigated (Keating et al., 1992); GPS coordinates of the sampled sections – D.8406: -64.002661, -58.363670; D.8403: -63.995561, -58.350487; D.8633: -63.858341, -58.101733; D.8751: -63.848775, -58.062067.

2. OBJECTIVES

The aim of this study is the detailed analysis of several alternating warm water/cold water conditions in the southern hemisphere (central- to southern Chile and western Antarctica) during the Late Jurassic and Early Cretaceous. The multidisciplinary approach is based on palynofacies analysis, but also includes TOC/TIC and CNS analysis, stable isotope analysis, the occurrence of micro-glendonite, occurrence of calpionellids and lithofacies. The extension from central Chile to Antarctica is intended to clarify whether these oscillations were regional events controlled by geotectonic processes in the hinterland (orogenesis of the Andes) or whether a supraregional and possibly global pattern can be identified, leading to climatic changes in the entire Southern Hemisphere. From the Northern Hemisphere, climatic cooling (glaciation?) is already known from this time interval, as evidenced by geochemical proxies, glaciogenic sediments and the appearance of glendonite, a carbonate mineral indicative of cold-water. From the Southern Hemisphere, on the other hand, no glendonite or other indicators for climatic cooling or glaciations are known from this time interval. As part of the project, the duration, and distribution of cooling phases in central Chile, southern Chile (Patagonia) and the Antarctic Peninsula are examined in detail. Palaeoenvironmental conditions are analysed and interpreted in a north-south transect over approximately 3,000 km along the south-western edge of Gondwana. On the basis of this high-resolution multidisciplinary and multistratigraphic analysis it will be clarified whether the variations in sea temperature in the Southern Hemisphere are controlled by large-scale factors and if they are of supraregional significance.

3. MATERIAL AND METHODS

The samples analysed from central Chile (Lo Valdés, Baños del Flaco) were provided by Dr. Christian Salazar (Universidad del Desarrollo, Santiago, Chile) and represent spare rock material of his PhD thesis in 2012. It was also possible to use his collection of thin sections from these sections. The material of Patagonia has been provided by the Chilean ENAP (Empresa Nacional del Petróleo) in Punta Arenas which granted access to their drilled cores. The sample material from Antarctica was stored at the British Antarctic Survey in Cambridge and has originally been collected by Alistair Crame. Selection of sample material of the Patagonia and Antarctica sections was carried out by Hartmut Jäger and Sven Brysch.

Optical analyses

Optical examinations were carried out with a transmitted light microscope (Leica DMLP & Olympus BX 51) and a fluorescence microscope (Leica Leitz DM RXP). Photographs of palynofacies samples were taken with an Olympus PEN E-PL7 camera attached to the microscopes. Magnification for palynofacies analyses was 400x (40x objective and 10x ocular). For illustrations of organic particles and micro-glendonites 630 x magnification was used.

3.1 Palynofacies

A total of 502 palynofacies samples were analysed for this thesis (250 samples of central Chile, 123 samples of Patagonia and 129 samples of Antarctica). Sample preparation was carried out at the chemical laboratory of the Institute of Earth Sciences, Heidelberg University. A piece of each sample was crushed with a mortar to a mean grain size between 2–5 mm in diameter. Each crushed rock sample was put into a plastic jar and filled with 500 ml of deionised water to remove particles of the dust fraction and contaminations of recent pollen or anthropogenic particles. Subsequently the carbonate minerals were dissolved using concentrated hydrochloride (36% HCl). Following neutralisation with deionised water, the silicate components were removed with hydrofluoric acid (53% HF). After the reaction was completed the acid unit was decanted and neutralised with NaOH dilution. This procedure of neutralisation was repeated until the HF-solution remaining in the plastic jar was neutral. Sample residues were then filtered through filter gauze with a mesh width of 15 µm and washed with deionised water. Because of the use of hydrofluoric acid, fluoric silicates crystallised out of the sample residues. To remove the fluoric silicates the samples were cleaned by boiling with HCl. Subsequently, the samples were neutralised with deionised water and repeatedly filtered through filter gauze. From each of the filter residues a strewn slide (size of 24 x 24 mm) was compounded to allow for examinations with a transmitted light and fluorescence microscope. Sample material was extracted from the aqueous solution with a pipette. To get a representative cross section of all contained components the sample cup was swivelled and the sample was taken out of the centre of the suspension of the particles. The extracted suspension was given onto a cover slip. After drying, the cover slip containing the organic material was glued onto an object plate with the artificial resin "Eukitt".

Particles contained in the slides were distinguished as shown in table 1. Each group of particles was counted in respect to its abundance (also size ratios were taken into account). Palynofacies preparations were analysed using a 40x magnification objective. The most representative area for analysis was chosen after analysing the sample with 20x magnification providing an overview. With the transmitted light microscope each strewn slide was counted until a minimum of 300–350 particles was reached. In samples with very homogenous compositions, the amount of counted particles was reduced to 250–300. In samples with very low organic matter content, compositions were usually very homogenous and around 100–150 particles were counted. The individual results are shown in the appendix. Quantities of organic matter only reflect the particles' amount in relation to the sum of all counted particles per strewn slide.

All organic particles were categorised into three groups depending on the preservation state (good/A, fair/B, poor/C). Phytoclasts are subdivided into three groups: the cutinites, the vitrinites and inertinites. They are differentiated due to their different stages of oxidation and degradation. Analysis of the opaque/translucent (OP/TR) ratio of phytoclasts is an approach which is derived from the palynofacies analysis. This approach was used in all sampled sections of the three study areas. The approach which uses the roundness/shape of phytoclasts to gain information about the palaeoenvironment was used in the sections with the poorest organic matter preservation, i.e. the Lo Valdés Formation (central Chile) and the upper Tobífera Formation (Patagonia). Samples were analysed randomly. Sporomorphs are generally found variously distorted and squashed flat which means that these fossils are not always spheres as idealistically drawn, but disk-like objects that twist and turn. In this thesis strongly degraded sporomorphs are classified as "spores indet". Organic matter

derived from fungi is grouped as “fungal remains”. The AOM was distinguished in fluorescent and non-fluorescent. Mineral remains were subdivided into the categories “quartz”, “pyrite” and “others”. Mineral remains (mainly quartz and heavy minerals) were counted the same way as the organic matter particles but registered separately. Detailed results of the palynofacies analysis are listed in the appendix (p. 235 ff.).

Study line (x/y)		Total amount of particles
1		
2		

Date	
No. of thin section	
Magnification	

Origin		Group	Component	Amount A	Amount B	Amount C	Sum
continental (allochtonous)	parts of vascular plants	Phytoclasts	Inertinite				
			Vitrinite				
			Cutinite				
	pollen	Sporomorphs (palynomorph)	nonsaccate				
			monosaccate				
			bisaccate				
	spores		monolete				
			trilete				
			Sporomorphs indet				
	AOM		terrestrial, translucent				
			terrestrial, opaque				
			marine/sensu stricto				
marine	marine Phytoplankton (palynomorph)		Dinocysts				
			Acritarchs				
			Prasinophytes (Tasmanites)				
			Leiospheres				
	Zoomorphs (palynomorph)		foraminiferal test linings				
	Zooclasts		Bivalves, Scolecodonts, Fungi				
diverse	others		*Botryococcus*				
			Filaments				
	mineral residues		Quartz				
			Pyrite				
			others				

Preservation	A = good	B = fair	C = poor

Table 1: Organic particle differentiation used in this thesis.

For palaeoenvironmental interpretation values obtained were plotted in Tri-Plot triangles (Fig. 19). Tri-plot is a Microsoft Excel based spreadsheet for the preparation of triangular (ternary) diagrams. The values of each sample were placed according to the classification of Tyson (1993) for AOM, phytoclasts and palynomorphs (Fig. 19). The key to the different palynofacies fields is given in table 2. Results of particle counting were used for palaeoenvironmental interpretation. The results of the palynofacies analysis is hence mainly based on the hydrodynamic properties of the individual particle groups, compiled and summarised by Tyson (1993, 1995) and McArthur et al. (2016a, b).

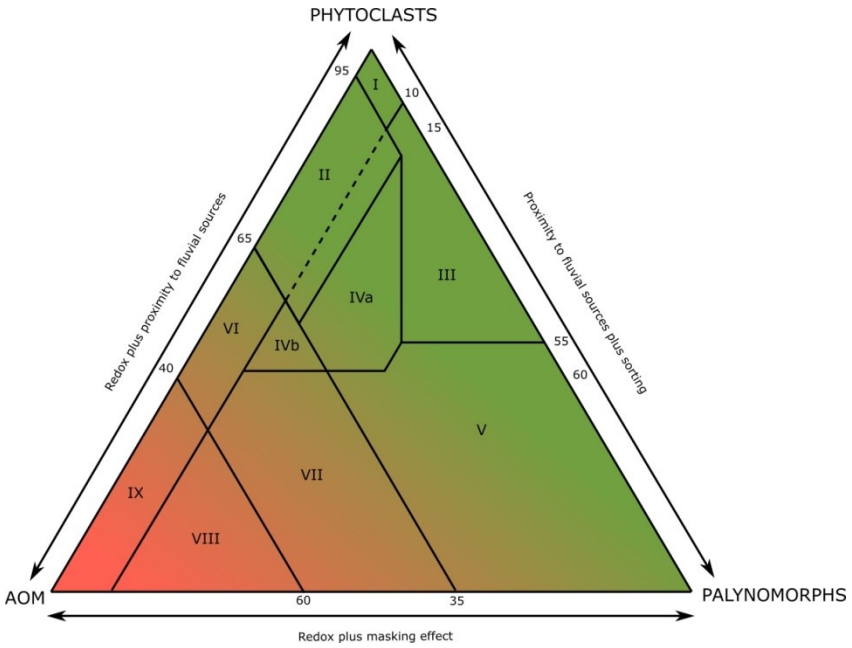

Figure 19: AOM-Phytoclast-palynomorph plot (modified after Tyson, 1993).

	Palynofacies field and environment	comments	Microplankton	Kerogen Type
I	Highly proximal shelf or basin	High phytoclast supply dilutes all o ther components	very low	III, gas prone
II	Marginal dysoxic-anoxic basin	AOM diluted by high phytoclast input but AOM preservation moderate to good. Amount of marine TOC dependent on basin redox state and dilution.	very low	III, gas prone
III	Heterolithic oxic shelf ('proximal shelf')	Generally low AOM preservation; absolute phytoclast abundance dependent on actual proximity to fluvio-deltaic source. Oxidation and reworking common.	common to abundant Dinocysts dominant	III or IV, gas prone
IV	Shelf to basin transition	Passage from shelf to basin in time (e.g. increased subsidence/water depth) or space (e.g. basin slope). Absolute phytoclast abundance depends on proximity to source and degree of redeposition. Amount of marine TOC depends on basin redox state. IVa dysoxic-suboxic, IVb suboxic-anoxic.	very low-low	II or III, mainly gas prone
V	Mud-dominated oxic shelf ('distal shelf')	Low to moderate AOM (usually degraded). Palynomorphs abundant. Light coloured bioturbated, calcareous mudstones are typical.	common to abundant Dinocysts dominant	III > IV, gas prone
VI	Proximal suboxic-anoxic shelf	High AOM preservation due to reducing basin conditions. Absolute phytoclast content may be moderate to high due to turbiditic input and/or general proximity to source.	low to common Dinocysts dominant	II, oil prone
VII	Distal dysoxic-anoxic 'shelf'	Moderate to good AOM preservation, low to moderate palynomorphs. Dark coloured slightly bioturbated mudstones are typical	moderate to common Dinocysts dominant	II, oil prone
VIII	Distal dysoxic-oxic shelf	AOM-dominated assemblages, excellent AOM preservation. Low to moderate palynomorphs (partly due to masking). Typical of organic-rich shales deposited under stratified shelf sea conditions.	low to moderate Dinocysts dominant, % prasinophytes increasing	II >> I, oil prone
IX	Distal suboxic-anoxic basin	AOM-dominated assemblages. Low abundance of palynomorphs due to masking. Frequently alginite-rich. Deep basin or stratified sfelf sea deposits, especially sediment starved basins.	generally low Prasinophytes often dominant	II > I, highly oil prone

Table 2: Key to the marine palynofacies fields of the phytoclast-AOM-palynomorph plot (Tyson, 1993).

3.2 Microfacies/Thin Section Analysis

The only sections in which carbonate rocks are the major constituent of the sedimentary succession and therefore are suitable for carbonate microfacies analysis are the LV and CM sections of central Chile. The sections of Patagonia and Antarctica mainly consist of clastic rocks. Composition, fabric and texture of carbonate rocks were studied in a total of 137 thin sections (76 CM section, 61 LV

section). For the investigation of the composition and fabrics of the samples, standard thin sections with a thickness of approximately 30 µm were used. These thin sections were usually cut perpendicular to the bedding (where bedding structures were recognisable) – the samples of the LV and CM sections were originally chosen by Christian Salazar for his PhD thesis.
Microfacies analysis was carried out following the models of Folk and Dunham. Photographs were taken with a Leica MZ16 and an attached Leica DFC480 stereomicroscope. Microfacies interpretation was based on the specifications of Flügel (2004). The same microscope was used to study occurrences of Calpionellids and to take pictures of the specimens.

Thin section analysis was performed on samples from the Byers Group, the only section that yielded usable rock material in addition to the Lo Valdés Formation. The thin sections were made in the preparation laboratory of the Institut für Geowisenschaften, Heidelberg University. Samples were analysed using a Leica DMLP & Olympus BX 51 microscopy. Detailed results of the microfacies/thin section analysis are listed in the appendix (p. 235 ff.).

3.3 Scanning Electron Microscopy

20 selected samples of the CM section were prepared for analyses with the scanning electron microscope (SEM) at the GeoZentrum Nordbayern of the FAU Erlangen-Nürnberg. Micro-glendonite clusters were analysed with Energy Dispersive X-Ray Analysis (EDX). The microscope used was a Tescan Vega XMU with an attached Oxford Instruments INCA analyser. A few drops of filter residue of the palynofacies samples were applied to a slide. After drying the slides were coated with gold using a sputter coater. Although filter residues were washed out thoroughly, the specimens were covered with a thin film of Na and F (side effect of the hydrofluoric acid treatment) wherefore information on the elemental composition of the mineral clusters was limited. It was tried to produce samples without the use of hydrofluoric acid but without the acid it was not possible to isolate micro-glendonite clusters out of the surrounding rock. Moving and additional cleaning of individual mineral clusters was not possible, because the clusters were very brittle and disintegrated by contact with any tool. Therefore the results from the element analysis were not used for further interpretation.

3.4 Carbon and oxygen isotope analysis of carbonate samples

Isotope ratios of $\delta^{13}C$ and $\delta^{18}O$ were measured on mostly bivalve carbonaceous shell material (44 samples CM section, 45 samples LV section) that was gained by drilling with a Merchantek Micromill (NewWave), on bulk rock samples (163 samples CM section, 120 samples LV section) and on isolated organic matter (77 samples CM section) that was taken from palynofacies residues. The MicroMill consists of a computer-controlled micro-drilling system, which is coupled to a microscope. Isotope analyses were performed by the Geozentrum Nordbayern of the Friedrich-Alexander-Universität Erlangen-Nürnberg. Carbonate powders were reacted with 100% phosphoric acid at 70 °C using a Gasbench II connected to a ThermoFisher Delta V Plus mass spectrometer. All values are reported in per mil relative to the V-PDB standard (Vienna-Pee Dee Belemnite). Reproducibility and accuracy was monitored by replicate analysis of laboratory standards calibrated to international standards NBS19 (TS-Limestone), NBS18 (Carbonatite) and LSVEC (Lithium Carbonate). Laboratory standards

were calibrated by assigning $\delta^{13}C$ values of +1.95‰ to NBS19 and -46.6‰ to LSVEC and by assigning $\delta^{18}O$ values of -2.20‰ to NBS19 and -23.2‰ to NBS18.
For analysis of isolated organic matter some of the material of the palynofacies filter residues was used. Carbon isotope analyses of organic carbon were performed on the same samples with a Flash EA 2000 elemental analyser connected online to a ThermoFinnigan Delta V Plus mass spectrometer. All carbon isotope values are reported in the conventional $\delta^{13}C$-notation in permil relative to V-^{13}C-PDB (Vienna-^{13}C-PDB). Nitrogen isotope values are reported in ‰ relative to atmospheric air. Accuracy and reproducibility of the analyses were checked by replicate analyses of laboratory standards calibrated to international standards USGS 40 and 41. Detailed results of the carbon and oxygen isotope analyses are listed in the appendix (p. 235 ff.).

3.5 Total organic carbon, total inorganic carbon, carbon/sulphur/nitrogen

Samples from all three study areas (central Chile: 216 samples, Patagonia: 123 samples, Antarctica: 84 samples) were analysed for total organic carbon (TOC), total inorganic carbon (TIC) and carbon/sulphur/nitrogen (CNS) contents. For this approach, the sample material was crushed to rock flour and subsequently weighed. For the analysis of CNS (see below) tungsten oxide was added as flux for the gas chromatograph. The samples of the TOC/TIC analysis were wet incinerated with sulphuric acid. The $CaCO_3$ abundance was calculated from the TIC content following the workflow of TDI-Brooks International, Inc. (compiled by Bernie B. Bernard, Heather Bernard, and James M. Brooks).
The determination of the carbon, nitrogen and sulphur contents was performed at the Institute of Geography at Heidelberg University with an ELEMENTAR CNS Max Analyser. The elements were analysed through the use of high temperature combustion (HTC), at a furnace temperature exceeding 1000 °C and admixed oxygen. Helium was used as the inert carrier gas. The detection of the combustion gases by quantitative separation of the combustion gases was followed by quantification with a thermal conductivity detector. Detailed results of the total organic carbon, total inorganic carbon and carbon/sulphur/nitrogen analyses are listed in the appendix (p. 235 ff.).

3.6 Thermal Maturity

Assessment of thermal alteration of the samples using clay was performed by Dr. Rüdiger Butz-Braun – tonmineralogische Beratung. X-ray diffractometric analyses of clay minerals after ethylene glycol treatment and thermal treatments at 120° C to 300° C in 20° steps. If present, this treatment leads to reactions in any smectite interlayers. The ethylene-glycol treatment produces a characteristic, X-ray diffractometrically detectable widening of the intermediate layers in smectites. This also applies to smectite layers within the mixed-layered illite/smectite minerals. Due to the thermal treatments, hydroxide complexes are displaced from their intermediate layers. As a result, it can be deduced to which temperatures the rock was previously exposed. Only by renewed weathering or hydrothermal processes OH groups could again reach the intermediate layers. Clay mineralogy for assessment of thermal alteration analyses were only carried out on the central Chilean samples. Due to only minor and mostly insufficient amounts of illite/smectite mixed-layer structures thermal maturation analysis

based on clay mineralogy was performed on three samples only. Those samples were suitable for the ethylene glycol treatment of the illite/smectite mixed-layers.

In all sections thermal maturation was additionally characterised using the Thermal Alteration Index (TAI) or Spore Coloration Index (SCI). The TAI & SCI are based on a temperature-related gradual change of organic matter colour in translucent white light (Tyson, 1995; Traverse, 2007) (Fig. 20). The TAI/SCI index was also used to infer temperature and maturation stage (Figs. 21, 22).

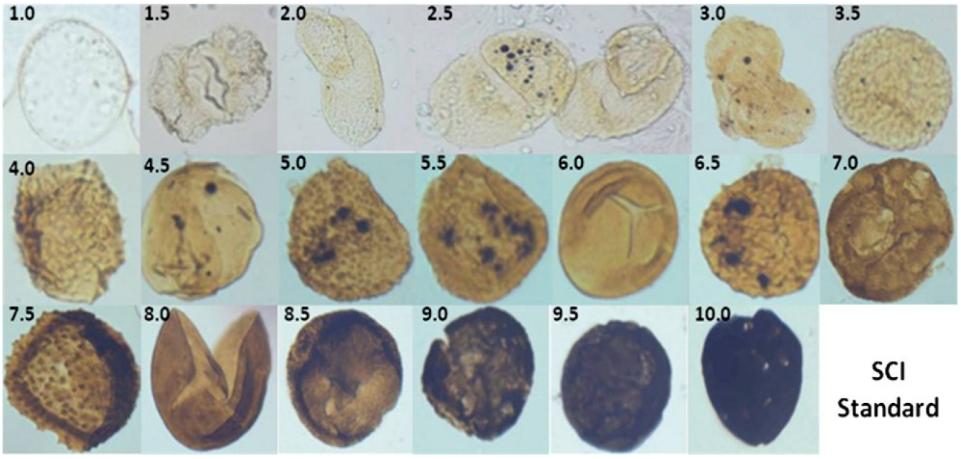

Figure 20: Spore Coloration Index (SCI) – spore colour change as a result of thermal alteration; scale proposed by Fischer et al. (1981).

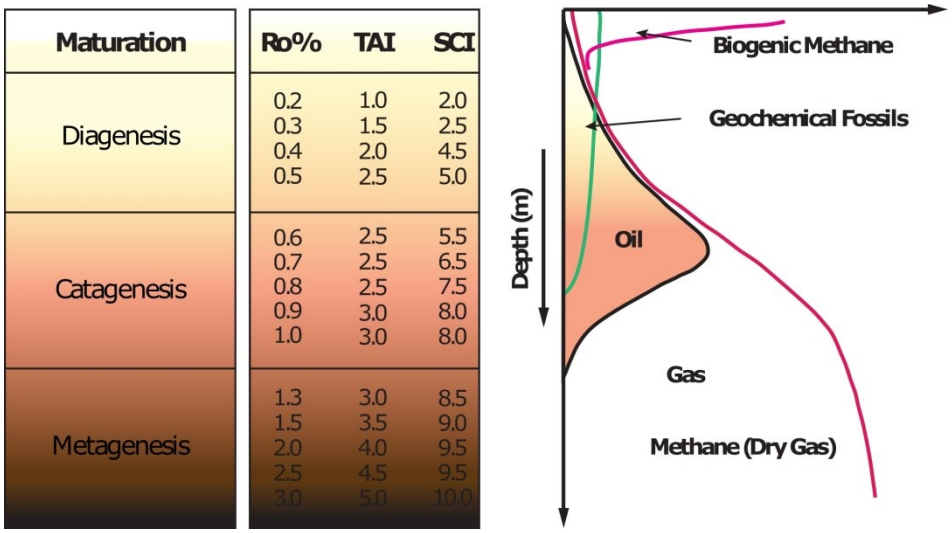

Figure 21: Correlation of palynomorph coloration changes as a function of increasing burial and rise in temperature (maturation). Correlation with vitrinite reflectance (Ro%) and spore coloration index (SCI) parameters (Suárez-Ruiz et al., 2012).

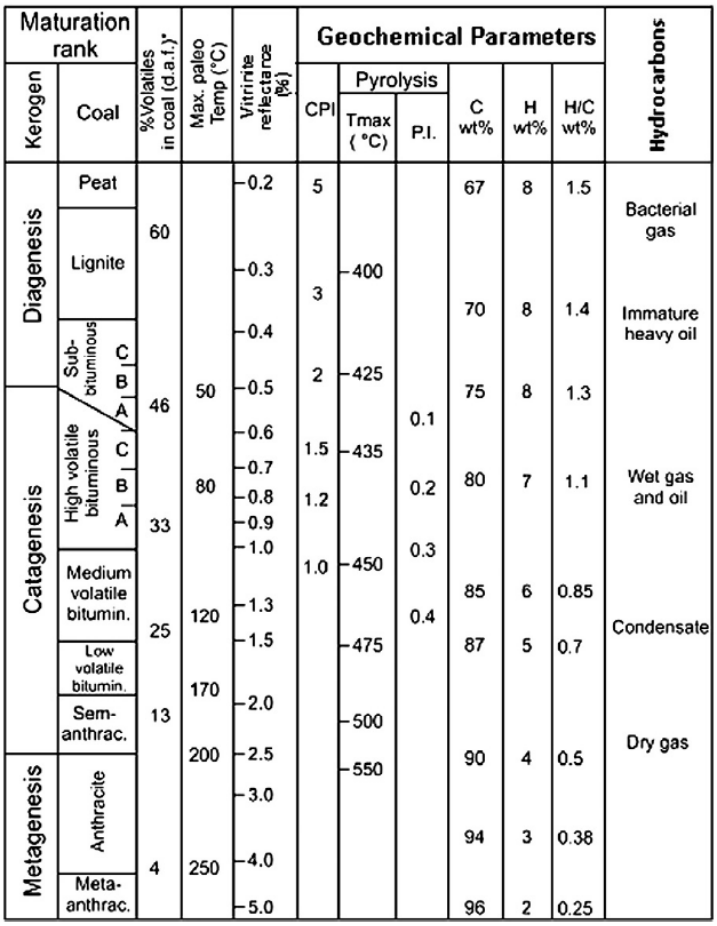

Figure 22: Correlation of vitrinite reflectance with max palaeotemperature (Suárez-Ruiz et al., 2012).

Biostratigraphy of the Nevenka 1 core

Data on the biostratigraphical subdivision of the Patagonian sections is limited. A biostratigraphical study on the Nevenka 1 core samples was therefore performed by Darrin Stead of Wellstrat Services Limited based on the diverse assemblage of dinoflagellate cysts and sporomorphs.

22 ditch cuttings samples over the interval 2104 m (NEV 63) – 2808 m (NEV 2) were analysed. Where possible a 200 specimen count has been made, followed by a scan of the slides to identify any species occurring outside the 200 count. The data has been entered into Stratabugs™ software. As the samples are ditch cuttings from a well section some caving of younger forms was noted.

4. RESULTS

4.1 CENTRAL CHILE

CAJÓN DEL MORADO

PALYNOFACIES ANALYSIS

166 samples of the CM section are analysed for their palynofacies composition. The value of the quantitative ratio of groups of particles of the total sedimentary organic matter (SOM) of each sample is given in % (Figs. 23–25). Note that SOM is intensively altered and that fluorescence microscopy is consequently not applicable to distinguish between AOM of algal/bacterial marine origin (AOMA) and AOM derived of strongly degraded terrestrial organic matter (phytoclasts, sporomorphs, fungal filaments) (AOMT). AOM is therefore differentiated into two groups, translucent and opaque, without reference to its origin. For simplification, the AOM proportion is added to the content of terrestrial organic matter.

Terrestrial organic matter

Sporomorphs, phytoclasts, fungal filaments and terrestrial derived AOM (AOMT) combine to the amount of terrestrial organic matter. In the CM section the amount of terrestrial organic matter dominates the organic matter composition throughout the section with a value ranging from 95.1 % to a maximum of 100 %. In the Tithonian section 38 samples are analysed with the content of terrestrial organic matter averaging at 99.1 % (SD=1.4 %). The Berriasian section that comprises 61 samples contains an averaged amount of 99.5 % of terrestrial organic matter (SD=0.85 %). 41 samples are analysed in the Valanginian section and terrestrial organic matter proportion averages 99.6 %, while standard deviation is 0.61 %. In total, 26 samples of the Hauterivian section are analysed and terrestrial organic matter content averages 99.4 % (SD=0.98 %).

Sporomorphs: Next to foraminiferal test linings, sporomorphs are the only palynomorphs that occur in the CM section. Preservation state of sporomorphs throughout the sample series of the CM section is predominantly poor, with only few specimens fairly preserved. The average sporomorph content in the Tithonian section is 2.5 % (SD=2.6 %). The proportion fluctuates intensely but shows higher abundance in the upper middle and upper part of the interval. The mean proportion of sporomorphs in the Berriasian section is 0.27 % (SD=0.62 %). A peak of 4.4 % is identified in the uppermost sample. A clear trend is not observed. Sporomorphs reach an average content of 2 % in the Valanginian section (SD=1.7 %). An intermittent peak of 8.7 % is identified in the upper middle part of the interval. No clear trend occurs. The Hauterivian section shows an average sporomorph content of 1.7 % (SD=1.3 %). Throughout the stage proportion increases from 0 % to 1.9 % but this increase appears erratic as several intermittent peaks occur.

Phytoclasts: Depending on their state of preservation each group of phytoclasts (inertinite, vitrinite and cutinite) is assigned to either category “A=good”, “B=fair” or “C=poor”. Poorly preserved phytoclasts are here counted as AOMT. Average phytoclast content of the Tithonian samples is 38.5 % (SD=18.1 %). Content increases discontinuously throughout the stage and varies between 4.5

% and 88.4 %. The Berriasian section of CM is characterised by a mean phytoclast content of 69.4 % (SD=19.1 %). No trend is observed in the lower part of the Berriasian. After a nadir of 6.6 % in the upper lower part of the Berriasian section content increases inhomogeneously to a maximum value of 99.8 % in the Middle Berriasian section. Subsequently, a discontinuous decrease is observed to 49.5 % which is reached towards the end of the stage. Phytoclast content in the Valanginian interval of the section shows no unequivocal trend. The amount varies between 32.1 % and 91.1 %. The average content for the Valanginian section is 58.6 % (SD=15.4 %). Phytoclast abundance of the Hauterivian section fluctuates intensely between 38.2 % and 94.8 %. Throughout the stage the content discontinuously decreases from 86.6 % to 56.0 %. A mean proportion of 73.6 % (SD=12.7 %) is identified.

Inertinite: Inertinite content in the Tithonian section varies between 0 % and 88.3 %, with an average amount of 29.4 % (SD=20.2 %). An inhomogeneous increasing trend is observed from 5.1 % to 88.3 %. The abundance of well-preserved (category A) inertinite increases throughout the Tithonian section from 5.1 % to 55.8 % but fluctuates highly between 0 % and 55.8 %. Several intermittent peaks are detected. The average content is 15.0 % (SD=14.5 %). Abundance of fairly (cat. B) preserved inertinite varies intensely between 0 % and 41.2 % and shows a discontinuous increase from 0 % to 32.5 %. The mean content is 14.5 % (SD=9.7 %). Throughout the Berriasian section of CM the abundance of inertinite varies strongly between 4.7 % and 90.3 %. A distinct trend is not observed and the average content of inertinite for the Berriasian section is 58.1 % (SD=20.4 %). Inertinite of category A shows no clear trend and proportion varies between 2.2 % and 82.7 %. The average content is 26.9 % with a SD of 17 %. In the Berriasian part of the CM section content of fairly (cat. B) preserved inertinite varies strongly between 0.66 % and 82.3 %. Highest proportion is reached in the lower upper part of the Berriasian section. A distinct trend is not observed. The average content is 31.3 % (SD=21 %). Samples of the Valanginian section shows an average inertinite abundance of 42 % (SD=16.4 %). A distinct trend is not observed and the content varies significantly between 12.1 % and 85.5 %. Proportion of well-preserved (cat. A) inertinite varies intensely between 5.4 % and 45.2 %. The average proportion is 20.5 % (SD=10.5%). A trend is not observed. Two intermittent peaks (79.2 % and 76.8 %) of fairly preserved inertinite are identified in the upper middle and lower upper part of the Valanginian section. Proportion varies between 1.9 % and 79.2 %. An unequivocal trend is not observed. The mean content is 21.5 % (SD=16.3 %). In the Hauterivian inertinite content varies significantly and decreases from 77.3 % to 32.8 %. The mean content is 60.2 % (SD=14.7 %). The stage is characterised by an initial discontinuous increase of well-preserved inertinite from 51.1 % to 72.2 % within the lower part of the interval. Subsequently the content decreases inhomogeneous throughout the middle and upper part of the Hauterivian section from 72.2 % to 20.9 %. In the Hauterivian well-preserved inertinite reaches a mean abundance of 43 % (SD=14.9 %). The content of fairly preserved (cat. B) inertinite ranges from 2.8 % to 33 % resulting in a mean value of 17.2 % (SD=9.9 %). A trend is not observed.

Vitrinite: Vitrinite content in the Tithonian section is comparatively low and varies between 0 % and 23.3 %. The mean content is 8.5 % (SD=8.6 %). The middle and lower upper part of the Tithonian section shows the highest content. In the Tithonian section well-preserved vitrinite shows a mean content of 0.64 % (SD=0.73 %). Frequency ranges from 0 % to 2.7 %. Several intermittent peaks occur. No distinct trend is observed. The proportion of vitrinite of category B varies between 0 % and 22.6 %. Proportion is highest in the middle and lower upper parts of the Tithonian section. The

mean content is 7.6 % (SD=8.2 %). In the Berriasian section the content of vitrinite varies significantly between 0 % and 45.5 %. Several intermittent peaks are present but a distinct trend is not observed. The mean content for this stage is 11.2 % (SD=12 %). Vitrinite of category A shows a mean frequency of 3.2 % (SD=4.4 %). The content ranges from 0 % to 19.5 %. Several intermittent peaks are identified and no distinct trend is observed. Throughout the Berriasian section the proportion of the fairly well preserved (cat. B) vitrinite varies strongly from 0 % to 35.1 %. A mean content of 8 % (SD=9.7 %) is detected. A clear trend is not observed. The content of vitrinite in the Valanginian section varies between 4.6 % and 36.1 %. The proportion fluctuates significantly and a distinct trend is not observed. The mean content is 16.5 % (SD=8.8 %). The mean content for well-preserved (cat. A) vitrinite is 3.4 % (SD=2.5 %). Frequency varies intensely between 0 % and 11 %. A trend is not observed. In the Valanginian interval of the CM section content of fairly preserved (cat. B) vitrinite ranges from 2.2 % to 30.3 %. A mean content of 13 % (SD=7.8 %) is detected. A distinct trend is not observed. In the Hauterivian interval of the CM section vitrinite content varies between 4.1 % and 35.6 %. A trend is not observed. The mean content is 12.9 % (SD=7.5 %). The frequency of well preserved (cat. A) vitrinite varies between 0.5 % and 14.7 %. No distinct trend is observed. A mean content of 4.6 % (SD=3.9 %) and 3 intermittent peaks are identified. Vitrinite of category B shows a mean content of 8.3 % (SD=5.3 %). Proportion varies between 1.6 % and 20.9 %. A clear trend is not observed.

Cutinite: Throughout the CM section the amount of cutinite is low and no differentiation was carried out according to the state of preservation. In the Tithonian of the CM section cutinite content varies between 0 % and 3.1 %. The mean content is 0.54 % (SD=0.82 %). An unequivocal trend is not observed. Throughout the Berriasian section content of cutinite remains low and ranges from 0% to 0.84 %. The average content is 0.10 % (SD=0.23 %). In the Valanginian section cutinite content remains low ranging between 0 % and 1.13 % and reaching an average of 0.19 % (SD=0.31 %). The samples of the Hauterivian section shows a mean content of 0.51 % (SD=0.77 %). A trend is not observed and proportion varies between 0 % and 3.3 %.

Fungal filaments: The content of fungal filaments varies considerably. On average, the Tithonian contains 1.8 % (SD=7.2 %) of fungal filaments whereas two samples of the lower Upper Tithonian section contain peaks of 19.8 % and 40.4 %, respectively. In the lower part of the Berriasian section one sample peaks at 21.4 %. The averaged value for the Berriasian is 0.58 % (SD=2.8 %). In the Valanginian 9 samples contain peaks of fungal filaments, between 10.5–45.9 %, with an average of 6 % (SD=11.8 %). 3 samples of the Hauterivian show peaks in fungal filament proportion (13.1–49.3 %) with a mean value of 3.8 % (SD=10.6 %).

Terrestrial AOM: Large amounts of the organic matter composition consist of AOMT. In the Tithonian average AOMT proportion is 54.2 % (SD=19.1%) for the translucent fraction and 2.5 % (SD=2.6 %) for the opaque fraction. A highly erratic decreasing trend of $AOMT_{total}$ is identified. The mean content of the Berriasian section is 24.4 % (SD=20.4 %) for translucent material and 5 % (SD=9.2 %) for opaque amorphous matter. The lower to middle part of the Berriasian section is characterised by several positive intermittent peaks. After a nadir of 0 % in the middle part of the Berriasian section $AOMT_{total}$ content increases discontinuously throughout the remainder of the interval reaching to 45.4 %. The samples of the Valanginian section contains a mean content of 31 % (SD=16.3 %) translucent and 1.9 % (SD=2.9 %) opaque AOMT, respectively. The distribution of

$AOMT_{total}$ shows no distinct trend. For the Hauterivian averaged proportion of 19.8 % (SD=9.8 %) (translucent) and 0.55 % (SD=0.79 %) (opaque) are acquired. A clear trend is not observed.

Marine organic matter

Due to the high thermal degradation of the sedimentary organic matter, fluorescence microscopy could not be applied to the Central Chilean sections to distinguish between terrestrial and marine AOM. In the samples analysed here, structured organic matter of marine origin is limited to 3 occurrences of acritarchs and a few more occurrences of foraminiferal test linings. All remaining marine organic matter is amorphous (AOM), without any indications of its former structured appearance and origin; in consequence, all AOM is counted as terrestrial organic matter.

Acritarchs: A total of 3 samples contain acritarchs. In the uppermost part of the Berriasian section 2 acritarch occurrences are identified in one sample. The average content for the stage is therefore 0.01 % (SD=0.09 %). In the lower(most) part of the Valanginian section 2 samples contain acritarchs, resulting in a mean content of 0.01 % (SD=0.06 %). Both the Tithonian and Hauterivian stages are free of acritarchs.

Foraminiferal test linings: In the Tithonian 15 samples contain foraminiferal remains leading to a content of structured marine organic matter (marine palynomorphs) for this stage of 0.5 % (SD=0.95 %). One sample of the lowermost Berriasian section contains foraminifera resulting in an average proportion of 0.005 % (SD=0.03 %). In the Valanginian section 3 samples contain foraminiferal remains. The averaged proportion is 0.04 % (SD=0.16 %). 2 samples of the Hauterivian section contain foraminiferal test linings leading to an average content of 0.03 % (SD=0.1 %).

Opaque/translucent ratio

For the Tithonian interval an OP/TR ratio of 3.5 is detected. The OP/TR ratio of the Berriasian section is 5.2. The OP/TR ratio of the Valanginian interval is 2.6. The OP/TR ratio of the Hauterivian section is 4.7.

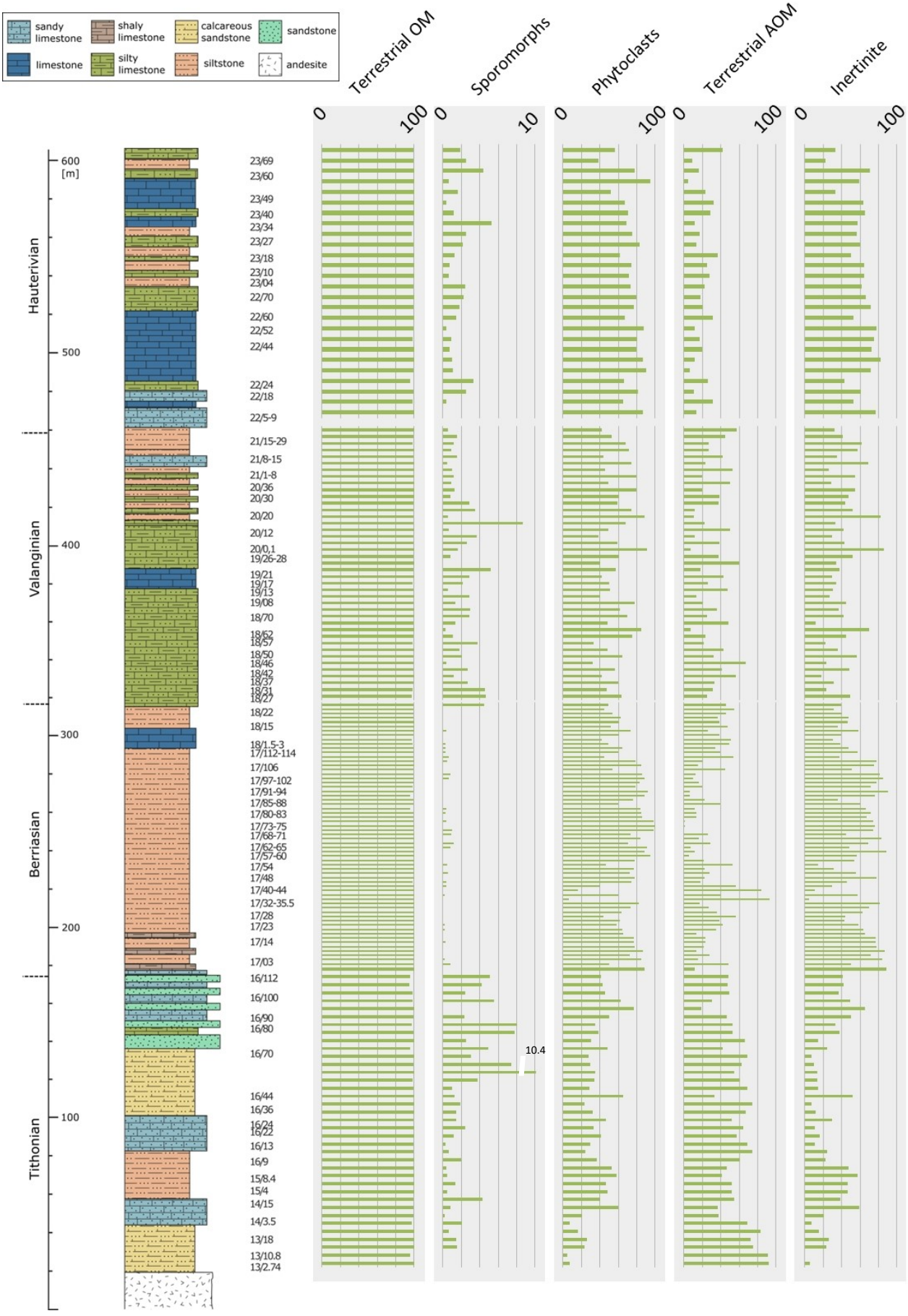

Figure 23: Sedimentary organic matter – terrestrial fraction; CM section. Values given in %, to increase visualisation, different scales are used. Statistical outliers are marked accordingly.

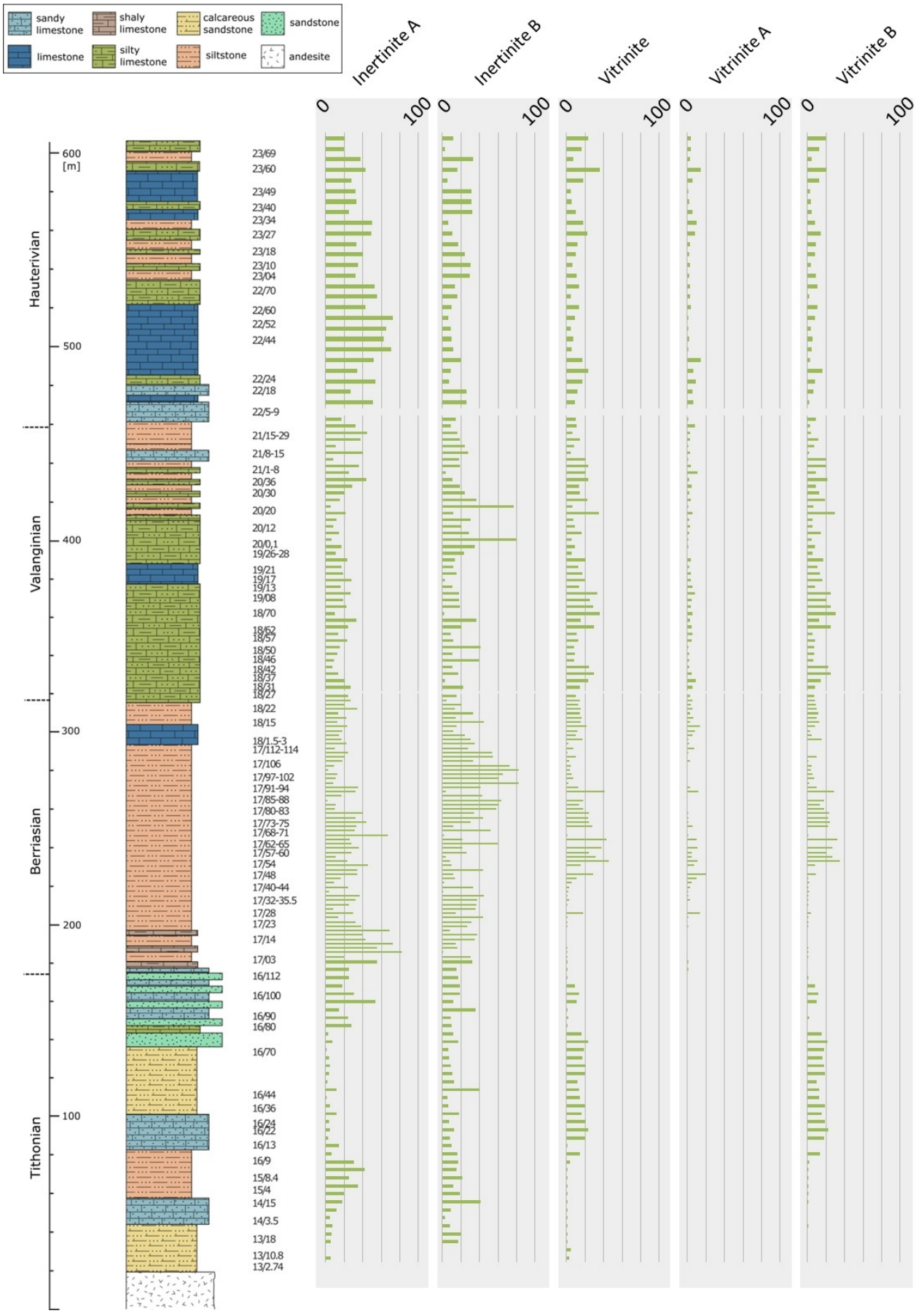

Figure 24: Sedimentary organic matter – terrestrial fraction continued; CM section. Values given in %, to increase visualisation, different scales are used.

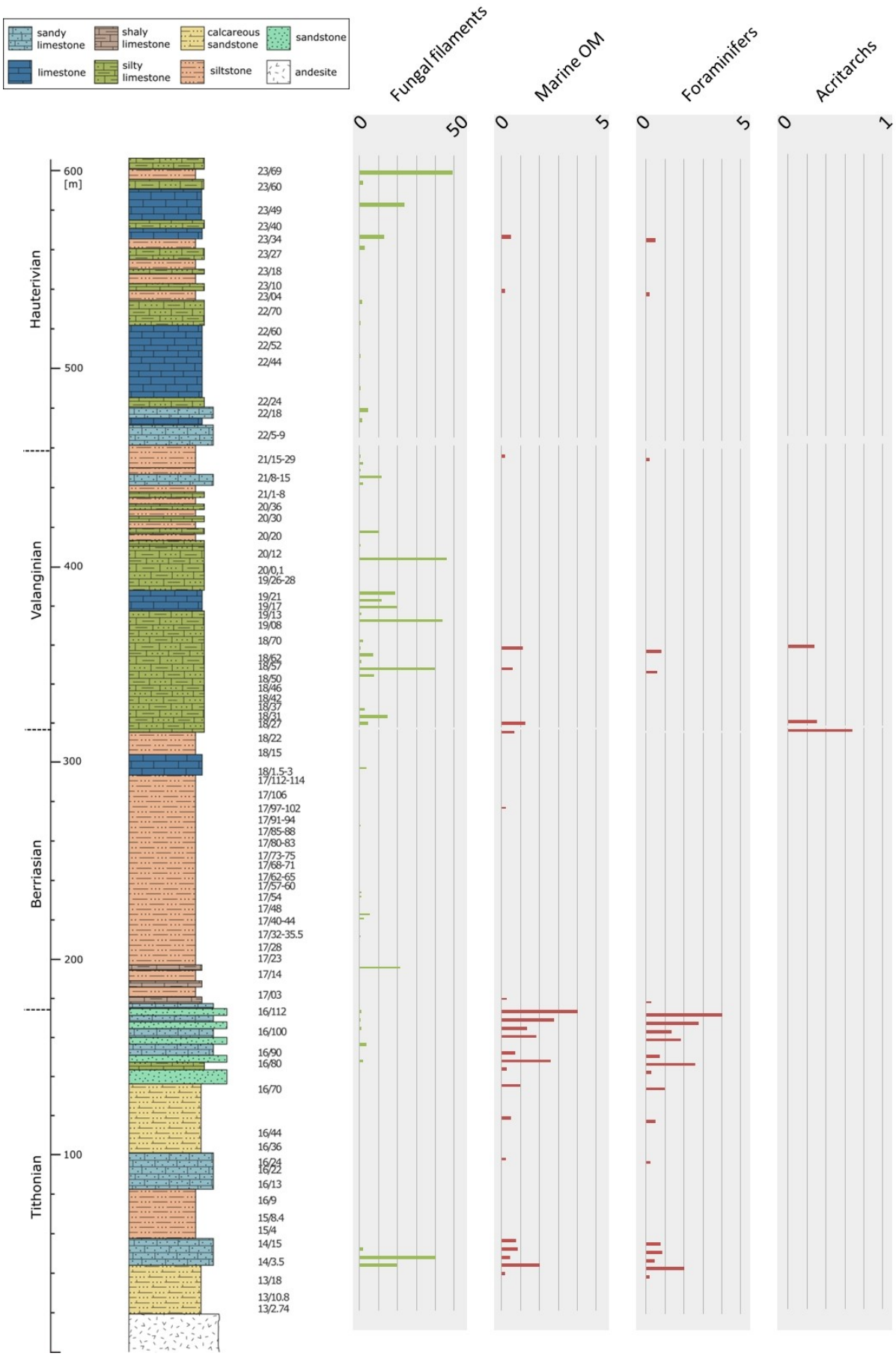

Figure 25: Sedimentary organic matter – fungal filaments and marine fraction; CM section. Values given in %, to increase visualisation, different scales are used.

LO VALDÉS

PALYNOFACIES ANALYSIS

84 samples of the LV section are analysed for palynofacies composition (Tithonian 29, Berriasian 31, Valanginian 12 and Hauterivian 12 samples) (Figs. 26–28). Values given in % always refer to the quantitative ratio of the described particle group within the total SOM of a sample. Procedure for very poorly preserved non-fluorescent organic matter is the same as in the CM section. All AOM derived from strongly degraded matter is added to the group of terrestrial origin (AOMT). AOMT is differentiated in two groups: translucent and opaque.

Terrestrial organic matter

As for the organic matter composition of the CM section, the LV section is characterised by a large amount of strongly degraded terrestrial organic matter. The abundance varies between 94.7–100 %. In the samples of the Tithonian section an average of 98.5 % (SD=1.4 %) of the organic matter composition is of terrestrial origin. Since there are no foraminiferal linings present and AOM is assigned to terrestrial organic matter, the proportion of the latter increases to 100 % (SD=0 %) in the samples of the Berriasian section. The samples of the Valanginian section contain on average 99.9 % (SD=0.1 %) of terrestrial organic matter. In the Hauterivian section the averaged abundance of terrestrial organic matter is 99.8 % (SD= 0.33 %).

Sporomorphs: Similar to the samples of the CM section, most sporomorphs of the LV section are poorly preserved and only a few are fairly well preserved. In the Tithonian section the averaged sporomorph abundance is 2.7 % (SD=2.6 %). A peak of 4.3 % is identified in the lower middle part of the Tithonian section. A clear trend is not observed. Only one sample in the uppermost part of the Berriasian section contains sporomorphs. Percentage of sporomorphs decreases in this stage to a mean of 0.04 % (SD=0.21 %). The sporomorph percentage of the Valanginian is 1.2 % (SD=2.3 %). A peak of 8.3 % is detected in the lower middle part of the Valanginian section. An inhomogeneous increasing trend from 0.27 % to 1.4 % is identified. Sporomorph abundance of the Hauterivian section averages 0.83 % (SD=1.7 %). A peak of 6 % is observed in the lowermost part of the Hauterivian section. A trend in the distribution pattern is not detected.

Phytoclasts: Phytoclasts are here subdivided into three groups (inertinite, vitrinite and cutinite). Depending on the state of preservation each particle of this group is assigned either to “A=good”, “B=fair” or “C=poor” in preservation. The preservation state of poorly preserved phytoclasts overlaps with that of AOMT and therefore is counted as such. The Tithonian samples reach a mean phytoclast content of 27.1 % (SD=20.1 %). After a sharp decrease (77.8 % to 0.39 %) in the lower part of the Tithonian section content increases discontinuously throughout the remainder of the stage to a maximum of 75.3 %. In the Berriasian section phytoclast content decreases inhomogeneous from 94.7 % to 19.7 %. The mean abundance increases to 64.7 % (SD=15.1 %). Mean phytoclast abundance in the Valanginian of the LV section is 51.7 % (SD=13.7 %). The content ranges from 25 % to 73 %. An inhomogeneous increasing trend is observed from 42.2 % to 66.1 %. The phytoclast proportion in the Hauterivian section shows a discontinuous increase from 39.2 % to 84 %. The value ranges from 39.2 % to 94.1 %. The mean content for this interval is 72.3 % (SD=18 %).

Inertinite: In the Tithonian of the LV section inertinite reaches a mean content of 19 % (SD=14.4 %). Value fluctuates highly between 0.4 % and 65.5 %. An indistinct increasing trend is identified. Intermittent peaks occur in the lower (57.4 %) and in the uppermost part of the Tithonian section (65.5 %). Well preserved (cat. A) inertinite shows a mean content of 3 % (SD=6.5 %). Throughout the lower, middle and lower upper part of the Tithonian section content varies on a low level between 0 % and 4.4 %. In the uppermost part of the section content increases significantly to 30 %. Abundance of fairly well preserved (cat. B) inertinite ranges from 0.4 % to 56.2 % (peak in the lower part of the interval). A mean content of 16 % (SD=11.7 %) is identified. An unequivocal trend is not observed. In the lower part of the Berriasian section inertinite frequency increases from 28.9 % to 85.9 %. Subsequently the content decreases towards the end of the stage until a minimum of 17.1 % is reached in the uppermost part of the Berriasian section. The mean content is 56.9 % (SD=16.9 %). Inertinite of category A reaches a mean proportion of 25.1 % (SD=8.4 %). The content fluctuates highly between 9.4 % and 38.8 % and increases throughout the lower and middle part of the Berriasian section. In the Late Berriasian a decreasing trend from 37.9 % to 9.4 % is observed. After a sharp increase from 15.5 % to 60.7 % in the lower part of the Berriasian section, the content of fairly preserved (cat. B) inertinite fluctuates on a high level between 27.9 % and 47.5 % throughout the remainder of the lower and middle part of the Berriasian section. In the upper part of the Berriasian section a decreasing trend from 47.5 % to 7.7 % is observed. The mean proportion for this stage is 31.8 % (SD=11.3 %). The Valanginian lacks a clear trend in inertinite proportion. Abundance varies between 13.9 % and 53.7 %. The content of well-preserved inertinite ranges from 10.1 % to 32.6 %. A trend is not observed. A mean content of 22.8 % (SD=6.8 %) is identified for the group of well-preserved inertinite. Abundance of fairly well preserved (cat. B) inertinite decreases discontinuously throughout the lower and lower middle part of the Valanginian section from 15.8 % to 3.7 %. Subsequently an indistinct increase to 22.1 % is detected. The mean content for this stage is 13.5 % (SD=6.2 %). For the Hauterivian of the LV section a mean inertinite content of 57.4 % (SD=18.5 %) is identified. The proportion fluctuates highly between 16.6 % and 79.4 %. A distinct trend is not observed. After a sharp increase from 9 % to 62.7 % and an immediate decrease to 31.8% in the lower part of the Hauterivian section well-preserved inertinite fluctuate between 23.3 % and 37.7 % for the remainder of the interval. A mean content of 30.3 % (SD=12.6 %) is observed and an unequivocal trend is not identified. Fairly well preserved inertinite ranges from 7.5 % to 46.3 %. The mean abundance is 27.1 % (SD=13.5 %). A discontinuous increasing trend from 7.5 % to 24.4 % is detected.

Vitrinite: In the lowermost part of the Tithonian interval of the LV section proportion of vitrinite decreases sharply from 64.7 % to 0.58 %. Until the middle upper part of the Tithonian section content varies on a low level between 0 % and 3.7 %. In the uppermost part of the Tithonian section the proportion increases significantly and ranges from 9.8 % to 25.1 %. The mean vitrinite proportion for the Tithonian section is 7.2 % (SD=16.1 %). The content of well-preserved (cat. A) vitrinite is continuously low throughout the interval and varies between 0 % and 1.1 %. In the uppermost part of the Tithonian section intermittent peaks of up to 7.5 % are observed. The mean proportion is 0.5 % (SD=1.5 %). The mean content of fairly well preserved vitrinite is significantly higher with 6.7 % (SD=15.7 %) abundance. In the lowermost part of the Tithonian section a sharp decrease from 64.3 % to 0.6 % is identified. A positive peak of 17.6 % is observed in the uppermost part of the Tithonian section. After a sharp decrease from 63.7 % to 1.4 % in the lowermost part of the Berriasian section the content increases inconsistently throughout the remainder of the interval. The mean proportion is

7.7 % (SD=11.1 %). The content of well-preserved vitrinite shows a marked decrease in the lowermost part of the Berriasian section (19.7 % to 0 %). An indistinct trend is not observed. The mean proportion of well-preserved vitrinite is 1.3 % (SD=3.5 %). A distinct decrease in fairly preserved vitrinite is detected in the lowermost part of the Berriasian section. Subsequently the content increases slightly throughout the remainder of the interval. The averaged content is 6.3 % (SD=7.7 %). Vitrinite proportion varies significantly throughout the Valanginian of the LV section between 4.3 % and 32.9 %. The mean proportion is 15.1 % (SD= 8.4 %). An unambiguous trend is not observed. Content of well-preserved vitrinite varies significantly between 0 % and 19.7 %. The mean proportion is (3.8 % (SD=5.8 %). A trend is not observed. Fairly preserved vitrinite of the Valanginian section shows an average content of 11.3 % (SD=5.2 %). The content ranges from 4.3 % to 24.8 %. No distinct trend is observed. Vitrinite proportion of the Hauterivian section varies between 2.9 % and 37.9 %. Intermittent positive peaks are present. The average proportion is 14.4 % (SD=11 %). The distribution pattern shows no clear trend. The content of well-preserved vitrinite decreases discontinuously throughout the lower and middle part of the Hauterivian section from 2.8 % to 0.7 %. A marked increase in well-preserved vitrinite is identified in the upper part of the Hauterivian section where the value rises to 6.7 %. A mean proportion of 2.9 % (SD=2.1 %) is observed. The proportion of fairly preserved vitrinite is significantly higher and varies between 1.9 % and 35.2 %. Intermittent peaks occur and a clear trend is not observed.

Cutinite: The Tithonian samples contain the highest amounts of cutinite. The proportion ranges from 0 % to 5.9 %. A distinct trend is not observed, although the value is higher in the lower part of the Tithonian section. The mean frequency for this stage is 0.89 % (SD=1.3 %). The proportion of cutinite in the Berriasian section varies between 0 % and 2.1 %. A trend is not observed. A mean content of 0.15 % (SD=0.42 %) is detected. In the Valanginian section the mean content of cutinite increases slightly to 0.26 % (SD=0.39 %). A trend in frequency distribution is not observed. In the Hauterivian section the average cutinite content is 0.5 % (SD=1.2 %). Sample content ranges from 0 % to 4 %. A trend is not observed.

Fungal filaments: Overall fluctuation of fungal filament content in the LV section is less intense than in the CM section. The average proportion is continuously low but highest in the Tithonian section where it reaches 2.9 % (SD=12.1 %), although with a single peak of 65.2 % in the middle part of the Tithonian section. Lowest abundance of fungal filaments is identified in the Berriasian with an average content of 0.05 % (SD=0.26 %). The content of the Valanginian section averages at 1.2 % (SD= 3.3 %) and for the Hauterivian section a proportion of 1.6 % (3.5 %) is identified. Individual peaks occur in the Late Valanginian section (11.4 %) and the Early Hauterivian section (11.7 %).

Terrestrial AOM: A large amount of organic matter of the LV section is composed of AOMT, either translucent or opaque. In the Tithonian section, the average translucent AOMT content accounts for 56.2 % (SD=22.5 %) of the total sedimentary organic matter composition. The content fluctuates between 7.7 % and 92.4 %. A trend is not observed. The proportion of opaque AOMT varies between 0 % and 19.3 %. A mean of 9.6 % (SD=4.7 %) is reached. No distinct trend is observed. The mean $AOMT_{total}$ proportion for the Tithonian section is 65.8 % (SD=21 %). In the Berriasian section the $AOMT_{translucent}$ content decreases to a mean of 33.3 % (SD=16.3 %) and $AOMT_{opaque}$ content decreases to a mean of 1.9 % (SD=6.5 %). Throughout the stage the content of translucent AOMT increases

discontinuously from 3.5 % to 79.9 %. For the opaque fraction of AOMT no trend is observed. The mean proportion of $AOMT_{total}$ is 35.2 % (SD= 15 %). An increase in mean $AOMT_{total}$ is identified in the Valanginian section where a value of 45.9 % (SD=16 %) is observed. The proportion varies intensely between 15.1 % and 74.3 %. A trend is not observed. No $AOMT_{opaque}$ is present in samples of the Valanginian section. In the Hauterivian section averaged abundance of $AOMT_{translucent}$ is 24.6 % (SD=16 %). Abundance ranges from 5.6 % to 52.3 %. A clear trend is not observed. For the opaque fraction the mean content is 0.55 % (SD=1.3 %). A peak of 4.4 % is detected in the uppermost Hauterivian section. Apart from that the content varies on a low level between 0 % and 0.69 %. The mean proportion of $AOMT_{total}$ in the Hauterivian section is 25.1 % (SD=15.6 %).

Marine organic matter

Similar to the CM section the sedimentary organic matter of the LV section shows a poor preservation state due to intense thermal alteration and/or oxidation. Aside from foraminiferal test linings all marine organic matter is amorphous (AOM) without any indications of its former structured appearance and origin. Since fluorescence microscopy shows no fluorescing AOM particles, a fluorescing fraction could not be distinguished. Therefore all AOM is counted as AOMT.

Foraminiferal test linings: 11 samples of the Tithonian section contain foraminiferal remains resulting in an average proportion for this stage of 0.29 % (SD=0.48 %). The frequency distribution shows no distinct pattern. No foraminiferal remains occur in the samples of the Berriasian section. The subsequent Valanginian section contains one sample with a single foraminiferal test lining leading to a mean proportion for this stage of 0.03 % (SD=0.1 %). The Hauterivian section contains 2 samples with foraminifers and the average proportion is 0.11 % (SD=0.29 %).

Opaque/translucent ratio

For the Tithonian section an OP/TR ratio of 2.6 is detected. The OP/TR ratio of the Berriasian interval is 7.4. The OP/TR ratio of the Valanginian interval is 2.4. The OP/TR ratio of the Hauterivian section is 4.

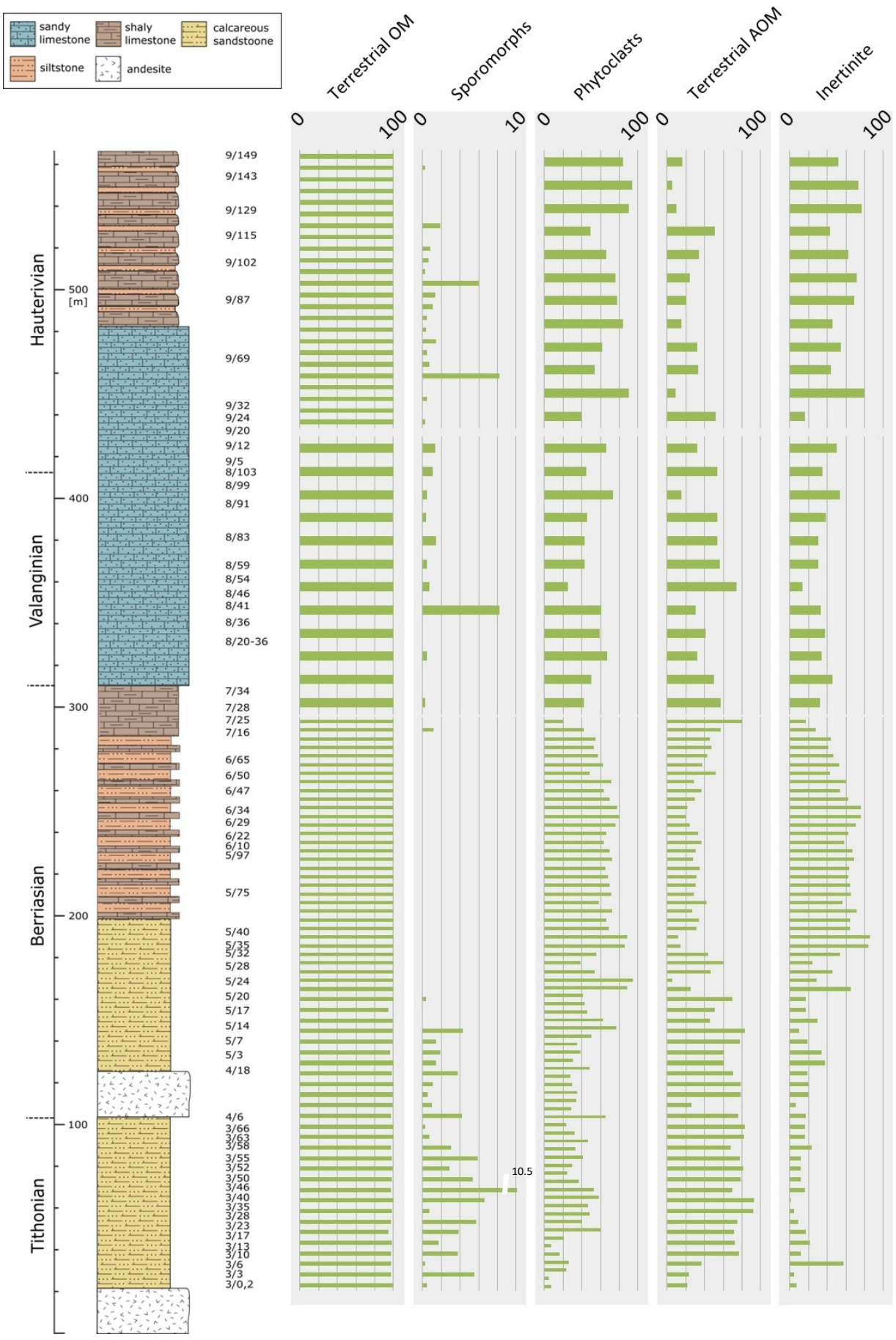

Figure 26: Sedimentary organic matter – terrestrial fraction; LV section. Values given in %, to increase visualisation, different scales are used. Statistical outliers are marked accordingly.

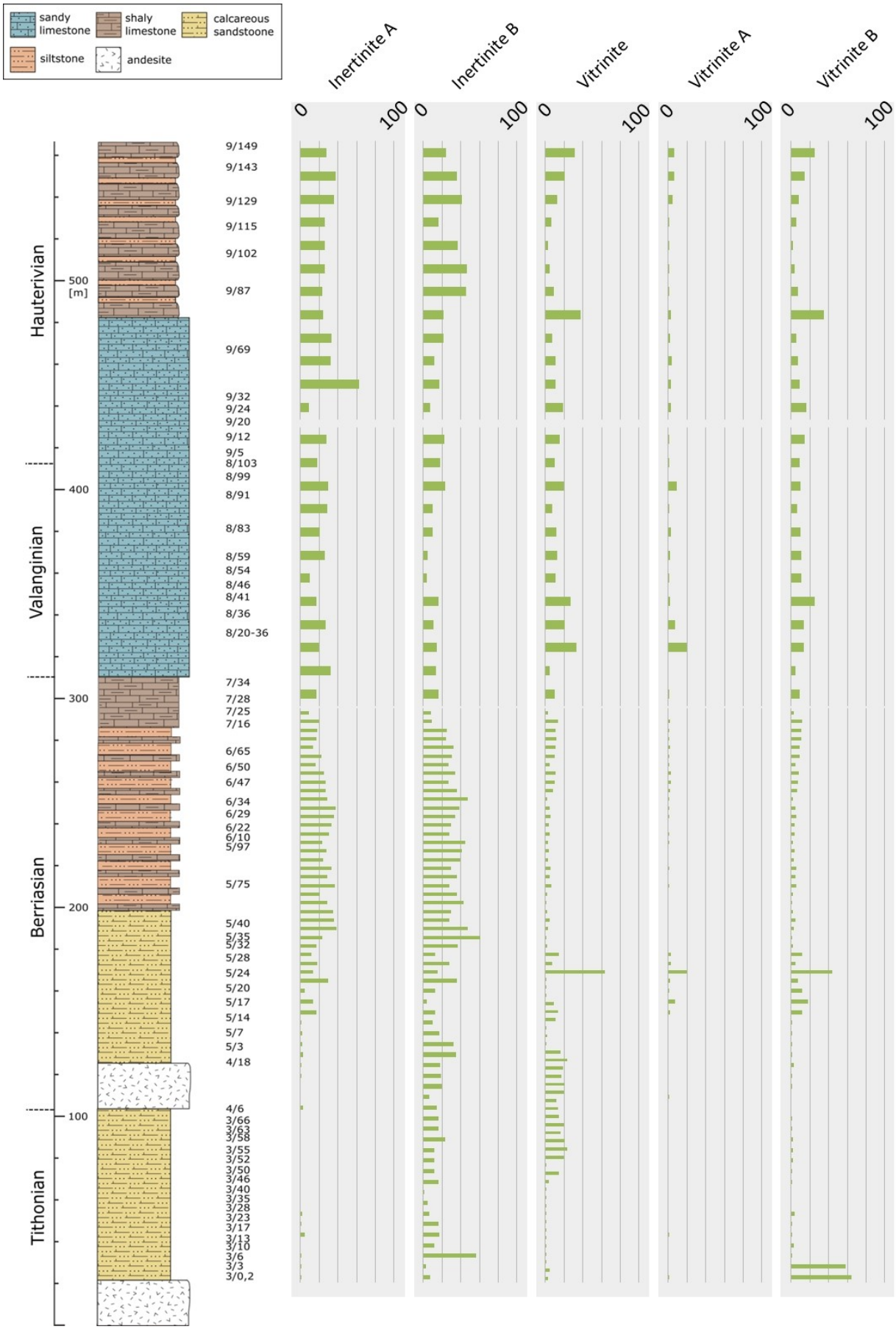

Figure 27: Sedimentary organic matter – terrestrial fraction continued; LV section. Values given in %, to increase visualisation, different scales are used.

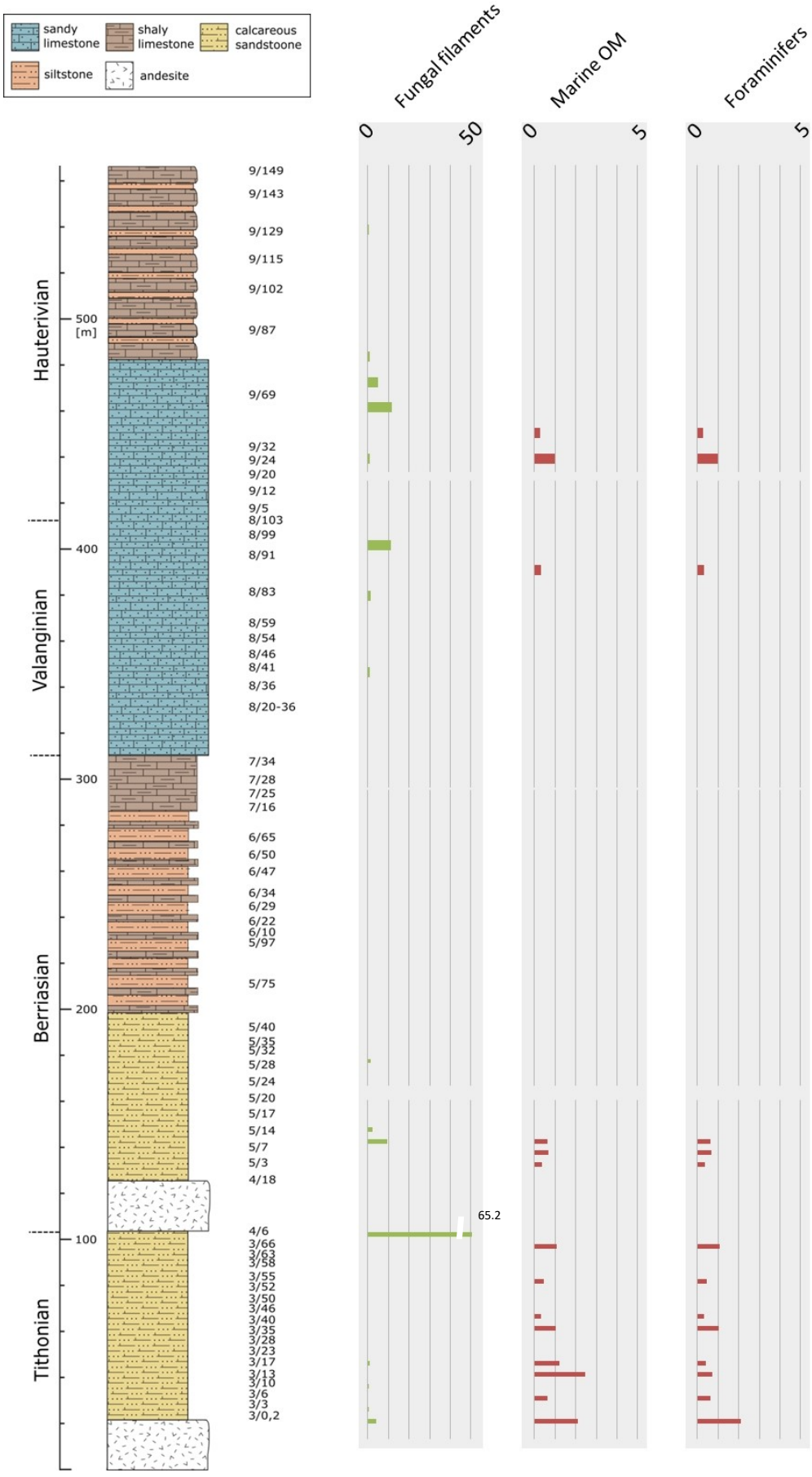

Figure 28: Sedimentary organic matter – fungal filaments and marine fraction; LV section. Values given in %, to increase visualisation, different scales are used. Statistical outliers are marked

AOM-PHYTOCLAST-PALYNOMORPH PLOT

CAJÓN DEL MORADO

Tithonian: Most samples of the Tithonian interval (CM 13/2.74–16/102) (Figs. 29–30) of the CM section plot in palynofacies field I – highly proximal shelf or basin. 10 samples plot in palynofacies field III – heterolithic oxic shelf ("proximal shelf"). Two samples of this interval plot in palynofacies field V – Mud-dominated oxic shelf ("distal shelf").

Berriasian: Almost all samples of the Berriasian section (CM 17/0.15–18/24) (Figs. 30–32) of CM plot in the palynofacies fields I – highly proximal shelf or basin. One sample plots in palynofacies field III – heterolithic oxic shelf ("proximal shelf").

Valanginian: Most samples of the Valanginian interval (CM 18/27–21/15-29) (Figs. 32–34) of the CM section plot in the palynofacies field I – highly proximal shelf or basin. 10 samples plot in the palynofacies field III – heterolithic oxic shelf ("proximal shelf"). 2 samples of this interval plot in the palynofacies field V – Mud-dominated oxic shelf ("distal shelf").

Hauterivian: Most samples of the Hauterivian section (CM 22/12–23/69) (Fig. 34) of the CM section plot in palynofacies field I – highly proximal shelf or basin. 2 samples plot in palynofacies field III – heterolithic oxic shelf ("proximal shelf") and one sample plots in field V – Mud-dominated oxic shelf ("distal shelf").

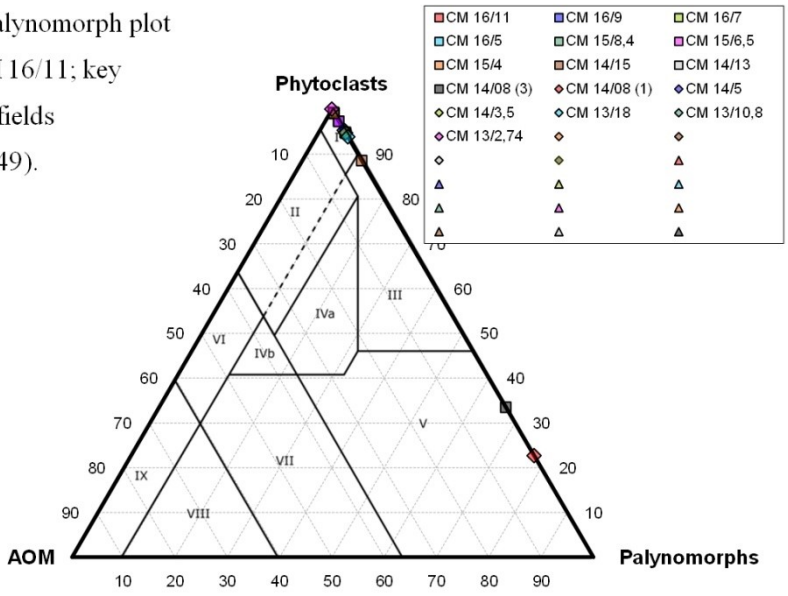

Figure 29: AOM-phytoclast-palynomorph plot of CM 13/2.74–CM 16/11; key to the palynofacies fields given in table 2 (p. 49).

Figure 30: AOM-phytoclast-palynomorph plot of CM 16/13–CM 17/8; key to the palynofacies fields given in table 2 (p. 49).

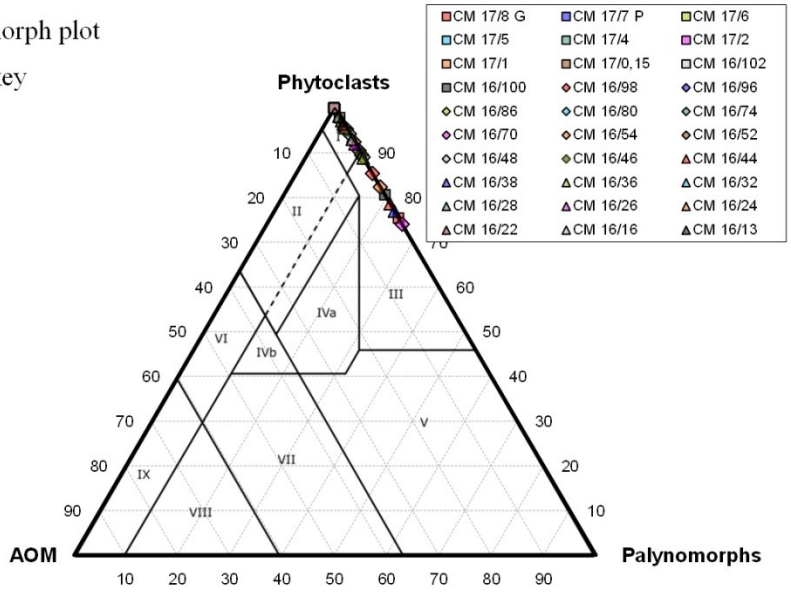

Figure 31: AOM-phytoclast-palynomorph plot of CM 17/14–CM 17/80; key to the palynofacies fields given in table 2 (p. 49).

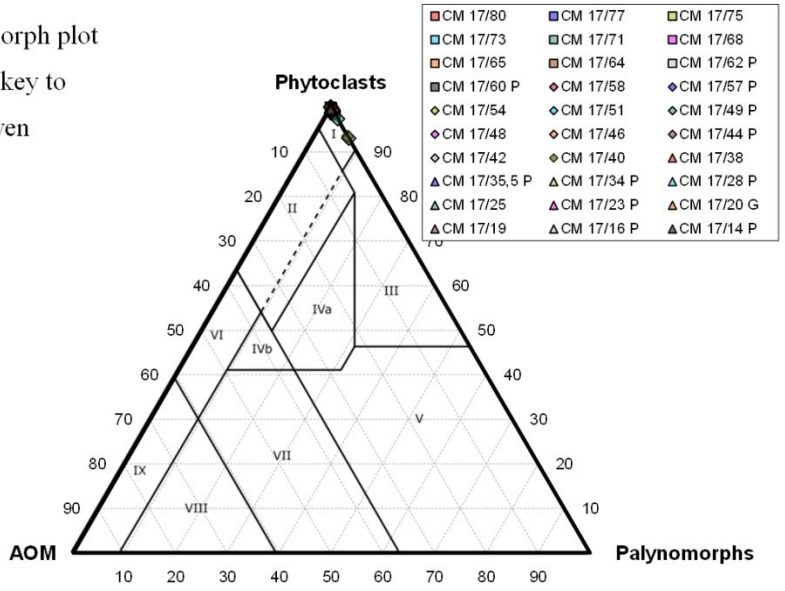

Figure 32: AOM-phytoclast-palynomorph plot of CM 17/81–CM 18/42; key to the palynofacies fields given in table 2 (p. 49).

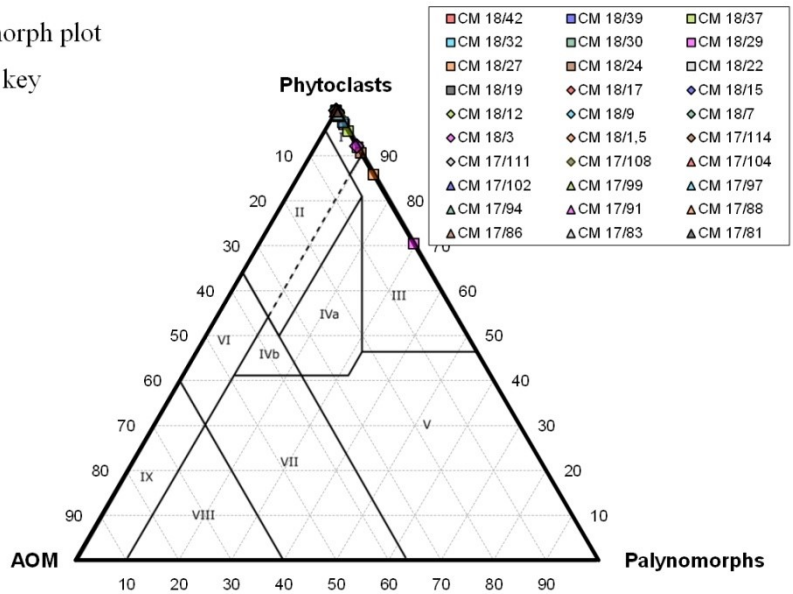

Figure 33: AOM-phytoclast-palynomorph plot of CM 18/45–CM 20/36; key to the palynofacies fields given in table 2 (p. 49).

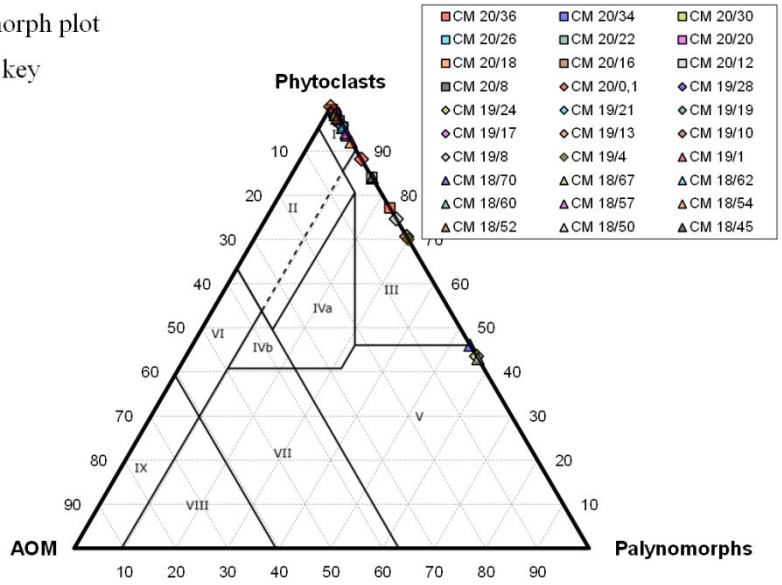

Figure 34: AOM-phytoclast-palynomorph plot of CM 21/1-8–CM 23/69; key to the palynofacies fields given in table 2 (p. 49).

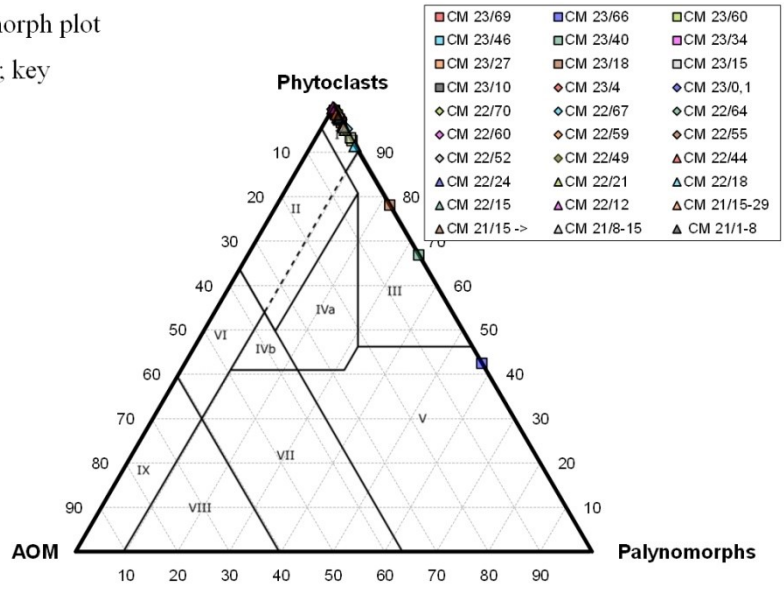

LO VALDÉS

Tithonian: 13 samples of the Tithonian interval (LV 3/0.2–3/66) (Figs. 35–36) of the LV section plot in palynofacies field I – highly proximal shelf or basin. 14 samples plot in palynofacies field III – heterolithic oxic shelf ("proximal shelf"). 2 samples plot in palynofacies field V – Mud-dominated oxic shelf ("distal shelf")

Berriasian: All samples of the Berriasian succession (LV 4/6–7/25) (Figs. 36–37) of the LV section plot in palynofacies field I – highly proximal shelf or basin.

Valanginian: 10 samples of the Valanginian interval (LV 7/28–8/103) (Fig. 37) of the LV section plot in palynofacies field I – highly proximal shelf or basin. 2 samples plot in palynofacies field III – heterolithic oxic shelf ("proximal shelf").

Hauterivian: Almost all samples of the Hauterivian interval (LV 9/5–9/149) (Fig. 37) of the LV section plot in palynofacies field I – highly proximal shelf or basin. 2 samples plots in palynofacies field III – heterolithic oxic shelf ("proximal shelf").

Figure 35: AOM-phytoclast-palynomorph plot of LV 3/0.2–LV 3/53; key to the palynofacies fields given in table 2 (p. 49).

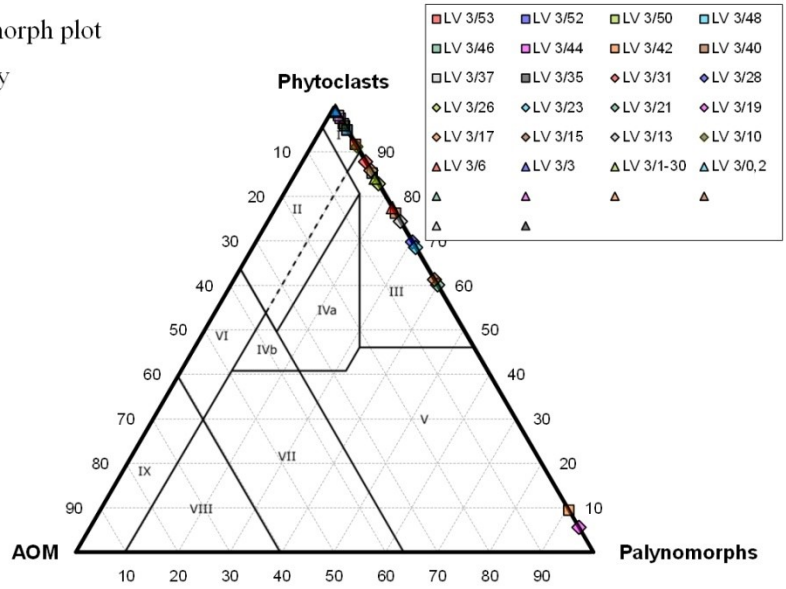

Figure 36: AOM-phytoclast-palynomorph plot of LV 3/55–LV 6/29; key to the palynofacies fields given in table 2 (p. 49).

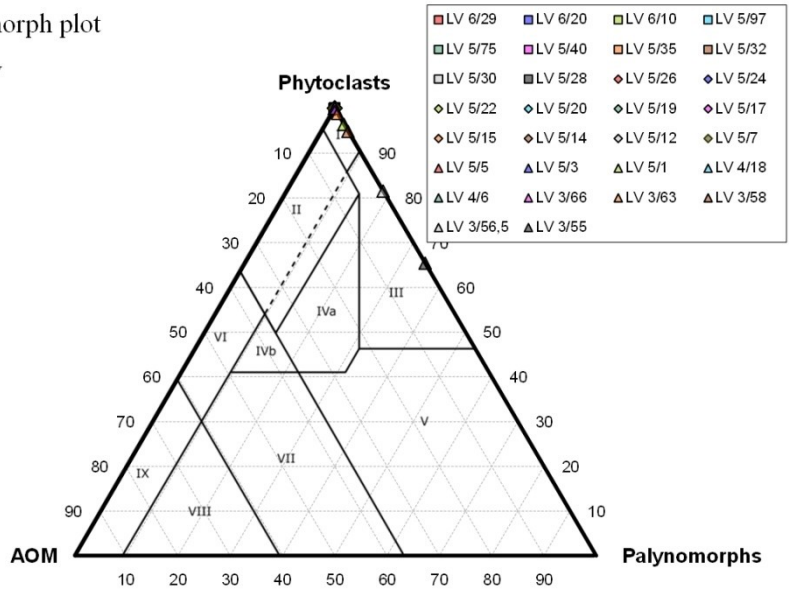

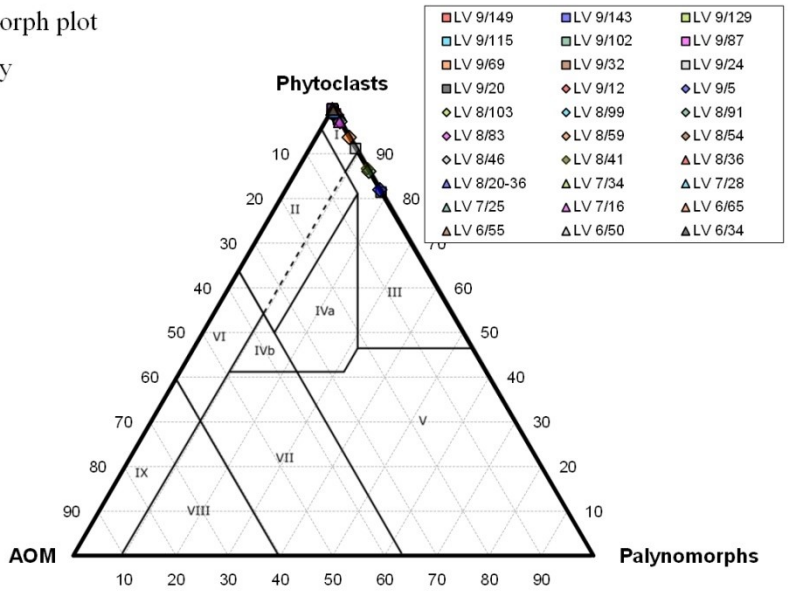

Figure 37: AOM-phytoclast-palynomorph plot of LV 6/34–LV 9/149; key to the palynofacies fields given in table 2 (p. 49).

STABLE ISOTOPE ANALYSIS

$\delta^{13}C$ and $\delta^{18}O$ isotopes – shell material

For the measurement of stable isotope the ratio on shell material, 44 carbonate samples of the CM section and 45 samples of the LV section were drilled using a MicroMill (cf. material and methods). The amount of samples per stage is directly linked to the abundance and accessibility of fossil remains (i.e. shell material). All samples are analysed concerning their $\delta^{13}C$ and $\delta^{18}O$ VPDB (Vienna PDB) ratio.

CAJÓN DEL MORADO

7 samples Tithonian of the CM section are analysed. $\delta^{13}C_{shell}$ value averages -3.16 ‰ (SD=5.7 ‰). The value varies strongly and throughout the Tithonian section it decreases from -0.31 ‰ to -14.35 ‰. In the 13 samples of the Berriasian section the ratio reaches a mean value of -0.25 ‰ (SD=1.7 ‰). Lowest $\delta^{13}C_{shell}$ value is observed in the Early Berriasian section (nadir of -4.40 ‰). In the middle to Late Berriasian section the ratio increases discontinuously from 0.26 ‰ to 1.96 ‰. In the latest Berriasian section the value is lower and decreases to 0.06 ‰. The 22 Valanginian samples shows a mean ratio of -0.34 ‰ (SD=1.51 ‰). Except for two stronger negative phases in the Early (-1.20 ‰, -5.99 ‰, -1.07 ‰) and Late (-0.86 ‰, -1.91 ‰, -1.13 ‰) Valanginian section, the value ranges between -0.44 ‰ and 1.60 ‰. The two samples of the Hauterivian section shows a mean $\delta^{13}C_{shell}$ ratio of -0.34 ‰ (SD=1.94 ‰) and varies between 1.03 ‰ and -1.71 ‰.

The $\delta^{18}O_{shell}$ value of the Tithonian section varies strongly between -5.49 ‰ and -10.20 ‰ and shows no clear trend (mean value of -8.17 ‰, SD=2.0 ‰). Although highly fluctuating, the value for the Berriasian section slightly increases throughout the stage from -8.31 ‰ to -3.65 ‰. The average ratio is -6.79 ‰ (SD=1.68 ‰). The opposite trend is observed in the $\delta^{18}O_{shell}$ ratio of the Valanginian

section. Again, the value is highly fluctuating but shows a decreasing trend. The ratio decreases from -4.16 ‰ in the Early Valanginian section to -7.82 ‰ in the Late Valanginian section (mean -5.68 ‰, SD=1.46 ‰). The value of the Hauterivian samples ranges from -4.16 ‰ to -7.36 ‰ (mean -5.76 ‰, SD=2.26 ‰).

LO VALDÉS

21 samples from the Tithonian of the Lo Valdés section contain carbonate shell remains that were isotopically analysed. Throughout the stage the ratio of $\delta^{13}C_{shell}$ fluctuates between 0.42 ‰ and -3.56 ‰ (mean -0.23 ‰, SD=0.83 ‰). One peak is detected in the Late Tithonian section (-3.56 ‰). 18 samples of the Berriasian section are analysed with regard to their $\delta^{13}C_{shell}$ ratio (mean -0.58 ‰, SD=1.59 ‰). This value shows three major peaks. A value of -3.72 ‰ was measured near the base of the stage. Immediately thereafter and still in the Early Berriasian section the ratio increases to 1.66 ‰. Upsection, the value decreases continuously until a highly fluctuating phase in the middle to Late Berriasian section which ends with a significant decrease to -4.42 ‰. Towards the end of the Berriasian section an increased ratio of -1.55 ‰ is detected. The 4 samples of the Valanginian shows no unequivocal trend and the ratio varies between 0.07 ‰ and -0.54 ‰ (mean -0.25 ‰, SD=0.29 ‰). The Hauterivian section is restricted to 2 samples which show a ratio between 1.70 ‰ and 1.89 ‰ (mean 1.80 ‰, SD=0.13 ‰).

The $\delta^{18}O_{shell}$ value of the Tithonian section varies strongly between -14.10 ‰ and 0.42 ‰ but slightly increases throughout the stage. The peak of 0.42 ‰ is reached in the Late Tithonian section and subsequently the ratio decreases to -11.78 ‰. The average ratio is -10.06 ‰ (SD=3.14 ‰). In the Berriasian section, the ratio varies even stronger but shows a similar trend as is identified for the Tithonian section. The Early Berriasian section starts with a value of -10.83 ‰; the ratio reaches a maximum of 0.42 ‰ in the Late Berriasian section and decreases subsequently to -7.67 ‰. The average ratio for the stage is -6.60 ‰ (SD=2.58 ‰). Samples of the Valanginian section show no clear trend in the $\delta^{18}O_{shell}$ ratio. The ratio varies between -6.25 ‰ and -9.10 ‰, with a mean value of -7.50 ‰ (SD=1.37). The ratio of the Hauterivian section is relatively homogenous and varies between -6.26 ‰ and -6.68 ‰ (mean -6.47 ‰, SD=0.30 ‰).

$\delta^{13}C$ isotope the ratio of isolated organic matter

$\delta^{13}C$ VPDB values were also measured on isolated sedimentary organic matter extracted from 78 TOC-rich samples of the CM section. 3 samples from the Tithonian part of the section show a decreasing trend from -25.30 ‰ to -27.7 ‰ (mean -26.7 ‰, SD=1.2 ‰). An increasing TOC content in the Berriasian interval of the CM section is evidenced by a series of 50 samples. The $\delta^{13}C_{iom}$ ratio varies strongly between -28.2 ‰ and -24.5 ‰ and shows a slight increase throughout the stage. The average value is -26.4 ‰ (SD=0.84 ‰). 14 samples analysed from the Valanginian part of the CM section show a slight and relatively homogenous decrease in $\delta^{13}C_{iom}$ ratio. In the Early Valanginian section, the least negative ratio is -25.9 ‰ and the most negative ratio occurs in the Late Valanginian section with -29.6 ‰ (mean -27 ‰, SD=1.46 ‰). In the Hauterivian of the CM section 10 samples are analysed. A mean ratio of -26.4 ‰ (SD=0.69 ‰) is observed. A $\delta^{13}C_{iom}$ ratio of -27.0 ‰ is identified in the Lower Hauterivian section. The ratio increases towards the Middle Hauterivian section where it

varies strongly between -26.4 ‰ and -25.5 ‰. The ratio decreases in the Late Hauterivian section to -27.8 ‰.

Isotope ratio of $\delta^{13}C$ and $\delta^{18}O$ – bulk rock

$\delta^{13}C$ and $\delta^{18}O$ the ratio were also measured on 283 bulk rock samples (163 CM section, 120 LV section) samples of the central Chilean CM and LV sections.

CAJÓN DEL MORADO

35 samples analysed of the Tithonian sediment sequence in the CM section present a mean $\delta^{13}C_{bulk}$ VPDB value of 0.30 ‰ (SD=0.78 ‰). A marked low of -3.13 ‰ in the Early Tithonian part of the section is subsequently followed by an increase to 0.98 ‰ in the Middle Tithonian and relatively continuous decrease to -0.70 ‰ in the Late Tithonian section. In the Berriasian section 63 samples are analysed (mean $\delta^{13}C_{bulk}$ of -0.82 ‰, SD=1.13 ‰). The lower and Middle Berriasian section is characterised by a wide variation of the ratio (between -3.3 ‰ and 0.44 ‰). The ratio is fluctuating less intensely throughout the late middle to Late Berriasian section and an increasing trend is identified for this interval (-1.68 ‰ to -0.07 ‰). A sharp decrease of the $\delta^{13}C_{bulk}$ ratio occurs in the uppermost sample of the latest Berriasian section where the value decreases from -0.07 ‰ to -3.28 ‰. 39 samples of the Valanginian section have a $\delta^{13}C_{bulk}$ mean value of -0.91 ‰ (SD=1.11 ‰). The value fluctuates significantly between -3.00 ‰ and 2.02 ‰. The Early and early Late Valanginian section is characterised by a lower ratio (between -1.28 ‰ and -3.00 ‰). Throughout the Middle Valanginian section the $\delta^{13}C_{bulk}$ value varies on a significantly higher level between -0.85 ‰ and 0.79 ‰. The Valanginian section shows a mean of -0.91 ‰ (SD=1.1 ‰). In the latest Valanginian section an intermittent peak of 2.02 ‰ is detected. From the lower to Middle Hauterivian section the $\delta^{13}C_{bulk}$ ratio fluctuates between 1.44 ‰ and 2.18 ‰. In the Middle Hauterivian section a sharp decrease from 1.42 ‰ to -0.32 ‰ is detected. After this nadir the value increases discontinuously towards the latest Hauterivian section to a value of 0.35 ‰.

The $\delta^{18}O_{bulk}$ value of the Tithonian in the CM section varies slightly throughout the stage from -8.68 ‰ in the Early to -9.80 ‰ in Late Tithonian section. From this nadir the $\delta^{18}O_{bulk}$ ratio increases again towards the end of the Tithonian section reaching -8.30 ‰. The mean ratio for this stage is -9.37 ‰ (SD=0.45 ‰). The value in the Berriasian part of the section shows a similar pattern. In the Early Berriasian section an intermittent nadir (-10.2 ‰) and an intermittent peak (-5.7 ‰) are identified. Upsection the value varies between -9.04 ‰ and -7.05 ‰. Throughout the latest Berriasian section the $\delta^{18}O_{bulk}$ ratio increases continuously to -7.23 ‰. The mean value for the Berriasian section is -8.06 ‰ (SD=0.62 ‰). Throughout the Early to Middle Valanginian section the ratio ranges between -7.44 ‰ and -6.43 ‰. After the high of -6.43 ‰ in the Middle Valanginian section the $\delta^{18}O_{bulk}$ ratio decreases relatively homogeneously to -8.14 ‰ in the Late Valanginian section. In the latest Valanginian section an intermittent peak of -4.86 ‰ is detected. The mean value for the Valanginian is -7.25 ‰ (SD=0.56 ‰). $\delta^{18}O_{bulk}$ results of the Hauterivian section shows no clear trend. In the Early Hauterivian interval an increase from -5.92 ‰ to -4.81 ‰ is detected. Throughout the rest of the stage the ratio varies only slightly and decreases to -6.09 ‰ in the latest Hauterivian section. The mean value for this stage is -5.59 ‰ (SD=0.40 ‰).

LO VALDÉS SECTION

The 28 samples of the Tithonian part of the LV section vary intensely and show no unequivocal trend. Overall the $\delta^{13}C_{bulk}$ ratio varies between -2.36 ‰ and 0.67 ‰. Two significant lows are identified. The first one is detected in the Early Tithonian section (-2.36 ‰) and the second in the Late Tithonian section (-1.49 ‰). The average value for this stage is -0.19 ‰ (SD=0.61 ‰). 67 samples are analysed from the Berriasian part of the section resulting in a mean $\delta^{13}C_{bulk}$ value of -1.45 ‰ (SD=1.58 ‰). Despite fluctuating widely, the value increases from -6.44 ‰ in the Early to 0.23 ‰ in the Late Berriasian section. Throughout the latest Berriasian section the value decreases discontinuously. 13 samples of the Valanginian section are analysed and show a relatively continuous increase in $\delta^{13}C_{bulk}$ ratio (mean -0.40 ‰, SD=1.05 ‰). The value decreases slightly to -1.50 ‰ within the Early Valanginian section and increases subsequently to 1.10 ‰ in the upper part of this section. 12 samples of the Hauterivian section are analysed. After a slight increase from 1.35 ‰ to 2.29 ‰ the $\delta^{13}C_{bulk}$ ratio decreases significantly to a minimum of -0.12 in the early Late Hauterivian section. The average value for this stage is 0.95 ‰ (SD=0.88 ‰).

The $\delta^{18}O_{bulk}$ value of the Tithonian section starts with a sharp increase from -14.55 ‰ to -10.85 ‰ and fall subsequently to -13.24 ‰. Throughout the rest of the Early to Middle Tithonian sequence a slight but continuous increase is detected. After a nadir in the Middle Tithonian section the $\delta^{18}O_{bulk}$ ratio increases discontinuously from -12.69 ‰ to -10.0 ‰. The mean value for this stage is -11.90 ‰ (SD=1.01 ‰). The $\delta^{18}O_{bulk}$ ratio of the earliest Berriasian section sharply increases from -14.14 ‰ to -11.05 ‰. Throughout the remainder of the stage the ratio increases discontinuously to -7.97 ‰ in the latest Berriasian section. For the Berriasian section an average $\delta^{18}O_{bulk}$ ratio of -9.63 ‰ (SD=1.30 ‰) is observed. The value increases discontinuously throughout the Valanginian section from -8.11 ‰ to -7.20 ‰. An intermittent low of -8.71 ‰ is identified in the Early Valanginian section. An intermittent peak (-5.97 ‰) is detected in the latest Valanginian section. The average value is -7.37 ‰ (SD=0.72). The Lower Hauterivian section shows a homogenous increase from -7.13 ‰ to -5.57 ‰. Throughout the rest of the stage the $\delta^{18}O_{bulk}$ value decreases continuously (with a sharp intermittent nadir of -8.51 ‰ in the late Middle Hauterivian section) to -7.20 ‰ in the latest Hauterivian section. The mean ratio is -6.62 ‰ (SD=0.78 ‰).

TOTAL ORGANIC CARBON, TOTAL INORGANIC CARBON, CARBON/SULPHUR/ NITROGEN

CAJÓN DEL MORADO

140 samples of the CM section are analysed for their CNS (carbon, nitrogen, sulphur) content (Tithonian 20, Berriasian 55, Valanginian 39 and Hauterivian 26 samples) (Fig. 38).

Total organic carbon: In the Tithonian part of the CM section, content of total organic carbon ranges between 0.07–0.82 %, with a mean value of 0.26 % (SD=0.19 %). A peak of 0.82 % is identified in the upper part of the Tithonian section. The Berriasian section shows an increased content of TOC ranging between 0.30–4.4 %. The mean value in the Berriasian section is 1.3 % (SD=0.77 %). Despite a major positive peak in the upper middle part of the sediment sequence of the Berriasian

section a distinct trend is not observed. The TOC content of the Valanginian section ranges between 0.06 % and 0.91 %, with 0.29 % (SD=0.17 %) as the mean value. TOC content of the Hauterivian section varies between 0.07–0.98 %. A major positive peak is detected in the upper middle part of the Hauterivian section. The mean proportion for this stage is 0.37 % (SD=0.21 %). A distinct trend is not observed.

Total inorganic carbon: The total inorganic carbon content of the Tithonian of the CM section varies between 2.8–9 %. A mean proportion of 5.4 % (SD=1.4 %) is identified. A highly discontinuously decreasing trend is observed. The TIC proportion of the Berriasian section varies between 4.4–10.5 %. An inhomogeneous increasing trend is identified from 6.6–8.5 %. The averaged content for this stage is 7.5 % (SD=1.4 %). The TIC content of the Valanginian section fluctuates significantly between 1.4–11.2 %. The mean proportion is 7.4 % (SD=2 %). The TIC content in the Hauterivian of the CM section varies between 6.9 % and 11.6 %. A slight and inhomogeneous decreasing trend is observed. The mean proportion is 9.9 % (SD=1.4 %).

$CaCO_3$: Tithonian $CaCO_3$ content varies between 23.1–74.8 %. The mean frequency is 45 % (SD=12 %). The Berriasian section shows an increased $CaCO_3$ proportion. The value ranges from 36.5–87.5 %. The mean content of this stage is 62.3 % (SD=12 %). The $CaCO_3$ content of the Valanginian section fluctuates significantly between 11.3–92.9 %. A mean proportion of 61.4 % (SD= 16.9 %) is observed. The $CaCO_3$ proportion of the Hauterivian is the highest of the Central Chilean sections. A mean content of 82.4 % (SD=11.5 %) is observed. The percentage of individual samples varies between 57.2–96.5 %.

Nitrogen: In the samples of the Tithonian nitrogen content is continuously low and varies between 0.007 % and 0.019 %. The mean value is 0.01 % (SD=0.005 %). The nitrogen content of the Berriasian section fluctuates widely and varies between 0.003 % and 0.16 %. Value increases towards the lower upper part of the Berriasian section. A marked low of 0.027 % is identified in the upper middle part of the Berriasian section. Subsequently, the value increases to 0.16 % and decreases highly inconsistently throughout the remainder of the section to 0.004 %. The average nitrogen content of the Berriasian section is 0.058 % (SD=0.042 %). Nitrogen content of the Valanginian samples shows no unequivocal trend. Except for several peaks in the lower (0.02 %) and upper/uppermost (0.014 % 0.032 %, 0.036 %, 0.011 %) Valanginian section the content varies between 0.003 % and 0.008 %. The mean content of the Valanginian is 0.006 % (SD=0.007 %). Throughout the lower and middle part of the Hauterivian section nitrogen content is continuously low and varies between 0.002 % and 0.005 %. From there on the content varies intensely and with no clear trend between 0.004 % and 0.033 %. The mean content is 0.01 % (SD=0.01 %).

Sulphur: After a peak of 0.1 % in the lower part of the Tithonian section, the sulphur content decreases towards a nadir in the Middle Tithonian section. Subsequently, the sulphur content increases with minor fluctuations to 0.03 % in the uppermost part of the Tithonian section. The mean sulphur content is 0.03 % (SD=0.03 %). The sulphur content of the Berriasian section varies intensely and shows no unequivocal trend. Two major peaks are detected in the lowermost (0.1 %) and upper (0.1 %) part of the Berriasian section. The mean content for this stage is 0.036 % (SD=0.019 %). Throughout the Valanginian sulphur content varies relatively homogenous between 0.01 % and 0.097 %. In the upper and uppermost part of the Valanginian section the content registers a phase of high fluctuation with peaks of 0.5 % and 1.65 %. The average sulphur content is 0.1 % (SD=0.27 %). The

sulphur content of the Hauterivian section varies strongly and shows no distinct trend. The content varies between 0.009 % and 0.57 %. Mean content is 0.056 % (SD=0.013 %).

C_{org}/N: Except for two intermittent peaks in the lowermost (83) and lower upper part (148) of the Tithonian section the C/N ratio of the CM section ranges from 4–35. The mean value is 28. In the Berriasian section the C/N ratio varies between 8 and 83. Several intermittent peaks (121, 136, 110 and 439) are observed. The ratio is highest in the upper part of the Berriasian sediment sequence. The averaged ratio is 42. Throughout the upper part of the Valanginian section the ratio varies intensely but on a high level between 11 and 319. The ratio is highest in the lower middle part of the Valanginian interval. A mean ratio of 73 is observed. The highest mean C/N ratio of the section occurs in the Hauterivian section where an averaged ratio of 81 is observed. The ratio varies between 15 and 224. A distinct trend is not evident.

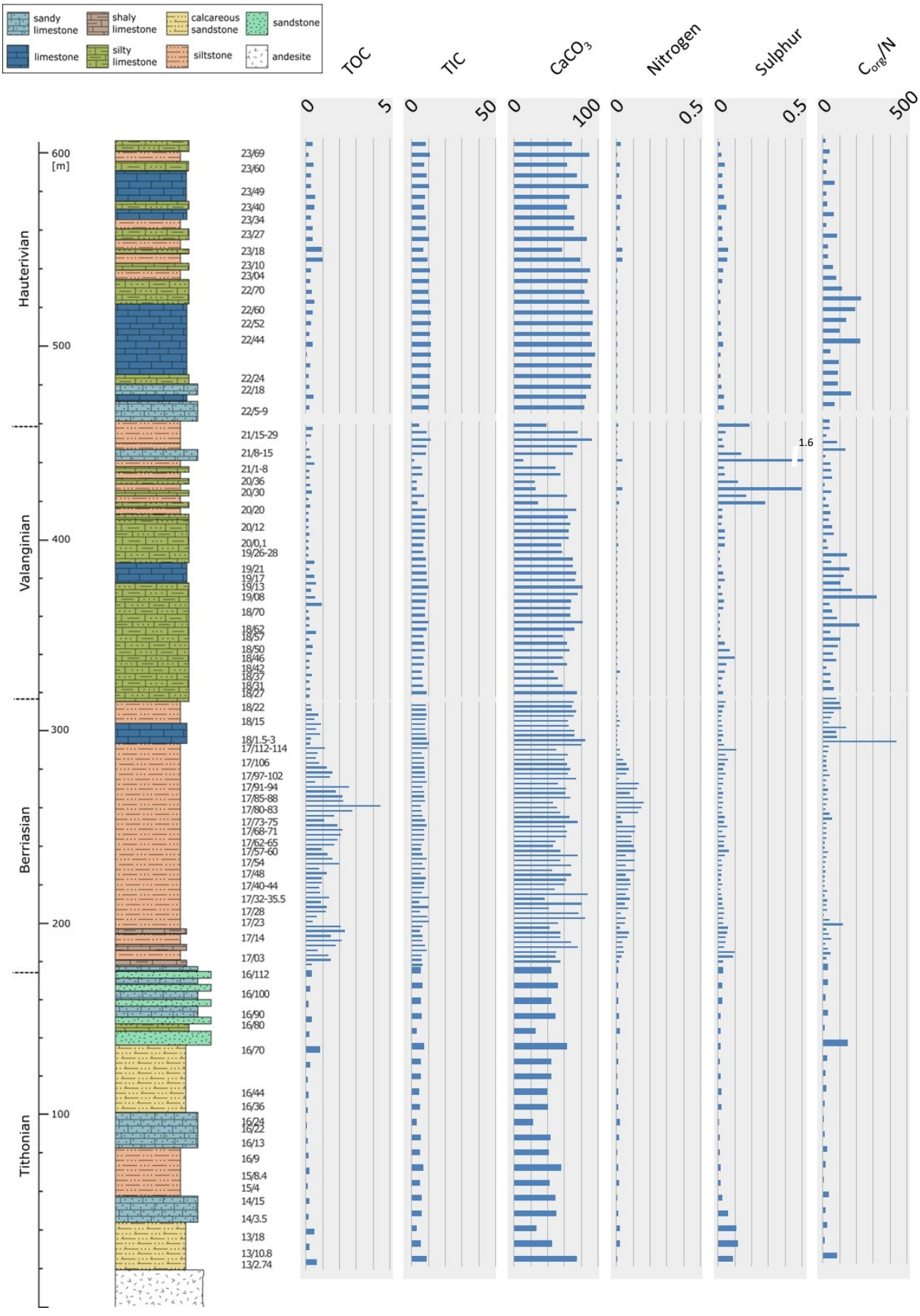

Figure 38: Results of the TOC, TIC and CNS analyses; CM section. Except for C_{org}/N, values given in %, to increase visualisation, different scales are used.

LO VALDÉS

76 samples of the LV section were analysed for their CNS content (Tithonian 3, Berriasian 66, Valanginian 3 and Hauterivian 4 samples).

Total organic carbon: In the Tithonian of the LV section, content of total organic carbon varies between 0.17–0.25 % (Fig. 39). The mean proportion is 0.22 % (SD=0.04 %). Similar to the CM section the Berriasian section of LV shows a significantly higher content of TOC than the previous Tithonian section. The proportion fluctuates intensely between 0.19–4.7 %. The averaged content of this interval is 1.87 % (SD=0.97 %). A distinct trend is not identified. The TOC content of the Valanginian varies between 0.14–0.25 %. A mean proportion of 0.21 % (SD=0.06 %) is detected. In the Hauterivian section the TOC content ranges from 0.44–1 %. The averaged proportion is 0.65 % (SD=0.24 %).

Total inorganic carbon: The total inorganic carbon content varies in the Tithonian of the LV section between 5.2–6.5 % (Fig. 39). A mean proportion of 5.9 % (SD=0.62 %) is observed. The TIC proportion of the Berriasian section varies between 0–9.9 %. The averaged content for this stage is 5.7 % (SD=2.2 %). A highly discontinuous increasing trend is identified. The TIC content of the Valanginian section varies between 7.2–10 %. The mean proportion is 8.4 % (SD=1.5 %). The TIC content in the Hauterivian of the LV section varies between 7.5 % and 10.6 %. The mean proportion is 8.4 % (SD= 1.4 %).

$CaCO_3$: In the Tithonian section of LV the content of $CaCO_3$ varies between 43.7–54 % (Fig. 39). The mean percentage is 49.2 % (SD=5.2 %). In the Berriasian section of LV a mean proportion of 47.2 % (SD=18.5 %) is identified. Throughout the Berriasian section the $CaCO_3$ content fluctuates intensely but shows an increasing trend from 0–69.4 %. The $CaCO_3$ content of the Valanginian section shows a mean proportion of 70 % (SD=12.2 %). Individual content varies between 59.9–83.6 %. In the Hauterivian section the $CaCO_3$ content varies between 62.5 % and 88.1 %. A mean proportion of 70.2 % (SD=12 %) is identified.

Nitrogen: The nitrogen content of the Tithonian in the LV section increases throughout the sampled interval from 0.003 % to 0.006 % (Fig. 39). The mean value is 0.004 % and the standard deviation is 0.002 %. The nitrogen content of the Berriasian section varies significantly between 0.004 % and 0.158 % but shows no unequivocal trend. In the mid-Berriasian section a marked peak of 0.77 % is identified. The mean N content of this stage is 0.08 % (SD=0.09 %). The N value of the Valanginian section shows a significant increase throughout the sampled interval from 0.003 % to 0.023 %. The mean nitrogen content for this stage is 0.01 % (SD=0.01 %). The nitrogen content of the Hauterivian section shows a marked decrease from 0.03 % to 0.01 %. The average N content of this stage is 0.021 % (SD=0.012 %).

Sulphur: The sulphur content in the Tithonian varies only marginally between 0.005 % and 0.01 % (Fig. 39). The mean sulphur content of this stage is 0.007 % (SD=0.003 %). The sulphur content of the Berriasian section shows no clear trend and varies significantly between 0 % and 2.4 % (mean of 0.76 %, SD=1.1 %). A marked peak of 7.97 % occurs in the mid-Berriasian section. A slight decrease of S content is observed in the Valanginian section. The value decreases from 0.03 % to 0.01 %. The mean sulphur content of the Valanginian is 0.02 % (SD=0.01 %). For the S content of the Hauterivian section no clear trend is identified. The value varies between 0.01–0.18 %. The mean sulphur content for this stage is 0.08 % (SD=0.07 %).

C_{org}/N: The C/N ratio of the Tithonian section ranges from 40–75 (Fig. 39). The mean value is 58. In the Berriasian interval the C/N ratio varies intensely between 6 and 110. The averaged ratio is 35. Two major peaks (107 and 110) are identified in the lowermost part of the Berriasian. An unequivocal trend is not detected. In the Valanginian interval the ratio varies between 6 and 90. A mean ratio of 35 is observed. The C/N ratio of the Hauterivian increases from 21 to 56. The averaged ratio is 37.

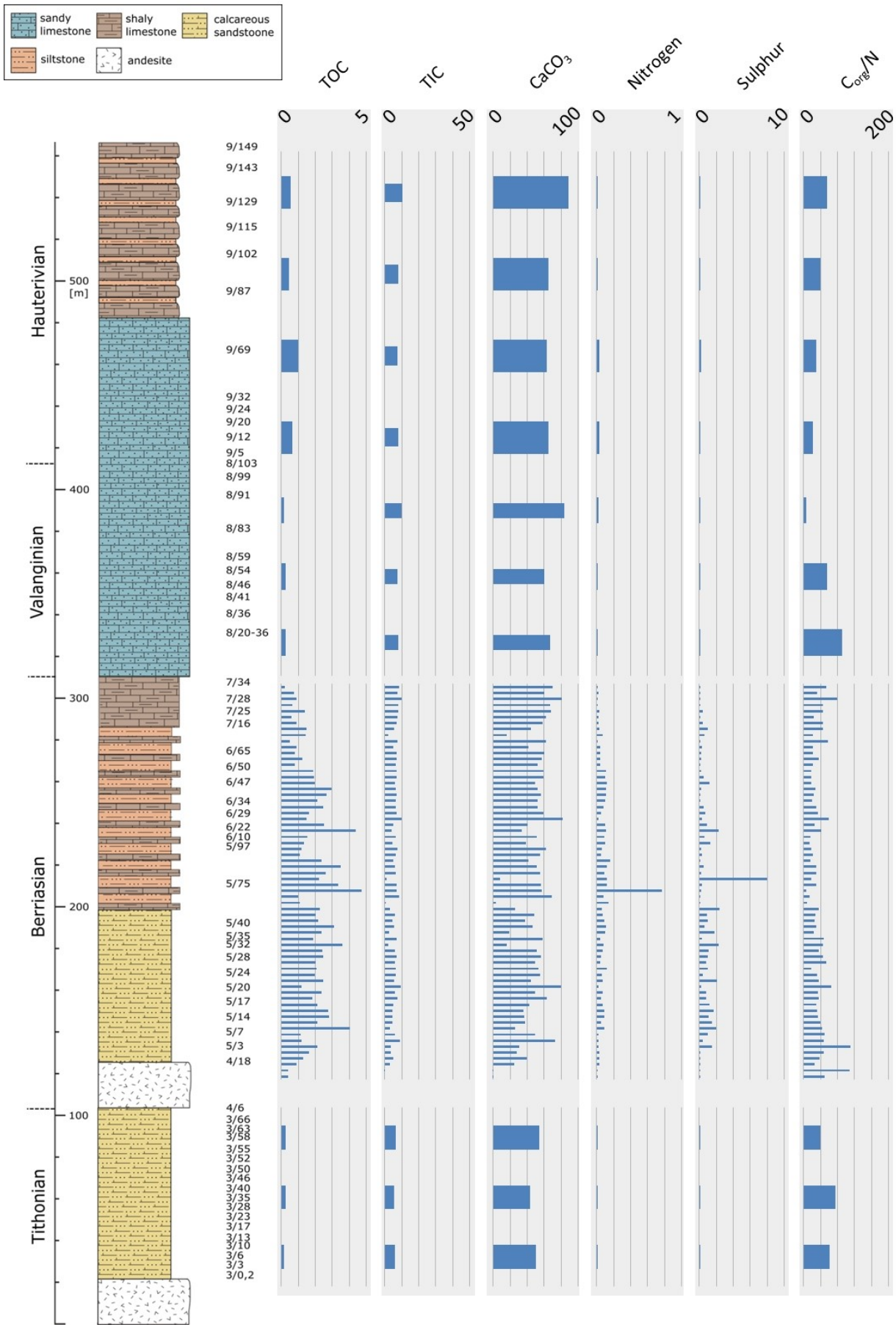

Figure 39: Results of the TOC, TIC and CNS analyses; LV section. Except for C_{org}/N, values given in %, to increase visualisation, different scales are used.

THERMAL MATURITY

Thermal maturation analysis based on clay mineralogy was only performed on three samples of the CM section due to only minor and mostly insufficient amounts of illite/smectite mixed-layer structures. Sample CM 23/4 was suitable for the use of ethylene glycol treatment of the illite/smectite mixed-layers. The analysis shows that temperatures must have reached 200–220 °C, which therefore indicates that the rocks reached the upper gas window (cf. Suárez-Ruiz et al., 2012). Thermal maturation is also characterised using the Thermal Alteration Index (TAI) and Spore Coloration Index (SCI). TAI/SCI analysis was performed on 8 samples (CM 14/15, CM 17/65, CM 19/24, CM 23/18, LV 3/55, LV 7/16, LV 8/41, LV 9/5). Samples show a TAI of approximately 4- to 4+ /SCI of 9.5 (Ro% 2–2.5). The suggested maturation stage is metagenesis (cf. Suárez-Ruiz et al., 2012).

MICROFACIES ANALYSIS

In the CM section microfacies analysis on 76 samples allowed for the identification of 11 different microfacies types (rmf=ramp microfacies types after Flügel (2004)). For the Tithonian part of the section samples indicate mid-ramp/outer ramp (rmf types 4/9) settings to mid-ramp (shoal) (rmf type 8) environments (Fig. 40). 3 samples in the lower and middle part of the Tithonian interval represent inner ramp-open marine (rmf type 14) environments. One sample from the upper part of the Tithonian section is characterised by a microfacies composition which reflects a mid-ramp to basin (rmf type 5) depositional environment. An evolution to deeper depositional environments is identified for the Berriasian section. Most samples of this stage represent mid-ramp (shoal)/outer ramp to basin (rmf types 5, 11, 28) environments (Fig. 42). One sample in the lower part of the Berriasian sediment sequence is characterised by an inner ramp/mid-ramp environment (rmf type 7). Mid-ramp to outer ramp environments (rmf types 3, 8, 9, 28) are also observed in the lower part of the Valanginian. In the mid-Valanginian part of the section shallow water environments are reflected by peritidal to inner ramp rmf types (7, 14, 19, 24) (Fig.44). Upsection and into the uppermost part of the Valanginian, samples vary between inner ramp to outer ramp environments (7, 8, 9, 14). The Hauterivian is characterised by microfacies types that reflect deeper depositional environments. Samples vary between mid-ramp (shoal) to outer ramp environments (rmf types 4, 11, 27) (Fig. 46).

In the LV section the lower to middle part of the sampled interval (61 samples) of the Tithonian is characterised by a mid-ramp/outer ramp depositional environment (rmf types 3, 9) (Fig. 41). In the upper part of the Tithonian section inner ramp/mid-ramp (shoal) environments are observed. An evolution to deeper environments occurs in the Berriasian. The lower to upper part of the Berriasian section is characterised by mid-ramp to basin microfacies types (2, 5, 9, 11) (Fig. 43). In the latest Berriasian a development is detected towards shallow environments. Here, microfacies samples vary between inner ramp to outer ramp settings (rmf types 3, 7, 13). The subsequent lowermost part of the Valanginian section is characterised by depositional environments of the mid-ramp to outer ramp (rmf type 3). Throughout the remainder of the stage mainly inner ramp to mid-ramp (shoal) (rmf types 7, 13, 26, 27, 28) environments are observed (Fig. 45). One interval in the uppermost part of the Valanginian stage reflects more distal environments and a microfacies type of mid-ramp to outer ramp (rmf types 9, 10) is observed. The Hauterivian stage is characterised by a change to more distal environments. Samples of the lower part of the Hauterivian section represent inner ramp to mid-ramp (shoal) (rmf types 14, 26, 27) environments (Fig. 47). Subsequently, in the middle part of the sampled

interval of the Hauterivian, microfacies samples represent outer ramp (rmf type 4) conditions. The three uppermost samples of the Hauterivian section represent mid-ramp to basin environments.

Figures 40 & 41: selected microfacies samples of the Tihonian interval of the CM section (CM 13/2.74) and the LV section (LV 3/40); scale bar is 0.5 mm.

Figures 42 & 43: selected microfacies samples of the Berriasian interval of the CM section (CM 17/35,5) and the LV section (LV 5/86); scale bar is 0.5 mm.

Figures 44 & 45: selected microfacies samples of the Valanginian interval of the CM section (CM 21/8-15) and the LV section (LV 8/59); scale bar is 0.5 mm.

Figures 46 & 47: selected microfacies samples of the Hauterivian interval of the CM section (CM 23/69) and the LV section (LV 9/69); scale bar is 0.5 mm.

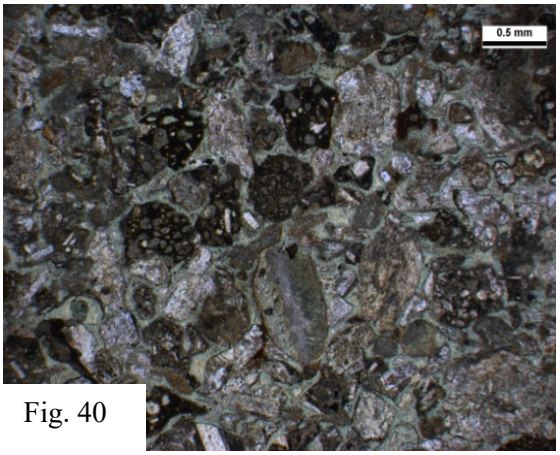

Fig. 40

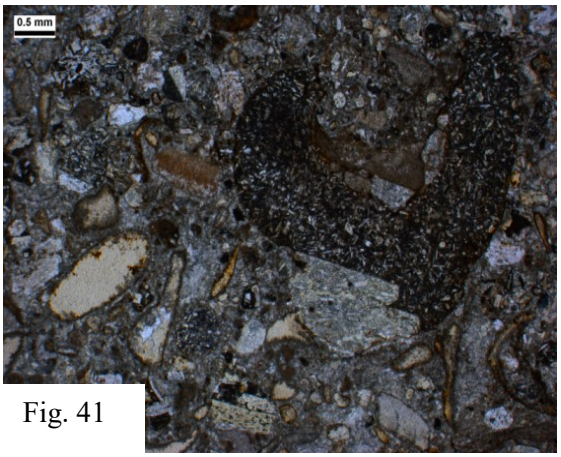

Fig. 41

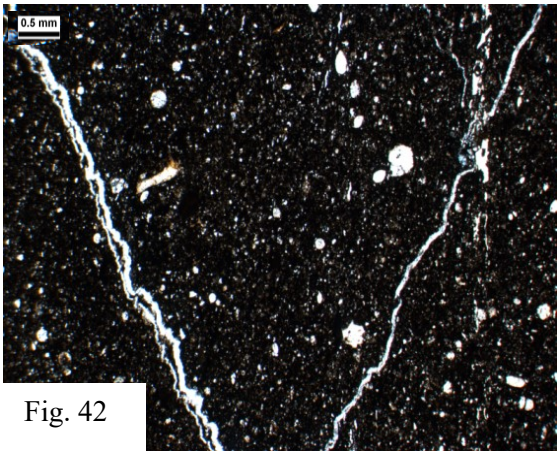

Fig. 42

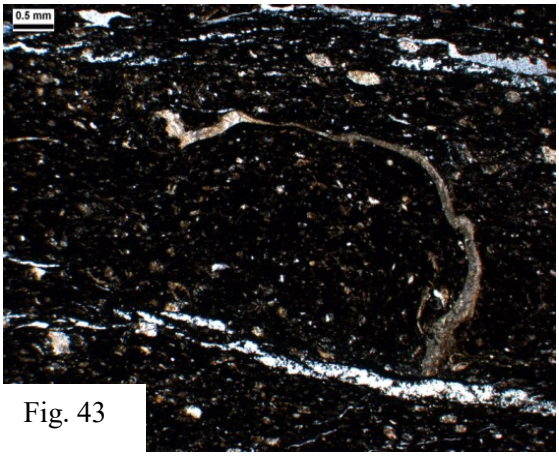

Fig. 43

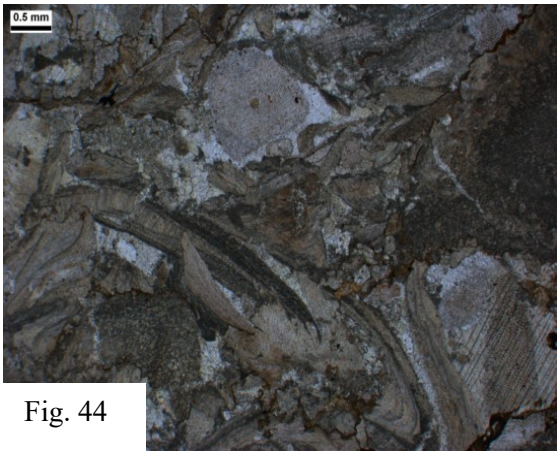

Fig. 44

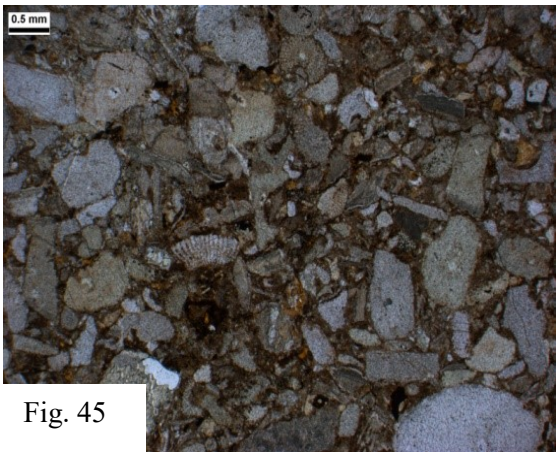

Fig. 45

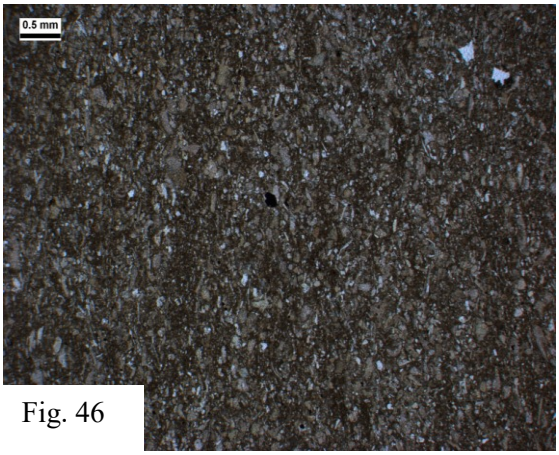

Fig. 46

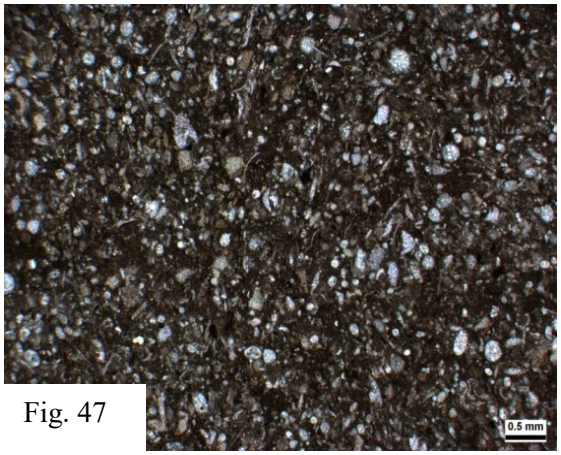

Fig. 47

MICRO-GLENDONITES

All samples analysed for sedimentary organic matter composition were also examined for occurrences of micro-glendonite mineral clusters. Photographs are only taken from the most representative specimens in each sample, i.e. the largest and/or the most distinctly structured mineral clusters. Where micro-glendonites occur, the frequency and size range of specimens are diverse. Therefore samples are recorded only qualitatively.

CAJÓN DEL MORADO

In the CM section 22 samples contain micro-glendonites (selected specimens shown in figures 48–51). Two samples in the lower part of the sampled interval of the Tithonian stage contain micro-glendonites. A total of 14 specimens are photographed and measured. They present a size range of 24–122 µm. The mean size is 56.5 µm (SD=25.4 µm). In the 7 samples from the middle part of the sampled interval of the Tithonian stage 26 micro-glendonites are recorded. The diameter ranges from 19–91 µm. The mean size is 50.3 µm (SD=17 µm). One sample in the lowermost Berriasian contains micro-glendonites. 4 specimens are recorded and their size ranges from 20–48 µm (mean of 37 µm, SD=12.1 µm). Micro-glendonites are detected in 11 samples of the Valanginian part of the CM section and are especially abundant in the lower and middle part of the interval. 39 specimens are recorded,

with individual diameters ranging from 22 µm to 162 µm and a mean size of 60.6 µm (SD=29.8 µm). Only one sample from the uppermost Valanginian interval of the CM section contains micro-glendonites. In this sample 4 specimens are photographed. The size of individual specimens ranges between 66–90 µm, resulting in a mean size of 78.5 µm (SD=12.8 µm). One sample in the middle part of the sampled interval of the Hauterivian stage contains micro-glendonites. 4 specimens are recorded. A mean diameter of 86.8 µm (SD=11.2 µm) are measured. Sizes of individual specimens vary between 76–101 µm.

Figures 48–51: Selected micro-glendonite specimens of the Cajón del Morado section – Fig. 48: CM 13/10,8; Fig. 49: CM 14/3,5; Fig. 50: CM 14/3,5; Fig. 51: CM 16/9; scale bars given in the photographs.

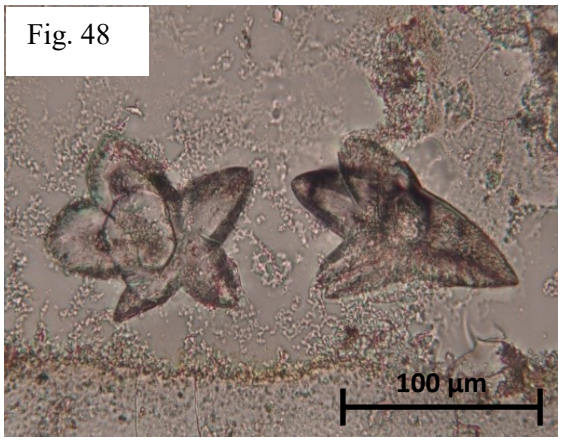

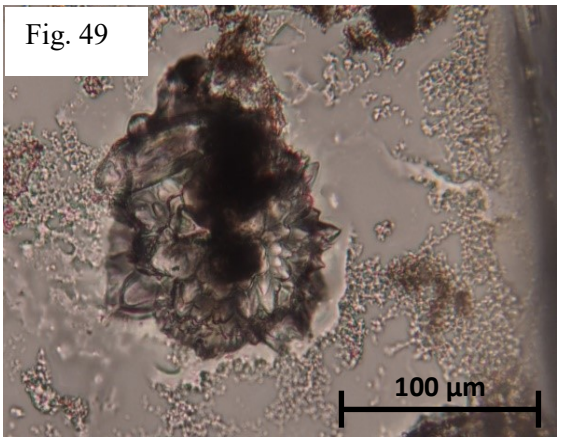

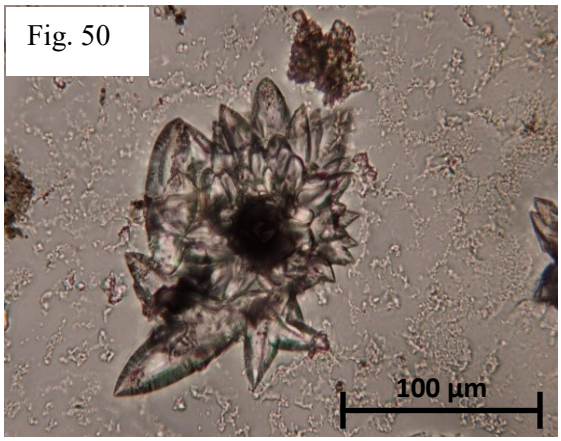

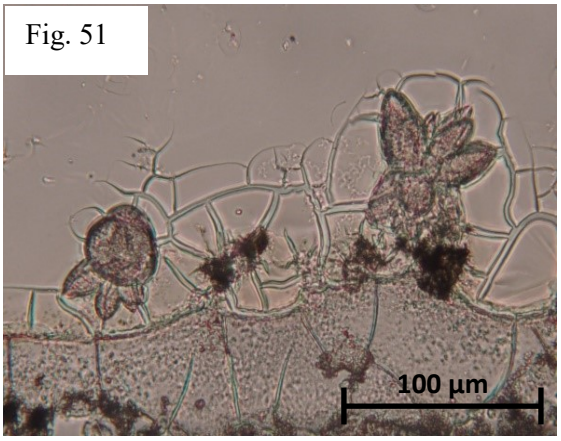

LO VALDÉS

20 samples of the LV section contain micro-glendonites (selected specimens shown in figures 52–55). In two samples of the lowermost part of the sampled interval of the Tithonian stage micro-glendonites are observed. A total of 15 specimens are recorded in this interval. Diameters range from 18 µm to 76 µm. The mean size of the measured mineral clusters is 48.9 µm (SD=17.2 µm). Another 12 samples which contain micro-glendonites are distributed throughout the remainder of the sampled interval of

the Tithonian. 141 specimens are recorded in this interval. Individual mineral clusters range in size from 13 µm to 172 µm. A mean size of 37.2 µm (SD=25.3 µm) is reached. Two samples of the sampled interval of the lowermost Berriasian contain micro-glendonites. 14 specimens are recorded. A mean size of 41.6 µm (SD=19.8 µm) is measured. Individual diameters range from 14 µm to 73 µm. In the Valanginian of the LV section 4 samples contain micro-glendonites of which 18 are photographed and measured. Individual mineral clusters vary in size between 24 µm to 70 µm. The average diameter is 35.9 µm (SD=13.2 µm). The Hauterivian stage is free of micro-glendonites.

Figures 52–55: Selected micro-glendonite specimens of the Lo Valdés section – Fig. 52: LV 3/6; Fig. 53: LV 3/35; Fig. 54: LV 3/35; Fig. 55: LV 3/44; scale bars given in the photographs.

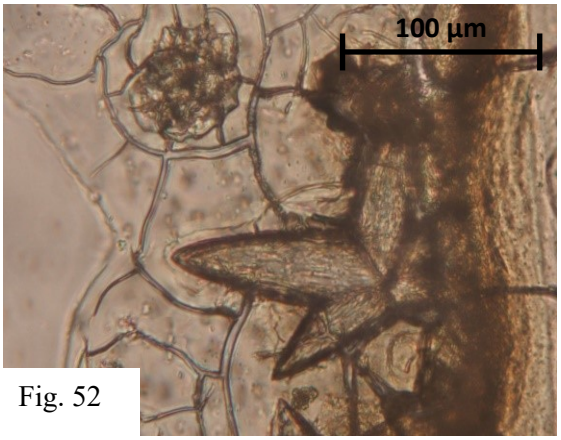

Fig. 52

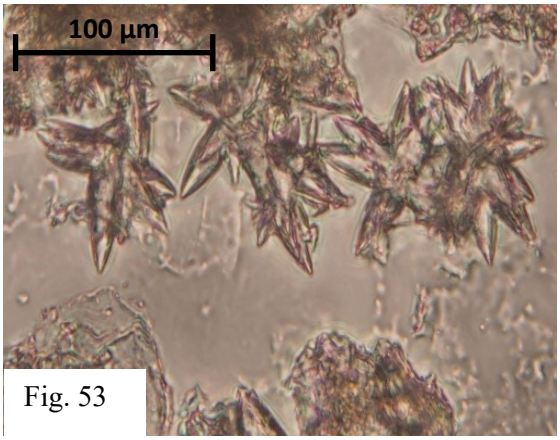

Fig. 53

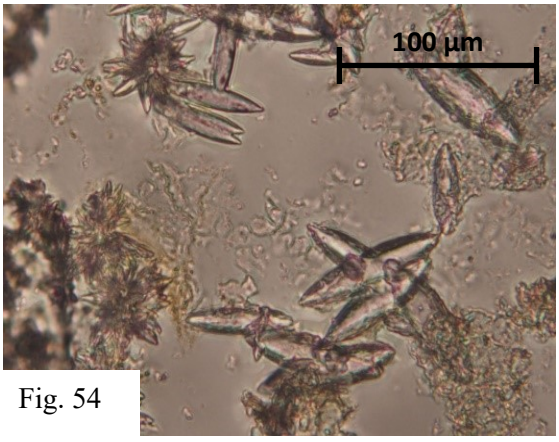

Fig. 54

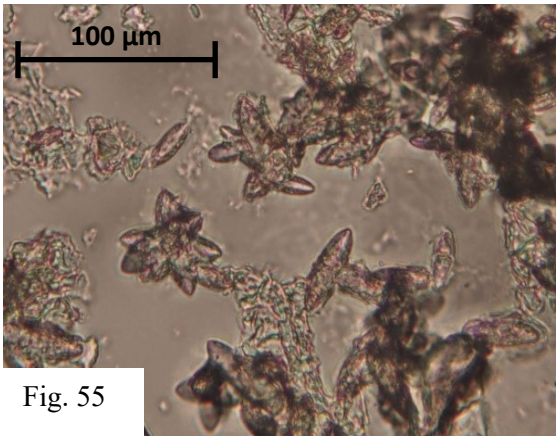

Fig. 55

CALPIONELLIDS

In Chile, preservation of calpionellids is poor. The dark fine grained and organic rich rocks, in which the specimens were found, impede precise classification to species level. Therefore, in the present thesis biostratigraphic assessment of the Jurassic/Cretaceous boundary remains on the definition of the J/K boundary based on ammonite species and lithostratigraphy (cf. Salazar and Stinnesbeck 2015a, b).

Occurrences of calpionellids are here rather considered as indicators of warm tropical climates (e.g. Tethyan influence).

Calpionellids are extremely rare and badly preserved in the two central Chilean sections, but isolated individuals were detected throughout the Berriasian sediment sequence. They are detected in 16 samples of the sampled interval of the Cajón del Morado section and in 15 samples of the sampled interval of the Lo Valdés section.

In the Cajón del Morado section this interval is approximately 129 m thick and in the Lo Valdés section, the interval extends over 89 m. Due to the poor preservation state of most calpionellid specimens and their low frequencies, with only a few specimens per sample, taxonomic assignation of individual genera or species remains incomplete and calpionellid assemblages are not assigned. Calpionellids are characteristically absent in sediments assigned to the Tithonian and Hauterivian

CAJÓN DEL MORADO

Early Berriasian

Zone 2 *Substeuoceras koeneni* – Zone 2a *Berriasella Jacobi* (Salazar, 2012)

4 samples (CM 17/23–CM 17/54) of the Lower Berriasian sediment sequence contain rare calpionellids. *Tintinnopsella carpathica* (Fig. 56) is present in four samples. Other specimens are tentatively identified as *Calpionella alpine* (Fig. 57)*, Crassicollaria colomi* (Fig. 58) and *Chitinoidella boneti* (Fig. 59). Scale bar is 100 µm.

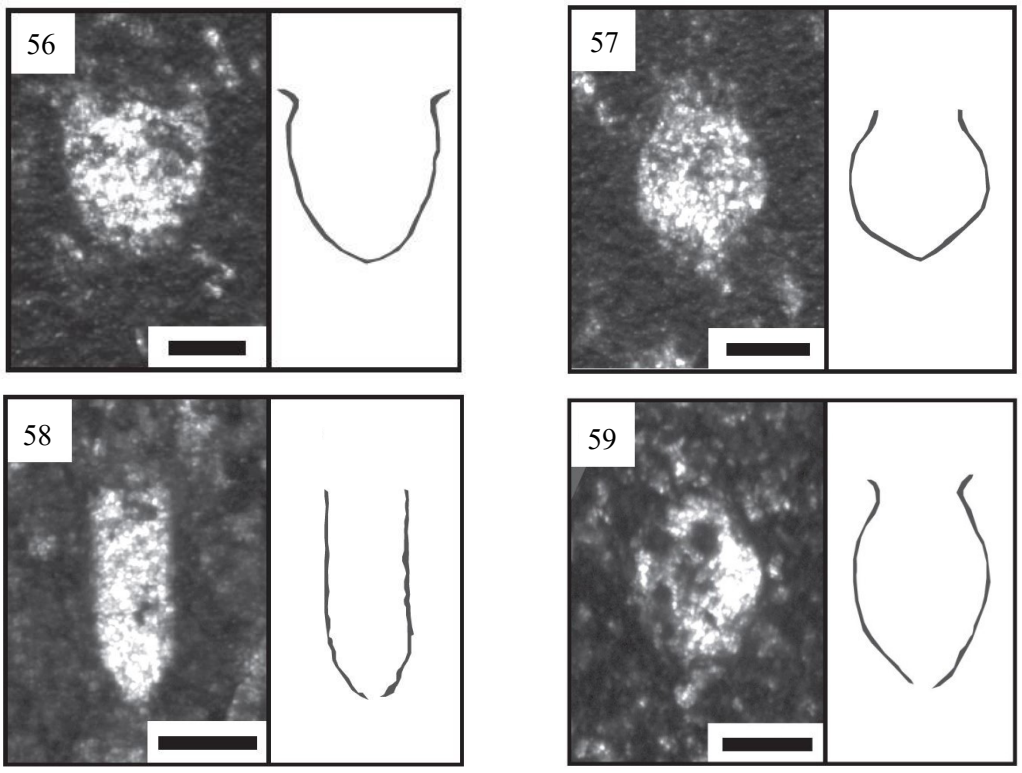

Late Berriasian

Zone 2 *Substeuoceras koeneni* – Zone 2b *Groebericeras riccardi* (Salazar, 2012)

In the sample series of the Upper Berriasian succession calpionellids occur in a total of 12 samples (CM 17/57-CM 18/3). *Tintinnopsella carpathica* (Fig. 60) is present in 7 samples, making it the most common specimen in this interval. *Calpionella alpina* (Fig. 61) is also present in this interval and *Remaniella ferasini* (Fig. 62) as well as *Crassicollaria parvula* (Fig. 63) occur in three samples, while *Remaniella catalanoi* (Fig. 64) and *Remaniella colomi* (Fig. 65) are detected in individual samples. Scale bar is 100 µm.

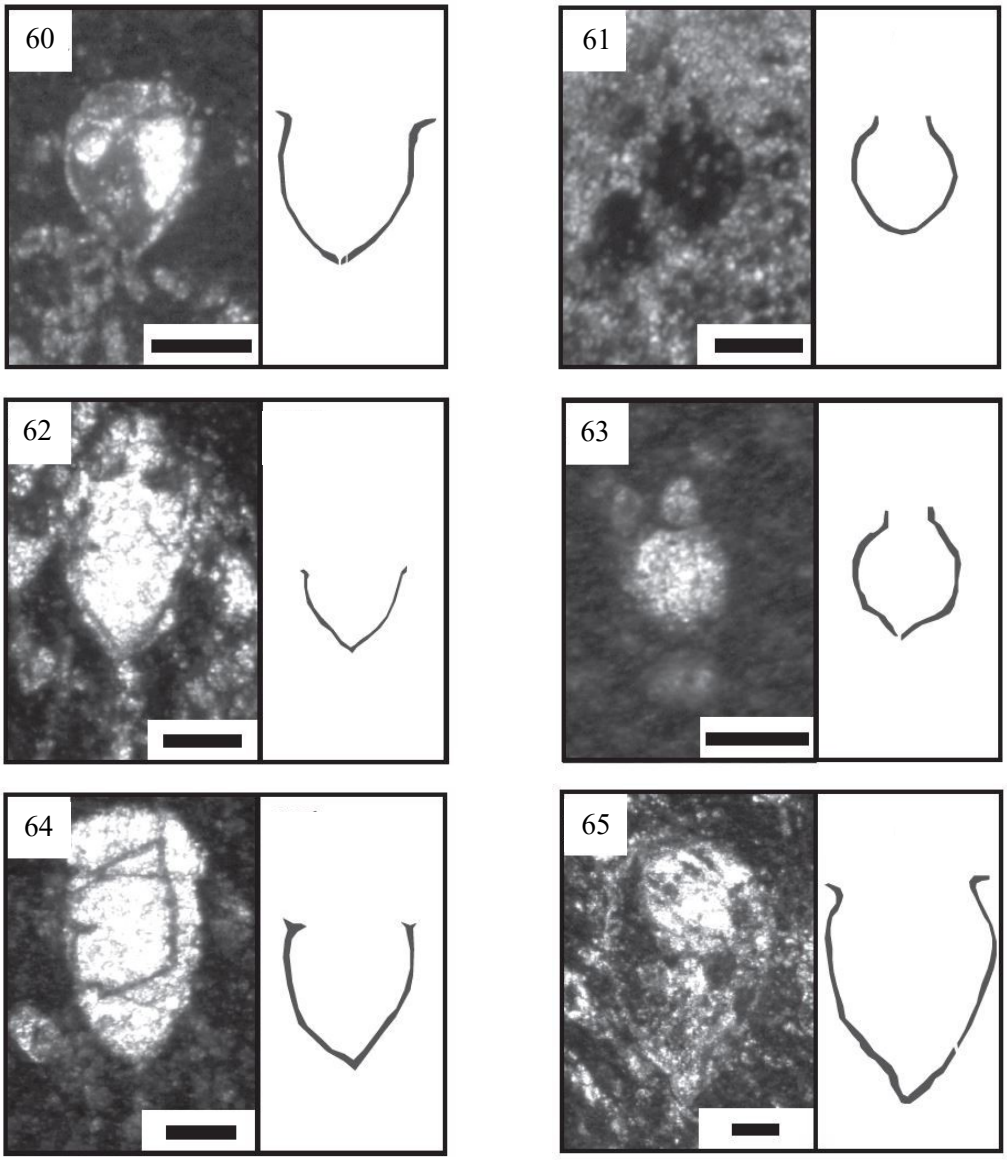

LO VALDÉS

Early Berriasian

Zone 2 *Substeuoceras koeneni* – Zone 2a *Berriasella jacobi* (Salazar, 2012)

Calpionellids are identified in 11 samples that cover the Lower Berriasian sediment sequence of the Lo Valdés section. They are relatively frequent faunal constituents in samples LV 5/24–LV 6/10 and are there assigned to *Tintinnopsella carpathica* (Fig. 66), *Calpionella alpine* (Fig. 67), *Calpionella elliptica* (Fig. 68), *Calpionella* sp. (Fig. 69), *Remaniella cadischinana* (Fig.70), *Remaniella filipescui* (Fig. 71), *Remaniella ferasini* (Fig. 72), *Calpionellopsis simplex* (Fig. 73), *Borzaiella atava* (Fig. 74), *Remaniella duranddelgai* (Fig. 75) and *Remaniella colomi* (Fig. 76). Scale bar is 100 μm.

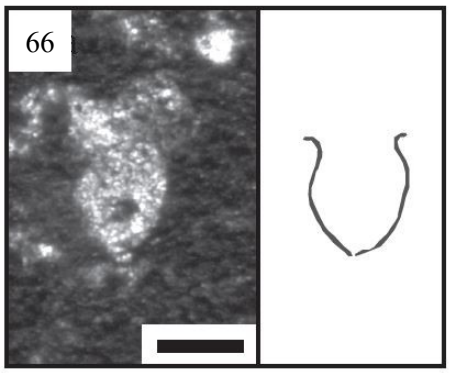

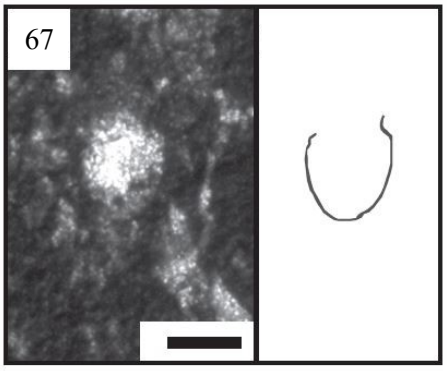

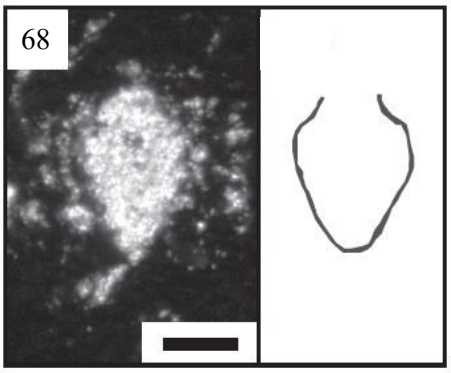

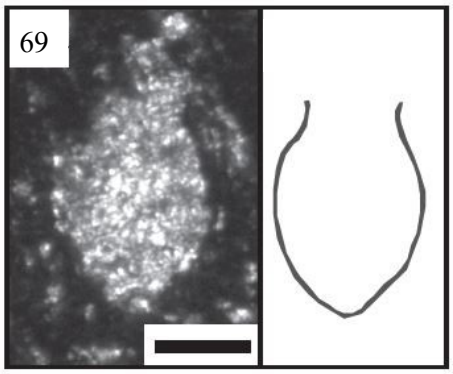

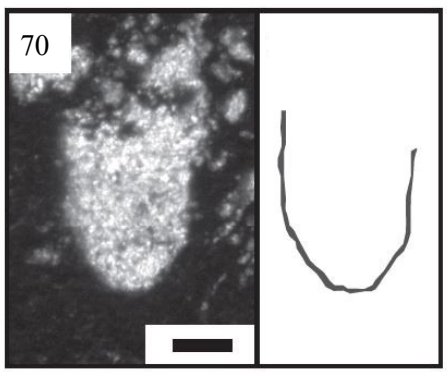

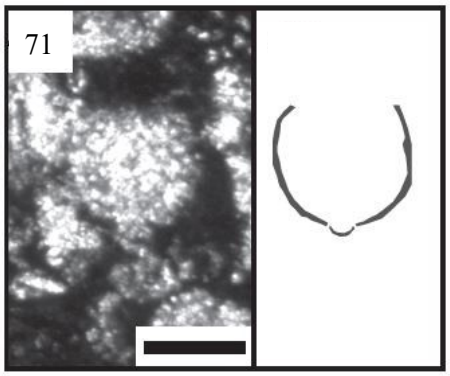

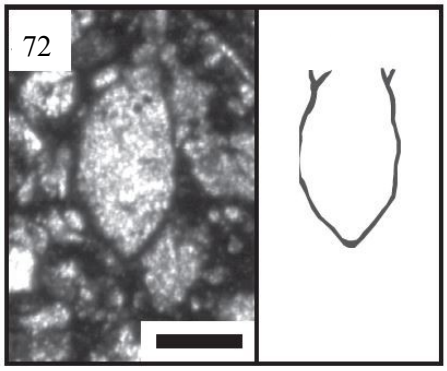

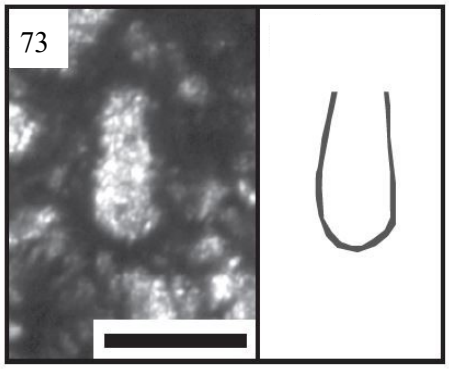

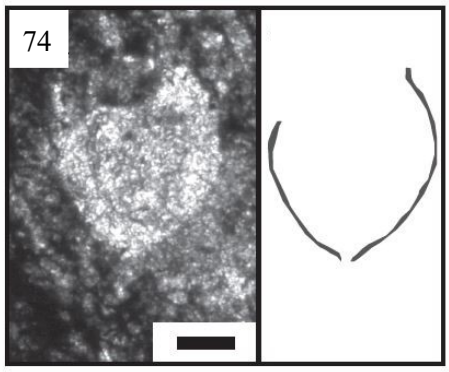

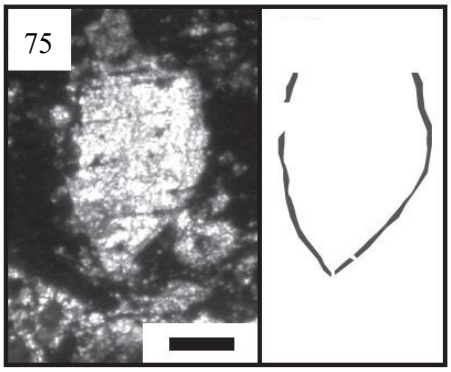

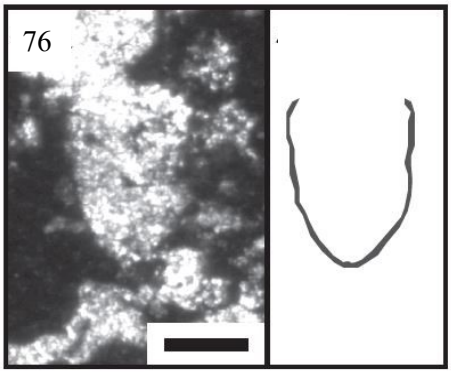

Late Berriasian

Zone 2 *Substeuoceras koeneni* – Zone 2b *Groebericeras rocardi* (Salazar, 2012)

In this Late Berriasian zone, 4 samples (LV 6/35–LV 6/53) contain calpionellids, among them *Tintinnopsella carpathica* (Fig. 77), *Calpionella* sp. (Fig. 78) and *Remaniella filipescui* (Fig. 79). Scale bar is 100 μm.

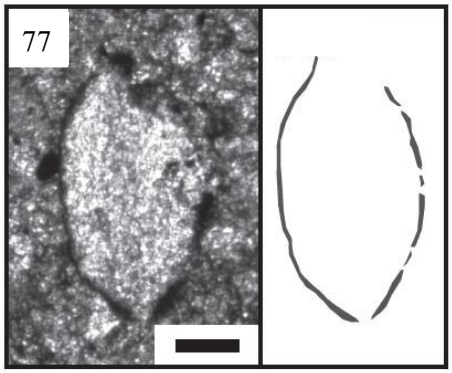

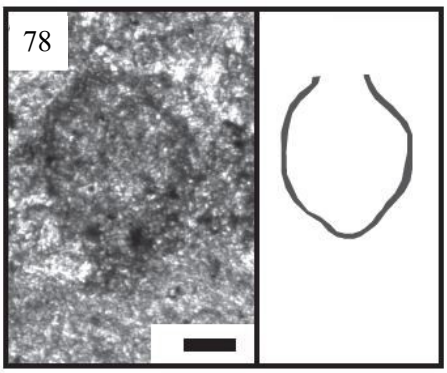

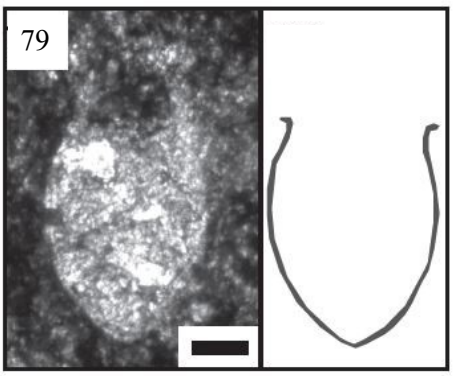

4.2 PATAGONIA

Two ENAP wells drilled in Patagonia, namely the Nevenka 1 and Sofia 1, are included in the present study. In this study area analyses include palynofacies, geochemical analysis, thermal maturity (optical), as well as occurrences of micro-glendonites.

Surface samples from the Lago Fagnano area of the Cordillera Darwin were not used here, as organic matter was poorly preserved and local faulting and shearing made continuous sampling impossible.

NEVENKA 1 CORE

Biostratigraphy of the Nevenka 1 core

The biostratigraphical results are based on a study on the Nevenka 1 core samples which was performed by Darrin Stead of Wellstrat Services Limited based on the diverse assemblage of dinoflagellate cysts and sporomorphs. Good assemblages have been recovered from most of the samples. Sporomorphs and dinoflagellate cysts are recovered. The overall numbers of each group varies, probably related to proximity of the shoreline. The assemblages include forms that appear to be derived from up-hole caving, and there is also a suggestion of some reworking. The assemblage interpreted as in situ is based on those forms that occur consistently. Based on this process the section is dated as Late Barremian to Early Aptian.

A summarised review of the results of Wellstrat Services Limited is presented here: The age can be constrained by the occurrence of *Palaeoperidinium cretaceum* in sample Nev 61. Nøhr-Hansen (1993) indicates an inception in the Barremian, likely Late Barremian. Davey (1988) also indicates a Late Barremian inception in Papua New Guinea. The first appearance datum of *Odontochitina operculata* is also recorded in this sample. Most records indicate an inception of the taxon in the Barremian, and increased abundance in the Aptian. Habib and Drugg (1987) suggest a first appearance datum as old as Hauterivian in the western margin of the North Atlantic. Stover et al. (1996) also shows this inception age, while Helby et al (1987) indicate sporadic occurrences in the Late Hauterivian to Barremian *Muderongia australis* Zone of Australia, but becoming persistent in the overlying *Odontochitina operculata* Zone, of Aptian age. Burger (1979, 1996) indicates an inception in the Barremian of

Australia, within the *Muderongia australis* Zone, while Nøhr-Hansen reports the form occurs consistently from the Late Barremian. A questionable specimen of *Systematophora areolata* is recorded. Helby et al. (1987) indicates an extinction of this species in Australia in the Aptian. The assemblage recovered from this sample suggests an age in the ranges Late Barremian to Aptian.

PALYNOFACIES ANALYSIS

63 samples of the Nevenka 1 core cuttings are analysed (NEV 1–63) for palynofacies interpretation (Figs. 80–84). The sequence is here biostratigraphically assigned to the Late Barremian (59 samples) and Aptian (4 samples) stage based on dinoflagellate occurrences:

The palynomorph assemblage identified in the Nevenka 1 core is much more diverse than that detected in the central Chilean sections. The marine fraction contains dinocysts, acritarchs, foraminifers, leiospheres and algae of unknown affiliation ("algae indet."). The terrestrial fraction of palynomorphs comprises sporomorphs and fungal filaments. The phytoclast group is differentiated in inertinite, vitrinite and cutinite. The fraction of AOM is subdivided into fluorescing matter (AOMA) and non-fluorescing particles (AOMT). Except for AOM, all organic matter types are subdivided according to preservation state, into "A=good", "B=fair" and "C=poor". Poorly preserved phytoclasts that shows no signs of the former structure are added to the group of AOMT.

Terrestrial organic matter

For the Upper Barremian part of the Nevenka 1 core the sedimentary organic matter composition is dominated by terrestrial organic matter. Content decreases discontinuously throughout the stage from 95.9 % to 41.7 %. The average percentage is 75.8 % (SD=16.9 %). The Lower Aptian interval of the section shows a mean proportion of terrestrial organic matter of 69.2 % (SD=11.6 %). The contents of individual samples range from 57.6–83 %.

Sporomorphs: In the Late Barremian of the Nevenka 1 core the content of sporomorphs fluctuates highly between 2.6 % and 35.1 % and shows no distinct trend. Several intermittent peaks are identified. A mean value of 11.3 % (SD=7.1 %) is observed. Overall, the abundance of well-preserved sporomorphs (cat. A) shows intermittent peaks and a highly discontinuous distribution with content fluctuating between 0.2–15.8 %. A mean proportion of 5.2 % (SD=3.4 %) is observed. Sporomorphs of category B vary strongly throughout the sampled interval from 0–20.9 % and shows highest fluctuations in the upper lower and middle part of the interval. The averaged proportion is 5.1 % (SD=4.8 %). The mean proportion of poorly preserved sporomorphs reaches 0.99 % (SD=1.9 %) and shows higher proportion in the lower part of the interval where the content fluctuates highly between 0–11.2 %. Throughout the remainder of the interval the content remains low and varies between 0–1 %. Proportion of sporomorphs in the Early Aptian section varies between 7.8 % and 31.8 %. Sporomorph abundance shows a sharp increase in the uppermost part of the interval where proportion increases from 9.8–31.8 %. A mean abundance of 14.8 % (SD=11.4 %) is observed. The content of sporomorphs of category A varies between 4.4–11.8 % (mean 6.7 %, SD=3.5 %). No clear trend in proportion is evident. Fairly preserved sporomorphs show a distinctly increasing trend from 3.3 to 20 % throughout the Lower Aptian interval. The average content of category B

sporomorphs is 7.9 % (SD=8.1 %). Sporomorphs of category C are present in one sample with a percentage of 0.54 % resulting in a mean abundance in the Lower Aptian section of 0.14 % (SD=0.27 %).

Phytoclasts: Throughout the Upper Barremian interval of the Nevenka 1 the average content of phytoclasts fluctuates significantly but shows a distinctly decreasing trend from 76.5 % to 18.7 %. The mean phytoclast content of this interval is 46.1 % (SD=19.2 %). In the Lower Aptian interval content varies between 21.9 % and 45.5 %. The mean proportion is 32 % (SD=11.4 %). A distinct trend is not observed.

Inertinite: The content of inertinite varies strongly between 8–67 % and shows a discontinuously decreasing trend throughout the Late Barremian section. The mean value is 27.6 % (SD=14.3 %). Content of well-preserved (cat. A) inertinite shows a discontinuous but significant decrease throughout the interval from 41.6 to 7.4 % (mean of 21.2 %, SD=10.8 %). Fairly (cat. B) preserved inertinite shows no clear trend. Content decreases sharply in the lowermost part of the Barremian section and subsequently varies intensely within the remainder of the interval. The average proportion is 6.4 % (SD=5.6 %). In the Lower Aptian part of the sequence inertinite distribution shows no clear trend and varies between 4.9–24.8 %. A mean content of 15.7 % (SD=8.3 %) is observed. Inertinite of category A shows an average content of 12.8 % (SD=7.3 %) that varies between 3.8–20.7 %. A distinct trend is not observed. Fairly preserved (cat. B) inertinite in this interval shows a varying content of 1.1–4.1 % and a mean value of 2.9 % (SD=1.5 %). The distribution pattern shows no clear trend.

Vitrinite: Content of vitrinite fluctuates highly throughout the Late Barremian section. The value varies between 4.6–37.3 % (average of 17.6 %, SD=8.2 %) and shows no clear trend except for a short interval of decreasing content in the uppermost part of the Barremian interval. Well-preserved (cat. A) vitrinite shows strongly varying content (1.5–29.4 %) and averages at 11.5 % (SD=6.2 %). In the upper part of the interval a decreasing trend is evident. Vitrinite of category B shows an intensely fluctuating content that varies between 1 % and 13.6 %. The mean proportion in the Late Barremian section is 6.2 % (SD=2.9 %). No unequivocal trend is observed in the vitrinite percentage of the Early Aptian section. The content varies between 7.3–18.8 % (mean of 15.1 %, SD=5.3 %). The proportion of the well-preserved (cat. A) vitrinite specimens ranges between 3.3–10.1 %. A trend is not observed and the average value for the Early Aptian section is 7.5 % with a SD of 3.1 %. Fairly (cat. B) preserved vitrinite shows a content of 4.1–9.0 % (mean of 7.6 %, SD=2.4 %). A trend is not observed.

Cutinite: In the Late Barremian section of the Nevenka 1 proportion of cutinite varies widely between 0 % and 4.1 %. A peak of 4.1 % occurs in the lower part of the interval. The mean content is 0.78 % (SD=0.84 %). A distinct trend is not observed. The Early Aptian section is characterised by cutinite proportion that is distributed between 0.82 % and 1.9 %. The average abundance for this interval is 1.24 % (SD=0.57 %).

Fungal filaments: The content of fungal filaments in the Late Barremian section ranges between 0 % and 3 %. A clear trend is not evident. The averaged proportion is 0.31 % (SD=0.61 %). In the Early Aptian section remains of fungal filaments are absent.

Terrestrial AOM: The content of terrestrial $AOMT_{translucent}$ in the Late Barremian section fluctuates highly and varies between 6.8 % and 51.5 %. A mean value of 18.2 % (SD=8.3 %) is identified. An indistinctly increasing trend is observed. The content of $AOMT_{opaque}$ is continuously low

and varies between 0 % and 0.71 % (mean of 0.07 %, SD=0.17 %). The mean proportion of $AOMT_{total}$ in the Late Barremian section is 36.5 % (SD=16.5 %). In the Early Aptian section an averaged $AOMT_{translucent}$ content of 22.3 % (SD=6.8 %) is observed. The value ranges from 14.6 % to 29.3 %. A distinct trend is not observed. The lowermost sample of the studied interval of the Early Aptian contains AOM_{opaque} and reaches an abundance of 0.51 % (mean of 0.08 %, SD=0.16 %). $AOMT_{total}$ value varies between 29.1 % and 58.6 % (mean 44.7 %, SD=13.7 %).

Marine organic matter

The content of marine organic matter varies strongly throughout the Nevenka 1 core. The Upper Barremian section of the Nevenka 1 core shows two peaks in the lower part of the interval where the proportion reaches 42.3 % and in the upper middle part where 58.1 % is reached. Despite strong variations in the proportion the content significantly increases from 3.4 % to 57.4 %. The mean content of the Upper Barremian is 23.8 % (SD=17 %). In the Lower Aptian section the content of marine organic matter varies between 17 % and 41.9 %. A mean value of 30.7 % (SD=11.5 %) is observed. No clear trend is identified for this interval.

Dinoflagellate cysts: Dinoflagellate cysts of the Upper Barremian section show no distinct trend. In the middle part of the interval abundance fluctuates highly and throughout the formation content varies between 0 % and 8.8 %. A mean value of 1.5 % and a SD of 1.7 % are detected. Well preserved dinocysts of category A show intensely varying abundance (0–4.5 %). A trend is not identified. The mean proportion is 0.68 % (SD=0.85 %). Fairly (cat. B) preserved dinocysts show an averaged content of 0.52 % (SD=0.62 %). The value fluctuates throughout the interval between 0 % and 3 %. A distinct trend is not observed. Poorly (cat. C) preserved dinoflagellate cysts vary widely between 0–1.6 %. A clear trend is not evident. The mean content reaches 0.32 % (SD=0.41 %). In the Early Aptian content of dinocysts averages at 2.5 % (SD=2.4 %). Proportion varies between 0 % and 5.1 %. Variations of 0–1.3 % are observed in the content of the well-preserved (cat. A) dinoflagellates. A trend is not observed and the averaged proportion is 0.90 % (SD=0.78 %). Proportion of fairly (cat. B) preserved dinocysts varies between 0–2.2 %. The averaged content in the Early Aptian section is 0.75 % (SD=1 %). Dinocysts of category C show a frequency between 0 % and 1.5 % (mean of 0.83 %, SD=0.70 %). A distinct trend is not observed.

Acritarchs: Although acritarchs are also subdivided into three groups depending on the preservation state, overall occurrences are so rare that abundances of acritarchs are mentioned here as a whole. Acritarch occurrence in the Late Barremian section varies between 0–3.9 %. This major peak of 3.9 % is detected in the uppermost part of the interval. A trend in frequency is not observed. The mean content of acritarchs in this interval is 0.38 % (SD=0.63 %). During the Early Aptian part of the sections acritarch abundance ranges between 0–0.82 %. An averaged proportion of 0.49 % (SD=0.38 %) is reached. A trend is not observed.

Algae indet.: Structured particles that show bright yellow to white fluorescence but show no unequivocal affiliation to any of the other marine palynomorphs are summarised in the group of algae indet. Algae indet. are not subdivided with regard to their preservation state. The proportion in the Late Barremian section fluctuates widely between 0 % and 5.7 %. A mean content of 1.4 % (SD=1.5 %) is observed. A clear trend in the distribution pattern is not observed. Early Aptian algae indet.

Abundance shows a mean of 1.4 % (SD=2.3 %). The content varies between 0 % and 4.7 %. A trend is not detected.

Foraminiferal test linings: Occurrences of foraminiferal linings are scarce. Throughout the studied interval of the Nevenka 1 core 4 samples from the Late Barremian interval of the section contain foraminiferal remains. Abundances of foraminiferal linings varies between 0.24–0.25 % (mean of 0.02 %, SD=0.06 %). No foraminifers are present in the Early Aptian part of the core.

Leiospheres: Leiospheres are absent in the lowermost and uppermost parts of the Late Barremian section. In the middle part of the Upper Barremian interval, leiosphere frequency varies between 0.23–1.5 %, reaching an average content of 0.17 % (SD=0.37 %). A trend in occurrence is not observed. In the Early Aptian leiospheres are absent.

Marine AOM: A discontinuous but significant increase in content of fluorescing AOM is observed for the Late Barremian (2.0–57.3 %). In the lower part of this interval a marked intermittent peak in AOMA content is detected reaching 38.6 %. The Late Barremian contains an average AOMA content of 20.2 % (SD=16.3 %). In the Lower Aptian, proportion of AOMA varies between 17–39.1 %. An averaged content of 26.3 % (SD=9.7 %) is reached. AOMA content of the Early Aptian shows no distinct trend

Opaque/translucent ratio

For the Upper Barremian interval an OP/TR ratio of 1.6 is detected. The OP/TR ratio of the Lower Aptian section is 1.

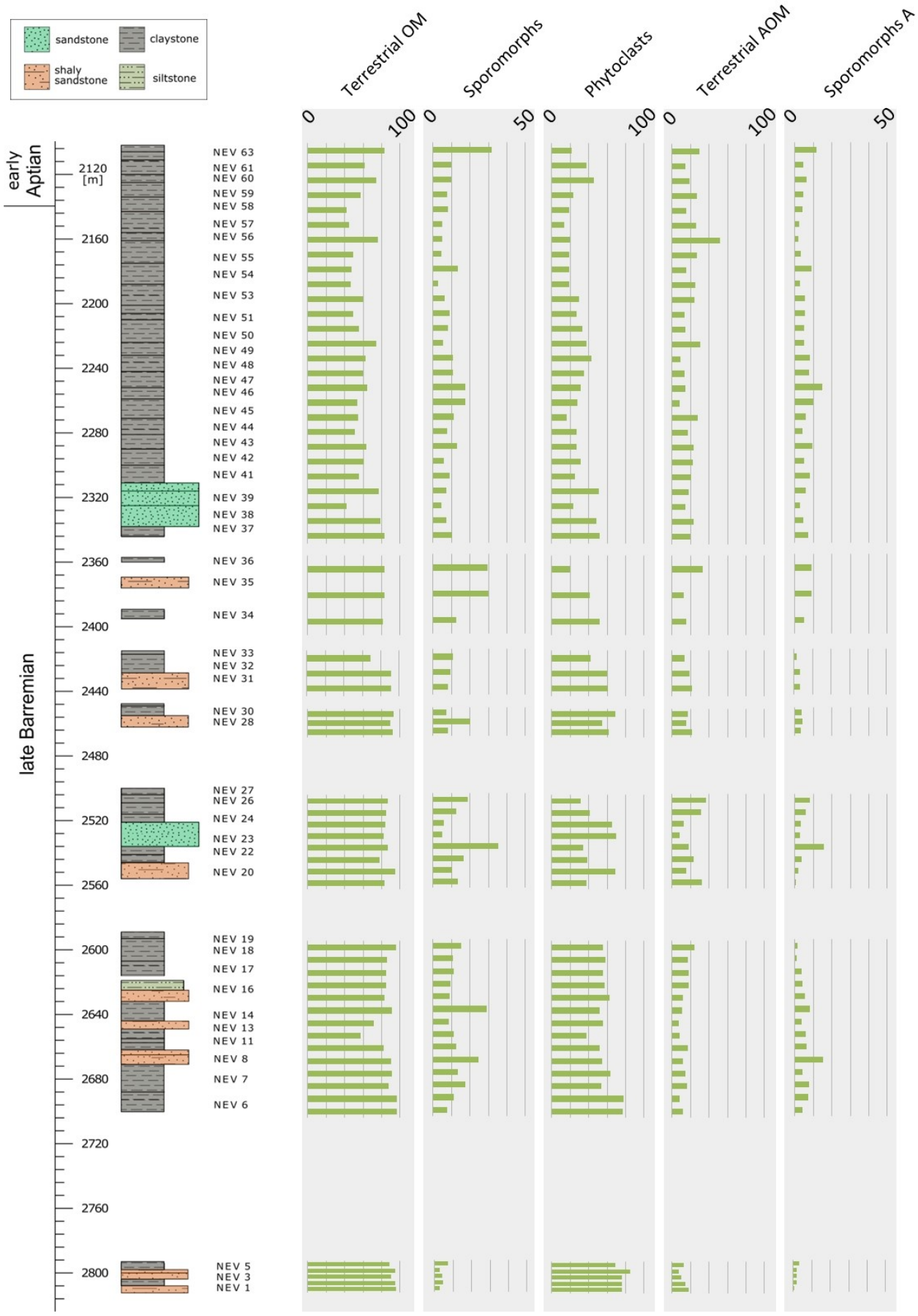

Figure 80: Sedimentary organic matter – terrestrial fraction continued; Nevenka 1 core. Values given in %, to increase visualisation, different scales are used.

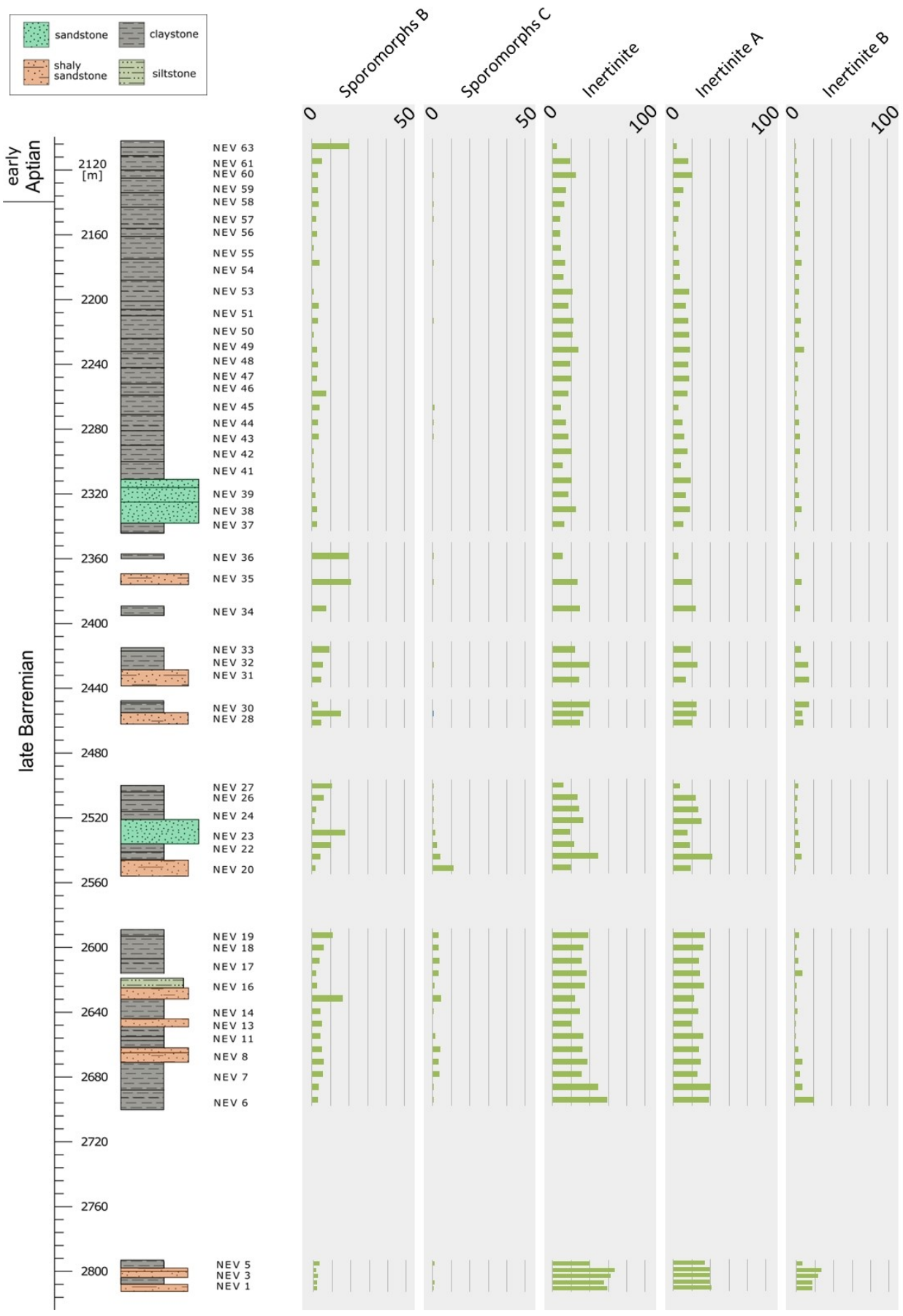

Figure 81: Sedimentary organic matter – terrestrial fraction continued; Nevenka 1 core. Values given in %, to increase visualisation, different scales are used.

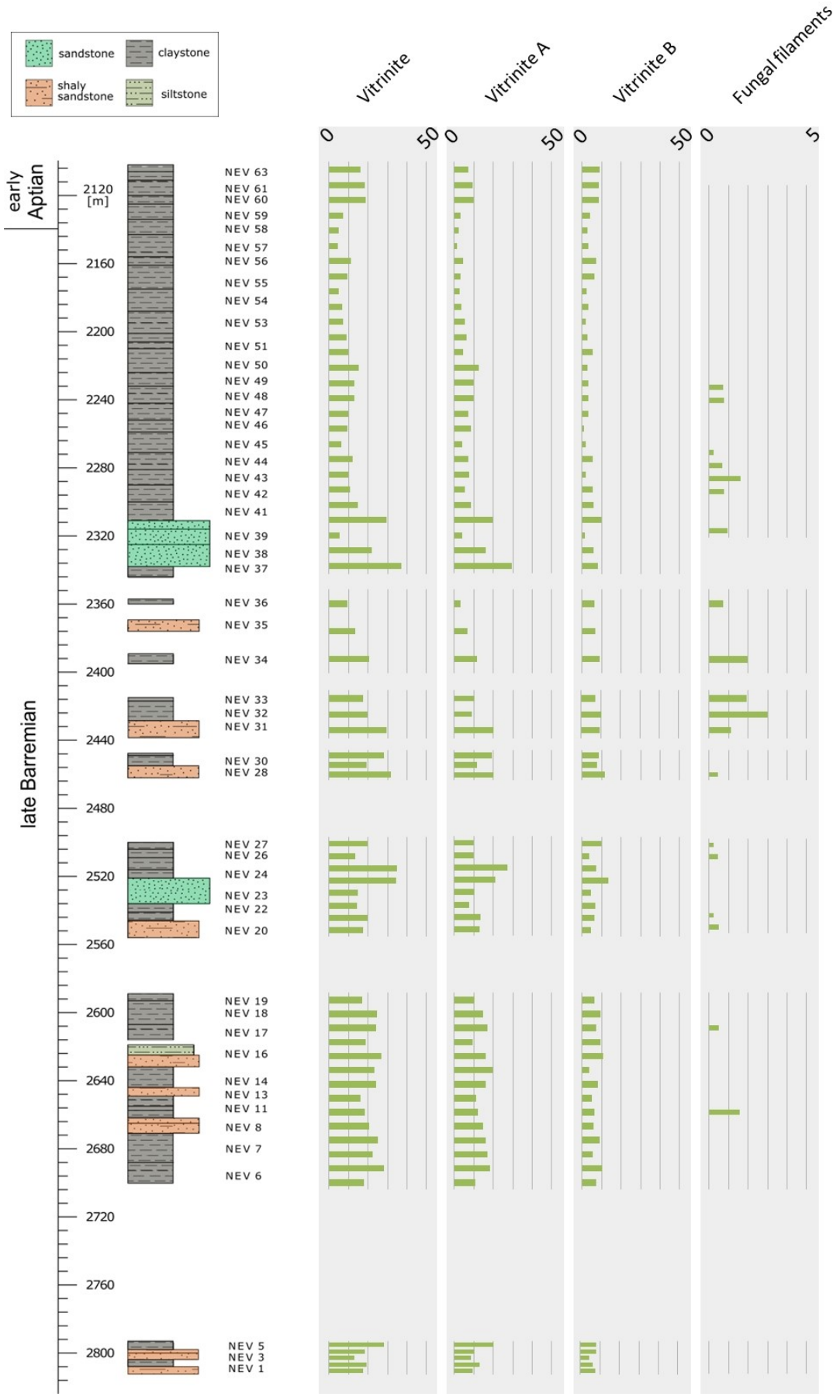

Figure 82: Sedimentary organic matter – terrestrial fraction continued; Nevenka 1 core. Values given in %, to increase visualisation, different scales are used.

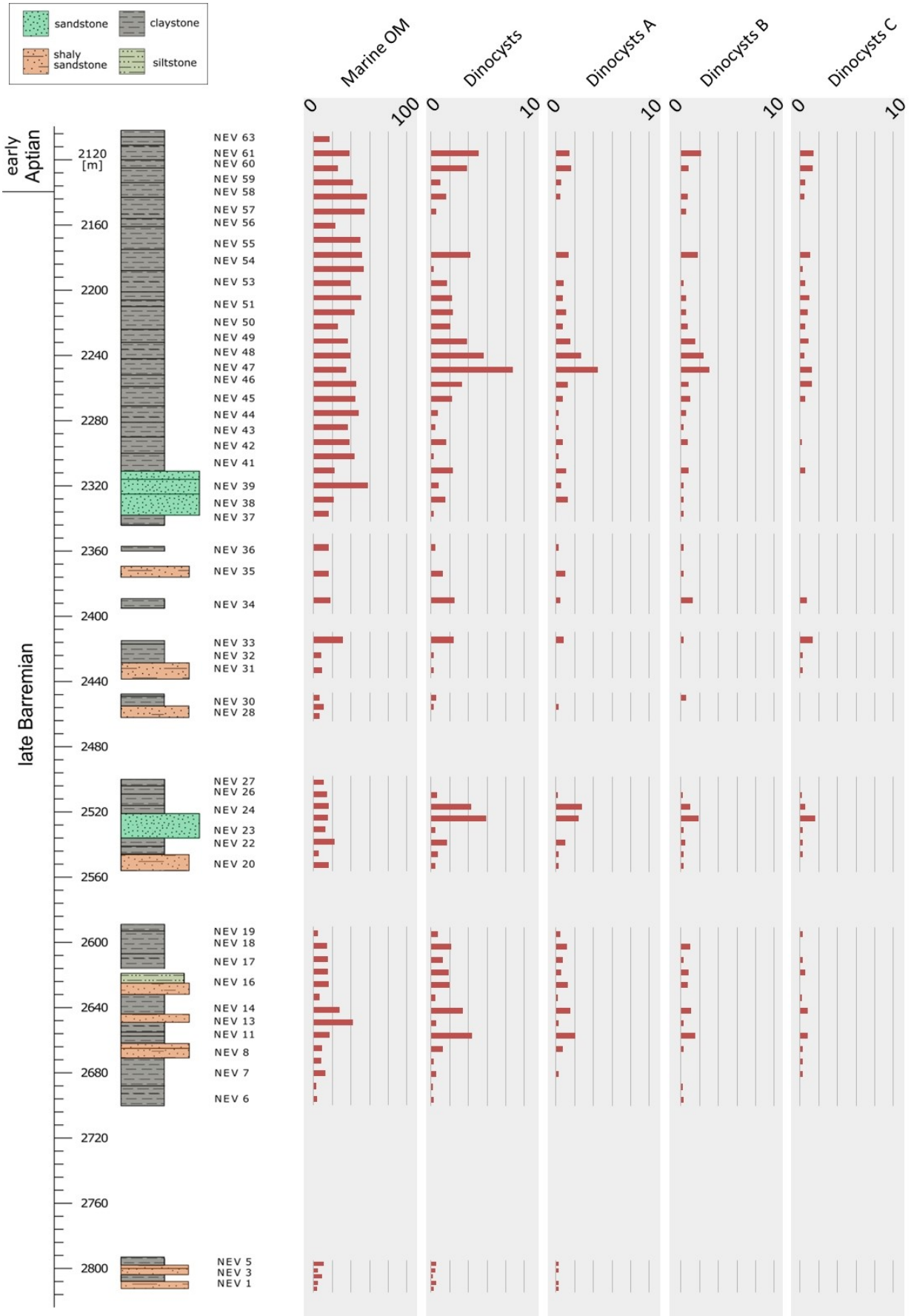

Figure 83: Sedimentary organic matter – marine fraction; Nevenka 1 core. Values given in %, to increase visualisation, different scales are used.

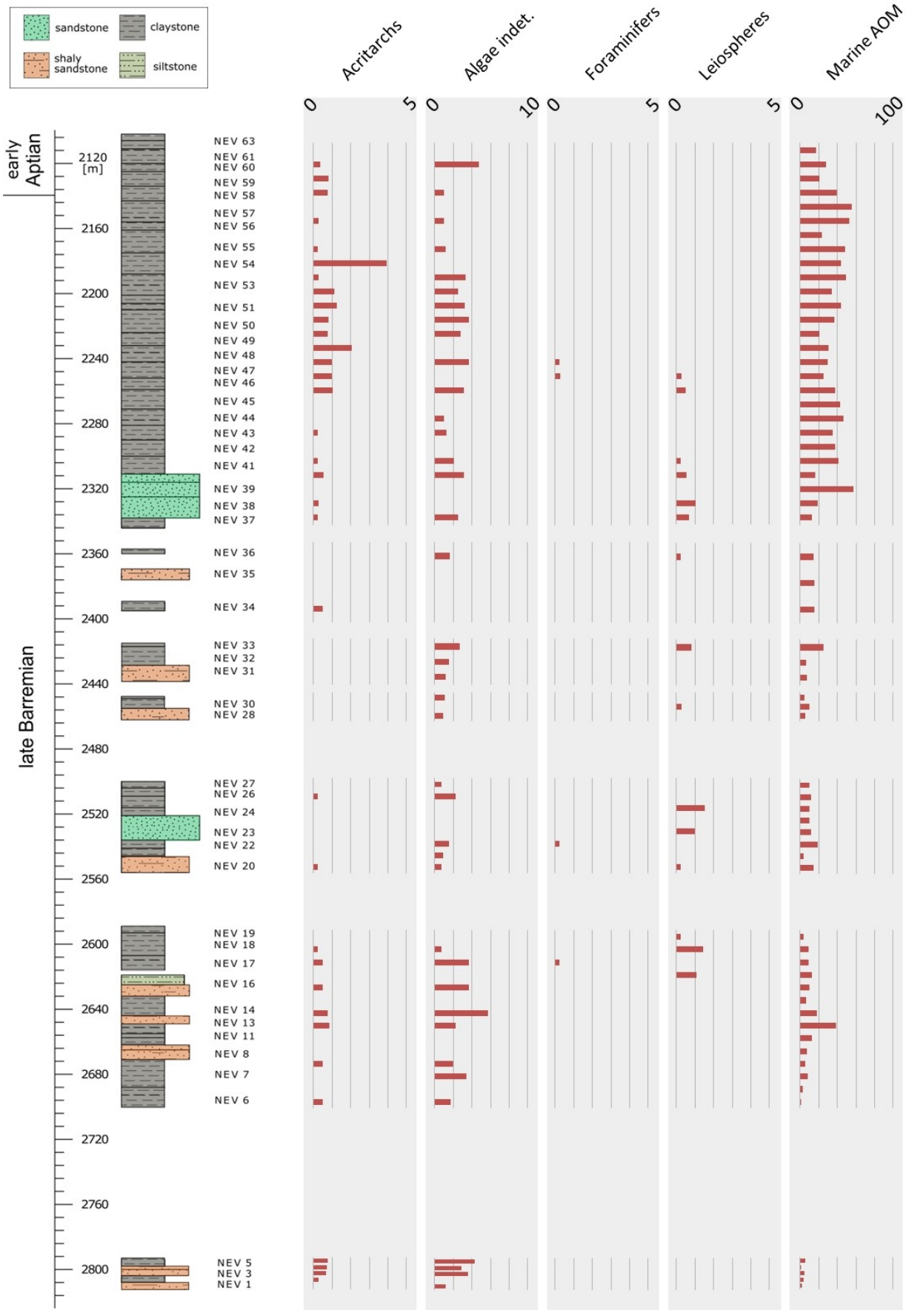

Figure 84: Sedimentary organic matter – terrestrial fraction; Nevenka 1 core. Values given in %, to increase visualisation, different scales are used.

AOM-PHYTOCLAST-PALYNOMORPH PLOT

Barremian–Aptian: In the lower to lower middle part of the Barremian–Aptian interval of the Nevenka 1 core samples plot in palynofacies field I – highly proximal shelf or basin over palynofacies fields II – marginal dysoxic-anoxic basin and III – heterolithic oxic shelf ("proximal shelf") to shelf to basin transition fields IVa/b (Figs. 85, 86). In the upper middle to upper part of the Barremian–Aptian interval of the Nevenka 1 core samples plot from palynofacies fields IVa/b – shelf to basin transition over field V – mud-dominated oxic shelf ("distal shelf") to field VII – distal dysoxic-anoxic "shelf" (Figs. 86, 87). In the upper part of the interval samples plot in palynofacies fields VII – distal dysoxic-anoxic "shelf", VIII – distal dysoxic-anoxic shelf and IX – distal suboxic-anoxic basin back to fields IVa/b –shelf to basin transition and V – mud-dominated oxic shelf ("distal shelf") (Fig. 87).

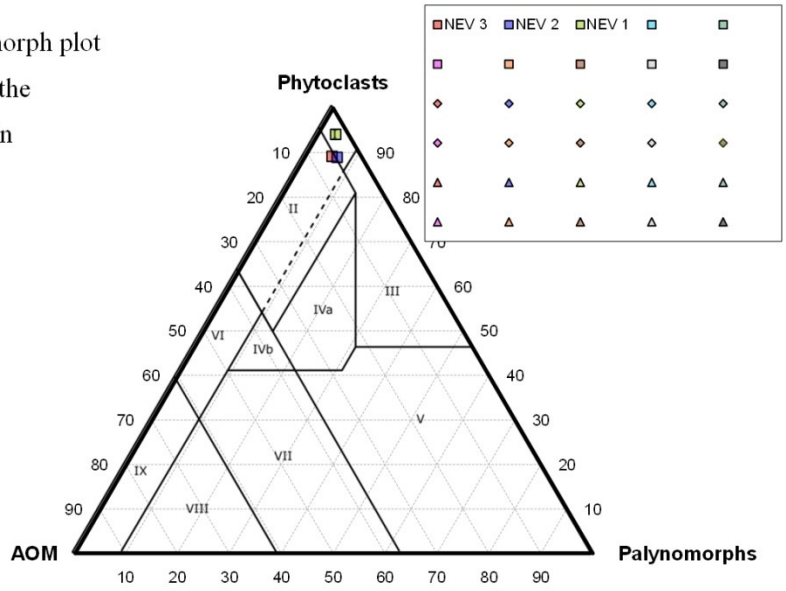

Figure 85: AOM-phytoclast-palynomorph plot of NEV 1–NEV 3; key to the palynofacies fields given in table 2 (p. 49).

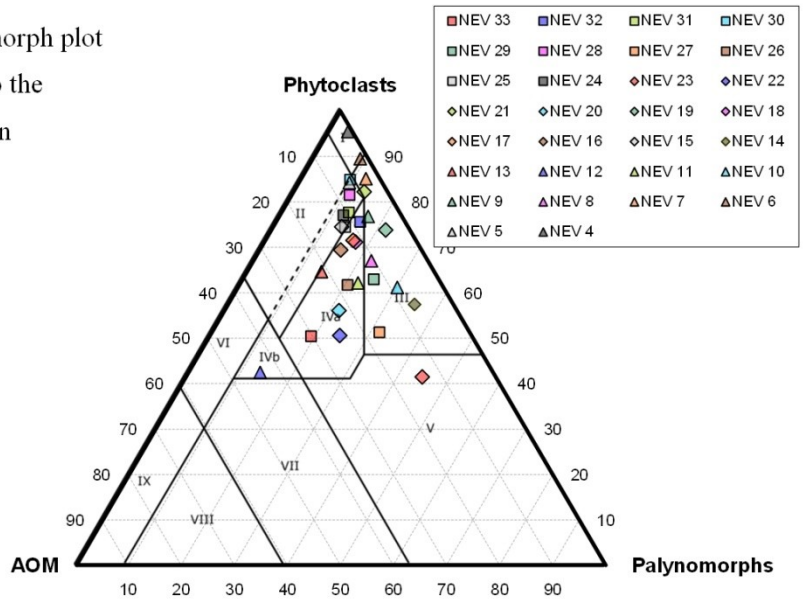

Figure 86: AOM-phytoclast-palynomorph plot of NEV 4–NEV 33; key to the palynofacies fields given in table 2 (p. 49).

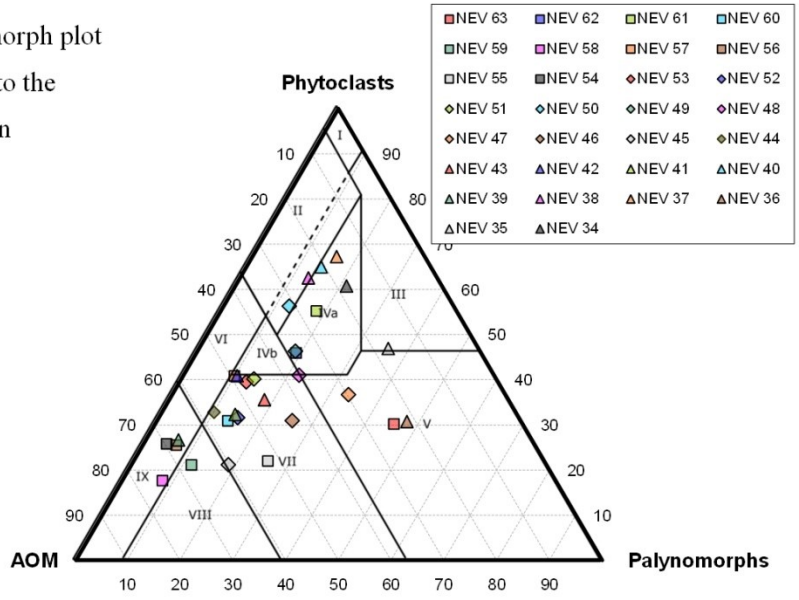

Figure 87: AOM-phytoclast-palynomorph plot of NEV 34–NEV 63; key to the palynofacies fields given in table 2 (p. 49).

TOTAL ORGANIC CARBON, TOTAL INORGANIC CARBON, CARBON/SULPHUR/ NITROGEN

63 samples of the Nevenka 1 were analysed for their carbon, nitrogen and sulphur content (Fig. 88).

Total organic carbon: TOC in the Late Barremian interval of the Nevenka 1 varies between 0.30 % and 9.2 %. Several intermittent peaks are observed. A mean proportion of 1.8 % (SD=1.8 %) is observed. The Early Aptian interval contains a lower mean proportion of 0.98 % (SD=1.2 %). The content of individual samples varies considerably between 0.25–2.7 %. A sharp increase is detected from 0.26 % to 2.7 % in the uppermost sample of the interval. An unequivocal trend is not observed.

Total inorganic carbon: In the Late Barremian section of the Nevenka 1 core TIC content is highest in the upper part of the interval where several peaks and a maximum of 3.9 % is identified. The overall proportion varies intensely between 0.3–3.9 %. The mean proportion for this interval is 1.1 % (SD=0.6 %). A distinct trend is not observed. The Early Aptian section contains a mean proportion of TIC of 0.92 % (SD=0.35 %). The content varies between 0.7 % and 1.4 %. A distinct trend is not evident.

$CaCO_3$: In the Late Barremian interval content of $CaCO_3$ ranges from 2.4–32.5 %. Several positive peaks are detected especially in the upper part of the section. A mean proportion of 9.4 % (SD=5.2 %) is observed. The Early Aptian section of the Nevenka 1 core shows a mean proportion of $CaCO_3$ of 7.6 % (SD=2.9 %). Individual contents vary between 5.8–12 %.

Nitrogen: In the samples of the Late Barremian section nitrogen content varies between 0.02 % and 0.17 %. The mean proportion is 0.05 % (SD=0.03 %). The content shows a highly discontinuously decreasing trend throughout the lower and middle part of the interval. Subsequently

an inhomogeneous increase is observed in the upper middle and upper part. The nitrogen content of the Early Aptian interval ranges from 0.02 % to 0.06 %. A trend is not observed.

Sulphur: Except for two peaks of 0.8 and 0.59 % in the lower and middle part of the Late Barremian section the sulphur content fluctuates in this section between 0.05 % and 0.36 %. In the upper middle and upper part of the interval the sulphur proportion fluctuates intensely on an increased level between 0.24–1.5 %. Overall a mean proportion of 0.49 % (SD=0.45 %) is detected. The Early Aptian section shows a mean proportion of 0.32 % (SD=0.17 %). Individual contents vary between 0.17–0.56 %. The distribution pattern shows no unequivocal trend.

C_{org}/N: C/N the ratio of the Late Barremian interval ranges from 9–84. In the middle part of the interval a positive peak of 84 is observed. The mean value is 32. In the Early Aptian interval of the Nevenka 1 C/N the ratio varies between 11 and 46. The averaged ratio is 23. An unequivocal trend is not observed.

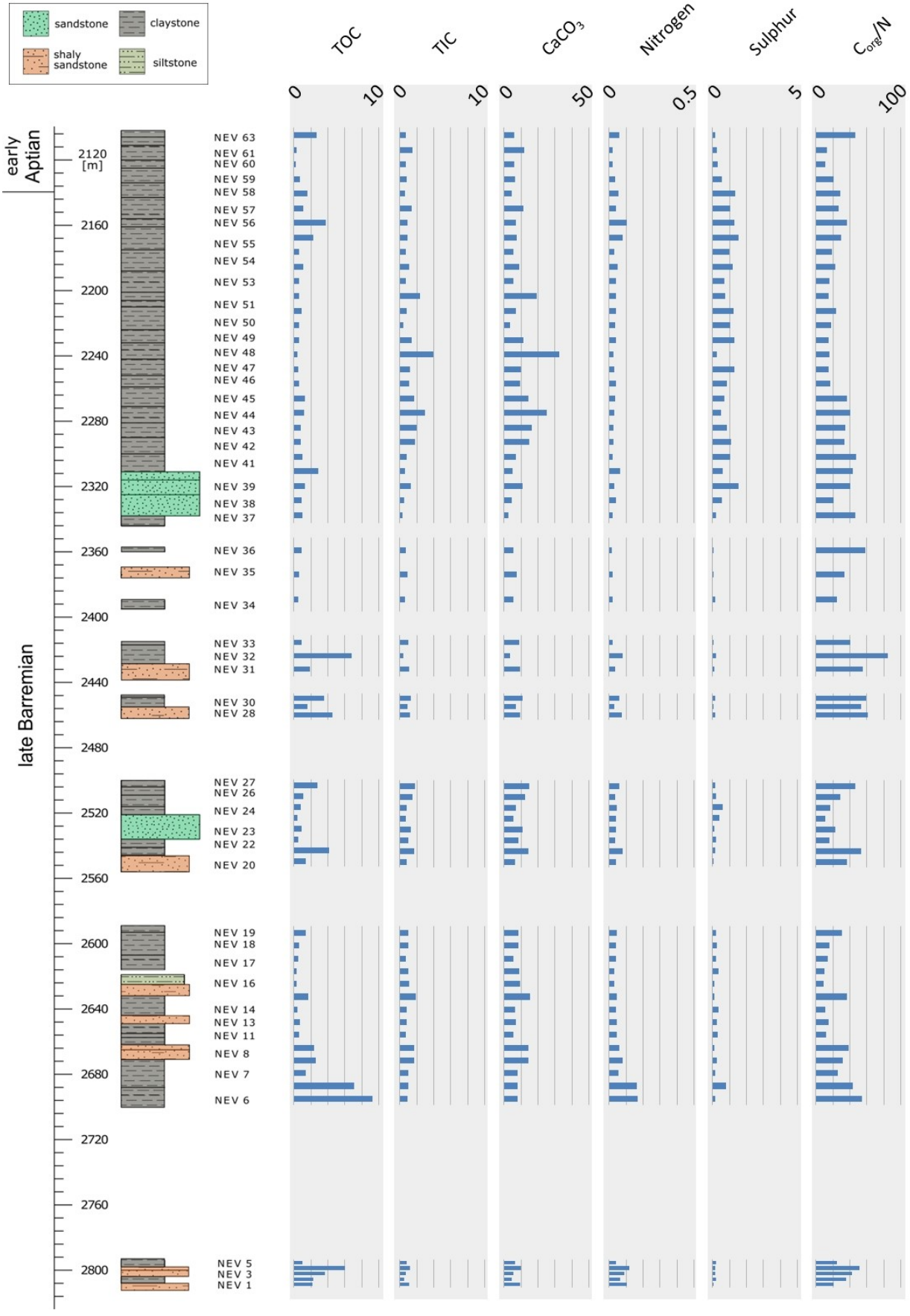

Figure 88: Results of the TOC, TIC and CNS analyses; Nevenka 1 core. Except for C_{org}/N, values given in %, to increase visualisation, different scales are used.

THERMAL MATURITY

In the Nevenka 1 core thermal maturation is determined using the Thermal Alteration Index (TAI) and Spore Coloration Index (SCI). Analysis was performed on 4 samples (NEV 5, NEV 22, NEV 43, NEV 62). Samples show a TAI ranging from approximately 2.5 to 3/SCI of 5.0-8.5 (Ro% 0.5–1.3). The resulting maturation stage is diagenesis to catagenesis (cf. Suárez-Ruiz et al., 2012).

MICRO-GLENDONITES

11 samples of the section of the Nevenka 1 core contain micro-glendonites. A total of 74 specimens are recorded (selected specimens shown in figures 89–92). The interval comprises the Late Barremian to Early Aptian. The exact position of the stage boundary is not known but is tentatively placed between samples 59 and 60. A total of 75 specimens are recorded. The mean size of the recorded micro-glendonites is 35.4 µm (SD=20.1 µm). Individual specimens range in diameter from 7 µm to 101 µm.

Figures 89–92: Selected micro-glendonite specimens of the Sofia 1 core – Fig. 89: NEV 49; Fig. 90: NEV 49; Fig. 91: NEV 50; Fig. 92: NEV 50; scale bars given in the photographs.

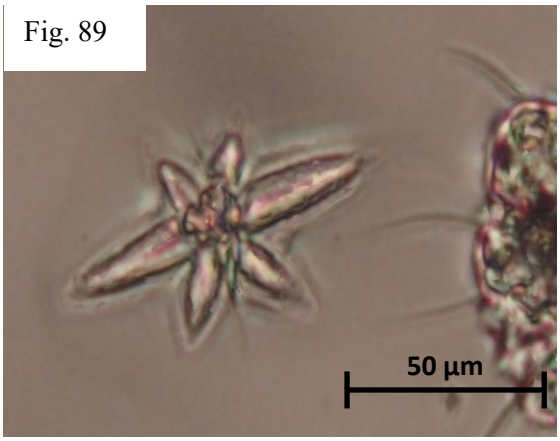

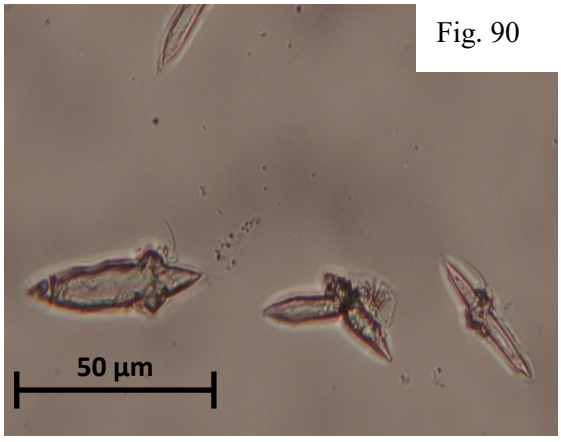

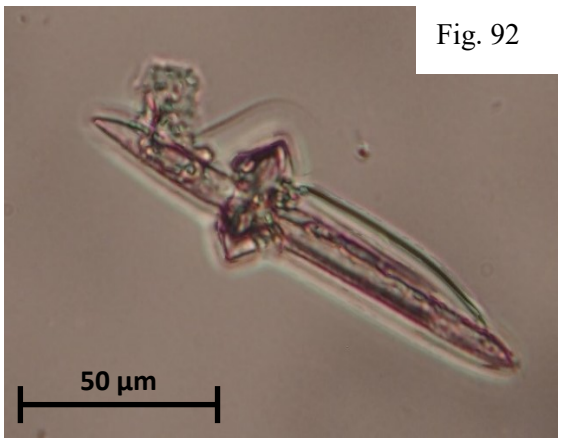

SOFIA 1 CORE

PALYNOFACIES ANALYSIS

60 samples of the Sofia 1 core cuttings have been available for palynofacies analysis (SOF 1–60) (Figs. 93–95). According to ENAP data (geophysical & lithostratigraphical data) 9 samples belong to the Late Tithonian, 13 samples to the Berriasian–Valanginian lower Zapata Formation and 38 samples were taken from the Hauterivian–Aptian middle Zapata Formation (cf. Fildani et al., 2003; Varela et al., 2012).

The palynofacies assemblage detected in the Sophia 1 is little diverse and contains only few groups of structured organic matter. The marine fraction consists exclusively of scarce dinocysts and acritarchs. Foraminifers and leiospheres are not present in the sampled interval. Also, no occurrences of aquatic/marine AOM are observed. The terrestrial fraction of structured organic particles is limited to sporomorphs and phytoclasts. The fraction of AOM is subdivided into translucent AOMT and opaque AOMT. The structured organic particles are subdivided according to its preservation state, into "A=good", "B=fair" and "C=poor". Poorly preserved phytoclasts that show no signs of its former structure are added to the group of AOMT.

Terrestrial organic matter

The palynofacies assemblage of samples of the Sofia 1 core is dominated by the occurrence of structured and unstructured terrestrial organic matter. Terrestrial organic matter contents of the Tithonian section average 99.9 % (SD=0.29 %). One sample only in the uppermost part of the interval contains less than 100 % terrestrial material. The same pattern is identified in the assemblage of the Berriasian–Valanginian interval where a negative peak of 98.0 % occurs in the upper part of the succession. A mean proportion of 99.8 % (SD=0.58 %) is detected. Content of terrestrial organic matter in the Hauterivian–Aptian section fluctuates on a high level between 95.7 % and 100 %. A marked low is identified in the lower middle part of the interval. A distinct trend in proportion is not observed. The section contains an average of 98.6 % (1.4 %) of terrestrial organic matter.

Sporomorphs: Distinctly decreasing sporomorph abundance from 2.5 % to 0 % is noted in the Tithonian interval of the Sofia 1 core. The averaged proportion is 0.79 % (SD=0.94 %). No well-preserved (cat. A) sporomorphs occur in the Tithonian section. Content of sporomorphs of category B varies between 0 % and 0.90 %. A clear trend for this organic matter type is not identified. The averaged frequency is 0.24 % (SD=0.33 %). A declining trend from 1.9 % to 0 % is observed for the proportion of poorly (cat. C) preserved sporomorphs in the succession of the Tithonian. The mean frequency is 0.55 % (SD=0.66 %). The Berriasian–Valanginian interval shows fluctuating contents of sporomorphs. Proportion varies from 0 % to 1.0 % but show no clear trend. An averaged content of 0.18 % (SD=0.29 %) is identified. In the Berriasian–Valanginian succession no sporomorphs of category A are present. In the lower and middle part of the interval fairly (cat. B) preserved sporomorphs are also absent. Content increases to 0.34 % in the upper part of the interval. A mean value of 0.07 % (SD=0.14 %) is observed. Poorly (cat. C) preserved sporomorphs show two peaks (1.0 %, 0.33 %) in the lower and middle part of the interval. A mean content of 0.1 % with a SD of 0.28 % is reached. The samples of the Hauterivian–Aptian contain significantly higher proportions of

sporomorphs. Content varies intensely between 0 % and 9.8 %. After a peak in the lower part of the interval of 8.8 % the content decreases irregularly to 0 % in the middle part of the section. Subsequently content rises to 2.9 % at the uppermost part of the sampled interval. Intermittent peaks of 7.9 % and 9.8 % are detected in this increasing phase of sporomorph content. The latter reaches an average of 2.7 % (SD=2.9 %) in the Hauterivian–Aptian section. Well-preserved (cat. A) sporomorphs show low abundance throughout the most of the Hauterivian–Aptian section that varies between 0–0.37 %. In the lower upper part of the section sporomorphs are more frequent with a varying content of 0–1.3 % (average for the whole interval is 0.12 %, SD=0.28 %). Sporomorphs of category B show a highly fluctuating proportion. Content varies between 0–5.2 %. Several peaks are detected in the lower and upper part of the interval. The middle part of the Hauterivian–Aptian succession contains lower amounts of sporomorphs. A clear trend is not observed. An average content of 1.2 % (SD=1.5 %) is identified. Relative abundances of poorly preserved sporomorphs vary intensely between 0–6.3 %. A marked peak (6.3 %) is detected in the upper part of the succession, a distinct trend is not evident. Contents for the Hauterivian–Aptian succession reach an average of 1.4 % (SD=1.5 %).

Phytoclasts: Content of phytoclasts increases slightly and relatively homogeneous throughout the Tithonian interval from 84.7 to 97.9 %. The averaged phytoclast content for this interval is 90.2 % (SD=5.7 %). For the Berriasian–Valanginian section a decreasing trend of phytoclast proportion from 96.3 % to 74.2 % is detected. For this interval, a mean value of 88.5 % (SD=8.0 %) is observed. The Hauterivian–Aptian interval shows an erratically decreasing content of phytoclast proportion from 88.9 % to 58.0 %. A mean proportion of 87 % (SD=10.9 %) is identified.

Inertinite: Despite minor fluctuations content of inertinite increases throughout the Tithonian interval from 80.3 % to 95.3 %. A mean content of 85.9 % (SD=7.7 %) is detected. Well-preserved inertinite shows varying content of 36.4 % to 45.6 %. An erratic decreasing trend is observed. The averaged content in this interval is 40.9 % (SD=2.9 %). Throughout the lower and middle part of the Tithonian succession abundance of fairly preserved inertinite remains relatively homogenous varying between 38.7 % and 36.3 %. Upsection a discontinuous increase to 58.9 % is identified in the upper part of the Tithonian interval. The mean frequency for this interval is 45 % (SD=9.6 %). Overall, inertinite proportion decreases throughout the Berriasian–Valanginian section from 95 % to 73.3 %. A mean content of 86.3 % (SD=9.5 %) is observed. Inertinite of category A shows a peak of 48.2 % in the upper middle part of the interval. An overall trend is not evident and the proportion varies between 21.2 % and 48.2 %. The averaged proportion is 37.4 % (SD=8.3 %). Content of fairly preserved inertinite varies between 34.8 and 68.7 %. A trend is not observed and the mean content is 48.8 % (SD=10.8 %). A discontinuously increasing trend is identified in the lower to middle part of the Hauterivian–Aptian section where inertinite content increases from 85.9–96.7 %. Subsequently the content decreases inhomogeneously towards the end of the succession to a value of 54.3 %. An averaged content of 83.1 % (SD=12.1 %) is noted for the Hauterivian–Aptian section. Well-preserved inertinite shows an inconsistently decreasing trend from 35.0 % to 11.9 % in the lower middle part of the succession. Upsection content increases highly discontinuous throughout the remainder of the interval to 32.9 %. An intermittent peak of 51.7 % is detected in the upper part of the Hauterivian–Aptian interval. The averaged proportion is 28.2 % (SD=7.7 %). Inertinite of category B increases erratically throughout the lower to middle part of the Hauterivian–Aptian section from 50.8 % to 78.6 %. Upsection inertinite proportion decreases to 21.4 % in the uppermost part of the section. An averaged content of 54.1 % (SD=16.1 %) is observed.

Vitrinite: Vitrinite content shows no clear trend throughout the Tithonian interval. Proportion varies between 0.7–10.5 % and reaches an averaged content of 4.2 % (SD=3.2 %). Content of well-preserved vitrinite ranges from 0 % to 4.7 % and fluctuates intensely. A trend is not observed and the averaged proportion for the Springhill Formation is 2.4 % (SD=1.6 %). Fairly preserved vitrinite shows a peak of 5.8 % in the lower part of the interval. Subsequently proportion decreases to 0.3 %. The averaged content of fairly preserved vitrinite in this interval is 1.8 % (SD=1.8%). Content of vitrinite in the Berriasian–Valanginian interval varies between 0% and 10.8 %. A distinct trend in proportion is not observed. For this interval a mean content of 2.2 % and a SD of 3 % are identified. Vitrinite of category A shows a varying proportion of 0 % to 9.3 %. A clear trend is not observed. The averaged content of well-preserved vitrinite in this interval is 1.7 % (SD=2.5 %). Content of fairly preserved vitrinite shows several peaks and no distinct trend. Proportion varies between 0–1.7 %. In the Berriasian–Valanginian section the average abundance for this organic matter type is 0.54 % (SD=0.65 %). Vitrinite content fluctuates intensely throughout the Hauterivian–Aptian interval. A marked low is detected in the middle part of the section. Overall the content varies between 0 % and 11.8 %. A distinct trend is not observed and the averaged vitrinite content of this interval is 3.8 % (SD=2.9 %). Several peaks (3.8–5.0 %) are identified for the proportions of well-preserved vitrinite. A clear trend is not observed. Overall content varies between 0–5 % and the averaged proportion for the Hauterivian–Aptian section is 1.4 % (SD=1.2 %). Despite a marked low in the middle part of the interval no distinct trend is noted for the fairly preserved content of vitrinite. Several intermittent positive and negative peaks are identified. The averaged content of fairly preserved vitrinite in this interval is 2.5 % (SD=2.2 %).

Terrestrial AOM: In the Tithonian interval the content of $AOMT_{translucent}$ is higher in the lower–middle part of the interval. The upper part of the section contains a lower amount of $AOMT_{translucent}$. Overall the content varies between 1.2 % and 18.5 %. The averaged content for this interval is 8.9 % (SD=5.5 %). Content of $AOMT_{opaque}$ remains low. A single sample in the upper part of the Tithonian interval contains a proportion of 0.59 % of $AOMT_{opaque}$ resulting in an averaged content of 0.07 % (SD=0.2 %). The $AOMT_{translucent}$ content shows an inhomogeneous increasing trend from 3.8 % to 25.5 % in the Berriasian–Valanginian interval. Overall the content varies from 1.0 % to 25.5 %. Averaged content for $AOMT_{translucent}$ in the Berriasian–Valanginian interval is 11.1 % (SD=7.7 %). $AOMT_{opaque}$ shows a peak of 2.0 % in the upper part of the succession. A mean value of 0.21 % (SD=0.58 %) is identified. Content of $AOMT_{translucent}$ shows a significant but discontinuous increase throughout the Hauterivian–Aptian succession. Proportion increases from 10.1 % to 37.1 %. Several intermittent peaks are observed. Proportion varies between 1.1 and 42.3 %. The averaged content of $AOMT_{translucent}$ in the Hauterivian–Aptian section is 8.9 % (SD=9.4 %). Content of $AOMT_{opaque}$ fluctuates intensely from 0 % to 4.3 % and shows several intermittent peaks. Content is highest in the upper lower to lower middle part of the succession. An overall distinct trend is not evident. The averaged content reaches 1.1 % (SD=1.3 %).

Marine organic matter

Throughout the analysed samples of the Sofia 1 core content of preserved marine organic matter is continuously low. One sample in the upper part of the Tithonian section contains marine organic matter with a relative abundance of 0.3 %. The average content for this interval is 0.03 % (SD=0.1 %). The same pattern is observed in the Berriasian–Valanginian section where a single sample in the upper part of the interval reaches a relative abundance of 0.6 % (mean of 0.04 %, SD=0.16 %). Occurrences of marine organic matter-bearing samples are highest in the Hauterivian–Aptian interval. 7 samples contain marine organic matter resulting in a mean content of 0.06 % (SD=0.14 %).

Dinoflagellate cysts: No dinocysts are contained in the samples of the Tithonian succession of the Sofia 1 core. A single sample in the upper part of the Berriasian–Valanginian section contains dinoflagellate cysts with a relative abundance of 0.29 %. The mean content for this interval is 0.02 % and the SD is 0.08 %. The lowermost and upper parts of the Hauterivian–Aptian interval contain dinocysts. Where present, the relative frequency varies between 0.29 % and 0.41 %. The upper lower and middle parts of the interval are free of dinocysts. Mean relative abundance for the Hauterivian–Aptian interval is 0.05 % (SD=0.13 %).

Acritarchs: Acritarchs occur once per sampled interval. In the Tithonian section the uppermost sample contains a relative proportion of 0.29 % of acritarchs resulting in a mean value of 0.03 % (SD=0.10 %) for the interval. In the uppermost part of the Berriasian–Valanginian section one sample with a relative abundance of 0.29 % is detected. This interval has a mean content of 0.02 % (SD=0.08 %). One sample in the upper part of the Hauterivian-Aptian section of the Sofia 1 core contains acritarchs with n abundance of 0.33 %. A mean value of 0.01 % (SD=0.05 %) is reached.

Opaque/translucent ratio

For the Tithonian section an OP/TR ratio of 20.3 is detected. The OP/TR ratio of the Berriasian–Valanginian interval is 38.8. The OP/TR ratio of the Hauterivian–Aptian interval is 21.8.

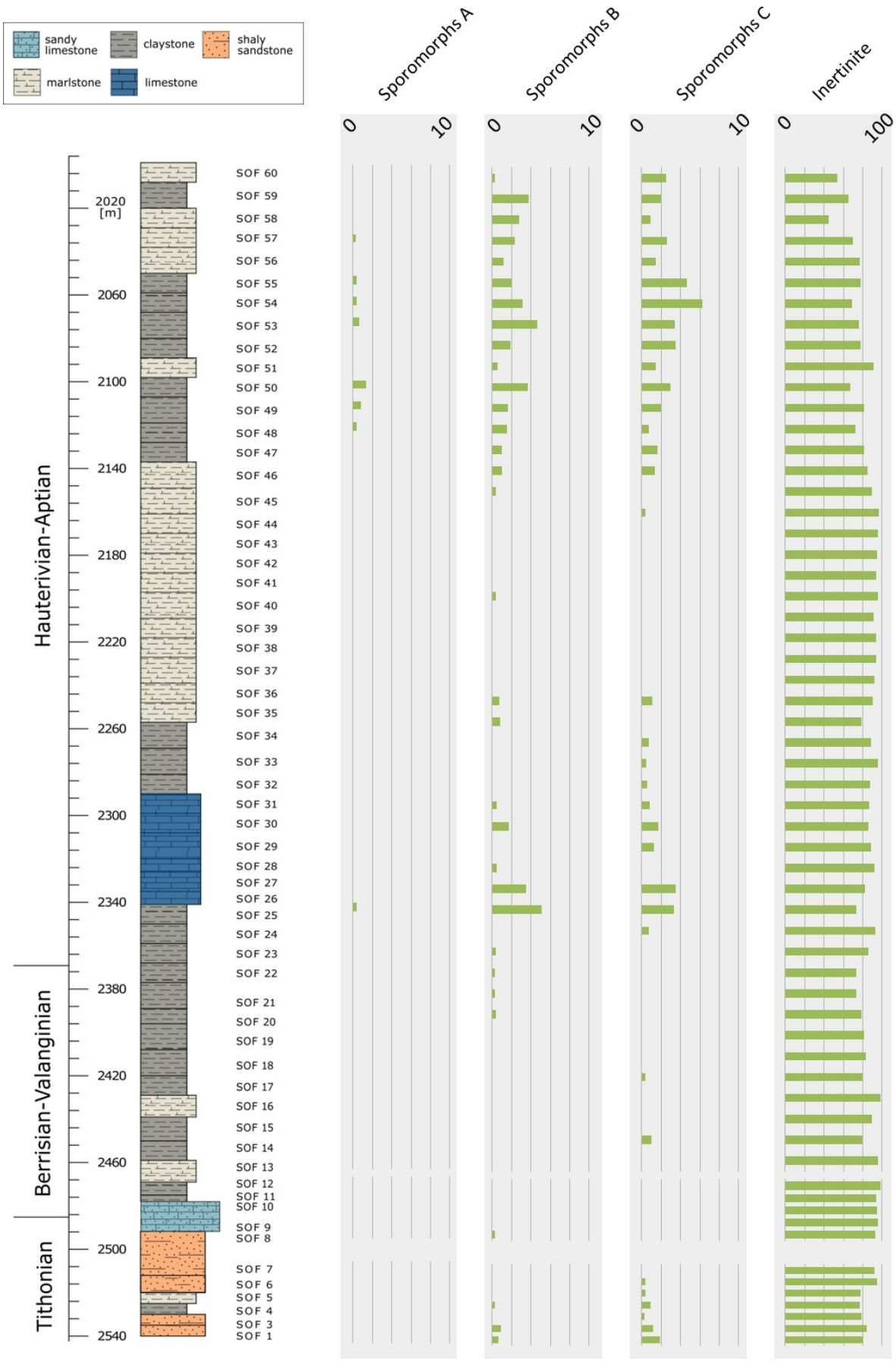

Figure 93: Sedimentary organic matter – terrestrial fraction; Sofia 1 core. Values given in %, to increase visualisation, different scales are used.

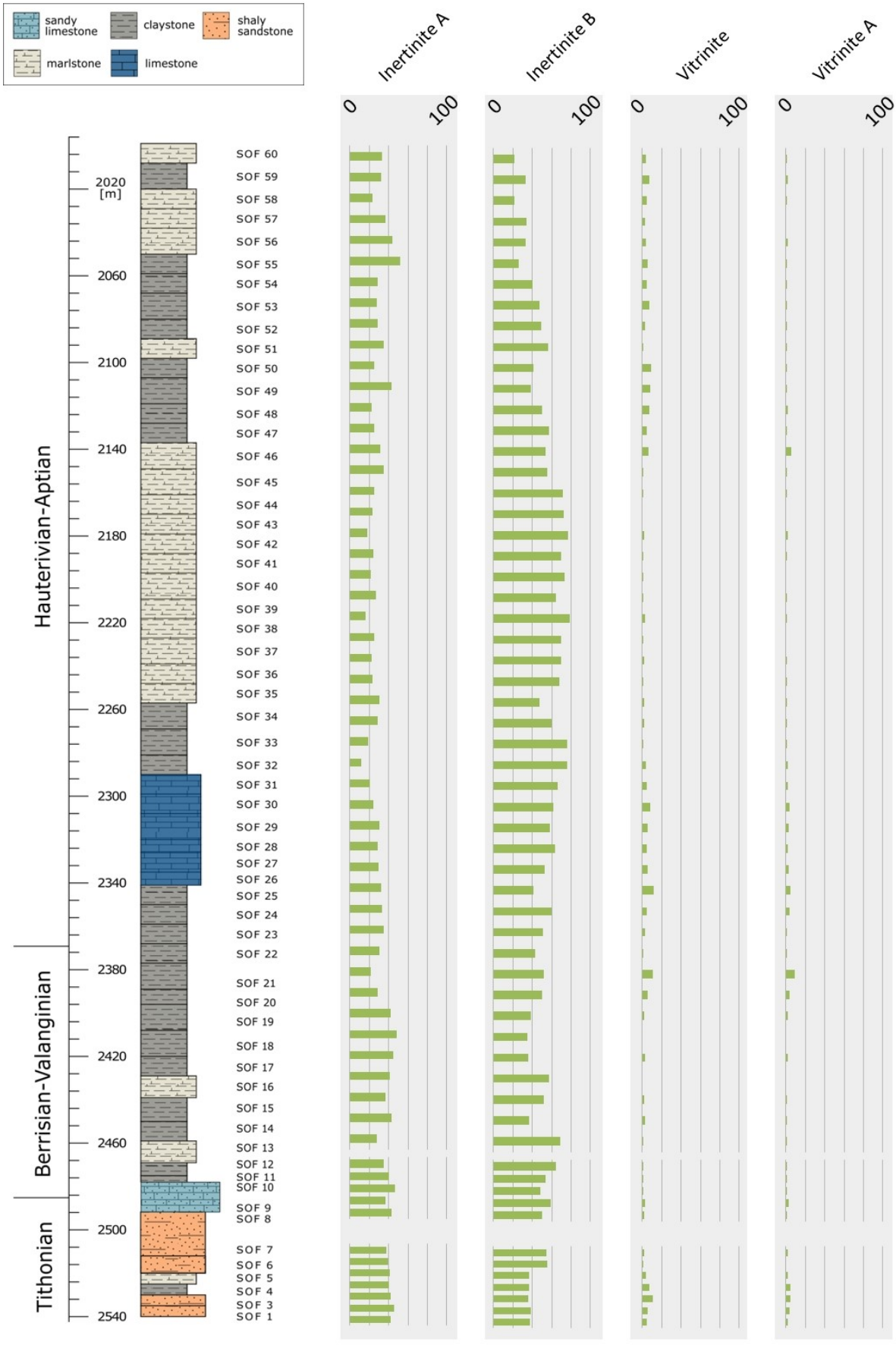

Figure 94: Sedimentary organic matter – terrestrial fraction continued; Sofia 1 core. Values given in %, to increase visualisation, different scales are used.

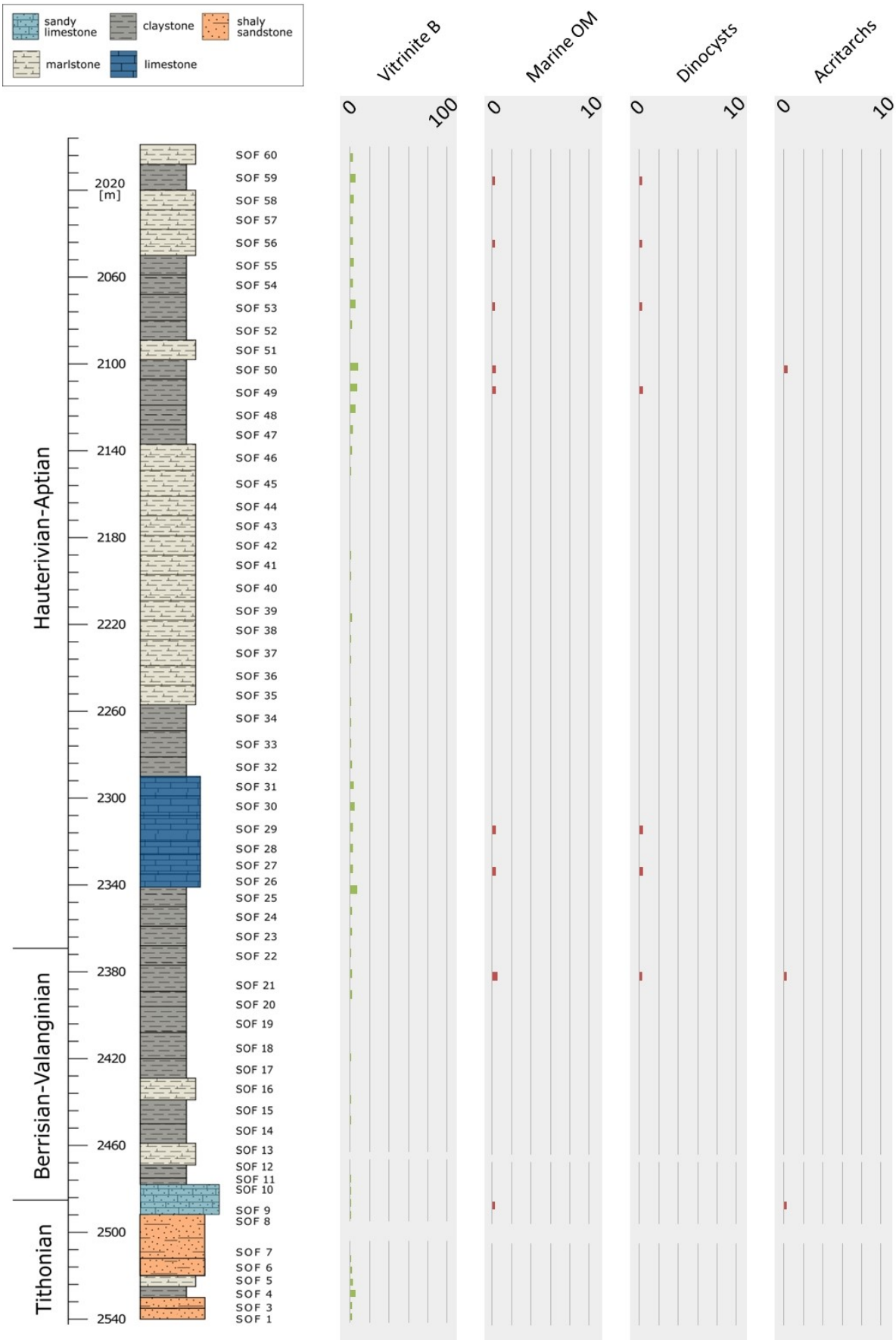

Figure 95: Sedimentary organic matter – Vitrinite B and marine fraction; Sofia 1 core. Values given in %, to increase visualisation, different scales are used.

AOM-PHYTOCLAST-PALYNOMORPH PLOT

Tithonian: All samples of the Tithonian interval (SOF 1–9) plot in palynofacies field I – highly proximal shelf or basin (Fig. 96).

Berriasian–Valanginian: The samples of the Berriasian–Valanginian section (SOF 10–22) plot exclusively in palynofacies field I – highly proximal shelf or basin (Fig. 96).

Hauterivian–Aptian: Most samples of the Hauterivian–Aptian interval (SOF 23–60) plot in palynofacies field I – highly proximal shelf or basin. One sample (SOF 54) plots in palynofacies field III – heterolithic oxic shelf ("proximal shelf") (Figs. 96, 97).

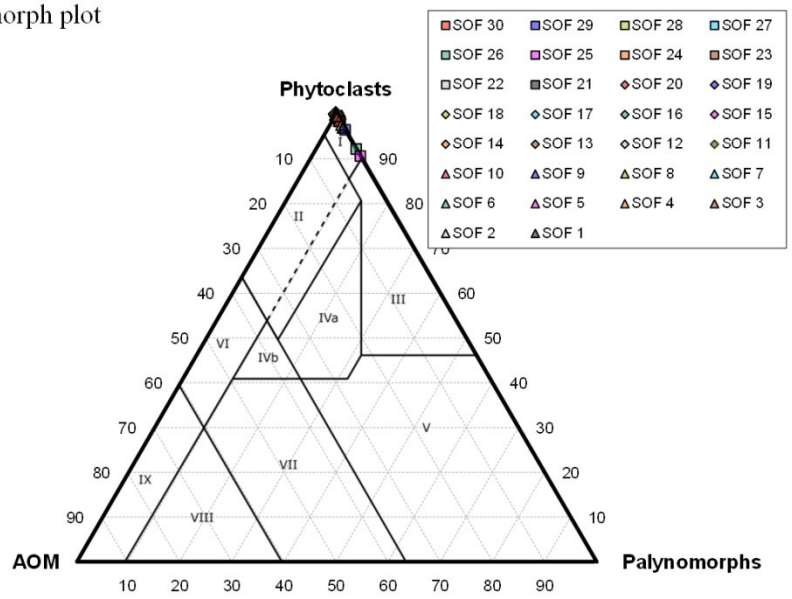

Figure 96: AOM-phytoclast-palynomorph plot of SOF 1–SOF 30; key to the palynofacies fields given in table 2 (p. 49).

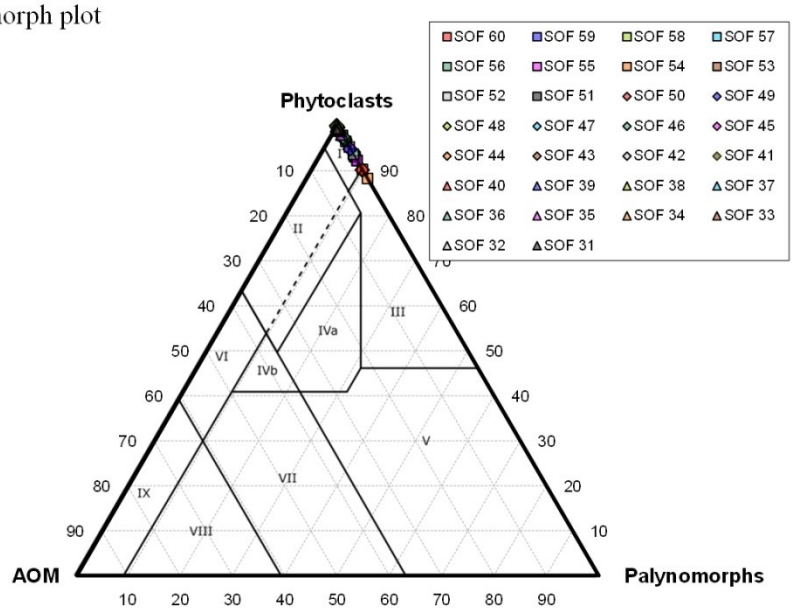

Figure 97: AOM-phytoclast-palynomorph plot of SOF 31–SOF 60; key to the palynofacies fields given in table 2 (p. 49).

TOTAL ORGANIC CARBON, TOTAL INORGANIC CARBON, CARBON/SULPHUR/ NITROGEN

60 samples of the Sofia 1 core were analysed for their carbon, nitrogen and sulphur content (Fig. 98).

Total organic carbon: The Tithonian section of the Sofia 1 shows a TOC content that varies between 0.13 % and 0.37 %. A mean proportion of 0.23 % (SD=0.07 %) is identified. A discontinuously increasing trend is identified. The Berriasian–Valanginian section of the Sofia 1 shows a TOC content that varies between 0.24 % and 1.9 %. After a peak of 1.9 % in the lower part of the section TOC content decreases inhomogeneous throughout the remainder of the interval. A mean proportion of 0.65 % (SD=0.46 %) is identified. The Hauterivian–Aptian section of the Sofia 1 shows a TOC content that varies intensely between 0.13% and 0.65 %. Several intermittent peaks are observed. A mean proportion of 0.27 % (SD=0.12 %) is identified. A distinct trend is not observed.

Total inorganic carbon: TIC content shows a peak in the lower part of the Tithonian interval where a maximum of 2.2 % is observed. Throughout the interval proportion varies significantly between 0.17–2.2 %. The mean proportion for this interval is 0.74 % (SD=0.65 %). A distinct trend is not observed. TIC content is highest in the lower part of the Berriasian–Valanginian interval where a peak of 2.5 % is identified. The proportion varies significantly between 0.16–2.5 %. The mean proportion for this interval is 0.72 % (SD=0.59 %). A distinct trend is not observed. In the Hauterivian–Aptian section TIC content is highest in the middle part of the analysed interval. Two peaks show a maximum of 4.1 % and 2.4 %. Proportion varies intensely between 0.34–4.1 %. The mean proportion for this interval is 1.3 % (SD=0.82 %). A distinct trend is not observed.

$CaCO_3$: In the lower part of the Tithonian interval the $CaCO_3$ content shows a peak of 18.5 %. Throughout the section the content varies intensely between 1.4–18.5 %. The mean proportion for this interval is 6.2 % (SD=5.4 %). A distinct trend is not observed. A significant peak of $CaCO_3$ content (20.5 %) is identified in the lower part of the Berriasian–Valanginian. Throughout the interval proportion varies significantly between 1.3–20.5 %. The mean proportion for this interval is 6 % (SD=4.9 %). A distinct trend is not observed. In the Hauterivian–Aptian section $CaCO_3$ content is highest in the middle part of the analysed interval. Two peaks are identified showing contents of 34.1 % and 24.2 %. Proportion varies intensely between 2.8–34.1 %. The mean proportion for this interval is 11 % (SD=6.9 %). A distinct trend is not observed.

Nitrogen: In the Tithonian interval nitrogen proportion increases inconsistently from 0.017 % to 0.028 %. The mean proportion is 0.002 % (SD=0.006 %). In the Berriasian–Valanginian section of the Sofia 1 core interval nitrogen proportion varies between 0.021–0.045 %. The mean proportion is 0.033 % (SD=0.008 %). A trend is not observed. In the Hauterivian–Aptian interval nitrogen proportion varies intensely between 0.003 % and 0.032 %. The mean proportion is 0.02 % (SD=0.01 %). A trend is not observed.

Sulphur: A peak of sulphur content is detected in the upper part of the Tithonian interval where a proportion of 2.2 % is reached. Overall, the content varies significantly between 0.33 % and 2.2 %. A mean proportion of 0.86 % (SD=0.57 %) is observed. The distribution pattern shows no unequivocal trend. In the Berriasian–Valanginian section sulphur content varies between 0.62 % and 1.3 %. A mean proportion of 0.87 % (SD=0.23 %) is observed. The distribution pattern shows no clear trend. Highest sulphur content in the Hauterivian–Aptian interval is detected in the lower middle–

middle part of the interval where a proportion of 1.5 % is reached. Content varies significantly between 0.11 % and 1.4 %. A mean proportion of 0.5 % (SD=0.47 %) is observed. The distribution pattern shows no unequivocal trend.

C_{org}/N: In the Tithonian section the C/N ratio is relatively homogenous and ranges from 13–17. A mean value of 15 is observed. An unequivocal trend is not identified. The C/N ratio of the Berriasian–Valanginian interval varies between 8 and 42 and is highest in the lower part of the interval. An average value of 19 is observed. An unequivocal trend is not identified. In the Hauterivian–Aptian section of the Sofia 1 the C/N ratio fluctuates intensely between 5 and 122. Peaks are identified in the middle (76) and uppermost (122) part of the interval. A mean value of 19 is observed. An unequivocal trend is not identified.

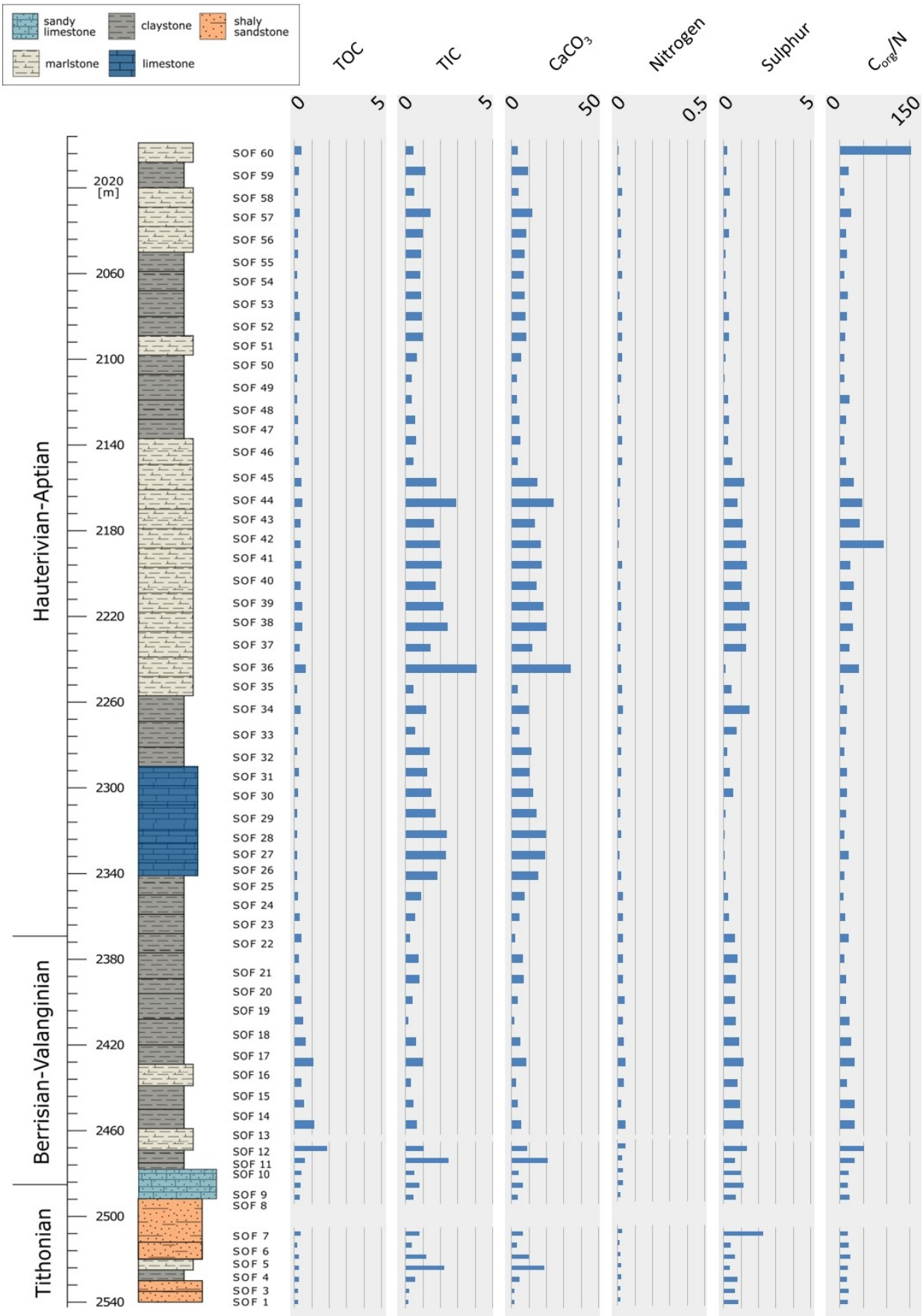

Figure 98: Results of the TOC, TIC and CNS analyses; Sofia 1 core. . Except for C_{org}/N, values given in %, to increase visualisation, different scales are used.

THERMAL MATURITY

Thermal maturation is characterised using the Thermal Alteration Index (TAI) or Spore Coloration Index (SCI). Analysis was performed on 4 samples (SOF 1, SOF 25, SOF 46, SOF 59). Samples show a TAI of approximately 4 to 5-/SCI of 9.5-10.0 (Ro% 2.5–3). The resulting maturation stage is metagenesis (cf. Suárez-Ruiz et al., 2012).

MICRO-GLENDONITES

17 samples contained micro-glendonites (selected specimens shown in figures 99–102). They are absent in the Tithonian and Berriasian part of the section, but occur relatively continuously throughout the Hauterivian–Aptian part of the interval. A total of 195 specimens are recorded and measured, with individual diameters ranging from 5 µm to 165 µm and a mean size of 60.1 µm (SD=27.2 µm).

Figures 99–102: selected micro-glendonite specimens of the Sofia 1 core – Fig. 99: SOF 33; Fig. 100: SOF 39; Fig. 101: SOF 39; Fig. 102: SOF 39; scale bars given in the photographs.

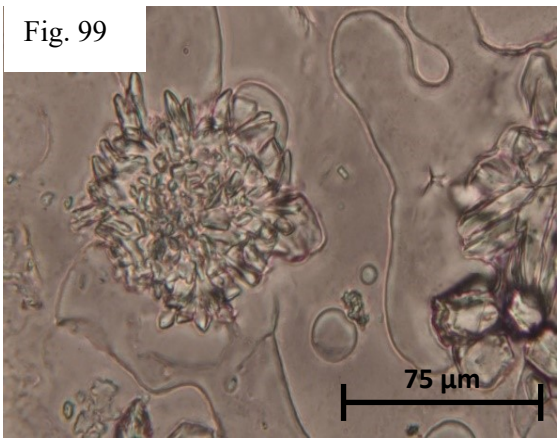

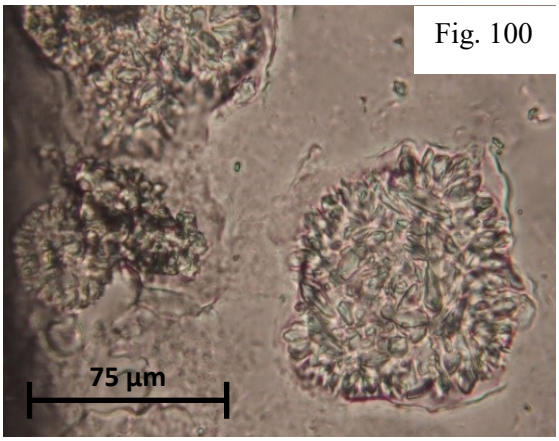

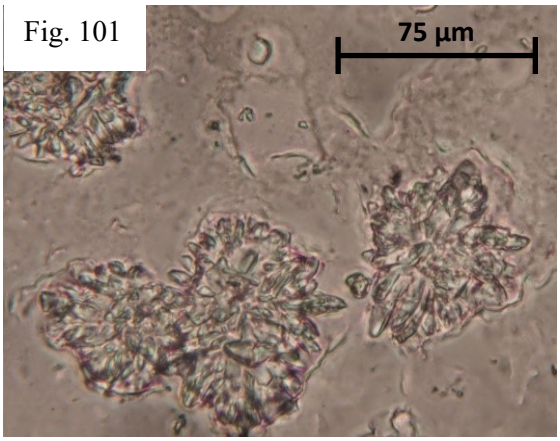

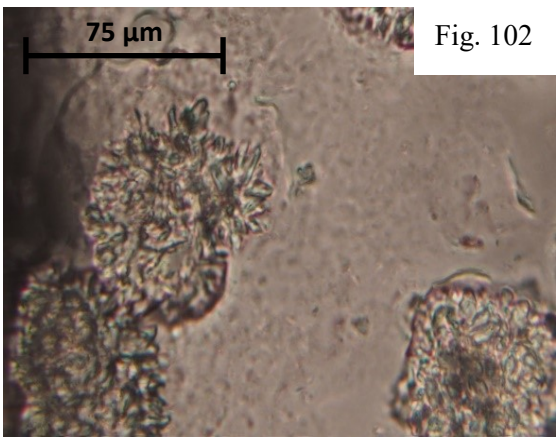

4.3 ANTARCTICA

A total of 129 samples are analysed from Middle Tithonian to Early Albian sediments of Antarctica. 98 samples belong to sections of Byers Group on Livingston and Snow Islands (Middle Tithonian–Middle Valanginian). 21 samples ranging from the Middle Tithonian to Late Aptian originate from the Fossil Bluff Group on Alexander Island. 10 samples were analysed from James Ross Island, including the Tithonian Nordenskjöld Formation and the Aptian/Albian Gustav Group.

BYERS GROUP

PALYNOFACIES ANALYSIS

Samples were analysed from 13 individual sections of the Byers Group. Results were combined to one composite section ranging from the Middle Tithonian to Middle Valanginian (cf. Pirrie & Crame, 1995; Duane, 1996; Hathway & Lomas, 1998) (Figs. 103–107). The Middle Tithonian interval is represented by sections P.2225 and P.2223 and comprises 21 samples. The Lower Berriasian–Middle Berriasian sediment sequence comprises the sections P.2183, P.2176, P.2222, P.2220 and P.2224. A total of 35 samples are analysed. The subsequent interval represents the Late Berriasian to Early Valanginian and contains a total of 19 samples of sections P.2171, P.2173, P.2172, P.2174 and P.2175. The uppermost 23 samples represent the Early to Middle Valanginian interval and comprise the P.2186 section of Snow Island.

Terrestrial organic matter

Anchorage Formation - Middle Tithonian

The organic matter composition of 19 samples assigned to the Middle Tithonian Anchorage Formation of Livingston Island is dominated by terrestrial organic matter. The content ranges between 69 % and 100 %. The 69 % low is detected in the upper middle part of the sampled section. A distinct trend in frequency distribution is not observed. The mean abundance of terrestrial organic matter is 96.7 % (SD=7.1 %). In two samples of this interval (P.2223.47 and P.2223.25 B) organic matter is absent and palynofacies preparations only consist of mineral detritus.

Sporomorphs: Sporomorph abundance varies between 0–1.8 %. Two intermittent positive peaks are identified and reach 16.5 % in the lowermost part of the interval and 8.8 % in the upper part of the section. A distinct trend is not observed. Sporomorphs reach an average abundance of 1.7 % (SD=4.1 %). The proportion of well-preserved sporomorphs varies between 0–8.9 %. A mean content of 0.98 % (SD=2.6 %) is reached. Two major positive peaks are detected. A distinct trend is not observed. Fairly preserved sporomorphs show a proportion that varies between 0 % and 5.9 %. A peak of 5.9 % is identified in the lowermost part of the interval. A mean content of 0.56 % (SD=1.4 %) is observed. The proportion of poorly preserved sporomorphs remains low and varies between 0–1.6 % (the most frequent occurrences are observed in the lower part of the interval). The mean content is 0.19 % (SD=0.41 %).

Phytoclasts: The proportion of phytoclasts varies significantly between 49.1 % and 92.1 %. The distribution pattern shows no unequivocal trend. The mean proportion of this interval is 73 % (SD=13.7 %).

Inertinite: Content of inertinite varies intensely between 44.3–88.9 %. A distinct trend is not observed. The mean proportion of this interval is 68 % (SD=14.6 %). Well-preserved inertinite shows a highly fluctuating content that ranges from 25.7 % to 59.5 %. A distinct trend is not observed. The mean content is 39.9 % (SD=9.2 %). The Middle Tithonian Anchorage Formation shows a mean content of fairly preserved inertinite of 28.1 % (SD=11.8 %). The abundance varies intensely between 8.9–48.3 %. A clear trend is not detected.

Vitrinite: Content of vitrinite ranges between 0–30 %. One intermittent peak is identified in the lowermost part of the section. A mean proportion of 4.4 % (SD=6.7 %) is observed. The frequency distribution shows no unequivocal trend. The content of well-preserved vitrinite varies between 0–4.3 %. The mean content is 0.49 % (SD=0.97 %). The proportion of well-preserved vitrinite shows no trend. A significant positive peak of 4.3 % is identified in the lowermost part of the interval. The content of fairly preserved vitrinite varies between 0–25.7 %. A major positive peak of 25.7 % is present in the lowermost part of the interval. A mean proportion of 3.9 % (SD=5.9 %) is detected.

Cutinite: Content of cutinite is continuously low and varies between 0–4.4 %. Several intermittent peaks are observed. A trend is not identified. The average proportion is 0.6 % (SD=1.3 %).

Fungal filaments: Only one sample of the lowermost part of the Middle Tihonian Anchorage Formation contains fungal remains, where a content of 2.4 % is reached. The rest of the interval is free of fungal filaments resulting in a mean content of 0.13 % (SD=0.56 %).

Terrestrial AOM: The proportion of $AOMT_{translucent}$ fluctuates intensely between 1 % and 50.5 %. A mean content of 20.35 % (SD=14.7 %) is detected and a trend in distribution pattern is not observed. Proportion of $AOMT_{opaque}$ varies between 0–8.7 %. The mean abundance is 1.43 % (SD=2.1 %). An indistinct trend is not detected. A mean content of 21.8 % (SD=14.7 %) is identified for the abundance of $AOMT_{total}$. The proportion varies between 1–50.9 %.

President Beaches Formation – Early–Middle Berriasian

The 35 samples of the Early Berriasian President Beaches Formation of Livingston Island are characterised by large amounts of terrestrial organic matter. The proportion varies between 69.8 % and 99.8 %. A strongly discontinuous trend is observed. The mean abundance of terrestrial organic matter in this interval is 88.8 % (SD=7.5 %).

Sporomorphs: Proportion of sporomorphs fluctuates intensely throughout the whole interval. Variations between 0 % and 35.5 % are observed. The mean content is 11.5 % (SD=9.3 %). The distribution pattern shows no clear trend. Well-preserved sporomorphs show a content ranging from 0–28 % resulting in a mean proportion of 4.7 % (SD=6.8 %). A distinct trend is not observed. The content of fairly preserved sporomorphs varies significantly between 0 % and 13.3 %. The frequency distribution shows no distinct trend. A mean content of 5.4 % (SD=4.1 %) is identified. The abundance of poorly preserved sporomorphs varies between 0–5.7 %. An unequivocal trend is not observed. The average proportion is 1.4 % (SD=1.6 %).

Phytoclasts: The proportion of phytoclasts varies between 42.9 % and 90.9 %. Several positive and negative peaks are observed. A mean abundance of 57.6 % (SD=15.5 %) is detected. The frequency distribution shows no clear trend.

Inertinite: Throughout the Early–Middle Berriasian interval the content of inertinite varies significantly between 2.6–87 %. Particularly the middle part of the interval is characterised by highly a fluctuating value. A clear trend is not observed. The mean proportion of this interval is 33.4 % (SD=23.3 %). Well-preserved inertinite reaches a mean proportion of 20.8 % (SD=12.1 %). A distinct rend is not observed. The content in the middle part of the interval fluctuates intensely between 3.5 % and 50.6 %. The overall content of well-preserved inertinite varies between 2.6–50.6 %. Content of fairly preserved inertinite shows an average of 12.6 % (SD=12.7 %). The proportion ranges from 0–45.9 %. A trend is not observed.

Vitrinite: The content of vitrinite in the Early–Middle Berriasian interval of Livingston Island fluctuates highly between 1.84 % and 46.1 %. The mean proportion is 22.8 % (SD=12.8 %). The frequency distribution shows no distinct trend. The content of well-preserved vitrinite ranges from 0–24.5 %. A trend is not observed and the average content of the interval is 8.7 % (SD=6.9 %). The content of fairly preserved vitrinite varies between 1.3 % and 42.3 %. The distribution pattern shows no unequivocal trend. The mean proportion of fairly preserved vitrinite in this section is 14.1 % (SD=8.9 %).

Cutinite: Where present, the proportion of cutinite varies between 0.3–11.2 %. A mean content of 1.4 % (SD=2.7 %) is detected. A clear trend is not observed.

Fungal filaments: The proportion of fungal remains varies between 0–2 %. Overall, the content remains low and an average of 0.31 % (SD=0.57 %) is observed. A distinct trend is not detected.

Terrestrial AOM: In the Early–Middle Berriasian section of Livingston Island $AOMT_{translucent}$ shows a mean content of 19.3 % (SD=9.3 %). The proportion fluctuates between 3 % and 39.6 %. The frequency distribution shows a discontinuously decreasing trend. Occurrences of $AOMT_{opaque}$ are scarce. Where present, samples reach a proportion between 0.31–2.3 %. The average content of this interval is 0.18 % (SD=0.45 %). The proportion of $AOMT_{total}$ varies between 3–39.6 %. The mean abundance of $AOMT_{total}$ is 19.4 % (SD=9.1 %).

Chester Cone Formation (Devils Point Member) – Late Berriasian–Early Valanginian

19 samples were analysed of the Late Berriasian to Early Valanginian Devils Point Member of the Chester Cone Formation of Livingston Island. Terrestrial organic matter shows a discontinuously increasing trend from 87.3 % to 97.1 %. The content varies between 85.7–100 %. The mean proportion for this interval is 94.1 % (SD=4.8 %).

Sporomorphs: Sporomorph abundance is highest in the lowermost part of the interval where the content varies between 15–25.3 %. Upsection, the proportion decreases to 1 % in the upper lower to lower middle part of the section. From there on the proportion varies between 0 % and 7.5 %. An overall discontinuously decreasing trend is observed. Sporomorphs reach an average content of 5.5 % (SD=7.8 %). Abundance of well-preserved sporomorphs varies between 0–19.4 %. Throughout the lower part of the interval the content decreases significantly from 19.4 % to 0.34 %. A mean content

of 3.1 % (SD=6 %) is identified. Fairly preserved sporomorphs show a highest proportion in the lower part of the interval where the percentage varies between 3.8–7.6 %. Subsequently the abundance remains low and varies between 0–1.2 %. A mean content of 1.4 % (SD=2.2 %) is detected. Except for two major peaks of 6.7 % and 5.4 % in the middle part of the interval the proportion of poorly preserved sporomorphs remains low and varies between 0–2 %. A mean content of 1 % (SD=2 %) is observed.

Phytoclasts: The proportion of phytoclasts fluctuates significantly between 16–95.5 %. The frequency distribution shows an inhomogeneous increasing proportion. A mean content of 66.6 % (SD=18.9 %) is identified.

Inertinite: Although significantly varying, the occurrence of inertinite in the lower part of the interval is significantly lower (4–13.9 %) than in the upper part where the content varies between 58–92.8 %. The average proportion for the whole interval is 53.6 % (SD=29.3 %). Well-preserved inertinite shows an average proportion of 31.8 % (SD=19.1 %). The content fluctuates intensely and ranges from 3.7 % to 60.2 %. A highly discontinuous increasing trend is observed. The abundance of fairly preserved inertinite varies significantly between 0.25 % and 49.7 %. The lower part of the section contains lower amounts of fairly preserved inertinite than the upper part of the section. After a peak of 49.7 % is reached in the middle part of the interval the proportion decreases inhomogeneous throughout the remainder of the succession. The average content of fairly preserved inertinite in the Upper Berriasian to Lower Valanginian Devils Point Member of the Chester Cone Formation is 21.9 % (SD=15.9 %).

Vitrinite: In the Late Berriasian to Early Valanginian section of Livingston Island content of vitrinite varies strongly between 0.32 % and 42.9 %. The lower part of this interval shows significantly higher abundance (35.9–42.9 %) than the middle and upper part where the content varies between 0.32–12.2 %. The mean content is 12.1 % (SD=14.4 %). The content of well-preserved vitrinite varies in the lower part of the interval between 24.2–31.8 %. Subsequently a sharp decrease to 0 % is identified. In the remainder of the interval the content varies between 0–5 %. An average proportion of 6.8 % (SD=11 %) is observed. Content of fairly preserved vitrinite fluctuates intensely between 0.32 % and 11.7 %. The highest proportion is identified in the lower part of the interval. A mean content of 5.3 % (SD=3.9 %) is observed.

Cutinite: In the lower part of the interval a sharp increase in abundance to 8.5 % is detected. Subsequently cutinite content varies between 0–0.35 %. Overall an average proportion of 0.93 % (SD=2.3 %) is identified.

Fungal filaments: Distribution of abundance of fungal remains shows two samples of increased value (29.3 % and 15.4 %) in the lower part of the interval. In the middle part of the succession a minor peak of 7.1 % is detected. A mean abundance of 3 % (SD=7.4 %) is observed. A trend in frequency distribution is not identified.

Terrestrial AOM: Throughout the Late Berriasian to Early Valanginian section of Livingston Island the content of $AOMT_{translucent}$ fluctuates intensely between 4.5–39.4 %. The mean content is 18.7 % (SD=8.7 %). The content of $AOMT_{opaque}$ is continuously low and reaches a maximum of 4.4 % in the lower middle part of the section. Apart from that the proportion varies between 0 % and 0-66 %. The average content for this interval is 0.34 % (SD=1 %). A distinct trend is not observed. The

proportion of $AOMT_{total}$ varies between 4.5 % and 53.7 %. The mean abundance is 19.1 % (SD=8.3 %).

Chester Cone Formation (Sealer Hill Member) – Early to Middle Valanginian

23 samples were analysed of the Early to Middle Valanginian Sealer Hill Member of the Chester Cone Formation on Snow Island. The organic matter content is dominated by terrestrial organic matter. The abundance varies between 77.8–92.1 %. The frequency distribution shows no distinct trend. The average proportion is 86.8 % (SD=4.1 %).

Sporomorphs: The occurrence of sporomorphs shows no distinct trend. A significant nadir of 1.2 % is identified in the lowermost part of the succession. The overall abundance of sporomorphs varies between 1.2–32.4 %. The proportion reaches an average content of 21.7 % (SD=6.7 %). Content of well-preserved sporomorphs fluctuates intensely between 0.3 % and 25.7 %. A mean content of 13.4 % (SD=6.3 %) is observed. The proportion of fairly preserved sporomorphs fluctuates intensely and ranges from 0–15 %. The distribution pattern shows no distinct trend. A mean content of 7.8 % (SD=4.3 %) is detected. The abundance of poorly preserved sporomorphs fluctuates intensely between 0–2.3 %. The content increases sharply in the uppermost part of the interval but a distinct trend is not observed. The mean content is 0.53 % (SD=64 %).

Phytoclasts: The content of phytoclasts is continuously high but decreases throughout the interval from 52.8 % to 29.9 %. Two peaks are detected in the lower (69 %) and upper (60.5 %) part of the section. The mean content is 44.3 % (SD=9 %).

Inertinite: Inertinite abundance varies between 2.9–65.5 %. Two positive peaks are identified in the lower (65.5 %) and upper (48 %) part of the succession. An average content of 15.5 % (SD=14.9 %) is observed. The proportion of well-preserved inertinite shows a maximum of 41.7 % in the lower part of the section. Throughout the remainder of the interval the proportion of well-preserved inertinite varies significantly between 3 % and 28.1 %. A mean content of 12.5 % (SD=9.5 %) is observed. Except for two peaks in the lower (23.8 %) and upper (19.9 %) part of the section, content of fairly preserved inertinite remains comparatively low and varies between 0–4.8 %. A mean content of 3 % (SD=6.1 %) is observed.

Vitrinite: The distribution of occurrence of vitrinite shows no distinct trend. The abundance ranges from 3.3–47 % and fluctuates intensely. A mean proportion of 26.9 % (SD=9.8 %) is observed. The content of well-preserved vitrinite varies significantly between 0.6 % and 29.1 %. A mean content of 17 % (SD=7 %) is identified. The distribution of occurrences shows no clear trend. Fairly preserved vitrinite shows an intensely fluctuating proportion (1.5–23.4 %). The mean content is 9.9 % (SD=6.1 %). An unequivocal trend is not observed.

Cutinite: Occurrences of cutinite are comparatively frequent. The proportion is highest in the middle part of the section but the value fluctuates intensely throughout the whole interval between 0–6.6 %. The average proportion for this stage is 1.9 % (SD=12 %). A distinct trend in distribution pattern is not observed.

Fungal filaments: Fungal remains are rare and the proportion varies between 0–1.1 %. A mean content of 0.22 % (SD=0.38 %) is identified. A distinct trend is not observed.

Terrestrial AOM: Throughout the Lower to Middle Valanginian section of the Chester Cone Formation the content of $AOMT_{translucent}$ fluctuates between 11.3–29.7 %. Except for the upper part where the content increases continuously the frequency distribution shows no distinct trend. The mean content for this interval is 20.6 % (SD=5.2 %). The content of AOM_{opaque} is continuously low. 2 samples in the lower part of the interval contain opaque AOM (0.60 % and 0.28 %). The average content for this interval is 0.04 % (SD=0.13 %). A distinct trend is not observed. The proportion of $AOMT_{total}$ ranges from 11.3 % to 29.7 %. The mean content is 20.6 % (5.2 %).

Marine organic matter

Anchorage Formation – Middle Tithonian

The proportion of marine organic matter in the Middle Tithonian section of Livingston Island is highest in the upper part of the interval. An individual peak of 31 % is identified in the upper middle part of the section. In the remainder of the interval abundance varies between 0 % and 8.3 %. The mean content of marine organic matter is 3.3 % (SD=7.2 %).

Dinoflagellate cysts: Content of dinocysts remains so low that the specimens are not differentiated according to the preservation state. Two samples of the upper middle and uppermost part of the interval contain dinoflagellate cyst remains with a proportion of 0.34 % and 0.30 %. A mean content of 0.03 % (SD=0.08 %) is detected for this section.

Acritarchs: One sample in the lower upper part of the Tithonian interval of Livingston Island contains acritarchs. Here, a content of 2 % is reached resulting in a mean content of 0.11 % (SD=0.46 %).

Algae indet.: Except for one sample in the lower upper part of the interval where undifferentiated algae reach an abundance of 28.6 %, the section is free of occurrences of algae indet. A mean proportion of 1.51 % (SD=6.6 %) is observed.

Marine AOM: The proportion of fluorescing AOM varies between 0–8.3 %. A mean content of 1.7 % (SD=2.5 %) is identified. The upper part of the interval shows a higher proportion of marine AOM but a distinct trend is not observed.

President Beaches Formation – Early–Middle Berriasian

Throughout the Early to Middle Berriasian section of Livingston Island, marine organic matter discontinuously increases from 3.3 % to 17.6 %. Several intermittent positive and negative peaks occur. A mean content of 10.5 % (SD=7.4 %) is detected.

Dinoflagellate cysts: In this interval dinocysts are observed in 8 samples ranging in abundance from 0.33–1.5 %. A mean content of 0.19 % (SD=0.39 %) is identified. A distinct trend in distribution pattern is not observed.

Acritarchs: The occurrence of acritarchs is restricted to 3 samples of the lower part of the interval. A mean content of 0.02 % (SD=0.08 %) is detected. Where present, the content of acritarchs varies between 0.23 % and 0.33 %. A clear trend is not observed.

Algae indet.: Throughout the lower, middle and lower upper part of the interval the content of undifferentiated algae varies significantly between 0–2.5 %. In the uppermost part of the section two peaks of 6.6 % and 7.1 % are detected. The distribution pattern is erratic. A mean proportion of 1.1 % (SD=1.6 %) is identified.

Foraminiferal test linings: Foraminiferal linings occur in 4 samples of this interval. Here, the abundance varies between 0.28 % and 0.50 % resulting in a mean content for this section of 0.04 % (SD=0.11 %). A pattern is not observed.

Leiospheres: One sample in the uppermost part of the Early to Middle Berriasian section contains leiospheres. A content of 0.60 % is detected. The mean proportion is 0.02 % (SD=0.10 %).

Marine AOM: Fluorescent marine AOM is identified in all samples of this interval. The proportion varies significantly between 0.2 % and 28.7 %. An average content of 9.1 % (SD=7.2 %) is detected. A distinct trend in distribution pattern is not observed.

Chester Cone Formation (Devils Point Member) – Late Berriasian–Early Valanginian

For the Late Berriasian–Early Valanginian section of Livingston Island marine organic matter shows a mean proportion of 5.3 % (SD=4.4 %). The content shows no clear trend and ranges from 0 % to 14.3 %.

Dinoflagellate cysts: Dinocysts are scarce and are only detected in two samples of the lower part of the section. The two samples contain a proportion of 0.95 % and 1 %. A mean content of 0.10 % (SD=0.31 %) is observed.

Acritarchs: Acritarchs occur in two samples of the lower part of the succession. Both samples reach a proportion of 0.27 %. The mean content of the interval is 0.03 % (SD=0.08 %).

Algae indet.: This group of sedimentary organic matter occurs mainly in the lowermost part of the section where the proportion decreases from 2.9 % to 0.54 %. Subsequently in the upper middle part if the interval one sample reaches a proportion of 0.66 %. A mean content of 0.37 % (SD=0.78 %) is observed.

Marine AOM: The proportion of marine AOM varies between 0–14.3 %. A maximum of 14.3 % is detected in the lower part of the succession. The content fluctuates intensely and shows no unequivocal trend. Several intermittent peaks are identified. A mean abundance of 4.8 % (SD=4 %) is observed.

Chester Cone Formation (Sealer Hill Member) – Early to Middle Valanginian

The content of marine organic matter fluctuates intensely between 7.3 % and 22.2 %. A strongly discontinuous increase from 9.4 % to 22.2 % is detected. The mean proportion for the Early to Middle Valanginian section of Snow Island is 12.4 % (SD=3.8 %).

Dinoflagellate cysts: Dinocysts occurrence is relatively frequent. The proportion remains low and varies between 0 % and 1.53 %. A mean content of 0.44 % (SD=0.48 %) is observed. The frequency distribution shows no distinct trend.

Acritarchs: 3 samples of the lower part and one sample in the middle part of the section contain acritarchs. Where present, proportion varies between 0.25–0.32 %. For the whole section an average abundance of 0.05 % (SD=0.11 %) is identified.

Algae indet.: Occurrences of undifferentiated algae are relatively frequent and fluctuate intensely between 0 % and 2.3 % The average content for the lower to Middle Valanginian sediment sequence of Snow Island is 0.98 % (SD=0.82 %).

Foraminiferal test linings: Foraminiferal remains are restricted to 3 samples in the lower part and one sample in the upper part of the interval. Proportion varies between 0.26 % and 0.32 %. A mean content of 0.05 % (SD=0.11 %) is detected. A trend is not observed.

Leiospheres: Content of leiospheres remains low and where present, the proportion reaches 0.22–0.81 %. A mean abundance of 0.12 % (SD=0.26 %) is identified for this interval. A trend is not observed.

Marine AOM: Content of marine AOM fluctuates intensely between 5.3–21.9 %. A positive peak is identified in the uppermost sample of this interval. A clear trend in distribution pattern is not observed. The mean content for this interval is 10.8 % (SD=4.1 %).

Opaque/translucent ratio

For the Middle Tithonian section an OP/TR ratio of 15.5 is detected. The OP/TR ratio of the lower–Middle Berriasian interval is 1.5. The OP/TR ratio of the Upper Berriasian–Lower Valanginian interval is 4.4. The OP/TR ratio of the lower–Middle Valanginian section is 0.6.

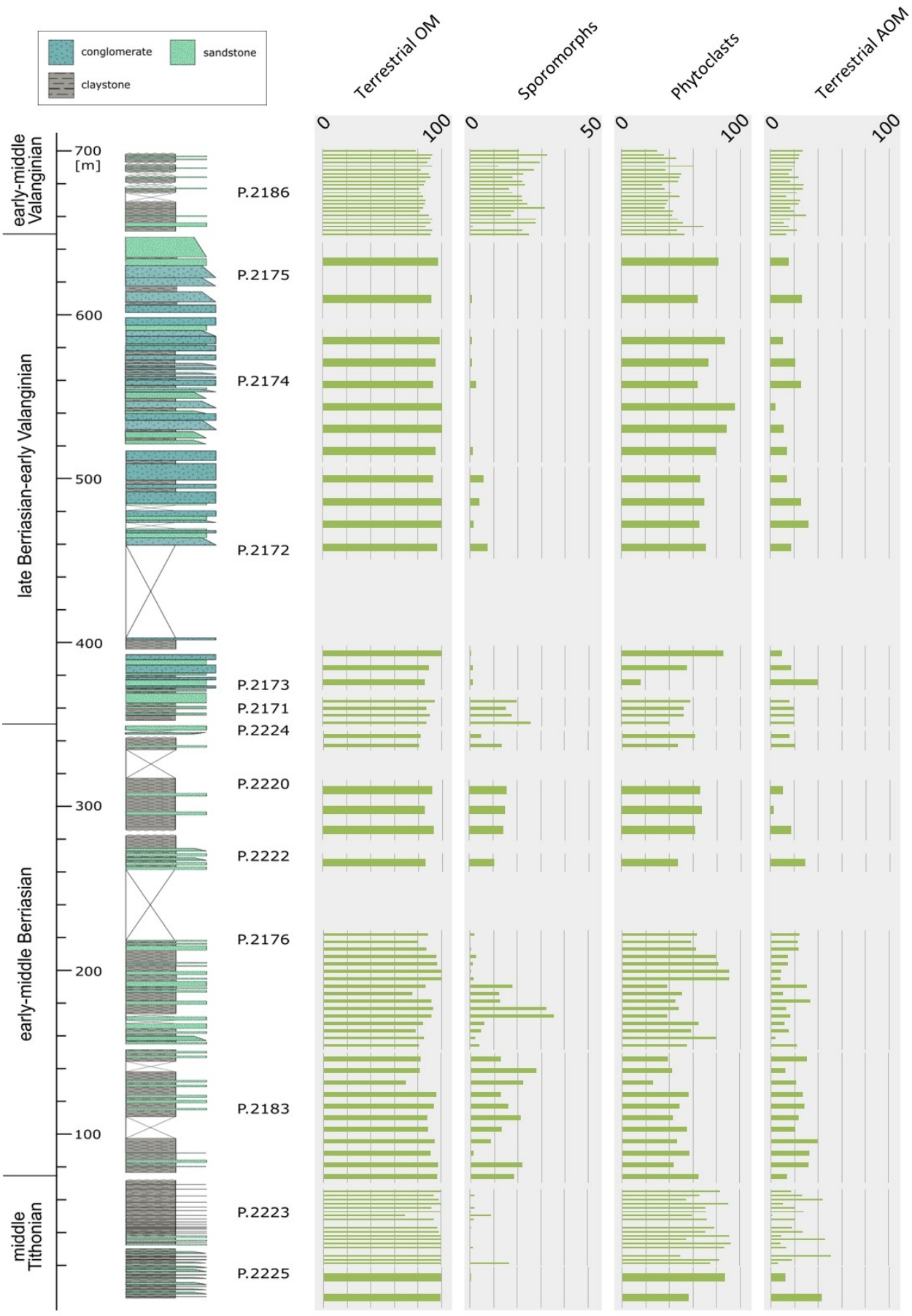

Figure 103: Sedimentary organic matter – terrestrial fraction; Byers Group. Values given in %, to increase visualisation, different scales are used.

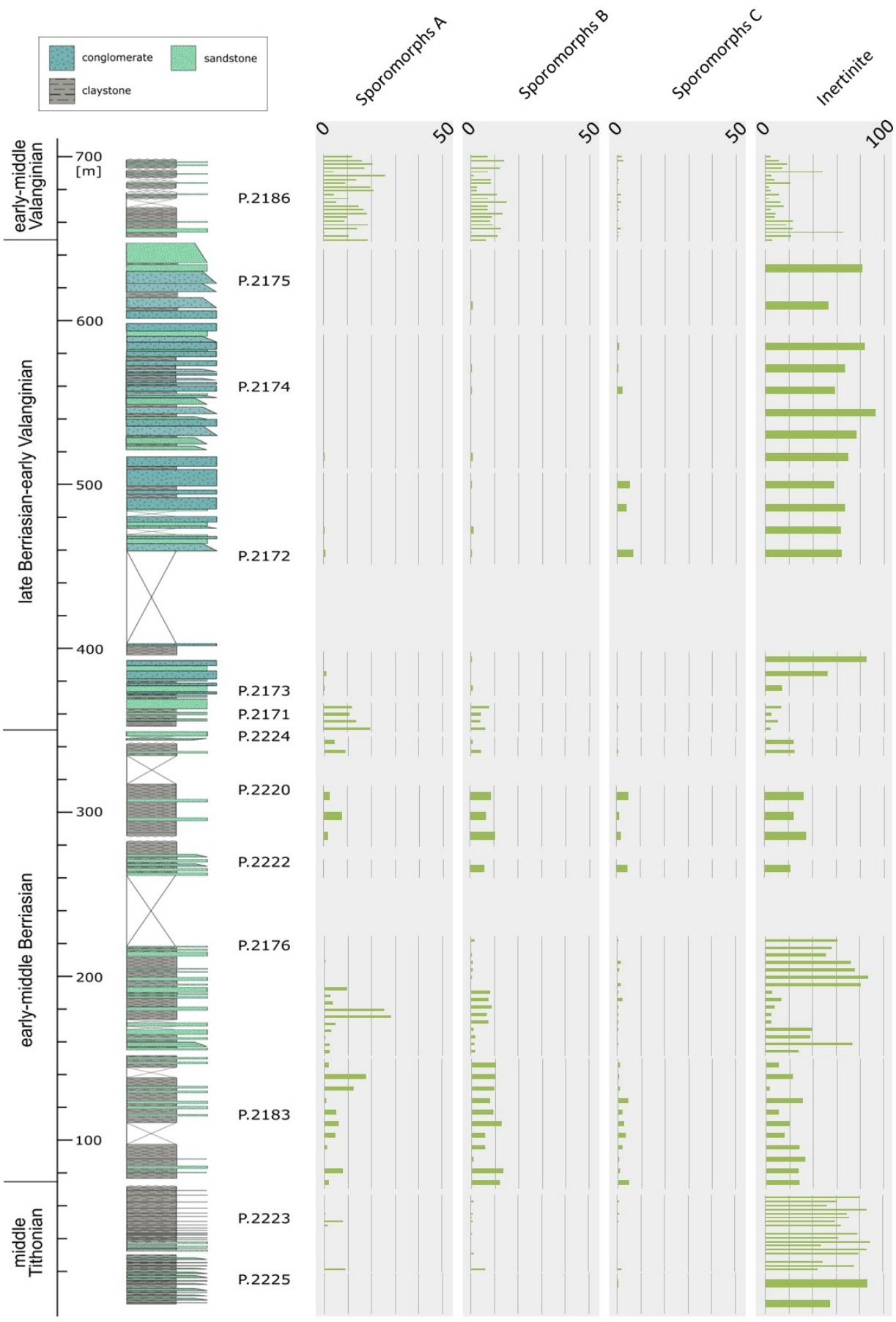

Figure 104: Sedimentary organic matter – terrestrial fraction continued; Byers Group. Values given in %, to increase visualisation, different scales are used.

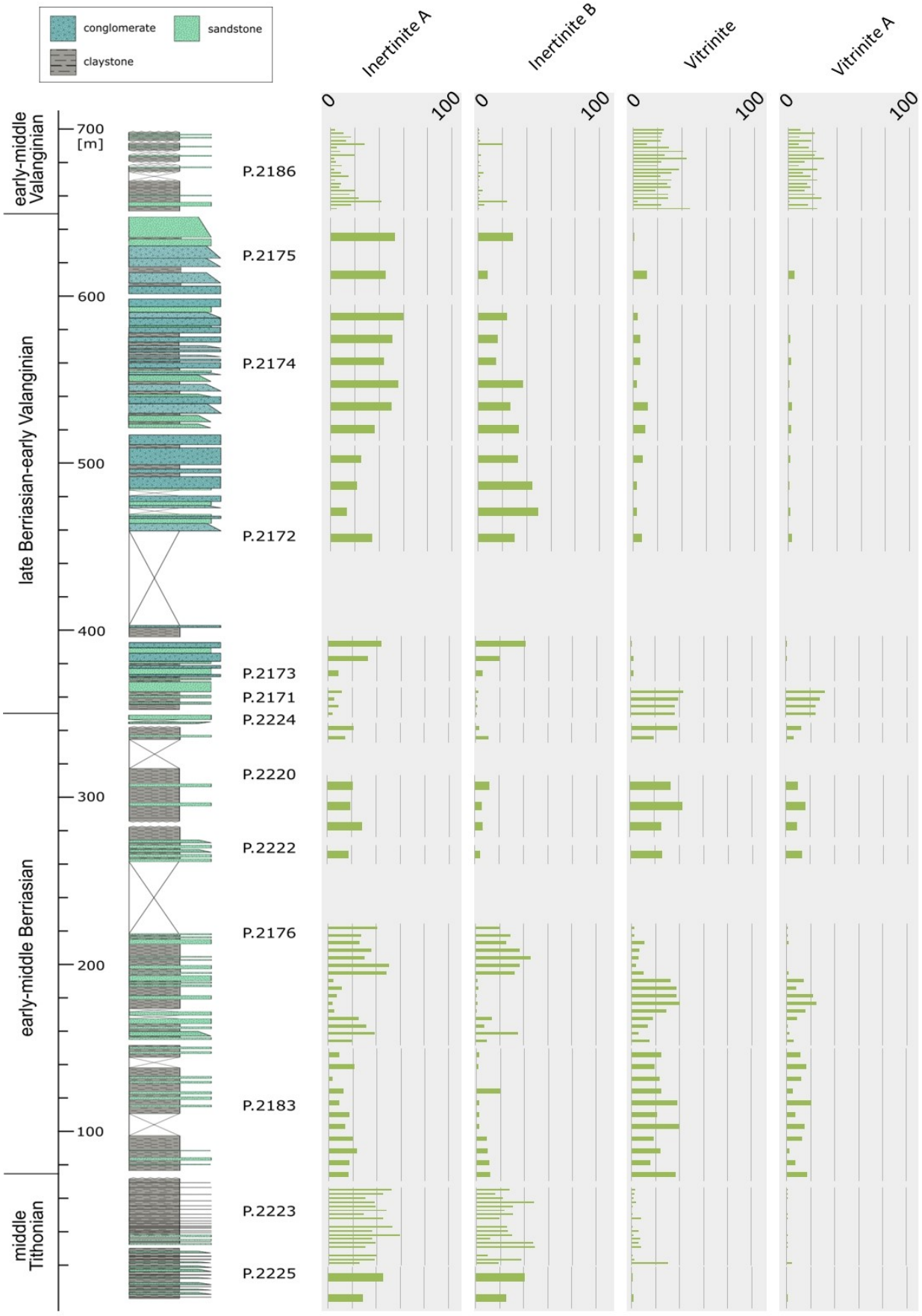

Figure 105: Sedimentary organic matter – terrestrial fraction continued; Byers Group. Values given in %, to increase visualisation, different scales are used.

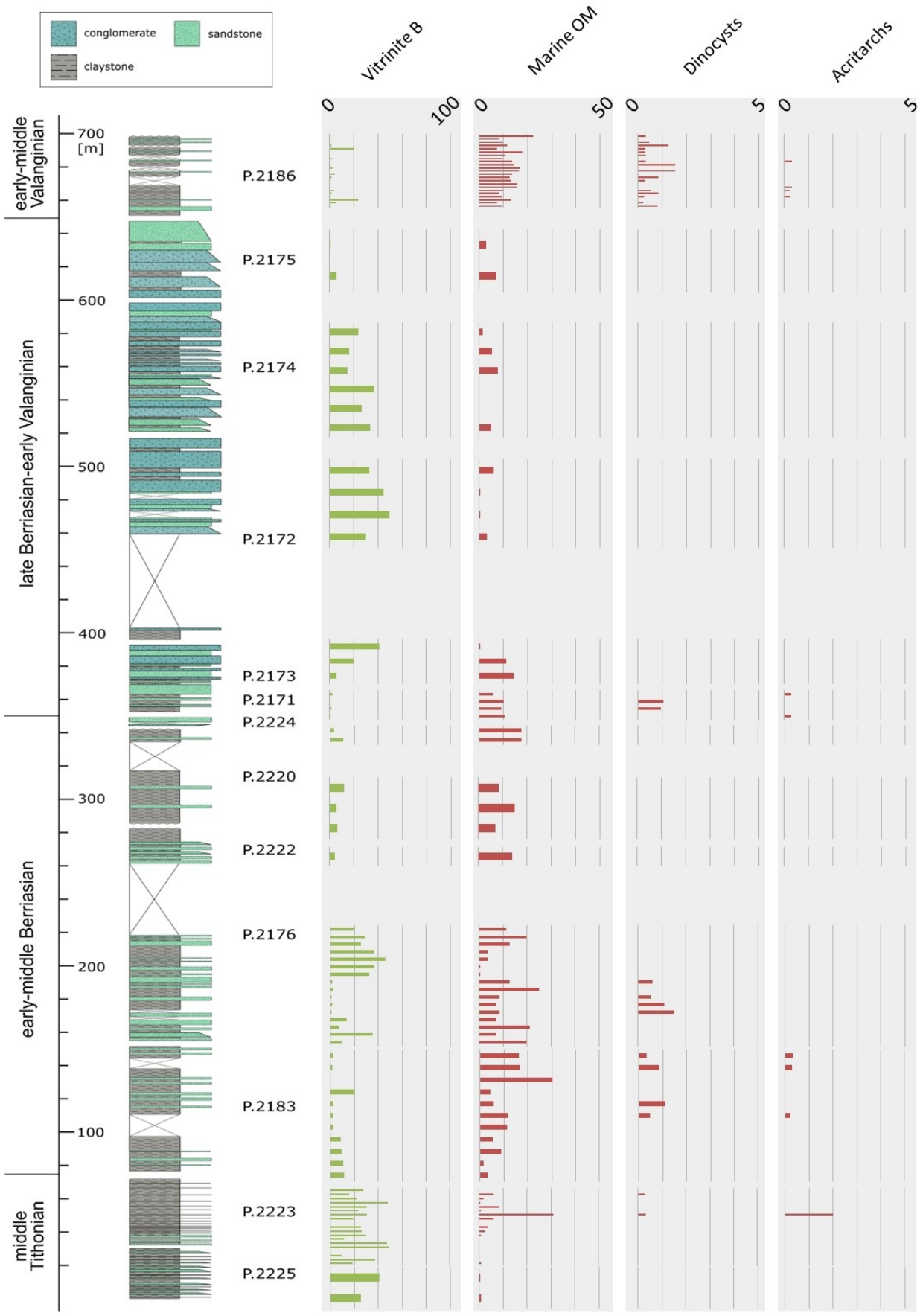

Figure 106: Sedimentary organic matter – Vitrinite B and marine fraction; Byers Group. Values given in %, to increase visualisation, different scales are used.

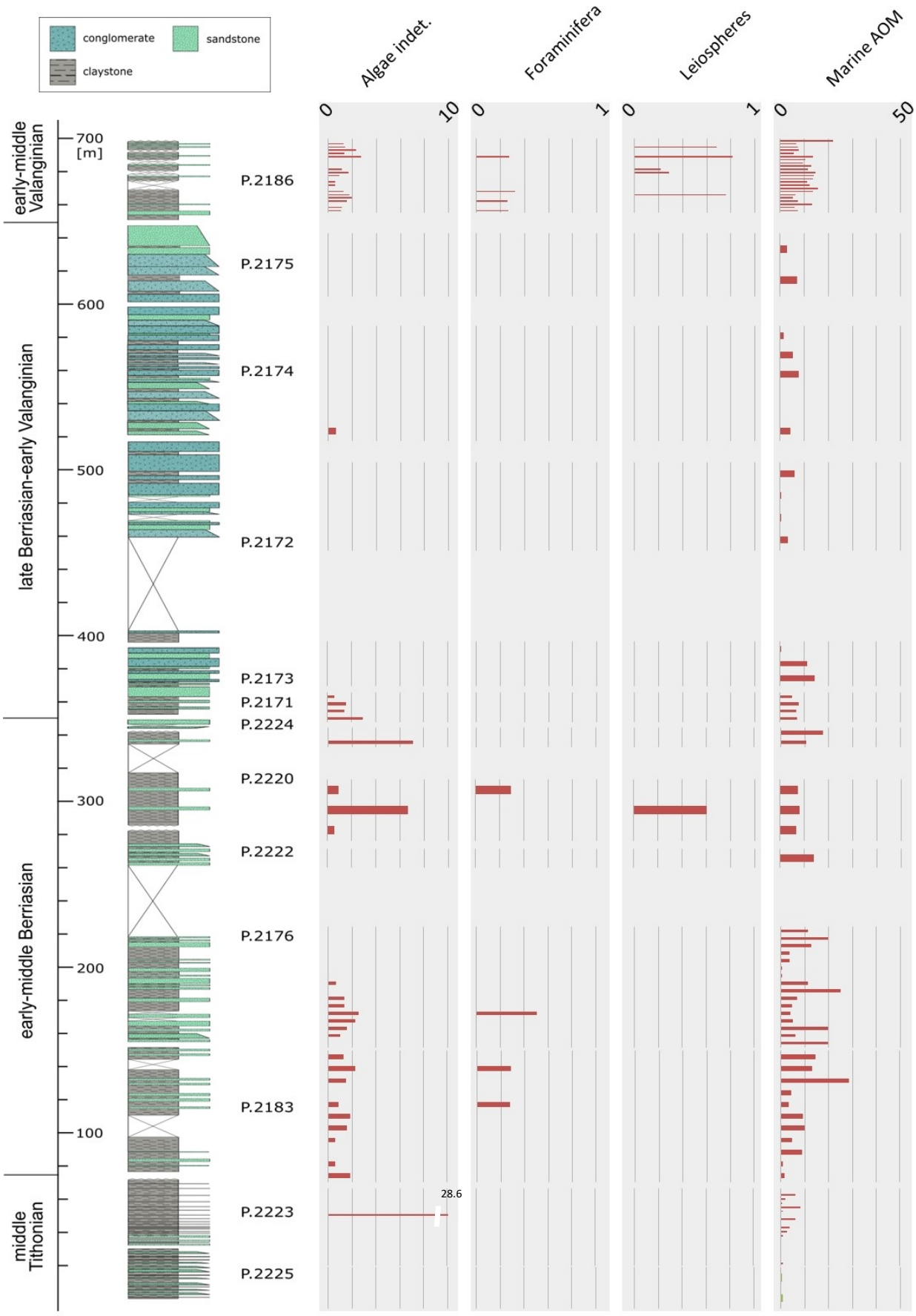

Figure 107: Sedimentary organic matter – marine fraction continued; Byers Group. Values given in %, to increase visualisation, different scales are used. Statistical outliers are marked accordingly.

AOM-PHYTOCLAST-PALYNOMORPH PLOT

Middle Tithonian: 15 samples of the Middle Tithonian interval (P.2225.3B–P.2223.72) plot in palynofacies field II – marginal dysoxic-anoxic basin. 2 samples plot in palynofacies field III – heterolithic oxic shelf ("proximal shelf") and 4 samples plot in palynofacies field VI – proximal suboxic-anoxic shelf (Fig. 108).

Early–Middle Berriasian: 14 samples of the Early–Middle Berriasian section (P.2183.1–P.2224.7) plot in palynofacies field II – marginal dysoxic-anoxic basin. Two samples plot in the palynofacies field III – heterolithic oxic shelf ("proximal shelf"). 11 samples plot in palynofacies fields IVa/b – shelf to basin transition. One sample plot in palynofacies field V – mud-dominated oxic shelf ("distal shelf"). 4 samples plot in palynofacies field VI – proximal suboxic-anoxic shelf and 3 samples plot in palynofacies field VII – distal dysoxic-anoxic "shelf" (Figs.109, 110).

Late Berriasian–Early Valanginian: One sample of the Late Berriasian–Early Valanginian section (P.2171.1–P.2175.7) plots in palynofacies field I – highly proximal shelf or basin. 12 samples plot in palynofacies field II – marginal dysoxic-anoxic basin. 5 samples plot in palynofacies fields IVa/b – shelf to basin transition and one sample plots in palynofacies field VII – distal dysoxic-anoxic "shelf" (Fig 111).

Early–Middle Valanginian: 2 samples of the Early–Middle Valanginian section (P.2186.1–P.2186.22) plot in palynofacies field II – marginal dysoxic-anoxic basin. One sample plots in palynofacies field III – heterolithic oxic shelf ("proximal shelf"). 12 samples plot in the palynofacies fields IVa/b – shelf to basin transition. 5 samples plot in the palynofacies field V – mud-dominated oxic shelf ("distal shelf"). 3 samples plot in palynofacies field VII – distal dysoxic-anoxic "shelf" (Fig. 112).

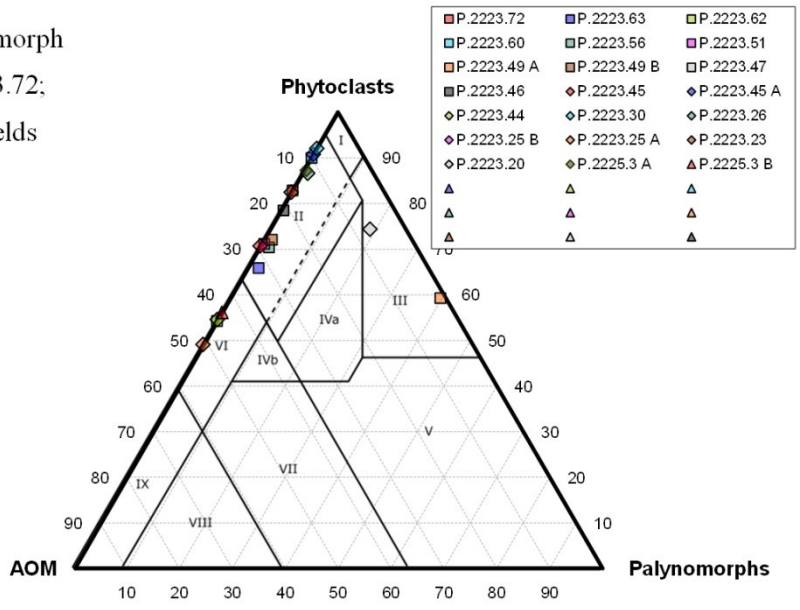

Figure 108: AOM-phytoclast-palynomorph plot of P.2225.3B–P.2223.72; key to the palynofacies fields given in table 2 (p. 49).

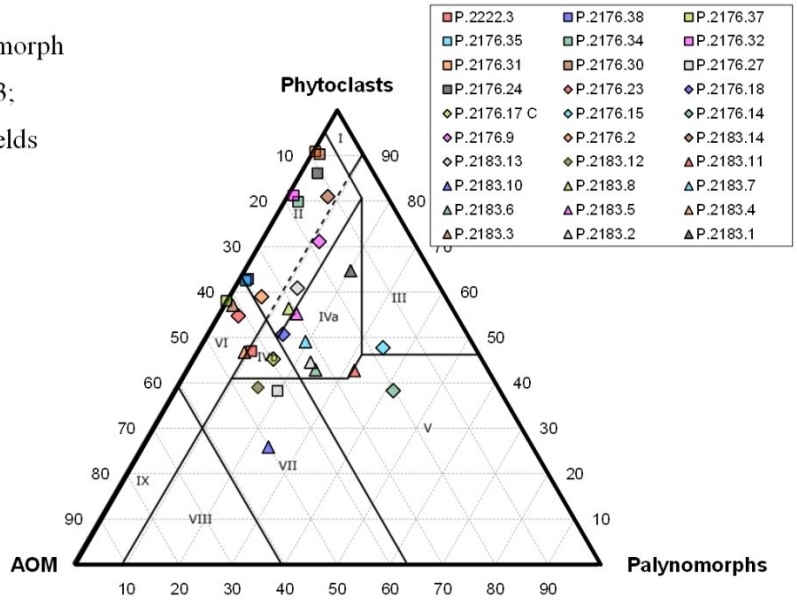

Figure 109: AOM-phytoclast-palynomorph plot of P.2183.1–P.2222.3; key to the palynofacies fields given in table 2 (p. 49).

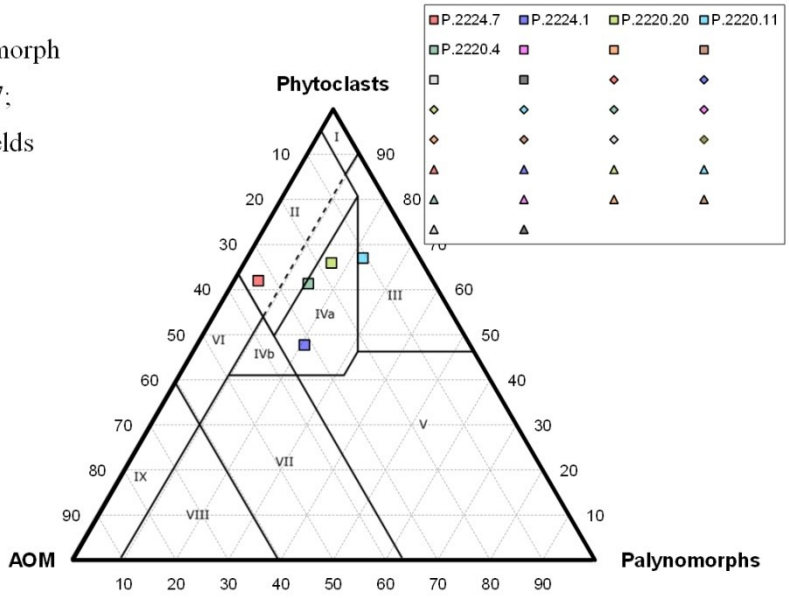

Figure 110: AOM-phytoclast-palynomorph plot of P.2220.4–P.2224.7; key to the palynofacies fields given in table 2 (p. 49).

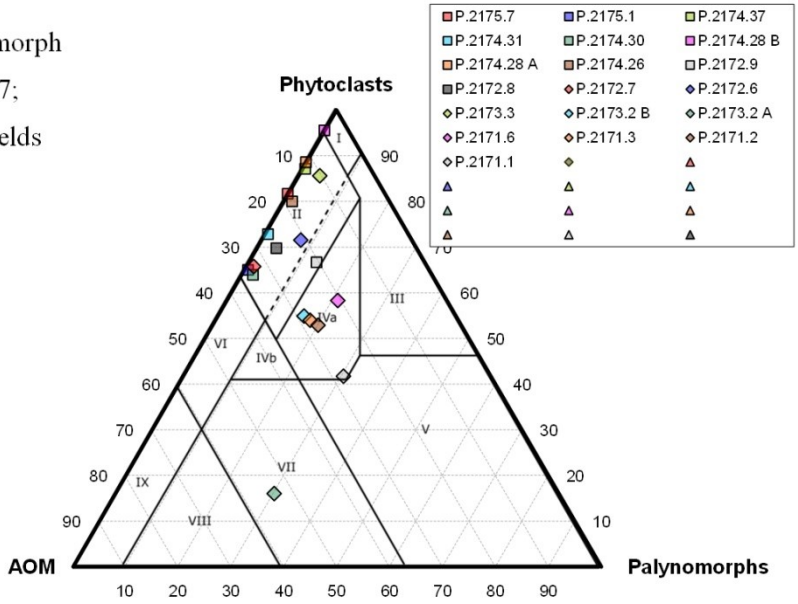

Figure 111: AOM-phytoclast-palynomorph plot of P.2171.1–P.2175.7; key to the palynofacies fields given in table 2 (p. 49).

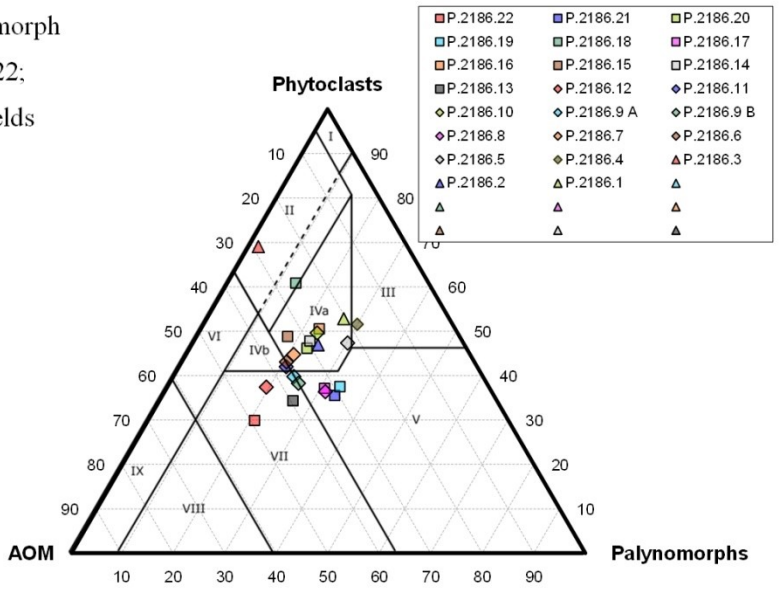

Figure 112: AOM-phytoclast-palynomorph plot of P.2186.1–P.2186.22; key to the palynofacies fields given in table 2 (p. 49).

THIN SECTION ANALYSIS

Thin section analysis was performed on 36 samples of the Byers Group. 12 samples were analysed from the Middle Tithonian interval, 11 samples originate from the lower–Middle Berriasian interval and 13 samples belong to the upper-Berriasian–Lower Valanginian sediment succession. Observations and remarks of individual samples are listed in the appendix, grain-size distribution and sedimentary features (if applicable) are described here:

Middle Tithonian: Most samples consist of mudstone. Sandstone interlayers are common. The lower–middle part of the interval is characterised by alternating normally graded sandstones and bioturbated mudstones.

Lower–Middle Berriasian: This interval is characterised by decreasing grain size. The lower part of the interval shows medium to coarse grained sandstones which subsequently are replaced by parallel laminated silt- and mudstones. Upsection, samples are characterised by fine-medium sized sandstones that show current ripple cross lamination. The upper part of the interval is characterised by a return to planar laminated mudstone.

Upper-Berriasian–Lower Valanginian: The lower part of the interval is composed of majorly mudstone to medium sized siltstone. Interlaminated mudstone/sandstone characterise the middle–upper part of the interval. One sample in the upper part of the interval consists of current ripple cross laminated silty mudstone and very fine sandstone.

TOTAL ORGANIC CARBON, TOTAL INORGANIC CARBON, CARBON/SULPHUR/ NITROGEN

68 samples from the Byers Group were analysed for their carbon, nitrogen and sulphur content (Fig. 113).

Total organic carbon: The Middle Tithonian interval of the Byers Group shows a relatively low content of TOC. The proportion varies on a low level between 0.08–0.45 %. A major positive peak of 1.92 % is detected in the upper part of the Tithonian section. A mean proportion of 0.32 % (SD=0.42 %) is identified. The Early–Middle Berriasian interval contains a mean proportion of 0.69 % (SD=0.31 %). The content of individual samples fluctuates intensely between 0.10–1.1 %. A distinct trend is not observed. In the Upper Berriasian to Lower Valanginian part of the sediment sequence the proportion is lower and the average content is 0.46 % (SD=0.17 %). Proportion ranges from 0.84–0.30 %. The distribution pattern shows no distinct trend. Another increase in proportion is observed for the Early–Middle Valanginian of the Snow Island. Here content averages at 0.80 % (SD=0.28 %). Throughout the interval the proportion fluctuates intensely between 0.10–1.09 %.

Total inorganic carbon: In the Middle Tithonian interval of the Byers Group TIC content is highest in the lowermost part of the interval where a maximum of 7.6 % is detected. Subsequently, the proportion decreases sharply to 0-63 %. Except for a minor positive peak of 3.3 % in the upper middle part of the interval the content varies on a low level between 0.29–1.2 %. The mean proportion for this interval is 1.4 % (SD=2 %). A distinct trend is not observed. The Early–Middle Berriasian section of the Byers Group contains a low amount of TIC ranging between 0.07 % and 5 %. A highly discontinuously increasing trend is observed throughout the middle and upper part of the interval. A mean content of 0.83 % (SD=1.3 %) is detected. The TIC content decreases sharply from 4.1 % to 0.39 % in the lowermost part of the Upper Berriasian to Lower Valanginian sediment sequence. Subsequently the content varies on a low level between 0.01–0.19 %. The mean proportion is 0.46 % (SD=1.2 %). In the Early–Middle Valanginian section on Snow Island TIC proportion is the lowest of all intervals studied of the Byers Group reaching a mean proportion of 0.32 % (SD=0.84 %). Except for two peaks of 1.3 % and 3.7 % in the lowermost part and one peak of 0.74 % in the upper part of the interval the content varies on a low level between 0–0.11 %. A trend is not observed.

$CaCO_3$: In the Middle Tithonian interval the content of $CaCO_3$ ranges from 2.4–63 %. 3 positive peaks are observed (35.7 % and 63 % in the lowermost part of the interval, 27.7 % in the upper middle part). The mean proportion is 11.3 % (SD=16.3 %). For the Early–Middle Berriasian of the Byers Group, the mean proportion of $CaCO_3$ is 6.9 % (SD=10.9 %). Individual content varies between 0.58–41.5 %. Several intermittent peaks are observed. The $CaCO_3$ proportion of the Upper Berriasian to Lower Valanginian interval of the sections varies between 0.06–33.7 %. The mean proportion is 3.9 % (SD=9.9 %). $CaCO_3$ is lowest in the Early–Middle Valanginian of Snow Island, only reaching 2.6 % (SD=7 %). The proportion varies between 0.01–30.9 %. Overall, $CaCO_3$ proportion decreases highly discontinuously throughout the Byers Group.

Nitrogen: In the Middle Tithonian samples nitrogen content varies between 0.006 % and 0.02 %. The mean proportion is 0.02 % (SD=0.015 %). The content shows a highly discontinuously increasing trend. The nitrogen content of the Early–Middle Berriasian interval fluctuates significantly and varies between 0.036 % and 0.13 %. Although highly inhomogeneous, the value shows a

decreasing trend throughout the interval. The average nitrogen content of the Early–Middle Berriasian is 0.08 % (SD=0.03 %). Especially in the upper lower, middle and lower upper parts of the Late Berriasian to Early Valanginian sequence nitrogen content shows an increasing trend. The mean proportion for this interval is 0.11 % (SD=0.07 %). The nitrogen content for the Early–Middle Valanginian of the Byers Group varies intensely between 0.01 % and 0.1 %. The mean content of the interval is 0.07 % (SD=0.03 %). A distinct trend is not observed.

Sulphur: The sulphur content of the Middle Tithonian of the Byers Group fluctuates significantly between 0.04–2.2 %. Several intermittent peaks are observed. An unequivocal trend is not detected. The mean proportion is 0.59 % (SD=0.71 %). The Early–Middle Berriasian interval shows a significantly decreased mean proportion of 0.09 % (SD=0.18 %). Individual content varies strongly between 0.004–0.61 %. The distribution pattern is characterised by several intermittent peaks. A clear trend is not observed. Throughout the lower and middle part of the Upper Berriasian to Lower Valanginian interval of the succession the abundance varies on a low level between 0.01–0.07 %. In the upper middle to upper part of the interval the content ranges on an increased level between 0.38–1.5 %. The average proportion of this interval is 0.32 % (SD=0.50 %). The sulphur content of the Early–Middle Valanginian interval varies between 0–0.38 %. A mean proportion of 0.04 % (SD=0.09 %) is detected for this interval.

C_{org}/N: The C/N ratio of the Middle Tithonian interval ranges from 6–27. In the lowermost part of the interval a major positive peak of 247 is detected. The mean value is 25. In the Early–Middle Berriasian section the C/N ratio varies intensely between 1 and 20. The averaged ratio is 9. An unequivocal trend is not observed. Throughout the Late Berriasian to Early Valanginian interval the ratio varies intensely between 1 and 13 and shows a highly discontinuously decreasing trend. A mean ratio of 6 is detected. The C/N ratio of the Early–Middle Valanginian section varies comparatively homogeneous between 8 and 13. The averaged ratio is 11.

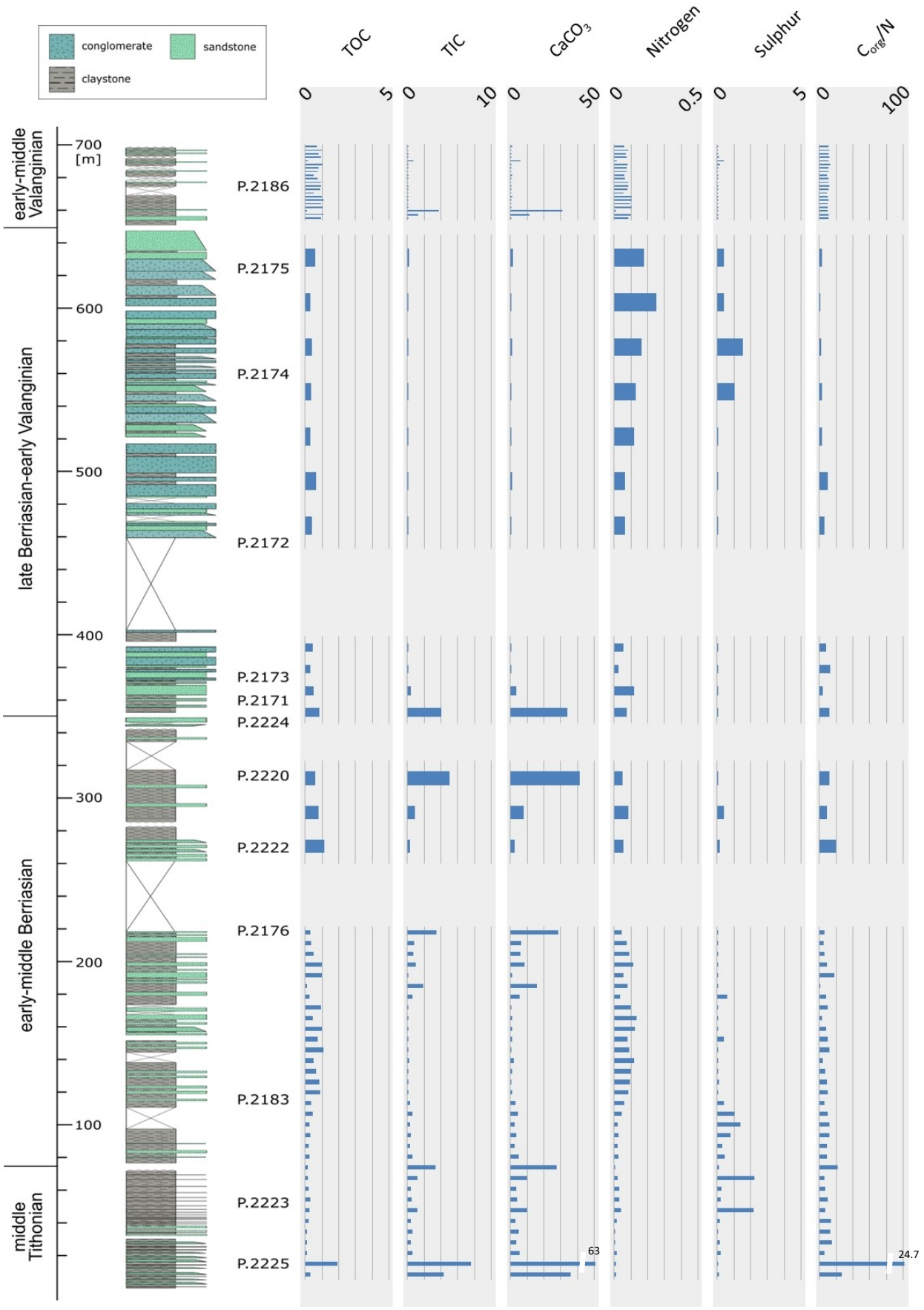

Figure 113: Results of the TOC, TIC and CNS analyses; Byers Group. Except for C_{org}/N, values given in %, to increase visualisation, different scales are used. Statistical outliers are marked accordingly.

THERMAL MATURITY

Determination of the thermal maturity is performed using the Thermal Alteration Index (TAI) and Spore Coloration Index (SCI) (Tyson, 1995; Traverse, 2007; Suárez-Ruiz et al., 2012).

Middle Tithonian: in this interval TAI analysis was performed on 2 samples (P.2223.30, P.2223.49 A). Sample P.2223.20 shows a TAI of approximately 3+ to 4/SCI of 9-9.5 (Ro% 1.5–2.5). Sample P.2223.49 A shows a significantly higher TAI of 5/SCI of 10 (Ro% >3). According to the results both samples represent the maturation stage of metagenesis (cf. Suárez-Ruiz et al., 2012).

Earliest Berriasian: in this interval TAI/SCI analysis was performed on 2 samples (P.2183.2, P.2183.11). Sample P.2183.2 shows a TAI of approximately 2+ to 3/SCI of 7.5-8.5 (Ro% 0.8–1.3). Sample P.2183.11 shows a similar TAI of 2+ to 3-/SCI of 6.5-8.5 (Ro% 0.6–1.1). Hence, both samples represent the maturation stage of catagenesis to early metagenesis (cf. Suárez-Ruiz et al., 2012).

Early to Middle Berriasian: in this interval TAI/SCI analysis was performed on 3 samples (P.2176.15, P.2176.27, P.2220.11). In the samples P.2176.15 and P.2176.27 TAI ranges approximately between 2- and 2+/SCI of 5-8 (Ro% 0.5–0.9). Hence, both samples represent the maturation stage of catagenesis (cf. Suárez-Ruiz et al., 2012). Sample P.2220.11 shows a higher TAI of approximately 3 to 3+/SCI of 8.5-9 (Ro% 1.3–1.7) and can be assigned to the stage of metagenesis.

Late Berriasian to Early Valanginian: TAI/SCI analysis was performed on 2 samples (P.2171.6, P.2174.30). Sample P.2171.6 shows a TAI of approximately 2 and 3-/SCI of 5-8.5 (Ro% 0.5–1.1). Hence the sample represents the maturation stage of diagenesis to catagenesis (cf. Suárez-Ruiz et al., 2012). Sample P.2174.30 shows a higher TAI of approximately 3+ to 4-/SCI of 9-9.5 (Ro% 1.7–2.0) and hence can be assigned to the stage of metagenesis.

Early to Middle Valanginian: in this interval TAI/SCI analysis was performed on 3 samples (P.2186.2, P.2186.11, P.2186.21). A TAI of approximately 2+ and 3-/SCI of 6.5-8.5 (Ro% 0.7–1.1) is observed. Maturation stage is thus catagenesis (cf. Suárez-Ruiz et al., 2012).

MICRO-GLENDONITES

32 samples of the Byers Group of Livingston Island and Snow Island contain micro-glendonites. A total of 135 specimens are recorded and measured (selected specimens shown in figures 114–117). 9 samples of the Middle Tithonian interval contain micro-glendonites. In the 33 recorded specimens, diameter ranges from 31 µm to 139 µm. The mean size of the measured mineral clusters is 80 µm (SD=32 µm). Another 9 samples which originate from the Early to Middle Berriasian interval contain micro-glendonites. 37 specimens are recorded. Individual mineral clusters ranges from 30 µm to 216 µm diameter. A mean size of 64.8 µm (SD=45.2 µm) is reached. In the Late Berriasian to Early Valanginian of Livingston Island 7 micro-glendonite-bearing samples are detected. 39 mineral clusters are recorded and measured. Individual diameters ranges from 26 µm to 238 µm, with a mean size of 65.2 µm (SD=41 µm). In the Early to Middle Valanginian interval 7 samples contain micro-glendonites, of which 26 specimens are recorded and measured. Individual mineral clusters vary in size between 30 µm to 140 µm. The average diameter is 64.8 µm (SD=25.5 µm).

Figures 114–117: Selected micro-glendonite specimens of the Byers Group – Fig. 114: P.2171.6; Fig. 115: P.2173.2; Fig. 116: P.2186.21; Fig. 117: P.2173.2.

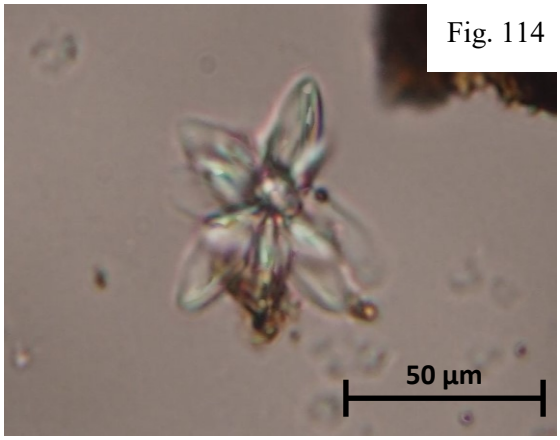

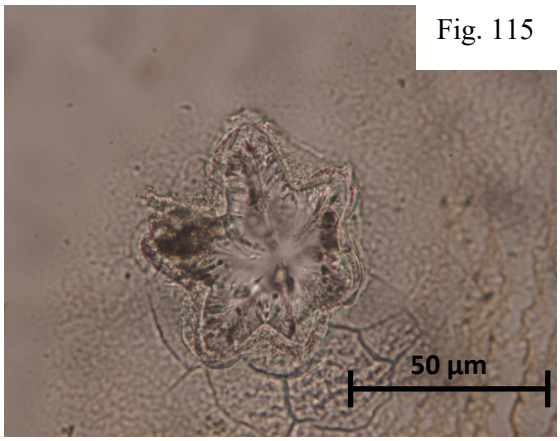

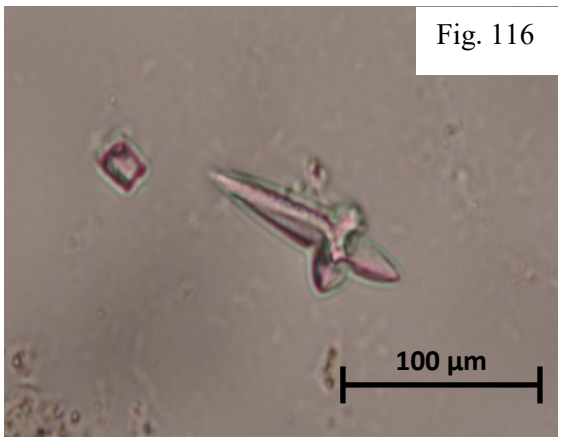

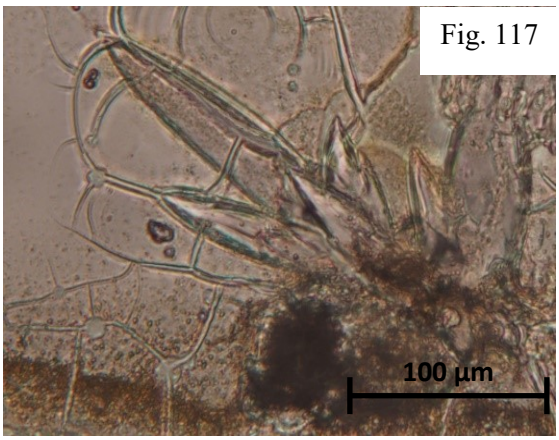

FOSSIL BLUFF GROUP

PALYNOFACIES ANALYSIS

The 21 samples from Alexander Island represent a stratigraphic range from the Middle Tithonian to Middle-Late Aptian (Butterworth et al., 1988). 9 samples originate from the Himalia Ridge Formation that ranges from the Middle Tithonian to Late Valanginian (Butterworth et al., 1988). 6 samples from the Spartan Glacier Formation represent the Valanginian to the ?Barremian. 6 samples were analysed from the Middle to Late Aptian Pluto Glacier Formation.

The palynofacies assemblage of the Alexander Island section shows relatively low diversity (Figs. 118–122). Marine environments are only reflected by acritarchs, undifferentiated algae and marine AOM. Dinocysts, foraminifera and leiospheres are absent. The terrestrial fraction of the sedimentary organic matter is restricted to phytoclasts, sporomorphs and terrestrial AOM. Fungal filaments are absent. AOM comprises structureless fluorescing particles (AOMA) and non-fluorescing amorphous matter (AOMT). Phytoclasts are subdivided according to preservation into 3 categories, “A=good”,

"B=fair" and "C=poor". Sporomorphs and structured marine organic matter are too low in numbers to allow for further subdivision. Poorly preserved phytoclasts that show no signs of its former structure are added to the group of AOMT. One sample (KG.2802.332) of the Upper Tithonian interval contains only mineral detritus.

Terrestrial organic matter

Himalia Ridge Formation – Middle–Late Tithonian to Berriasian

Throughout the Middle–Late Tithonian to Berriasian of Alexander Island, terrestrial organic matter shows a continuously high content that varies between 96.8–100 %. The mean content is 98.9 % (SD=1.1 %).

Sporomorphs: Sporomorphs are low in number ranging between 0–2 %. The mean content is 0.80 % (SD=0.79 %). A distinct trend is not observed.

Phytoclasts: The content of phytoclasts varies from 31.4 % to 96 %. The mean abundance is 70.1 % (SD=24.8 %). A distinct trend is not observed.

Inertinite: The content of inertinite varies between 26.8–90.1 %. The average is 56 % (SD=22.8 %). A distinct distribution pattern is not observed. Abundance of well-preserved inertinite fluctuates significantly between 11 % and 54.2 %. A distinct trend in distribution pattern is not observed. The mean content is 28.1 % (SD=14.8 %). The proportion of fairly preserved inertinite fluctuates significantly between 10.4–59.6 %. A clear trend is not observed. The mean proportion is 27.8 % (SD=17.7 %).

Vitrinite: The average proportion of vitrinite in the Middle–Upper Tithonian to Berriasian sediment sequence of Alexander Island is 14.1 % (SD=11.8 %). Samples show a proportion that varies between 3.2 % and 36.8 %. A distinct trend is not observed. The content of well-preserved vitrinite fluctuates between 1.1–8.6 %. A trend is not observed and the average abundance is 2.7 % (SD=2.4 %). The proportion of fairly preserved vitrinite is significantly higher and varies between 1.8–28.2 %. The average content is 11.4 % (SD=9.9 %).

Cutinite: Occurrences of cutinite are not observed in the sampled interval.

Terrestrial AOM: $AOMT_{translucent}$ average is 27.8 % (SD=23.3 %). Proportion fluctuates intensely between 4 % and 65.2 %. A distinct trend is not observed. Two samples of uppermost part of the interval contain $AOMT_{opaque}$ of 0.46– 0.79 %. The mean content is 0.16 % (SD=0.30 %). $AOMT_{toatal}$ abundance varies between 0–65.2 %. The mean proportion is 24.9 % (SD=23.8 %).

Spartan Glacier Formation – Valanginian–?Barremian

The proportion of terrestrial organic matter is continuously high in the Valanginian to ?Barremian interval of Alexander Island. The content varies between 93.6–100 % and reaches a mean abundance of 98.6 % (SD=2.5 %).

Sporomorphs: Occurrences of sporomorphs are rare. The proportion varies between 0–2.4 %. The mean abundance is 0.64 % (SD=0.91 %). A distinct trend is not observed.

Phytoclasts: Proportion of phytoclasts varies significantly between 40.2–95 %. The mean abundance for this interval is 70.1 % (SD=24.8 %). A distinct trend in the distribution pattern is not observed.

Inertinite: The content of inertinite varies between 26.3–74.3 %. The mean proportion is 50.9 % (SD=17.5 %). A distinct trend is not observed. Well-preserved inertinite shows a discontinuous increase throughout the interval. The proportion increases from 17.8 % to 31.8 %. The highest content is observed in the middle part of the interval where an abundance of 43.6 % is identified. The mean proportion is 30.4 % (SD=10 %). The content of fairly preserved inertinite shows a sharp decrease in the lowermost part of the section from 56.4 % to 4.8 %. A mean content of 20.6 % (SD=18.4 %) is detected.

Vitrinite: The content of vitrinite shows a slight and inhomogeneous decreasing trend from 20.8 % to 16.1 %. The overall proportion varies between 9.3–20.8 %. The mean abundance is 15.9 % (SD=3.9 %). Content of well-preserved vitrinite increases inhomogeneous but distinctly throughout the interval from 0–4.7 %. A mean proportion of 2.1 % (SD=1.5 %) is observed. The proportion of fairly preserved vitrinite is significantly higher than of well-preserved specimens. A discontinuous decrease from 20.8–11.3 % is detected. The mean abundance is 13.7 % (SD=4.6 %).

Cutinite: One sample in the middle part of the interval contains cutinite. A proportion of 0.77 % is observed resulting in a mean abundance for the interval of 0.13 % (SD=0.32 %).

Terrestrial AOM: Since no $AOMT_{opaque}$ is present in the interval, $AOMT_{toatal}$ content equal those of $AOMT_{translucent}$. The proportion of AOM fluctuates significantly between 5–51.3 %. The mean abundance for the Valanginian–?Barremian interval of Alexander Island is 31 % (SD=18.9 %). The distribution of occurrences shows no distinct trend.

Middle–Late Aptian – Pluto Glacier Formation

Terrestrial organic matter content is high, ranging between 90.4–100 %. The distribution pattern shows no distinct trend. The mean proportion is 94.2 % (SD=3.3 %).

Sporomorphs: Content of sporomorphs is highest in the upper lower to middle part of the interval. Here the proportion varies between 1.9–5.4 %. In the remainder of the interval content varies between 0–0.7 %. A mean proportion of 2.2 % (SD=2.3 %) is identified.

Phytoclasts: In the Middle–Late Aptian section of Alexander Island phytoclasts show a discontinuously increasing content from 32.2 % to 74.6 %. The content varies between 27.3–74.6 %. A mean proportion of 42.5 % (SD=17.9 %) is reached.

Inertinite: Proportion of inertinite varies between 10.7–40.4 %. The mean abundance is 25.7 % (SD=10.8 %). A distinct trend is not observed. Well-preserved inertinite shows a proportion that varies between 8.5–33.3 %. The mean proportion is 19.1 % (SD=9.3 %). The frequency distribution shows no unequivocal trend. Content of fairly preserved inertinite is significantly lower and varies between 2.2–14 %. In this interval a mean proportion of 6.5 % (SD=4.1 %) is detected.

Vitrinite: The proportion of vitrinite increases discontinuously throughout the Middle-Late Aptian section of Alexander Island. The proportion increases from 11.2 % to 34.2 %. A mean proportion of 16.9 % (SD=9.5 %) is identified. The content of well-preserved vitrinite decreases continuously throughout the lower and middle part of the interval from 5.1–1.9 %. In the subsequent upper part of the interval a significant increase to 8.2 % is detected. The mean proportion is 3.8 %

(SD=2.5 %). The proportion of fairly preserved vitrinite is distinctly higher. An inhomogeneous increase from 6.2 % to 26 % is detected. The mean proportion is 13.1 (SD=7.8 %).

Cutinite: Occurrences of cutinite are not observed in the interval.

Terrestrial AOM: The proportion of $AOMT_{translucent}$ varies on a relatively high level between 40.7 % and 64.9 % throughout the lower and middle part of the interval until a sharp decrease in the upper part when abundance decreases to 19 %. A mean proportion of 49.4 % (SD=17.3 %) is identified. One sample in the middle part of the interval contains $AOMT_{opaque}$. A content of 0.78 % is observed resulting in a mean abundance for this interval of 0.13 5 (SD=0.32 %). $AOMT_{toatal}$ proportion varies between 19.1–64.9 %. The mean content is 49.5 % (SD=17.3 %).

Marine organic matter

Himalia Ridge Formation – Middle–Late Tithonian to Berriasian

The content of marine organic matter is continuously low and varies between 0–3.2 %. A mean content of 1.1 % (SD=1.1 %) is observed. Frequency distribution shows no clear trend.

Marine AOM: Proportion of fluorescent AOM shows a fluctuating value that ranges from 0 % to 3.2 %. A mean abundance of 1.1 % (SD=1.1 %) is identified. A distinct trend is not observed.

Spartan Glacier Formation – Valanginian–?Barremian

The proportion of marine organic matter increases significantly from 0 % to 6.4 % in the lowermost part of the section. Subsequently the content decreases continuously to 0 % in the upper part of the interval. The mean abundance is 1.4 % (SD=2.5 %).

Algae indet.: One sample in the lower part of the interval contains occurrences of undifferentiated algae. A proportion of 2.4 % is reached in this sample leading to a mean abundance for the interval of 0.40 % (SD=0.99 %).

Marine AOM: Proportion of fluorescent AOM shows an increase in the lower part of the interval where the proportion increases from 0–4 %. Subsequently the content decreases throughout the remainder of the interval to 0 %. A mean content of 1 % (SD=1.6 %) is detected.

Pluto Glacier Formation – Aptian

Proportion of marine organic matter is significantly higher than in the previous intervals and varies between 0–9.6 %. A mean abundance of 5.8 % (SD=3.3 %) is observed. A distinct trend is not identified.

Acritarchs: One sample in the uppermost part of the interval contains occurrences of acritarchs. A proportion of 0.58 % is reached in this sample leading to a mean abundance for the Middle-Late Aptian interval of 0.10 % (SD=0.24 %).

Algae indet.: The proportion of undifferentiated algae varies between 0–4.5 %. A mean abundance of 1.9 % (SD=1.7 %) is observed. The distribution pattern shows no distinct trend.

Marine AOM: Content of fluorescent AOM varies significantly between 0–6.3 %. The mean proportion is 3.8 % (SD=2.3 %). A distinct trend is not observed.

Opaque/translucent ratio

For the middle–Upper Tithonian section an OP/TR ratio of 3.4 is detected. The OP/TR ratio of the Berriasian–Valanginian interval is 5.6. The OP/TR ratio of the Valanginian–Barremian section is 3.2. The OP/TR ratio of the Aptian interval is 1.8.

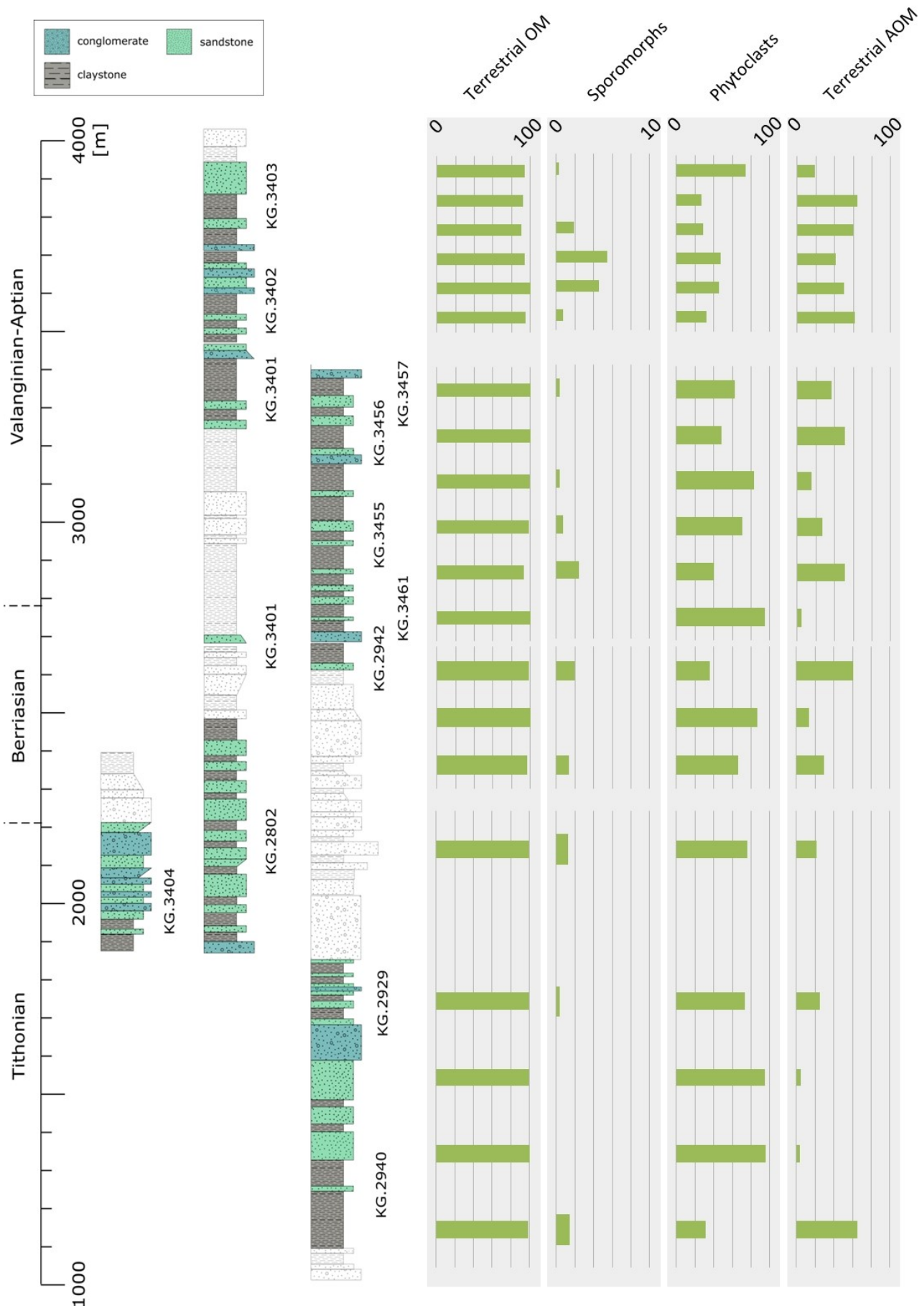

Figure 118: Sedimentary organic matter – terrestrial fraction; Fossil Bluff Group. Values given in %, to increase visualisation, different scales are used.

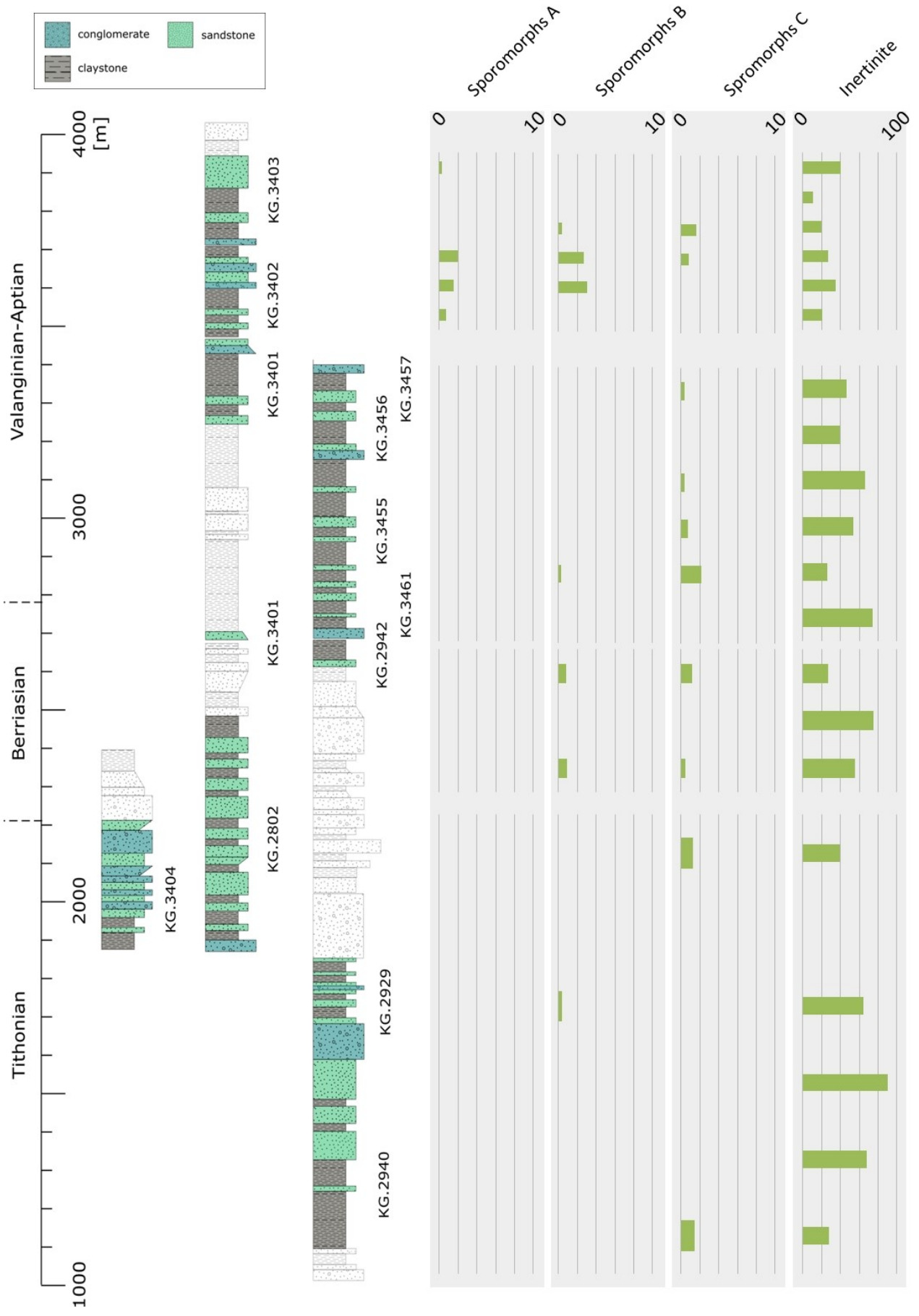

Figure 119: Sedimentary organic matter – terrestrial fraction continued; Fossil Bluff Group. Values given in %, to increase visualisation, different scales are used.

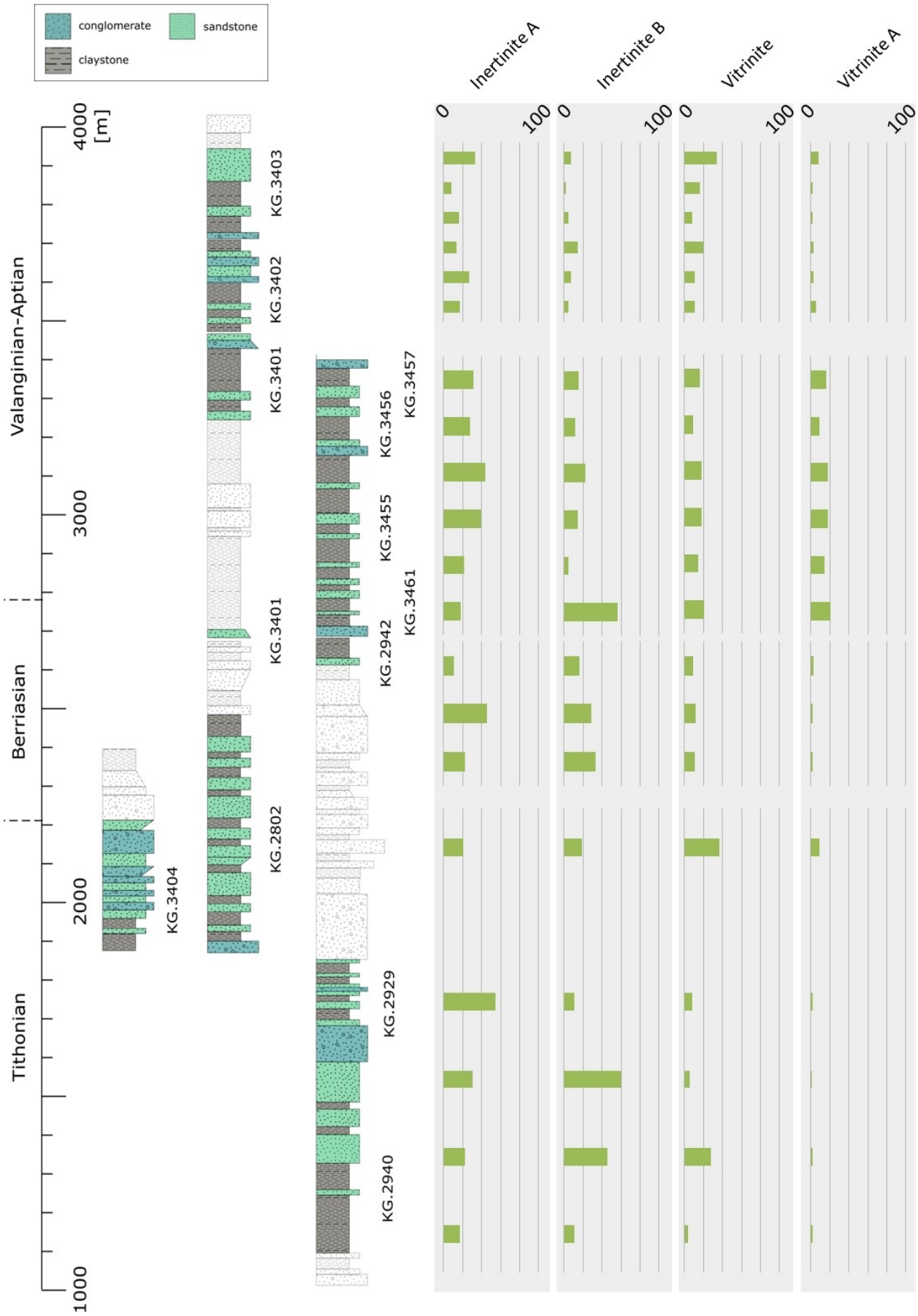

Figure 120: Sedimentary organic matter – terrestrial fraction continued; Fossil Bluff Group. Values given in %, to increase visualisation, different scales are used.

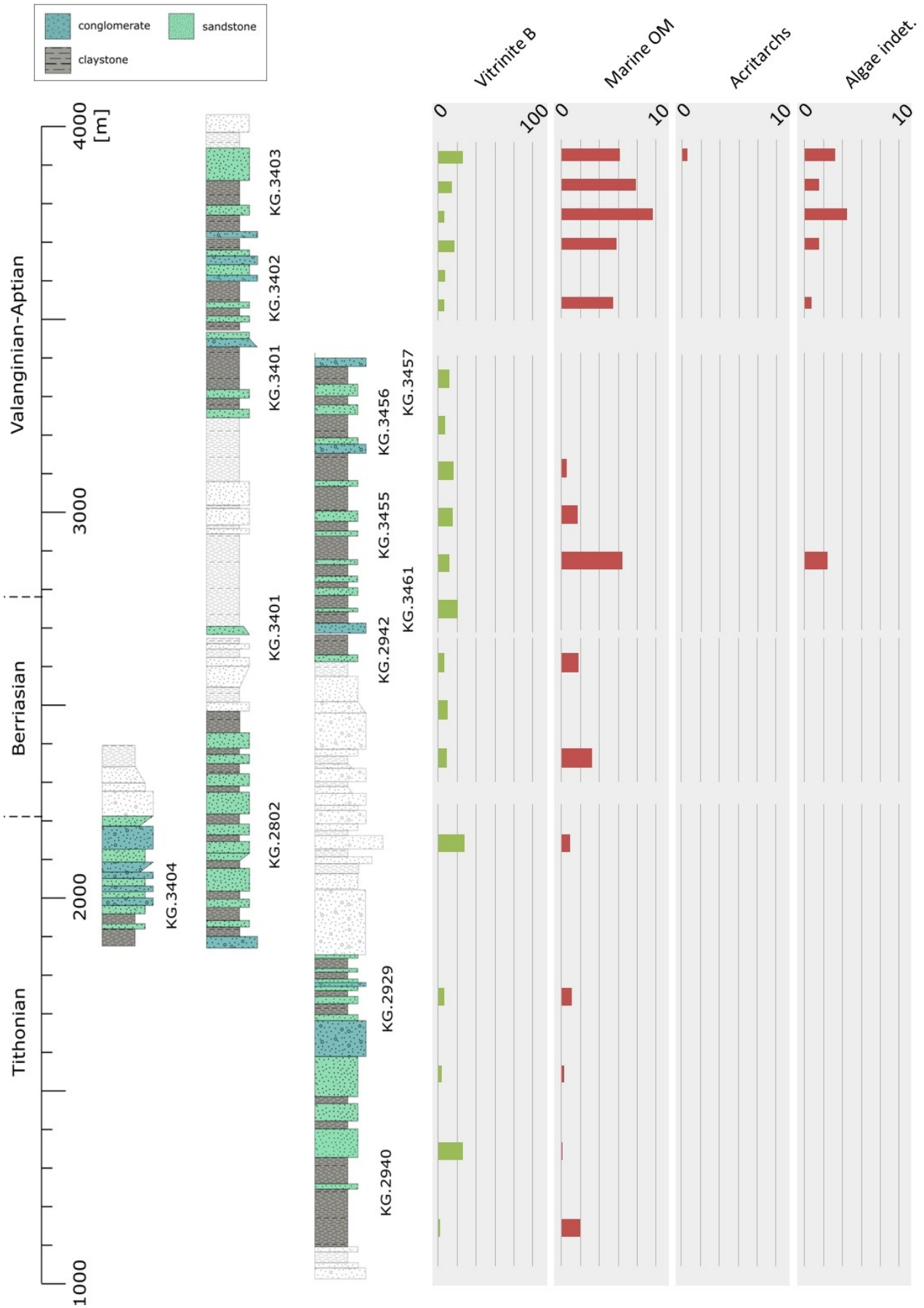

Figure 121: Sedimentary organic matter – Vitrinite B and marine fraction; Fossil Bluff Group. Values given in %, to increase visualisation, different scales are used.

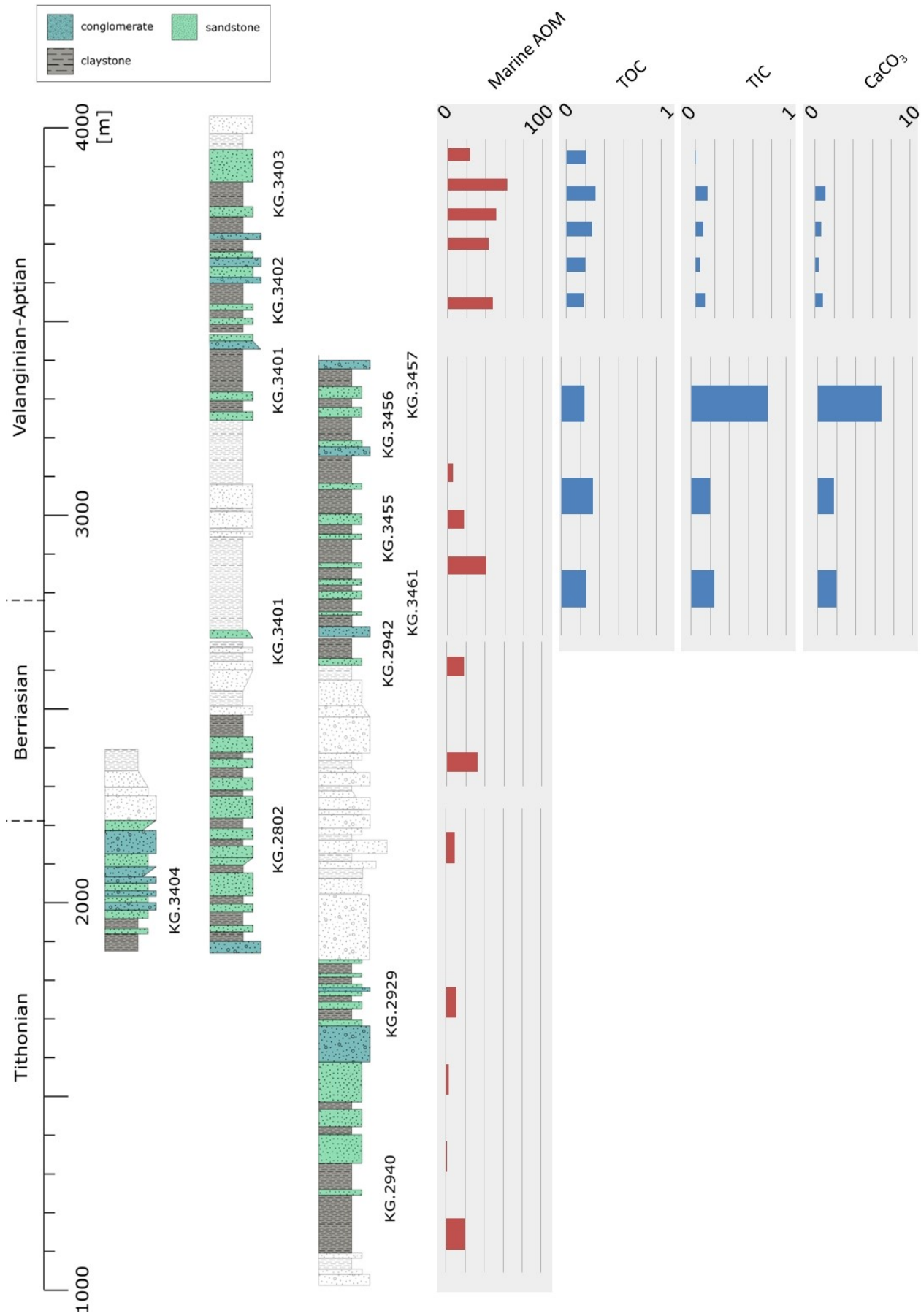

Figure 122: Sedimentary organic matter – marine AOM and results of the TOC and TIC analyses Fossil Bluff Group. Values given in %, to increase visualisation, different scales are used.

AOM-phytoclast-palynomorph plot

Tithonian: Two samples of the Tithonian interval (KG.2940.10–KG2929.1) of the Fossil Bluff Group plot in palynofacies field I – highly proximal shelf or basin. Another 2 samples plot in palynofacies field II – marginal dysoxic-anoxic basin (Fig. 123). The lowermost sample plots in palynofacies field IX – distal suboxic-anoxic basin.

Berriasian–Early Valanginian: Two samples of the Berriasian–Early Valanginian section (KG.2802.662–KG.2942.10) plot in palynofacies field II – marginal dysoxic-anoxic basin (Fig. 123). One sample plots in palynofacies field IX– distal suboxic-anoxic basin.

Valanginian–Barremian: One sample of the Valanginian–Barremian interval (KG.3461.26–KG.3457.54) plots in in palynofacies field I – highly proximal shelf or basin. Two samples plot in palynofacies field II – marginal dysoxic-anoxic basin. 3 samples plot in palynofacies field VI – proximal suboxic-anoxic shelf (Fig. 123).

Aptian: One sample of the Aptian section (KG.3402.16–KG.3403.213) of the Fossil Bluff Group plots in palynofacies field II – marginal dysoxic-anoxic basin. Two samples plot in palynofacies field VI – proximal suboxic-anoxic shelf. 3 samples plot in palynofacies field IX – distal suboxic-anoxic basin (Fig. 123).

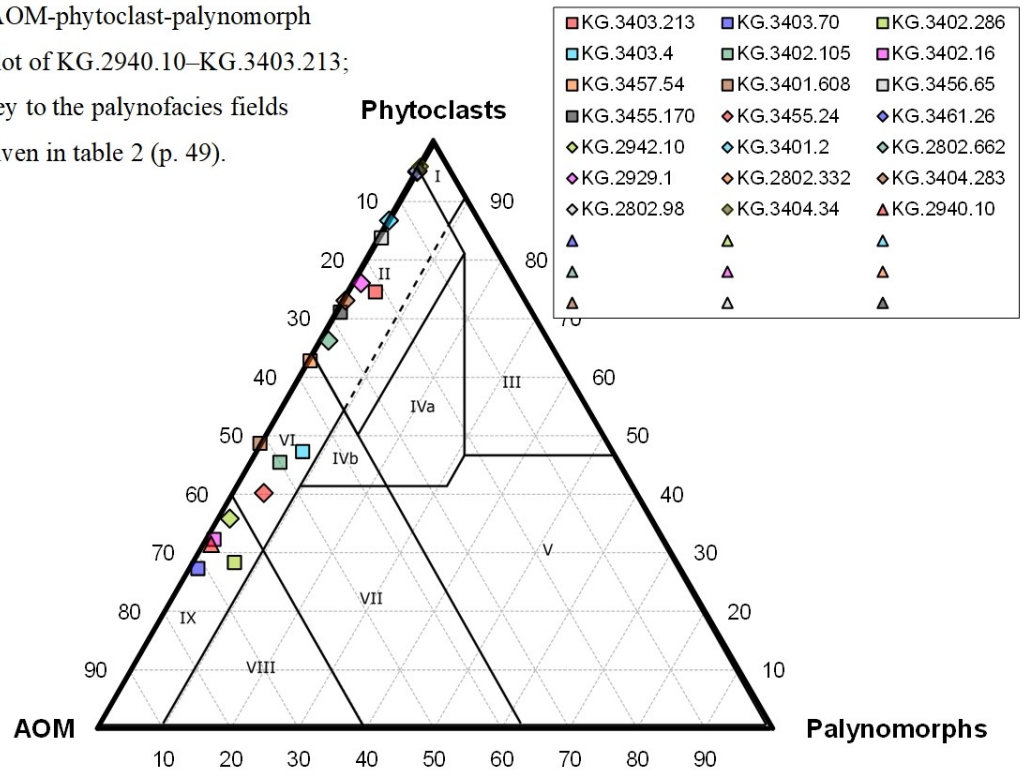

Figure 123: AOM-phytoclast-palynomorph plot of KG.2940.10–KG.3403.213; key to the palynofacies fields given in table 2 (p. 49).

TOTAL ORGANIC CARBON, TOTAL INORGANIC CARBON, CARBON/SULPHUR/ NITROGEN

3 samples of the Spartan Glacier Formation and 5 samples of the Pluto Glacier Formation of Alexander Island are analysed for their carbon, nitrogen and sulphur content (Figs. 122, 124).

Total organic carbon: The TOC content of the Valanginian–?Barremian section of Alexander Island varies between 0.24–0.33 %. The mean proportion is 0.28 % (SD=0.04 %). The Aptian samples contain a mean TOC proportion of 0.23 % (SD=0.05 %). The content varies between 0.20–0.31 %. An unequivocal trend is not observed.

Total inorganic carbon: In the Valanginian–?Barremian section the proportion of TIC varies between 0.20–0.80 %. The mean abundance is 0.42 % (SD=0.34 %). In the Aptian interval of Alexander Island TIC proportion varies between 0–0.13 %. The mean content is 0.07 % (SD=0.05 %).

$CaCO_3$: In the Valanginian–?Barremian of Alexander Island $CaCO_3$ proportion ranges from 1.7 % to 6.7 %. The averaged abundance for this interval is 3.5 % (SD=2.8 %). The Aptian interval shows a proportion that varies between 0–1.1 %. The mean content is 0.58 % (SD=0.42 %).

Nitrogen: The samples of the Valanginian–?Barremian section of the Spartan Glacier Formation of the Fossil Bluff Group contains a nitrogen content that varies between 0.028 % and 0.033 %. The average proportion is 0.03 % (SD=0.004 %). The nitrogen content of the Aptian Pluto Glacier Formation varies between 0.013 % and 0.036 %. Although highly discontinuous, the value shows a decreasing trend. The average nitrogen content of the Aptian interval of the section is 0.02 % (SD=0.01 %).

Sulphur: The sulphur content of the Valanginian–?Barremian section fluctuates between 0.06–0.40 %. The mean proportion is 0.22 % (SD=0.17 %). The Aptian interval shows a mean proportion of 0.10 % (SD=0.10 %). Individual contents vary significantly between 0.008–0.25 %. A distinct distribution pattern is not observed.

C_{org}/N: The C/N ratio of the Valanginian–?Barremian interval ranges from 8–13. The averaged value is 10. In the Aptian section of the Fossil Bluff Group the C/N ratio varies between 5 and 16. The averaged ratio is 11. A comparatively continuous increase in C/N ratio is observed.

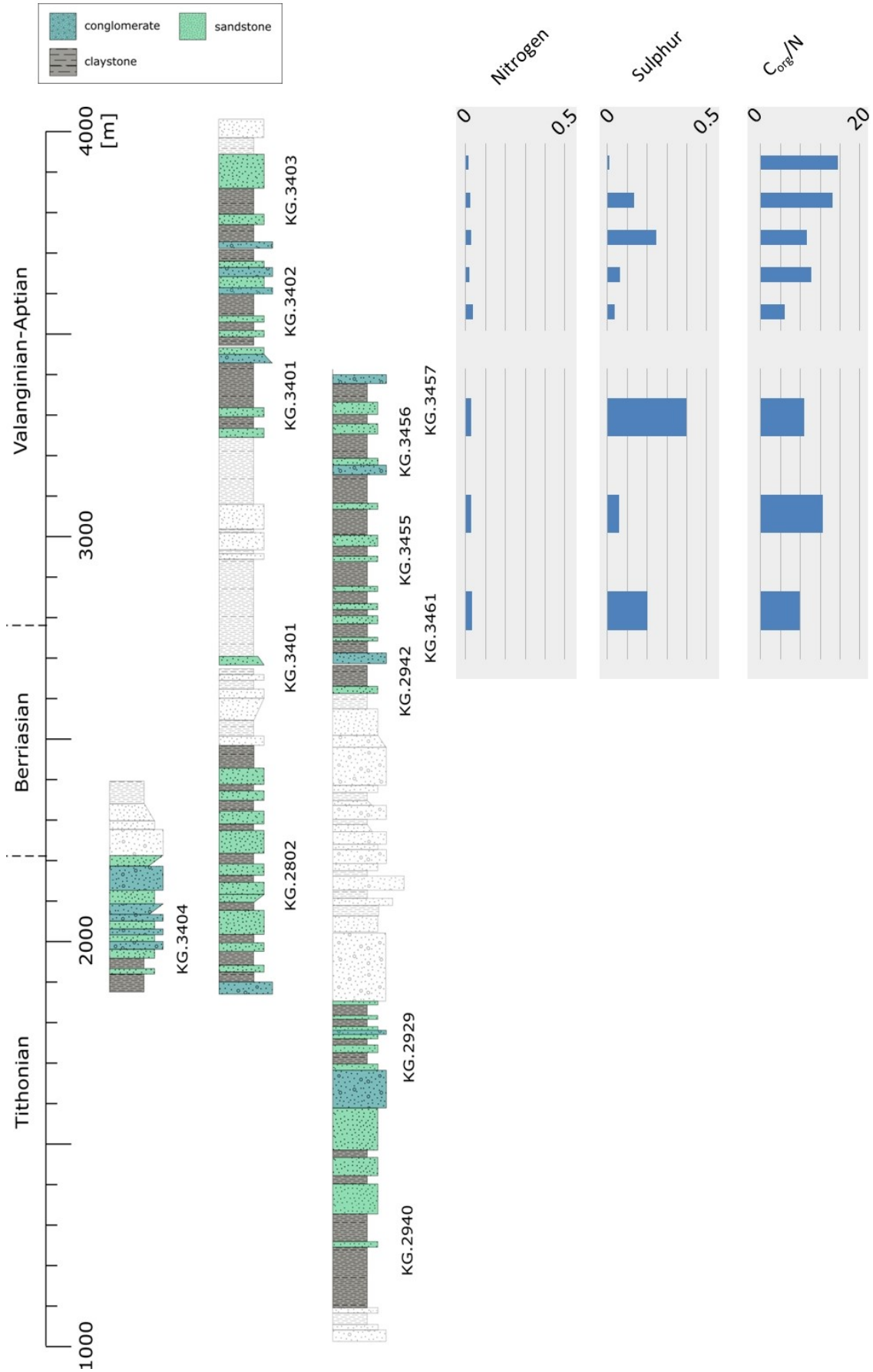

Figure 124: Results of the TOC, TIC and CNS analyses continued Fossil Bluff Group. Except for C_{org}/N, values given in %, to increase visualisation, different scales are used.

THERMAL MATURITY

Middle Tithonian to Berriasian: in this interval TAI/SCI analysis is performed on 3 samples (KG.2940.10, KG.2929.1, KG.2802.662) Samples show a TAI of approximately 4- to 4+/SCI of 9.5 (Ro% 2.0–2.7). The samples represent the maturation stage of metagenesis (cf. Suárez-Ruiz et al., 2012).

Valanginian to Barremian: in this interval TAI/SCI analysis is performed on 3 samples (KG.2942.10, KG.3455.24, KG.3457.54) Samples show a TAI of approximately 4- to 4+/SCI of 9.5 (Ro% 2.0–2.7). The samples represent the maturation stage of metagenesis (cf. Suárez-Ruiz et al., 2012).

Aptian: in this interval TAI/SCI analysis is performed on 2 samples (KG.3403.4, KG.3402.286) Samples show a TAI of approximately 3+ to 4/SCI of 9-9.5 (Ro% 1.5–2.3). The samples represent the maturation stage of catagenesis to metagenesis (cf. Suárez-Ruiz et al., 2012).

MICRO-GLENDONITES

In the section of Alexander Island occurrence of micro-glendonites is observed in 12 samples. A Total of 39 specimens is recorded and measured (selected specimens shown in figures 125–128). In the Tithonian of the Himalia Ridge Formation 4 samples contain micro-glendonites. 12 specimens are recorded and measured. The mean size of the specimens is 60.1 µm (SD=30.8 µm). Individual mineral clusters vary in size between 23–117 µm. One sample of the Late Berriasian–Early Valanginian of the Himalia Ridge Formation contains micro-glendonites. 4 specimens are recorded. The mean diameter of these mineral clusters is 64.3 µm (SD=25.9 µm). Specimens range in size from 49 µm to 103 µm. In the subsequent Valanginian to ?Barremian Spartan Glacier Formation 5 samples contain micro-glendonites. A total of 13 specimens are recorded and measured. A mean size of 84.6 µm (SD=34.2 µm) is detected. The diameter of individual crystals varies between 38 µm and 145 µm. The Early–Middle Aptian Pluto Glacier Formation contains 2 micro-glendonite bearing samples. A total of 8 specimens are recorded. The mean diameter is 32.1 µm (SD=28.5 µm). The mineral clusters vary in size between 12–89 µm.

Figures 125–128 (Page 152): Selected micro-glendonite specimens of the Fossil Bluss Group – Fig. 125: KG.2802.332; Fig. 126: KG.2940.10; Fig. 127: KG.3404.283; Fig. 128: KG.3404.283; scale bars given in the photograph.

Fig. 125

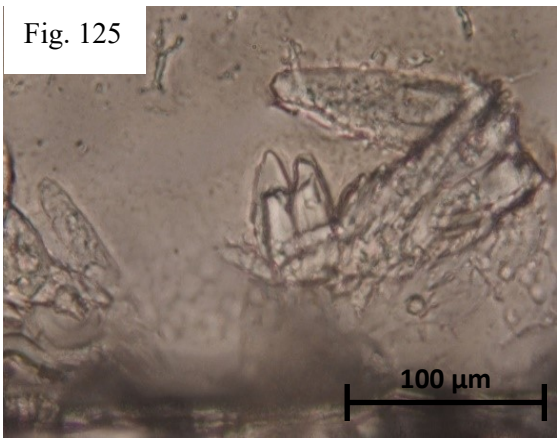

Fig. 126

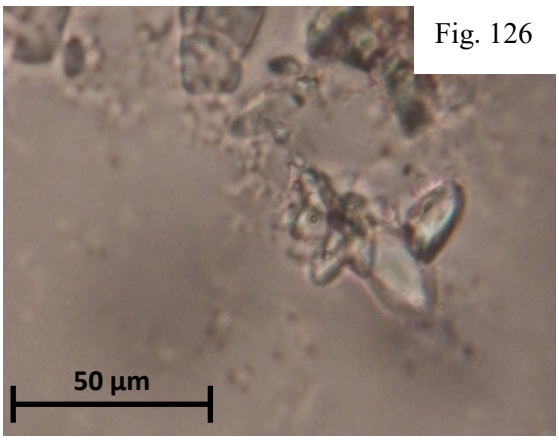

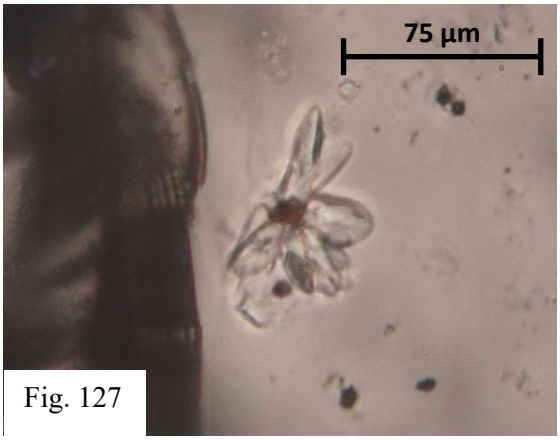

Fig. 127

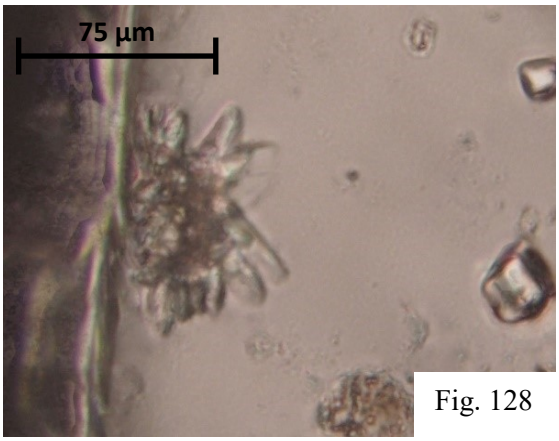

Fig. 128

NORDENSKJÖLD FORMATION AND KOTICK POINT FORMATION

PALYNOFACIES ANALYSES

10 samples of the section on James Ross Island are analysed. 4 samples belong to the Tithonian Nordenskjöld Formation. Another 6 samples represent the Late Aptian–Early Albian section of the Kotick Point Formation.

The palynomorph assemblage of the sections on James Ross Island shows a comparatively high diversity (Figs. 129–134). All representatives of the marine fraction that are used for analyses in this thesis (dinocysts, acritarchs, undifferentiated algae, foraminifera and leiospheres) occur in this interval. Of the terrestrial fraction of sedimentary organic matter phytoclasts, sporomorphs, fungal filaments and terrestrial AOM are present. The fraction of AOM is subdivided into structureless fluorescing particles (AOMA) and non-fluorescing amorphous matter (AOMT). Sporomorphs and phytoclasts are subdivided into the three preservation-dependent categories “A=good”, “B=fair” and “C=poor”. Numbers of structured marine organic matter are so low that a further subdivision is not realised. Poorly preserved phytoclasts that show no signs of its former structure are added to the group of AOMT.

Terrestrial organic matter

Nordenskjöld Formation – Tithonian

Terrestrial organic matter of the middle Tithonian interval varies between 57.5–85.5 %. A clear trend is not observed. The average content for this interval is 66.4 % (SD=13 %).

Sporomorphs: In the middle Tithonian interval sporomorphs reach a mean proportion of 13.9 % (SD=1.7 %). The content varies between 12.6–16.4 %. The distribution pattern shows no clear trend. Well-preserved sporomorphs have a mean content of 8.6 % (SD=1.6 %). Samples show a varying content that ranges from 7.2 % to 10.8 %. A trend is not observed. Fairly preserved sporomorphs reach a mean proportion of 4.1 % (SD=0.6 %). An inconsistent slight increase from 3.6 % to 4.1 % is detected. The frequency distribution of poorly preserved sporomorphs shows a discontinuously decreasing trend from 1.5 % to 0 %. A peak of 2.5 % is observed. The mean proportion is 1.2 % (SD=1.1 %).

Phytoclasts: The content of phytoclasts ranges from 39 % to 62.9 %. A distinct distribution pattern is not observed. The mean proportion is 48.8 % (SD=10.4 %).

Inertinite: The Tithonian samples show an average inertinite content of 28 % (SD=7.3 %). Abundance ranges from 21–38.2 %. A clear trend is not observed. The proportion of well-preserved inertinite varies between 16.8 % and 34.1 %. The frequency distribution shows no distinct trend. A mean content of 24.8 % (SD=7.1 %) is identified. Fairly preserved inertinite shows a significantly lower proportion that varies between 1.7–4.2 %. A continuous increasing trend is detected. The mean proportion is 3.2 % (SD=1.2 %).

Vitrinite: In the Tithonian interval of James Ross Island vitrinite shows a mean proportion of 19.5 % (SD=4 %). An unequivocal pattern of distribution is not observed. The samples shows a proportion that varies between 15.8–24.2 %. The proportion of well-preserved vitrinite varies between 6.4–13.2 %. The mean content is 8.8 % (SD=3 %). Content of fairly preserved vitrinite increases discontinuously from 8.1 % to 10.3 %. A mean proportion of 10.7 % (SD=2.3 %) is observed.

Cutinite: Content of cutinite remains low and varies between 0.54–2.3 %. The mean proportion is 1.3 % (SD=0.72 %). A distinct trend is not observed.

Fungal filaments: One sample in the lowermost part of the interval contains fugal remains. Here a proportion of 1.1 % is identified resulting in a mean abundance for the interval of 0.27 % (SD=0.53 %).

Terrestrial AOM: Content of $AOMT_{translucent}$ varies between 0.83–6.2 %. The proportion is higher in the upper part of the interval. A mean content of 3.3 % (SD=2.8 %) is observed. A distinct trend is not identified. One sample in the uppermost part of the Tithonian interval contains $AOMT_{opaque}$. A proportion of 0.65 % is observed. The mean content is 0.16 % (SD=0.32 %). Abundance of $AOMT_{toatal}$ varies between 0.83 % and 6.2 %. The mean content is 3.5 % (SD=2.9 %).

Kotick Point Formation – Late Aptian–Early Albian

The organic matter composition of the Late Aptian–Early Albian of James Ross Island contains an average of 73.4 % (SD=16 %) of terrestrial organic matter. The proportion varies between 58.3–93.5 %. An unequivocal trend is not observed.

Sporomorphs: In the Upper Aptian–Lower Albian sediment sequence of James Ross Island sporomorphs reach an average abundance of 10.7 % (SD=5.6 %). The content varies significantly between 4.8–19 %. An unequivocal trend in distribution is not observed. Well-preserved sporomorphs have a mean content of 6.7 % (SD=4.4 %). Samples show a proportion that varies between 2.8 % and 12.6 %. A trend is not observed. Fairly preserved sporomorphs reach an average abundance of 3.3 % (SD=1.8 %). The content varies between 1.5 and 6.3 %. The proportion of poorly preserved sporomorphs ranges from 0–1.3 %. The frequency distribution shows no distinct trend. The mean proportion is 0.6 % (SD=0.5 %).

Phytoclasts: Phytoclasts reach a mean proportion of 55.2 % (SD=9.7 %). The content varies between 45.3–69.8 %. A distinct distribution pattern is not observed.

Inertinite: Abundance of inertinite ranges from 7.7 % to 32.6 %. After a sharp decrease in the lower part of the section (21.7–7.7 %) a distinct increase in the lower middle to upper part of the interval is observed. The mean proportion is 16.9 % (SD=9.3 %). The content of well-preserved inertinite ranges from 6.7 % to 25.6 %. In the lower part of the interval a sharp decrease from 21.5 % to 6.7 % is identified. Subsequently the proportion increases continuously throughout the remainder of the interval. A mean proportion of 14.7 % (SD=7.7 %) is detected. The distribution pattern of fairly preserved inertinite shows an inhomogeneous increase from 0.3 % to 7 %. A mean proportion of 2.2 % (SD=2.5 %) is observed.

Vitrinite: The content of vitrinite shows a continuously decreasing trend throughout the Late Aptian–Early Albian section of James Ross Island. The proportion decreases from 46.7 % to 29.2 %. The mean proportion is 36.3 % (SD=5.8 %). For the well-preserved vitrinite an erratic decrease from 26.6 % to 9.3 % is detected. A positive peak of 24.6 % is identified in the upper part of the interval. The average proportion is 20.9 % (SD=6 %). Fairly preserved vitrinite shows a decreasing trend throughout the lower and middle part of the interval (20.1–9.6 %). In the upper part of the section a sharp increase to 19.9 % is observed. The mean proportion is 15.5 % (SD=4.1 %).

Cutinite: The proportion of cutinite remains comparatively low and varies between 0–6.2 %. A mean proportion of 1.9 % (SD=2.3 %) is observed. A distinct trend is not identified.

Fungal filaments: One sample in the middle part of the interval contains fungal remains. The proportion amounts to 1 % leading to a mean of 0.17 (SD=0.43 %) in the interval.

Terrestrial AOM: Occurrence of AOM is restricted to translucent amorphous masses. The proportion varies between 1.4–15.9 %. A mean content of 7.4 % (SD=6.4 %) is observed. The distribution pattern shows no distinct trend. The content of $AOMT_{toatal}$ is similar to this of $AOMT_{translucent}$.

Marine organic matter

Nordenskjöld Formation – Tithonian

In the Tithonian section of James Ross Island the marine organic matter proportion varies between 14–40.9 %. A trend is not observed. The average proportion is 32.7 % (SD=12.7 %).

Dinoflagellate cysts: Dinocysts reach a mean proportion of 2.2 % (SD=0.08 %). The content varies only slightly between 2.15–2.35 %. A distribution pattern is not observed. The highest mean content is observed in the group of well-preserved dinocysts (1.13 % to 1.05 % of fairly preserved dinocysts, and 0.07 % of poorly preserved specimens).

Acritarchs: In the Tithonian interval of James Ross Island the proportion of Acritarchs is relatively high and varies between 2.4–31 %. A mean proportion of 19.5 % (SD=12.1 %) is observed. A distinct trend is not detected.

Algae indet.: Undifferentiated algae reach a mean proportion of 1.5 % (SD=2.1 %). The pattern of distribution shows no clear trend. Proportion varies between 0–4.5 %.

Foraminiferal test linings: The proportion of foraminiferal linings remains low and varies between 0–0.28 % leading to a mean content of 0.12 % (SD=0.14 %). Only the lower 2 samples contain foraminiferal remains.

Leiospheres: The proportion of leiospheres averages at 2.4 % (SD=2.8 %). Content varies between 0–5.1 %. Occurrence of leiospheres is restricted to the lower 2 samples.

Marine AOM: The proportion of fluorescing AOM shows a discontinuously increasing trend from 6.4 % to 7.7 %. The mean content is 6.9 % (SD=1.2 %).

Kotick Point Formation – Late Aptian–Early Albian

The content of marine derived organic matter of the Upper Aptian–Lower Albian sediment sequence of James Ross Island varies between 6 % and 41.3 %. The mean proportion is 26.3 % (SD=16.1 %). A distinct trend in the pattern of distribution is not observed.

Dinoflagellate cysts: Dinoflagellate remains reach a mean proportion of 1 % (SD=0.88 %). A discontinuously increasing trend is identified (with a peak of 2.2 % in the lower part of the interval). Highest proportion is observed in the group of fairly preserved dinocysts, where a mean of 0.51 % is detected. Well-preserved dinocysts have a mean proportion of 0.33 % and poorly preserved specimens of 0.17 %.

Acritarchs: The proportion of acritarchs remains low and varies between 0–0.83 %. A mean content of 0.56 % (SD=0.30 %) is observed. The distribution pattern shows no clear trend.

Algae indet.: Where present content of undifferentiated algae varies between 1.6–4.9 %. A mean abundance of 1.7 % (SD=2.2 %) is identified. An unequivocal trend is not observed.

Foraminiferal test linings: The proportion of foraminiferal linings varies between 0–0.90 %. A mean abundance of 0.42 % (SD=0.33 %) is observed. A distinct trend is not detected.

Leiospheres: Proportion of Leiospheres is fluctuating intensely. The content varies between 0–38.6 %. The mean abundance is 17.7 % (SD=19.4 %). No distinct trend is observed.

Marine AOM: Marine derived AOM reaches a mean proportion of 4.9 % (SD=3.9 %). The content varies significantly between 0.3 % and 11.3 %. The frequency distribution shows no distinct trend.

Opaque/translucent ratio

The OP/TR ratio of the Berriasian–Valanginian interval is 5. For the Middle Tithonian section an OP/TR ratio of 0.5 is detected.

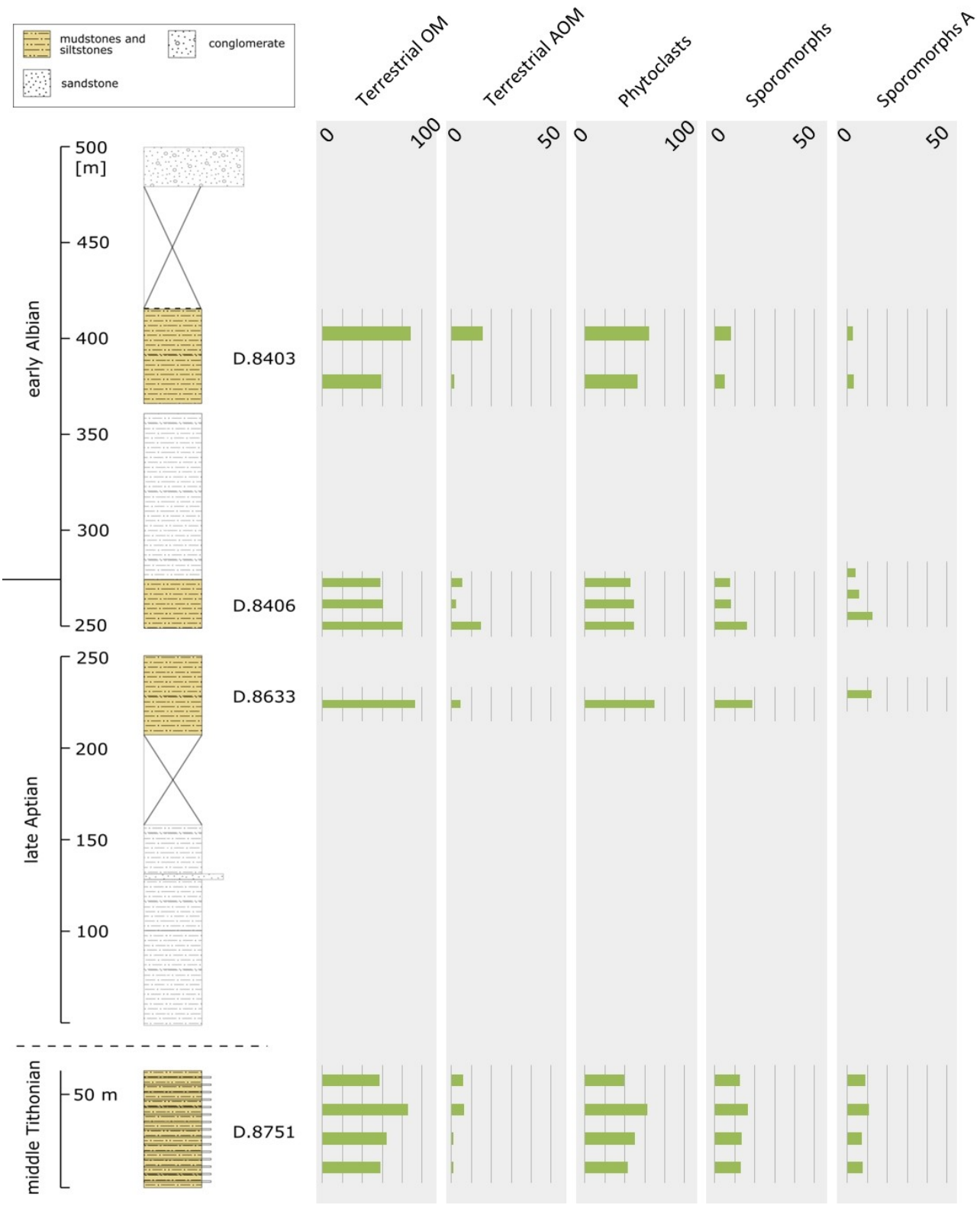

Figure 129: Sedimentary organic matter – terrestrial fraction; Nordenskjöld and Kotick Point Formations. Values given in %, to increase visualisation, different scales are used.

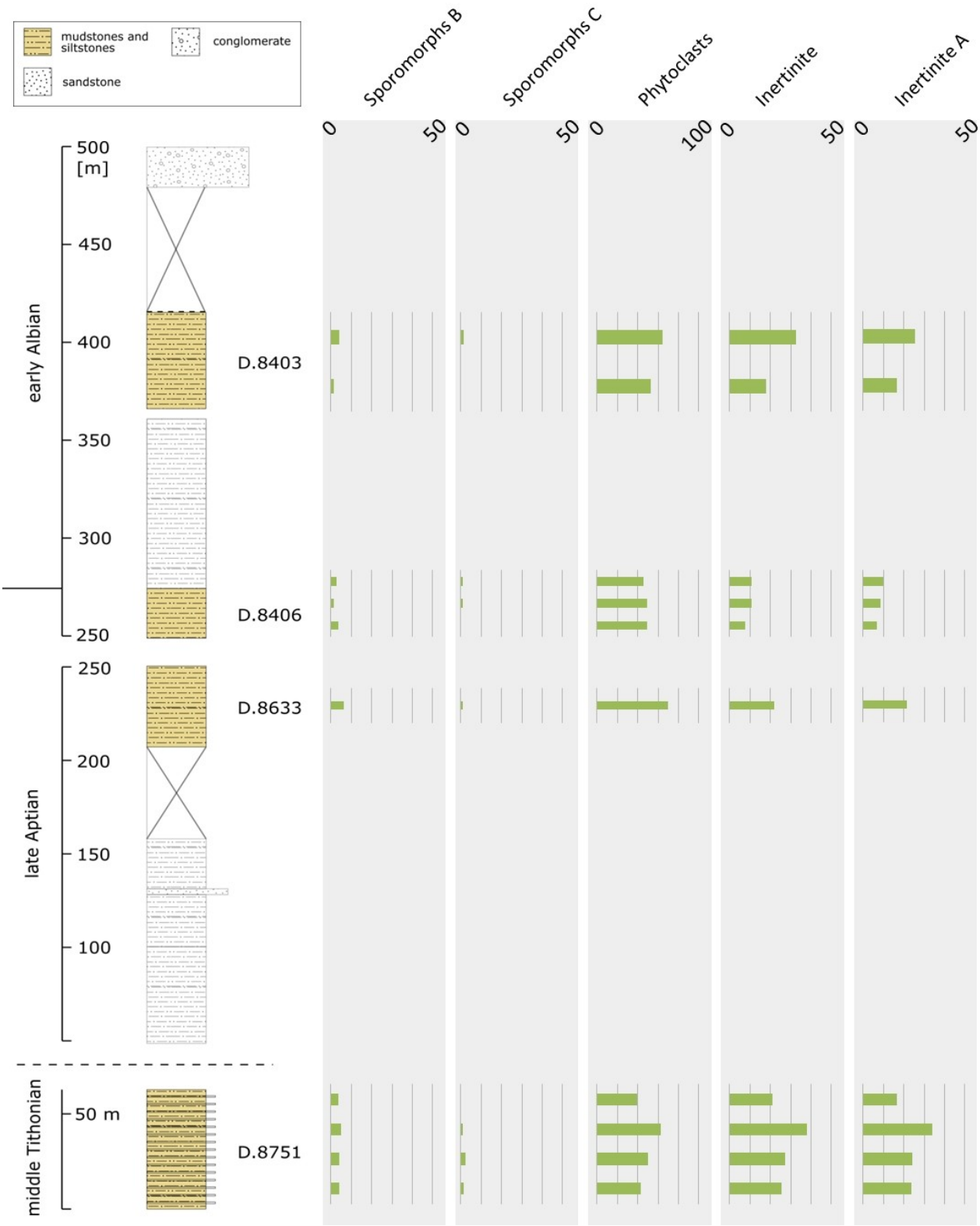

Figure 130: Sedimentary organic matter – terrestrial fraction continued; Nordenskjöld and Kotick Point Formations. Values given in %, to increase visualisation, different scales are used.

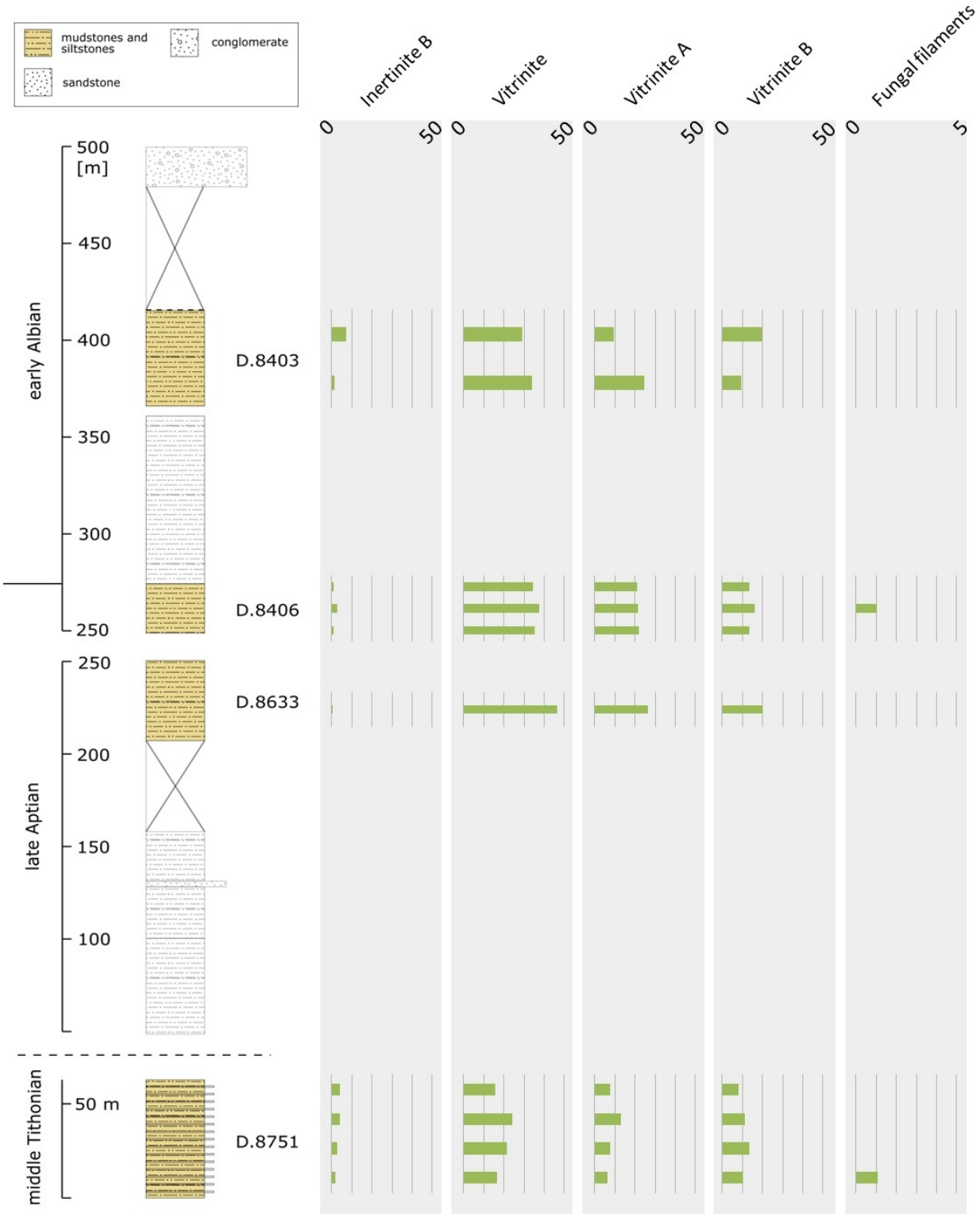

Figure 131: Sedimentary organic matter – terrestrial fraction continued; Nordenskjöld and Kotick Point Formations. Values given in %, to increase visualisation, different scales are used.

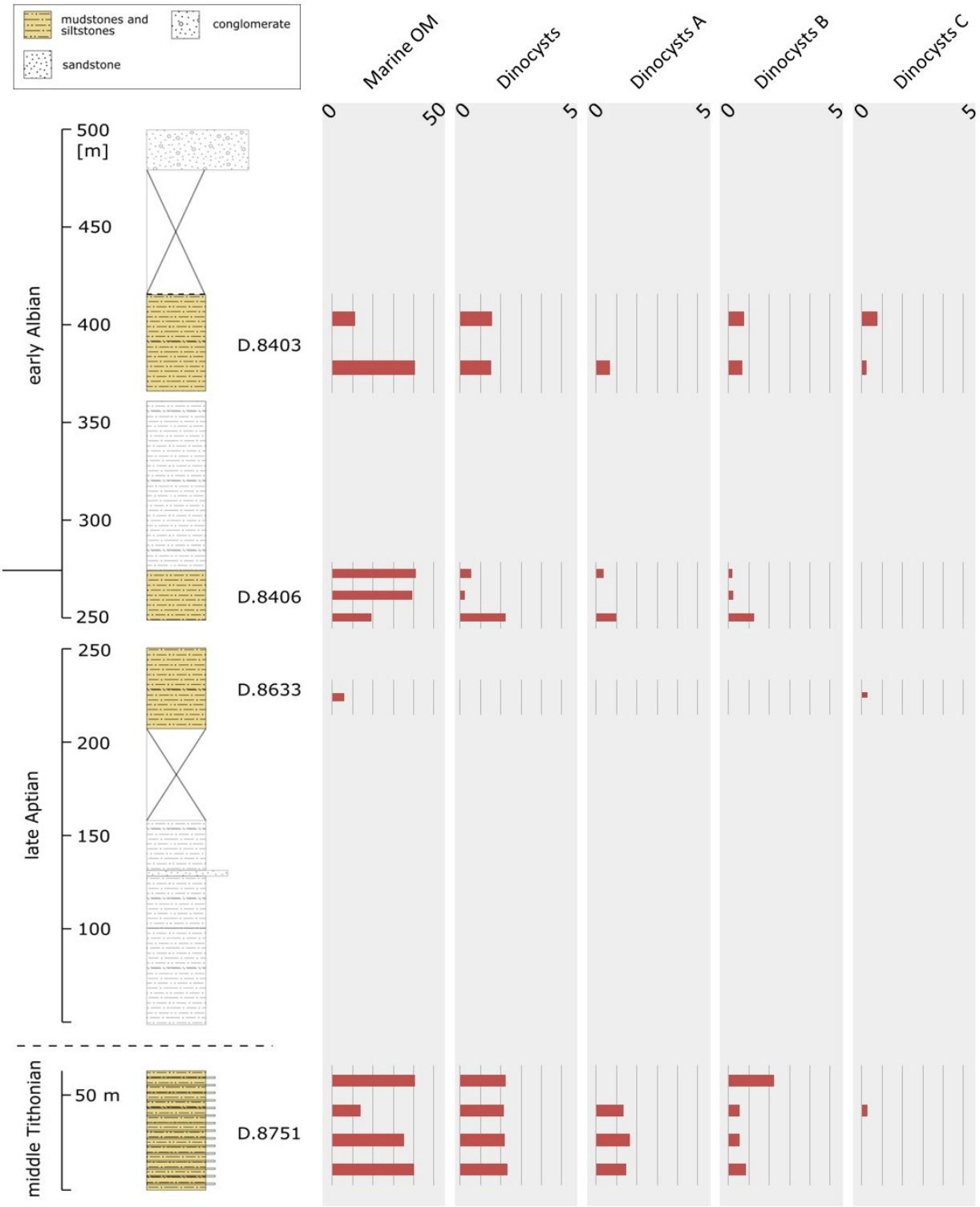

Figure 132: Sedimentary organic matter – marine fraction; Nordenskjöld and Kotick Point Formations. Values given in %, to increase visualisation, different scales are used.

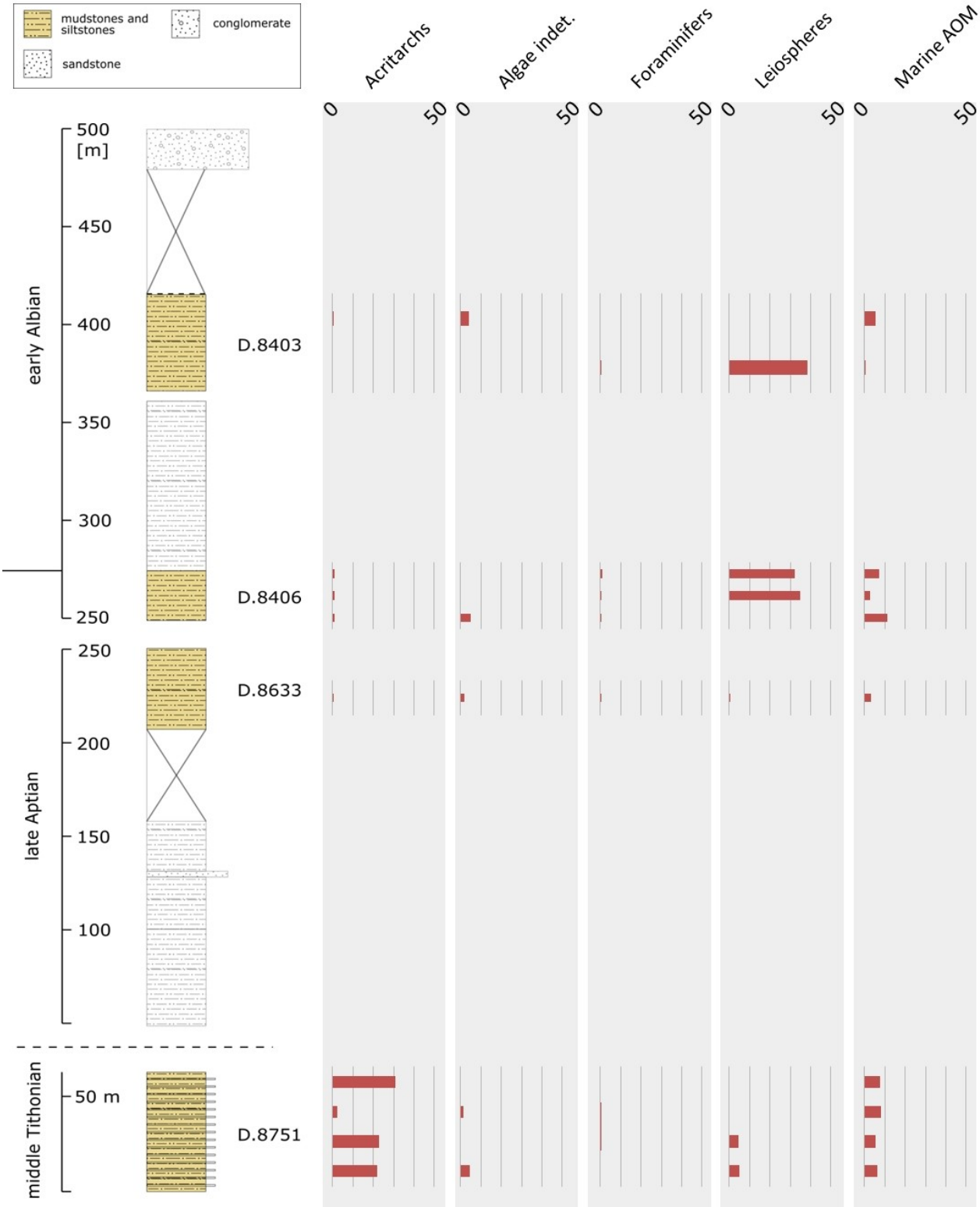

Figure 133: Sedimentary organic matter – marine fraction continued; Nordenskjöld and Kotick Point Formations. Values given in %, to increase visualisation, different scales are used.

AOM-phytoclast-palynomorph plot

Middle Tithonian: One sample each of the Middle Tithonian interval (D.8751.1–D.8751.4) of the Nordenskjöld Formation plots in palynofacies field III – heterolithic oxic shelf ("proximal shelf") and in palynofacies field IVa – shelf to basin transition. Two samples plot in palynofacies field V – proximal suboxic-anoxic shelf (Fig. 134).

Late Aptian: Three Samples of the Late Aptian section (D.8633.10–D.8406.6) of the Kotick Point Formation plot in palynofacies field III – heterolithic oxic shelf ("proximal shelf"). One sample plots in palynofacies field IVa & IVb – shelf to basin transition (Fig. 134).

Early Albian: One sample of the Early Albian section (D.8403.65 & D.8403.30) of the Kotick Point Formation plots in palanofacies feld II – Marginal dysoxic-anoxic basin. Another sample plots in palynofacies field III – heterolithic oxic shelf ("proximal shelf") (Fig. 134).

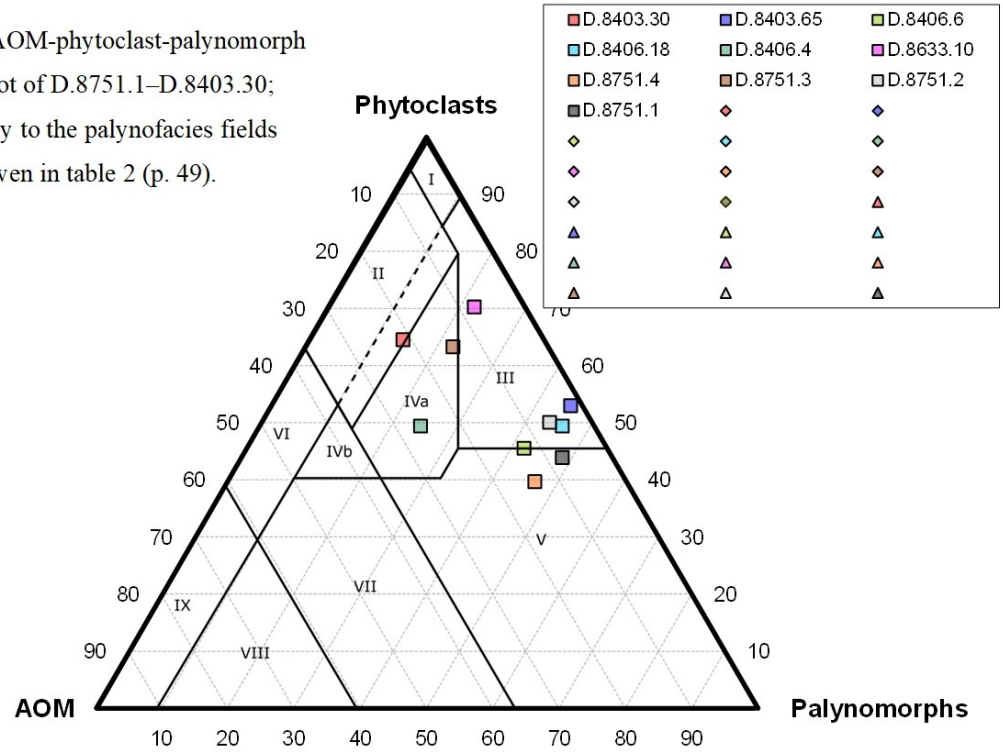

Figure 134: AOM-phytoclast-palynomorph plot of D.8751.1–D.8403.30; key to the palynofacies fields given in table 2 (p. 49).

TOTAL ORGANIC CARBON, TOTAL INORGANIC CARBON, CARBON/SULPHUR/ NITROGEN

In the Tithonian Nordenskjöld Formation of James Ross Island 3 samples were analysed (Fig. 135). Of the Late Aptian–Early Albian succession 5 samples were selected for carbon, nitrogen and sulphur analyses (Fig. 135).

Total organic carbon: In the Tithonian part of the section proportion of TOC ranges from 0.39–0.66 %. An average proportion of 0.51 5 (SD=0.14 %) is idnetified. The Late Aptian–Early Albian shows a mean abundance of TOC of 0.60 % (SD=0.16 %). Throughout the interval the proportion varies between 0.35–0.76 %.

Total inorganic carbon: The content of TIC varies in the Tithonian interval between 5.4–5.6 %. The mean abundance is 5.5 % (SD=0.13 %). The Late Aptian–Early Albian section of James Ross Island shows a mean abundance of TIC of 5.6 % (SD=3.3 %). Samples show a content that varies on a relatively high level between 5.4–8.1 % throughout the lower, middle and lower upper part of the section. The uppermost sample shows a sharp decrease in TIC content from 8.1 % to 0.08 %.

$CaCO_3$: In the Tithonian interval of James Ross Island the $CaCO_3$ proportion varies between 44.8–46.9 %. The interval reaches an averaged abundance of 45.8 % (SD=1.1 %). In the Late Aptian–Early Albian interval the content varies between 0.69–67.6 %. The mean proportion reaches 46.5 % (SD=27.1 %).

Nitrogen: The samples of the Nordenskjöld Formation on James Ross Island contain a nitrogen content that varies between 0.015 % and 0.020 %. A mean proportion of 0.018 % (SD=0.002 %) is identified. The nitrogen content of the Upper Aptian to Lower Albian Kotick Point Formation varies between 0.012 % and 0.052 %. The distribution pattern shows no clear trend. The average nitrogen content of this interval is 0.03 % (SD=0.015 %).

Sulphur: The sulphur content of the Tithonian Nordenskjöld Formation varies between 0.008–0.086 %. The mean proportion is 0.04 % (SD=0.04 %). The Late Aptian–Early Albian section shows a mean proportion of 0.21 % (SD=0.28 %). Individual content varies between 0.02–0.71 %. A distinct distribution pattern is not observed.

C_{org}/N: The C/N ratio of the Tithonian interval varies between 22 and 43. The averaged value is 30. In the Late Aptian to Early Albian section of the Kotick Point Formation the C/N ratio ranges from 12 to 64. An averaged ratio of 29 is detected. A trend is not observed.

S/C_{org}: In the Tithonian interval the ratio of sulphur/C_{org} varies between 0.01 and 0.22. The mean ratio is 0.10. The S/C ratio of the Late Aptian–Early Albian section shows the highest ratio in the middle part of the interval. The ratios of individual samples range from 0.03–1.2. An average ratio of 0.37 is observed.

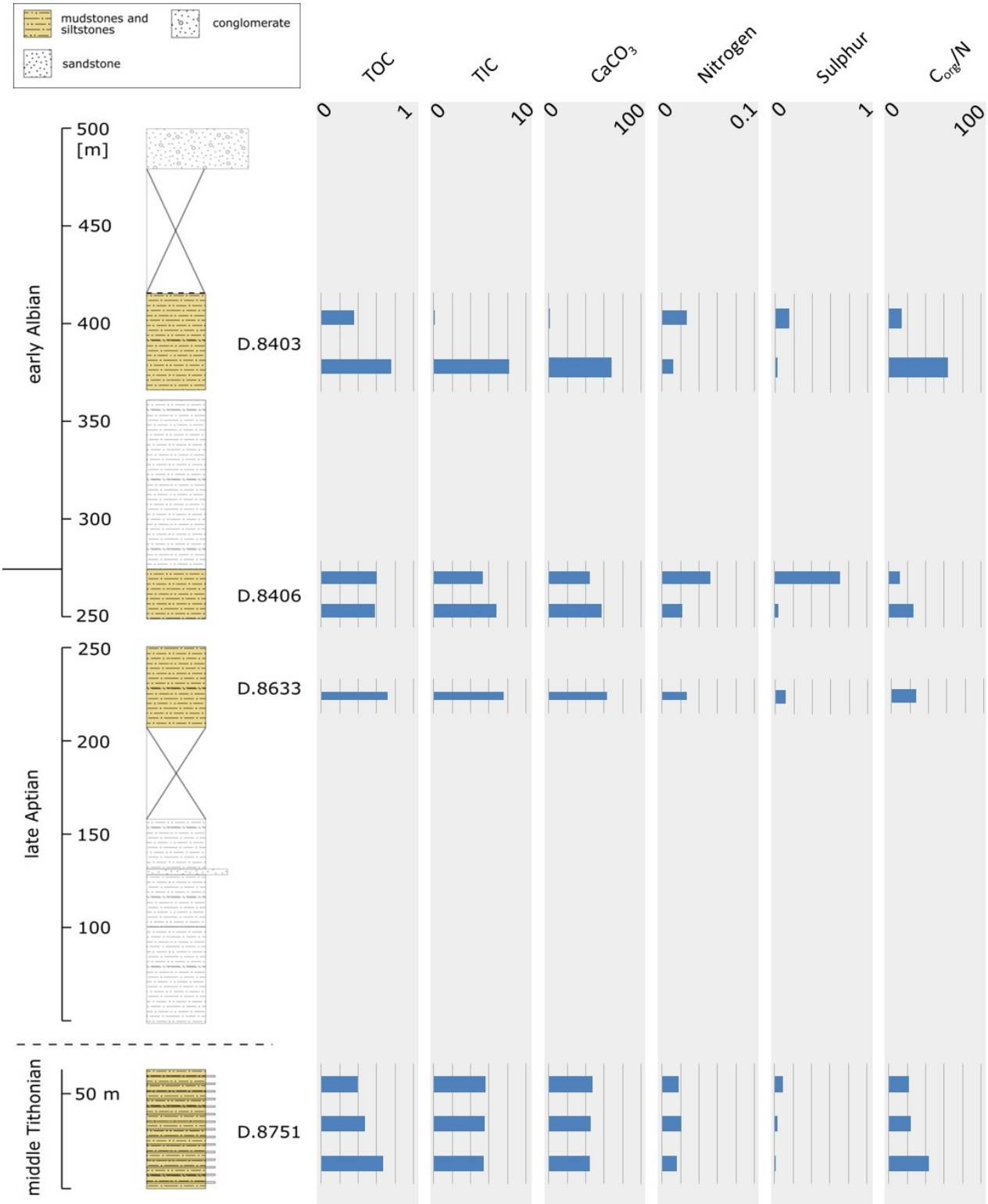

Figure 135: Results of the TOC, TIC and CNS analyses; Byers Group. Except for C_{org}/N, values given in %, to increase visualisation, different scales are used.

THERMAL MATURITY

Tithonian: in this interval TAI/SCI analysis was performed on 2 samples (D.8751.1, D.8751.3). Results show a TAI of approximately 2- to 3-/SCI of 2.5-8 (Ro% 0.5–1.1). The samples represent the maturation stage of diagenesis to catagenesis (cf. Suárez-Ruiz et al., 2012).

Late Aptian to Early Albian: in this interval TAI/SCI analysis was performed on 2 samples (D.8633.10, D.8406.18). Samples show a TAI of approximately 2- to 3-/SCI of 2.5-8 (Ro% 0.5–1.1). Hence the samples represent the maturation stage of diagenesis to catagenesis (cf. Suárez-Ruiz et al., 2012).

MICRO-GLENDONITES

In the sections of James Ross Island one sample contains micro-glendonites. The sample originates from the Early Albian interval. Here 6 specimens are recorded (selected specimens shown in figures 136–139). A mean diameter of 66.2 µm (SD=19 µm) is observed. The specimens range in size from 41 µm to 88 µm.

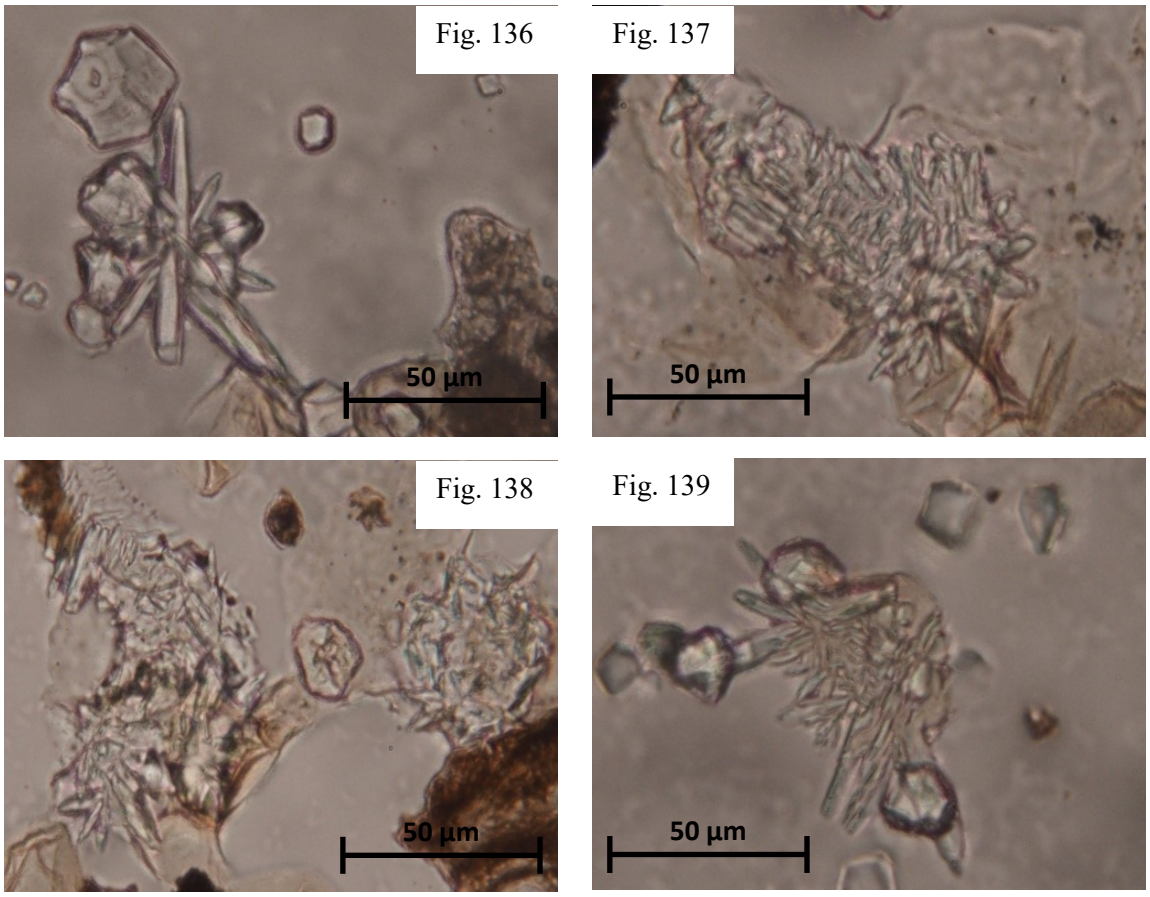

Figures 136–139: selected micro-glendonite specimens of the Nordenskjöld and Kotick Point Formations – Fig. 136: D.8403.65; Fig. 137: D.8403.65; Fig. 138: D.8403.65; Fig. 139: D.8403.65; scale bars given in the photograph

5. DISCUSSION

A North-South transect of sections from central to southern Chile and into Antarctica is here studied for the Tithonian to Albian palaeoenvironmental and climatic history. The approach is multidisciplinary and based on microfloral assemblages, palynofacies analysis, TOC-, TIC-, carbon/ nitrogen/sulphur-analysis, the occurrence of micro-glendonite and carbonate microfacies.
The following chapter will discuss the results obtained by the application of the above methodologies and evaluates the results of these different approaches regarding their palaeoenvironmental and palaeoclimatic significance.

5.1 Palaeoenvironment

The palaeoenvironmental interpretation is mainly based on the composition and preservation of the palynofacies assemblage, composition and abundance of mineral detritus in the palynofacies samples, and results of geochemical (C/N/S) and microfacies analyses.

TITHONIAN

ANTARCTICA

Most samples of the Tithonian interval of the Antarctic sections originate from the Anchorage Formation (Byers Group), Himalia Ridge Formation (Fossil Bluff Group) and Nordenskjöld Formation and are of Middle Tithonian age. Only three samples of the upper Himalia Ridge Formation belong to the Upper Tithonian. Therefore, the Middle Tithonian results are discussed detached from those of the Upper Tithonian succession of the Lo Valdés Formation in central Chile and the Tobífera Formation in Patagonia.

Byers Group – Anchorage Formation

Terrestrial organic matter dominates the sedimentary organic matter composition of the Middle Tithonian sediments with a proportion of 69–100 %. Content of inertinite varies on a high level, resulting in a high (15.5) but strongly varying opaque:translucent (OP/TR) ratio (1.5–175), indicating varying lengths of transport (Tyson, 1993). The carbon:nitrogen (C/N) ratio varies intensely and also suggests a mixture of organic matter (degraded terrestrial – leaves and wood – particles, degraded marine – macrophytes and marine plankton-derived – particles (Tyson, 1995)). Abundance of terrestrial AOM is high, reflecting intense alteration of terrestrial organic matter. Four samples show occurrences of well-preserved sporomorphs. Coexistence of various stages of alteration in both the terrestrial and marine fraction of organic matter (fluorescent AOM and marine palynomorphs) indicate a mixture of material with i) longer ways of transport (inertinite and AOM) and ii) a more autochthonous origin (well-preserved sporomorphs and marine palynomorphs). The amount of siliciclastic detritus in the palynofacies preparations varies but is ubiquitous. In some samples siliciclastic detritus vastly exceeds the amount of organic particles reflecting the low TOC content with a mean of 0.32 wt %. This is generally attributed to dilution effects due to high influx of

siliciclastic material in a near-shore depositional environment (cf. Tyson, 1995). Usually, high proportion of inertinite in association with coarse-grained sediment reflects high energy proximal oxygenated organic-poor facies (e.g., Fisher, 1980; Denison & Fowler, 1980; Parry et al., 1981; Batten, 1982; Whitaker, 1984; Boulter & Riddick, 1986; Bustin, 1988). However, most of the mudstone of the Anchorage Formation was interpreted by Pirrie and Crame (1995) as a hemipelagic deposit. Hemipelagic material is often associated with turbidity currents (Nichols, 2009). After the mixing of the density current water with that of the ocean, the provenance and hence the general composition of the hemipelagic deposit will be the same as that of the turbidite (Nichols, 2009). Low density turbidity currents were reported for the Anchorage Formation by Pirrie and Crame (1995). Turbidite material is also indicated by thin section analysis of samples of the Middle Tithonian interval which show that radiolarian-rich mudstone (facies 3 of Pirrie & Crame, 1995) is interbedded with thin layers of un- to normally graded sandstone (facies 2 of Pirrie & Crame, 1995) and tuff (facies 1 of Pirrie & Crame, 1995). Infrequent occurrences of bioturbated levels are detected in the radiolarian-rich mudstone indicating oxygenated or at least dysaerobic conditions. Sandstone interbeds are rare and reflect oxidised shallow water facies that was transported into the basin by turbidity currents (cf. Pirrie & Crame, 1995). Analysis of the organic matter composition confirms this assumption: the composition of the organic matter assemblages with dominance of terrestrial organic matter in the distal continental margin environment is the result of activity of turbidites (next to the thermal degradation). The reworked organic matter of the sampled intervals most likely originated from a proximal marine environment. These sediments were transported to the area of deposition by the low-density turbidity currents. Although continuously rare, occurrences of particulate marine organic matter such as dinocysts and acritarchs in the upper part of the interval either indicate an increasingly distal marine environment (Tyson, 1993), or reduced dilution by turbidity currents, or both. The occasional high content of disseminated pyrite indicates activity of sulphate-reducing bacteria in depositional settings such as salt-marsh peats (Howarth, 1979) or marginal marine oxygen-depleted basins in which the inflow of oxygenated bottom water is obstructed by a barrier, e.g. a sill (Killops & Killops, 2005). Anoxic conditions in the Anchorage Formation are reported for the early Kimmeridgian with subsequent development to dysaerobic-aerobic conditions in the Early Tithonian (Pirrie & Crame, 1995). Results therefore suggest that at least in part, euxinic bottom water conditions still occurred within the Middle Tithonian of the Anchorage Formation.

Farquharson (1983) and Hathway (2000) suggested that the Antarctic Peninsula formed a discontinuous archipelago during the Late Jurassic, with increasing emergence during the Berriasian due to arc uplift. Previous work suggested that deposition of the Middle Tithonian succession of the Anchorage Formation took place within an extended anoxic, shallow marine basin (Crame et al., 1993). An uplifted landmass (Crame et al., 1993) to the north (Botany Bay Group; Millar et al., 1990) acted as the source for the terrestrial organic matter of the palynofacies samples. Duane (1996) suggested that a high geothermal gradient was responsible for the dominance of phytoclasts (as a result of selective preservation, cf. Tyson, 1995; Batten et al., 1996; Traverse, 2007). This is also observed in the thermal alteration index (TAI) of the analysed samples which varies between 3+ and >5 (Ro% 1.9–3; c. 170–220°C; metagenesis–overmature). Miller and McDonald (2004) argued that the high geothermal gradient resulted either from rifting during basin formation or from a late-stage arc migration event. A depositional environment that varies between dominantly marginal marine to occasionally more fully marine conditions for the whole Late Jurassic-Early–Cretaceous Byers Group

was recognised by Duane (1994) based on the high terrestrial:marine palynomorph ratio. Occurrences of dinoflagellate cysts and the acritarch species *Nummus similis* (Cookson and Eisenack) Burger and *Corrolina* Maljawkina pollen (Backhouse, 1988; Mayagilo, 1992) further implies that the palaeooceanographic setting varied from dominantly marginal marine to occasionally more fully marine conditions (Duane, 1994).

It is here suggested that the organic matter composition represents a mixture of proximal (sandstone turbidites) and distal marine (radiolarian-rich mudstone) environments, with the diversity of components being altered by high thermal gradients (cf. Tyson, 1995; Batten et al., 1996; Duane, 1996; Traverse, 2007). Results point to a Middle Tithonian depositional environment that is characterised by continental margin settings (continental slope to continental rise) (Figs. 140, 145). Occasional influences of distal suboxic-anoxic shelf environments are observed.

Nordenskjöld Formation – Longing Member

In the analysed sediments of the Middle Tithonian Nordenskjöld Formation the majority (66.4 %) of the organic matter composition is of terrestrial origin. The TAI of approximately 2- to 3- (Ro% 0.5–1.1; c. 50–100 °C; diagenesis–catagenesis) indicates that the organic matter composition is not significantly influenced by selective preservation of phytoclast material (cf. Tyson, 1995; Batten et al., 1996; Traverse, 2007). The C/N ratio represents an organic matter composition characterised by terrestrial organic detritus after degradative processing or terrigenous humic acids (Tyson, 1995). The C/N ratio is also in the modal range of marine macrophytes (Tyson, 1995). Since the nitrogen content is continuously low, the C/N ratio might also indicate marine plankton-derived organic matter like N-starved plankton (Tyson, 1995). The organic matter composition throughout the Middle Tithonian interval is composed of up to 31 % of acritarchs which confirms plankton-derived C/N ratios. In Mesozoic sediments abundance of acritarchs in shallow water marginal marine facies is often only dominant when dinocysts are inhibited by brackish and/or hypersaline conditions (Wall, 1965; Downie et al., 1971; Davey, 1971; Riley, 1970, 1974; Burger, 1980; Schrank, 1984; Tyson, 1993). Since acritarchs are the most salinity-tolerant kind of marine phytoplankton (Tyson, 1995) the high amount of acritarchs points to a proximal environment with saline influences (cf. Hancock & Fisher, 1981; Tyson, 1993). The presence of foraminiferal remains within the lower part of the Middle Tithonian interval suggests normal marine conditions (Muller 1959; Hoffmeister 1960; Tschudy 1969; Martinez-Hernandez et al. 1980; Courtinat 1989; Tyson, 1993). Usually, the abundance of foraminiferal linings decreases with increasing water depth (Melia 1984; Tyson, 1993), pointing to proximal open marine environments. In the lowermost samples of the Middle Tithonian interval, the increased occurrence of leiospheres points to a more distal marine depositional environment (Tyson, 1993). Contents of both terrestrial and marine AOM are low in the lower part of the Middle Tithonian Nordenskjöld Formation, with increasing abundance in the upper part of the section. Abundance of fluorescent AOMA exceeds the non-fluorescent AOMT. Increased proportion of AOMA is often correlated with areas of oxygen-depleted bottom waters in distal environments or marginal marine settings with restricted basins (Davey & Rogers 1975, Tissot & Pelet, 1981, Summerhayes 1983; Tyson 1993; Killops & Killops, 2005). The continuously low TOC and sulphur contents, however, rather point to an oxygenated water body (cf. Tyson, 1995). Nevertheless, frequent occurrences of disseminated pyrite in combination with low sedimentation rates (Hathway, 2000) indicate oxygen-reduced euxinic

bottom water within the Middle Tithonian interval of the Nordenskjöld Formation. Hathway (2000) reported that the main cause for anoxia in the area is likely to have been rift-topography and/or transgression-related stagnation. Transition from dysaerobic to aerobic conditions occurred in the Late Tithonian–Early Berriasian transition (Pirrie & Crame, 1995). The organic matter composition, with reduced abundance of phytoclasts and increased occurrence of marine palynomorphs, corresponds well to the hydrodynamic properties of a more distal marine environment (cf. McArthur et al., 2016a, b). However, increased abundance of well-preserved sporomorphs suggests a proximal environment with short ways of transport (Tyson, 1995). The OP/TR ratio is low and distinctly homogenous reflecting incomplete sorting and short ways of transport (Tyson, 1993; McArthur et al., 2016a, b). Based on the AOM-Phytoclast-Palynomorph plot the samples represent a depositional environment of the shelf to basin transition with occasional influence from a heterolithic oxic shelf. Whitham (1993) and Hathway (2000) suggested that the Nordenskjöld Formation represents a hemipelagic setting with reduced deposition rates. Abundance of siliciclastic detritus in the palynofacies preparations of the Nordenskjöld Formation is reduced which in combination with the low TOC content suggests low influx and reduced sedimentation rates. In this interpretation, deposition of the Nordenskjöld Formation took place in a quiet-water anoxic barred basin with restricted circulation and intermittent ash-falls (Doyle & Whitham, 1991; Whitham, 1993). Farquharson (1983) describes the sediments of the Nordenskjöld Formation as a succession of alternating radiolarian-rich laminated mudstone and ash-fall tuff. The macrofossil assemblage is dominated by pelagic and pseudoplanktonic species (Doyle & Whitham, 1991).

It is suggested that deposition of the Tithonian sediment succession of the Nordenskjöld Formation took place in an epicontinental sea with restricted basins and occasional oxygen reduced conditions.

Fossil Bluff Group – Himalia Ridge Formation

The palynofacies assemblage of the Middle Tithonian Himalia Ridge Formation is devoid of any particulate marine organic matter. The fluorescent portion of the total AOM most likely represents degraded marine plankton-derived organic matter (cf. Tyson, 1995). The organic matter composition with dominance of non-fluorescing material is suggested to be either the result of selective preservation of the more resistant phytoclast material (cf. Tyson, 1995; Batten et al., 1996; Traverse, 2007), or results from oxidation processes during transport, or both (cf. Tyson, 1995; McArthur et al., 2016a, b). The OP/TR ratio varies significantly between 1.1 and 17.5, reflecting varying lengths of transport of the terrestrial organic matter. A higher mean OP/TR ratio is observed in the Middle Tithonian interval pointing to increased lengths of transport in this interval. The organic matter composition can be divided into two groups, based on the difference in alteration intensity: i) terrestrial organic matter which experienced oxidation during transport – the TAI is approximately 4- to 4+ (Ro% 2.0–2.7; catagenesis–metagenesis) and thus equivalent to c. 175–210 °C, while the presence of fluorescent AOM suggests the existence of a less degraded and much less abundant group of organic matter – ii) marine AOM which was only altered to a level where the constituents lost their structure but not their fluorescence (AOM loses its fluorescence above 150–160 °C; Tyson, 1995). Miller and Macdonald (2004) reported thermal alteration of the organic matter in the Himalia Ridge Formation of up to 100–140 °C. It is likely that the fluorescent marine AOM represents the autochthonous portion of the sedimentary organic matter and that the much larger proportion of

terrestrial organic matter results from both the degree of thermal alteration processes and reworking caused by influx of turbidity currents (cf. Streel & Bless, 1980; Tyson, 1993, 1995; Traverse, 2007). It is therefore suggested that the depositional environment of the unstable continental slope (cf. Butterworth, 1985) was characterised by input of material with a more near-shore palynofacies composition. Two samples in the lowermost and middle part of the interval show increased amounts of disseminated pyrite. Content of dispersed pyrite is indicative of sulphate-reducing bacteria in depositional settings such as marginal marine oxygen-depleted basins in which the inflow of oxygenated bottom water is reduced (Killops & Killops, 2005). However, TOC is low throughout the sampled interval (reflected also by very low proportions of organic matter in the palynofacies preparations); the high abundance of phytoclasts and siliciclastic detritus simultaneously indicate a depositional environment with high influx of terrestrial material (cf. Tyson, 1995). A lowered OP/TR ratio and increased abundance of mineral detritus in the Upper Tithonian section suggests a more proximal depositional environment for this part of the interval.
The Himalia Ridge Formation is a highly variable stratigraphic unit with a wide range of facies and lateral variation. Previously suggested depositional settings for the Fossil Bluff Group range from inter-deltaic and shallow shelf environments (Horne, 1969), via tidal flat, sub-littoral and deeper water environments (based on lithofacies) (Elliott, 1975), to a complex environment roughly corresponding to inter-deltaic facies (Horne, 1969; Taylor et al., 1979). Butterworth et al. (1985) found evidence for low-density turbidity currents; these turbidites were deposited within submarine fans on an unstable slope below wave base. Distribution and preservation of organic matter in turbidite systems are mostly controlled by currents, local vegetation, oxygenation and especially density sorting during transport (Caratini, 1994; Tyson, 1995; Jäger & McLean, 2008; McArthur et al. 2016). The analysed samples originate from interbedded facies and are at least partly derived from turbidites (cf. Macdonald et al., 1993), which is also reflected in the organic matter composition.

For the Middle Tithonian interval a continental margin (continental slope to continental rise) setting with input of reworked organic matter by turbidites and at times suboxic conditions is suggested by the organic matter composition and the AOM-Phytoclast-Palynomorph plot. The Upper Tithonian interval is characterised by more proximal continental margin settings.

CENTRAL CHILE

Lo Valdés Formation

Large intervals of the Tithonian sediment succession of the central Chilean Cajón del Morado and Lo Valdés sections show inertinite-dominated organic matter compositions. Opaque phytoclast material is mainly derived from the oxidation of translucent wood material during prolonged transport or post-depositional alteration (Tyson 1993). Tyson (1993) states that shoreface environments are often characterised by a phytoclast-dominated organic matter composition. The ecological conditions reflected here point to a near shore depositional environment for the phytoclast-dominated deposits of the Tithonian section of the Lo Valdés Formation. The scarcity of marine palynomorphs (limited occurrence of foraminifers) in the palynofacies samples, and the absence of fluorescing AOM in both the CM and the LV sections, is most likely caused by increased thermal alteration: analyses of the illite/smectite mixed-layers and the TAI both indicate that the organic matter was altered, in the Lo

Valdés Formation, to the point of metagenesis (> 200 °C, cf. Suárez-Ruiz et al., 2012). This resulted in a selective preservation of degradation-resistant particles, i.e. phytoclasts (cf. Tyson, 1995; Batten et al., 1996; Traverse, 2007) and indicates that marine facies indicators which existed in the palynofacies assemblage prior to thermal degradation were lost during oxidation or became part of the non-fluorescing AOM (cf. Traverse, 2007). It is this intense alteration that impedes a detailed and comprehensive interpretation of the palaeoenvironment in the central Chilean sections (CM and LV) based on the organic matter assemblage. In such cases, the OP/TR ratio of phytoclasts and the shape of inertinite particles (rounded or blade-shaped) provide better evidence for the evaluation of the depositional environment (Tyson, 1995). Several indications were observed for a proximal high-energy depositional environment throughout the Upper Tithonian sediment succession: i) low OP/TR ratios (CM: 3.5, LV: 2.6) of phytoclasts, ii) high abundance of equant (round) inertinite which additionally show no distinct decrease in size, iii) frequent occurrence of cross- or horizontal lamination (Salazar, 2012), iv) occurrences of authigenic glauconite and ooids in microfacies samples (indicating shallow shelf and high energy environments; Chafetz & Reid, 2000; Nichols, 2009), v) coarse sandy lithofacies and low TOC content (0.26 wt % (CM), 0.22 wt % (LV)) suggest deposition in a near-shore oxidising environment, vi) increased abundance of sporomorphs – sporomorphs are characterised by intermediate buoyancy between phytoclasts and marine palynomorphs (McArthur et al., 2016a, b) and vii) microfacies analysis that shows an inner ramp-open marine environment for the middle part of the Upper Tithonian succession. A mid-ramp depositional environment is indicated for the Early and Late Tithonian. The infrequent occurrence and at times increased abundance of fungal remains in the Tithonian palynofacies samples of the Lo Valdés Formation points to intervals with increased fungal activity similar to those found in swamp environments (Cohen et al., 1989; Tyson, 1995). However, the co-occurrences of well-preserved vitrinite indicate varying periods of oxidation and fungal mouldering of the phytoclasts. Reworking processes of the fungal remains are therefore suggested to have occurred in a near shore environment rather than a swamp setting (cf. Tyson, 1995). The brown colour of the fungal filaments (as a result of thermal alteration) rule out fungal growth in Recent times (Tyson, 1995). Reworking is also indicated by the high proportion of non-fluorescing AOM in the Tithonian deposits, which may have been caused by processes of bacterial activity (cf. Tyson, 1995; Batten et al., 1996; Traverse, 2007). A terrestrial origin of the vast majority of organic matter of the Tithonian sediments and therefore a proximal depositional environment (cf. Tyson, 1995) is also indicated by the results of the geochemical analysis. Sediments are characterised by varying C/N ratios that show that most of the organic matter is derived from terrigenous humic acids, leaves and herbaceous plants, and only to a minor extent from marine macrophytes (Tyson, 1995). The C/N ratio of some samples of the middle part of the Tithonian sediment succession also indicates marine plankton-derived organic matter (Tyson, 1995). The results of the geochemical analyses correspond well to the optical observations and also indicate a proximal depositional environment. However, as C-N bonds are much weaker than C-C bonds (Tyson, 1995 and references therein), a preferential loss of nitrogen is expected by alteration processes such as diagenesis (Tyson, 1995). Because of the intense thermal maturation of the central Chilean sections, an alteration of the C/N ratio is likely and the results are here interpreted only as an additional indicator of terrestrial-dominated organic matter and, in conclusion, a proximal marine depositional environment. Salazar (2012) found evidence for deposition in shallow sandy seas and shoreface facies - horizontal lamination, cross lamination and few ooids – distributed across a storm-dominated shelf (cf. Nichols 2009).

The Tithonian sediment succession of the Lo Valdés Formation is thus characterised by a proximal high-energy depositional environment, namely reflecting inner ramp-open marine to mid-ramp settings.

PATAGONIA

Upper Tobífera Formation

The Sofia 1 core is the only Patagonian section studied here that contains deposits of Tithonian age (upper Tobífera Formation). Due to the lack of biostratigraphical data, it is not possible to determine to which part of the Tithonian interval the sampled section of the Sofia 1 core corresponds. A Late Tithonian age is here used for the interpretation of the results.

In this core, the palynofacies assemblage is dominated by structured and unstructured terrestrial organic matter. However, due to the high thermal alteration of approximately TAI 4 to 5- (Ro% 2.5–3.5; c. 200–230°C) it is likely that the high abundance of terrestrial organic matter and especially inertinite is also the result of post-depositional oxidation of the organic matter. Since it is likely that the high thermal alteration resulted in the selective preservation of degradation-resistant phytoclasts and a loss of marine palynomorphs (lowered resistance to degradation processes, cf. Tyson (1995); Batten et al. (1996); Traverse (2007)), the validity of the terrestrial dominated palynofacies assemblage is limited. Therefore special focus is given to the OP/TR ratio and the shape of inertinite particles. Most terrestrial organic matter is deposited near the mouths of rivers and remains trapped in the inner part of the shelf (Hedges & Parker 1976, Tyson 1995). The high OP/TR ratio of 20.3 is either the result of a near-shore highly oxidised depositional environment or oxidation and fractionation of phytoclasts during prolonged ways of transport (Tyson, 1993; McArthur et al., 2016a, b). Roundness and size of the inertinite particles vary indicating incomplete sorting. Therefore a near shore environment is indicated by the morphologies of inertinite particles (cf. Tyson, 1995). The high content of phytoclasts (mean value of 90 %) correlates with coarse silt to very fine sand facies (Reyre 1973; Tyson, 1993) indicating a shelf marine depositional environment for the interval. The high amount of siliciclastic mineral detritus in the palynofacies preparations, together with the low TOC content of the Tithonian deposits, indicate a well-oxygenated near shore environment (siliciclastic dilution, cf. Tyson, 1995). Occurrences of terrestrial palynomorphs are restricted to scarce occurrences of sporomorphs. Well-preserved specimens are absent and throughout the section content of miospores decreases significantly. The absence of well-preserved sporomorphs results from increased degradation by thermal alteration or prolonged transport, or both (cf. Tyson, 1995). A post-depositional alteration of the sporomorphs is indicated by the high thermal alteration. The absence of light saccate pollen grains indicates a sporomorph composition representative of a near shore environment (Tyson, 1995; MacArthur et al., 2016 a, b). In the AOM-phytoclast-palynomorph plot all Tithonian samples indicate a highly proximal shelf environment but samples are affected by the thermal degradation. A more distal fully marine environment in the upper part of the sampled interval is indicated by the decrease in miospore abundance throughout the interval, the occurrence of acritarchs in the uppermost sample and the decreasing amounts of siliciclastic mineral detritus in the palynofacies preparations. In the Tithonian sediments the C/N ratio is reduced and homogenous and ranges from 13–17. Although the ratio is in the range of terrestrial organic matter such as degraded detritus and terrigenous humic acids or marine macrophyte material, the low ratio points to a more

fully marine organic matter composition (Tyson, 1995). However, nitrogen was lost by alteration processes and original amounts cannot be assessed, wherefore results likely represent a mixture of terrestrial and proximal marine organic matter.

A conclusive determination of the depositional environment of the Tithonian upper Tobífera Formation of the Sofia 1 core is difficult to establish because of the poor preservation state of organic matter and the tectonically active arc setting (extensional tectonics creating asymmetric hemigrabens) (Schwarz et al., 2011). The sampled material of the Sofia 1 core exclusively consists of cuttings. Therefore no sedimentary structures are available for a conclusive interpretation of the depositional environment. The organic-rich shales of Late Jurassic and Early Cretaceous ages are assigned to anoxic marine environments (Stinnesbeck et al., 2014; EIA, 2015). A TOC-rich anoxic environment is not reflected in the results of the present study which is attributed to the fact that the analysed samples are shale and siltstone which were mostly deposited in shallow water (Fildani & Hessler, 2005). Changes in depositional regimes and sediment dispersal of the Late Jurassic–Early Cretaceous extensional Rocas Verdes backarc basin (Tobífera and Zapata formations) are related to the onset of Andean contraction and transition to the Magallanes retroarc foreland basin (Rabinowitz & La Brecque, 1979; Dalziel, 1986; Ramos, 1988; Fildani & Hessler, 2005). Based on the results a shallow water shelf marine environment is suggested for most of the Tithonian interval of the upper Tobífera Formation with a potentially increasingly distal setting towards the Berriasian.

Summary

The depositional settings of the Middle Tithonian interval in Antarctica (Anchorage Formation, Nordenskjöld Formation and Himalia Ridge Formation) show more distal marine affinities. The Late Tithonian shows a change towards majorly proximal depositional settings of the Himalia Ridge Formation, Tobífera Formation and Lo Valdés Formation (Figs. 140, 145).

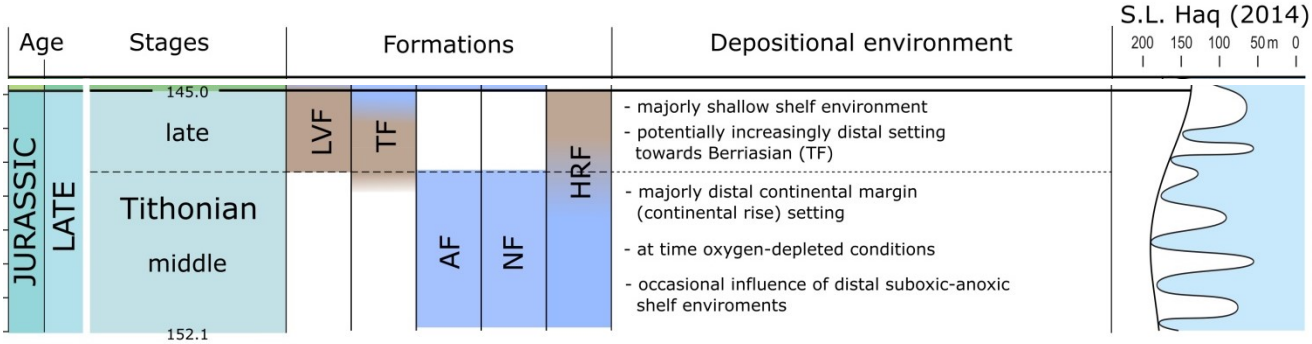

Figure 140: Depositional settings during the Tithonian interval; Formations: LVF=Lo Valdés, TF=Tobífera, AF=Anchorage, NF=Nordenskjöld, HRF=Himalia Ridge; S.L.=sea level; brown=proximal environment, blue=distal environment; global sea level curve from Haq (2014).

BERRIASIAN

CENTRAL CHILE

Lo Valdés Formation

The organic matter composition in Berriasian deposits of the central Chilean Lo Valdés Formation resembles that of the underlying Tithonian sediments. Terrestrial organic matter dominates the palynofacies assemblage. In the CM section, the lowermost and uppermost Berriasian palynofacies samples contain marine facies indicators (foraminifers and acritarchs) which are absent in the LV section. The organic matter composition of the LV section is thus completely composed of terrestrial organic matter (AOMT, phytoclasts, sporomorphs and rare fungal remains). The presence of ammonites (Salazar & Stinnesbeck, 2015b), frequent occurrences of echinoderms in the microfacies samples and increased carbonate content indicate marine depositional environments. The low abundance of sporomorphs and their poor preservation state indicate an increased distance to the sediment provenance and suggest a stable stratified water mass (Tyson, 1995). The increased (CM: 5.2, LV: 7.4) OP/TR ratio is characteristic for a more distal depositional environment with prolonged fractionation during transport (Tyson, 1993; McArthur et al., 2016a, b). Samples show high TOC values and disseminated pyrite indicating a more distal environment with oxygen-depleted (euxinic) bottom water, enhanced bioproductivity and low sedimentation rates (Didyk et al. 1978; Tourtelot 1979; Tyson, 1995; Killops & Killops, 2005). Oxygen-depleted bottom water in distal environments, or marginal marine settings with barred basins, are often correlated with an increased content of AOM (Davey & Rogers 1975, Tissot & Pelet 1981; Summerhayes 1983; Tyson 1993; Killops & Killops, 2005). This is reflected in the central Chilean Berriasian sediment succession by increased proportions of AOM. The TAI of approximately 4- to 4+ (Ro% 2–2.5; c. 175–200 °C) suggests maturation to metagenesis (cf. Suárez-Ruiz et al., 2012). The intense alteration of the organic matter results in a relative accumulation of degradation-resistant particles (cf. Tyson, 1995; Batten et al., 1996; Traverse, 2007) which explains the dominance of terrestrial organic matter in a supposedly distal shelf marine environment. The less resistant marine palynomorphs were removed from the total sedimentary organic matter by oxidation, bacterial activity and thermal alteration (cf. Tyson, 1995; Batten et al., 1996; Traverse, 2007) and became part of the AOM, which is also reflected in the few occurrences of low C/N ratios. Some samples of the Berriasian deposits yield exceedingly low C/N ratios indicating that a significant amount of the amorphous organic matter is marine plankton-derived (Tyson, 1995). In the majority of the samples C/N ratios are high suggesting terrestrial-derived organic matter like terrigenous humic acids and remains of leaves and herbaceous plants, but the latter may also be derived from marine macrophytes (cf. Tyson, 1995). The absence of foraminifers in the Berriasian deposits might indicate a more distal environment – foraminifers are larger and heavier than marine algae and are thus reported to be transported less easily into deep-marine systems (Tyson, 1993, McArthur et al., 2016a, b). For the Berriasian section of the Lo Valdés Formation the microfacies analysis indicates a more distal marine environment (mid-ramp (shoal)/outer ramp to basin, cf. Flügel (2004)) with common horizontal lamination which was also observed by Salazar (2012). The results of the AOM-Phytoclast-Palynomorph plot were not adduced for the interpretation of the palaeoenvironment due to the poor preservation state of organic matter.

For the Berriasian interval of the central Chilean section results suggest a more distal shelf

environment (mid-ramp to outer ramp) with high organic matter preservation and temporal oxygen-reduced conditions. This observation is in agreement with Salazar (2012) who described this interval as offshore transition facies in a low oxygen and low energy environment.

PATAGONIA

Lower part of the lower Zapata Formation

The original data provided by ENAP for the Sofia 1 core do not allow for a subdivision of the section into a Berriasian and Valanginian interval. Even though, based on differences in the organic matter composition and the results of the geochemical analysis, a tentative subdivision is possible into a lower (potentially Berriasian) and an upper part (potentially Valanginian). The lower part of the lower Zapata Formation is discussed below, whereas the upper part is discussed in the Valanginian paragraph.

The palynofacies assemblage in the lower part of the lower Zapata Formation is dominated by terrestrial organic matter, especially by phytoclasts. The OP/TR ratio is exceedingly high (101.8), indicating either a highly oxidised near-shore depositional environment, or intense oxidation and fractionation of phytoclasts during prolonged transport (Tyson, 1993; McArthur et al., 2016a, b). Another reason for the high abundance of phytoclasts, especially inertinite, is a high degree of selective preservation: abundance of phytoclasts is often encountered in sections with intense thermal degradation, in which the highly resistant (refractory) nature of lignin leads to the enhanced preservation of wood debris (Tyson, 1993). Analysis of thermal alteration shows TAI/SCI values equivalent to Ro% 2.5–3 (c. 200–220 °C, cf. Suárez-Ruiz et al., 2012) which points to increased selective preservation of phytoclasts. Abundance of sporomorphs is low and specimens are poorly preserved, which further indicates increased distance to the sediment provenance (Tyson, 1993; McArthur et al., 2016a, b). Marine organic matter is absent in the deposits of the lower part of the Lower Zapata Formation. It is suggested that high thermal stress led to a degradation-induced structure loss of the marine organic matter fraction and hence to a conversion into AOMA (cf. Tyson, 1995). Since the organic matter was thermally altered by more than 200 °C, fluorescence of marine AOM is no longer expected (cf. Tyson, 1995), making it impossible to differentiate between marine AOMA and terrestrial AOMT. Proportion of siliciclastic detritus varies strongly. Especially in the lower part of the interval, content is significantly reduced in contrast to the underlying Tithonian sediment succession. The reduced amount of siliciclastic mineral detritus in the palynofacies preparations – in combination with increased TOC content – indicates a more distal depositional setting with reduced influence of siliciclastic dilution (Tyson, 1995). In the AOM-phytoclast-palynomorph plot, the sediments of the lower part of the lower Zapata Formation reflect a proximal basin environment. However, alteration of the composition is expected due to the poor preservation of the organic matter composition. The C/N ratio varies significantly between 12–42, thus indicating organic matter derived from degraded detritus and terrigenous humic acids or marine macrophyte material and benthic macroalgal detritus (Tyson, 1995). In contrast to the underlying Tithonian section, nitrogen content is increased. Higher nitrogen content is often connected to marine plankton-derived organic matter (cf. Tyson, 1995) but influx of inorganic N caused by volatilisation through volcanism also influences the N content (Holloway et al., 2002).

A conclusive determination of the depositional environment of the lower part of the lower Zapata

Formation is difficult because of the poor preservation state of the organic matter and the tectonically active arc. The onset of Andean contraction and transition to the Magallanes retroarc foreland basin (Tobífera and Zapata formations) during the Late Jurassic–Early Cretaceous (Rabinowitz & La Brecque, 1979; Dalziel, 1986; Ramos, 1988; Fildani & Hessler, 2005) impede comprehensive assessment of the depositional environment. However, changes in organic matter composition and differences in the results of the geochemical and optical approaches suggest a potentially distal shelf to proximal basin environment for the lower (?Berriasian) part of the lower Zapata Formation.

ANTARCTICA

Fossil Bluff Group – Himalia Ridge Formation

The organic matter composition shows little fluctuation, except for variations in the abundance of well- and fairly preserved phytoclasts. The TAI analysis shows values of approximately 4- to 4+ (Ro% 2.0-2.7; c. 170-220 °C), whereas vitrinite reflectance (Ro) data of Miller & Macdonald (2004) range from 2.3 % to 3.7 % (>250 °C). Variations in the results of the thermal alteration analysis of individual samples may result from turbidity currents that caused a mixture of organic matter with different degradation states. The high values of alteration suggest selective preservation of phytoclast material resulting in a general absence of marine palynomorphs (cf. Tyson, 1995; Batten et al., 1996; Traverse, 2007). The OP/TR ratio is erratic indicating mixed lengths of transport (Tyson, 1993, 1995; McArthur et al., 2016a, b), which also reflects a mixture of particle transport by low density turbidity currents (Macdonald et al., 1993). High proportion of siliciclastic detritus in the palynofacies samples, reflects influx of near-shore material (siliciclastic dilution, cf. Tyson, 1995) and further points to activity of turbidity currents. The low abundance of sporomorphs and their poor preservation reflect increased distance to the sediment provenance and alteration processes during transport (Tyson, 1995; McArthur et al., 2016a, b). Together with the occurrence of turbidites a continental margin (continental rise) environment is indicated. The AOM-Phytoclast-Palynomorph plot shows a highly proximal basin composition with a tendency to a marginal dysoxic-anoxic basin setting, but values are affected by the high thermal alteration and selective preservation.

According to Butterworth et al. (1988) and Butterworth (1991) the deposits of the Himalia Ridge Formation represent a submarine fan complex, in which arenites/rudites represent tectonic pulses resulting from arc uplift. Gradual basin shallowing was reported by the authors. Bioturbation is frequent indicating oxygenated bottom water conditions (Crame & Howlett, 1988). The combination of low TOC content and low abundance of pyrite in the palynofacies samples suggests an oxygenated water body (Tyson, 1995). Siliciclastic detritus is ubiquitous in the samples used for palynofacies; this is also reflected by the low numbers of organic particles in the palynofacies samples (dilution effects due to high influx of siliciclastic material). Rather than reflecting a proximal depositional environment, it is here suggested that the high abundance of siliciclastic detritus results from turbidites.

The depositional environment of the Berriasian HRF is characterised by low-density turbidites in a submarine fan setting, as already suggested by Butterworth (1985, 1988). Deposition on the continental rise is suggested for the Berriasian Himalia Ridge Formation.

Byers Group – President Beaches Formation

The organic matter composition of the deposits of the PBF is dominated by terrestrial organic matter. The OP/TR ratio varies intensely indicating varying lengths of transport and different intensities of oxidation and degradation for the phytoclast group (Tyson, 1993; 1995; McArthur et al., 2016a, b). All marine palynomorphs are present but abundance is low (between 0.02–1.1 %). The abundance of fluorescent AOMA is high (up to 29 %), reflecting the presence of marine palynomorphs after degradation-induced structure loss (cf. Tyson, 1995) and points to bacterial degradation (cf. Williams 1984; Glikson & Taylor 1986; Tyson, 1995), whereas at times largely increased abundance of fungal filaments points to fungal mouldering of organic matter that contributed to the increased proportion of terrestrial AOM (cf. Tyson, 1995). Since the C/N ratio is also continuously very low, indicating a larger amount of marine plankton-derived organic matter (e.g., marine humic acids, zooplankton faecal pellets) (Tyson, 1995), the scarcity of marine palynomorphs may be the result of selective preservation which favoured the conservation of degradation-resistant phytoclast material (cf. Tyson, 1995; Batten et al., 1996; Traverse, 2007). The intensity of thermal degradation varies significantly throughout the Berriasian interval between Ro% 0.8–1.7 (85–165 °C); it is hence suggested to reflect the variety in preservation state and composition in the organic matter assemblage. The preservation state of sporomorphs varies significantly and indicates various lengths of transport that supposedly originated from turbidity currents (cf. McArthur et al., 2016a, b). The sedimentary organic matter composition represents a mixture of proximal terrestrial-dominated material and *in situ* marine organic matter, both in various stages of preservation. Thin section analysis shows that the lower part of the Berriasian interval is characterised by medium-to-coarse grained sandstone which is superseded by parallel laminated mudstone which in turn gives way to rippled cross-bedded fine-to-medium grained sandstone. This alternation in grain size and sedimentary structures points to varying distance to the shoreline (Boggs, 2014) but is also common in the Bouma sequences of low- and medium density turbidity currents (Nichols, 2009). Lomas (1999) reported that the sandstone was probably deposited by low-density turbidity currents. Rather than being caused by sustained discharges, Lomas (1999) suggested that most of the turbidites were deposited from discrete surge-type events. Widespread slope instability is indicated by locally slump and slope collapse zones and thick mud debrites (Duane, 1997). The AOM-Phytoclast-Palynomorph plot indicates highly proximal basin to marginal dysoxic-anoxic basin conditions. The abundance of disseminated pyrite varies strongly, but slightly increased TOC contents (0.1–1.1 wt %) suggest an oxygen-restricted environment. In contrast to the euxinic bottom waters in the Berriasian sections of central Chile, occurrences of benthic foraminifers and individual samples with general absence of pyrite indicate that anoxic conditions were not permanent. However, occurrences of benthic foraminifera might also result from input of turbidity currents. The mudstones of the PBF are finely laminated, with a restricted benthic macrofauna and little bioturbation, indicating inhospitable seafloor environments (Duane, 1996; Lomas, 1999). Lomas (1999) concluded that oxygen depletion was not the primary limiting factor on the benthic biomass; rather, key stress factors may have been a soft substrate, rapid sedimentation and turbid bottom waters. The abundance of terrestrial plant debris in the mostly fine-grained slope-apron deposits indicates both, a well-vegetated source area and a substantial fluvial input to the basin (Lomas, 1999). According to Duane (1996), the spore and pollen assemblages reflect diverse land vegetation and a humid temperate climate.

According to Lomas (1999), the PBF represents a rapidly deposited mud-rich deep-water slope apron derived from an arc terrain to the south-east. This interpretation is largely consistent with the results of the present study in which it is suggested that organic matter influx was influenced by turbidity currents. The early–Middle Berriasian section represents continental slope environments in the lowermost part of the interval (earliest Berriasian) to proximal continental rise settings with at times oxygen-depleted bottom water conditions.

Byers Group – Chester Cone Formation (Devils Point Member)

In the lower part of the Late Berriasian interval of the Chester Cone Formation, proportions of marine organic matter are increased indicating a fully marine environment (Tyson, 1995; Traverse, 2007). Reduced abundance of mineral detritus in the palynofacies samples in the lower part further points to a distal marine environment (Tyson, 1995). Thin section analysis shows majorly mudstone sedimentation for the lower part of the DPM reflecting a depositional environment with low water energy (Boggs, 2014). Grainsize increases towards the Berriasian–Valanginian transition indicating higher water energy . The organic matter composition of the middle–upper part of the Berriasian interval of the CCF is dominated by an organic matter composition indicative of a proximal shallow marine depositional environment. This interpretation is in agreement with previous studies (Duane, 1996; Hathway & Lomas, 1998; Lomas, 1999). High content of siliciclastic detritus in the palynofacies samples indicates preferred input of near-shore material (siliciclastic dilution, cf. Tyson, 1995). The poor preservation state of the organic matter likely results from a high geothermal gradient as was suggested by Duane (1996). TAI/SCI analysis of the deposits of the Late Berriasian Chester Cone Formation shows that the results are in the range of Ro% 0.5–1.1 (c. 50–100 °C; catagenesis; cf. Suárez-Ruiz et al., 2012). Hence, it is considered unlikely that the organic matter composition was significantly altered by selective reservation linked to thermal alteration (cf. Tyson, 1995; Batten et al., 1996; Traverse, 2007). In the AOM-Phytoclast-Palynomorph plot this interval shows characteristics of the heterolithic oxic shelf, the shelf to basin transition and mud-dominated distal shelf.
A stressed sea floor is implied by the general lack of bioturbation and scarcity of benthos (Duane, 1996). The author suggests that shallow-water conditions and/or high levels of volcaniclastic input may be the forcing mechanisms of this stress. In the Late Berriasian sediments abundance of disseminate pyrite varies widely throughout the sampled section and several samples show significantly increased amounts. However, the low TOC content (0.3–0.8 wt %) is indicative of an oxygenated water mass and absence of anoxia. The OP/TR ratio which varies intensely between 0.1–257 indicates various lengths of transport and oxidation of the phytoclast material (Tyson, 1993, 1995; McArthur et al., 2016a, b). An oxygenated water body is also indicated by the high abundance of inertinite. However, C/N ratios are continuously low indicating dominantly marine plankton-derived organic matter. This does not correspond to the results of the optical analysis with a terrestrial-dominated organic matter composition. It is therefore suggested that the significantly increased nitrogen content is the result of higher contents of inorganic nitrogen. This might be caused by weathering of nitrogen-bearing bedrock or volatilisation through volcanism (Holloway et al., 2002). Duane (1996) reports high levels of volcaniclastic input in the Devils Point Member of the CCF. The reduced C/N ratios of especially the middle–upper part of the interval are therefore suggested to be the result of relative enrichment through influx of inorganic N, rather than representing nearly exclusively

marine plankton-derived organic matter (cf. Tyson, 1995).
According to Lomas (1999), deposition in the area was characterised by a discontinuous transition from pelagic/hemipelagic sedimentation of the Anchorage Formation through deep slope apron of the President Beaches Formation to shallow marine systems of the Chester Cone Formation. The DPM mainly consists of sediment-gravity-flow-deposited conglomerate and sandstone with remobilised shoreface/beach gravels (Pirrie, 1991; Pirrie & Crame, 1995; Duane, 1996; Hathway & Lomas, 1998). It is unclear whether the conglomerates represent the submarine portion of a fan delta or if they fill part of a large submarine channel (Pirrie & Crame, 1995; Duane, 1996; Hathway & Lomas, 1998). Undulating stratification in the thicker-bedded sandstones indicates storm-produced deposition above storm wave-base (cf. Dott & Bourgeois, 1982).
A more distal fully marine environment is indicated for the lower part of the Late Berriasian CCF part whereas a proximal shelf marine depositional setting is suggested for the middle-upper part based on the results of the present study.

Summary

The majority of the Berriasian sections of central Chile (Lo Valdés Formation), Patagonia (Lower Zapata Formation) and Antarctica (President Beaches Formation and Himalia Ridge Formation) were deposited in a distal fully marine environment (Figs. 141, 145). Only the lowermost Berriasian of the Lo Valdés Formation and the middle-upper part of the Late Berriasian Chester Cone Formation is characterised by a proximal shallow marine environment (Figs. 141, 145).

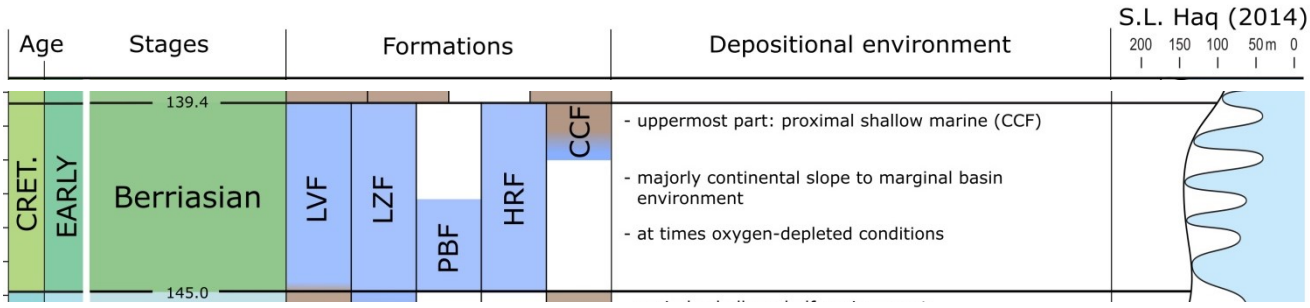

Figure 141: Depositional settings during the Berriasian interval; Formations: LVF=Lo Valdés, LZF=Lower Zapata, PBF=President Beaches, HRF=Himalia Ridge, CCF=Chester Cone; description same as figure 140.

VALANGINIAN

CENTRAL CHILE

Lo Valdés Formation

Sporomorph abundance increases significantly in the Valanginian sediments of the Lo Valdés Formation. The intermediate buoyancy of sporomorphs (McArthur et al., 2016a, b) indicates a more proximal depositional environment (Tyson, 1993). A decreased (CM: 2.6, LV: 2.4) OP/TR ratio of

phytoclasts indicates short ways of transport with reduced intensity of oxidation and degradation. An elevated content of translucent phytoclasts is typical in proximal depositional environments since reduced lengths of transport result in a less intense oxidation and fractionation (Tyson, 1993; McArthur et al., 2016a, b). High amounts of siliciclastic mineral detritus in the palynofacies samples and a low TOC content (mean of 0.21–0.29 wt %) indicate well-oxygenated near-shore high-energy environments (siliciclastic dilution, cf. Tyson, 1995). Microfacies samples with frequent skeletal grains, echinoderms and burrows provide evidence for inner ramp to mid-ramp (shoal) environments and therefore further indicate a proximal depositional setting (cf. Flügel, 2004). In the earliest and latest Valanginian interval, a more distal environment is reflected in the microfacies composition (mid-ramp to outer ramp).

Increasing carbonate content, occurrence of abundant ammonites (Salazar, 2012) and the presence of rare marine palynomorphs are indicators for a marine environment. Foraminifers are rare indicating a proximal marine environment (Tyson, 1995). The high TAI/SCI value (Ro% 2–2.5; c. 175–200 °C) indicates possible post-depositional oxidation and selective preservation of phytoclast material (cf. Tyson, 1995; Batten et al., 1996; Traverse, 2007). Occurrences of fungal filaments are exceedingly abundant and non-fluorescent AOMT is simultaneously high, suggesting that intense fungal mouldering of phytoclasts contributed to the degradation of organic matter (cf. Tyson, 1995). The C/N ratio of the Valanginian samples is increased but a few samples also show low values. This indicates an organic matter composition derived from leaves and herbaceous plants, terrigenous humic acids, and marine macrophytes, but also minor amounts of marine plankton (Tyson, 1995). The results of the AOM-Phytoclast-Palynomorph plot integrate well with the previously discussed results but are affected by the poor preservation state of the organic matter.

For the Valanginian interval of the Lo Valdés Formation a proximal depositional environment is proposed (Figs. 142, 145. Occasional influence of more distal shelf settings in the earliest and latest Valanginian are observed.

PATAGONIA

Upper part of the lower Zapata Formation

The palynofacies assemblage detected in the upper part of the lower Zapata Formation is dominated by terrestrial organic matter, especially by phytoclasts. The OP/TR ratio is high (33), but significantly reduced when compared to the lower (potentially Berriasian) part of the section. This either indicates a highly oxidised near-shore depositional environment, or intense oxidation and fractionation of phytoclasts during prolonged transport (Tyson, 1993; McArthur et al., 2016a, b). The abundance of highly oxidised phytoclasts may also have resulted from selective preservation (cf. Tyson, 1995; Batten et al., 1996; Traverse, 2007) due to high TAI/SCI values equivalent to Ro% 2.5–3 (c. 200–220 °C). Compared to the lower part of the interval, the abundance of sporomorphs is increased and specimens are significantly better preserved which indicates reduced lengths of transport and proximity to the source area (Tyson, 1993; McArthur et al., 2016a, b). Occurrences of marine organic matter are restricted to individual occurrences of dinocysts and acritarchs in the uppermost lower Zapata Formation. It is suggested that thermal alteration resulted in a degradation-induced structure loss of the marine organic matter fraction and hence to a conversion into AOMA (cf. Tyson, 1995). Due to the high level of thermal alteration of more than 200 °C, fluorescence of marine AOM is no

longer existent (cf. Tyson, 1995). The increased amount of siliciclastic mineral detritus in the palynofacies preparations of the lower and middle part of the studied interval and the reduced TOC content in the upper interval of the lower Zapata Formation indicates a more proximal depositional setting with increased influence of siliciclastic dilution and increased proximity to the sediment provenance (cf. Tyson, 1995). The results of the AOM-phytoclast-palynomorph plot are affected by the poor preservation state of the organic matter composition. In the upper part of the lower Zapata Formation the C/N ratio is low and varies between 8–19, indicating organic matter derived from terrigenous humic acids, marine macrophyte material and benthic macroalgal detritus or degraded plankton and marine humic acids (Tyson, 1995). It is suggested that the reduced C/N ratios which indicate a more marine organic matter composition, either represent the marine organic matter fraction which became part of the non-fluorescent AOM, or they are caused by the increased nitrogen content which in turn may be influenced by weathering of nitrogen-bearing bedrock or volatilisation through volcanism (cf. Holloway et al., 2002).

The Berriasian–Valanginian lower Zapata Formation of the Sofia 1 core was deposited proximate to the Andean orogen, and is now located close to the fold-thrust belt (Fildani & Hessler, 2005). The proximity to the volcanic arc resulted in increased thermal stress which caused the poor preservation state of the organic matter. Here, the sampled interval of the lower Zapata Formation is roughly divided into a lower and an upper part. Differentiation is based on differences in the organic matter composition and the results of the geochemical and optical analysis, and not by means of stratigraphical approaches (due to lack of data).

Determination of the depositional environment is difficult in the upper part of the lower Zapata Formation because of the poor preservation of the organic matter. During the Late Jurassic–Early Cretaceous changes in the depositional setting are influenced by the onset of Andean contraction and transition to the Magallanes retroarc foreland basin (Tobífera and Zapata formations) (Rabinowitz & La Brecque, 1979; Dalziel, 1986; Ramos, 1988; Fildani & Hessler, 2005). Based on the changes in organic matter composition and differences in the results of the geochemical and optical approaches, a more proximal shelf environment is suggested for the upper part of the lower detritus and the occurrence of marine palynomorphs indicate a more distal shelf marine environment in the uppermost part of the lower Zapata Formation (Figs. 142, 145).

ANTARCTICA

Fossil Bluff Group – Spartan Glacier Formation

Precise age control on the sample series of the Spartan Glacier Formation is not given. A tentatively Valanginian, Late Valanginian–Early Hauterivian and Late Hauterivian–Barremian subdivision of the sample series is used, based on the lithostratigraphic results of Butterworth et al. (1988). The interval is discussed as a whole due to the limited sample amount. The palynofacies assemblage is dominated by terrestrial organic matter. Particulate marine organic matter is mostly absent and limited to a single sample that contains undifferentiated algae (Valanginian). Abundance of marine AOM is highest in the middle part of the interval (Late Valanginian–Early Hauterivian). In contrast to the underlying Berriasian HRF, the OP/TR ratio is continuously low (3.2) in the Valanginian–Barremian deposits of the SGF. This reduction reflects reduced levels of fractionation and therefore points to a more proximal marine environment (Tyson, 1993; McArthur, 2016a, b). The dominance of phytoclast

material is suggested to be linked to effects of selective preservation, as TAI/SCI analysis is equivalent to Ro% 2.0–2.7 (c. 175–220 °C) and resulted in conversion of marine organic matter to fluorescent AOM (cf. Tyson, 1995). The co-occurrence of particles that show thermal alteration above 175 °C and fluorescent AOM (AOM loses its fluorescence above 150–160 °C; Tyson, 1995) indicates differences in the length of transport and a mixture of organic matter with allochthonous and autochthonous origin due to reworking. The C/N ratio is continuously low, indicating a mixture of organic matter derived from degraded terrestrial material, terrigenous humic acids, marine macrophytes, but also from degraded plankton and marine humic acids (Tyson, 1995). The AOM-Phytoclast-Palynomorph plot indicates "highly proximal shelf or basin" to "marginal dysoxic-anoxic basin" environments, but values are affected by thermal alteration. Doubleday and Storey (1998) reported that the sediments of the SGF were deposited within mud lobes on the outer shelf.

The Spartan Glacier Formation is composed of grey mudstone and siltstone with only a few intercalated swarms of sandstone dykes (Butterworth et al., 1988). Upsection, sediments gradually become coarser and suggest a shallower environment (Macdonald et al., 1993). The significant increase in grain size points to a general shallowing-upward trend (Crame & Howlett, 1988). Disseminated pyrite is frequent in all analysed samples of the SGF but abundance is not increased. An oxygenated near-shore environment is indicated by continuously low TOC contents and high abundances of siliciclastic mineral detritus in the palynofacies samples (cf. Tyson, 1995; Duane, 1996). Butterworth et al. (1988) reported frequent bioturbation, further indicating an oxygenated water body. The Valanginian section of the Spartan Glacier Formation was deposited in an outer shelf setting (Figs. 142, 145). Siliciclastic detritus is reduced in the Late Valanginian–Early Hauterivian interval (Figs. 142, 143, 145). Together with the increased abundance of marine AOM, a more distal marine depositional environment is suggested for this interval. Increased abundance of siliciclastic detritus and absence of any marine facies indicators in the palynofacies assemblage indicate a more proximal depositional setting for the Late Hauterivian–Barremian interval (Figs. 143, 144, 145).

Byers Group – Chester Cone Formation (Sealer Hill Member)

In contrast to the DPM, the SHM yields a much more diverse palynofacies assemblage: although generally low in numbers, dinocysts, acritarchs, algae indet., foraminifers, leiospheres and marine AOM are present. Although the analysed section is still dominated by terrestrial organic matter, low TAI/SCI values (equivalent to Ro% 0.7–1.1; c. 75–100 °C) indicate that the organic matter shows the original (unaltered) composition (cf. Tyson, 1995; Batten et al., 1996; Traverse, 2007). Increased content of well-preserved sporomorphs and a low OP/TR ratio (0.6) indicate short distances of transport (Tyson, 1993; McArthur et al., 2016a, b). Compared to the underlying DPM, the amount of marine AOM is increased, but so is the amount of terrestrial AOM. The average abundance of fungal filaments is lower in the SHM (to the DPM) but fungal remains occur more frequent in the palynofacies samples indicating that the organic matter was exposed to fungal mouldering and bacterial activity (cf. Demaison & Moore, 1980; Tyson, 1995). With an average of 11 the C/N ratio represents a mixture of components that derived from origins like leaves and herbaceous plants, terrigenous humic acids, marine macrophytes, but also from marine plankton (Tyson, 1995). In contrast to the deposits of the DPM the absolute nitrogen content is reduced, indicating reduced influx from weathering processes, volcanic volatilisation and/or a more marine organic matter composition

(cf. Tyson, 1995; Holloway et al., 2002; Montross et al., 2013). TOC content of the CCF is the highest of the Byers Group. Except for significant peaks in two samples, pyrite content is continuously low providing no evidence of euxinic bottom water conditions (cf. Tyson, 1995). The AOM-Phytoclast-Palynomorph plot indicates a proximal shelf setting for the majority of the samples, with occasional shifts to marginal basin environments and shelf to basin transition settings.

Compared to the DPM, the SHM is characterised by a slightly more proximal environment indicated by current ripple cross laminated silty mudstone and fine sandstone which is restricted to the lowermost part of the SHM. Reduced abundance of siliciclastic detritus reflects transition to lower water energy for the remainder of the interval. The succession is dominated by mudstone deposits in which sandstone beds are interpreted by Duane (1996) as storm-generated sediment incursions into a low-energy marine shelf environment above storm wave base. The upper member (SHM) of the Chester cone Formation consists of finely laminated mudstone of Early–Middle Valanginian age (Hathway & Lomas, 1998). Deposition was penecontemporaneous with the emergence and expansion of the arc. Tectonic uplift was accompanied by a discontinuous transition from pelagic/hemipelagic sedimentation of the Anchorage Formation to shallow marine systems of the Chester Cone Formation (Lomas, 1999).

Results suggest a proximal fully marine depositional environment for the Early-Middle Valanginian Chester Cone Formation (Figs. 142, 145). Occasional influences of lower energy marginal basin settings are also indicated.

Summary

The Valanginian sections in Central Chile (Lo Valdés Formation), Patagonia (Lower Zapata Formation) and Antarctica (Chester Cone Formation and Spartan Glacier Formation) show majorly proximal depositional settings that range from well-oxygenated near shore environments to outer/distal continental shelf settings.

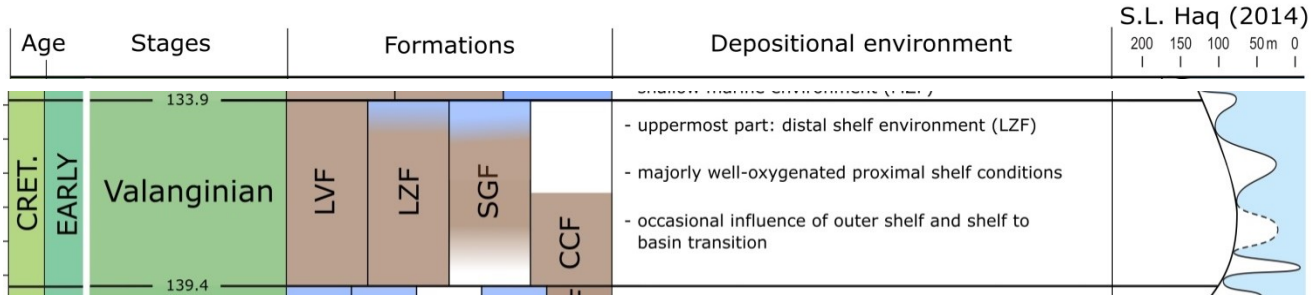

Figure 142: Depositional settings during the Valanginian interval; Formations: LVF=Lo Valdés, LZF=Lower Zapata, SGF=Spartan Glacier, CCF=Chester Cone; description same as figure 140.

HAUTERIVIAN

CENTRAL CHILE

Lo Valdés Formation

The organic matter composition is dominated by terrestrial organic matter. Marine facies indicators are absent. Similar to the Tithonian, Berriasian and Valanginian stages of the central Chilean sections, the absence of marine palynomorphs results from selective preservation of phytoclasts caused by intense thermal alteration (cf. Tyson, 1995; Batten et al., 1996; Traverse, 2007). Analysis of the TAI/SCI shows values equivalent to Ro% 2–2.5 (c. 175–200 °C). Thermal stress resulted in degradation-induced structure loss of marine palynomorphs with subsequent incorporation in fluorescent AOMA (cf. Tyson, 1995). However, the increased level of thermal degradation of the sediments resulted in loss of fluorescence of the marine AOM fraction (Tyson 1995). Compared to the deposits of the underlying Valanginian section, samples of the Hauterivian deposits are characterised by a higher OP/TR ratio indicating increased fractionation and oxidation during transport (Tyson, 1993; McArthur et al., 2016a, b); they hence point to a more distal shelf marine environment. Occurrences of fungal filaments are frequent and abundance of non-fluorescent AOM is simultaneously high, indicating that fungal mouldering of phytoclasts contributed to the degradation of the organic matter (cf. Tyson, 1995). According to Jones (1988) and Tyson (1995) fungi may also play a significant role in marine biodegradation, including the degradation of marine organic matter. The C/N ratio shows a mean value of 37 but varies significantly (15–224) throughout the sampled interval. The ratio is increased in the deposits of the lower–middle part of the Hauterivian interval, indicating a terrestrial derived organic matter composition (i.e. detritus of wood, leaves and herbaceous plants) (Tyson, 1995). The middle–upper part of the Hauterivian section is characterised by lower C/N ratios, indicating organic matter derived from terrigenous humic acids and marine macrophytes. Some samples also indicate shares of marine plankton-derived organic matter (zooplankton faecal pellets and/or marine humic acids) (Tyson, 1995). The abundance distribution of siliciclastic detritus in the palynofacies samples shows a similar pattern. In the lower–middle part of the Hauterivian interval the abundance vastly exceeds that of the middle-upper part. This indicates an increased distance to the sediment provenance and lower influence of terrestrial settings for the upper part of the Hauterivian interval (cf. Tyson, 1995). Disseminated pyrite is frequent throughout the deposits of the Hauterivian section of the Lo Valdés Formation but TOC content is only slightly increased. A euxinic environment is therefore considered unlikely (cf. Tyson, 1995). Although the sediments show increased contents of skeletal grains and carbonate debris, microfacies characteristics (including grain size) are in an intermediate range between those of the Berriasian and the Valanginian: Microfacies analysis indicates a development from inner ramp to mid-ramp environments in the lower part of the Hauterivian section to outer ramp/basin settings in the upper part (cf. Flügel, 2004). Due to the intense thermal degradation and hence selective preservation of the phytoclast material, the results of the AOM-Phytoclast-Palynomorph plot are prone to alteration and thus considered unreliable.

Results suggest a proximal depositional environment for the lower part of the Hauterivian interval. In the middle–upper interval of the Hauterivian section a more distal marine environment is indicated (Figs. 143, 145).

PATAGONIA

Middle Zapata Formation

Based on data provided by ENAP, the upper interval of the sampled section of the Sofia 1 core is assigned to the Hauterivian–Aptian, or middle Zapata Formation. Results show a tripartite subdivision of the Hauterivian–Aptian interval and allow a tentatively division in a lower (potentially Hauterivian), middle (potentially Barremian) and upper (potentially Aptian) interval. A detailed subdivision based on stratigraphic data is not possible, wherefore the whole interval is discussed in this paragraph.

The organic matter composition of the deposits of the Hauterivian–Aptian interval of the Sofia 1 core is dominated by terrestrial organic matter. Well-preserved particles are restricted to dinocysts, sporomorphs and phytoclasts. Abundance of sporomorphs is significantly increased in the lower and upper part of the interval, indicating proximity to the sediment provenance (Tyson, 1993; McArthur et al., 2016a, b). Sporomorphs are rare to absent in the middle part, indicating a more distal marine depositional environment (Tyson, 1993, 1995; McArthur et al., 2016 a, b). A tripartite subdivision of the interval is also reflected in the OP/TR ratio. In the lower and upper part of the interval the ratio is significantly reduced compared to the middle part. This indicates less fractionation and oxidation of the organic matter in the lower and upper part of the interval and hence a more proximal depositional environment (Tyson, 1993; McArthur et al., 2016a, b). Samples of the lower and upper part of the interval also show a significantly increased proportion of siliciclastic detritus. This indicates high influx of siliciclastic material in proximity to the sediment provenance (cf. Tyson, 1995). Occurrences of dinocysts and acritarchs are restricted to the lower and upper part of the sampled interval and indicate fully marine environments (Tyson, 1993, 1995; McArthur et al., 2016 a, b). In this core the proximity to the volcanic arc (Fildani & Hessler, 2005) resulted in increased thermal stress. The co-occurrence of fluorescent particles and TAI of 4 to 5- (equivalent to Ro% 2.5–3; c. 200–220 °C) indicates a mixed allochthonous and autochthonous organic matter composition, but might also result from caving during the process of core-drilling. A tripartite subdivision becomes also apparent in the results of the geochemical analysis. The reduced TOC contents (in combination with increased siliciclastic detritus) indicate a well-oxygenated near shore environment for the lower and upper parts of the interval (siliciclastic dilution, cf. Tyson, 1995). TOC content is higher and siliciclastic detritus is reduced in the deposits of the middle part of the interval which indicates a more stable water body in a distal marine environment (Tyson, 1995). Combined with increased TOC contents, high abundance of pyrite and reduced siliciclastic detritus, an oxygen depleted low-energy euxinic water body is indicated for the middle part of the interval (cf. Tyson, 1995). The C/N ratio is reduced in the lower and upper part of the section, pointing to marine-derived organic matter (Tyson, 1995). The middle part of the interval is characterised by higher C/N ratios that indicate a mixed terrestrial-marine organic matter composition. This observation contradicts the previously discussed subdivision of proximal environments for the lower and upper part of the interval and a more distal marine setting for the middle part. Volatilisation through volcanism and/or weathering of nitrogen-bearing bedrock could have influenced the nitrogen content (cf. Holloway et al., 2002) but no significant change in N-content throughout the interval is observed. It is suggested that the intense thermal alteration resulted in loss of Nitrogen and hence to a lower C/N ratio. The results of the AOM-Phytoclast-Palynomorph plot indicate a continuously proximal shelf or basin environment. However, because of the poor

preservation state of the organic matter, the results are of limited reliability.
Fildani and Hessler (2005) suggested that the Zapata Formation was deposited in a shallow-water marine environment which was tectonically influenced by the Andean orogeny. A highly irregular basin partitioned by horsts is indicated by sand deposition confined to sub-basins closer to the arc (Fildani & Hessler, 2005). A conclusive determination of the depositional environment of the Hauterivian–Aptian interval of the Zapata Formation is difficult because of the poor preservation state of the organic matter, the tectonically active arc and consequent highly irregular morphology of the area (cf. Fildani & Hessler, 2005).
Based on the results proximal depositional environments are suggested for the lower (?Hauterivian) and upper (?Aptian) part of the sampled interval (Figs. 143, 144, 145). The middle (?Barremian) part of the interval is characterised by a distal oxygen-depleted low-energy setting (Figs. 144, 145).

ANTARCTICA

Spartan Glacier Formation

The depositional environment of the SGF is discussed as a whole in the Valanginian paragraph due to the limited sample amount. The interpretation of the Hauterivian interval is thus only briefly summarised here. For the Early Hauterivian section a more distal marine depositional environment is suggested. For the Late Hauterivian interval a more proximal depositional setting is indicated (Figs. 143, 145).

Summary

For the Hauterivian interval, shifts in proximity of the depositional settings are observed in all three sections (Figs. 143, 145). However, a uniformly trend in palaeoenvironmental development for the Hauterivian interval cannot be inferred from the present data.

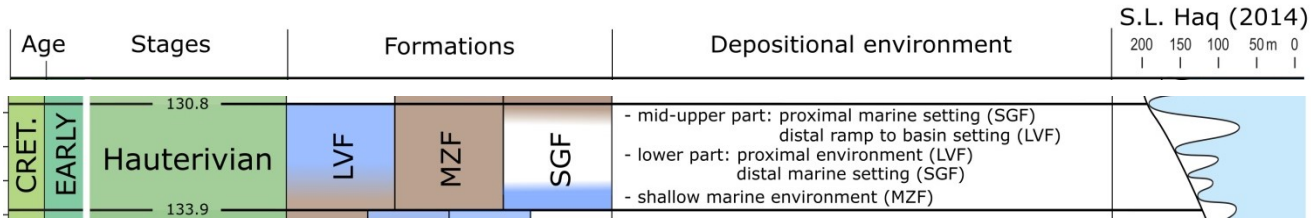

Figure 143: Depositional settings during the Hauterivian interval; Formations: LVF=Lo Valdés, MZF=Middle Zapata, SGF=Spartan Glacier; description same as figure 140.

BARREMIAN–APTIAN

PATAGONIA

Springhill/Río Mayer Formation

The palynofacies assemblages identified in the Nevenka 1 core are dominated by terrestrial organic matter. The OP/TR ratio varies significantly but is continuously low (mean of 1.5) indicating a near shore depositional environment with short ways of transport and limited degrees of oxidation and fractionation (Tyson, 1993, 1995; McArthur et al., 2016a, b). The great variety of particle sizes that was observed in the phytoclast remains further reflects insufficient lengths of transport and incomplete sorting, an observation that is typical in proximal assemblages (Tyson 1995). Terrestrial organic matter is usually deposited near the mouths of rivers and remains trapped in the inner part of the shelf (Hedges & Parker, 1976; Wollast, 1983; Tyson, 1995). The TAI/SCI ratio of the Barremian–Aptian interval of the Nevenka 1 core is equivalent to Ro% values of 0.5–1.3 (c. 50–115 °C), providing no indication for increased selective preservation of phytoclasts (Tyson, 1993). Throughout the lower part of the interval contents of phytoclasts decrease significantly and this matter was replaced by AOMT and AOMA. Commonly, the relative and absolute abundance of AOM is strongly correlated with distal areas of oxygen-reduced bottom water conditions (Davey & Rogers, 1975; Tissot & Pelet, 1981; Summerhayes, 1983; Tyson, 1993). Throughout the section abundance of both fluorescent AOMA and non-fluorescent AOMT fluctuate on a high level and show an increasing trend and hence, a more distal depositional setting. Intervals with increased TOC content are restricted to the lower, middle and lower upper part of the interval and show concurrently decreased abundance of siliciclastic detritus and sporomorphs. The TOC-rich intervals represent confined phases of distal marine settings in which the depositional environment is characterised by lower energy and oxygen-deficiency (cf. Tyson, 1995). Abundances of dinocysts and acritarchs fluctuate intensely but show higher values in the upper part of the interval further indicating progressive tendency towards fully marine settings (Tyson, 1993, 1995; McArthur et al., 2016 a, b). Occurrences of leiospheres (referred to division Prasinophyta of the green algae (Tappan, 1980; Guy-Ohlson, 1996; Traverse, 2007)) are only present in the middle part of the interval where they reflect more distal marine depositional environments (Tyson, 1993). Results of the AOM-Phytoclast-Palynomorph plot point to depositional settings that reflect alternating distances to the sediment provenance from marginal basin to shelf to basin transition (lower to upper part of the Upper Barremian). The same pattern is observed in the Lower Aptian interval where the plot shows a transition from distal suboxic-anoxic basin settings back to the shelf to basin transition and the mud-dominated oxic shelf. Concurrent increase in abundance of sporomorphs and phytoclasts reflect a transition to proximal depositional settings (Tyson, 1993, 1995).

The sampled interval of the Springhill/Río Mayer was deposited during Late Barremian–Early Aptian times and is composed of fluvial, marginal-marine, coastal and shallow-marine siliciclastic deposits (Kielbowicz et al., 1984; Biddle et al., 1986; Arbe and Fernández Bell Fano, 2002; Schwarz et al., 2011). The vast majority of the sampled interval of the Nevenka 1 core belongs to the Upper Barremian Springhill Formation based on the dinocyst assemblage. In the uppermost interval of the studied section of the Nevenka 1 core the dinocyst assemblage shows an Early Aptian age and is assigned to the Río Mayer Formation (cf. Archangelsky et al., 2009).

Schwarz et al. (2011) suggest deposition as incised valley fills for the most part of the Springhill Formation. The dominance of thermally unaltered terrestrial organic matter in the analysed section also suggests deposition on the shelf. Throughout the sampled section a fluctuating depositional environment is suggested with an increasingly proximal shelf marine setting. In the lowermost Aptian, a temporary shift towards more distal marine settings is superseded by proximal depositional environment (Figs. 144, 145).

ANTARCTICA

Spartan Glacier Formation

The depositional environment of the SGF is discussed as a whole in the Valanginian paragraph due to the limited sample amount. For the Barremian interval a more proximal depositional setting is indicated (Figs. 144, 145).

Summary

Based on the results a majorly distal marine depositional setting is suggested for the Middle–Upper Barremian interval. Both analysed sections from Patagonia indicate distal shelf marine settings with intervals of more proximal settings in the Springhill/Río Mayer Formation. Results further point to oxygen-depleted low-energy settings for the lower–middle part of the Barremian interval. The results from Antarctica (SGF) suggest a proximal depositional environment for the Lower Barremian, although age control is poor.

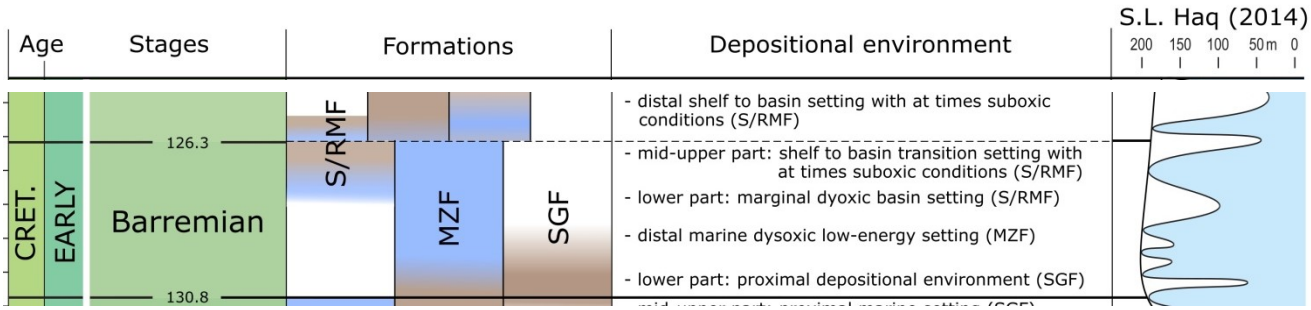

Figure 144: Depositional settings during the Barremian-Aptian interval; Formations: S/RMF=Springhill/Río Mayer, MZF=Middle Zapata, SGF=Spartan Glacier; description same as figure 140.

APTIAN–ALBIAN

ANTARCTICA

Fossil Bluff Group – Pluto Glacier Formation (Aptian)

Except for the occurrences of acritarchs in the uppermost part of the interval, and undifferentiated algae throughout the section, structured marine organic matter is absent. Compared to the sediments of the other lithostratigraphic units of the Fossil Bluff Group content of fluorescent AOM is significantly

increased. Nonetheless, terrestrial organic matter dominates the palynofacies assemblage. The OP/TR ratio of the deposits is very low (1.8) reflecting decreased fractionation and oxidation and short ways of transport (Tyson, 1993, 1995; McArthur et al., 2016a, b). Well- to fairly preserved sporomorphs are abundant in the PGF indicating short distances to the source area (Tyson, 1993, 1995; McArthur et al., 2016a, b). Fungal remains are absent which indicates that the high amount of terrestrial AOM is not the result of intense fungal mouldering (cf. Tyson, 1995). Although an increase in abundance of fluorescing AOM is an indicator for distal depositional environment (Tyson, 1993), this interpretation is unlikely in the present context because of the low amount of fluorescing AOMA compared to terrestrial AOMT (3.8% to 49.4 %). Non-fluorescing AOM has been reported as also being produced by the activity of benthic filamentous cyanobacteria in shallow waters (Williams, 1984; Glikson & Taylor, 1986; Tyson, 1993, McArthur et al., 2016a, b). Levels of thermal alteration of the sediments reached TAI/SCI values equivalent to Ro% 1.5–2.3 (c. 140–185 °C). These high degrees of thermal degradation and coexisting fluorescent marine organic matter indicate a mixture of organic matter with both allochthonous and autochthonous origins. The low C/N ratio (mean of 11) indicates an organic matter composition which originates from a mixture of degraded material like terrestrial humic acids, marine macrophytes and marine plankton-derived organic matter (Tyson, 1995). Abundance of both disseminated pyrite and TOC is low whereas content of siliciclastic detritus is continuously high, indicating an oxygenated depositional environment (e.g. Ineson, 1989; Tyson, 1995). The majority of the Pluto Glacier Formation (PGF) consists of alternating units of thick-bedded sandstone and siltstone. The siltstone units are interbedded with sandstone of various grain-sizes (Butterworth et al., 1988). The sandstone units are usually intensely bioturbated and some intervals present herringbone cross-stratification. The sandstone units are considered as shallow marine deposits representing basin shallowing (Doubleday & Storey, 1998) into the tidal zone (cf. Nichols, 2009). The palynofacies assemblage also indicates a depositional setting in proximity to the shoreline. The results of the AOM-Phytoclast-Palynomorph plot indicate a depositional environment that alternates between proximal and distal shelf settings. Results are characterised by settings of highly proximal shelf or basin, marginal dysoxic-anoxic basin to shelf to basin transition.

For the Aptian interval of the Pluto Glacier Formation results indicate a shallow shelf marine depositional environment. Confined intervals of more distal shelf environments are indicated by the results of the AOM-Phytoclast-Palynomorph plot and the C/N ratio (Fig. 145).

Gustav Group – Kotick Point Formation (Aptian, Albian)

Although dominated by terrestrial organic matter, marine palynomorphs and fluorescent AOM are abundant. In the middle part of the interval leiosphere abundance is increased. With a relative abundance of 32–39 % leiospheres are the dominant type of palynomorphs and hence indicate restricted oxygen-depleted shallow water (cf. Bernier & Courtinat, 1979; Hunt, 1987). Pyrite content is low while TOC values are slightly increased giving no indication of a euxinic environment. Siliciclastic detritus is significantly reduced and at times absent. This point to either increased distance to the sediment provenance or a proximal low energy environment The C/N ratio (mean of 29) of the deposits of the Kotick Point Formation is increased compared to values detected in the Aptian Pluto Glacier Formation. Organic matter composition is derived from degraded leaves and herbaceous plants, terrigenous humic acids, marine macrophytes and degraded plankton and marine humic acids

(Tyson, 1995). A very low OP/TR ratio of 0.5 indicates short ways of transport and limited degrees of fractionation and oxidation (Tyson, 1993, 1995; McArthur et al., 2016a, b). A TAI/SCI equivalent to Ro% 0.5–1.1 (c. 50–100 °C) indicates that the organic matter composition is not significantly altered by selective preservation of phytoclast material (cf. Tyson, 1995; Batten et al., 1996; Traverse, 2007). Abundance of well-preserved sporomorphs is high, further indicating short ways of transport. Except for the peaks in leiosphere abundance marine palynomorphs are rare though diverse indicating a fully marine environment (cf. Tyson, 1995). The organic matter composition thus represents a mixture of allochthonous terrestrial and an *in situ* assemblage of marine palynomorphs. This could be the result of activity of low-density turbidity currents which were reported by Ineson (1989). Abundance of AOM is low indicating less intense alteration by bacterial activity and typically proximal depositional settings (cf. Tyson, 1995; Batten et al., 1996; Traverse, 2007). All samples of the Aptian/Albian sediments of the Kotick Point Formation indicate a proximal shelf environment when plotted in the AOM-Phytoclast-Palynomorph plot.

The Kotick Point Formation is largely composed of interbedded sandstone and mudstone. These lithologies include muddy mass flow deposits and allochthonous glide blocks of the Gustav Group (Ineson, 1989). The strata are interpreted as gravelly submarine fan deposits; and mud- and sandstone-dominated slope apron deposits characterised by low-density turbidity currents (Farquharson et al. 1984; Ineson 1989; Pirrie et al. 1991). Ineson (1987) suggested a low-energy environment in an aerobic to dysaerobic marine setting based on the ichnofauna present. Sampling of the silt- to fine sand sized material which was part of turbidites may have led to the indication of a higher-energy environment that differs from the low-energy dysaerobic environment suggested by Ineson (1987). However, dominance of leiospheres in the middle–upper part of the interval and low abundance of siliciclastic mineral detritus suggests low-energy oxygen-reduced conditions (cf. Bernier & Courtinat, 1979; Hunt, 1987). It is therefore suggested that the analysed samples of the Kotick Point Formation represent deposition by turbidites and therefore reflect continental margin settings ranging from continental slope to continental rise with at times oxygen-depleted conditions (Fig. 145).

Summary

In the present study the majority of the Aptian interval is characterised by a shallow shelf depositional setting (Middle Zapata Formation and Pluto Glacier Formation). Confined intervals of more distal marine environments (distal shelf to marginal basin) are observed in the Early Aptian of the Springhill Formation and occasionally throughout the Pluto Glacier Formation. For the Springhill/Río Mayer Formation a subsequent transition to more proximal settings is observed. Continuously more distal marine settings are observed in the Late Aptian to Early Albian Kotick Point Formation which is characterised by continental slope to continental rise settings.

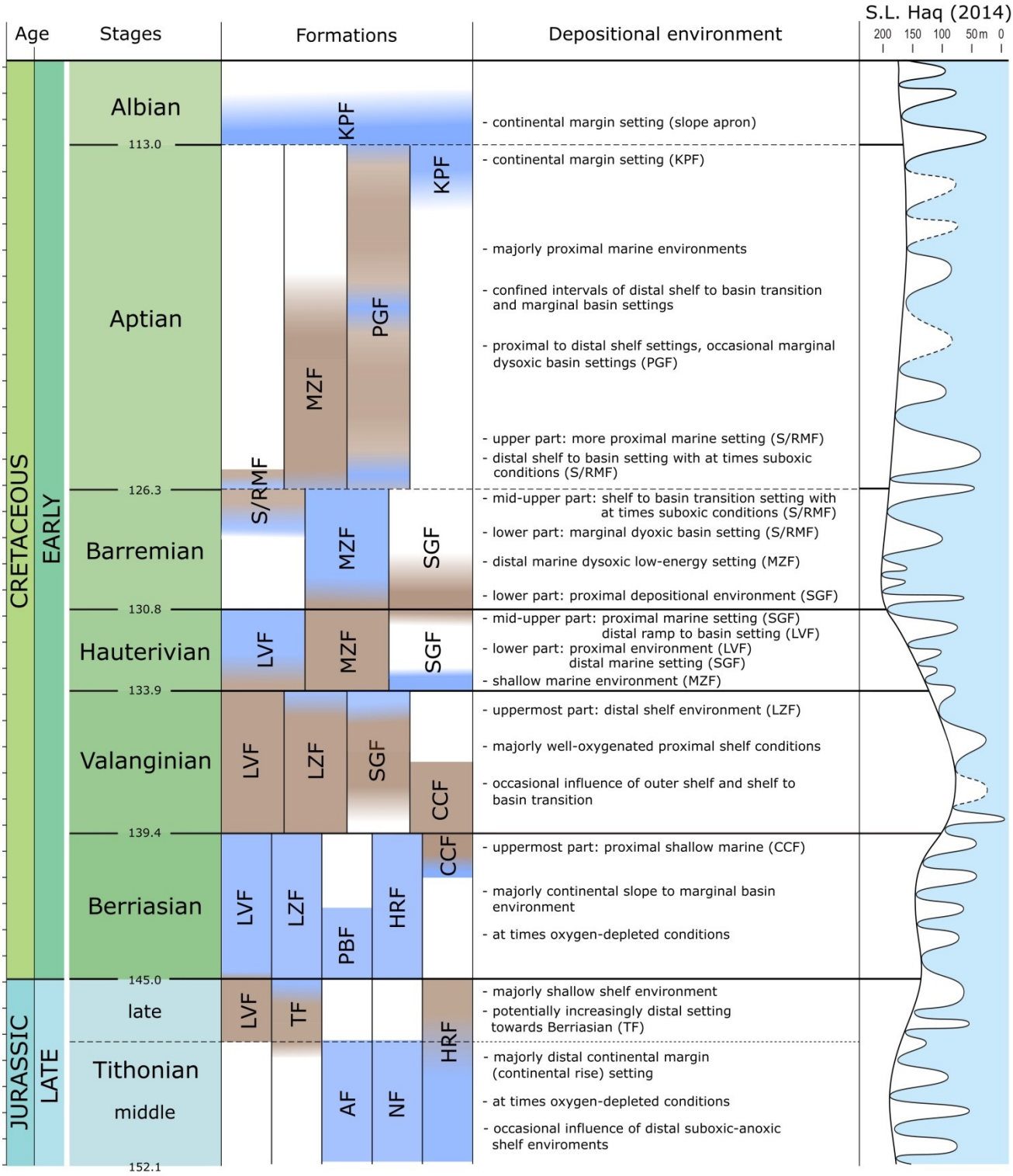

Figure 145: Development of depositional settings in the present study, including the Aptian-Albian interval; Formations: LVF= Lo Valdés, TF=Tobífera, AF=Anchorage, NF=Nordenskjöld, HRF=Himalia Ridge, LZF=Lower Zapata, PBF=President Beaches, CCF=Chester Cone, SGF=Spartan Glacier, PGF=Pluto Glacier, S/RMF=Springhill/Río Mayer, MZF=Middle Zapata, KPF=Kotick Point; description same as figure 140.

5.2 Sea level fluctuations and Palaeoclimate

Over the last 30 years, the understanding of the Latest Jurassic and Early Cretaceous paleoclimate has changed from that of an equable, warm-temperate greenhouse world (e.g., Frakes, 1979; Hallam, 1981, 1985) to a more varied climatic history including icehouse periods (e.g., Kemper, 1987; Weissert & Lini, 1991; Price et al., 2000; Steuber et al., 2005; McArthur et al., 2007; Grabowski et al., 2013; Tennant et al., 2016). The earliest Cretaceous climate might be characterised as a warm greenhouse world with interludes of short cooling ('cold snaps') (Kessels et al., 2006).

In the present study palaeoclimatic interpretation is mainly based on sea level interpreted from the depositional environment as well as the presence of micro-glendonites as a direct indicator of cold water, as well as the presence, or absence, of calpionellids of subtropical Tethyan origin.

TITHONIAN

Most samples of the Anchorage, Nordenskjöld and Himalia Ridge Formations in Antarctica were here informally assigned to the Middle Tithonian and represent hemipelagic and distal basin environments (cf. Butterworth et al., 1985; Pirrie & Crame, 1995; Hathway, 2000). The scarcity of marine facies indicators in the palynofacies assemblages of the Anchorage and Himalia Ridge Formations was most likely caused by the high thermal alteration of the organic matter of up to 220 °C (cf. Suárez-Ruiz et al., 2012). Only in the Nordenskjöld Formation the organic matter composition shows higher proportions of marine organic matter. In this section, thermal alteration was limited to approximately 100 °C which supported the preservation of the less degradation-resistant marine palynomorphs (Tyson, 1993). It is therefore suggested that this section shows the most representative and primary organic matter composition for the Middle Tithonian interval of the Antarctica sections. Reduced siliciclastic input in most of the samples reflects a position with increased distance to the sediment provenance. When compared to the long term sea level curve of Haq (2014) the distal depositional environments indicate increased sea level for the Middle Tithonian sections (Figs. 146, 152). The general absence of micro-glendonites in the Middle Tithonian Nordenskjöld and Himalia Ridge Formations suggests increased sea level which coincided with warm water conditions. Concurrent occurrences of micro-glendonites in the Middle Tithonian Anchorage Formation indicate influence of cool bottom water in the hemipelagic environment of the intra-arc basin (continental slope and rise) (cf. Selleck et al., 2007). Occurrences of well-developed and large micro-glendonite specimens are restricted to the lower-middle part of the section. It is possible that these occurrences represent short-termed cooling which was not recorded in the sample series of the Nordenskjöld- and Himalia Ridge Formation.

The sampled material of the Sofia 1 core exclusively consists of cuttings and thus no sedimentary structures are available for a conclusive interpretation of the depositional environment. A tentative middle–Late Tithonian age is suggested for the analysed section based on similarities to the results of the sections of middle–Late Tithonian age from the Antarctica study area. Stinnesbeck et al. (2014) and the U.S. Energy Information Administration EIA, (2015) assigned the organic C-rich shales of Late Jurassic and Early Cretaceous ages to anoxic marine environments. Such an oxygen-depleted environment is not reflected in the results of the present study. This is attributed to the fact that the succession of silicic pyroclastic rocks (mostly tuffaceous deposits) which are interbedded by black

shales and shale and siltstone deposits described by Fildani and Hessler (2005) as shallow water deposits. A proximal depositional environment is thus indicated for the upper Tobífera Formation of Patagonia. It cannot be decided, however, whether the potentially lower sea level represents the Late Tithonian regressive cycle reported by Oliveros et al. (2012), or a Late Tithonian cooling phase, or both. This is because of the uncertainties in precise stratigraphic affiliation and the absence of micro-glendonites. The absence of micro-glendonites in the deposits Tithonian upper Tobífera Formation might result from decreased carbonate content and hence reduced alkalinity, the major prerequisite for ikaite formation (cf. De Lurio & Frakes, 1999; Selleck et al., 2007; Hu et al., 2014). In addition it is not known to what extent the onset of Andean contraction and transition to the Magallanes retroarc foreland basin (Rabinowitz & La Brecque, (1979); Dalziel, (1986); Ramos, (1988); Fildani & Hessler, (2005)) influenced the depositional environment and hence sea level.

A proximal depositional environment is identified for the Late Tithonian interval of the central Chilean Lo Valdés Formation. This setting may be linked to the regressive cycle in the Andes mentioned by Oliveros et al. (2012). The authors suggested the presence of a Late Jurassic marine regression and suggested that this event was synchronous over a large portion of the Andean margin, based on correlation of the Lagunillas and Tordillo-Río Damas Formations in Chile. The proximal depositional environment may therefore reflect a lowered sea level. For the Late Tithonian interval of the Himalia Ridge Formation, a proximal continental margin environment and hence lowered sea-level is suggested. Cluster-shaped micro-glendonites are observed throughout the Upper Tithonian interval of both the Lo Valdés Formation and the Himalia Ridge Formation. In the Lo Valdés Formation, specimens of the Late Tithonian are small but micro-glendonite size increases in the latest Tithonian. The abundance and size increase of these minerals in the latest Tithonian points to a connection of lowered sea level and cold climate (cf. Selleck et al., 2007). $\delta^{13}C$ and $\delta^{18}O$ analyses presented here from central Chile contradict this interpretation. With a mean of -3.16 ‰ for $\delta^{13}C$ and -8.17 ‰ for $\delta^{18}O$, values are significantly reduced and would indicate warm climatic conditions (Mutterlose et al., 2009; Stanley, 2010) or influence of fresh water (Ravelo & Hillaire-Marcel, 2007). However, due to the scarcity of shell material, diagenetic screening of the analysed samples of the highly thermally altered Lo Valdés Formation was not feasible. Therefore the results of the $\delta^{13}C$ and $\delta^{18}O$ analyses are considered unreliable for the palaeoenvironmental interpretation.

Haq et al. (1987) and Haq (2014) reported on a long-term sea-level decrease towards the J/K boundary, with a short-term sea level low of approximately 70 m above present at the end of the Nannofossil Zone NJ18 (~145 Ma, Late Tithonian, Gradstein et al., 2012). Grabowksi et al. (2013) suggested regressive sea level intervals for the Upper Tithonian/lowermost Berriasian pelagic carbonates in the Central Western Carpathians. Regression and associated relative sea level fall was also detected by Hesselbo (2008) for the Late Tithonian of the onshore British Jurassic. Tennant et al. (2016) linked the patterns of extinctions of shallow marine low latitude shelf assemblages of Hallam (1986) and Alroy (2010), to a significant eustatic sea level fall in the latest Jurassic. During the Tithonian there is an increase in glacial tillites and dropstones on the margins of the Boreal and southern Austral seas (Moore et al., 1992), of which so far no accompanying occurrences of glendonites are reported (Price, 1999). In the present study, occurrences of micro-glendonites were observed in the deposits of the Middle Tithonian Anchorage Formation and in the Upper Tithonian succession of the Lo Valdés Formation and the Himalia Ridge Formation. For the first time glacial tillites and dropstones reported by Moore et al., (1992) from the Southern Hemisphere coincide with

glendonites for the Upper Tithonian interval, clearly indicating a phase of cool climate. The occurrence of micro-glendonites in combination with the reported lowered sea level in the present study and from higher latitudes (e.g. Haq, 1987; Hallam, 1986; Alroy, 2010; Oliveros et al., 2012; Grabowksi et al., 2013) are suggested to reflect a temporal cooling during the Late Tithonian in central Chile, Patagonia and Antarctica. It is suggested that this cooling event was not only of local importance, but a global phenomenon during the Tithonian–Berriasian transition.

Summary

Distal depositional settings and the absence of micro-glendonites in the Middle Tithonian interval indicate higher sea level and warm water. Occurrences of micro-glendonites in the Anchorage Formation point to short-termed intervals of cool bottom water. Agglomerated occurrences of micro-glendonites in the Late Tithonian and concurrent lowered sea level (as compared with the Middle Tithonian) indicate cold sea water and a glacioeustatic influence on sea level (Figs. 146, 152). Climatic cooling is suggested for the Late Tithonian as already proposed by previous studies for the wider region (e.g. Moore et al., 1992; Oliveros et al., 2012; Grabowksi et al., 2013)

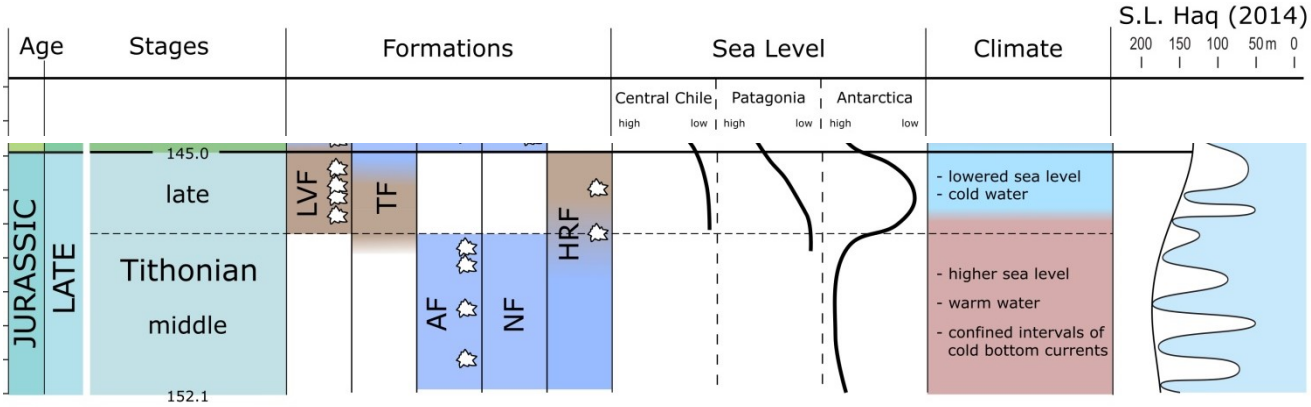

Figure 146: Sea level/palaeoclimatic interpretation of the Tithonian interval; Formations: LVF=Lo Valdés, TF=Tobífera, AF=Anchorage, NF=Nordenskjöld, HRF=Himalia Ridge; brown=proximal environment, blue=distal environment, light blue=cold climate; red=warm climate; S.L.=sea level; global sea level curves from Haq (2014), = micro-glendonite occurrence.

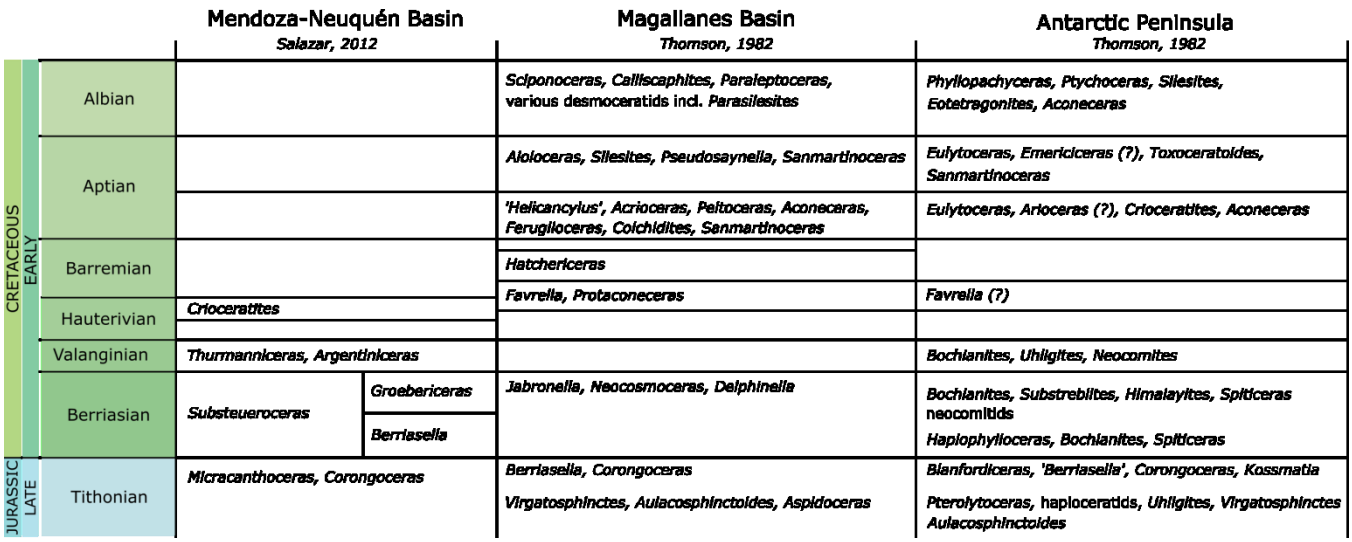

Figure 147: Simplified ammonite stratigraphy of the Late Jurassic–Early Cretaceous interval of the Mendoza-Neuquén Basin (Salazar, 2012), the Magallanes Basin (Thomson, 1983) and the Antarctic Peninsula (Thomson, 1983).

BERRIASIAN

For the lower–Middle Berriasian President Beaches Formation the results of the present study indicate a proximal continental margin (continental slope) setting (the dinoflagellate cyst assemblage is indicative of the *Kalyptea wisemaniae* Interval Zone of Early Berriasian age; Crame et al., 1993). Scarce occurrences of small micro-glendonites in the lowermost Berriasian (lower Zone 2 *Substeueroceras koeneni*, i.e. Zone 2a – *Berriasella jacobi* of Salazar, 2012; Fig. 147) of the Lo Valdés Formation correspond well to the frequent findings of larger micro-glendonites in the Lower Berriasian of the President Beaches Formation. Proximal depositional environments in combination with occurrences of micro-glendonites suggest cool climate connected to low sea level during the earliest Berriasian in central Chile and the early–Middle Berriasian in Antarctica.

Contemporaneous occurrences of oxygen-depleted euxinic facies and calpionellids in a distal marine environment are observed in the lower–middle and Upper Berriasian samples of the Lo Valdés Formation. This presence of calpionellids throughout the Berriasian sediments of the central Chilean sections is suggested to reflect warm water conditions, at least for the upper water column (cf. Bolli et al. 2007). The proximal settings and micro-glendonite occurrences of the lowermost Berriasian are followed by a sea level rise from the Lower Berriasian onwards which is indicated by distal microfacies and a low-energy TOC-rich euxinic environment inferred from the palynofacies analysis. In the Lo Valdés Formation, the transition from inner- to mid-ramp (shoreface to offshore transition, cf. Salazar, 2012) environment is marked by an abrupt change from fine-grained calcareous sandstone to calcareous siltstone. The offshore transition facies of the Berriasian Lo Valdés Formation is characterised by common horizontal laminated siltstone, calcareous siltstone and silty limestone. Conglomerate and sandstone are typically absent and increased carbonate content, abundant organic matter and disseminated pyrite are observed. For the Berriasian interval of the Lo Valdés Formation, Salazar (2012) reported a faunal assemblage consisting of ammonoids, calcispheres, echinoderms,

foraminifers, radiolarians, inoceramids and other bivalves. In the Patagonian lower Zapata Formation data presented here indicate a potentially distal shelf environment for the Berriasian interval and hence support the concept of a higher sea level for most of this time interval.
Occurrences of micro-glendonites in the latest Berriasian–Early Valanginian of the Chester Cone Formation in Antarctica suggest decreasing water temperatures coinciding well with the proximal depositional environment in this time interval. The presence of micro-glendonites in the latest Berriasian is suggested to represent the onset of cooling in Antarctica. In central Chile calpionellids also occur in the Late Berriasian. Since no indications for sediment reworking are observed, calpionellid occurrences suggest: i) that during this time cold water in the Southern Hemisphere was restricted to Antarctica, or ii) that there was no pathway for cold Antarctic water to reach central Chile, or iii) that a layered water body resulted in the co-occurrence of cold bottom water and warm surface water. The Upper Berriasian interval of the Himalia Ridge Formation consists of one sample only. The absence of micro-glendonites in this sample is therefore not suggested to reflect warmer climate in Antarctica.

Grabowski et al. (2013) observed that abrupt magnetic susceptibility (MS) variations correlate well with relative sea-level changes. The authors report on MS highs that occur in the lowermost and Upper Berriasian and indicate regressive intervals. A transgressive interval (MS low) occurs in the lower to Middle Berriasian (Grabowski et al., 2013). Haq (2014) proposed a long-term sea level rise during the Berriasian but for the short-term curve, he proposed a distinct sea level drop for the Early Berriasian nannofossil zone CC1 (145–144 Ma). Langrock et al. (2003) found quartz grains with diameters of 60–200 µm that were patchily distributed in the earliest Berriasian of the Barents Sea that could not have been transported along with the common claystone facies. Therefore, the authors proposed ice rafting as a possible mechanism for the input of these large sand grains. A cool lower(most) Berriasian is indicated by the faunal provincialism across the Jurassic–Cretaceous boundary which might have been caused by a significant temperature gradient (Price & Mutterlose, 2004).
For the early and Middle Berriasian of the lower latitudes (Poland) oxygen-depleted waters with enhanced palaeoproductivity are supposedly linked to progressively warmer conditions (the "*Nannoconus* world" of Tremolada et al., 2006) (Grabowski et al., 2013). The organic-rich shale deposits of the Berriasian in central Chile suggest high primary productivity and organic matter burial (cf. Dera et al., 2011) during warm conditions. In the Western Tethys Grabowski et al. (2013) report increased productivity and oxygen deficiency for the early and Middle Berriasian, which corresponds to low MS values and calpionellid-bearing limestone sedimentation. Occurrences of calpionellids in the Lo Valdés Formation and the more distal depositional environments in central Chile, Patagonia and Antarctica, suggest increased sea level and warm climate for the early–Middle Berriasian interval. An increased sea level during that time period fits well to the suggestion of a long-term sea level rise for the Berriasian by Haq (2014).
Haq (2014) suggests a regressive long-term sea level from the Late Berriasian onward and Grabowksi et al. (2013) reported regressive sea level intervals (MS highs) for the Upper Berriasian of the Western Carpathians. Rogov et al. (2017) further suggest glacioeustatic cooling accompanied by a long-term sea-level fall in the Late Berriasian to Hauterivian based on glendonite findings from the Late Berriasian of north eastern Siberia. The authors suggest the initiation of this high-latitude cooling in the Late Berriasian. Episodes of cool climate were also suggested for the earliest Cretaceous Boreal realm by Price et al. (2000) and Mutterlose et al. (2003). Evidence for polar ice in the Early

Cretaceous comes also from occurrences of glacial diamictite, dated palynologically as Berriasian-to-Valanginian, in the Cadna-owie Formation of South Australia (Alley & Frakes, 2003). For this interval cooling is also indicated by a decrease in CO_2 (Royer, 2006). In the present study proximal depositional environments and occurrences of micro-glendonites suggest regressive intervals for the lowermost and Upper Berriasian that are linked to cold climates in the higher latitudes (Figs. 148, 152)

Summary

A warmer climate with associated increased sea level throughout the lower–Middle Berriasian is indicated by the presence of calpionellids, the absence of micro-glendonites and the more distal depositional environments in the studied sections (Fig. 141). Intermittent phases of lower sea level in the lowermost and upper(most) Berriasian and associated short-termed cooling periods are indicated by the occurrences of micro-glendonites in the central Chilean Lo Valdés Formation and the Chester Cone Formation in Antarctica. Occurrences of micro-glendonites in the Middle Berriasian of the President Beaches Formation are restricted to a few specimens and might reflect local short-termed cooling restricted to Antarctica. The increased sea-level in the Berriasian and a warmer lower–Middle Berriasian climate occurring in wide regional extension is indicated by the temperature increase throughout the Berriasian.

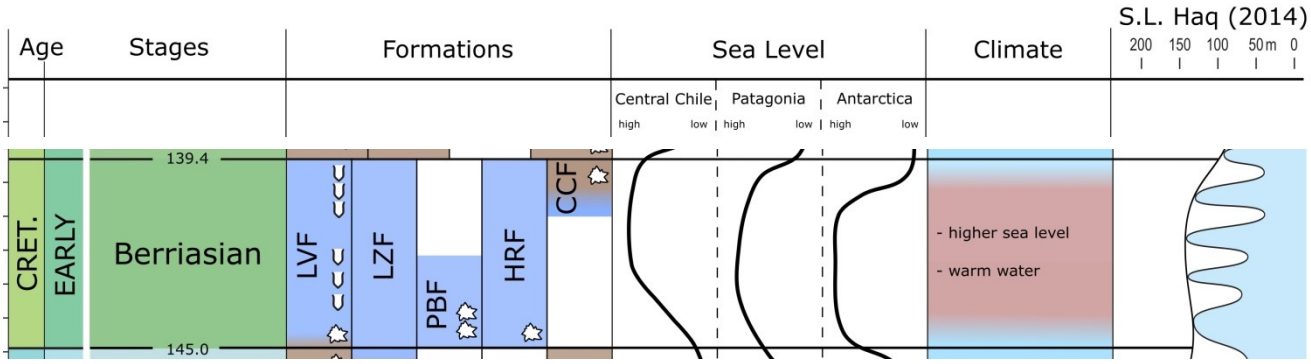

Figure 148: Sea level/palaeoclimatic interpretation of the Berriasian interval; Formations: LVF=Lo Valdés, LZF=Lower Zapata, PBF=President Beaches, HRF=Himalia Ridge, CCF=Chester Cone; description same as figure 146, ∪ = calpionellid occurrence.

VALANGINIAN

A return to proximal depositional environments and consequently lower sea-level is detected in the Valanginian interval of all sections analysed here from central Chile, Patagonia and Antarctica (Figs. 149, 152). For the Spartan Glacier Formation in Antarctica, a general shallowing trend was previously reported by Crame & Howlett (1988) and Macdonald et al. (1993), while Lomas (1999) suggested shallow marine environments for the Chester Cone Formation. A regressive interval in the Valanginian is indicated for the lower Zapata Formation by proximal depositional environments, following the distal depositional setting of the underlying Berriasian. For the Valanginian interval of

the Lo Valdés Formation inner ramp to mid-ramp (shoal) microfacies suggest a return to proximal depositional settings (cf. Flügel, 2004) after the mid–outer ramp to basin setting of the underlying Berriasian. A lower sea level for the Valanginian period was already reported by other authors (Southern Andes: Haq et al., 1987; Tethys: Chatalov et al., 2015). These observations of proximal depositional environments correlate well with the frequent clustered occurrence of micro-glendonites in lower–Middle Valanginian samples. These are abundant in the central Chilean Lo Valdés Formation (medium–large specimens) as well as the Chester Cone (medium–large specimens) and Spartan Glacier (large specimens) formations of Antarctica. The absence of micro-glendonites in the lower Zapata Formation of Patagonia may again result from low alkalinity observed in the geochemical analysis.

Regressive sequences were reported for the Early Valanginian Andean and Austral Basins of southern South America (Riccardi, 1988). Other authors (e.g., Immenhauser & Scott, 2002; Gréselle & Pittet, 2005, 2010; Bover-Arnal et al., 2009, 2014; Rameil et al., 2012; Maurer et al., 2013) suggest glacioeustasy as the cause for extensive and rapid global sea level fluctuation during certain intervals of the Early Cretaceous, i.a. the Late Valanginian. 'Disaster deposits' (sensu Groves et al. (2003): microbialites, oolites and calcimudstones which formed during pronounced phases of bio-calcification crisis) from the Berriasian–Lower Valanginian in the Tethys Ocean were reported by Chatalov et al. (2015) as a result of local but dramatic sea level fall and cooling. The formation of these disaster deposits in the Valanginian of the Tethyan realm was caused by rapid sea level fall, atmospheric CO_2 drawdown and the decrease of carbonate production leading to seawater carbonate supersaturation (Chatalov et al., 2015). The reasons proposed for decreased atmospheric CO_2 include i) increased primary productivity and hence increased organic carbon burial (Dromart et al., 2003a; McAnena et al., 2013; Bodin et al., 2015), ii) enhanced sequestration of organic carbon (Dromart et al., 2003a), or iii) storage of organic carbon in coastal areas and/or enhanced preservation within stratified waters in high-latitude basins (Price & Mutterlose, 2004). A temperature decrease through the *S. verrucosum* Zone immediately precedes intense faunal changes in the *N. peregrinus* Zone, which supports the view that climate controlled, at least in part, the migration of Boreal ammonoid faunas in the Valanginian of Western Europe (Kemper, 1987; Rawson, 1994; Reboulet & Atrops, 1995; Reboulet, 1996). An abundance peak of Boreal nannofossils (Melinte & Mutterlose, 2001) occurs during this time of relative cold in which Boreal ammonites occur commonly in SE France (Besse et al., 1986; Thieuloy et al., 1990; Bulot et al., 1993, Reboulet & Atrops, 1995; Reboulet, 1996). Faunal migration between the Tethys and the eastern Pacific was also reported by Salazar (2012). This cooling resulted in the presence of Boreal ammonites (*Argentiniceras fasciculatum*) in the Lower Valanginian of central Chile (Salazar, 2012) and indicates migration processes of ammonite faunas. McArthur et al. (2007) used Mg/Ca ratios and faunal migration to deduce climatic perturbations during the Valanginian. The lowest temperatures were reported from the Late Valanginian–Early Hauterivian *P. michalskii–H. bojarkensis* zones. From an analysis of calcareous nannoplankton, Kessels et al. (2006) reported a distinctive southward migration of the endemic cold water species *C. salebrosum* into low latitudes from the Valanginian to Early Hauterivian which was interpreted as an indicator of climatic cooling within the Northern Hemisphere (McArthur et al., 2007).

Valanginian glendonites are widely distributed across the present-day Arctic (Kemper & Schmitz, 1981; Kemper, 1987; Kaplan, 1978; Zlobina et al., 2014) and were also briefly described from West Siberia (Rogov & Zakharov, 2010). In Antarctica, glendonite occurrences have so far been reported

from the Late Berriasian–Middle Valanginian (Varela & Cisternas, 2015). Price and Nunn (2010) used oxygen isotope data from well-preserved Valanginian glendonites to infer the oxygen isotope composition of ambient seawater. Integrated with the oxygen isotope compositions of coexisting belemnites, palaeotemperatures were calculated to 4–7 °C, which is in agreement with temporary glacial polar conditions during the Cretaceous greenhouse (Price & Nunn, 2010). Based on a belemnite clumped-isotope study, Price and Passey (2013) provide further evidence for a cooler Late Valanginian with existence of polar ice. Hardenbol et al. (1998) report on a sea level fall and recovery of 90 m within the Early Valanginian which was one of the largest third-order excursions of sea level in the Mesozoic Era. This rapid sea level change was of a duration so short that it could have been caused only by the waxing and waning of polar ice (cf. McArthur et al., 2007).

Summary

Cooling episodes are suggested for most of the Valanginian based on the presence of micro-glendonites throughout the sections of central Chile and Antarctica (especially early and Middle Valanginian – central Chile: *Thurmaniceras thurmanni/Argentiniceras fasciculatum* zone, cf. Salazar, 2012, fig. 147; Antarctica: *Bochianites, Uhligites* and *Neocomites* ammonite assemblage, Covacevich, 1976; Crame et al., 1993, fig. 147) and associated lower sea level in central Chile, Patagonia and Antarctica. A brief cooling episode is also suggested for the Late Valanginian (Zone 4, of Salazar, 2012) by infrequent occurrences of micro-glendonites (Figs. 149, 152).

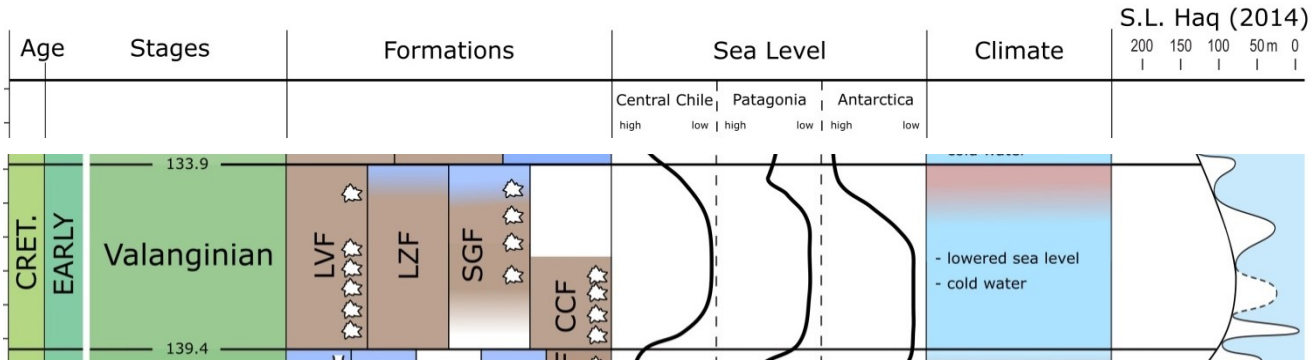

Figure 149: sea level/palaeoclimatic interpretation of the Valanginian interval; Formations: LVF=Lo Valdés, LZF=Lower Zapata, SGF=Spartan Glacier, CCF=Chester Cone; description same as figure 146.

HAUTERIVIAN

Throughout the different study areas of the present thesis, palaeoenvironmental development and sea level change for the Hauterivian interval are inconsistent. Results indicate more distal depositional environments for the Hauterivian interval of the central Chilean samples compared to the underlying Valanginian and hence suggest a higher sea level. This observation is in agreement with Haq (2014) who proposes on-going transgression for the Hauterivian. Results indicate a higher sea level from the

Early–Middle Hauterivian onwards (central Chile), mainly based on the distal depositional environment indicated by microfacies and by palynofacies compositions. Absence of micro-glendonites combined with the higher sea level suggests a warm climate. The occurrence of large micro-glendonites in one sample of the lower-middle part of the Hauterivian in the analysed interval of the CM section points to local short-term cooling which is coherent with an Early Hauterivian cooling phase (McArthur et al., 2007). In Patagonia samples show increased carbonate content. However, micro-glendonite is absent which is here interpreted as indication for warm climate although analyses show proximal depositional settings for the Hauterivian interval. The tectonically active arc and hence highly irregular morphology of the area (cf. Fildani & Hessler, 2005) might have masked a potential sea level change. The samples of the Spartan Glacier Formation of Antarctica are restricted to the lower and Upper Hauterivian sediment succession. Results suggest higher sea level in the Early Hauterivian and lower sea level in the Late Hauterivian. Micro-glendonite occurrences lack continuously pointing to warmer water. However, absence of micro-glendonite might also be connected to lowered alkalinity. From the results of the present study the Hauterivian interval is not characterised by a uniformly development of sea level and palaeoclimate.

Bodin et al. (2015) state that one of the episodes of cool climate that punctuated the Early Cretaceous greenhouse occurred during the Late Valanginian–earliest Hauterivian. Several authors propose that coolest temperatures of the Early Cretaceous were reached in the Early Hauterivian, i.e. in the *P. michalskii–H. bojarkensis* zones (Podlaha et al., 1998; Veizer et al., 2000; Huber et al., 2002; Price & Mutterlose, 2004; Kessels et al., 2006; Keller, 2008). Bodin et al. (2015) suggested that the cool episode was triggered by enhanced organic-carbon burial on a global scale, as reflected by coeval short-term positive $\delta^{13}C$ excursions in belemnite rostra, micrite, and organic carbon. Kessels et al. (2006) observed a similar distinctive trend for the Valanginian to Hauterivian interval which points to a general decrease of water temperature in this time interval. This decrease of temperature is supported by the southward migration of the high latitudinal cold water nannofossil *Crucibiscutum salebrosum* to lower latitudes. Based on measurements of $\delta^{18}O_{sw}$, computed from Mg/Ca and $\delta^{18}O_c$, McArthur et al. (2007) proposed the formation of substantial amounts of polar ice after a period of global cooling through the Late Valanginian and Early Hauterivian.

The cool phase of the Early Hauterivian was followed by warming throughout the Middle and Late Hauterivian: increasing Mg/Ca ratios indicate a substantial warming which led to the retreat of the previously established ice (McArthur et al., 2007). Temperature increase and associated less positive values of $\delta^{18}O_{sw}$ are indicated through the Middle-to-Upper Hauterivian. Reduced polar ice volumes are indicated by significant warming for the Hauterivian (based on $\delta^{18}O_c$ and Mg/Ca) (McArthur et al., 2007). Continental volcanism in the Paraná-Etendeka region (Paraná traps in the Paraná Basin in central-eastern South America and the Etendeka traps in northwest Namibia and southwest Angola) is suggested as the key driver for this temperature increase, although the eruptive volumes were probably small (0.21 $km^3\ y^{-1}$; Stewart et al., 1996) (McArthur et al., 2007). Nevertheless, volcanic activity may have supported the melting of polar ice through the release of carbon dioxide reported by previous studies (e.g. Podlaha et al., 1998; Veizer et al., 2000; Huber et al., 2002; Kessels et al., 2006; Keller, 2008). A warm Hauterivian in the middle latitudes is suggested by Mutterlose et al. (2014). The authors proposed sea surface temperatures in a range of 24–27 °C for the Lower Saxony Basin (~39° N) throughout the Hauterivian based on Tex_{86} derived temperatures.

Summary

Results suggest an Early Hauterivian cooling phase indicated by few occurrences of micro-glendonites and proximal depositional environment in the Lo Valdés Formation. This cooling phase is followed by increased sea level and warm climate in the Middle–Upper Hauterivian in which micro-glendonites are generally absent (Figs. 150, 152). In Patagonia, the influence of the tectonically active arc and the irregular morphology of the area (cf. Fildani & Hessler, 2005) make it difficult to assess the extent of sea level and climatic change. The sample series of the Spartan Glacier Formation covers only a limited interval of the Hauterivian. The sample series of central Chile provides the most comprehensive data set and points to a warm climate during the middle-Late Hauterivian. Previous studies support this interpretation.

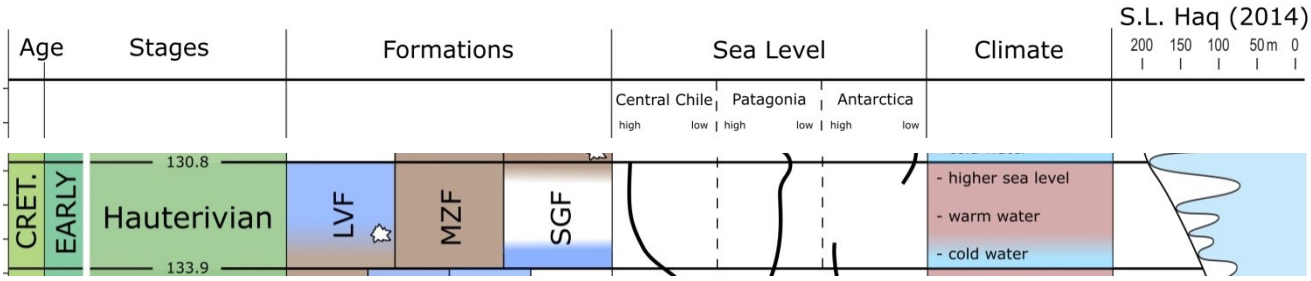

Figure 150: Sea level/palaeoclimatic interpretation of the Hauterivian interval; Formations: LVF=Lo Valdés, MZF=Middle Zapata, SGF=Spartan Glacier; description same as figure 146.

BARREMIAN–APTIAN

Results suggest a distal low energy depositional environment for the middle (?Barremian) part of the middle Zapata Formation. Frequent occurrences of medium to large sized micro-glendonites in the distal depositional environment indicate cold bottom water conditions during the Barremian time interval, although this stratigraphic assignation is not well defined in Patagonia. The palaeoenvironmental development of the Upper Barremian–Lower Aptian (Barremian *Muderongia australis* Zone of Australia, and overlying *Odontochitina operculata* Zone of Aptian age) interval of the Springhill/Río Mayer Formation is characterised by increasingly distal shelf marine environments. The uppermost part of the Lower Aptian shows a return to more proximal marine conditions. Confined intervals of reduced sea level also occur in the upper part of the Upper Barremian which is indicated by increased proportions of siliciclastic mineral detritus and contemporaneous agglomerations of small micro-glendonites. Co-occurrence of (medium sized) micro-glendonites (cold water) and increased siliciclastic detritus (proximal depositional environment) is also evident in the samples of the Barremian interval of the Spartan Glacier Formation of Antarctica.

Distinctive provincialism of belemnites during the Barremian–Aptian interval was interpreted by Price and Mutterlose (2004) to be a result of palaeobiogeographical isolation. The authors suggested that

substantial temperature gradients and hence low polar temperatures may in part explain the observed provincialism. High temperature seasonality was recorded in stable isotope analyses of Barremian–Aptian rudist bivalves which supposedly resulted from the existence of polar ice sheets (Steuber et al., 2005). According to Steuber et al. (2005) the presence of seasonal temperature extremes at 17–25 °N during the Late Barremian–Middle-Albian requires the presence of polar ice. The authors suggest the existence of ice sheets with one third the extent of today. When adjusted to ice-free conditions the $\delta^{18}O_{sw}$ indicates sea surface temperatures lower than today for the period from 100–130 Ma (Steuber et al., 2005). The oxygen isotope signature of belemnite guards from the Boreal Barremian at a palaeolatitude of northeastern England and northwestern Germany shows three different phases of climatic evolution (Malkoč & Mutterlose, 2010). An earliest Barremian cool phase (*Praeoxyteuthis pugio* belemnite Zone) is followed by a distinctive warming event in the late Early Barremian (*Aulacoteuthis spp.* belemnite Zone). Steuber et al. (2005) also observed negative (=warm) values for the Early Barremian of northern Germany based on the high-resolution $\delta^{18}O$ record gained from belemnite guards throughout a complete succession of Barremian–Early Aptian mudstone. The Late Barremian (*Oxyteuthis brunsvicensis, O. germanica*, and *O. depressa* belemnite Zones) is characterised by another cooling interval (Malkoč & Mutterlose, 2010). Stable isotope analysis of shark teeth showed positive $\delta^{18}O$ values and suggest a cooling in the Late Barremian–Early Aptian (Pucéat et al., 2003). This palaeotemperature interpretation based on oxygen data is supported by the Mg/Ca trends (Malkoč and Mutterlose, 2010), but also by micro-glendonite occurrences in the Lower Barremian. Cool temperatures are indicated by belemnopseid belemnites *B. alexandri, B. gladiatoris, B.* cf. *madagascariensis*; Crame & Howlett, 1988) in Antarctica and the upper(most) Barremian–Lower Aptian in Patagonian and Antarctica, as indicated by bivalve *A. andina-radiatostriata* gp. (Crame & Howlett, 1988).

Summary

Micro-glendonite occurrences in the Lower Barremian middle Zapata Formation of Patagonia and in coeval Lower Barremian section of Antarctica reflect a cooling episode that was restricted to high latitudes (Figs. 151, 152). An Early Barremian cooling phase correlates well with the reduced short-term sea level curve of Haq (2014). A subsequent Late Barremian–Early Aptian cooling has been observed in the Springhill/Río Mayer Formation of Patagonia, but also in Tethyan sections (Mutterlose et al., 2009). In consequence, this latter cooling phase is considered to reflect a global trend.

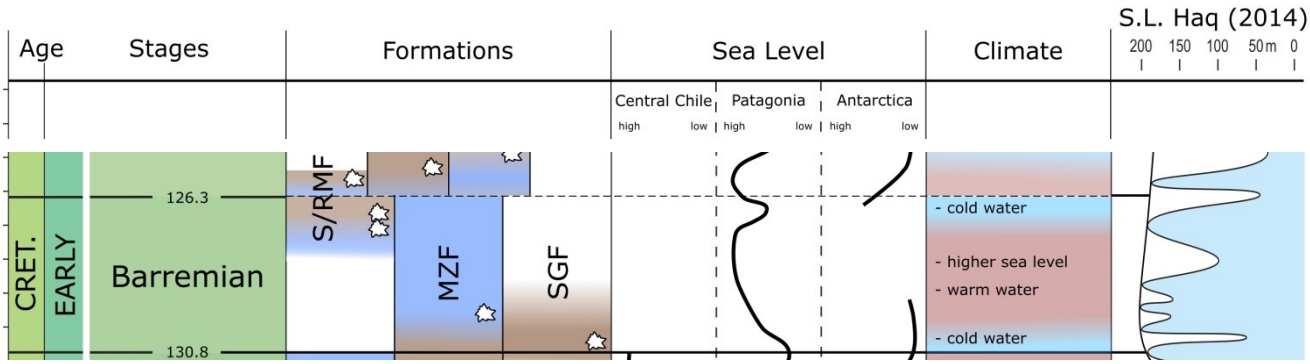

Figure 151: sea level/palaeoclimatic interpretation of the Barremian-Aptian interval; Formations: LVF=Lo Valdés, LZF=Lower Zapata, PBF=President Beaches, HRF=Himalia Ridge, CCF=Chester Cone; description same as figure 146.

APTIAN–ALBIAN

For the Aptian interval of the middle Zapata Formation a proximal shallow marine depositional setting is indicated. For the majority of the Pluto Glacier Formation results also suggest a shallow shelf marine depositional environment. Confined intervals of more distal environments (marginal dysoxic-anoxic shelf) are identified. In the Aptian–Albian interval of the Kotick Point Formation, the analysed samples originate from turbidite material indicating more distal marine settings. The organic-matter composition reflects a higher energy depositional environment than that reported by Ineson (1987). Samples of the Kotick Point Formation represent deposition by turbidites on the continental margin and reflect mixed terrestrial-marine conditions ranging from shallow near-shore to slope apron environments (cf. Farquharson et al. 1984; Ineson 1989; Pirrie et al. 1991). Micro-glendonite occurrences are here identified in: i) the Lower Aptian of the Springhill/Río Mayer Formation with intensely clustered and relatively large clusters; ii) the Aptian middle Zapata Formation with frequent occurrences and agglomerations in the middle–upper part where also the largest specimens are observed; iii) the lower (infrequent occurrences and small specimens) and Middle Aptian Pluto Glacier Formation (scarce occurrences and large specimens) and iv) the Lower Albian Kotick Point Formation (high numbers, medium sized and intensely clustered specimens). In the Aptian interval micro-glendonite occurrences coincide with increased content of siliciclastic mineral detritus and proximal depositional environments. This points to concurrent intervals of reduced sea level and cold water and hence a glacioeustatic control on the sea level. In the Early Albian interval samples are restricted to the Kotick Point Formation where micro-glendonite occurrences are observed in distal environments. Increased sea level and occurrences of micro-glendonites point to cold bottom water conditions.

For the Aptian–Albian interval glendonite occurrences have previously been reported from numerous locations in the northern hemisphere: in the Arctic region of Canada (Upper Aptian–Lower Albian of Sverdrup Basin, see Kemper, 1987; Upper Aptian–Lower Albian of Christopher Formation, Schröder-

Adams et al., 2014), in Spitsbergen (lowermost Upper Aptian, Rogov & Zakharov, (2010); Upper Aptian–Lower Albian, Maher et al., (2004) and Vickers et al., (2016)) and the Early Albian of Kamchatka, eastern NE Russia (Alabushev, 1995). Aptian glendonites are also known from the southern hemisphere, including the Late Aptian Bulldog Shale in the Eromanga Basin, Australia (Sheard, 1991; de Lurio & Frakes, 1999) and the Aptian of the South Shetland Islands (Varela & Cisternas, 2015). Peaks in glendonite distribution correlate well with episodes of global climatic cooling, with one of the most prominent temperature lows occurring in the Late Aptian – a cooling which also corresponds to long-term sea level fall supposedly caused by glacioeustatic control (Rogov et al., 2017). Extensive and rapid global sea level fluctuations were observed during certain intervals of the Aptian–Albian (e.g., Immenhauser & Scott, 2002; Gréselle & Pittet, 2005, 2010; Bover-Arnal et al., 2009, 2014; Rameil et al., 2012; Maurer et al., 2013). These studies suggest polar glaciation and therefore glacioeustasy as the cause for the sea level fluctuations. Husinec et al. (2012) proposed a significant glacioeustatic component of sea level fall during cool episodes of the Aptian greenhouse: The authors corrected the Phanerozoic temperature curve of Royer et al. (2004) (based on oxygen isotopes) for pH, changes in Ca^{2+}, CO_2 and $CaCO_3$ saturation and showed significant cooling in the Aptian. Husinec et al. (2012) concluded that the Adriatic platform was characterised by attributes of transitional icehouse. Significant sea level falls in the Aptian have also been documented in Oman and Spain (Greselle & Pittet, 2005; Bover-Arnal et al., 2009).

Wang et al. (2013) suggested that the Aptian was most likely punctuated by several brief cool periods based on evidence from both paleobotany and paleosols. The cool periods correspond well with documented intervals of low CO_2 (Royer, 2006). For example, the marine palaeotemperature record of Steuber et al. (2005) is consistent with a cool interval during the Early Aptian (Royer, 2006). The low CO_2 levels in the Aptian–Albian interval and their decrease after OAE1a coincide with oxygen isotope data (Veizer et al., 2000; Weissert & Erba, 2004) that indicate a cool late Early Cretaceous. The cooling was likely caused by increased organic-carbon burial on a global scale. McAnena et al. (2013) suggest that the emerging Southern Ocean, Atlantic Ocean and Tethys Ocean basins served as global carbon sinks during the Late Aptian, resulting in increased pCO_2 drawdown and associated global cooling.

The Aptian–Albian transition contained intervals of global cooling, leading to disruption of the warm and equable climate conditions of the latest Early Cretaceous period (Kemper, 1987; Weissert & Lini, 1991; Mutterlose et al., 2008, 2009; Jenkyns et al., 2012). Further evidence for Late Aptian–Early Albian climate perturbation includes indications for cold climates like decline in pCO_2 (Hong and Lee, 2012), occurrences of erratic lithologies and diamictites (Price, 1999) and a major biotic crisis that affected carbonate producers on a global scale (Leckie et al., 2002; Herrle & Mutterlose, 2003; Föllmi et al., 2006). No substantial temperature variation between South America and Antarctica existed in the Early Albian, a time in which the shelf seas of Gondwana were cool and a distinct marine Austral realm was present (Pirrie et al., 2004). However, the exact timing of these climatic perturbations is still poorly constrained (McAnena et al., 2013).

Summary

Although a precise stratigraphic subdivision is not possible, the shallow environments and associated lower sea level combined with the occurrences of micro-glendonites reflect phases of climatic cooling

and episodes of glacioeustatic control on the sea level during the Aptian–Albian interval in the studied sections (Fig. 152). In the present study, the Aptian–Albian interval was only accessible in the Patagonian and Antarctica sections. However, in the Chilean Central Andes (Pabellón and Arqueros Formations of the Chañarcillo basin north of Santiago) Masse et al. (2015) suggested that oceanographic conditions of the Chilean Pacific margin during the Aptian–Albian were characterised by a cool greenhouse regime.

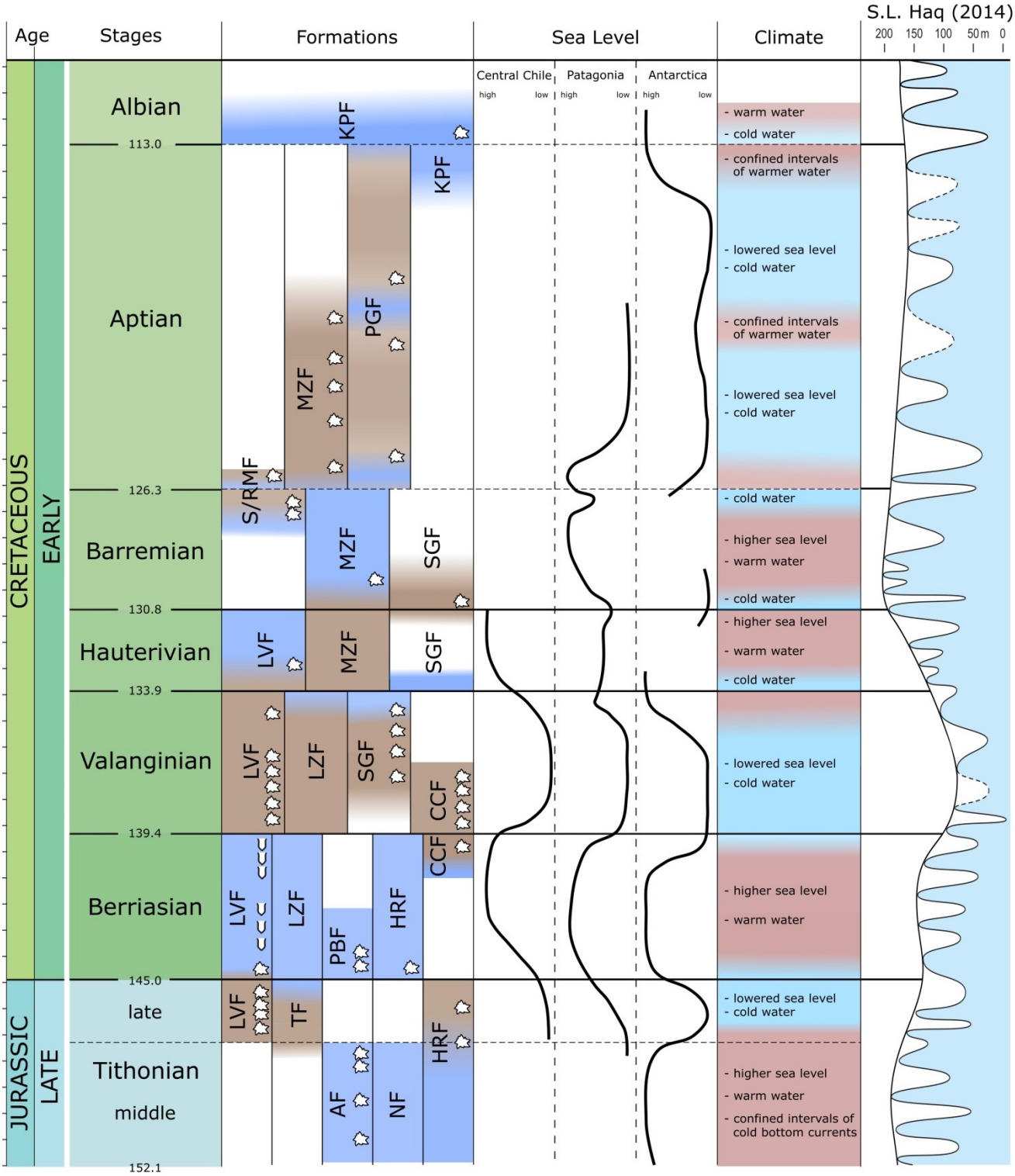

Figure 152: Sea level/palaeoclimatic interpretation of the present study; Formations: LVF= Lo Valdés, TF=Tobífera, AF=Anchorage, NF=Nordenskjöld, HRF=Himalia Ridge, LZF=Lower Zapata, PBF=President Beaches, CCF=Chester Cone, SGF=Spartan Glacier, PGF=Pluto Glacier, S/RMF=Springhill/Río Mayer, MZF=Middle Zapata, KPF=Kotick Point; description same as figures 146 and 148.

6. CONCLUSIONS

Tithonian

In the present study, the Middle Tithonian interval is restricted to the Antarctica study area. Presence of turbidites and the results of the palynofacies and geochemical analyses of the Anchorage-, Himalia Ridge- and Nordenskjöld Formation show a majorly distal continental margin (continental slope to continental rise) setting with at times oxygen-depleted conditions and input of reworked organic matter. Occasional influences of distal suboxic-anoxic shelf environments are observed. Indications for climatic cooling are absent in the Himalia Ridge- and Nordenskjöld Formation suggesting a connection of distal depositional environment and increased sea level. Occurrence of microscopic glendonite in the time equivalent Anchorage Formation indicates influence of cool bottom water in the intra-arc during times of warm climate and high sea level.

The Upper Tithonian interval is present in all three study areas (central Chile, Patagonia and Antarctica). The interval shows a shift towards more proximal depositional settings. The Upper Tithonian sediment succession of the central Chilean Lo Valdés Formation is characterised by a proximal high-energy depositional environment. For the upper Tobífera Formation (Patagonia) and the Himalia Ridge Formation (Antarctica) proximal continental margin depositional settings are observed. Agglomerated occurrences of micro-glendonites in the deposits of the Upper Tithonian and concurrent lowered sea level point to glacioeustatic control of the sea level. Integrated with the results of previous studies, a climatic cooling of the Southern Hemisphere during the Late Tithonian is suggested.

Berriasian

The central Chilean sections show a shift towards more distal shelf environments during the Berriasian. This interval is characterised by high organic matter preservation and temporal oxygen-reduced conditions. The results of the present study don't allow for a precise stratigraphic subdivision of the sedimentary succession of the lower Zapata Formation. Correct assessment of the environmental changes (depositional setting and climate) for the lower part (?Berriasian) of the lower Zapata Formation is impeded by the poor preservation state of the organic matter and the onset of Andean contraction and transition to the Magallanes retroarc foreland basin during the Late Jurassic–Early Cretaceous. Nevertheless, results suggest a potentially distal shelf to proximal basin environment for this interval. In the Antarctic study area results also point to a more distal marine depositional setting and a higher sea level during the Berriasian. The depositional environment of the Berriasian Himalia Ridge Formation is characterised by low-density turbidites in a submarine fan setting. In this interval the formation shows a shift towards settings of the continental rise to abyssal plain. The early–Middle Berriasian President Beaches Formation represents a distal continental margin (slope to rise) environment with at times oxygen-depleted bottom water conditions. A more distal fully marine environment is also observed for the lower part of the Late Berriasian Chester Cone Formation whereas a proximal shelf marine depositional setting is suggested for the middle-upper part.

The majority of the Berriasian sections of central Chile (Lo Valdés Formation), Patagonia (Lower Zapata Formation) and Antarctica (President Beaches Formation and Himalia Ridge Formation) therefore show an increased sea level with deposition in distal fully marine environments. Only the

uppermost Berriasian Devils Point Member of the Chester Cone Formation is characterised by a proximal shallow marine environment. In the studied sections a warmer climate with associated increased sea level throughout the lower–Middle Berriasian is indicated by the presence of calpionellids (central Chile), the absence of micro-glendonites and the more distal depositional environments. Intermittent phases of lower sea level in the earliest and latest Berriasian and associated short-termed cooling periods are indicated by the occurrences of micro-glendonites in the central Chilean Lo Valdés Formation and the Chester Cone Formation in Antarctica. Occurrences of micro-glendonites in the Middle Berriasian of the President Beaches Formation reflect local short-termed cooling restricted to Antarctica.

Valanginian

For the Valanginian interval of the Lo Valdés Formation a proximal depositional environment with occasional shifts to more distal shelf settings during the earliest and latest Valanginian are observed. Microscopic glendonites are present throughout the Valanginian and are most frequent in the lower–middle part of the section. Poor preservation of the organic matter and the onset of Andean contraction and transition to the Magallanes retroarc foreland basin mask the changes of the depositional environment in the upper part of the Patagonian lower Zapata Formation. Nevertheless, changes in organic matter composition and differences in the results of the geochemical and optical approaches point to a more proximal shelf environment for the upper part of the lower Zapata Formation (?Valanginian). Results indicate a more distal shelf marine environment in the uppermost part of the lower Zapata Formation. Throughout the Valanginian interval of the Spartan Glacier Formation a significant increase in grain size points to a general shallowing-upward trend. An oxygenated near-shore environment is indicated by continuously low TOC contents and high abundances of siliciclastic mineral detritus in the palynofacies samples. Previous studies reported frequent bioturbation which further indicates an oxygenated water body. The Valanginian section of the Spartan Glacier Formation was deposited in an outer continental shelf setting. The Sealer Hill Member of the Chester Cone Formation consists of finely laminated mudstone of Early–Middle Valanginian age and is characterised by a more proximal but a lower-energy setting compared to the underlying Devils Point Member. Results suggest a proximal fully marine depositional environment for the Early-Middle Valanginian Chester Cone Formation with occasional influences of lower energy marginal basin settings.

The Valanginian sections in central Chile (Lo Valdés Formation), Patagonia (Lower Zapata Formation) and Antarctica (Chester Cone Formation and Spartan Glacier Formation) show proximal depositional settings that range from well-oxygenated near shore environments to outer continental shelf settings. Presence of micro-glendonites throughout the sections of central Chile and Antarctica and associated lower sea level in central Chile, Patagonia and Antarctica give strong evidence for episodes of climatic cooling during most of the Valanginian (especially Early and Middle Valanginian). A brief cooling episode is also suggested for the Late Valanginian by infrequent occurrences of micro-glendonites.

Hauterivian

The central Chilean sediment succession is characterised by a proximal depositional environment during the earliest Hauterivian and shows a shift to more distal marine settings within the Early Hauterivian and throughout the remainder of the stage. A brief interval of cold bottom water coinciding with the increased sea level is indicated by micro-glendonite occurrence in the Middle Hauterivian. In contrast to the Lo Valdés Formation, the middle Zapata Formation is characterised by a continuously proximal depositional environment for the presumable Hauterivian interval. For the Patagonian Zapata Formation previous studies suggest a shallow-water marine environment which was tectonically influenced by the Andean orogeny resulting in a highly irregular morphology of the area. Occurrences of micro-glendonites are not observed which might reflect influence of tectonic processes on the sea level rather than climatic cooling and glacioeustasy. The sample series of the Spartan Glacier Formation is restricted to the Lower and Upper Hauterivian sediment succession. A more distal marine depositional environment is suggested for the Early Hauterivian. The sedimentary succession of the Late Hauterivian Spartan Glacier Formation records the return to proximal depositional environments.

A cooling phase during the earliest Hauterivian is indicated by occurrences of micro-glendonite in the central Chilean sections. This cooling phase is followed by increased sea level and warm climate in the Middle–Upper Hauterivian with no occurrences of micro-glendonite. Reliable correlation of the Hauterivian intervals of central Chile, Patagonia and Antarctica is obstructed by the poor age control.

Barremian–Aptian

The sampled interval of the Springhill/Río Mayer Formation is composed of fluvial, marginal-marine, coastal and shallow-marine siliciclastic deposits which were deposited as incised valley fills. The sampled section shows a depositional environment which is characterised by increased distance to the sediment provenance and hence higher sea level in the early Late Barremian and the earliest Aptian. During the latest Barremian and especially the upper interval of the Early Aptian shifts to proximal depositional settings are observed. This high-frequent sea level change is influenced by the Andean orogeny in combination with glacioeustatic effects which is shown by micro-glendonite occurrences. In the middle Zapata Formation of Patagonia a distal low energy depositional environment and concurrent and frequent occurrences of medium to large micro-glendonites are observed. This suggests a scenario of cold bottom water conditions in an environment with increased sea level. In the Lower Barremian interval of the Spartan Glacier Formation of Antarctica, increased siliciclastic detritus and concurrent occurrence of micro-glendonite point to cold water and a lowered sea level caused by glacioeustatic effects.

Micro-glendonite occurrences in the Lower Barremian middle Zapata Formation of Patagonia and in the time equivalent Lower Barremian section of Antarctica reflect a cooling episode that was restricted to higher latitudes. A subsequent Late Barremian–Early Aptian cooling has been observed in the Springhill/Río Mayer Formation and the Spartan Glacier Formation, but also in Tethyan sections. In consequence, this cooling is considered to reflect a global trend.

Aptian–Albian

The majority of the Aptian interval is characterised by a shallow shelf depositional setting (Middle Zapata Formation and Pluto Glacier Formation). Confined intervals of shifts towards more distal marine environments (distal shelf to marginal basin) are observed in the Early Aptian of the Springhill Formation and occasionally within the Pluto Glacier Formation. Continuously more distal marine settings are observed in the Late Aptian to Early Albian Kotick Point Formation. The analysed samples represent deposition by turbidites and therefore reflect continental margin settings ranging from continental slope to continental rise with at times oxygen-depleted conditions.
The shallow environments and associated lower sea level combined with the occurrences of micro-glendonites reflect phases of climatic cooling and episodes of glacioeustatic control on the sea level during the Aptian interval in the studied sections. The Aptian–Albian Kotick Point Formation is characterised by distal marine settings and scarce occurrence of micro-glendonite. Previous studies of the Chilean Central Andes observed oceanographic conditions of the Chilean Pacific margin during the Aptian–Albian were characterised by a cool greenhouse regime.

Micrometre-sized glendonite crystals are here recorded from all three study areas (central Chile, Patagonia and Antarctica). The findings of micro-glendonites in the present study extend the stratigraphic range of those pseudomorphs after ikaite in the Southern Hemisphere to the Late Jurassic–Early Cretaceous. Until now glendonites from this age have only been known from the northern high latitudes. Their occurrences in specific levels of the Tithonian to Aptian succession which are majorly concurrent with proximal depositional settings provide strong evidence for episodes of glacioeustatic control of the sea level. The new data from Chile and Antarctica point to repeated small scale glaciations in the Southern Hemisphere. These cold episodes in the Upper Tithonian, lowermost Berriasian, Valanginian, lowermost Hauterivian, Lower Barremian, Aptian and Lower Albian punctuated the Late Jurassic and Early Cretaceous greenhouse climate in both the Northern and Southern Hemispheres and must thus have been global events.

7. OUTLOOK

The discovery of micrometre-sized glendonites in palynofacies samples might prove a useful tool for investigations of palaeoclimate. Future studies could focus on well-known phases of climatic cooling and try to prove the existence of micro-glendonites in the same time intervals and depositional settings. Focus should also be given on how size and shape of micro-glendonite crystals depends on the ocean chemistry and water temperature. Selection of sections with well-preserved organic matter compositions would further increase in-depth knowledge of palaeoenvironmental changes.
Future studies could also focus on stratigraphic correlation of the different cooling episodes in the study areas of the present study. Especially for the study area in Patagonia a more reliable (bio-) stratigraphic classification would be of great use.

8. REFERENCES

Adatte, T., Stinnesbeck, W., Remane, J., Hubberten, H., 1996b. Paleoceanographic changes at the Jurassic-Cretaceous boundary in the Western Tethys, northeastern Mexico: Cretac. Res., 17, p. 671–689.

Aguirre, L.L., 1960. Geología de los Andes de Chile central – provincia de Aconcague, Santiago: Inst. Invest. Geol., Bol., 9, 70 pp.

Alabushev, A., 1995. Ammonite faunas and biostratigraphy of the Albian to Middle Cenomanian (Cretaceous) in western Korjak-Kamchatka, NE Russia: Neues Jahrbuch für Gelogie und Paläontologie, Abhandlungen 196, p. 109–139.

Allemann, F., Catalano, R., Fares, F. & Remane, J. 1971. Standard calpionellid zonation of the western Mediterranean province: Proceedings of the Second Planktonic Conference, Rome 1970 2, p. 1337–1340.

Alley, N.F. and Frakes, L.A., 2003. First known Cretaceous glaciation: Livingston Tillite Member of the Cadna-owie Formation, South Australia: Australian Journal of Earth Sciences 50, p. 139–144.

Alroy, J., 2010. Geographical, environmental and intrinsic biotic controls on Phanerozoic marine diversification: Palaeontology 53, p. 1211–1235

Andreini, G., Caracuel, J.E., Parisi, G., 2007. Calpionellid biostratigraphy of the Upper Tithonian-Upper Valanginian interval inWestern Sicily (Italy): Swiss J. Geoscien. 100 (2), p. 179–198.

Arbe, H., Fernández Bell Fano, F., 2002. Formación Springhill en el área costa afuera. In: Schiuma, M., Hinterwimmer, G., Vergani, G. (Eds.), Rocas Reservorio de las Cuencas Productivas Argentinas, p. 75–89. V Congreso de Exploración y Desarrollo de Hidrocarburos, Mar del Plata.

Archangelsky, S., Barreda, V., Passalia, M. G., Gandolfo, M., Pramparo, M., Romero, E., Cúneo, R., Zamuner, A., Iglesias, A., Llorens, M., Puebla, G.G., Quattrochio, M., Volkheimer, W. 2009. Early angiosperm diversification: evidence from southern South America. Cretaceous Research, 30(5), p. 1073-1082.

Arcos, R., 1987. Geología del Cuadrángulo Termas del Flaco, provincia de Colchagua, VI Región, Chile. Thesis: Departamento de Geología, Universidad de Chile.

Armstrong, H.A. and Brasier, M.D., 2004. Microfossils, Stable Isotopes and Ocean-Atmosphere History: Microfossils, Second Edition, Blackwell Publishing, Malden, MA USA. p. 25–34.

Arthur, M.A. & Sageman, B.B., 1994. Marine black shales: depositional mechanisms and environments of ancient deposits: Annual Review of Earth and Planetary Sciences, 22, p. 499–551.

Atwater, T., Severinghaus, J., 1990. Tectonic maps of the northeast Pacific. In: Winterer, E.L., Hussong, D.M., Decker, R.W. (Eds.), The Eastern Pacific Ocean and Hawaii, Volume N, The Geology of North America: Geological Society of America, Boulder, Colorado, p. 15–20.

Barclay, R.S., McElwain, J.C., Sageman, B.B., 2010. Carbon sequestration activated by a volcanic CO2 pulse during Ocean Anoxic Event 2. Nature Geoscience.

Barker, P.F., Lonsdale, M.J., 1991. A multichannel seismic profile across the Weddell Sea margin of the Antarctic Peninsula: regional tectonic implications. In: Thomson, M.R.A, Crame, J.A., Thomson, J.W. (Eds.), Geological Evolution of Antarctica. Cambridge, Cambridge Univ. Press, pp. 237–241.

Barral, A., Gomez, B., Fourel, F., Daviero-Gomez, V., & Lécuyer, C, 2017. CO_2 and temperature decoupling at the million-year scale during the Cretaceous Greenhouse: Scientific Reports, 7(1), 8310.

Barron, E.J., 1983. A warm equable Cretaceous: the nature of the problem: Earth-Sci. Rev. 19, p. 305–338.

Batten, D.J. and Stead, D.T., 2005. Palynofacies Analysis and its Stratigraphic Application, In: E.A.M Koutsoukos (Ed.): Applied Stratigraphy, p. 203–226.

Batten, D.J., 1973. Use of palynologic assemblagetypes in Wealden correlation: Palaeontology, 16, p. 1–40.

Batten, D.J., 1975. Wealden palaeoecology from the distribution of plant fossils: Proceedings of the Geologists' Association, London, 85, p. 433–458, pl. 13.

Batten, D.J., 1981. Palynofacies, organic maturation and source potential for petroleum; in: Brooks, J. (ed.), Organic maturation studies and fossil fuel exploration; Academic Press, London, p. 201–223, pl. 1–6.

Batten, D.J., 1982. Palynofacies, palaeoenvironments, and petroleum: Journal of Micropalaeontology, 1, p. 107–114.

Batten, D.J., 1983. Identification of amorphous sedimentary organic matter by transmitted light microscopy: Geological Society, London, Special Publications, 12(1), p. 275–287.

Batten, D.J., 1985. Coccolith moulds in sedimentary organic matter and their use in palynofacies analysis: Journal of Micropalaeontology, 4(2), p. 111–116, pl. 1, 2.

Batten, D.J., Jansonius, J. and McGregor, D.C., 1996. Palynofacies. Palynology: Principles and Applications. AASP, Dallas, Texas, p. 1011–1064.

Bennett, M.R., Doyle, P., Mather, A.E., 1996. Dropstones – their origin and significance: Palaeogeogr. Palaeoclimatol. Palaeoecol. 121, p. 331–339.

Bernier, P. and Courtinat, B., 1979. Le microplankton (Leiosphaeridia) et la matiere organique des calcaires d'arrier-recif du Kimmeridgien Superieur dans le Jura Meridional, Systematique, conditions de genese et d'environment: Documents du Laboratoire Geologique, Faculte des Sciences Lyon, 75, p. 95–117.

Bertrand, P. and Lallier-Vergès, E., 1993. Past sedimentary organic matter accumulation and degradation controlled by productivity: Nature, 364, p. 786–788.

Bertrand, P., Pittion, J.-L. and Bernaud, C, 1986. Fluorescence of sedimentary organic matter in relation to its chemical composition: Organic Geochemistry, 10, p. 641–647.

Besairie, H. and Collignon, M., 1956. Le système Crétacé à Madagascar: Tramux du Bureau Géologique de Madagascar, 77, 66 pp.

Besse, J., Boisseau, T., Arnaud-Vanneau, A., Arnaud, H., Mascle, G. and Thieuloy, J.P., 1986. Modifications sédimentaires, renouvellement des faunes et inversions magnétiques dans le Valanginien de l'hypostratotype d'Angles: Bulletin Centres Recherche Exploration Production Elf-Aquitaine, 10, p. 365–368.

Biddle, K.; Uliana, M.; Mitchum, R. Jr.; Fitzgerald, M.; Wright, R., 1986. The stratigraphic and structural evolution of central and eastern Magallanes Basin, Southern America. In Foreland basins (Allen, P.; Homewood, P.; editors). International Association of Sedimentologists, Special Publication 8, p. 41–61.

Biro-Bagóczky, L., 1964. Estudio sobre el límite Titoniano y el Neocomiano en la Formación Lo Valdés, Provincia de Santiago, principalmente en base a ammonoideos, Región Metropolitana, Chile: Departamento de Geología, Universidad de Chile, Memoria.

Bjørlykke, K., 1985. Glaciations, preservation of the sedimentary record and sea level changes – a discussion based on the late Precambrian and Lower Palaeozoic sequences in Norway: Palaeogeogr. Palaeoclimatol. Palaeoecol., 51, p. 197–207.

Boch, R., Dietzel, M., Reichl, P., Leis, A., Baldermann, A., Mittermayr, F. Pölt, P., 2015. Rapid ikaite ($CaCO_3 \cdot 6H_2O$) crystallization in a man-made river bed: Hydrogeochemical monitoring of a rarely documented mineral formation: Applied Geochemistry, 63, p.366–379.

Bodin, S., Meissner, P., Janssen, N.M.M., Steuber, T. and Mutterlose, J., 2015. Large igneous provinces and organic carbon burial: Controls on global temperature and continental weathering during the Early Cretaceous: Global and Planetary Change, 133, p. 238–253.

Boggs Jr, S., 2014. Principles of sedimentology and stratigraphy. Pearson Education. 662 pp.

Bombardiere, L., Gorin, G.E., 1998. Sedimentary organic matter in condensed sections from distal oxic environments: examples from the Mesozoic of SE France Sedimentology, 45, p. 771–788.

Bornemann, A., Norris, R.G., Friedrich, O., Beckmann, B., Schouten, S., Sinninghe Damsté, J.S., Vogel, J., Hofmann, P., Wagner, T., 2008. Isotopic evidence for glaciation during the Cretaceous Supergreenhouse: Science, 319, p. 189–192.

Bostick, N.H., 1979. Microscopic measurement of the level of catagenesis of solid organic matter in sedimentary rocks to aid exploration for petroleum and to determine former burial ternperatures – a review; in: Scholle, P.A. & Schluger, P.R. (Eds.), Aspects of diagenesis: Society of Economic Paleontologists and Mineralogists, Special Publication, 26, p. 17–43, ca. 3 pl.

Boulter, M.C. and Riddick, A., 1986. Classification and analysis of palynodebris from the Palaeocene sediments of the Forties Field: Sedimentology, 33, p. 871–886, 2 pl.

Bover-Arnal, T., Salas, R., Moreno-Bedmar, J.A., and Bitzer, K., 2009. Sequence stratigraphy and architecture of a late Early-Middle Aptian carbonate-platform succession from the western Maestrat Basin (Iberian chain, Spain): Sedimentary Geology, 219, p. 280–301.

Bover-Arnal, T., Salas, R., Guimerà, J., Moreno-Bedmar, J.A., 2014. Deep incision in an Aptian carbonate succession indicates major sea-level fall in the Cretaceous: Sedimentology, 61, p. 1558–1593.

Bradley, W.H., 1966. Tropical lakes, copropel, and oil shale: Geological Society of America, Bulletin, 77, p. 1333–1337, pl. 1-3.

Bradshaw, R.H.W. and Webb, T. III., 1985. Relationships between contemporary pollen and vegetation data from Wisconsin and Michigan, USA: Ecology, 66, p. 721–737.

Bradshaw, M.T., Brakel, A.T., Parrish, J.T., Totterdell, J.M., and Yeates, A.N., 1995. Paleoclimatology of Australia during the Pangaean interval (abstract): SEPM and American Association of Petroleum Geologists, Annual Meeting Abstracts, 4, 12 p.

Brandley, R.T., and Krause, F.F., 1994. Thinolite-type pseudomorphs after ikaite: indicators of cold water on the subequatorial western margin of Lower Carboniferous, North America, In: Beauchamp, B., Embry, A.F., and Glass, D., (Eds.), Pangea: Global Environments and Resources: Canadian Society of Petroleum Geologists, Memoir, 17, p. 333–344.

Brandt, K., 1986. Glacioeustatic cycles in the Early Jurassic?: Neues Jahrbuch für Geologie und Palaontologie, Monatshefte, 5, p. 257–274.

Brooks, K., 2016. Ikaite: enigmatic crystals of cold waters. Geology Today, 32(2), p. 75–78.

Bujak, J.P. and Davies, E.H., 1983. Fluorescence helps find oil: Geos, 12(1), p. 5–8, 1 pl.

Bulot, L.G., Thieuloy, J.-P., Blanc, E., Klein, J., 1993. Le cadre stratigraphique du Valanginien supérieure et de l'Hauterivien du Sud-Est de la France: Définition des biochronozones et caractérisation de nouveaux biohorizons: Géologie Alpine, 68, p. 13–56.

Burger, D., 1980. Palynological studies in the Lower Cretaceous of the Surat Basin, Australia: Bureau of Mineral Resources Geology and Geophysics Bulletin, 189, 106 pp.

Bustin, R.M., 1988. Sedimentology and characteristics of dispersed organic matter in Tertiary Niger Delta: origin of source rocks in a deltaic environment: American Association of Petroleum Geologists Bulletin, 72, p. 277–298.

Butterworth, P. J., 1985. Sedimentology of Ablation Valley, Alexander Island: British Antarctic Survey Bulletin, 66, p. 73–82.

Butterworth, P.J., Crame, J.A., Howlett, P.J. and Macdonald, D.I.M., 1988. Lithostratigraphy of Upper Jurassic-Lower Cretaceous strata of eastern Alexander Island Antarctica: Cretaceous Research, 9, p. 249–264.

Calderón, M., Fildani, A., Hervé, F., Fanning, C.M., Weislogel, A., and Cordani, U., 2007. Late Jurassic bimodal magmatism in the northern sea-floor remnant of the Rocas Verdes Basin, southern Patagonian Andes: Journal of the Geological Society of London, 164, p. 1011–1022.

Calvert, S.E. and Pedersen, T.F., 1992. Organic carbon accumulation and preservation in marine sediments: how important is anoxia?, In: Whelan, J.K. and Farrington, J.W. (Eds.), Organic matter: productivity, accumulation, and preservation in recent and ancient sediments: Columbia University Press, New York, p. 231–263.

Cande, S.C., Larson, R.L., LaBrecque, J.L., 1978. Magnetic lineations in the Pacific Jurassic Quiet Zone: Earth and Planetary Science Letters, 41, p. 434–440.

Caratini, C., 1994. Palynofacies of some recent marine sediments: the role of transportation. In: Traverse, A. (Ed.), Sedimentation of Organic Particles: Cambridge University Press, Cambridge, p. 129–139.

Carr, P.F., Jones, B.G. and Middleton, R.G., 1989. Precursor and formation of glendonites in the Sydney Basin: Australian Mineralogist, 4, p. 3–12.

Carvalho, M.A., Ramos, R.R.C., Crud, M.B., Witovisk, L., Kellner, Alexander A.W., Silva, H.D.P., Grillo, O.N., Riff, D. and Romano, P.S.R., 2013. Palynofacies as indicators of paleoenvironmental changes in a Cretaceous succession from the Larsen Basin, James Ross Island, Antarctica: Sedimentary Geology, 295, p. 53–66.

Casey, R. and Rawson, P.F., 1973. (Eds.), The Boreal Lower Cretaceous: Geological Journal Special Issue, 5, 448 pp.

Cassens, C., 1999. Palynofazies, Mikrofazies und Sequenzanalyse im Dogger (Bajocium) der Bohrung Hasental (Ostalb): Fachbereich Geowissenschaften. Darmstadt, Technische Universität Darmstadt, Diploma: 112.

Cecioni, G., 1981. Jurassic Flamenco and Seno Rodrigues Formations of southern Chile, In: Hambrey, M.J., Harland, W.B. (Eds.), Earth's Pre-Pleistocene Glacial Record: Cambridge Univ. Press, p. 835–836.

Charrier, R., Pinto, L. and Rodríguez, M.P., 2007. Tectonostratigraphic evolution of the Andean Orogen in Chile. In: Moreno, T. & Gibbons, W. (Eds.), The Geology of Chile: Geological Society, London, p. 21–114.

Charrier, R., Ramos, V.A., Tapia, F. and Sagripanti, L., 2014. Tectono-stratigraphic evolution of the Andean Orogen between 31 and 37 S (Chile and Western Argentina): Geological Society, London, Special Publications, 399(1), p. 13–61.

Chatalov, A., Bonev, N. and Ivanova, D., 2015. Depositional characteristics and constraints on the mid-Valanginian demise of a carbonate platform in the intra-Tethyan domain, Circum-Rhodope Belt, northern Greece: Cretaceous Research, 55, p. 84–115.

Chen, Y.Y., 1978. Jurassic and Cretaceous palynostratigraphy of a Madagascar well. Ph.D. thesis: University of Arizona, 264 pp. [Unpublished].

Chumakov, N.M., 1995. The problem of the warm biosphere: Stratigraphy and Correlation, 3, p. 205–215.

Scott, A., Cripps, J.A., Collinson, M.E., Nichols, G.J., 2000. The taphonomy of charcoal following a recent heathland fire and some implications for the interpretation of fossil charcoal deposits. Palaeogeography, Palaeoclimatology, Palaeoecology 164: 1–31.

Cohen, A.D., Raymond, R. Jr., Ramirez, A, Morales, Z. and Ponce, F., 1989. The Changuinola peat deposit of northwestern Panama: a tropical, back-barrier, peat (coal)-forming environment: International Journal of Coal Geology, 12, p. 157–192, 3 pl.

Combaz, A., 1964. Les palynofacies: Revue de Micropaleontologie, 7, p. 205–218.

Courtinat, B. and Méon, H., 1991. Les microforaminiferes (Scytinascia), un groupe palynologique meconnu (historique). Leur analyse dans le Cenomanien-Turonien de Vergons (Bassin vocontien, France): Geobios, 24, p. 559–567, pl. 1.

Courtinat, B., 1989. Les organoclastes des formations lithologiques du Malm dans le Jura meridional. Systematique, biostratigraphie et elements d'interpretation paleoecologique; Documents des Laboratoires de Geologie, Lyon, 105, p. 1–361, pl. 1-35.

Covacevich, V., Varela, J. and Vergara, M., 1976. Estratigrafía y sedimentación de la Formación Baños del Flaco al sur del rio Tinguiririca, Cordillera de los Andes, provincia de Curicó, Chile: I Congreso Geológico Chileno, Santiago, 1, p. A191–A211.

Covacevich, V., 1976. Fauna valanginiana de Peninsula Byers, Isla Livingston, Antarctica: Rev. geol. Chile, 3, p. 25–46.

Crame, J.A. and Howlett, P.J., 1988. Late Jurassic and Early Cretaceous biostratigraphy of the Fossil Bluff Formation, Alexander Island: Scientific reports-British Antarctic Survey, 78, p. 1–35

Crame, J.A., Pirrie, D., Crampton, J.S. and Duane, A.M., 1993. Stratigraphy and regional significance of the Upper Jurassic-Lower Cretaceous Byers Group, Livingston Island, Antarctica: J. Geol. Soc. London, 150, p. 1075–1087.

Crame J.A., 1985. New Late Jurassic oxytomid bivalves from the Antarctic Peninsula region: British Antarctic Survey Bulletin, 69, p. 35–55.

Crame, J.A., 1986. Late Mesozoic bipolar bivalve faunas, Geological Magazine, 123, p. 611–618.

Cross, A.T., Thompson, G.G., Zaitzeff, J.B., 1966. Source and distribution of palynomorphs in bottom sediments, southern part of Gulf of California: Marine Geology, 4, p. 467–524, pl. 1.

Crowley, T.J., North, G.R., 1991. Paleoclimatology: Oxford Univ. Press, New York, 339 pp.

Dalziel, I.W.D., de Wit, M.J. and Palmer, K.F., 1974. Fossil marginal basin in the southern Andes: Nature, 250, p. 291–294.

Dalziel, I.W.D., 1981. Back-arc extension in the southern Andes: A review and critical reappraisal: Royal Society of London Philosophical Transactions, 300, p. 319–335.

Dalziel, I.W.D., 1986. Collision and cordilleran orogenesis: An Andean perspective, in Coward, M.P., and Ries, A.C., (Eds.), Collision Tectonics: Geological Society of London Special Publication, 19, p. 389–404.

Davey, R.J., Rogers, J., 1975. Palynomorph distribution in Recent offshore sediments along two traverses off South West Africa: Mar. Geol., 18, p. 213–225.

Davey, R.J., 1971. Palynology and palaeo-environmental studies, with special reference to the continental-shelf sediments of South Africa. In: Farinacci, A. (Ed.): Proceedings of the Second Planktonic Conference, Roma, p. 331–347.

Davey, R.J., 1988. Palynological zonation of the Lower Cretaceous, Upper and uppermost Middle Jurassic in the Northwestern Papuan Basin of Papua New Guinea: Geological Survey Papua New Guinea, Memoir, 13, p. 1–77.

Davies, E.H., Bujak, J.P. and Williams, G.L., 1982. The application of dinoflagellates to paleoenvironmental problems: Third North American Paleontological Convention, Proceedings, 1, p. 125–131.

De Lurio, J.L. and Frakes, L.A., 1999. Glendonites as a paleoenvironmental tool: implications for Early Cretaceous high latitude climates in Australia: Geochimica et Cosmochimica Acta, 63, p. 1039–1048.

Del Valle, R.A. and Fourcade, N.H., 1992. Sedimentary basins on the east flank of the Antarctic Peninsula: proposed nomenclature: Antarctic Science, 4, p. 477–478.

Demaison G.J. and Moose, G.T., 1980. Anoxic marine environments and oil source bed genesis: American Association of Petroleum Geologists Bulletin, 64, p. 1179–1209.

Denison, C. and Fowler, R.M., 1980. Palynological identification of facies in a deltaic environment. In: Proceedings of the Meeting on the Sedimentation of North Sea Reservoir Rocks, Geilo, Norsk Petroleumsforening, Paper XII, p. 1–22.

Dera, G., Brigaud, B., Monna, F., Laffont, R., Puceat, E., Deconinck, J.-F., Pellenard, P., Joachimski, M.M., Durlet, C., 2011. Climatic ups and downs in a disturbed Jurassic world: Geology, 39, p. 215–218.

Dickinson, C.H., Wallace, B. and Given, P.H., 1974. Microbial activity in Florida Everglades peat: New Phytologist, 73, p. 107–113.

Didyk B.M., Simoneit B.R.T., Brassell S.C. and Eglinton G., 1978. Organic geochemical indicators of palaeoenvironmental conditions of sedimentation: Nature, 272, p. 216–22.

Dieckmann, G.S., Nehrke, G., Papadimitriou, S., Göttlicher, J., Steininger, R., Kennedy, H., Wolf-Gladrow, D. and Thomas, D.N., 2008. Calcium carbonate as ikaite crystals in Antarctic sea ice: Geophysical Research Letters, 35, L08501.

Dieckmann, G.S., Nehrke, G., Uhlig, C., Göttlicher, J., Gerland, S., Granskog, M.A., Thomas, D.N., 2010, Ikaite ($CaCO_3 \cdot 6H_2O$) discovered in Arctic sea ice: The Cryosphere, 4, p. 227–230.

Ditchfield, P.W., Marshall, J.D., Pirrie, D., 1994. High latitude paleotemperature variation: new data from the Tithonian to Eocene of James Ross Island, Antarctica: Palaeogeography, Palaeoclimatology, Palaeoecology, 107, p. 79–101.

Donnadieu, Y., Dromart, G., Goddéris, Y., Pucéat, E., Brigaud, B., Dera, G., Dumas, C. and Olivier, N., 2011. A mechanism for brief glacial episodes in the Mesozoic greenhouse: Paleoceanography, 26, PA3123

Dott, R.H. Jr and Bourgeois, J., 1982. Hummocky stratification: significance of its variable bedding sequences: Geological Society of America, Bulletin, 93, p. 663–680.

Doubleday, P.A. and Storey, B.C., 1998. Deformation history of a Mesozoic forearc basin sequence on Alexander Island, Antarctic Peninsula: Journal of South American Earth Sciences, 11, p. 1–21.

Downie, C., Hussain, M.A. and Williams, G.L., 1971. Dinoflagellate cyst and acritarch associations in the Paleogene of Southeast England: Geoscience and Man, 3, p. 29–35, pl. 1, 2.

Doyle, P. and Whitham, A.G., 1991. Palaeoenvironments of the Nordenskjöld Formation: an Antarctic Late Jurassic-Early Cretaceous black shale-tuff sequence. In: R.V. Tyson and T.H., Pearson (Eds.), Modern and Ancient Continental Shelf Anoxia: Geol. Soc. London Spec. Pub1., 58, p. 397–414.

Doyle, P., 1987. The Cretaceous Dimitobelidae (Belemnitida) of the Antarctic Peninsula region: Palaeontology 30, p. 147–177.

Dromart, G., Garcia, J.P., Picard, S., Atrops, F., Lécuyer, C. and Sheppard, S.M.F., 2003a. Ice age at the Middle-Late Jurassic transition?: Earth and Planetary Science Letters, 213, p. 205– 220.

Dromart, G., Garcia, J. P., Gaumet, F., Picard, S., Rousseau, M., Atrops, F., Lecuyer, C., Sheppard, S. M., 2003b. Perturbation of the carbon cycle at the Middle/Late Jurassic transition: geological and geochemical evidence: American Journal of Science, 303(8), p. 667–707.

Duane, A.M., 1994. Preliminary palynological investigations of the Byers Group (Late Jurassic–Early Cretaceous), Livingston Island, Antarctic Peninsula: Review of Palaeobotany and Palynology, 84, p. 113–120.

Duane, A.M., 1996. Palynology of the Byers Group (Late Jurassic-Early Cretaceous) of Livingston and Snow Islands, Antarctic Peninsula: its biostratigraphical and palaeoenvironmental significance: Review of Palaeobotany and Palynology, 91, p. 241–281.

Edwards, C.W., 1980. The geology of eastern Alexander Island, Antarctica, PhD thesis: University of Birmingham, 228 pp. [Unpublished].

EIA, U., 2015. Technically Recoverable Shale Oil and Shale Gas Resources, September 2015.: U.S. Energy Information Administration, 27 pp.

Elliott, M.H., 1975. The stratigraphy and sedimentary petrology of the Ablation Point area, Alexander Island. MSc thesis: University of Birmingham, 93 pp. [Unpublished].

Elliot, D.H., 1988. Tectonic setting and evolution of the James Ross Basin, northern Antarctic Peninsula, In: Feldmann, R.M., and Woodburne, M.O., (Eds.), Geology and Paleontology of Seymour Island, Antarctic Peninsula. Geological Society of America Memoir, 169, p. 541–555.

Elsik, W.C., 1992. The morphology, taxonomy, classification and geologic occurrence of fungal palynomorphs, A short course presented under the auspices of the American Association of Stratigraphic Palynologists. Houston, Texas, 287 pp. [Unpublished].

Ercegovac, M. and Kostić, A., 2006. Organic facies and palynofacies: nomenclature, classification and applicability for petroleum source rock evaluation: International Journal of Coal Geology, 68, p. 70–78.

Farquharson, G.W, 1983. The Nordenskjold Formation of the northern Antarctic Peninsula: an Upper Jurassic Radiolarian mudstone and tuff sequence: Bull. Br. Antarct. Suro., 60, p. 1–22.

Farquharson, G.W, Hamer, R.D. and Ineson, J.R., 1984. Proximal volcaniclastic sedimentation in a Cretaceous back-arc basin, northern Antarctic Peninsula, In: Kokelaar, B.P. and Howells, M.F (Eds.), Marginal Basin Geology, Spec. Publs geol. SOC. London, 16, p. 219–229.

Farr, K.M., 1989. Palynomorph and palynodebris distributions in modern British and Irish estuarine sediments, In: Batten, D.J. and Keen, M.C. (Eds.), Northwest European micropalaeontology and palynology: British Micropalaeontological Society Series, Ellis Horwood, Chichester, p. 265–285, pl. 1.

Fildani, A., Cope, T.D., Graham, S.A. and Wooden, J.L., 2003. Initiation of the Magallanes foreland basin: Timing of the southernmost Patagonian Andes orogeny revised by detrital zircon provenance analysis: Geology, 31, n. 12, p. 1081–1084.

Fildani, A. and Hessler, A.M., 2005. Stratigraphic record across a retroarc basin inversion: Rocas Verdes – Magallanes Basin, Patagonian Andes: Geological Society of America Bulletin, 117, p. 1596–1614.

Fildani, A., Romans, B., Fosdick, J., Crane, W. and Hubbard, S., 2008. Orogenesis of the Patagonian Andes as reflected by basin evolution in southernmost South America: Arizona Geological Society Digest, 22, p. 259–268.

Fisher, M.J., 1980. Kerogen distribution and depositional environments in the Middle Jurassic of Yorkshire U.K., In: Bharadwaj, D.C., Singh, H.P. and Tiwari, R.S., (Eds.), Proceedings of the 4th International Palynological Conference, Lucknow 1976-1977, 2, p. 574–580.

Flügel, E., 2004. Microfacies of Carbonate Rocks: Springer, Erlangen, 984 pp.

Fosdick, J.C., Romans, B.W., Fildani, A., Bernhardt, A., Calderón, M. and Graham, S.A., 2011. Kinematic evolution of the Patagonian retroarc fold-and-thrust belt and Magallanes foreland basin, Chile and Argentina, 51º30'S: Geological Society of America Bulletin, 123, p. 1679–1698.

Frakes, L.A. and Francis, J.E., 1988. A guide to Phanerozoic cold polar climates from high-latitude ice-rafting in the Cretaceous: Nature, 333, p. 547–549

Frakes, L.A., Francis, J.E. and Syktus, J.I., 1992. Climate modes of the Phanerozoic: The history of the Earth's climate over the past 600 million years: Cambridge, United Kingdom, Cambridge University Press, 274 p.

Frakes, L.A., 1979. Climates Through Geological Time: Elsevier, Amsterdam, 310 p.

Frakes, L.A., 1999. Estimating the global thermal state from Cretaceous sea surface and continental temperature data, in Evolution of the Cretaceous ocean-climate system: Geological Society of America Special Paper, 332, p. 49–57.

Francis, J.E. and Frakes, L.A., 1993. Cretaceous Climates. In: Wright, V.P. (Ed.), PRIS Sedimentology Review, vol. 1: Wiley-Blackwell, Oxford, p. 17–30.

Gale, A. S., Hardenbol, J., Hathway, B., Kennedy, W. J., Young, J. R. and Phansalkar, V., 2002. Global correlation of Cenomanian (Upper Cretaceous) sequences: Evidence for Milankovitch control on sea level: Geology, 30(4), p. 291–294.

Galeazzi, J.S., 1998. Structural and stratigraphic evolution of the western Malvinas Basin, Argentina: American Association of Petroleum Geologists Bulletin, 82, p. 596–636.

Galloway, J.M., Tullius, D.N., Evenchick, C.A., Swindles, G.T., Hadlari, T. and Embry, A., 2015. Early Cretaceous vegetation and climate change at high latitude: Palynological evidence from Isachsen Formation, Arctic Canada: Cretaceous Research, 56, p. 399–420.

Gastaldo, R.A. and Huc, A.-Y., 1992. Sediment facies, depositional environments, and distribution of phytoclasts in the Recent Mahakam River delta, Kalimantan, Indonesia: Palaios, 7, p. 574–590, 2 pl.

Given, P.H., Spackman, W., Imbalzano, J.R., Casagrande, D.J., Lucas, A.J., Cooper, W. and Exarchos, C., 1983. Physicochemical characteristics and levels of microbial activity in some Florida peat swamps: International Journal of Coal Geology, 3, p. 77–99.

Glikson, M. and Taylor, G.H., 1986. Cyanobacterial mats; major contributors to the organic matter in Toolebuc Formation oil shales, In: Gravestock, D.I., Moore, P.S. and Pitt, G.M. (Eds.), Contributions to the Geology and Hydrocarbon Potential of the Eromanga Basin: Geological Society of Australia Special Publication, 12, p. 273–86

Goldhammer, R.K., Dunn, P.A., Hardie, L.A., 1987. High frequency glacio-eustatic sea level oscillations with Milankovitch characteristics recorded in Middle Triassic platform carbonates in northern Italy: Am. J. Sci. 287, 853–892.

González, O., 1963. Observaciones geológicas en el valle del Río Volcán: Revista Minerales, Santiago, 17(81), p. 20–61.

González, O. and Vergara, M., 1962. Reconocimiento geológico de la Cordillera de los Andes entre los paralelos 35° y 38° latitude: S. Instituto de Geología, Universidad de Chile, Santiago, Publicación, 24.

González, L., Herrero, C., Kelm, U., 1998. Springhill Formation, Magellan Basin, Chile: formation water characteristics and mineralogy. Marine and Petroleum Geology 15, 661–666

Goodall, J.G.S., Coles, G.P. and Whitaker, M.F., 1992. An integrated palynological, palynofacies and micropalaeontological study of the pre-salt formations of the South Gabon Subbasin and the Congo Basin; In: Curnelle, R. (Ed.), Geologie Africaine: Colloques de geologie de Libreville, 6–8 Mai 1991, recueil des publications: Centres de Recherehes Exploration-Production Elf Aquitaine, Memoire, 13, p. 365–399, pl. 1-10.

Goodarzi, F., 1984. Chitinous fragments in coal: Fuel, 63, p. 1504–1507, 2 pl.

Gordon, D.C., Jr., 1970. A microscopic study of organic particles in the North Atlantic Ocean: Deep-Sea Research, 17, p. 175–185.

Grabowski, J., Schnyder, J., Sobień, K., Koptikova, L., Krzemiński, L., Pszczółkowski, A., Hejnar, J. and Schnabl, P., 2013. Magnetic susceptibility and spectral gamma logs in the Tithonian–Berriasian pelagic carbonates in the Tatra Mts (Western Carpathians, Poland): palaeoenvironmental changes at the Jurassic/Cretaceous boundary: Cretaceous Research, 43, p. 1–17.

Gradstein, F., Ogg, J. and Smith, A., 2004. A Geological Time Scale, 2004: CUP 2004, 589 pp.

Gregory, W.A. and Hart, G.F., 1992. Towards a predictive model for the palynologic response to sea-level changes: Palaios, 7, p. 3–33, 6 pl.

Gréselle, B., Pittet, B., 2005. Fringing carbonate platforms at the Arabian Plate margin in northern Oman during the Late Aptian–Middle Albian: Evidence for high-amplitude sea-level changes: Sedimentary Geology, 175, p. 367–390.

Gréselle, B., Pittet, B., 2010. Sea-level reconstruction from the Peri-Vocontian Zone (South-east France) point to Valanginian glacio-eustasy: Sedimentology, 57, p. 1640–1684.

Groves, J.R., Altiner, D., Boyce, M. Craig, B.J., 2003. “Disaster oolites” in the Permian–Triassic boundary interval, Tauride Mountains (Turkey): Geological Society of America, North-Central Section, Abstracts with Programs, 35, p. 48.

Guy-Ohlson, D., 1996. Prasinophycean algae, In: Jansonius, J. and McGregor, D.C. (Eds.), Palynology: Principles and Applications, vol.1, Dallas, Am. Assoc. Strat. Palynol. Found., p. 181–189.

Guy-Ohlson, D. and Norling, E., 1988. Upper Jurassic litho- and biostratigraphy of NW Scania, Sweden: Sveriges Geologiska Undersokning, Ser. Ca, 72, 37 pp.

Habib, D., 1983. Sedimentation-rate-dependent distribution of organic matter in the North Atlantic Jurassic-Cretaceous: Initial Reports of the Deep Sea Drilling Project, 76, p. 781–794, pl. 1, 2.

Habib, D. and Drugg, W.S., 1987. Palynology of Sites 603 and 605, Leg 93, Deep Sea Drilling Project. In: van Hinte, J.E. et al., Deep Sea Drilling Project, Washington, Initial Reports, v.92, p.751-775, pl.1-9.

Habib, D. and Miller, J.A., 1989. Dinoflagellate species and organic facies evidence of marine transgression and regression in the Atlantic Coastal Plain: Palaeogeography, Palaeoclimatology, Palaeoecology, 74, p. 23–47.

Hallam, A., 1981. A revised sea-level curve for the early Jurassic: J. Geol. Soc. London, 138, p. 735–743.

Hallam, A., 1985. A review of Mesozoic climates: J. Geol. Soc. London, 142, p. 433–445.

Hallam, A., 1986. The Pliensbachian and Tithonian extinction events: Nature, 319, p. 765–768.

Hallam, A., 1993. Jurassic climates as inferred from the sedimentary and fossil record: Phil. Trans. R. Soc. London, B 341, p. 287–296.

Hallam, A., Biró-Bagóczky, L. and Pérez, E., 1986. Facies analysis of the Valdés Formation (Tithonian–Hauterivian) of the High Cordillera of Central Chile, and the Paleogeographic evolution of the Andean Basin: Geological Magazine, 123, p. 425–435.

Holloway, J.M. and Dahlgren, R.A., 2002. Nitrogen in rock: occurrences and biogeochemical implications: Global Biogeochemical Cycles, 16(4).

Hancock, N.J. and Fisher, M.J., 1981. Middle Jurassic North Sea deltas with particular reference to Yorkshire, In: Illing, L.V. and Hobson, G.D. (Eds.), Petroleum geology of the continental shelf of North-West Europe: Institute of Petroleum, London, p. 186–195.

Haq, B.U., 2014. Cretaceous eustasy revisited. Global and Planetary Change 113, p. 44–58.

Haq, B., Hardenbol, J. and Vail, P., 1987. Chronology of fluctuating sea levels since the Triassic: Science, 23, p. 1156–1167.

Hardenbol, J. A.N., Thierry, J., Farley, M.B., Jacquin, T., De Graciansky, P.C., & Vail, P.R, 1998. Mesozoic and Cenozoic Sequence Stratigraphy of European Basins: SEPM Special Publication, 60, p. 3–13.

Hathway, B. and Lomas, S.A., 1998. The Jurassic–Lower Cretaceous Byers Group, South Shetland Islands, Antarctica: revised stratigraphy and regional correlations: Cretaceous Research, 19(1), p. 43–67.

Hathway, B., 2000. Continental rift to back-arc basin: Jurassic–Cretaceous stratigraphical and structural evolution of the Larsen Basin, Antarctic Peninsula: Journal of the Geological Society, London, 157, p. 417–432.

Hedges, J.I. and Parker, P.L., 1976, Land-derived organic matter in surface sediments from the Gulf of Mexico: Geochimica et Cosmochimica Acta, 40, p. 1019–1029.

Helby, R., Morgan, R. and Partridge, A.D., 1987. A palynological zonation of the Australian Mesozoic. In: Jell, P.A., (Ed.), Studies in Australian Mesozoic Palynology: Memoir of the Association of Australasian Palaeontologists, 4, p. 1–94.

Herrle, J.O. and Mutterlose, J., 2003. Calcareous nannofossils from the Aptiane–Lower Albian of southeast France: palaeoecological and biostratigraphic implications: Cretaceous Research 24, p. 1–22.

Herrle, J.O., Schröder-Adams, C.J., Davis, W., Pugh, A.T., Galloway, J.M. and Fath, J., 2015. Mid-Cretaceous High Arctic stratigraphy, climate, and Oceanic Anoxic Events: Geology 43, p. 403–406.

Hesselbo, S.P., 2008. Sequence stratigraphy and inferred relative sea-level change from the onshore British Jurassic: Proceedings of the Geologists' Association, 119(1), p. 19–34.

Hoffmeister, W.S., 1960. Palynology has important role in oil exploration: World Oil, 150, p. 101–104.

Hollis, C.J., Tayler, M.J.S., Andrew, B., Taylor, K.W., Lurcock, P., Bijl, P.K., Kulhanek, D.K., Crouch, E.M., Nelson, C.S., Pancost, R.D., Huber, M., Wilson, G.S., Ventura, G.T., Crampton, J.S., Schioler, P. and Phillips, A., 2014. Organic-rich sedimentation in the South Pacific Ocean associated with Late Paleocene climatic cooling: Earth-Science Reviews, 134, p. 81–97.

Honjo, S. and Roman, M.R., 1978, Marine copepod fecal pellets: production, preservation and sedimentation: Journal of Marine Research, 36, p. 45–57.

Horne, R.R., 1969. Sedimentology and palaeogeography of the Lower Cretaceous depositional trough of south-eastern Alexander Island: British Antarctic Survey Bulletin, 22, p. 61–76.

Horne, R.R. and Taylor, B.J., 1969. Calcareous concretions in the Lower Cretaceous sediments of southeastern Alexander Island: British Antarctic Survey Bulletin, 21, p. 19–32.

Howarth, R.W., 1979. Pyrite: its rapid formation in a salt marsh and its importance in ecosystem metabolism: Science, 203(4375), p. 49–51.

Howlett, P.J., 1986. Olcostephanus (Ammonitina) from the Fossil Bluff Formation, Alexander Island, and its stratigraphical significance: British Antarctic Survey Bulletin, 70, p. 71–77.

Hu, X., Wagreich, M. and Yilmaz, I.O., 2012. Marine rapid environmental/climatic change in the Cretaceous greenhouse world: Cretaceous Research, 38, p. 1–6.

Hu, Y.-B., Wolf-Gladrow, D.A., Dieckmann G.S., Völker C. and Nehrke G., 2014. A laboratory study of ikaite ($CaCO_3 \cdot 6H_2O$) precipitation as a function of pH, salinity, temperature and phosphate concentration: Mar. Chem., 162, p. 10–18.

Huber, B., Norris, R.D. and MacLeod, K.G., 2002. Deep-sea paleotemperature record of extreme warmth during the Cretaceous: Geology, 30, p. 123–126.

Huc, A.Y., 1980. Origin and formation of organic matter in recent sediments and its relation to kerogen; in: Durand, B. (Ed.), Kerogen: insoluble organic matter from sedimentary rocks: Editions Technip, Paris, p. 445–474.

Huggett, J.M., Schultz, B.P., Shearman, D.J. and Smith, A.J., 2005. The petrology of ikaite pseudomorphs and their diagenesis: Proc. Geol. Assoc., 116, p. 207–220.

Hunt, C.O., 1987. Dinoflagellate cyst and acritarch assemblages in shallow-marine and marginal marine carbonates; the Portland Sand Portland Stone and Purbeck Formations (Upper Jurassic–Lower Cretaceous) of southern England and northern France, In: Hart, M.B. (Ed.) Micropalaeontology of Carbonate Environments: British Micropalaeontological Society Series, Ellis Horwood, Chichester, p. 208–225.

Husinec, A., Harman, C.A., Regan, S.P., Mosher, D.A., Sweeney, R.J. Read, J.F., 2012. Sequence development influenced by intermittent cooling events in the Cretaceous Aptian greenhouse, Adriatic platform, Croatia: AAPG bulletin, 96(12), p. 2215–2244.

Immenhauser, A. and Scott, R.W., 2002. An estimate of Albian sea-level amplitudes and its implication for the duration of stratigraphic hiatuses: Sedimentary Geology, 152, p. 19–28.

Ineson, J.R., 1985. Submarine glide blocks from the Lower Cretaceous of the Antarctic Peninsula: Sedimentology, 32, p. 659–670.

Ineson, J.R., 1987. Trace fossils from a submarine fan-slope apron complex in the Cretaceous of James Ross Island, Antarctica: Bull. Br. Antarct. Sum., 14, p. 1–16.

Ineson, J.R., 1989. Coarse-grained submarine fan and slope apron deposits in a Cretaceous back-arc basin, Antarctica: Sedimentology, 36(5), p. 793–819.

Ineson, J. R., Crame, J. A., & Thomson, M. R. A., 1986. Lithostratigraphy of the Cretaceous strata of west James Ross Island, Antarctica. Cretaceous Research, 7(2), p. 141–159.

Jäger, H. and McLean, D., 2008. Palynofacies and spore assemblage variations of upper Viséan (Mississippian) strata across the southern North Sea: Review of Palaeobotany and Palynology, 148(2), p. 136–153.

Jaenicke, R., 2005. Abundance of cellular material and proteins in the atmosphere: Science, 308, 73 pp.

James, N.P., Narbonne, G.M., Dalrymple, R.W. and Kyser, T.K., 2005. Glendonites in Neoproterozoic low-latitude, interglacial, sedimentary rocks, northwest Canada: insights into the Cryogenian ocean and Precambrian cold-water carbonates: Geology, 33, p. 9–12.

Jansen, J.H.F., Woensdregt, C.F., Kooistra, M.J. and van der Gaast, S.J., 1987. Ikaite pseudomorphs in the Zaire deep-sea fan: an intermediate between calcite and porous calcite: Geology, 15, p. 245–248.

Jarvis, I., Lignum, J.S., Gröcke, D.R., Jenkyns, H.C. and Pearce, M.A., 2011. Black shale deposition, atmospheric CO_2 drawdown, and cooling during the Cenomanian–Turonian Oceanic Anoxic Event: Paleoceanography 26, PA3201.

Jenkyns, H., Schouten-Huibers, L., Schouten, S. and Damsté, J.S.S., 2012. Warm Middle Jurassice–Early Cretaceous high-latitude sea-surface temperatures from the Southern Ocean: Climate of the Past, 8, p. 215–226.

Jewell, P.W., 1992. Hydrodynamic controls of anoxia in shallow lakes. Organic Matter; Productivity, Accumulation, and Preservation in Recent and Ancient Sediments, p. 201–228.

Johnston, J.D., 1995, Pseudomorphs after ikaite in a glaciomarine sequence in the Dalradian of Donegal, Ireland: Scottish Journal of Geology, 31, p. 3–9.

Jones, E.B.G., 1988. Do fungi occur in the sea? The Mycologist, 2, 150–157

Kaplan, M.E., 1978. Calcite pseudomorphs from the Jurassic and Lower Cretaceous deposits of northern east Siberia: Proceedings of the Academy of Sciences of the USSR, Siberian Branch, Geology and Geophysics, 12, p. 62–70.

Kaplan, M.E., 1979. Calcite pseudomorphs (pseudogaylussite, jarrowite, thinolite, glendonite, gennoishi, White Sea hornlets) in sedimentary rocks: origins of the pseudomorphs: Lithology and Mineral Resources, 14, p. 623–636.

Katz, H.R., 1963. Revision of Cretaceous stratigraphy in Patagonian cordillera of Ultima Esperanza, Magallanes Province, Chile: American Association of Petroleum Geologists Bulletin, 47, p. 506–524.

Keating, J.M., Spencer-Jones, M. and Newham, S., 1992. The stratigraphical palynology of the Kotick Point and Whisky Bay formations, Gustav Group (Cretaceous), James Ross Island: Antarctic Science, 4, p. 279–292.

Keller, G., 2008. Cretaceous climate, volcanism, impacts, and biotic effects: Cretac. Res., 29 (5–6), p. 754–771.

Kemper, E., 1987. Das Klima der Kreide-Zeit: Geologisches Jahrbuch Reihe A, 96, p. 5–185.

Kemper, E. and Schmitz, H.H., 1975. Stellate nodules from the upper Deer Bay Formation (Valanginian) of Arctic Canada: Geological Survey of Canada, Paper 75–1C, p. 109–119.

Kemper, E. and Schmitz, H.H., 1981. Glendonite – Indikatoren des polarmarinen Ablagerungsmilieus: Geologische Rundshau, 70, p. 759–773.

Kessels, K., Mutterlose, J. and Michalzik, D., 2006. Early Cretaceous (Valanginian–Hauterivian) calcareous nannofossils and isotopes of the northern hemisphere: proxies for the understanding of Cretaceous climate: Lethaia, 39, p. 157–171.

Kielbowicz, A., Ronchi, D. and Stach, N., 1984. Foraminíferos y ostrácodos valanginianos de la Formación Springhill, Patagonia Austral: Revista de la Asociación Geológica Argentina, 38, p. 313–339.

Kietzmann, D.A., 2017. Chitinoidellids from the Early Tithonian–Early Valanginian Vaca Muerta Formation in the Northern Neuquén Basin, Argentina: Journal of South American Earth Sciences, 76, p. 152–164.

Killops, S.D. and Killops, V.J., 2005. Introduction to organic geochemistry. Second edition: Blackwell Publishing, 406 pp.

Klohn, G., 1960. Geología de Santiago, O'Higgins, Colchagua y Curicó: Instituto de Investigaciones Geológicas Chile, 8, 95 pp.

Langrock, U., Stein, R., Lipinski, M. and Brumsack, H.-J., 2003. Late Jurassic to Early Cretaceous black shale formation and paleoenvironment in high northern latitudes: Examples from the Norwegian-Greenland Seaway: Paleoceanography 18, PA1074.

Larsen, D., 1994. Origin and paleoenvironmental significance of calcite pseudomorphs after ikaite in the Oligocene Creede Formation, Colorado: J. Sediment. Res. A 64, p. 593–603.

Larson, R.L., 1976. Late Jurassic and Early Cretaceous evolution of the Western Central Pacific Ocean: Journal of Geomagnetism and Geoelectricity 28, p. 219–236.

Leckie, R.M., Bralower, T.J. and Cashman, R.C., 2002. Oceanic anoxic events and plankton evolution: biotic response to tectonic forcing during the mid-Cretaceous: Paleoceanography, 17(3), p. 13-1–13-29.

Lippert, P., 2004. A cold start to the Cretaceous: defining climate history near the north pole: Journal of Undergraduate Research, 2 (2), p. 42–48.

Lister, J.K. and Batten, D.J., 1988. Stratigraphical and palaeoenvironmental distribution of Early Cretaceous dinoflagellate cysts in the Hurlands Farm Borehole, West Sussex, England: Palaeontographica, 210 B, p. 9–89.

Lomas, S.A., 1999. A Lower Cretaceous clastic slope succession, Livingston Island, Antarctica: Sand body characteristics, depositional processes and implications for slope apron depositional systems: Sedimentology, 46, p. 477–504.

López-Martínez, R., Barragán, R. and Reháková, D., Cobiella-Reguera, J.L., 2013. Calpionellid distribution and microfacies across the Jurassic/Cretaceous boundary in western Cuba (Sierra de los Organos): Geologica Carpathica, 64, 3, p. 195–208.

López-Martínez, R., Barragán, R., Reháková, D., Martini, M. and Eguiluz de Antunano, S., 2015. Calpionellid biostratigraphy, U-Pb geochronology and microfacies of the Upper Jurassic-Lower Cretaceous Pimienta Formation (Tamazunchale, San Luis Potosí, central-eastern Mexico): Boletín de la Sociedad Geológica Mexicana, 67(1).

Macdonald, D.I.M., Barker, P.F., Garrett, S.W., Ineson, J.R., Pirrie, D., Storey, B.C., Whitham, A.G., Kinghorn, R.R.F. and Marshall, J.E.A., 1988. A preliminary assessment of the hydrocarbon potential of the Larsen Basin, Antarctica: Marine and Petroleum Geology, 5, p. 34–53.

Macdonald, D.I.M., Moncrieff, A.C.M. and Butterworth, P.J., 1993. Giant slide deposits from a Mesozoic fore-arc basin Alexander Island, Antarctica: Geology, 21, p. 1047–1050.

Maher Jr., H.D., Hays, T., Shuster, R. and Mutrux, J., 2004. Petrography of Lower Cretaceous sandstones on Spitsbergen: Polar Research, 23(2), p. 147–165.

Malkoč, M. and Mutterlose, J., 2010. The Early Barremian warm pulse and the Late Barremian cooling: a high-resolution geochemical record of the Boreal Realm: Palaios, 25(1), p. 14–23.

Markwick, P.J. and Rowley, D.B., 1998. The geological evidence for Triassic to Pleistocene glaciations: Implications for eustasy, In: Pindell, J., Drake, C.L., (Eds.), Paleogeographic Evolution and Non-Glacial Eustasy, Northern South America: SEPM Special Publication, 58, p. 17–43.

Marland, G., 1975. The stability of $CaCO_3 \cdot 6H_2O$ (Ikaite): Geochim. Cosmochim. Acta, 39, p. 83–91.

Marshall, K.L. and Batten, D.J., 1988. Dinoflagellate cyst associations in Cenomanian-Turonian 'black shale' sequences of northern Europe: Review of Palaeobotany and Palynology, 54, p. 85–103.

Martinez-Hernandez, E., Almeida-Leftero, L., Reyes-Salas, M. and Betancourt-Aguilar, Y., 1980. Estudio palinologico para la determinacion de ambientes en la Cuenca Fuentes Rio Escondido (Cretacico Superior), Region de Piedras Negras, Coahulia: Revista Instituto de Geologia, Universidad Nacional Autonoma de Mexico, 4, p. 167–85.

Masetti, D., Neri, C. and Bosellini, A., 1991. Deep-water asymmetric cycles and progradation of carbonate platforms governed by high-frequency eustatic oscillations – Triassic of the Dolomites, Italy: Geology, 19, p. 336–339.

Matthews, R. K. and Frohlich, C., 1991. Orbital forcing of low-frequency glacioeustasy: Journal of Geophysical Research: Solid Earth, 96(B4), p. 6797–6803.

Maurer, F., van Buchem, F.S.P., Eberli, G.P., Pierson, B.J., Raven, M.J., Larsen, P.-H., Al-Husseini, M.I. and Vincent, B., 2013. Late Aptian long-lived glacio-eustatic lowstand recorded on the Arabian Plate: Terra Nova, 25, p. 87–94.

McAnena, A., Flögel, S., Hofmann, P., Herrle, J.O., Griesand, A., Pross, J., Talbot, H.M., Rethemeyer, J., Wallmann, K. and Wagner, T., 2013. Atlantic cooling associated with a marine biotic crisis during the mid-Cretaceous period: Nature Geoscience, 6, p. 558–561.

McArthur, J.M., Janssen, N.M.M., Reboulet, S., Leng, M.J., Thirlwall, M.F., Van de Schootbrugge, B., 2007. Palaeo-temperatures, polar ice-volume, and isotope stratigraphy (Mg/Ca, $\delta^{18}O$, $\delta^{13}C$, $^{87}Sr/^{86}Sr$): the Early Cretaceous (Berriasian, Valanginian, Hauterivian): Palaeogeography, Palaeoclimatology, Palaeoecology, 248, p. 391–430.

McArthur, A. D., Kneller, B. C., Souza, P. A., & Kuchle, J., 2016a. Characterization of deep-marine channel-levee complex architecture with palynofacies: An outcrop example from the Rosario Formation, Baja California, Mexico. Marine and Petroleum Geology, 73, p. 157–173.

McArthur, A. D., Kneller, B. C., Wakefield, M. I., Souza, P. A. and Kuchle, J., 2016b. Palynofacies classification of the depositional elements of confined turbidite systems: Examples from the Gres d'Annot, SE France: Marine and Petroleum Geology, 77, p. 1254–1273.

Melia, M.B., 1984. The distribution and relationship between palynomorphs in aerosols and deep-sea sediments off the coast of northwest Africa. Marine Geology, 58, p. 345–371.

Melinte, M. and Mutterlose, J., 2001. A Valanginian (Early Cretaceous) Boreal nannoplankton excursion in sections from Romania: Marine Micropaleontology, 43, p. 1–25.

Middlemiss, F.A., 1984. Cretaceous terebratulid events inwestern and southern Europe and their relation to the stage boundaries: Cretaceous Research, 5, p. 345–348.

Miller, S. and Macdonald, D.I.M., 2004. Metamorphic and thermal history of a fore-arc basin: The Fossil Bluff Group, Alexander Island: Antarctica. Journal of Petrology, 45(7), p. 1453–1465.

Miller, K.G.,Wright, J.D. and Browning, J.V., 2005a. Visions of ice sheets in a greenhouse world: Mar. Geol., 217, p. 215–231.

Miller, K.G., Kominz, M.A., Browning, J.V., et al., 2005b. The Phanerozoic record of global sea-level change. Science 312, 1293–1298

Montross, G.G., McGlynn, B.L., Montross, S.N. and Gardner, K.K., 2013. Nitrogen production from geochemical weathering of rocks in southwest Montana, USA: Journal of Geophysical Research: Biogeosciences, 118(3), p. 1068–1078.

Moore, G.T., Hayashida, D.N., Ross, C. and Jacobson, S.R., 1992. Paleoclimate of the Kimmeridgian/Tithonian (Late Jurassic) world: I. Results using a general circulation model: Palaeogeogr. Palaeoclimatol. Palaeoecol., 93, p. 113–150.

Mpodozis, C. and Ramos, V., 1989. The Andes of Chile and Argentina, in Geology of the Andes and its relations to energy and mineral resources, (Eds.: Ericksen, G.E., Canas Pinochet, M.T., and Reinemund, J.A.), Circum-Pacific Council for Energy and Mineral Resources: Earth Science Series, 11, p. 59–90.

Muller, J., 1959. Palynology of Recent Orinoco delta and shelf sediments: reports of the Orinoco Shelf expedition; volume 5: Micropalaeontology, 5, p. 1–32.

Mutterlose, J. and Harding, I., 1987. Phytoplankton from the anoxic sediments of the Barremian (Lower Cretaceous) of North–West-Germany: Abhandlungen Geologische Bundes-Anstalt, 39, p. 177–215.

Mutterlose, J., Bornemann, A., Luppold, F.W., Owen, H.G., Ruffell, A., Weiss, W. and Wray, D., 2003. The Vöhrum section (northwest Germany) and the Aptian/Albian boundary: Cretaceous Research, 24, p. 203–252.

Mutterlose, J., Bornemann, A. and Herrle, J., 2008. The Aptian–Albian cold snap: Evidence for "mid" Cretaceous icehouse interludes: N. Jb. Geol. Paläont. Abh., 252, p. 217–225.

Mutterlose, J., Pauly, S. and Steuber, T., 2009. Temperature controlled deposition of early Cretaceous (Barremian–Early Aptian) black shales in an epicontinental sea: Palaeogeography, Palaeoclimatology, Palaeoecology, 273, p. 330–345.

Mutterlose, J., Bottini, C., Schouten, S. and Damsté, J.S.S., 2014. High sea-surface temperatures during the Early Aptian Oceanic Anoxic Event 1a in the Boreal Realm: Geology, 42(5), p. 439–442.

Nakanishi, M. and Winterer, E.L., 1998. Tectonic history of the Pacific–Farallon–Phoenix triple junction from late Jurassic to early Cretaceous: an abandoned Mesozoic spreading system in the central Pacific basin: Journal of Geophysical Research-Solid Earth, 103, p. 12453–12468.

Oboh, F.E., 1992a. Multivariate statistical analyses of palynodebris from the Middle Miocene of the Niger Delta and their environmental significance: Palaios, 7, p. 559–573, 3 pl.

Oboh, F.E, 1992b. Middle Miocene palaeoenvironments of the Niger Delta: Palaeogeography, Palaeoclimatology, Palaeoecology, 92, p. 55–84, 2pl.

Oboh, F.E., Salami, M.B. and Chapman, J.L., 1992 Palynological interpretation of the palaeoenvironments of Miocene strata of the well Igbomotoru-1, Niger Delta: Journal of Micropalaeontology, 11, p. 1–6.

Oldham, T.C.B., 1976. Flora of the Wealden plant debris beds of England: Palaeontology, 19, p. 437–502, pl. 55-80.

Oliveros, V., Labbé , M., Rossel, P., Charrier, R. and Encinas, A., 2012. Late Jurassic paleogeographic evolution of the Andean back-arc basin: new constrains from the Lagunillas Formation, northern Chile (27 30′–28 30′S): Journal of South American Earth Sciences, 37, p. 25–40.

Oyarzun, R., Doblas, M., Lopez Ruiz, J., Cebria, J.M. and Youbi, N., 1999. Tectonically-induced icehouse-greenhouse climate oscillations during the transition from the Variscan to the Alpine cycle – Carboniferous to Triassic: Bull. Soc. Géol. Fr., 170, p. 3–11.

Pacton, M., Gorin,G.E. and Vasconcelos, C., 2011. Amorphous organicmatter – experimental data on formation and the role of microbes: Review of Palaeobotany and Palynology, 166, p. 253–267.

Pankhurst, R.J., 1982. Rb-Sr geochronology of Graham Land, Antarctica: Journal of the Geological Society, 139(6), p. 701–711.

Parrish, J.T., Daniel, I.L., Kennedy, E.M. and Spicer, R.A., 1998. Palaeoclimatic significance of mid-Cretaceous floras from the middle Clarence Valley, New Zealand: Palaios, 13, p. 149–159.

Parry, C.C., Whitley, P.K.J. and Simpson, R.D.H., 1981. Integration of palynological and sedimentological methods in facies analysis of the Brent Formation; in: Illing, L.V. and Hobson, G.D. (Eds.), Petroleum geology of the continental shelf of North-West Europe: Institute of Petroleum, London, p. 205–215.

Pauly, H., 1963. "Ikaite", a New Mineral from Greenland: Arctic, 16(4), p. 263.

Peroni, G., Cagnolatti, M. and Pedrazzini, M., 2002. Cuenca Austral: Marco geológico y resena histórica de la actividad petrolera. In: Schiuma, M., Hinterwimmer, G. and Vergani, G. (Eds.), Rocas Reservorio de las Cuencas Productivas Argentinas: V Congreso de Exploración y Desarrollo de Hidrocarburos, Mar del Plata, p. 11–19.

Philippe, M. and Thevenard, F., 1996. Distribution and palaeoecology of the Mesozoic wood genus Xenoxylon: palaeoclimatological implication for the Jurassic of western Europe: Rev. Palaeobot. Palynol., 91, p. 353–370.

Pilskaln, C. H. and Honjo, S., 1987. The fecal pellet fraction of biogeochemical particle fluxes to the deep sea: Global Biogeochemical Cycles, 1, p. 31–48.

Pirrie, D., Whitham, A.G. and Ineson, J.R., 1991. The role of tectonics and eustasy in the evolution of a marginal basin: Cretaceous–Tertiary Larsen Basin, Antarctica. In: Macdonald, D.I.M., (Ed.), Sedimentation, Tectonics and Eustacy: IAS Spec. Publ., 12, p. 293–305.

Pirrie, D., Duane, A.M. and Riding, J.B., 1992. Jurassic-Tertiary stratigraphy and palynology of the James Ross Basin; review and introduction: Antarct. Sci., 4, p. 259–266.

Pirrie, D. and Crame, J.A., 1995. Late Jurassic palaeogeography and anaerobic-dysaerobic sedimentation in the northern Antarctic Peninsula region: Journal of the Geological Society, 152(3), p. 469–480.

Pirrie, D., Marshall, J.D., Doyle, P. and Riccardi, A.C., 2004. Cool Early Albian climates; new data from Argentina: Cretaceous Research, 25, p. 27–33.

Podlaha, O.G., Mutterlose, J. and Veizer, J., 1998. Preservation of $d^{18}O$ and $d^{13}C$ in belemnite rostra from the Jurassic/Early Cretaceous successions: American Journal of Science, 298, p. 324–347.

Porter, K.G. and Robbins, E.I., 1981. Zooplankton fecal pellets link fossil fuel and phosphate deposits: Science, 212, p. 931–933, 1 pl.

Powell, A.J., Dodge, J.D. and Lewis, J., 1990. Late Neogene to Pleistocene palynological facies of the Peruvian continental margin upwelling, Leg 112; In: Suess, E., Von Huene, R. et al.: Proceedings of the Ocean Drilling Program, Scientific Results, 112, p. 297–321.

Prentice, M.L. and Matthews, R.K., 1991. Tertiary ice sheet dynamics: The Snow Gun Hypothesis: J. Geophys. Res., 96(B4), p. 6811–6827.

Price, G.D., 1999. The evidence and implications of polar-ice during the Mesozoic: Earth-Science Reviews, 48, p. 183–210.

Price, G.D., Ruffell, A.H., Jones, C.E., Kalin, R.M., and Mutterlose, J., 2000, Isotopic evidence for temperature variation during the early Cretaceous (late Ryazanian–mid-Hauterivian): Journal of the Geological Society, 157, p. 335– 343.

Price, G.D. and Mutterlose, J., 2004. Isotopic signals from late Jurassic–early Cretaceous (Volgian–Valanginian) sub-Arctic belemnites, Yatria River, Western Siberia: Journal of the Geological Society, 161(6), p. 959–968.

Price, G.D. and Nunn, E.V., 2010. Valanginian isotope variation in glendonites and belemnites from the Arctic Svalbard: transient glacial temperatures during the Cretaceous greenhouse: Geology, 38, p. 251–254.

Price, G.D. and Passey, B.H., 2013. Dynamic polar climates in a greenhouse world: Evidence from clumped isotope thermometry of Early Cretaceous belemnites: Geology, 41, p. 923–926.

Pucéat, E., Lécuyer, C., Sheppard S.M.F, Dromart, G., Reboulet, S. and Grandjean, P., 2003. Thermal evolution of Cretaceous Tethyan marine waters inferred from oxygen isotope composition of fish tooth enamels: Paleoceanography, 18, 1029.

Rabinowitz, P.D. and La Brecque, J., 1979. The Mesozoic South Atlantic Ocean and evolution of its continental margin: Journal of Geophysical Research, 84, p. 5973–6002.

Rameil, N., Immenhauser, A., Csoma, A.É. and Warrlich, G.M.D., 2012. Surfaces with a long history: the Aptian top Shu'aiba Formation unconformity, Sultanate of Oman: Sedimentology, 59, p. 212–248.

Ramos, V.A., 1988. The Tectonics of Central Andes: 30° to 33°S latitude, In: Clark, S. and Burchfiel, D. (Eds.), Processes in Continental Lithospheric Deformation: Geological Society of America, Special Paper, 218, p. 31–54.

Ramos, V.A., 1989. Andean foothills structures in Northern Magallanes Basin, Argentina: American Association of Petroleum Geologists, 73, p. 887–903.

Rawson, P.F., 1973. Lower Cretaceous (Ryazanian–Barremian) marine connections and cephalopod migrations between the Tethyan and Boreal Realms, In: Casey, R. and Rawson, P.F. (Eds.), The Boreal Lower Cretaceous. Geological Journal special issue, 5: Seel House Press, Liverpool, p. 131–144.

Rawson, P.F., 1994. Sea level changes and their influence on ammonite biogeography in the European Early Cretaceous: Palaeopelagos Sp. Pu., 1, Proceed. 3rd Pergola International Symposium, p. 317–326.

Raynaud, J.-F. and Robert, P., 1976. Les methods d'etude optique de la matiere organique: Bulletin de Centre Recherche Pau-Societe National Production Aquitaine, 10, p. 109–127.

Reboulet, S., 1996. L'évolution des ammonites du Valanginien-Hauterivien inférieur du bassin vocontien et de la plate-forme provençale (Sud-Est de la France): relations avec la stratigraphie séquentielle et implications biostratigraphique: Documents des Laboratoires de Géologie de Lyon, 137, 371 pp.

Reboulet, S. and Atrops, F., 1995. Rôle du climat sur les migrations et la composition des peuplements d'ammonites du Valanginien supérieur du bassin vocontien (S–E de la France): Geobios, 18, p. 357–365.

Rehakova, D. and Michalík, J., 1997. Evolution and distribution of calpionellids – The most characteristic constituents of Lower Cretaceous Tethyan microplankton: Cretaceous Research, 18, p. 493–504.

Remane, J., 1964. Untersuchungen zur Systematik und Stratigraphie der Calpionellen in den Jura-Kreide-Grenzschichten des Vocontischen Troges: Palaeontographica, A 123, p. 1–57.

Remane, J., 1965. Neubearbeitung der Gattung Calpionellopsis COL. 1948 (Protozoa, Tintinnina ?): N. Jb. Geol. Paläont. Abh., 122, p. 27–49.

Reyre, Y., 1973. Palynologie du Mesozoique Saharien. Traitment des donnes par l'Informatique et applications a la Stratigraphie et a la Sedimentologie: Memoires du Museum National d'Histoire Naturelle, Paris, C27, 284 pp.

Rhoads, D.C. and Morse, J.W., 1971. Evolutionary and ecologic significance of oxygen deficient marine basins: Lethaia, 4, p. 413–428.

Riccardi, A., 2015. Remarks on the Tithonian–Berriasian ammonite biostratigraphy of west central Argentina: Volumina Jurassica, 13, p. 23–52.

Rice, A.L., Billet, D.S.M., Fry, J., John, A.W.G., Lampitt, R.S., Mantoura, R.F.C. and Morris, R.J., 1986. Seasonal deposition of phytodetritus to the deep-sea floor: Proceedings of the Royal Society of Edinburgh, 888, p. 265–279.

Riley, G.A., 1970. Particulate organic matter in seawater: Adv. Mar. Biol., 8, p. 1–118.

Riley, L.A., 1974. A palynological investigation of Upper Jurassic–Basal Cretaceous sediments from England, France, and Iberia, PhD Thesis: The Open University, Milton Keynes, 289 pp. [Unpublished].

Robinson, J.M., 1990. Lignin, land plants and fungi: biological evolution affecting Phanerozoic oxygen balance: Geology, 15, p. 607–610.

Rogov, M.A. and Zakharov, V.A., 2010. Jurassic and Lower Cretaceous glendonite occurrences and their implication for Arctic paleoclimate reconstructions and stratigraphy: Earth Science Frontiers, 17, Special Issue, p. 345–347.

Rogov, M. A., Ershova, V. B., Shchepetova, E. V., Zakharov, V. A., Pokrovsky, B. G. and Khudoley, A. K., 2017. Earliest Cretaceous (Late Berriasian) glendonites from Northeast Siberia revise the timing of initiation of transient Early Cretaceous cooling in the high latitudes: Cretaceous Research, 71, p. 102–112.

Romans, B.W., Fildani, A., Graham, S.A., Hubbard, S.M. and Covault, J.A., 2010. Importance of predecessor basin history on sedimentary fill of a retroarc foreland basin: Provenance analysis of the Cretaceous Magallanes basin, Chile (50–52°S): Basin Research, 22, p. 640–658.

Romans, B.W., Fildani, A., Hunnard, S., Covault, J., Fosdick, J. and Graham, S., 2011. Evolution of deep-water stratigraphic architecture, Magallanes Basin, Chile: Marine and Petroleum Geology, 29, p. 824–842.

Rossel, P., Oliveros, V., Mescua, J., Tapia, F., Ducea, M. N., Calderón, S., Hoffman, D., 2014. La Formación Rio Damas-Tordillo (338–35,58S): antecedentes sobre petroge´nesis, proveniencia e implicancias tectónicas. Andean Geology.

Rowley, D.B. and Markwick, P.J., 1992. Haq et al. eustatic sea level curve: implications for sequestered water volumes: J. Geol. 100(6), p. 103–715.

Royer, D.L., 2006. CO_2-forced climate thresholds during the Phanerozoic: Geochimica et Cosmochimica Acta, 70(23), p. 5665–5675.

Royer, D.L., Berner, R.A., Montañez, I.P., Tabor, N.J. and Beerling, D.J., 2004. CO_2 as primary driver of Phanerozoic climate: Geological Society of America Today, 14, p. 4–10.

Sachse, V. F., Strozyk, F., Anka, Z., Rodriguez, J. F. and Primio, R., 2016. The tectono-stratigraphic evolution of the Austral Basin and adjacent areas against the background of Andean tectonics, southern Argentina, South America: Basin Research, 28(4), p. 462–482.

Salazar, C., 2012. The Jurassic–Cretaceous boundary (Tithonian–Hauterivian) in the Andean Basin of central Chile: Ammonites, bio- and sequence stratigraphy and palaeobiogeography, PhD thesis: Heidelberg, Germany, Ruprecht-Karls Universität, 388 pp.

Salazar, C. and Stinnesbeck, W., 2015a. Redefinition, stratigraphy and facies of the Lo Valdés Formation (Upper Jurassic–Lower Cretaceous) in central Chile: Boletín del Museo Nacional de Historia Natural, Chile, 64, p. 41–68.

Salazar, C. and Stinnesbeck, W., 2015b. Tithonian–Berriasian ammonites from the Baños del Flaco Formation, central Chile: Journal of Systematic Palaeontology, p. 1–34.

Schrank, E., 1984. Organic-walled microfossils and sedimentary facies in the Abu Tartur phosphates (Late Cretaceous, Egypt): Berliner Geowissenschaftliche Abhandlungen, A, 50, p. 177–187, pl. 1.

Schröder-Adams, C.J., Herrle, J.O., Embry, A.F., Haggart, J.W., Galloway, J.M., Pugh, A.T. and Harwood, D.M., 2014. Aptian to Santonian foraminiferal biostratigraphy and paleoenvironmental change in the Sverdrup Basin as revealed at glacier Fiord, Axel Heiberg Island, Canadian Arctic Archipelago: Palaeogeography, Palaeoclimatology, Palaeoecology, 413, p. 81–100.

Schultz, B.P., 1998. The relationship between ikaite and glendonite type pseudomorphs. MSc thesis, Aarhus University, Denmark

Schwarz, E., Veiga, G.D., Spalletti, L.A. and Massaferro, J.L., 2011. The transgressive infill of an inherited-valley system: The Springhill Formation (lower Cretaceous) in southern Austral Basin, Argentina: Marine and Petroleum Geology, 28(6), p. 1218–1241.

Selleck, B.W., Carr, P.F. and Jones, B.G., 2007. A review and synthesis of glendonites (pseudomorphs after ikaite) with new data: assessing applicability as recorders of ancient coldwater conditions: Journal of Sedimentary Research, 77 (11), p. 980–991.

Sellwood, B.W., Valdes, P.J. and Price, G.D., 2000. Geological evaluation of multiple general circulation model simulations of Late Jurassic palaeoclimate: Palaeogeogr. Palaeoclimatol. Palaeoecol., 156, p. 147–160.

Seton, M., Müller, R. D., Zahirovic, S., Gaina, C., Torsvik, T., Shephard, G., Taslma, A., Guurnis, M., Turner, M., Maus, S. and Chandler, M., 2012. Global continental and ocean basin reconstructions since 200 Ma.: Earth-Science Reviews, 113(3), p. 212–270.

Sheard, M.J., 1990. Glendonites from the southern Eromanga Basin in South Australia: palaeoclimatic indicators for Cretaceous ice: Geological Survey of South Australia: Quarterly Geological Notes, 114, p. 17–21.

Sheard, M.J., 1990. Glendonites from the southern Eromanga Basin in South Australia: palaeoclimatic indicators for Cretaceous ice. Geological Survey of South Australia: Quarterly Geological Notes, 114, p. 17–23.

Shi, G.R., 2001. Possible influence of Gondwanan glaciation on low-latitude carbonate sedimentation and trans-equatorial faunal migration: the Lower Permian of South China: Geosciences Journal, 5, p. 57–63.

Smellie, J.L., Davies, R.E.S. and Thomson, M.R.A., 1980. Geology of a Mesozoic intra-arc sequence on Byers Peninsula, Livingston Island, South Shetland Islands: British Antarctic Survey Bulletin, 50, p. 55–76.

Snape, M.G., 1992. Dinoflagellate cysts from an allochthonous block of Nordenskjöld Formation (Upper Jurassic), north-west James Ross Island: Antarctic Science, 4, p. 267–278.

Spielhagen, R.F. and Tripati, A., 2009. Evidence from Svalbard for near freezing temperatures and climate oscillations in the Arctic during the Paleocene and Eocene: Palaeogeography, Palaeoclimatology, Palaeoecology, 278, p. 48–56.

Stach, E., 1982. The macerals of coal, In: Stach, E., Mackowsky, M.T., Teichmüller, M., Taylor, G.H., Chandra, D., Teichmüller, R., Murchison, D.G. and Zierke, F. (Eds.), Stach's Textbook of Coal Petrology, 3rd edn: Gebruder Bomtraeger, Berlin, p. 87–140.

Stancliffe, R.P.W., 1989. Microforaminiferal linings: their classification, biostratigraphy and paleoecology, with special reference to specimens from British Oxfordian sediments: Micropaleontology, 35, p. 337–352.

Stein, C.L. and Smith, A.J., 1986. Authigenic carbonate nodules in the Nankai Trough, Site 583: :Initial Reports of the Deep Sea Drilling Project, 87, p. 659–668.

Steuber, T., Rauch, M., Masse, J.-P., Graaf, J. and Malkoc, M., 2005. Low-latitude seasonality of Cretaceous temperatures in warm and cold episodes: Nature, 437, p. 1341–1344.

Stevens, G.R., 1973. Cretaceous belemnites, In: Hallam, A. (Ed.), Atlas of Paleobiogeography: Elsevier, Amsterdam, p. 385–401.

Stinnesbeck, W., Frey, E., Rivas, L., Pérez, J.P., Cartes, M.L., Salazar, C.S. and Lobos, P.Z., 2014. A Lower Cretaceous ichthyosaur graveyard in deep marine slope channel deposits at Torres del Paine National Park, southern Chile: Geol. Soc. Am. Bull. 126(9–10), p. 1317–1339.

Stoll, H.M. and Schrag, D.P., 1996. Evidence of glacial control of rapid sea level changes in the Early Cretaceous: Science, 272, p. 1771–1774.

Stoll, H.M. and Schrag, D.P., 2000. High-resolution stable isotope record from Upper Cretaceous rocks of Italy and Spain: glacial episodes in a greenhouse planet?: Geol. Soc. Am. Bull,. 112, p. 308–319.

Storey, B.C. and Nell, P.A.R., 1988. Role of strike-slip faulting in the tectonic evolution of the Antarctic Peninsula: Journal of the Geological Society, London, 145, p. 333–337.

Storey, B.C., Vaughan, A.P.M. and Millar, I.L., 1996. Geodynamic evolution of the Antarctic Peninsula during Mesozoic times and its bearing on Weddell Sea history. In: Storey, B.C., King, E.C. and Livermore, R.A. (Eds.), Weddell Sea Tectonics and Gondwana Break-up: Geological Society Special Publication, 108, p. 87–103.

Streel, M. and Bless, M.J.M., 1980. Occurrence and significance of reworked palynomorphs: Mededelingen-Rijks Geologische Dienst, 32(10), p. 69–80.

Styan, W.B. and Bustin, R.M., 1983. Petrography of some Fraser River delta peat deposits: coal maceral and microlithotype precursors in temperate-climate peats: International Journal of Coal Geology, 2, p. 321–370.

Suess, E., Balzer, W., Hesse, K.F., Moller, P.J. and Wefer, G., 1982. Calcium carbonate hexahydrate from organic rich sediments of the Antarctic Shelf: Precursor of glendonites: Science, 1216, p. 1128–1131.

Summerhayes, C.P., 1983. Sedimentation of organic matter in upwelling regimes, In: Thiede J. and Suess E. (Eds.), Coastal Upwelling – Its Sediment Record. Part B: Sedimentary Records of Ancient Coastal Upwelling, p. 29–72.

Swainson, I.P. and Hammond, R.P., 2001. Ikaite, $CaCO_3 \cdot 6H_2O$: cold comfort for glendonites as paleothermometers: American Mineralogist, 86, p. 1530–1533.

Chafetz, H. S., & Reid, A., 2000. Syndepositional shallow-water precipitation of glauconitic minerals. Sedimentary Geology, 136(1-2), 29-42.Tappan, H., 1980. The Paleobiology of Plant Protists: Freeman, San Francisco, 1028 pp.

Taylor, T.N., 1982. Ultrastructural studies of Paleozoic seed fern pollen: sporoderm development: Rev. Palaeobot. Palynol., 37, p. 29–53.

Taylor, P.D., 1990. Preservation of soft-bodied and other organisms by bioimmuration – a review: Palaeontology, 33, p. 1–17.

Taylor, B.J., Thomson, M.R.A. and Willey, L.E., 1979. The geology of the Ablation Point-Keystone Cliffs area, Alexander Island: British Antarctic Survey Scientific Reports, 82, 65 pp.

Teichmüller, M. 1982. Origin of the petrographic constituents of coal, In: Stach, E., Mackowsky, M.-TH., Teichmüller, M., Taylor, G.H., Chandra, D. and Teichmüller, R. (Eds.), Stach' s textbook of coal petrology; 3rd edition, Gebrüder Borntraeger, Berlin, p. 219–294.

Tennant, J.P., Mannion, P.D., Upchurch, P., Sutton, M.D. and Price, G.D., 2017. Biotic and environmental dynamics through the Late Jurassic–Early Cretaceous transition: evidence for protracted faunal and ecological turnover: Biological Reviews, 92(2), p. 776–814.

Thiele, R. and Cubillos, E., 1980. Hoja Santiago, región metropolitana Instituto de Investigaciones Geológicas: Carta Geológica de Chile, 21 pp.

Thieuloy, J.-P., Fuhr, M. and Bulot, L.G., 1990. Biostratigraphie de Crétacé inférieur de l'Arc de Castellane (SE de la France). 1: Faunes d'ammonites du Valanginien supérieur et âge de l'horizon de 'La Grande Lumachelle': Geologie Méditerranéenne, 17, p. 55–99.

Thomas, B.M., 1982. Land-plant source rocks for oil and their significance in Australian basins: Australian Petroleum Exploration Association Journal, 22, p. 164–78.

Thomson, M.R.A., 1979. Upper Jurassic and Lower Cretaceous ammonite faunas of the Ablation Point Area, Alexander Island: British Antarctic Survey, Scientific Reports, 97, p. 1–37.

Thomson, M.R.A., 1983. Late Jurassic ammonites from the Orville Coast, Antarctica. In: Oliver, R.L. et al. (Eds.), Antarctic Earth Science: Australian Academy of Science & Cambridge University Press, Canberra, p. 315–319.

Tissot, B. and Pelet, R., 1981. Sources and fate of organic matter in ancient sediments. Oceanologica Acta, Special Issue, Actes 26th Congres International de Geologie: Colloque Geologie des Oceans, Paris 1980, p. 97–103.

Tissot, B.P. and Welte, D.H., 1984. Petroleum Formation and Occurrence, 2nd edn, SpringerVerlag, Berlin, 699 pp.

Tourtelot, H.A., 1979. Black shale – its deposition and diagenesis: Clays and Clay Minerals 27(5), p. 313–321.

Traverse, A., 1992. Organic fluvial sediment: palynomorphs and 'palynodebris' in the lower Trinity River, Texas: Annals of the Missouri Botanical Gardens, 79, p. 110–125.

Traverse, A., 2007. Paleopalynology, Second Edition, Topics in Geobiology, 28, Springer, Dordrecht, The Netherlands, 813 pp.

Traverse, A. and Ginsburg, R.N., 1966. Palynology of the surface sediments of Great Bahama Bank, as related to water movement and sedimentation: Marine Geology, 4, p. 417–459.

Tremolada, F., Bornemann, A., Bralower, T.J., Koeberl, C. and Van de Schootbrugge, B., 2006. Paleoceanographic changes across the Jurassic/Cretaceous boundary: the calcareous phytoplankton response: Earth and Planetary Science Letters, 241, p. 361–371.

Tschudy, R.H., 1961. Palynomorphs as indicators of facies environments in Upper Cretaceous and Lower Tertiary strata, Colorado and Wyoming: Wyoming Geological Society 16th Annual Field Conference, Guidebook, p. 53–59.

Tschudy, R.H., 1969. Relationship of palynomorphs to sedimentation, In: Tschudy, R.H. and Scott, R.A. (Eds.), Aspects of Palynology, Wiley, New York, p. 79–96.

Turner, J.T. and Ferrante, J.G., 1979. Zooplankton fecal pellets in aquatic ecosystems: Bioscience, 29, p. 670–676.

Tyson, R.V., 1984. Palynofacies investigation of Callovian (Middle Jurassic) sediments from DSDP Site 534, Blake-Bahama Basin, western Central Atlantic: Marine and Petroleum Geology, 1, p. 3–13.

Tyson, R.V., 1993. Palynofacies analysis, In: Jenkins, D.J. (Ed.), Applied Micropalaeontology, Kluwer, Dordrecht, p. 153–191.

Tyson, R.V., 1995. Abundance of organic matter in sediments: TOC, hydrodynamic equivalence, dilution and flux effects. In: Sedimentary organic matter, p. 81–118, Springer, Dordrecht.

Tyson, R.V., Wilson, R.C. and Downie, C., 1979. A stratified water column environmental model for the Kimmeridge Clay: Nature, 277, p. 377–380.

Tyson, R.V. and Pearson, T.H., 1991. Modem and ancient continental shelf anoxia: and overview, In: Tyson, R.V. and Pearson, T.H. (Eds.), Modern and Ancient Continental Shelf Anoxia: Geological Society of London Special Publication, 58, p. 1–24.

Vakhrameyev, V.A., 1982. Classopollis pollen as an indicator of Jurassic and Cretaceous climate. International Geology Review 24 (10), p. 1190–1196.

Valdes, P.J., Sellwood, B.W. and Price, G.D., 1995. Modelling Jurassic Milankovitch climate variations. In: House, M.R. and Gale, A.S. (Eds.), Orbital Forcing Timescales and Cyclostratigraph.: Geol. Soc. London Spec. Publ., 85, p. 115–132.

Van Waveren, I.M., 1993. Planktonic organic matter in surficial sediments of the Banda Sea (Indonesia): a palynological approach: Geologica Ultraiectina, Mededelingen van de Faculteit Aardwetenschappen Universiteit Utrecht, 104, p. 1–237, 23 pl.

Varela, A.N., Poiré, D.G., Martin, T., Gerdes, A., Goin, F.J., Gelfo, J.N. and Hoffmann, S., 2012. U-Pb zircon constraints on the age of the Cretaceous Mata Amarilla Formation, Southern Patagonia, Argentina: its relationship with the evolution of the Austral Basin. Andean Geology, 39(3).

Varela, N. and Cisternas, M.E., 2015. Ikaite pseudomorphs as cool water proxies in the Lower Cretaceous of the South Shetland Islands, Antarctic Peninsula: Abstract Book of 31st IAS Meeting of Sedimentology, 22–25 June, 2015, Kraków, Poland, p. 551.

Veizer, J., Godderis, Y. and Francois, L.M., 2000. Evidence for decoupling of atmospheric CO_2 and global climate during the Phanerozoic eon: Nature, 408, p. 698–701.

Vickers, M.L., Price, G.D., Jerrett, R.M. and Watkinson, M., 2016. Stratigraphic and geochemical expression of Barremian–Aptian global climate change in Arctic Svalbard: Geosphere 12(5), p. 1–12.

Wang, Y., Huang, C., Sun, B., Quan, C., Wu, J. and Lin, Z., 2014. Paleo-CO_2 variation trends and the Cretaceous greenhouse climate: Earth-Science Reviews, 129, p. 136–147.

Waples, D.W., 1983. Reappraisal of anoxia and organic richness, with emphasis on Cretaceous of North Atlantic: American Association of Petroleum Geologists Bulletin, 67, p. 963–978.

Weissert, H., 1989. C-isotope stratigraphy, a monitor of paleoenvironmental change: a case study from the early Cretaceous: Surveys in Geophysics, 10, p. 1–61.

Weissert, H. and Lini, A., 1991. Ice age interludes during the time of Cretaceous greenhouse climate? In: Müller, D., MacKenzie, J.A. and Weissert, H. (Eds.), Controversies in Modern Geology: Academic Press, London, p. 173–191.

Weissert, H. and Erba, E., 2004. Volcanism, CO_2 and palaeoclimate: a Late Jurassic–Early Cretaceous carbon and oxygen isotope record: Journal of the Geological Society, London, 161, p. 695–702.

Whitaker, M.F., 1984. The usage of palynology in definition of Troll Field geology, In: Reduction of Uncertainties in Innovative Reservoir Geomodelling, 6th Offshore Northern Seas Conference and Exhibition, Stavanger 1984, Norsk Petroleumsforening, Paper G6, 44 pp.

Whitham, A.G., 1993. Facies and depositional processes in an Upper Jurassic to Lower Cretaceous pelagic sedimentary sequence, Antarctica: Sedimentology, 40, p. 331–349.

Whitham, A.G. and Doyle, P., 1989. Stratigraphy of the Upper Jurassic–Lower Cretaceous Nordenskjöld Formation of eastern Graham Land, Antarctica: Journal of South American Earth Sciences, 2, p. 371–384.

Williams, L.A., 1984. Subtidal stromatolites in Monterey Formation and other organic-rich rocks as suggested source contributors to petroleum formation: American Association of Petroleum Geologists Bulletin, 68, p. 1879–1893.

Wilson, J.L., 1975. Carbonate Facies in Geologic History: Springer, Berlin, 471 pp.

Wilson, T.J., 1991. Transition from back-arc to foreland basin development in the southernmost Andes: Stratigraphic record from the Ultima Espiranza District, Chile: Geological Society of America Bulletin, 103, p. 98–111.

Wimbledon, W.A.P., Reháková D., Pszczółkowski, A., Casellato, C.E., Halásová, E., Frau, C., Bulot, L.G., Grabowski, J., Sobień, K., Pruner, P., Schnabl, P. and Čížková, K., 2013. An account of the bio-and magnetostratigraphy of the Upper Tithonian–Lower Berriasian interval at Le Chouet, Drôme (SE France): Geologica Carpathica, 64(6), p. 437–460.

Wollast, R., 1983. Interactions in estuaries and coastal waters, In: Bolin, B. and Cook, R.B. (Eds.), The Major Biogeochemical Cycles and Their Interactions: Wiley, New York, p. 385–407.

Woolnough, W.G., David, T.W.E., 1926. Cretaceous glaciation in central Australia: Quat. J. Geol. Soc. London. 82, p. 332–351.

Yan, J., 1996. Ikaite pseudomorphs, cold water indicators in the Chihsia Formation (Early Permian) of South China (abstract): 30th International Geological Congress, Abstracts, 30, 97 p.

Zakharov, V.A., and Rogov, M.A., 2003. Boreal-Tethyan mollusk migrations at the Jurassic-Cretaceous boundary time and biogeographic ecotone position in the Northern Hemisphere. Stratigraphy and Geological Correlation, 11(2), p. 152–171.

Zell, P., Stinnesbeck, W., Beckmann, S., Adatte, T. and Hering, F., 2015. The Berriasian–Valanginian (Early Cretaceous) boundary transition at Santa Catarina Ticuá, Oaxaca state, southern Mexico: Ammonites, bivalves, calpionellids and their paleobiogeographic significance: Journal of South American Earth Sciences, 62, p. 33–57.

Zlobina, O.N., Marinov, V.A., Kugakolov, S.A. and Perepyolkin, A.S., 2014. Lithology and paleogeography of the Lower Cretaceous deposits of the Anabar-Khatanga saddle (norther Middle Siberia): Geology and Mineral Resources of Siberia, 2c, p. 88–98.

9. ACKNOWLEDGEMENTS

First and foremost I would like to thank my supervisors Wolfgang Stinnesbeck and Hartmut Jäger without whom this project would not have been possible. I would like to thank them for their continuous support, dedication and contributions that have greatly helped to realise this thesis.

I gratefully acknowledge the German Research Ministry for funding this project. I'm in great debt to Alistair Crame from the BAS for providing access to sample material of Antarctica. Furthermore I would like to thank ENAP and Pablo Mella for granting access to subsurface material of southern Chile and an interesting time in Punta Arenas. Furthermore Thanks to Christian Salazar for providing access to his rock samples and thin sections.

Special thanks goes to Mercelo Leppe who very much helped me during my stays in Punta Arenas but also contributed to the progress of this thesis with many helpful discussion and especially with his friendly being.

I will never forget the staff of the Institute of Earth Sciences, especially Margit Brückner, Francisco Cueto, Torsten Hoffmann, Ayten Eicher, Ilona Fin, Oliver Wienand and Hans Ebert. Thank you very much!

Thanks to my colleagues, Fabio Hering, Seija Beckmann, Christian Lorson, Georg Miernik, Till Drews, Melissa Perner and Thomas Reutner, who made the time at the Institute so memorable and made sure that every low was succeeded by a high.

I would also like to thank my family and friends who always believed in me and without whom I would not be where I am today.

Last but not least I would like to thank my wife Lena, who was with me all the time in every way possible and helped me consciously and unconsciously to accomplish this work. This thesis is dedicated to you.

Eidesstattliche Versicherung gemäß §8 der Promotionsordnung der Naturwissenschaftlich-Mathematischen Gesamtfakultät der Universität Heidelberg

1. Bei der eingereichten Dissertation zu dem Thema

   Changes in climate and palaeoenvironment during the Late Jurassic–Early Cretaceous in southern South America and western Antarctica

   handelt es sich um eine eigenständig erbrachte Leistung.

2. Ich habe nur die angegebenen Quellen und Hilfsmittel benutzt und mich keiner unzulässigen Hilfe Dritter bedient. Insbesondere habe ich wörtlich oder sinngemäß aus anderen Werken übernommene Inhalte als solche kenntlich gemacht.

3. Die Arbeit oder Teile davon habe ich bislang nicht an einer Hochschule des In- oder Auslands als Bestandteil einer Prüfungs- oder Qualifikationsleistung vorgelegt.

4. Die Richtigkeit der vorstehenden Erklärungen bestätige ich.

5. Die Bedeutung der eidesstattlichen Versicherung und die strafrechtlichen Folgen einer unrichtigen oder unvollständigen eidesstattlichen Versicherung sind mir bekannt.

   Ich versichere an Eides statt, dass ich nach bestem Wissen die reine Wahrheit erklärt und nichts verschwiegen habe.

Heidelberg, 20.08.2018

Ort und Datum Unterschrift

Appendix

Palynofacies Analysis

I–LXVII

Cajón del Morado

Age	Preservation		terrestrial																														AOM
			parts of vascular plants												Pollen						Spores												
			phytoclasts												Sporomorphs																		
			Inertinite				Vitrinite				Cutinite				nonsaccate	monosaccate				bisaccate	monolete				trilete				indet				terrestrial, translucent
	Sample	Depth (m)	A	B	C	sum	A	B	C	sum	A	B	C	sum		A	B	C	sum		A	B	C	sum	A	B	C	sum	A	B	C	sum	
Hautervian	CM 23/69	588	110	63	0	173	18	103	0	121	1	0	0	1	0	0	0	0	0	0	0	0	0	0	0	0	0	0	0	2	8	10	220
	CM 23/66	575	127	18	0	145	22	80	0	102	0	0	0	0	0	0	0	0	0	0	0	0	0	0	0	0	0	0	0	1	15	16	60
	CM 23/60	570	165	144	0	309	11	20	0	31	0	0	0	0	0	0	0	0	0	0	0	0	0	0	0	0	2	4	6	0	2	11	13	65
	CM 23/46	555	139	54	0	193	48	68	0	116	0	0	0	0	0	0	0	0	0	0	0	0	0	0	0	0	0	0	0	0	0	2	2	14
	CM 23/40	552	139	25	0	164	26	64	0	90	2	0	0	2	0	0	0	0	0	0	0	0	0	0	0	0	0	0	0	1	4	3	8	112
	CM 23/34	548	165	158	0	323	7	14	0	21	0	0	0	0	0	0	0	0	0	0	0	0	0	0	0	0	0	0	0	0	0	2	2	161
	CM 23/27	540	171	162	0	333	9	20	0	29	0	0	0	0	0	0	0	0	0	0	0	0	0	0	0	0	0	0	0	0	2	4	6	142
	CM 23/18	528	100	127	0	227	21	19	0	40	3	4	0	7	0	0	0	0	0	0	0	0	0	0	0	0	0	3	3	1	7	10	18	43
	CM 23/15	526	221	29	0	250	45	35	0	80	2	1	0	3	0	0	0	0	0	0	0	0	0	0	0	0	1	0	1	1	5	4	10	74
	CM 23/10	524	183	41	0	224	30	52	0	82	3	3	0	6	0	0	0	0	0	0	0	0	0	0	0	0	0	0	0	0	2	6	8	51
	CM 23/4	520	158	80	0	238	11	43	0	54	0	0	0	0	0	0	0	0	0	0	0	0	0	0	0	0	0	0	0	0	0	6	6	173
	CM 23/0,1	518	235	138	0	373	10	46	0	56	0	0	0	0	0	0	0	0	0	0	0	0	0	0	0	0	0	1	1	0	0	3	3	144
	CM 22/70	511	214	186	0	400	17	24	0	41	0	0	0	0	0	0	0	0	0	0	0	0	0	0	0	0	0	0	0	0	2	2	4	166
	CM 22/67	508	79	72	0	151	5	22	0	27	0	2	0	2	0	0	0	0	0	0	0	0	0	0	0	0	0	1	1	0	0	5	5	55
	CM 22/64	505	166	44	0	210	8	34	0	42	0	1	0	1	0	0	0	0	0	0	0	0	0	0	0	0	2	1	3	0	1	3	4	56
	CM 22/60	501	248	74	0	322	14	7	0	21	0	1	0	1	0	0	0	0	0	0	0	0	0	0	0	0	0	1	1	0	0	7	7	82
	CM 22/59	500	121	27	0	148	9	30	0	39	0	0	0	0	0	0	0	0	0	0	0	0	0	0	0	0	0	1	1	0	0	3	3	89
	CM 22/55	496	216	18	0	234	3	25	0	28	0	0	0	0	0	0	0	0	0	0	0	0	0	0	0	0	0	0	0	0	0	1	1	35
	CM 22/52	493	225	32	0	257	3	13	0	16	1	1	0	2	0	0	0	0	0	0	0	0	0	0	0	0	0	0	0	0	0	3	3	59
	CM 22/49	490	182	29	0	211	5	16	0	21	0	0	0	0	0	0	0	0	0	0	0	0	0	0	0	0	0	0	0	1	0	1	2	56
	CM 22/44	485	149	24	0	173	1	10	0	11	0	0	0	0	0	0	0	0	0	0	0	0	0	0	0	0	0	0	0	0	0	2	2	25
	CM 22/24	464	233	91	0	324	66	13	0	79	6	0	0	6	0	0	0	0	0	0	0	1	0	1	0	0	2	2	0	0	2	2	21
	CM 22/21	462	92	24	0	116	17	45	0	62	0	1	0	1	0	0	3	3	0	0	0	0	0	0	0	1	2	3	0	4	2	6	70
	CM 22/18	459	147	20	0	167	26	22	0	48	6	13	0	9	0	0	0	0	0	0	0	0	0	0	0	1	1	2	3	6	30
	CM 22/15	456	81	78	0	159	17	18	0	35	1	2	0	3	0	0	0	0	0	0	0	0	0	0	0	0	0	0	0	0	0	1	1	91
	CM 22/12	453	283	145	0	428	36	12	0	48	3	1	0	4	0	0	0	0	0	0	0	0	0	0	0	0	0	0	0	0	0	0	0	58
Valanginian	CM 21/15-29	439	59	51	0	110	4	31	0	35	0	1	0	1	0	0	0	0	0	0	0	0	0	0	0	0	0	0	0	0	1	1	2	197
	CM 21/15 ->	433	170	48	0	218	42	13	0	55	2	2	0	4	0	0	0	0	0	0	0	0	0	0	0	0	0	0	0	1	3	4	8	225
	CM 21/8-15	430	150	55	0	205	8	12	0	20	0	1	0	1	0	0	0	0	0	0	0	0	0	0	0	0	0	0	0	0	2	2	4	89
	CM 21/1-8	425	170	85	0	255	11	53	0	64	0	0	0	0	0	0	0	0	0	0	0	0	0	0	0	0	0	0	0	0	2	2	4	106
	CM 20/36	416	44	97	0	141	4	30	0	34	0	2	0	2	0	0	0	0	0	0	0	0	0	0	0	0	0	0	0	0	2	4	6	170
	CM 20/34	414	166	116	0	282	10	9	0	19	3	0	0	3	0	0	0	0	0	0	0	0	0	0	0	0	0	0	0	1	1	0	2	94
	CM 20/30	410	25	55	0	80	2	62	0	64	0	0	0	0	0	0	0	0	0	0	0	0	0	0	0	0	0	0	0	0	1	2	3	166
	CM 20/26	405	96	50	0	146	10	52	0	62	1	2	0	3	0	0	0	0	0	0	0	0	0	0	0	0	0	0	0	0	0	3	3	45
	CM 20/22	399	80	12	0	92	35	30	0	65	0	0	0	0	0	0	0	0	0	0	0	0	0	0	0	0	0	0	0	0	1	2	3	157
	CM 20/20	397	136	34	0	170	7	66	0	73	0	2	0	2	0	0	0	0	0	0	0	0	0	0	0	0	1	0	1	0	0	3	3	59
	CM 20/18	393	71	47	0	118	11	23	0	34	0	0	0	0	0	0	0	0	0	0	0	0	0	0	0	0	0	0	0	0	0	2	2	91
	CM 20/16	390	72	84	0	156	6	45	0	51	0	0	0	0	0	0	0	0	0	0	0	0	0	0	0	0	0	1	1	0	4	5	9	130
	CM 20/12	385	43	104	0	147	11	53	0	64	0	0	0	0	0	0	0	0	0	0	0	0	0	0	0	0	0	0	0	0	5	5	10	28
	CM 20/8	383	21	301	0	322	1	24	0	25	0	0	0	0	0	0	0	0	0	0	0	0	0	0	0	0	0	1	1	0	0	1	1	39
	CM 20/0,1	375	87	47	0	134	21	119	0	140	0	0	0	0	0	0	0	0	0	0	0	1	0	1	0	5	0	5	1	25	3	29	86
	CM 19/28	369	37	93	0	130	5	16	0	21	0	0	0	0	0	0	0	0	0	0	0	0	0	0	0	0	0	0	0	0	2	2	151
	CM 19/24	367	41	103	0	144	15	28	0	43	0	1	0	1	0	0	0	0	0	0	0	0	0	0	0	2	1	3	0	2	13	15	49
	CM 19/21	364	61	122	0	183	7	62	0	69	0	0	0	0	0	0	0	0	0	0	0	0	0	0	0	0	0	0	0	0	1	10	11	159
	CM 19/19	361	24	301	0	325	4	16	0	20	0	1	0	1	0	0	0	0	0	0	0	1	0	1	0	0	0	0	0	0	1	4	5	28
	CM 19/17	359	61	124	0	185	3	30	0	33	0	0	0	0	0	0	0	0	0	0	0	0	0	0	0	0	0	0	0	0	0	3	3	134
	CM 19/13	356	32	70	0	102	0	17	0	17	0	0	0	0	0	0	0	0	0	0	0	0	0	0	0	0	0	0	0	0	0	0	0	179
	CM 19/10	352	69	40	0	109	10	49	0	59	0	0	0	0	0	0	0	0	0	0	0	0	0	0	0	0	4	1	5	1	5	4	10	35
	CM 19/8	349	73	50	0	123	8	45	0	53	0	2	0	2	0	0	0	0	0	0	0	0	0	0	0	0	2	1	3	1	3	5	9	170
	CM 19/4	346	89	70	0	159	17	62	0	79	0	0	0	0	0	0	0	0	0	0	0	0	0	0	0	0	0	7	7	0	2	1	3	95
	CM 19/1	345	105	11	0	116	15	61	0	76	0	0	0	0	0	0	0	0	0	0	0	0	0	0	0	0	0	1	1	0	0	1	1	178
	CM 18/70	340	71	48	0	119	24	36	0	60	0	0	0	0	0	0	0	0	0	0	1	2	0	3	0	0	0	0	0	0	5	5	10	56
	CM 18/67	336	98	64	0	162	29	90	0	119	1	0	0	1	0	0	0	0	0	0	0	1	0	1	0	0	1	1	1	0	1	2	3	60
	CM 18/62	333	77	71	0	148	18	81	0	99	0	0	0	0	0	0	0	0	0	0	0	1	1	2	0	0	0	0	1	2	7	10	134
	CM 18/60	331	85	73	0	158	14	94	0	108	0	0	0	0	0	0	0	0	0	0	0	0	0	0	0	0	0	0	0	1	3	7	11	91
	CM 18/57	328	37	7	0	44	21	110	0	131	0	0	0	0	0	0	0	0	0	0	0	0	0	0	0	0	0	0	0	1	2	2	5	177
	CM 18/54	324	109	120	0	229	8	42	0	50	0	0	0	0	0	0	0	0	0	0	0	0	0	0	0	0	0	0	0	0	0	1	1	20
	CM 18/52	322	90	74	0	164	17	91	0	108	2	0	0	2	0	0	0	0	0	0	0	0	0	0	0	0	0	0	0	0	0	4	4	70
	CM 18/50	320	69	44	0	113	27	28	0	55	2	0	0	2	0	0	0	0	0	0	0	1	0	1	1	1	0	2	3	0	7	8	15	105
	CM 18/45	315	80	40	0	120	14	28	0	42	0	0	0	0	0	0	0	0	0	0	0	0	0	0	0	1	2	0	3	1	1	1	3	142
	CM 18/42	312	52	143	0	195	2	26	0	28	0	0	0	0	0	0	0	0	0	0	0	0	0	0	0	0	0	1	1	0	1	5	6	107
	CM 18/39	309	38	32	0	70	5	22	0	27	0	0	0	0	0	0	0	0	0	0	0	0	0	0	0	0	0	0	0	0	0	1	1	203
	CM 18/37	307	30	132	0	162	6	22	0	28	0	0	0	0	0	0	0	0	0	0	0	0	0	0	0	0	0	0	0	0	1	7	9	95
	CM 18/32	302	27	37	0	64	6	79	0	85	0	0	0	0	0	0	0	0	0	0	0	0	0	0	0	0	0	0	0	0	0	4	4	200
	CM 18/30	300	46	58	0	104	15	84	0	99	0	0	0	0	0	0	0	0	0	0	0	0	0	0	0	0	1	0	1	0	2	6	8	109
	CM 18/29	299	78	9	0	87	35	52	0	87	3	1	0	4	0	0	0	0	0	0	0	0	0	0	0	0	0	5	5	0	7	5	12	109
	CM 18/27	297	87	72	0	159	19	27	0	46	1	0	0	1	0	0	0	0	0	0	1	0	0	1	0	0	2	2	0	4	8	12	39
Berriasian	CM 18/24	294	71	44	0	115	8	22	0	30	0	0	0	0	0	0	0	0	0	0	0	0	0	0	0	2	1	3	0	8	2	10	94
	CM 18/22	292	80	13	0	93	17	25	0	42	0	0	0	0	0	0	0	0	0	0	0	0	0	0	0	0	0	0	0	0	0	0	0	160
	CM 18/19	289	66	66	0	132	13	28	0	41	0	0	0	0	0	0	0	0	0	0	0	0	0	0	0	0	0	0	0	0	0	0	0	149
	CM 18/17	287	90	35	0	125	15	25	0	40	0	0	0	0	0	0	0	0	0	0	0	0	0	0	0	0	0	0	0	0	0	0	0	94
	CM 18/15	285	50	118	0	168	11	41	0	52	0	0	0	0	0	0	0	0	0	0	0	0	0	0	0	0	0	0	0	0	0	0	0	139
	CM 18/12	282	71	45	0	116	19	33	0	52	0	0	0	0	0	0	0	0	0	0	0	0	0	0	0	0	0	0	0	0	0	0	0	154
	CM 18/9	279	39	136	0	175	8	38	0	46	0	0	0	0	0	0	0	0	0	0	0	0	0	0	0	0	0	0	0	0	1	0	1	64
	CM 18/7	277	68	45	0	113	38	23	0	61	0	0	0	0	0	0	0	0	0	0	0	0	0	0	0	0	0	0	0	0	0	0	0	76
	CM 18/3	275	66	43	0	109	31	11	0	42	3	0	0	3	0	0	0	0	0	0	0	0	0	0	0	0	0	0	0	0	0	0	0	49
	CM 18/1,5	274	58	97	0	155	23	17	0	40	1	0	0	1	0	0	0	0	0	0	0	0	0	0	0	0	0	0	0	0	0	1	1	192
	CM 17/114	272	61	109	0	170	5	55	0	60	0	0	0	0	0	0	0	0	0	0	0	0	0	0	0	0	0	0	0	0	0	1	1	111

Cajón del Morado

AOM		marine												Diverse												
		marine phytoplankton				Zoomorphs				Zooclasts				others		mineral residues										
terrestrial opaque	marine/sensu stricto	Dinocysts	Acritarchs	Prasinophytes	Leiospheres	foraminiferal test linings				Bivalves, Scolecodonts, Fungi				Botryococcus	Filaments	Quartz	Pyrite	others	Glendonites							
						A	B	C	sum	A	B	C	sum							Totals	Dinocysts	%	Acritarchs	%	Foraminifers	%
0	0	0	0	0	0	0	0	0	0	0	2	0	2	0	0	2	12	5		527	0,00	0,00	0,00	0,00	0,00	0,03
0	0	0	0	0	0	0	0	0	0	0	3	2	5	0	319	15	3	15		647	0,00	0,00	0,00	0,00	0,00	0,10
4	0	0	0	0	0	0	0	0	0	0	0	0	0	0	8	7	24	0		436	0,00		0,00		0,00	
1	0	0	0	0	0	0	0	0	0	0	0	0	0	0	0	270	46	14		326	0,00		0,00		0,00	
3	0	0	0	0	0	0	0	0	0	0	0	0	0	0	118	228	24	16		497	0,00		0,00		0,00	
3	0	0	0	0	0	0	0	0	0	0	0	0	0	0	0	0	16	0		510	0,00		0,00		0,00	
3	0	0	0	0	0	0	0	0	0	0	0	0	0	0	0	14	30	5		513	0,00		0,00		0,00	
4	0	0	0	0	0	0	1	1	2	0	0	0	0	0	52	44	14	3		396	0,00		0,00		0,51	
3	0	0	0	0	0	0	0	0	0	0	9	0	9	0	13	11	36	5		443	0,00		0,00		0,00	
0	0	0	0	0	0	0	0	0	0	0	2	0	2	0	0	5	5	2		373	0,00		0,00		0,00	
0	0	0	0	0	0	0	0	0	0	0	0	0	0	0	0	125	12	3		471	0,00		0,00		0,00	
1	0	0	0	0	0	0	0	0	0	0	0	1	1	0	0	1	11	2		579	0,00		0,00		0,00	
5	0	0	0	0	0	0	0	1	1	0	0	0	0	0	0	0	14	3		617	0,00		0,00		0,16	
0	0	0	0	0	0	0	0	0	0	0	2	0	2	0	3	132	207	32		246	0,00		0,00		0,00	
0	0	0	0	0	0	0	0	0	0	0	0	0	0	0	0	263	19	141		316	0,00		0,00		0,00	
11	0	0	0	0	0	0	0	0	0	0	0	2	2	0	1	74	22	2	x	448	0,00		0,00		0,00	
0	0	0	0	0	0	0	0	0	0	0	0	0	0	0	0	221	14	8		280	0,00		0,00		0,00	
0	0	0	0	0	0	0	0	0	0	0	1	0	1	0	0	175	43	5		299	0,00		0,00		0,00	
0	0	0	0	0	0	0	0	0	0	0	4	0	4	0	2	225	134	149		343	0,00		0,00		0,00	
0	0	0	0	0	0	0	0	0	0	0	0	0	0	0	0	82	151	13		290	0,00		0,00		0,00	
0	0	0	0	0	0	0	0	0	0	0	0	0	0	0	0	104	123	14		211	0,00		0,00		0,00	
9	0	0	0	0	0	0	0	0	0	0	3	2	5	0	3	30	12	21		452	0,00		0,00		0,00	
1	0	0	0	0	0	0	0	0	0	1	5	6	12	0	0	23	15	2		271	0,00		0,00		0,00	
0	0	0	0	0	0	0	0	0	0	0	1	0	1	0	13	29	99	225		275	0,00		0,00		0,00	
3	0	0	0	0	0	0	0	0	0	0	3	3	6	0	4	37	591	40		302	0,00		0,00		0,00	
16	0	0	0	0	0	0	0	0	0	0	0	0	0	0	0	19	16	2		554	0,00		0,00		0,00	
0	0	0	0	0	0	0	0	0	0	0	0	0	0	0	0	285	47	19		345	0,00	0,00	0,00	0,01	0,00	0,04
12	0	0	0	0	0	0	1	0	1	0	2	0	2	0	2	125	43	7		527	0,00	0,00	0,00	0,06	0,19	0,16
1	0	0	0	0	0	0	0	0	0	0	3	3	6	0	6	475	155	222	x	332	0,00		0,00		0,00	
15	0	0	0	0	0	0	0	0	0	0	0	1	1	0	3	263	11	6		448	0,00		0,00		0,00	
0	0	0	0	0	0	0	0	0	0	0	0	2	2	0	46	155	13	14		401	0,00		0,00		0,00	
3	0	0	0	0	0	0	0	0	0	0	0	0	0	0	8	58	15	4		411	0,00		0,00		0,00	
0	0	0	0	0	0	0	0	0	0	0	0	0	0	0	0	258	84	6		313	0,00		0,00		0,00	
7	0	0	0	0	0	0	0	0	0	0	0	0	0	0	0	412	72	47		266	0,00		0,00		0,00	
2	0	0	0	0	0	0	0	0	0	0	0	0	0	0	0	334	46	8		319	0,00		0,00		0,00	
1	0	0	0	0	0	0	0	0	0	0	0	0	0	0	0	128	25	2		309	0,00		0,00		0,00	
4	0	0	0	0	0	0	0	0	0	0	0	0	0	0	0	796	21	32		249	0,00		0,00		0,00	
3	0	0	0	0	0	0	0	0	0	0	1	1	2	0	0	150	84	13		352	0,00		0,00		0,00	
5	0	0	0	0	0	0	0	0	0	0	1	0	1	0	30	215	98	29		285	0,00		0,00		0,00	
3	0	0	0	0	0	0	0	0	0	0	1	0	1	0	0	217	72	10		392	0,00		0,00		0,00	
6	0	0	0	0	0	0	0	0	0	0	1	0	1	0	2	88	59	26		404	0,00		0,00		0,00	
2	0	0	0	0	0	0	0	0	0	0	0	0	0	0	0	718	27	9		306	0,00		0,00		0,00	
8	0	0	0	0	0	0	0	0	0	0	2	0	2	0	225	140	16	26		490	0,00		0,00		0,00	
6	0	0	0	0	0	0	0	0	0	0	1	0	1	0	0	135	28	3	x	429	0,00		0,00		0,00	
0	0	0	0	0	0	0	0	0	0	0	0	0	0	0	0	121	18	7	x	380	0,00		0,00		0,00	
0	0	0	0	0	0	0	0	0	0	0	1	0	1	0	0	265	9	2		356	0,00		0,00		0,00	
0	0	0	0	0	0	0	0	0	0	0	0	0	0	0	0	530	5	4	x	298	0,00		0,00		0,00	
17	0	0	0	0	0	0	0	0	0	0	1	0	1	0	55	369	4	6		291	0,00		0,00		0,00	
11	0	0	0	0	0	0	0	0	0	0	0	0	0	0	48	16	14	6		419	0,00		0,00		0,00	
28	0	0	0	0	0	0	0	0	0	8	0	0	8	0	92	9	75	7		471	0,00		0,00		0,00	
2	0	0	0	0	0	0	0	0	0	0	1	0	1	0	3	0	63	0		378	0,00		0,00		0,00	
3	0	0	0	0	0	0	0	0	0	0	0	0	0	0	197	13	22	13	x	449	0,00		0,00		0,00	
13	0	0	0	0	0	0	0	0	0	0	1	0	1	0	0	2	8	5	x	361	0,00		0,00		0,00	
8	0	0	0	0	0	0	0	0	0	0	0	0	0	0	0	6	23	3	x	401	0,00		0,00		0,00	
4	0	0	0	0	0	0	0	0	0	0	0	0	0	0	7	39	138	4		379	0,00		0,00		0,00	
0	0	0	1	0	0	0	0	3	3	0	0	0	0	0	2	6	0	2	x	363	0,00		0,28		0,83	
5	0	0	0	0	0	0	0	0	0	0	0	0	0	0	23	87	40	24		328	0,00		0,00		0,00	
14	0	0	0	0	0	0	0	0	0	0	1	0	1	0	3	11	4	4		366	0,00		0,00		0,00	
3	0	0	0	0	0	2	1	0	3	0	4	2	6	0	201	8	1	5	x	507	0,00		0,00		0,59	
2	0	0	0	0	0	0	0	0	0	0	0	0	0	0	25	224	5	7		337	0,00		0,00		0,00	
4	0	0	0	0	0	0	0	0	0	0	2	1	3	0	0	8	80	5	x	344	0,00		0,00		0,00	
0	0	0	0	0	0	0	0	0	0	0	0	1	1	0	0	291	27	2		302	0,00		0,00		0,00	
43	0	0	0	0	0	0	0	0	0	0	1	0	1	0	0	77	67	11	x	338	0,00		0,00		0,00	
0	0	0	0	0	0	0	0	0	0	0	0	0	0	0	0	118	9	0		353	0,00		0,00		0,00	
3	0	0	0	0	0	0	0	0	0	0	1	2	3	0	9	0	4	32		336	0,00		0,00		0,00	
7	0	0	0	0	0	0	0	0	0	0	6	0	6	0	56	0	5	6		373	0,00		0,00		0,00	
41	0	0	1	0	3	0	0	0	0	0	3	0	3	0	15	0	162	56		324	0,00		0,31		0,00	
39	0	0	2	0	0	0	0	0	0	0	0	0	0	0	0	0	372	18		293	0,00	0,00	0,68	0,01	0,00	0,00
3	0	0	0	0	0	0	0	0	0	0	0	1	1	0	0	0	241	24		299	0,00	0,00	0,00	0,09	0,00	0,04
0	0	0	0	0	0	0	0	0	0	0	0	2	2	0	0	0	5	22		324	0,00		0,00		0,00	
3	0	0	0	0	0	0	0	0	0	0	0	2	2	0	0	0	5	59		264	0,00		0,00		0,00	
0	0	0	0	0	0	0	0	0	0	0	0	0	0	0	0	0	2	6		359	0,00		0,00		0,00	
0	0	0	0	0	0	0	0	0	0	0	0	0	0	0	0	0	3	14		322	0,00		0,00		0,00	
15	0	0	0	0	0	0	0	0	0	0	0	0	0	0	0	0	0	5		301	0,00		0,00		0,00	
34	0	0	0	0	0	0	0	0	0	0	0	3	3	0	0	0	7	44		287	0,00		0,00		0,00	
137	0	0	0	0	0	0	0	0	0	0	3	6	9	0	13	0	24	39		362	0,00		0,00		0,00	
6	0	0	0	0	0	0	0	0	0	1	4	0	5	0	0	0	7	5		400	0,00		0,00		0,00	
10	0	0	0	0	0	0	0	0	0	0	2	1	3	0	0	0	12	7		355	0,00		0,00		0,00	

Cajón del Morado

Age	Sample	Depth (m)	Leiospheres	%	marine AOM	%	terrestrial AOM translucent	%	terrestrial AOM opaque	%	AOMT total	%	Sporomorphs
Hautervian	CM 23/69	588	0,00	0,00	0,00	0,00	41,75	19,77	0,0	0,55	41,75	20,32	10
	CM 23/66	575	0,00	0,00	0,00	0,00	9,27	9,77	0,0	0,79	9,27	9,60	16
	CM 23/60	570	0,00		0,00		14,91		0,9		15,83		19
	CM 23/46	555	0,00		0,00		4,29		0,3		4,60		2
	CM 23/40	552	0,00		0,00		22,54		0,6		23,14		8
	CM 23/34	548	0,00		0,00		31,57		0,6		32,16		2
	CM 23/27	540	0,00		0,00		27,68		0,6		28,27		6
	CM 23/18	528	0,00		0,00		10,86		1,0		11,87		21
	CM 23/15	526	0,00		0,00		16,70		0,7		17,38		11
	CM 23/10	524	0,00		0,00		13,67		0,0		13,67		8
	CM 23/4	520	0,00		0,00		36,73		0,0		36,73		6
	CM 23/0,1	518	0,00		0,00		24,87		0,2		25,04		4
	CM 22/70	511	0,00		0,00		26,90		0,8		27,71		4
	CM 22/67	508	0,00		0,00		22,36		0,0		22,36		6
	CM 22/64	505	0,00		0,00		17,72		0,0		17,72		7
	CM 22/60	501	0,00		0,00		18,30		2,5		20,76		8
	CM 22/59	500	0,00		0,00		31,79		0,0		31,79		4
	CM 22/55	496	0,00		0,00		11,71		0,0		11,71		1
	CM 22/52	493	0,00		0,00		17,20		0,0		17,20		3
	CM 22/49	490	0,00		0,00		19,31		0,0		19,31		2
	CM 22/44	485	0,00		0,00		11,85		0,0		11,85		2
	CM 22/24	464	0,00		0,00		4,65		2,0		6,64		5
	CM 22/21	462	0,00		0,00		25,83		0,4		26,20		9
	CM 22/18	459	0,00		0,00		10,91		0,0		10,91		7
	CM 22/15	456	0,00		0,00		30,13		1,0		31,13		1
	CM 22/12	453	0,00		0,00		10,47		2,9		13,36		0
Valangian	CM 21/15-29	439	0,00	0,02	0,00	0,00	57,10	30,97	0,0	1,91	57,10	32,89	2
	CM 21/15 ->	433	0,00	0,14	0,00	0,00	42,69	16,31	2,3	2,87	44,97	15,51	8
	CM 21/8-15	430	0,00		0,00		26,81		0,3		27,11		4
	CM 21/1-8	425	0,00		0,00		23,66		3,3		27,01		4
	CM 20/36	416	0,00		0,00		42,39		0,0		42,39		6
	CM 20/34	414	0,00		0,00		22,87		0,7		23,60		2
	CM 20/30	410	0,00		0,00		53,04		0,0		53,04		3
	CM 20/26	405	0,00		0,00		16,92		2,6		19,55		3
	CM 20/22	399	0,00		0,00		49,22		0,6		49,84		3
	CM 20/20	397	0,00		0,00		19,09		0,3		19,42		4
	CM 20/18	393	0,00		0,00		36,55		1,6		38,15		2
	CM 20/16	390	0,00		0,00		36,93		0,9		37,78		10
	CM 20/12	385	0,00		0,00		9,82		1,8		11,58		10
	CM 20/8	383	0,00		0,00		9,95		0,8		10,71		2
	CM 20/0,1	375	0,00		0,00		21,29		1,5		22,77		35
	CM 19/28	369	0,00		0,00		49,35		0,7		50,00		2
	CM 19/24	367	0,00		0,00		10,00		1,6		11,63		18
	CM 19/21	364	0,00		0,00		37,06		1,4		38,46		11
	CM 19/19	361	0,00		0,00		7,37		0,0		7,37		6
	CM 19/17	359	0,00		0,00		37,64		0,0		37,64		3
	CM 19/13	356	0,00		0,00		60,07		0,0		60,07		0
	CM 19/10	352	0,00		0,00		12,03		5,8		17,87		15
	CM 19/8	349	0,00		0,00		40,57		2,6		43,20		12
	CM 19/4	346	0,00		0,00		20,17		5,9		26,11		10
	CM 19/1	345	0,00		0,00		47,09		0,5		47,62		2
	CM 18/70	340	0,00		0,00		12,47		0,7		13,14		13
	CM 18/67	336	0,00		0,00		16,62		3,6		20,22		5
	CM 18/62	333	0,00		0,00		33,42		2,0		35,41		12
	CM 18/60	331	0,00		0,00		24,01		1,1		25,07		11
	CM 18/57	328	0,00		0,00		48,76		0,0		48,76		5
	CM 18/54	324	0,00		0,00		6,10		1,5		7,62		1
	CM 18/52	322	0,00		0,00		19,13		3,8		22,95		4
	CM 18/50	320	0,00		0,00		20,71		0,6		21,30		19
	CM 18/45	315	0,00		0,00		42,14		0,6		42,73		6
	CM 18/42	312	0,00		0,00		31,10		1,2		32,27		7
	CM 18/39	309	0,00		0,00		67,22		0,0		67,22		1
	CM 18/37	307	0,00		0,00		28,11		12,7		40,83		9
	CM 18/32	302	0,00		0,00		56,66		0,0		56,66		4
	CM 18/30	300	0,00		0,00		32,44		0,9		33,33		9
	CM 18/29	299	0,00		0,00		29,22		1,9		31,10		17
	CM 18/27	297	0,93		0,00		12,04		12,7		24,69		15
Berriasian	CM 18/24	294	0,00	0,00	0,00	0,00	32,08	24,37	13,3	4,95	45,39	29,32	13
	CM 18/22	292	0,00	0,03	0,00	0,00	53,51	20,36	1,0	9,18	54,52	19,16	0
	CM 18/19	289	0,00		0,00		45,99		0,0		45,99		0
	CM 18/17	287	0,00		0,00		35,61		1,1		36,74		0
	CM 18/15	285	0,00		0,00		38,72		0,0		38,72		0
	CM 18/12	282	0,00		0,00		47,83		0,0		47,83		0
	CM 18/9	279	0,00		0,00		21,26		5,0		26,25		1
	CM 18/7	277	0,00		0,00		26,48		11,8		38,33		0
	CM 18/3	275	0,00		0,00		13,54		37,8		51,38		0
	CM 18/1,5	274	0,00		0,00		48,00		1,5		49,50		1
	CM 17/114	272	0,00		0,00		31,27		2,8		34,08		1

Cajón del Morado

Age	Sample	Depth (m)	Sporomorphs %		Cutinite %		Inertinite A	%	Inertinite B	%	Inertinite total	%	Vitrinite A	%	Vitrinite B	%
Hautervian	CM 23/69	588	1,9	1,66	0,19	0,51	20,9	43,04	12,0	17,19	32,8	60,22	3,4	4,62	19,5	8,25
	CM 23/66	575	2,5	1,27	0,00	0,77	19,6	14,87	2,8	9,87	22,4	14,71	3,4	3,93	12,4	5,25
	CM 23/60	570	4,4		0,00		37,8		33,0		70,9		2,5		4,6	
	CM 23/46	555	0,6		0,00		42,6		16,6		59,2		14,7		20,9	
	CM 23/40	552	1,6		0,40		28,0		5,0		33,0		5,2		12,9	
	CM 23/34	548	0,4		0,00		32,4		31,0		63,3		1,4		2,7	
	CM 23/27	540	1,2		0,00		33,3		31,6		64,9		1,8		3,9	
	CM 23/18	528	5,3		1,77		25,3		32,1		57,3		5,3		4,8	
	CM 23/15	526	2,5		0,68		49,9		6,5		56,4		10,2		7,9	
	CM 23/10	524	2,1		1,61		49,1		11,0		60,1		8,0		13,9	
	CM 23/4	520	1,3		0,00		33,5		17,0		50,5		2,3		9,1	
	CM 23/0,1	518	0,7		0,00		40,6		23,8		64,4		1,7		7,9	
	CM 22/70	511	0,6		0,00		34,7		30,1		64,8		2,8		3,9	
	CM 22/67	508	2,4		0,81		32,1		29,3		61,4		2,0		8,9	
	CM 22/64	505	2,2		0,32		52,5		13,9		66,5		2,5		10,8	
	CM 22/60	501	1,8		0,22		55,4		16,5		71,9		3,1		1,6	
	CM 22/59	500	1,4		0,00		43,2		9,6		52,9		3,2		10,7	
	CM 22/55	496	0,3		0,00		72,2		6,0		78,3		1,0		8,4	
	CM 22/52	493	0,9		0,58		65,6		9,3		74,9		0,9		3,8	
	CM 22/49	490	0,7		0,00		62,8		10,0		72,8		1,7		5,5	
	CM 22/44	485	0,9		0,00		70,6		11,4		82,0		0,5		4,7	
	CM 22/24	464	1,1		1,33		51,5		20,1		71,7		14,6		2,9	
	CM 22/21	462	3,3		0,37		33,9		8,9		42,8		6,3		16,6	
	CM 22/18	459	2,5		3,27		53,5		7,3		60,7		9,5		8,0	
	CM 22/15	456	0,3		0,99		26,8		25,8		52,6		5,6		6,0	
	CM 22/12	453	0,0		0,72		51,1		26,2		77,3		6,5		2,2	
Valangian	CM 21/15-29	439	0,6	2,03	0,29	0,19	17,1	20,49	14,8	21,46	31,9	41,95	1,2	3,44	9,0	13,03
	CM 21/15 ->	433	1,5	1,68	0,76	0,31	32,3	10,47	9,1	16,32	41,4	16,38	8,0	2,50	2,5	7,80
	CM 21/8-15	430	1,2		0,30		45,2		16,6		61,7		2,4		3,6	
	CM 21/1-8	425	0,9		0,00		37,9		19,0		56,9	2,55	2,5		11,8	
	CM 20/36	416	1,5		0,50		11,0		24,2		35,2		1,0		7,5	
	CM 20/34	414	0,5		0,73		40,4		28,2		68,6		2,4		2,2	
	CM 20/30	410	1,0		0,00		8,0		17,6		25,6		0,6		19,8	
	CM 20/26	405	1,1		1,13		36,1		18,8		54,9		3,8		19,5	
	CM 20/22	399	0,9		0,00		25,1		3,8		28,8		11,0		9,4	
	CM 20/20	397	1,3		0,65		44,0		11,0		55,0		2,3		21,4	
	CM 20/18	393	0,8		0,00		28,5		18,9		47,4		4,4		9,2	
	CM 20/16	390	2,8		0,00		20,5		23,9		44,3		1,7		12,8	
	CM 20/12	385	3,5		0,00		15,1		36,5		51,6		3,9		18,6	
	CM 20/8	383	0,5		0,00		5,4		76,8		82,1		0,3		6,1	
	CM 20/0,1	375	8,7		0,00		21,5		11,6		33,2		5,2		29,5	
	CM 19/28	369	0,7		0,00		12,1		30,4		42,5		1,6		5,2	
	CM 19/24	367	3,7		0,20		8,4		21,0		29,4		3,1		5,7	
	CM 19/21	364	2,6		0,00		14,2		28,4		42,7		1,6		14,5	
	CM 19/19	361	1,6		0,26		6,3		79,2		85,5		1,1		4,2	
	CM 19/17	359	0,8		0,00		17,1		34,8		52,0		0,8		8,4	
	CM 19/13	356	0,0		0,00		10,7		23,5		34,2		0,0		5,7	
	CM 19/10	352	5,2		0,00		23,7		13,7		37,5		3,4		16,8	
	CM 19/8	349	2,9		0,48		17,4		11,9		29,4		1,9		10,7	
	CM 19/4	346	2,1		0,00		18,9		14,9		33,8		3,6		13,2	
	CM 19/1	345	0,5		0,00		27,8		2,9		30,7		4,0		16,1	
	CM 18/70	340	2,9		0,00		15,8		10,7		26,5		5,3		8,0	
	CM 18/67	336	1,4		0,28		27,1		17,7		44,9		8,0		24,9	
	CM 18/62	333	3,0		0,00		19,2		17,7		36,9		4,5		20,2	
	CM 18/60	331	2,9		0,00		22,4		19,3		41,7		3,7		24,8	
	CM 18/57	328	1,4		0,00		10,2		1,9		12,1		5,8		30,3	
	CM 18/54	324	0,3		0,00		33,2		36,6		69,8		2,4		12,8	
	CM 18/52	322	1,1		0,55		24,6		20,2		44,8		4,6		24,9	
	CM 18/50	320	3,7		0,39		13,6		8,7		22,3		5,3		5,5	
	CM 18/45	315	1,8		0,00		23,7		11,9		35,6		4,2		8,3	
	CM 18/42	312	2,0		0,00		15,1		41,6		56,7		0,6		7,6	
	CM 18/39	309	0,3		0,00		12,6		10,6		23,2		1,7		7,3	
	CM 18/37	307	2,7		0,00		8,9		39,1		47,9		1,8		6,5	
	CM 18/32	302	1,1		0,00		7,6		10,5		18,1		1,7		22,4	
	CM 18/30	300	2,7		0,00		13,7		17,3		31,0		4,5		25,0	
	CM 18/29	299	4,6		1,07		20,9		2,4		23,3		9,4		13,9	
	CM 18/27	297	4,6		0,31		26,9		22,2		49,1		5,9		8,3	
Berriasian	CM 18/24	294	4,4	0,27	0,00	0,10	24,2	26,85	15,0	31,27	39,2	58,11	2,7	3,17	7,5	7,98
	CM 18/22	292	0,0	0,62	0,00	0,23	26,8	16,98	4,3	20,98	31,1	20,35	5,7	4,41	8,4	9,67
	CM 18/19	289	0,0		0,00		20,4		20,4		40,7		4,0		8,6	
	CM 18/17	287	0,0		0,00		34,1		13,3		47,3		5,7		9,5	
	CM 18/15	285	0,0		0,00		13,9		32,9		46,8		3,1		11,4	
	CM 18/12	282	0,0		0,00		22,0		14,0		36,0		5,9		10,2	
	CM 18/9	279	0,3		0,00		13,0		45,2		58,1		2,7		12,6	
	CM 18/7	277	0,0		0,00		23,7		15,7		39,4		13,2		8,0	
	CM 18/3	275	0,0		0,83		18,2		11,9		30,1		8,6		3,0	
	CM 18/1,5	274	0,3		0,25		14,5		24,3		38,8		5,8		4,3	
	CM 17/114	272	0,3		0,00		17,2		30,7		47,9		1,4		15,5	

Cajón del Morado

Age	Sample	Depth (m)	Vitrinite % total		Phytoclasts %		Filaments %		marine OM %		terrestrial OM %		Palynomorphs %	OP/TR
Hautervian	CM 23/69	588	23,0	12,87	56,0	73,60	0,0	3,83	0,0	0,03	99,6	99,42	1,90	4,68
	CM 23/66	575	15,8	7,45	38,2	12,71	49,3	10,63	0,0	0,10	99,2	0,98	51,78	
	CM 23/60	570	7,1		78,0		1,8		0,0		100,0		6,19	
	CM 23/46	555	35,6		94,8		0,0		0,0		100,0		0,61	
	CM 23/40	552	18,1		51,5		23,7		0,0		100,0		25,35	
	CM 23/34	548	4,1		67,5		0,0		0,0		100,0		0,39	
	CM 23/27	540	5,7		70,6		0,0		0,0		100,0		1,17	
	CM 23/18	528	10,1		69,2		13,1		0,5		99,5		18,94	
	CM 23/15	526	18,1		75,2		2,9		0,0		98,0		5,42	
	CM 23/10	524	22,0		83,6		0,0		0,0		99,5		2,14	
	CM 23/4	520	11,5		62,0		0,0		0,0		100,0		1,27	
	CM 23/0,1	518	9,7		74,1		0,0		0,0		99,8		0,69	
	CM 22/70	511	6,6		71,5		0,0		0,2		99,8		0,81	
	CM 22/67	508	11,0		73,2		1,2		0,0		99,2		3,66	
	CM 22/64	505	13,3		80,1		0,0		0,0		100,0		2,22	
	CM 22/60	501	4,7		76,8		0,2		0,0		99,6		2,01	
	CM 22/59	500	13,9		66,8		0,0		0,0		100,0		1,43	
	CM 22/55	496	9,4		87,6		0,0		0,0		99,7		0,33	
	CM 22/52	493	4,7		80,2		0,6		0,0		98,8		1,46	
	CM 22/49	490	7,2		80,0		0,0		0,0		100,0		0,69	
	CM 22/44	485	5,2		87,2		0,0		0,0		100,0		0,95	
	CM 22/24	464	17,5		90,5		0,7		0,0		98,9		1,77	
	CM 22/21	462	22,9		66,1		0,0		0,0		95,6		3,32	
	CM 22/18	459	17,5		81,5		4,7		0,0		99,6		7,27	
	CM 22/15	456	11,6		65,2		1,3		0,0		98,0		1,66	
	CM 22/12	453	8,7		86,6		0,0		0,0		100,0		0,00	
Valanginian	CM 21/15-29	439	10,1	16,47	42,3	58,61	0,0	6,03	0,0	0,08	100,0	99,56	0,58	2,55
	CM 21/15 ->	433	10,4	8,75	52,6	15,38	0,4	11,83	0,2	0,27	99,4	0,61	2,09	
	CM 21/8-15	430	6,0		68,1		1,8		0,0		98,2		3,01	
	CM 21/1-8	425	14,3		71,2		0,7		0,0		99,8		1,56	
	CM 20/36	416	8,5		44,1		11,5		0,0		99,5		12,97	
	CM 20/34	414	4,6		74,0		1,9		0,0		100,0		2,43	
	CM 20/30	410	20,4		46,0		0,0		0,0		100,0		0,96	
	CM 20/26	405	23,3		79,3		0,0		0,0		100,0		1,13	
	CM 20/22	399	20,4		49,2		0,0		0,0		100,0		0,94	
	CM 20/20	397	23,6		79,3		0,0		0,0		100,0		1,29	
	CM 20/18	393	13,7		61,0		0,0		0,0		100,0		0,80	
	CM 20/16	390	14,5		58,8		0,0		0,0		99,4		2,84	
	CM 20/12	385	22,5		74,0		10,5		0,0		99,6		14,04	
	CM 20/8	383	6,4		88,5		0,0		0,0		99,7		0,51	
	CM 20/0,1	375	34,7		67,8		0,5		0,0		99,8		9,16	
	CM 19/28	369	6,9		49,3		0,0		0,0		100,0		0,65	
	CM 19/24	367	8,8		38,4		45,9		0,0		99,6		49,59	
	CM 19/21	364	16,1		58,7		0,0		0,0		99,8		2,56	
	CM 19/19	361	5,3		91,1		0,0		0,0		100,0		1,58	
	CM 19/17	359	9,3		61,2		0,0		0,0		99,7		0,84	
	CM 19/13	356	5,7		39,9		0,0		0,0		100,0		0,00	
	CM 19/10	352	20,3		57,7		18,9		0,0		99,7		24,05	
	CM 19/8	349	12,6		42,5		11,5		0,0		100,0		14,32	
	CM 19/4	346	16,8		50,5		19,5		0,0		98,3		21,66	
	CM 19/1	345	20,1		50,8		0,8		0,0		99,7		1,32	
	CM 18/70	340	13,4		39,9		43,9		0,0		99,8		46,77	
	CM 18/67	336	33,0		78,1		0,0		0,0		99,7		1,39	
	CM 18/62	333	24,7		61,6		0,0		0,0		100,0		2,99	
	CM 18/60	331	28,5		70,2		1,8		0,0		100,0		4,75	
	CM 18/57	328	36,1		48,2		0,6		1,1		98,9		3,03	
	CM 18/54	324	15,2		85,1		7,0		0,0		100,0		7,32	
	CM 18/52	322	29,5		74,9		0,8		0,0		99,7		1,91	
	CM 18/50	320	10,8		33,5		39,6		0,6		98,2		43,98	
	CM 18/45	315	12,5		48,1		7,4		0,0		100,0		9,20	
	CM 18/42	312	8,1		64,8		0,0		0,0		99,1		2,03	
	CM 18/39	309	8,9		32,1		0,0		0,0		99,7		0,33	
	CM 18/37	307	8,3		56,2		0,0		0,0		99,7		2,66	
	CM 18/32	302	24,1		42,2		0,0		0,0		100,0		1,13	
	CM 18/30	300	29,5		60,4		2,7		0,0		99,1		5,36	
	CM 18/29	299	23,3		47,7		15,0		0,0		98,4		19,57	
	CM 18/27	297	14,2		63,6		4,6		1,2		97,5		10,49	
Berriasian	CM 18/24	294	10,2	11,16	49,5	69,37	0,0	0,58	0,7	0,02	99,3	99,54	5,12	5,21
	CM 18/22	292	14,0	11,99	45,2	19,08	0,0	2,84	0,0	0,10	99,7	0,85	0,00	
	CM 18/19	289	12,7		53,4		0,0		0,0		99,4		0,00	
	CM 18/17	287	15,2		62,5		0,0		0,0		99,2		0,00	
	CM 18/15	285	14,5		61,3		0,0		0,0		100,0		0,00	
	CM 18/12	282	16,1		52,2		0,0		0,0		100,0		0,00	
	CM 18/9	279	15,3		73,4		0,0		0,0		100,0		0,33	
	CM 18/7	277	21,3		60,6		0,0		0,0		99,0		0,00	
	CM 18/3	275	11,6		42,5		3,6		0,0		97,5		3,59	
	CM 18/1,5	274	10,0		49,0		0,0		0,0		98,8		0,25	
	CM 17/114	272	16,9		64,8		0,0		0,0		99,2		0,28	

Cajón del Morado

Age	Preservation		terrestrial																														AOM
			parts of vascular plants												Pollen						Spores												
			phytoclasts												Sporomorphs																		
			Inertinite				Vitrinite				Cutinite				nonsaccate	monosaccate				bisaccate	monolete				trilete				indet				terrestrial, translucent
	Sample	Depth (m)	A	B	C	sum	A	B	C	sum	A	B	C	sum		A	B	C	sum		A	B	C	sum	A	B	C	sum	A	B	C	sum	
Berriasian	CM 17/111	269	82	125		207	8	0	0	8	0	0	0	0	0	0	0	0	0	0	0	0	0	0	0	0	0	0	0	1	0	1	139
	CM 17/108	266	35	93		128	23	0	0	23	0	0	0	0	0	0	0	0	0	0	0	0	0	0	0	0	0	0	0	0	2	2	176
	CM 17/104	262	104	234		338	2	0	0	2	0	0	0	0	0	0	0	0	0	0	0	0	0	0	0	0	0	0	0	0	2	2	59
	CM 17/102	260	71	190		261	0	33	0	33	0	0	0	0	0	0	0	0	0	0	0	0	0	0	0	0	0	0	0	0	0	0	33
	CM 17/99	258	66	124		190	9	2	0	11	0	0	0	0	0	0	0	0	0	0	0	0	0	0	0	0	0	0	0	0	0	0	139
	CM 17/97	256	34	278		312	0	17	0	17	0	0	0	0	0	0	0	0	0	0	0	0	0	0	0	0	0	0	0	2	1	3	0
	CM 17/94	253	13	365		378	0	15	0	15	0	0	0	0	0	0	0	0	0	0	0	0	0	0	0	0	0	0	0	2	1	3	0
	CM 17/91	250	43	228		271	0	18	0	18	0	0	0	0	0	0	0	0	0	0	0	0	0	0	0	0	0	0	0	0	0	0	0
	CM 17/88	247	52	286		338	0	34	0	34	0	0	0	0	0	0	0	0	0	0	0	0	0	0	0	0	0	0	0	0	0	0	0
	CM 17/86	245	25	255		280	0	7	0	7	0	0	0	0	0	0	0	0	0	0	0	0	0	0	0	0	0	0	0	0	0	0	0
	CM 17/83	242	115	134		249	9	31	0	40	0	0	0	0	0	0	0	0	0	0	0	0	0	0	0	0	0	0	0	0	0	0	0
	CM 17/81	240	89	9		98	33	80	0	113	0	0	0	0	0	0	0	0	0	0	0	0	0	0	0	0	0	0	0	0	0	0	62
	CM 17/80	238	50	124		174	0	0	0	0	0	0	0	0	0	0	0	0	0	0	0	0	0	0	0	0	0	0	0	0	0	0	109
	CM 17/77	235	6	173		179	0	49	0	49	0	0	0	0	0	0	0	0	0	0	0	0	0	0	0	0	0	0	0	0	1	1	2
	CM 17/75	232	45	256		301	0	57	0	57	0	0	0	0	0	0	0	0	0	0	0	0	0	0	0	0	0	0	0	0	1	1	3
	CM 17/73	230	42	256		298	0	80	0	80	0	0	0	0	0	0	0	0	0	0	0	0	0	0	0	0	0	0	0	0	0	0	5
	CM 17/71	228	201	171		372	2	118	0	120	0	2	0	2	0	0	0	0	0	0	0	0	0	0	0	0	0	0	0	2	2	5
	CM 17/68	226	172	235		407	3	122	0	125	0	3	0	3	0	0	0	0	0	0	0	0	0	0	0	0	0	0	0	0	0	0	1
	CM 17/65	223	174	119		293	1	96	0	97	0	0	0	0	0	0	0	0	0	0	0	0	0	0	0	0	0	1	1	0	0	3	3	0
	CM 17/64	222	108	39		147	17	74	0	91	0	0	0	0	0	0	0	0	0	0	0	0	0	0	0	0	0	0	0	0	3	3	85
	CM 17/62 P	220	108	180		288	0	0	0	0	0	1	0	1	0	0	0	0	0	0	0	0	0	0	0	0	0	0	0	0	0	0	56
	CM 17/60 P	218	111	3		114	1	1	0	2	0	1	0	1	0	0	0	0	0	0	0	0	0	0	0	0	0	0	0	0	2	2	45
	CM 17/58	216	63	52		115	24	78	0	102	2	0	0	2	0	0	0	0	0	0	0	0	0	0	0	0	0	0	0	0	2	2	18
	CM 17/57 P	215	128	276		404	0	0	0	0	0	0	0	0	0	0	0	0	0	0	0	0	0	0	0	0	0	0	0	0	0	0	53
	CM 17/54	212	325	196		521	97	244	0	341	1	5	0	6	0	0	0	0	0	0	0	0	0	0	0	0	0	0	0	0	0	0	47
	CM 17/51	208	140	130		270	21	103	0	124	0	0	0	0	0	0	0	0	0	0	0	0	0	0	0	0	0	0	0	0	0	0	108
	CM 17/49 P	206	27	8		35	10	65	0	75	0	1	0	1	0	0	0	0	0	0	0	0	0	0	0	0	0	0	0	0	1	1	126
	CM 17/48	206	95	33		128	42	142	0	184	0	0	0	0	0	0	0	0	0	0	0	0	0	0	0	0	0	0	0	0	0	0	91
	CM 17/46	204	169	36		205	28	30	0	58	0	3	0	3	0	0	0	0	0	0	0	0	0	0	0	0	0	0	0	0	2	2	99
	CM 17/44 P	202	148	190		338	0	0	0	0	0	0	0	0	0	0	0	0	0	0	0	0	0	0	0	0	0	0	0	0	0	0	81
	CM 17/42	199	85	30		115	49	23	0	72	0	0	0	0	0	0	0	0	0	0	0	0	0	0	0	0	0	0	0	0	1	1	43
	CM 17/40	195	84	71		155	54	4	0	58	0	0	0	0	0	0	0	0	0	0	0	0	0	0	0	0	0	0	0	0	2	2	296
	CM 17/38	195	41	8		49	20	7	0	27	0	0	0	0	0	0	0	0	0	0	0	0	0	0	0	0	0	0	0	0	0	0	388
	CM 17/35,5 P	195,5	158	214		372	17	1	0	18	0	0	0	0	0	0	0	0	0	0	0	0	0	0	0	0	0	0	0	0	1	1	252
	CM 17/34 P	194	12	2		14	1	5	0	6	0	0	0	0	0	0	0	0	0	0	0	0	0	0	0	0	0	0	0	0	0	0	280
	CM 17/28 P	188	267	320		587	6	1	0	7	0	0	0	0	0	0	0	0	0	0	0	0	0	0	0	0	0	0	0	0	0	0	101
	CM 17/25	185	221	255		476	16	4	0	20	0	0	0	0	0	0	0	0	0	0	0	0	0	0	0	0	0	0	0	0	0	0	160
	CM 17/23 P	183	79	115		194	0	4	0	4	0	0	0	0	0	0	0	0	0	0	0	0	0	0	0	0	0	0	0	0	0	0	95
	CM 17/20 G	180	35	156		191	0	0	0	0	0	0	0	0	0	0	0	0	0	0	0	0	0	0	0	0	0	0	0	0	0	0	4
	CM 17/19	179	180	86		266	85	25	0	110	0	2	0	2	0	0	0	0	0	0	0	0	0	0	0	0	0	0	0	0	0	0	229
	CM 17/16 P	176	87	281		368	1	1	0	2	0	0	0	0	0	0	0	0	0	0	0	0	0	0	0	0	0	0	1	0	0	1	260
	CM 17/14 P	174	147	144		291	0	4	0	4	0	0	0	0	0	0	0	0	0	0	0	0	0	0	0	0	0	0	0	1	1	149
	CM 17/8 G	168	184	129		313	1	1	0	2	0	1	0	1	0	0	0	0	0	0	0	0	0	0	0	0	0	0	0	0	0	0	61
	CM 17/7 P	167	195	23		218	0	0	0	0	0	0	0	0	0	0	0	0	0	0	0	0	0	0	0	0	0	0	0	0	0	0	58
	CM 17/6	166	155	148		303	0	0	0	0	0	0	0	0	0	0	0	0	0	0	0	0	0	0	0	0	0	0	0	1	1	86
	CM 17/5	165	160	130		290	0	0	0	0	0	0	0	0	0	0	0	0	0	0	0	0	0	0	0	0	0	0	0	0	0	0	79
	CM 17/4	164	266	52		318	0	0	0	0	0	0	0	0	0	0	0	0	0	0	0	0	0	0	0	0	0	0	0	0	0	0	46
	CM 17/2	162	238	70		308	0	4	0	4	0	0	0	0	0	0	0	0	0	0	0	0	0	0	0	0	0	0	0	0	0	0	109
	CM 17/1	161	578	7		585	0	9	0	9	0	0	0	0	0	0	0	0	0	0	0	0	0	0	0	0	0	0	0	1	1	1	91
	CM 17/0,15	160,5	70	109		179	0	2	0	2	0	0	0	0	0	0	0	0	0	0	0	0	0	0	0	0	0	0	0	1	2	3	168
Tithonian	CM 16/102	150	290	169		459	0	0	0	1	0	0	0	0	0	0	0	0	0	0	0	0	0	0	0	0	0	0	0	0	0	0	60
	CM 16/100	148	69	43		112	0	0	0	1	0	1	0	1	0	0	0	0	0	0	1	0	0	1	0	0	1	1	0	1	11	12	123
	CM 16/98	146	120	79		199	3	1	0	4	0	0	0	0	0	0	0	0	0	0	10	0	0	10	0	0	0	0	0	0	10	10	199
	CM 16/96	144	82	84		166	6	35	0	41	0	0	0	0	0	0	0	0	0	0	0	0	0	0	0	0	0	0	2	9	11	207
	CM 16/86	134	99	61		160	6	38	0	44	0	0	0	0	0	0	1	8	9	0	0	4	4	8	0	0	1	1	0	0	0	0	82
	CM 16/80	128	85	18		103	2	15	0	17	0	1	0	1	0	0	0	0	0	0	0	0	0	0	0	0	0	0	0	0	0	0	25
	CM 16/74	122	60	150		210	0	0	0	1	0	0	0	0	0	0	0	0	0	0	0	0	0	0	0	0	0	0	0	2	8	10	190
	CM 16/70	118	83	33		116	0	6	0	6	0	0	0	0	0	0	0	1	1	0	0	2	1	3	0	0	0	0	0	3	21	24	170
	CM 16/54	102	95	35		130	0	0	0	1	1	2	0	3	0	0	0	1	1	0	0	1	0	1	0	1	0	1	0	10	14	24	180
	CM 16/52	100	9	36		45	3	49	0	52	0	0	0	0	0	0	0	0	0	0	0	0	0	0	0	0	0	1	1	4	0	3	7	206
	CM 16/48	98	30	68		98	9	86	0	95	2	2	0	4	0	0	0	0	0	0	0	1	0	1	0	0	0	0	6	4	9	19	163
	CM 16/46	96	2	20		22	3	54	0	57	2	2	0	4	0	0	0	0	0	0	0	0	0	0	0	0	0	0	1	8	9	203
	CM 16/44	94	11	22		33	3	52	0	55	2	4	0	6	0	0	0	0	0	0	0	0	0	0	0	0	0	1	10	13	24	199
	CM 16/38	86	17	33		50	10	67	0	77	0	2	0	2	0	0	0	0	0	0	0	0	0	0	0	0	0	8	23	7	38	200
	CM 16/36	84	14	44		58	4	81	0	85	0	2	0	2	0	0	0	4	4	0	0	0	0	0	0	0	0	1	6	5	12	236
	CM 16/32	80	5	37		42	3	30	0	33	0	9	0	9	0	0	0	0	0	0	0	0	0	0	0	0	0	0	2	1	3	203
	CM 16/28	78	38	131		169	2	42	0	44	0	0	0	0	0	0	0	0	0	0	0	0	0	0	0	0	0	0	0	4	4	101
	CM 16/26	76	3	12		15	3	28	0	31	0	5	0	5	0	0	0	0	0	0	0	0	0	0	0	0	0	0	2	2	4	161
	CM 16/24	74	20	28		48	3	79	0	82	0	4	0	4	0	0	0	0	0	0	0	0	0	0	0	0	0	0	1	5	6	281
	CM 16/22	70	49	75		124	4	63	0	67	0	2	0	2	0	0	0	0	0	0	0	0	0	0	0	0	0	0	1	5	6	207
	CM 16/16	66	11	25		36	6	64	0	70	0	4	0	4	0	0	0	0	0	0	0	0	0	0	0	0	0	0	3	5	8	215
	CM 16/13	63	14	42		56	2	77	0	79		6	0	6	0	0	0	0	0	0	0	0	0	0	0	0	0	0	1	3	4	196
	CM 16/11	61	10	27		37	5	62	0	67	0	0	0	0	0	0	0	0	0	0	0	0	0	0	0	0	0	0	0	1	1	240
	CM 16/9	57	43	31		74	0	0	0	1	0	0	0	0	0	0	0	0	0	0	0	0	0	0	0	0	0	0	1	1	2	225
	CM 16/7	58	23	56		79	2	49	0	51	0	0	0	0	0	0	0	0	0	0	0	0	0	0	0	0	0	0	1	6	7	216
	CM 16/5	56	94	53		147	3	7	0	10	0	8	0	8	0	0	0	0	0	0	0	0	0	0	0	0	0	0	0	1	1	145

Cajón del Morado

AOM		marine												Diverse						Totals	Dinocysts %		Acritarchs %		Foraminifera %	
		marine phytoplankton				Zoomorphs				Zooclasts				others		mineral residues										
terrestrial opaque	marine/sensu stricto	Dinocysts	Acritarchs	Prasinophytes	Leiospheres	foraminiferal test linings				Bivalves, Scolecodonts, Fungi				Botryococcus	Filaments	Quartz	Pyrite	others	Glendonites							
						A	B	C	sum	A	B	C	sum													
3	0	0	0	0	0	0	0	0	0	0	1	0	1	0	0	0	18	4		359	0,00		0,00		0,00	
7	0	0	0	0	0	0	0	0	0	0	2	0	2	0	0	0	10	0		338	0,00		0,00		0,00	
31	0	0	0	0	0	0	0	0	0	0	1	0	1	0	0	0	3	0		433	0,00		0,00		0,00	
19	0	0	0	0	0	0	0	0	0	0	0	0	0	0	0	0	6	2		346	0,00		0,00		0,00	
30	0	0	0	0	0	0	0	0	0	4	0	0	4	0	0	0	5	1		374	0,00		0,00		0,00	
50	0	0	0	0	0	0	0	0	0	0	2	0	2	0	0	0	0	0		384	0,00		0,00		0,00	
43	0	0	0	0	1	0	0	0	0	0	3	0	3	0	0	0	3	1		443	0,00		0,00		0,00	
57	0	0	0	0	0	0	0	0	0	0	3	0	3	0	0	0	0	1		349	0,00		0,00		0,00	
95	0	0	0	0	0	0	0	0	0	0	3	3	6	0	0	0	0	0		473	0,00		0,00		0,00	
21	0	0	0	0	0	0	0	0	0	0	2	0	2	0	0	0	0	0		310	0,00		0,00		0,00	
21	0	0	0	0	0	0	0	0	0	5	6	3	14	0	2	0	8	19		326	0,00		0,00		0,00	
0	0	0	0	0	0	0	0	0	0	0	1	2	3	0	0	0	12	21		276	0,00		0,00		0,00	
4	0	0	0	0	0	0	0	0	0	0	1	0	1	0	0	0	6	0		288	0,00		0,00		0,00	
29	0	0	0	0	0	0	0	0	0	0	4	7	11	0	0	0	0	0		271	0,00		0,00		0,00	
55	0	0	0	0	0	0	0	0	0	2	1	0	3	0	0	0	9	1		420	0,00		0,00		0,00	
55	0	0	0	0	0	0	0	0	0	0	3	0	3	0	0	0	0	0		441	0,00		0,00		0,00	
0	0	0	0	0	0	0	0	0	0	0	1	1	2	0	0	1	5	2		503	0,00		0,00		0,00	
0	0	0	0	0	0	0	0	0	0	0	0	0	0	0	0	1	2	1		536	0,00		0,00		0,00	
0	0	0	0	0	0	0	0	0	0	1	0	0	1	0	0	1	1	0		395	0,00		0,00		0,00	
0	0	0	0	0	0	0	0	0	0	0	0	0	0	0	0	295	7	3		326	0,00		0,00		0,00	
0	0	0	0	0	0	0	0	0	0	0	0	0	0	0	0	3	4	6		345	0,00		0,00		0,00	
2	0	0	0	0	0	0	0	0	0	0	0	0	0	0	0	7	4	8		166	0,00		0,00		0,00	
0	0	0	0	0	0	0	0	0	0	0	0	0	0	0	0	0	3	6		239	0,00		0,00		0,00	
1	0	0	0	0	0	0	0	0	0	0	0	0	0	0	0	0	3	2		458	0,00		0,00		0,00	
2	0	0	0	0	0	0	0	0	0	0	0	0	0	0	0	21	2	42		917	0,00		0,00		0,00	
0	0	0	0	0	0	0	0	0	0	0	0	0	0	0	4	15	10	30		506	0,00		0,00		0,00	
0	0	0	0	0	0	0	0	0	0	0	0	0	0	0	2	351	3	20		240	0,00		0,00		0,00	
1	0	0	0	0	0	0	0	0	0	0	0	0	0	0	0	16	5	17		404	0,00		0,00		0,00	
2	0	0	0	0	0	0	0	0	0	0	0	0	0	0	0	26	6	27		369	0,00		0,00		0,00	
16	0	0	0	0	0	0	0	0	0	0	0	0	0	0	0	4	3	1		435	0,00		0,00		0,00	
3	0	0	0	0	0	0	0	0	0	0	4	0	4	0	13	11	7	140		251	0,00		0,00		0,00	
3	0	0	0	0	0	0	0	0	0	0	0	0	0	0	13	11	7	23		527	0,00		0,00		0,00	
4	0	0	0	0	0	0	0	0	0	0	0	0	0	0	0	31	5	81		468	0,00		0,00		0,00	
9	0	0	0	0	0	0	0	0	0	0	0	0	0	0	0	2	4	9		652	0,00		0,00		0,00	
1	0	0	0	0	0	0	0	0	0	0	0	0	0	0	0	958	4	23		301	0,00		0,00		0,00	
24	0	0	0	0	0	0	0	0	0	0	0	0	0	0	2	3	2	1		721	0,00		0,00		0,00	
22	0	0	0	0	0	0	0	0	0	0	0	0	0	0	0	1	3	0		678	0,00		0,00		0,00	
17	0	0	0	0	0	0	0	0	0	0	0	0	0	0	0	3	3	13		310	0,00		0,00		0,00	
240	0	0	0	0	0	0	0	0	0	0	0	0	0	0	0	0	7	2		435	0,00		0,00		0,00	
9	0	0	0	0	0	0	0	0	0	0	0	0	0	0	0	32	3	72		616	0,00		0,00		0,00	
5	0	0	0	0	0	0	0	0	0	0	0	0	0	0	0	47	48	5		636	0,00		0,00		0,00	
12	0	0	0	0	0	0	0	0	0	0	0	0	0	0	0	9	9	6		457	0,00		0,00		0,00	
2	0	0	0	0	0	0	0	0	0	0	0	0	0	0	103	0	4	1		482	0,00		0,00		0,00	
7	0	0	0	0	0	0	0	0	0	0	0	0	0	0	0	0	5	3		283	0,00		0,00		0,00	
5	0	0	0	0	0	0	0	0	0	0	0	0	0	0	0	0	4	1		395	0,00		0,00		0,00	
2	0	0	0	0	0	0	0	0	0	0	0	0	0	0	0	0	5	2		371	0,00		0,00		0,00	
3	0	0	0	0	0	0	0	0	0	0	0	0	0	0	0	0	10	6		367	0,00		0,00		0,00	
10	0	0	0	0	0	0	0	0	0	0	0	0	0	0	0	0	4	2	x	431	0,00		0,00		0,00	
13	0	0	0	0	0	0	0	0	0	0	0	0	0	0	0	0	5	0		699	0,00		0,00		0,00	
7	0	0	0	0	0	0	0	1	1	0	0	0	0	0	0	3	13	2		360	0,00		0,00		0,28	
0	0	0	0	0	0	0	0	0	0	0	0	0	0	0	0	0	11	0		520	0,00	0,00	0,00	0,00	0,00	0,51
9	0	0	0	0	0	0	4	7	11	0	0	0	0	0	2	6	22	45		274	0,00	0,00	0,00	0,00	4,01	0,95
24	0	0	0	0	0	0	5	8	13	0	0	0	0	0	2	6	10	209		471	0,00		0,00		2,76	
13	0	0	0	0	0	0	3	3	6	0	0	0	0	0	5	24	13	129		449	0,00		0,00		1,34	
16	0	0	0	0	0	1	2	3	6	0	0	0	0	0	0	0	15	11		326	0,00		0,00		1,84	
5	0	0	0	0	0	0	0	0	0	0	0	0	0	0	0	6	19	15	227	157	0,00		0,00		0,00	
8	0	0	0	0	0	0	2	1	3	0	0	0	0	0	0	0	2	10	4	422	0,00		0,00		0,71	
14	0	0	0	0	0	2	3	4	9	0	0	0	0	0	6	3	8	8		349	0,00		0,00		2,58	
3	0	0	0	0	0	1	0	0	1	0	0	0	0	0	0	23	5	35		345	0,00		0,00		0,29	
3	0	0	0	0	0	0	0	0	0	0	0	0	0	0	0	0	0	0		314	0,00		0,00		0,00	
9	0	0	0	0	0	1	1	2	4	7	4	3	14	0	0	0	4	0	x	407	0,00		0,00		0,98	
2	0	0	0	0	0	0	0	0	0	0	0	0	0	0	0	0	0	0		297	0,00		0,00		0,00	
2	0	0	0	0	0	0	0	0	0	3	0	0	3	0	0	0	0	0		322	0,00		0,00		0,00	
0	0	0	0	0	0	0	0	0	0	0	0	0	0	0	0	0	0	0	x	367	0,00		0,00		0,00	
19	0	0	0	0	0	1	0	1	2	2	1	0	3	0	0	0	2	0		421	0,00		0,00		0,48	
0	0	0	0	0	0	0	0	0	0	3	0	0	3	0	0	0	1	0	x	293	0,00		0,00		0,00	
8	0	0	0	0	0	0	0	0	0	0	0	0	0	0	0	0	2	0		326	0,00		0,00		0,00	
0	0	0	0	0	0	0	0	0	0	0	0	0	0	0	0	0	4	0		216	0,00		0,00		0,00	
0	0	0	0	0	0	0	0	0	0	0	0	0	0	0	0	0	0	0		421	0,00		0,00		0,00	
6	0	0	0	0	0	0	1	0	1	0	0	0	0	0	0	340	15	21	x	413	0,00		0,00		0,24	
0	0	0	0	0	0	0	0	0	0	0	0	0	0	0	0	0	2	0		333	0,00		0,00		0,00	
0	0	0	0	0	0	0	0	0	0	0	0	0	0	0	0	0	0	0	x	341	0,00		0,00		0,00	
0	0	0	0	0	0	0	0	0	0	0	2	0	2	0	0	0	2	0	x	347	0,00		0,00		0,00	
3	0	0	0	0	0	0	0	0	0	1	0	0	1	0	0	420	7	16	x	306	0,00		0,00		0,00	
0	0	0	0	0	0	0	0	0	0	0	0	0	0	0	0	0	0	0		353	0,00		0,00		0,00	
1	0	0	0	0	0	0	0	0	0	0	0	0	0	0	0	237	4	14		312	0,00		0,00		0,00	

Cajón del Morado

Age	Sample	Depth (m)	Leiospheres	%	marine AOM	%	terrestrial AOM translucent	%	terrestrial AOM opaque	%	AOMT total	%	Sporomorphs
Berriasian	CM 17/111	269	0,00		0,00		38,72		0,8		39,55		1
	CM 17/108	266	0,00		0,00		52,07		2,1		54,14		2
	CM 17/104	262	0,00		0,00		13,63		7,2		20,79		2
	CM 17/102	260	0,00		0,00		9,54		5,5		15,03		0
	CM 17/99	258	0,00		0,00		37,17		8,0		45,19		0
	CM 17/97	256	0,00		0,00		0,00		13,0		13,02		3
	CM 17/94	253	0,23		0,00		0,00		9,7		9,71		3
	CM 17/91	250	0,00		0,00		0,00		16,3		16,33		0
	CM 17/88	247	0,00		0,00		0,00		20,1		20,08		0
	CM 17/86	245	0,00		0,00		0,00		6,8		6,77		0
	CM 17/83	242	0,00		0,00		0,00		6,4		6,44		0
	CM 17/81	240	0,00		0,00		22,46		0,0		22,46		0
	CM 17/80	238	0,00		0,00		37,85		1,4		39,24		0
	CM 17/77	235	0,00		0,00		0,74		10,7		11,44		1
	CM 17/75	232	0,00		0,00		0,71		13,1		13,81		1
	CM 17/73	230	0,00		0,00		1,13		12,5		13,61		0
	CM 17/71	228	0,00		0,00		0,99		0,0		0,99		2
	CM 17/68	226	0,00		0,00		0,19		0,0		0,19		0
	CM 17/65	223	0,00		0,00		0,00		0,0		0,00		4
	CM 17/64	222	0,00		0,00		26,07		0,0		26,07		3
	CM 17/62 P	220	0,00		0,00		16,23		0,0		16,23		0
	CM 17/60 P	218	0,00		0,00		27,11		1,2		28,31		2
	CM 17/58	216	0,00		0,00		7,53		0,0		7,53		2
	CM 17/57 P	215	0,00		0,00		11,57		0,2		11,79		0
	CM 17/54	212	0,00		0,00		5,13		0,2		5,34		0
	CM 17/51	208	0,00		0,00		21,34		0,0		21,34		0
	CM 17/49 P	206	0,00		0,00		52,50		0,0		52,50		1
	CM 17/48	206	0,00		0,00		22,52		0,2		22,77		0
	CM 17/46	204	0,00		0,00		26,83		0,5		27,37		2
	CM 17/44 P	202	0,00		0,00		18,62		3,7		22,30		0
	CM 17/42	199	0,00		0,00		17,13		1,2		18,33		1
	CM 17/40	195	0,00		0,00		56,17		0,6		56,74		2
	CM 17/38	195	0,00		0,00		82,91		0,9		83,76		0
	CM 17/35,5 P	195,5	0,00		0,00		38,65		1,4		40,03		1
	CM 17/34 P	194	0,00		0,00		93,02		0,3		93,36		0
	CM 17/28 P	188	0,00		0,00		14,01		3,3		17,34		0
	CM 17/25	185	0,00		0,00		23,60		3,2		26,84		0
	CM 17/23 P	183	0,00		0,00		30,65		5,5		36,13		0
	CM 17/20 G	180	0,00		0,00		0,92		55,2		56,09		0
	CM 17/19	179	0,00		0,00		37,18		1,5		38,64		0
	CM 17/16 P	176	0,00		0,00		40,88		0,8		41,67		1
	CM 17/14 P	174	0,00		0,00		32,60		2,6		35,23		1
	CM 17/8 G	168	0,00		0,00		12,66		0,4		13,07		0
	CM 17/7 P	167	0,00		0,00		20,49		2,5		22,97		0
	CM 17/6	166	0,00		0,00		21,77		1,3		23,04		1
	CM 17/5	165	0,00		0,00		21,29		0,5		21,83		0
	CM 17/4	164	0,00		0,00		12,53		0,8		13,35		0
	CM 17/2	162	0,00		0,00		25,29		2,3		27,61		0
	CM 17/1	161	0,00		0,00		13,02		1,9		14,88		1
	CM 17/0,15	160,5	0,00		0,00		46,67		1,9		48,61		3
Tithonian	CM 16/102	150	0,00	0,00	0,00	0,00	11,54	54,17	0,0	2,14	11,54	56,31	0
	CM 16/100	148	0,00	0,00	0,00	0,00	44,89	19,13	3,3	2,69	48,18	17,81	14
	CM 16/98	146	0,00		0,00		42,25		5,1		47,35		20
	CM 16/96	144	0,00		0,00		46,10		2,9		49,00		11
	CM 16/86	134	0,00		0,00		25,15		4,9		30,06		18
	CM 16/80	128	0,00		0,00		15,92		3,2		19,11		0
	CM 16/74	122	0,00		0,00		45,02		1,9		46,92		10
	CM 16/70	118	0,00		0,00		48,71		4,0		52,72		28
	CM 16/54	102	0,00		0,00		52,17		0,9		53,04		27
	CM 16/52	100	0,00		0,00		65,61		1,0		66,56		8
	CM 16/48	98	0,00		0,00		40,05		2,2		42,26		20
	CM 16/46	96	0,00		0,00		68,35		0,7		69,02		9
	CM 16/44	94	0,00		0,00		61,80		0,6		62,42		24
	CM 16/38	86	0,00		0,00		54,50		0,0		54,50		38
	CM 16/36	84	0,00		0,00		56,06		4,5		60,57		16
	CM 16/32	80	0,00		0,00		69,28		0,0		69,28		3
	CM 16/28	78	0,00		0,00		30,98		2,5		33,44		4
	CM 16/26	76	0,00		0,00		74,54		0,0		74,54		4
	CM 16/24	74	0,00		0,00		66,75		0,0		66,75		6
	CM 16/22	70	0,00		0,00		50,12		1,5		51,57		6
	CM 16/16	66	0,00		0,00		64,56		0,0		64,56		8
	CM 16/13	63	0,00		0,00		57,48		0,0		57,48		4
	CM 16/11	61	0,00		0,00		69,16		0,0		69,16		1
	CM 16/9	57	0,00		0,00		73,53		1,0		74,51		2
	CM 16/7	58	0,00		0,00		61,19		0,0		61,19		7
	CM 16/5	56	0,00		0,00		46,47		0,3		46,79		1

Cajón del Morado

Age	Sample	Depth (m)	Sporomorphs %		Cutinite %		Inertinite A %		Inertinite B %		Inertinite total %		Vitrinite A %		Vitrinite B %	
Berriasian	CM 17/111	269	0,3		0,00		22,8		34,8		57,7		2,2		0,0	
	CM 17/108	266	0,6		0,00		10,4		27,5		37,9		6,8		0,0	
	CM 17/104	262	0,5		0,00		24,0		54,0		78,1		0,5		0,0	
	CM 17/102	260	0,0		0,00		20,5		54,9		75,4		0,0		9,5	
	CM 17/99	258	0,0		0,00		17,6		33,2		50,8		2,4		0,5	
	CM 17/97	256	0,8		0,00		8,9		72,4		81,3		0,0		4,4	
	CM 17/94	253	0,7		0,00		2,9		82,4		85,3		0,0		3,4	
	CM 17/91	250	0,0		0,00		12,3		65,3		77,7		0,0		5,2	
	CM 17/88	247	0,0		0,00		11,0		60,5		71,5		0,0		7,2	
	CM 17/86	245	0,0		0,00		8,1		82,3		90,3		0,0		2,3	
	CM 17/83	242	0,0		0,00		35,3		41,1		76,4		2,8		9,5	
	CM 17/81	240	0,0		0,00		32,2		3,3		35,5		12,0		29,0	
	CM 17/80	238	0,0		0,00		17,4		43,1		60,4		0,0		0,0	
	CM 17/77	235	0,4		0,00		2,2		63,8		66,1		0,0		18,1	
	CM 17/75	232	0,2		0,00		10,7		61,0		71,7		0,0		13,6	
	CM 17/73	230	0,0		0,00		9,5		58,0		67,6		0,0		18,1	
	CM 17/71	228	0,4		0,40		40,0		34,0		74,0		0,4		23,5	
	CM 17/68	226	0,0		0,56		32,1		43,8		75,9		0,6		22,8	
	CM 17/65	223	1,0		0,00		44,1		30,1		74,2		0,3		24,3	
	CM 17/64	222	0,9		0,00		33,1		12,0		45,1		5,2		22,7	
	CM 17/62 P	220	0,0		0,29		31,3		52,2		83,5		0,0		0,0	
	CM 17/60 P	218	1,2		0,60		66,9		1,8		68,7		0,6		0,6	
	CM 17/58	216	0,8		0,84		26,4		21,8		48,1		10,0		32,6	
	CM 17/57 P	215	0,0		0,00		27,9		60,3		88,2		0,0		0,0	
	CM 17/54	212	0,0		0,65		35,4		21,4		56,8		10,6		26,6	
	CM 17/51	208	0,0		0,00		27,7		25,7		53,4		4,2		20,4	
	CM 17/49 P	206	0,4		0,42		11,3		3,3		14,6		4,2		27,1	
	CM 17/48	206	0,0		0,00		23,5		8,2		31,7		10,4		35,1	
	CM 17/46	204	0,5		0,81		45,8		9,8		55,6		7,6		8,1	
	CM 17/44 P	202	0,0		0,00		34,0		43,7		77,7		0,0		0,0	
	CM 17/42	199	0,4		0,00		33,9		12,0		45,8		19,5		9,2	
	CM 17/40	195	0,4		0,00		15,9		13,5		29,4		10,2		0,8	
	CM 17/38	195	0,0		0,00		8,8		1,7		10,5		4,3		1,5	
	CM 17/35,5 P	195,5	0,2		0,00		24,2		32,8		57,1		2,6		0,2	
	CM 17/34 P	194	0,0		0,00		4,0		0,66		4,7		0,3		1,7	
	CM 17/28 P	188	0,0		0,00		37,0		44,4		81,4		0,8		0,1	
	CM 17/25	185	0,0		0,00		32,6		37,6		70,2		2,4		0,6	
	CM 17/23 P	183	0,0		0,00		25,5		37,1		62,6		0,0		1,3	
	CM 17/20 G	180	0,0		0,00		8,0		35,9		43,9		0,0		0,0	
	CM 17/19	179	0,0		0,32		29,2		14,0		43,2		13,8		4,1	
	CM 17/16 P	176	0,2		0,00		13,7		44,2		57,9		0,2		0,2	
	CM 17/14 P	174	0,2		0,00		32,2		31,5		63,7		0,0		0,9	
	CM 17/8 G	168	0,0		0,21		38,2		26,8		64,9		0,2		0,2	
	CM 17/7 P	167	0,0		0,00		68,9		8,1		77,0		0,0		0,0	
	CM 17/6	166	0,3		0,00		39,2		37,5		76,7		0,0		0,0	
	CM 17/5	165	0,0		0,00		43,1		35,0		78,2		0,0		0,0	
	CM 17/4	164	0,0		0,00		72,5		14,2		86,6		0,0		0,0	
	CM 17/2	162	0,0		0,00		55,2		16,2		71,5		0,0		0,9	
	CM 17/1	161	0,1		0,00		82,7		1,00		83,7		0,0		1,3	
	CM 17/0,15	160,5	0,8		0,00		19,4		30,3		49,7		0,0		0,6	
Tithonian	CM 16/102	150	0,0	2,49	0,00	0,54	55,8	14,98	32,5	14,45	88,3	29,42	0,0	0,64	0,0	7,63
	CM 16/100	148	5,1	2,58	0,36	0,82	25,2	14,54	15,7	9,65	40,9	20,19	0,0	0,73	0,0	8,20
	CM 16/98	146	4,2		0,00		25,5		16,8		42,3		0,6		0,2	
	CM 16/96	144	2,4		0,00		18,3		18,7		37,0		1,3		7,8	
	CM 16/86	134	5,5		0,00		30,4		18,7		49,1		1,8		11,7	
	CM 16/80	128	0,0		0,64		54,1		11,5		65,6		1,3		9,6	
	CM 16/74	122	2,4		0,00		14,2		35,5		49,8		0,0		0,0	
	CM 16/70	118	8,0		0,00		23,8		9,5		33,2		0,0		1,7	
	CM 16/54	102	7,8		0,87		27,5		10,1		37,7		0,0		0,0	
	CM 16/52	100	2,5		0,00		2,9		11,5		14,3		1,0		15,6	
	CM 16/48	98	4,9		0,98		7,4		16,7		24,1		2,2		21,1	
	CM 16/46	96	3,0		1,35		0,7		6,7		7,4		1,0		18,2	
	CM 16/44	94	7,5		1,86		3,4		6,8		10,2		0,9		16,1	
	CM 16/38	86	10,4		0,54		4,6		9,0		13,6		2,7		18,3	
	CM 16/36	84	3,8		0,48		3,3		10,5		13,8		1,0		19,2	
	CM 16/32	80	1,0		3,07		1,7		12,6		14,3		1,0		10,2	
	CM 16/28	78	1,2		0,00		11,7		40,2		51,8		0,6		12,9	
	CM 16/26	76	1,9		2,31		1,4		5,6		6,9		1,4		13,0	
	CM 16/24	74	1,4		0,95		4,8		6,7		11,4		0,7		18,8	
	CM 16/22	70	1,5		0,48		11,9		18,2		30,0		1,0		15,3	
	CM 16/16	66	2,4		1,20		3,3		7,5		10,8		1,8		19,2	
	CM 16/13	63	1,2		1,76		4,1		12,3		16,4		0,6		22,6	
	CM 16/11	61	0,3		0,00		2,9		7,8		10,7		1,4		17,9	
	CM 16/9	57	0,7		0,00		14,1		10,1		24,2		0,0		0,0	
	CM 16/7	58	2,0		0,00		6,5		15,9		22,4		0,6		13,9	
	CM 16/5	56	0,3		2,56		30,1		17,0		47,1		1,0		2,2	

Cajón del Morado

Age	Sample	Depth (m)	Vitrinite % total		Phytoclasts %		Filaments %		marine OM %		terrestrial OM %		Palynomorphs %	OP/TR
Berriasian	CM 17/111	269	2,2		59,9		0,0		0,0		99,7		0,28	
	CM 17/108	266	6,8		44,7		0,0		0,0		99,4		0,59	
	CM 17/104	262	0,5		78,5		0,0		0,0		99,8		0,46	
	CM 17/102	260	9,5		85,0		0,0		0,0		100,0		0,00	
	CM 17/99	258	2,9		53,7		0,0		0,0		98,9		0,00	
	CM 17/97	256	4,4		85,7		0,0		0,0		99,5		0,78	
	CM 17/94	253	3,4		88,7		0,0		0,2		99,1		0,90	
	CM 17/91	250	5,2		82,8		0,0		0,0		99,1		0,00	
	CM 17/88	247	7,2		78,6		0,0		0,0		98,7		0,00	
	CM 17/86	245	2,3		92,6		0,0		0,0		99,4		0,00	
	CM 17/83	242	12,3		88,7		0,6		0,0		95,7		0,61	
	CM 17/81	240	40,9		76,4		0,0		0,0		98,9		0,00	
	CM 17/80	238	0,0		60,4		0,0		0,0		99,7		0,00	
	CM 17/77	235	18,1		84,1		0,0		0,0		95,9		0,37	
	CM 17/75	232	13,6		85,2		0,0		0,0		99,3		0,24	
	CM 17/73	230	18,1		85,7		0,0		0,0		99,3		0,00	
	CM 17/71	228	23,9		98,2		0,0		0,0		99,6		0,40	
	CM 17/68	226	23,3		99,8		0,0		0,0		100,0		0,00	
	CM 17/65	223	24,6		98,7		0,0		0,0		99,7		1,01	
	CM 17/64	222	27,9		73,0		0,0		0,0		100,0		0,92	
	CM 17/62 P	220	0,0		83,8		0,0		0,0		100,0		0,00	
	CM 17/60 P	218	1,2		70,5		0,0		0,0		100,0		1,20	
	CM 17/58	216	42,7		91,6		0,0		0,0		100,0		0,84	
	CM 17/57 P	215	0,0		88,2		0,0		0,0		100,0		0,00	
	CM 17/54	212	37,2		94,7		0,0		0,0		100,0		0,00	
	CM 17/51	208	24,5		77,9		0,8		0,0		100,0		0,79	
	CM 17/49 P	206	31,3		46,3		0,8		0,0		100,0		1,25	
	CM 17/48	206	45,5		77,2		0,0		0,0		100,0		0,00	
	CM 17/46	204	15,7		72,1		0,0		0,0		100,0		0,54	
	CM 17/44 P	202	0,0		77,7		0,0		0,0		100,0		0,00	
	CM 17/42	199	28,7		74,5		5,2		0,0		98,4		5,58	
	CM 17/40	195	11,0		40,4		2,5		0,0		100,0		2,85	
	CM 17/38	195	5,8		16,2		0,0		0,0		100,0		0,00	
	CM 17/35,5 P	195,5	2,8		59,8		0,0		0,0		100,0		0,15	
	CM 17/34 P	194	2,0		6,6		0,0		0,0		100,0		0,00	
	CM 17/28 P	188	1,0		82,4		0,3		0,0		100,0		0,28	
	CM 17/25	185	2,9		73,2		0,0		0,0		100,0		0,00	
	CM 17/23 P	183	1,3		63,9		0,0		0,0		100,0		0,00	
	CM 17/20 G	180	0,0		43,9		0,0		0,0		100,0		0,00	
	CM 17/19	179	17,9		61,4		0,0		0,0		100,0		0,00	
	CM 17/16 P	176	0,3		58,2		0,0		0,0		100,0		0,16	
	CM 17/14 P	174	0,9		64,6		0,0		0,0		100,0		0,22	
	CM 17/8 G	168	0,4		65,6		21,4		0,0		100,0		21,37	
	CM 17/7 P	167	0,0		77,0		0,0		0,0		100,0		0,00	
	CM 17/6	166	0,0		76,7		0,0		0,0		100,0		0,25	
	CM 17/5	165	0,0		78,2		0,0		0,0		100,0		0,00	
	CM 17/4	164	0,0		86,6		0,0		0,0		100,0		0,00	
	CM 17/2	162	0,9		72,4		0,0		0,0		100,0		0,00	
	CM 17/1	161	1,3		85,0		0,0		0,0		100,0		0,14	
	CM 17/0,15	160,5	0,6		50,3		0,0		0,3		99,7		1,11	
Tithonian	CM 16/102	150	0,2	8,52	88,5	38,49	0,0	1,83	0,0	0,51	100,0	99,12	0,00	3,45
	CM 16/100	148	0,4	8,57	41,6	18,12	0,7	7,20	4,0	0,95	95,6	1,43	9,85	
	CM 16/98	146	0,8		43,1		0,4		2,8		95,1		7,43	
	CM 16/96	144	9,1		46,1		1,1		1,3		98,7		4,90	
	CM 16/86	134	13,5		62,6		0,0		1,8		98,2		7,36	
	CM 16/80	128	10,8		77,1		3,8		0,0		100,0		3,82	
	CM 16/74	122	0,2		50,0		0,0		0,7		99,3		3,08	
	CM 16/70	118	1,7		35,0		1,7		2,6		97,4		12,32	
	CM 16/54	102	0,3		38,8		0,0		0,3		99,7		8,12	
	CM 16/52	100	16,6		30,9		0,0		0,0		100,0		2,55	
	CM 16/48	98	23,3		48,4		0,0		1,0		95,6		5,90	
	CM 16/46	96	19,2		27,9		0,0		0,0		100,0		3,03	
	CM 16/44	94	17,1		29,2		0,0		0,0		99,1		7,45	
	CM 16/38	86	21,0		35,1		0,0		0,0		100,0		10,35	
	CM 16/36	84	20,2		34,4		0,0		0,5		98,8		4,28	
	CM 16/32	80	11,3		28,7		0,0		0,0		99,0		1,02	
	CM 16/28	78	13,5		65,3		0,0		0,0		100,0		1,23	
	CM 16/26	76	14,4		23,6		0,0		0,0		100,0		1,85	
	CM 16/24	74	19,5		31,8		0,0		0,0		100,0		1,43	
	CM 16/22	70	16,2		46,7		0,0		0,2		99,8		1,69	
	CM 16/16	66	21,0		33,0		0,0		0,0		100,0		2,40	
	CM 16/13	63	23,2		41,3		0,0		0,0		100,0		1,17	
	CM 16/11	61	19,3		30,0		0,0		0,0		99,4		0,29	
	CM 16/9	57	0,3		24,5		0,0		0,0		99,7		0,65	
	CM 16/7	58	14,4		36,8		0,0		0,0		100,0		1,98	
	CM 16/5	56	3,2		52,9		0,0		0,0		100,0		0,32	

Cajón del Morado			terrestrial																													AOM
			parts of vascular plants												Pollen						Spores											
			phytoclasts												Sporomorphs																	
			Inertinite				Vitrinite				Cutinite				nonsaccate	monosaccate				bisaccate	monolete				trilete				indet				terrestrial, translucent
Age	Preservation		A	B	C	sum	A	B	C	sum	A	B	C	sum		A	B	C	sum		A	B	C	sum	A	B	C	sum	A	B	C	sum	
	Sample	Depth (m)																															
Tithonian	CM 15/8,4	46,4	195	70	0	265	0	2	0	2	0	1		1	0	0	0	0	0	0	0	0	0	0	0	0	0	0	0	0	2	2	182
	CM 15/6,5	44	95	83	0	178	0	1	0	1	0	0		0	0	0	0	0	0	0	0	0	0	0	0	0	0	0	0	2	3	5	183
	CM 15/4	42	166	55	0	221	0	6	0	6	0	0		0	0	0	0	0	0	0	0	0	0	0	0	0	0	0	0	0	2	2	224
	CM 14/15	35	78	75	0	153	0	2	0	2	0	4		4	0	0	0	0	0	0	0	0	0	0	0	0	0	0	0	14	3	17	193
	CM 14/13	30	64	147	0	211	0	4	0	4	0	0		0	0	0	0	0	0	0	0	0	0	0	0	0	0	0	0	0	3	3	109
	CM 14/08 (3)	27	52	43	0	95	0	0	0	1	0	0		0	0	0	0	0	0	0	0	0	0	0	0	0	0	0	0	0	1	1	113
	CM 14/08 (1)	27	15	9	0	24	0	0	0	1	0	0		0	0	0	0	0	0	0	0	0	0	0	0	0	0	0	0	1	6	7	224
	CM 14/5	25	36	39	0	75	1	5	0	6	0	0		0	0	0	0	0	0	0	0	0	0	0	0	0	0	0	0	0	3	3	411
	CM 14/3,5	25	22	67	0	89	0	0	0	1	0	0		0	0	0	0	0	0	0	0	0	0	0	0	0	0	0	0	0	5	5	250
	CM 13/18	20	15	46	0	61	0	0	0	1	0	0		0	0	0	0	0	0	0	0	0	0	0	0	0	0	0	0	0	4	4	200
	CM 13/10,8	10	0	0	0	0	0	0	0	1	0	0		0	0	0	0	0	0	0	1	0	0	0	0	0	0	0	0	0	0	0	20
	CM 13/2,74	0	2	0	0	2	0	0	0	1	0	0		0	0	0	0	0	0	0	0	0	0	0	0	0	0	0	0	0	0	0	37

Cajón del Morado

AOM		marine												Diverse							
		marine phytoplankton				Zoomorphs				Zooclasts				others		mineral residues					
terrestrial opaque	marine/sensu stricto	Dinocysts	Acritarchs	Prasinophytes	Leiospheres	foraminiferal test linings				Bivalves, Scolecodonts, Fungi				Botryococcus	Filaments	Quartz	Pyrite	others	Glendonites	Totals	Dinocysts %	Acritarchs %	Foraminifera %
						A	B	C	sum	A	B	C	sum										
10	0	0	0	0	0	0	0	0	0	0	0	0	0	0	0	0	10	86		462	0,00	0,00	0,00
14	0	0	0	0	0	0	0	0	0	0	0	0	0	0	0	121	9	0		381	0,00	0,00	0,00
20	0	0	0	0	0	0	0	0	0	0	0	0	0	0	0	0	20	86		473	0,00	0,00	0,00
24	0	0	0	0	0	1	1	1	3	0	0	0	0	0	0	0	5	50		396	0,00	0,00	0,76
21	0	0	0	0	0	0	1	2	3	0	0	0	0	0	6	0	4	19		357	0,00	0,00	0,84
62	0	0	0	0	0	0	0	2	2	0	0	0	0	0	186	0	6	16		460	0,00	0,00	0,43
13	0	0	0	0	0	0	2	5	7	0	0	0	0	0	68	0	5	13		344	0,00	0,00	2,03
8	0	0	0	0	0	0	0	1	1	0	0	0	0	0	0	0	7	11		504	0,00	0,00	0,20
0	0	0	0	0	0	0	0	0	0	0	0	0	0	0	0	0	3		x	345	0,00	0,00	0,00
0	0	0	0	0	0	0	0	0	0	0	0	0	0	0	0	0	0			266	0,00	0,00	0,00
0	0	0	0	0	0	0	0	0	0	0	0	0	0	0	0	0	0		x	22	0,00	0,00	0,00
0	0	0	0	0	0	0	0	0	0	0	0	0	0	0	0	0	0			40	0,00	0,00	0,00

Cajón del Morado

Age	Sample	Depth (m)	Leiospheres %	marine AOM %	terrestrial AOM % translucent	terrestrial AOM % opaque	AOMT % total	Sporomorphs
Tithonian	CM 15/8,4	46,4	0,00	0,00	39,39	2,2	41,56	2
	CM 15/6,5	44	0,00	0,00	48,03	3,7	51,71	5
	CM 15/4	42	0,00	0,00	47,36	4,2	51,59	2
	CM 14/15	35	0,00	0,00	48,74	6,1	54,80	17
	CM 14/13	30	0,00	0,00	30,53	5,9	36,41	3
	CM 14/08 (3)	27	0,00	0,00	24,57	13,5	38,04	1
	CM 14/08 (1)	27	0,00	0,00	65,12	3,8	68,90	7
	CM 14/5	25	0,00	0,00	81,55	1,6	83,13	3
	CM 14/3,5	25	0,00	0,00	72,46	0,0	72,46	5
	CM 13/18	20	0,00	0,00	75,19	0,0	75,19	4
	CM 13/10,8	10	0,00	0,00	90,91	0,0	90,91	0
	CM 13/2,74	0	0,00	0,00	92,50	0,0	92,50	0

Cajón del Morado

Age	Sample	Depth (m)	Sporomorphs %	Cutinite %	Inertinite A %	Inertinite B %	Inertinite total %	Vitrinite A %	Vitrinite B %
Tithonian	CM 15/8,4	46,4	0,4	0,22	42,2	15,2	57,4	0,0	0,4
	CM 15/6,5	44	1,3	0,00	24,9	21,8	46,7	0,0	0,3
	CM 15/4	42	0,4	0,00	35,1	11,6	46,7	0,0	1,3
	CM 14/15	35	4,3	1,01	19,7	18,9	38,6	0,0	0,5
	CM 14/13	30	0,8	0,00	17,9	41,2	59,1	0,0	1,1
	CM 14/08 (3)	27	0,2	0,00	11,3	9,3	20,7	0,0	0,0
	CM 14/08 (1)	27	2,0	0,00	4,4	2,6	7,0	0,0	0,0
	CM 14/5	25	0,6	0,00	7,1	7,7	14,9	0,2	1,0
	CM 14/3,5	25	1,4	0,00	6,4	19,4	25,8	0,0	0,0
	CM 13/18	20	1,5	0,00	5,6	17,3	22,9	0,0	0,0
	CM 13/10,8	10	0,0	0,00	0,0	0,0	0,0	0,0	0,0
	CM 13/2,74	0	0,0	0,00	5,0	0,0	5,0	0,0	0,0

Cajón del Morado

Age	Sample	Depth (m)	Vitrinite % total	Phytoclasts %	Filaments %	marine OM %	terrestrial OM %	Palynomorphs %	OP/TR
Tithonian	CM 15/8,4	46,4	0,4	58,0	0,0	0,0	100,0	0,43	
	CM 15/6,5	44	0,3	47,0	0,0	0,0	100,0	1,31	
	CM 15/4	42	1,3	48,0	0,0	0,0	100,0	0,42	
	CM 14/15	35	0,5	40,2	0,0	0,8	99,2	5,05	
	CM 14/13	30	1,1	60,2	1,7	0,8	99,2	3,36	
	CM 14/08 (3)	27	0,2	20,9	40,4	0,4	99,6	41,09	
	CM 14/08 (1)	27	0,3	7,3	19,8	2,0	98,0	23,84	
	CM 14/5	25	1,2	16,1	0,0	0,2	99,8	0,79	
	CM 14/3,5	25	0,3	26,1	0,0	0,0	100,0	1,45	
	CM 13/18	20	0,4	23,3	0,0	0,0	100,0	1,50	
	CM 13/10,8	10	4,5	4,5	0,0	0,0	95,5	0,00	
	CM 13/2,74	0	2,5	7,5	0,0	0,0	100,0	0,00	

Lo Valdés			terrestrial																																AOM	
			parts of vascular plants												Pollen						Pollen	Spores															
			phytoclasts												Sporomorphs																						
			Inertinite				Vitrinite				Cutinite				nonsaccate	monosaccate					bisaccate	monosaccate	monolete				trilete				indet				terrestrial, translucent	terrestrial opaque
Age	Preservation		A	B	C	sum	A	B	C	sum	A	B	C	sum		A	B	C	sum			A	B	C	sum	A	B	C	sum	A	B	C	sum		
	Sample	Depth (m)																																		
Hauterivian	LV 9/149	539	125	110	0	235	30	112	0	142	0	1	0	1	0	0	0	0	0	0	0	0	0	0	0	0	0	0	0	0	0	0	0	0	52	20
	LV 9/143	533	161	152	0	313	28	61	0	89	0	0	0	0	0	0	0	0	0	0	0	0	0	0	0	0	0	0	0	0	0	1	0	1	24	0
	LV 9/129	519	132	150	0	282	18	29	0	47	0	2	0	2	0	0	0	0	0	0	0	0	0	0	0	0	0	0	0	0	0	0	0	0	36	0
	LV 9/115	505	113	71	0	184	3	25	0	28	0	0	0	0	0	0	0	0	0	0	0	0	0	0	0	0	0	0	0	0	0	0	0	0	219	0
	LV 9/102	492	125	177	0	302	5	9	0	14	0	0	0	0	0	0	0	0	0	0	0	0	0	0	0	0	0	0	0	0	0	0	0	0	161	2
	LV 9/87	477	112	202	0	314	2	16	0	18	0	0	0	0	0	0	0	0	0	0	0	0	0	0	0	0	0	0	0	0	0	0	0	0	101	3
	LV 9/69	459	99	195	0	294	6	31	0	37	0	0	0	0	0	0	0	0	0	0	0	0	0	0	0	0	0	0	0	0	0	1	7	8	85	1
	LV 9/32	422	80	70	0	150	9	116	0	125	0	0	3	3	0	0	0	0	0	0	0	0	0	0	0	0	0	0	0	0	0	0	0	0	48	1
	LV 9/24	414	117	75	0	192	5	20	0	25	0	0	0	0	0	0	0	0	0	0	0	0	0	0	0	0	0	0	0	0	0	0	3	3	114	0
	LV 9/20	410	49	18	0	67	5	11	0	16	0	0	0	0	0	0	0	0	0	0	0	0	0	0	0	0	0	0	0	0	0	1	0	1	51	0
	LV 9/12	402	237	63	0	300	9	33	0	42	0	0	1	1	0	0	0	0	0	0	0	0	0	0	0	0	0	0	0	0	0	0	1	1	31	2
	LV 9/5	395	36	30	0	66	11	63	0	74	1	8	7	16	0	0	0	0	0	0	0	3	0	2	0	2	0	0	0	0	0	16	6	22	208	0
Valanginian	LV 8/103	388	101	81	0	182	3	54	0	57	0	0	3	3	0	0	0	0	0	0	0	0	0	1	0	1	0	0	0	0	0	1	3	4	119	0
	LV 8/99	384	64	63	0	127	2	32	0	34	0	0	0	0	0	0	0	0	0	0	0	0	0	0	1	1	0	0	0	0	0	1	2	3	194	0
	LV 8/91	376	129	102	0	231	39	44	0	83	0	0	0	0	0	0	0	0	0	0	0	0	0	0	0	0	0	0	0	0	0	0	2	2	65	0
	LV 8/83	368	88	29	0	117	4	18	0	22	0	0	0	0	0	0	0	0	0	0	0	0	0	0	0	0	0	0	0	0	0	0	1	1	162	0
	LV 8/59	344	72	33	0	105	9	33	0	42	0	0	2	2	0	0	0	0	0	0	0	0	0	0	0	0	0	0	1	1	0	1	3	4	187	0
	LV 8/54	339	105	18	0	123	7	45	0	52	0	0	0	0	0	0	0	0	0	0	0	0	0	0	0	0	0	0	0	0	0	2		2	227	0
	LV 8/46	331	41	15	0	56	3	42	0	45	0	0	0	0	0	0	0	0	0	0	0	0	0	0	0	0	0	1	0	1	0	0	2	2	300	0
	LV 8/41	326	53	51	0	104	6	78	0	84	0	0	3	3	0	0	0	0	0	0	0	0	1	0	1	1	0	1	1	2	0	8	15	23	95	0
	LV 8/36	321	102	43	0	145	28	51	0	79	0	0	3	3	0	0	0	0	0	0	0	0	0	0	0	0	0	0	0	0	0	0	0	0	157	0
	LV 8/20-36	310	45	33	0	78	45	30	0	75	0	0	0	0	0	0	0	0	0	0	0	0	0	0	0	0	0	0	0	0	0	0	1	1	74	0
	LV 7/34	285	61	25	0	86	0	8	0	8	0	0	0	0	0	0	0	0	0	0	0	0	0	0	0	0	0	0	0	0	0	0	0	0	93	0
	LV 7/28	279	62	58	0	120	1	34	0	35	0	0	0	0	0	0	0	0	0	0	0	0	0	0	0	0	0	0	0	0	0	0	1	1	211	0
Berriasian	LV 7/25	276	22	18	0	40	0	6	0	6	0	0	0	0	0	0	0	0	0	0	0	0	0	0	0	0	0	0	0	0	0	0	0	0	187	1
	LV 7/16	267	66	30	0	96	5	40	0	45	0	2	0	2	0	0	0	0	0	0	0	0	0	0	0	0	0	0	0	0	0	2	2	4	195	0
	LV 6/65	258	81	112	0	193	1	46	0	47	0	0	0	0	0	0	0	0	0	0	0	0	0	0	0	0	0	0	0	0	0	0	0	0	201	0
	LV 6/55	248	80	112	0	192	5	49	0	54	0	0	0	0	0	0	0	0	0	0	0	0	0	0	0	0	0	0	0	0	0	0	0	0	222	0
	LV 6/50	243	76	177	0	253	8	50	0	58	0	1	0	1	0	0	0	0	0	0	0	0	0	0	0	0	0	0	0	0	0	0	0	0	235	0
	LV 6/34	227	113	154	0	267	3	46	0	49	0	0	0	0	0	0	0	0	0	0	0	0	0	0	0	0	0	0	0	0	0	0	0	0	191	0
	LV 6/29	222	63	102	0	165	3	16	0	19	0	0	0	0	0	0	0	0	0	0	0	0	0	0	0	0	0	0	0	0	0	0	0	0	200	0
	LV 6/20	213	91	123	0	214	10	30	0	40	0	3	0	3	0	0	0	0	0	0	0	0	0	0	0	0	0	0	0	0	0	0	0	0	100	2
	LV 6/10	203	112	113	0	225	10	31	0	41	0	0	0	0	0	0	0	0	0	0	0	0	0	0	0	0	0	0	0	0	0	0	0	0	152	0
	LV 5/97	197	117	154	0	271	7	27	0	34	0	0	0	0	0	0	0	0	0	0	0	0	0	0	0	0	0	0	0	0	0	0	0	0	130	0
	LV 5/75	169	132	219	0	351	2	8	0	10	0	0	0	0	0	0	0	0	0	0	0	0	0	0	0	0	0	0	0	0	0	0	0	0	100	0
	LV 5/40	134	210	212	0	422	2	23	0	25	0	0	0	0	0	0	0	0	0	0	0	0	0	0	0	0	0	0	0	0	0	0	0	0	107	0
	LV 5/35	129	154	147	0	301	1	23	0	24	0	0	0	0	0	0	0	0	0	0	0	0	0	0	0	0	0	0	0	0	0	0	0	0	103	0
	LV 5/32	126	133	120	0	253	0	13	0	13	0	0	1	1	0	0	0	0	0	0	0	0	0	0	0	0	0	0	0	0	0	0	0	0	134	0
	LV 5/30	124	130	119	0	249	3	17	0	20	0	0	1	1	0	0	0	0	0	0	0	0	0	0	0	0	0	0	0	0	0	0	0	0	157	0
	LV 5/28	122	96	185	0	281	2	8	0	10	0	0	0	0	0	0	0	0	0	0	0	0	0	0	0	0	0	0	0	0	0	0	0	0	125	0
	LV 5/26	120	125	187	0	312	0	17	0	17	0	0	0	0	0	0	0	0	0	0	0	0	0	0	0	0	0	0	0	0	0	0	0	0	125	0
	LV 5/24	118	102	165	0	267	0	10	0	10	0	0	0	0	0	0	0	0	0	0	0	0	0	0	0	0	0	0	0	0	0	0	0	0	146	0
	LV 5/22	116	153	135	0	288	3	23	0	26	0	0	0	0	0	0	0	0	0	0	0	0	0	0	0	0	0	0	0	0	0	0	0	0	146	0
	LV 5/20	114	135	166	0	301	0	22	0	22	0	0	0	0	0	0	0	0	0	0	0	0	0	0	0	0	0	0	0	0	0	0	0	0	142	0
	LV 5/19	113	171	129	0	300	3	26	0	29	0	0	0	0	0	0	0	0	0	0	0	0	0	0	0	0	0	0	0	0	0	0	0	0	133	0
	LV 5/17	111	100	176	0	276	0	10	0	10	0	0	0	0	0	0	0	0	0	0	0	0	0	0	0	0	0	0	0	0	0	0	0	0	206	0
	LV 5/15	109	131	193	0	324	0	3	0	3	0	0	0	0	0	0	0	0	0	0	0	0	0	0	0	0	0	0	0	0	0	0	0	0	123	0
	LV 5/14	108	148	126	0	274	0	7	0	7	0	0	0	0	0	0	0	0	0	0	0	0	0	0	0	0	0	0	0	0	0	0	0	0	141	2
	LV 5/12	106	133	102	0	235	0	17	0	17	0	0	0	0	0	0	0	0	0	0	0	0	0	0	0	0	0	0	0	0	0	0	0	0	113	2
	LV 5/7	101	149	181	0	330	0	10	0	10	0	0	0	0	0	0	0	0	0	0	0	0	0	0	0	0	0	0	0	0	0	0	0	0	33	11
	LV 5/5	99	121	312	0	433	0	7	0	7	0	0	0	0	0	0	0	0	0	0	0	0	0	0	0	0	0	0	0	0	0	0	0	0	8	66
	LV 5/3	97	82	174	0	256	0	8	0	8	0	0	0	0	0	0	0	0	0	0	0	0	0	0	0	0	0	0	0	0	0	0	0	0	48	162
	LV 5/1	95	50	52	0	102	11	49	0	60	0	0	0	0	0	0	0	0	0	0	0	0	0	0	0	0	0	0	0	0	0	0	0	0	241	8
	LV 4/18	91	70	112	0	182	11	18	0	29	1	1	0	2	0	0	0	0	0	0	0	0	0	0	0	0	0	0	0	0	0	0	0	0	171	14
	LV 4/6	79	38	44	0	82	56	125	0	181	3	3	0	6	0	0	0	0	0	0	0	0	0	0	0	0	0	0	0	0	0	0	0	0	10	5
Tithonian	LV 3/66	56	52	62	0	114	4	13	0	17	0	0	0	0	0	0	0	0	0	0	0	0	0	0	0	0	0	0	0	0	0	0	0	0	14	29
	LV 3/63	53	14	38	0	52	2	35	0	37	0	0	3	3	0	0	0	0	0	0	0	0	0	0	0	0	0	0	0	0	0	1	0	1	208	7
	LV 3/58	48	42	10	0	52	23	54	0	77	0	0	0	0	0	0	0	0	0	0	0	0	0	0	0	0	0	0	0	0	0	0	0	0	140	16
	LV 3/56,5	46,5	55	40	0	95	7	39	0	46	0	2	0	2	0	0	0	0	0	0	0	0	0	0	0	0	0	0	0	0	0	0	0	0	114	33
	LV 3/55	45	2	29	0	31	0	3	0	3	0	0	0	0	0	0	0	0	0	0	0	0	0	1	0	1	0	0	1	1	0	0	11	11	224	27
	LV 3/53	43	6	47	0	53	0	2	0	2	0	0	1	1	0	0	0	0	0	0	0	0	0	0	0	0	0	1	0	1	0	0	3	3	195	22
	LV 3/52	42,6	4	87	0	91	0	1	0	1	0	0	0	0	0	0	0	0	0	0	0	0	0	0	1	1	0	0	0	0	0	0	4	4	122	43
	LV 3/50	42,3	7	96	0	103	0	1	0	1	0	0	0	0	0	0	0	0	0	0	0	0	0	0	0	0	0	0	0	0	0	0	4	4	114	53
	LV 3/48	42	2	39	0	41	0	5	0	5	0	2	4	6	0	0	0	0	0	0	0	0	0	0	0	0	0	0	0	0	0	4	4	8	130	21
	LV 3/46	41,5	3	52	0	55	0	1	0	1	0	0	0	0	0	0	0	0	0	0	0	0	0	0	0	0	0	0	0	0	0	0	3	3	178	38
	LV 3/44	41	0	77	0	77	0	1	0	1	0	0	0	0	0	0	0	0	0	0	0	0	0	0	0	0	0	0	0	0	0	0	2	2	261	41
	LV 3/42	40,5	0	19	0	19	1	0	0	1	0	0	0	0	0	0	0	0	0	0	0	0	0	0	1	1	0	0	0	0	0	1	1	2	69	6
	LV 3/40	40	7	41		48	0	0	0	0	0	0	0	0	0	0	0	0	0	0	0	1	0	0	0	0	0	0	2	2	0	2	8	10	176	40

Lo Valdés

AOM	marine												diverse													
	rine phytoplankt				Zoomorphs				Zooclasts					mineral residues												
marine/sensu stricto	Dinocysts	Acritarchs	Prasinophytes	Leiospheres	foraminiferal test linings				Bivalves, Scolecodonts, Fungi				Filaments	Quartz	Pyrite	others	Glendonites									
					A	B	C	sum	A	B	C	sum						Totals	Dinocysts	%	Acritarchs	%	Foraminifera	%	Leiospheres	%
0	0	0	0	0	0	0	0	0	0	0	0	0	0	77	0	0		450	0,00	0,00	0,00	0,00	0,00	0,11	0,00	0,00
0	0	0	0	0	0	0	0	0	0	0	0	0	0	85	3	1		427	0,00	0,00	0,00	0,00	0,00	0,29	0,00	0,00
0	0	0	0	0	0	0	0	0	0	0	0	0	1	100	6	0		368	0,00		0,00		0,00		0,00	
0	0	0	0	0	0	0	0	0	0	0	0	0	0	170	7	0		431	0,00		0,00		0,00		0,00	
0	0	0	0	0	0	0	0	0	0	0	0	0	0	80	21	0		479	0,00		0,00		0,00		0,00	
0	0	0	0	0	0	0	0	0	0	0	0	0	0	140	29	0		436	0,00		0,00		0,00		0,00	
0	0	0	0	0	0	0	0	0	0	0	0	0	0	68	43	1		425	0,00		0,00		0,00		0,00	
0	0	0	0	0	0	0	0	0	0	0	0	0	3	15	12	15		330	0,00		0,00		0,00		0,00	
0	0	0	0	0	0	0	0	0	0	0	0	0	18	98	5	4		352	0,00		0,00		0,00		0,00	
0	0	0	0	0	0	0	0	0	1	0	0	1	18	93	12	39		154	0,00		0,00		0,00		0,00	
0	0	0	0	0	0	0	1	1	0	0	0	0	0	145	5	6		378	0,00		0,00		0,26		0,00	
0	0	0	0	0	2	1	1	4	0	0	0	0	3	28	7	7		398	0,00		0,00		1,01		0,00	
0	0	0	0	0	0	0	0	0	0	0	0	0	0	72	11	25		366	0,00	0,00	0,00	0,00	0,00	0,03	0,00	0,00
0	0	0	0	0	0	0	0	0	0	0	0	0	0	15	35	38		359	0,00	0,00	0,00	0,00	0,00	0,10	0,00	0,00
0	0	0	0	0	0	0	0	0	0	0	0	0	49	46	7	8	x	430	0,00		0,00		0,00		0,00	
0	0	0	0	0	0	0	1	1	0	0	0	0	0	345	13	9	x	303	0,00		0,00		0,33		0,00	
0	0	0	0	0	0	0	0	0	0	0	0	0	5	488	10	15		346	0,00		0,00		0,00		0,00	
0	0	0	0	0	0	0	0	0	0	0	0	0	0	584	13	9		404	0,00		0,00		0,00		0,00	
0	0	0	0	0	0	0	0	0	0	0	0	0	0	612	6	3		404	0,00		0,00		0,00		0,00	
0	0	0	0	0	0	0	0	0	0	0	0	0	3	409	93	43	x	315	0,00		0,00		0,00		0,00	
0	0	0	0	0	0	0	0	0	0	0	0	0	0	152	8	2		384	0,00		0,00		0,00		0,00	
0	0	0	0	0	0	0	0	0	0	0	0	0	0	679	18	35	x	228	0,00		0,00		0,00		0,00	
0	0	0	0	0	0	0	0	0	0	0	0	0	0	518	62	3		187	0,00		0,00		0,00		0,00	
0	0	0	0	0	0	0	0	0	0	0	0	0	0	335	22	1		367	0,00		0,00		0,00		0,00	
0	0	0	0	0	0	0	0	0	0	0	0	0	0	352	0	3		234	0,00	0,00	0,00	0,00	0,00	0,00	0,00	0,00
0	0	0	0	0	0	0	0	0	0	0	0	0	0	209	129	11		342	0,00	0,00	0,00	0,00	0,00	0,00	0,00	0,00
0	0	0	0	0	0	0	0	0	0	0	0	0	0	22	39	0		441	0,00		0,00		0,00		0,00	
0	0	0	0	0	0	0	0	0	0	0	0	0	0	22	33	0		468	0,00		0,00		0,00		0,00	
0	0	0	0	0	0	0	0	0	0	0	0	0	0	8	2	3		547	0,00		0,00		0,00		0,00	
0	0	0	0	0	0	0	0	0	0	0	0	0	0	175	47	62		507	0,00		0,00		0,00		0,00	
0	0	0	0	0	0	0	0	0	0	0	0	0	0	131	43	0		384	0,00		0,00		0,00		0,00	
0	0	0	0	0	0	0	0	0	0	0	0	0	0	242	195	17		359	0,00		0,00		0,00		0,00	
0	0	0	0	0	0	0	0	0	0	0	0	0	0	40	22	12		418	0,00		0,00		0,00		0,00	
0	0	0	0	0	0	0	0	0	0	0	0	0	0	35	13	9		435	0,00		0,00		0,00		0,00	
0	0	0	0	0	0	0	0	0	0	0	0	0	0	0	0	0		461	0,00		0,00		0,00		0,00	
0	0	0	0	0	0	0	0	0	0	0	0	0	0	0	5	0		554	0,00		0,00		0,00		0,00	
0	0	0	0	0	0	0	0	0	0	0	0	0	0	0	2	0		428	0,00		0,00		0,00		0,00	
0	0	0	0	0	0	0	0	0	0	0	0	0	0	0	5	0		401	0,00		0,00		0,00		0,00	
0	0	0	0	0	0	0	0	0	0	0	0	0	0	0	7	0		427	0,00		0,00		0,00		0,00	
0	0	0	0	0	0	0	0	0	0	0	0	0	0	0	2	0		416	0,00		0,00		0,00		0,00	
0	0	0	0	0	0	0	0	0	0	0	0	0	0	0	0	0		454	0,00		0,00		0,00		0,00	
0	0	0	0	0	0	0	0	0	0	0	0	0	0	0	2	0		423	0,00		0,00		0,00		0,00	
0	0	0	0	0	0	0	0	0	0	0	0	0	0	0	2	0		460	0,00		0,00		0,00		0,00	
0	0	0	0	0	0	0	0	0	0	0	0	0	0	0	1	0		465	0,00		0,00		0,00		0,00	
0	0	0	0	0	0	0	0	0	0	0	0	0	0	0	0	0		462	0,00		0,00		0,00		0,00	
0	0	0	0	0	0	0	0	0	0	0	0	0	0	0	9	2		492	0,00		0,00		0,00		0,00	
0	0	0	0	0	0	0	0	0	0	0	0	0	0	0	4	0		450	0,00		0,00		0,00		0,00	
0	0	0	0	0	0	0	0	0	0	0	0	0	0	0	15	0		424	0,00		0,00		0,00		0,00	
0	0	0	0	0	0	0	0	0	0	0	0	0	0	0	9	3		367	0,00		0,00		0,00		0,00	
0	0	0	0	0	0	0	0	0	0	0	0	0	0	0	4	0		384	0,00		0,00		0,00		0,00	
0	0	0	0	0	0	0	0	0	0	0	0	0	0	0	0	0		514	0,00		0,00		0,00		0,00	
0	0	0	0	0	0	0	0	0	0	0	0	0	0	0	0	0	x	474	0,00		0,00		0,00		0,00	
0	0	0	0	0	0	0	0	0	0	0	0	0	6	0	0	0		417	0,00		0,00		0,00		0,00	
0	0	0	0	0	0	0	0	0	0	0	0	0	0	0	2	0		398	0,00		0,00		0,00		0,00	
0	0	0	0	0	0	0	0	0	0	0	0	0	0	0	0	0	x	284	0,00		0,00		0,00		0,00	
0	0	0	0	0	0	0	0	0	0	0	0	0	0	0	1	0	x	174	0,00	0,00	0,00	0,00	0,00	0,29	0,00	0,09
0	0	0	0	0	0	0	0	0	0	0	0	0	0	0	6	0		308	0,00	0,00	0,00	0,00	0,00	0,48	0,00	0,36
0	0	0	0	0	0	0	0	0	15	0	0	15	7	0	0	0	x	307	0,00		0,00		0,00		0,00	
0	0	0	0	0	2	0	0	2	0	0	0	0	30	0	4	0	x	322	0,00		0,00		0,62		0,00	
0	0	0	0	0	0	0	2	2	0	0	0	0	0	0	6	1	x	300	0,00		0,00		0,67		0,00	
0	0	0	0	0	0	0	1	1	0	1	0	1	0	0	3	0		279	0,00		0,00		0,36		0,00	
0	0	0	0	0	0	0	0	0	0	3	5	8	0	0	9	3	x	270	0,00		0,00		0,00		0,00	
0	0	0	0	0	0	0	0	0	0	0	0	0	0	0	18	7	x	275	0,00		0,00		0,00		0,00	
0	0	0	0	0	0	0	0	0	0	2	1	3	0	0	16	0	x	214	0,00		0,00		0,00		0,00	
0	0	0	0	0	0	0	0	0	0	0	0	0	0	0	8	10		275	0,00		0,00		0,00		0,00	
0	0	0	0	0	0	0	0	0	3	0	0	3	0	0	5	13	x	385	0,00		0,00		0,00		0,00	
0	0	0	0	0	0	0	0	0	0	0	3	3	189	0	7	9		290	0,00		0,00		0,00		0,00	
0	0	0	0	0	1	1	1	3	0	0	3	3	0	0	20	6	x	283	0,00		0,00		1,06		0,00	

Lo Valdés

Age	Sample	Depth (m)	marine AOM	%	terrestrial AOM translucent	%	terrestrial AOM opaque	%	AOMT total	%	Sporomorphs	Sporomorphs %		Cutinite %	
Hauterivian	LV 9/149	539	0,00	0,00	11,56	24,59	4,44	0,55	16,00	25,14	0	0,00	0,83	0,22	0,50
	LV 9/143	533	0,00	0,00	5,62	15,98	0,00	1,25	5,62	15,64	1	0,23	1,73	0,00	1,15
	LV 9/129	519	0,00		9,78		0,00		9,78		0	0,00		0,54	
	LV 9/115	505	0,00		50,81		0,00		50,81		0	0,00		0,00	
	LV 9/102	492	0,00		33,61		0,42		34,03		0	0,00		0,00	
	LV 9/87	477	0,00		23,17		0,69		23,85		0	0,00		0,00	
	LV 9/69	459	0,00		20,00		0,24		20,24		8	1,88		0,00	
	LV 9/32	422	0,00		14,55		0,30		14,85		0	0,00		0,91	
	LV 9/24	414	0,00		32,39		0,00		32,39		3	0,85		0,00	
	LV 9/20	410	0,00		33,12		0,00		33,12		1	0,65		0,00	
	LV 9/12	402	0,00		8,20		0,53		8,73		1	0,26		0,26	
	LV 9/5	395	0,00		52,26		0,00		52,26		24	6,03		4,02	
Valanginian	LV 8/103	388	0,00	0,00	32,51	45,86	0,00	0,00	32,51	45,86	5	1,37	1,24	0,82	0,26
	LV 8/99	384	0,00	0,00	54,04	16,04	0,00	0,00	54,04	16,04	4	1,11	2,26	0,00	0,39
	LV 8/91	376	0,00		15,12		0,00		15,12		2	0,47		0,00	
	LV 8/83	368	0,00		53,47		0,00		53,47		1	0,33		0,00	
	LV 8/59	344	0,00		54,05		0,00		54,05		5	1,45		0,58	
	LV 8/54	339	0,00		56,19		0,00		56,19		2	0,50		0,00	
	LV 8/46	331	0,00		74,26		0,00		74,26		3	0,74		0,00	
	LV 8/41	326	0,00		30,16		0,00		30,16		26	8,25		0,95	
	LV 8/36	321	0,00		40,89		0,00		40,89		0	0,00		0,78	
	LV 8/20-36	310	0,00		32,46		0,00		32,46		1	0,44		0,00	
	LV 7/34	285	0,00		49,73		0,00		49,73		0	0,00		0,00	
	LV 7/28	279	0,00		57,49		0,00		57,49		1	0,27		0,00	
Berriasian	LV 7/25	276	0,00	0,00	79,91	33,32	0,43	1,91	80,34	35,23	0	0,00	0,04	0,00	0,15
	LV 7/16	267	0,00	0,00	57,02	16,28	0,00	6,45	57,02	15,00	4	1,17	0,21	0,58	0,42
	LV 6/65	258	0,00		45,58		0,00		45,58		0	0,00		0,00	
	LV 6/55	248	0,00		47,44		0,00		47,44		0	0,00		0,00	
	LV 6/50	243	0,00		42,96		0,00		42,96		0	0,00		0,18	
	LV 6/34	227	0,00		37,67		0,00		37,67		0	0,00		0,00	
	LV 6/29	222	0,00		52,08		0,00		52,08		0	0,00		0,00	
	LV 6/20	213	0,00		27,86		0,56		28,41		0	0,00		0,84	
	LV 6/10	203	0,00		36,36		0,00		36,36		0	0,00		0,00	
	LV 5/97	197	0,00		29,89		0,00		29,89		0	0,00		0,00	
	LV 5/75	169	0,00		21,69		0,00		21,69		0	0,00		0,00	
	LV 5/40	134	0,00		19,31		0,00		19,31		0	0,00		0,00	
	LV 5/35	129	0,00		24,07		0,00		24,07		0	0,00		0,00	
	LV 5/32	126	0,00		33,42		0,00		33,42		0	0,00		0,25	
	LV 5/30	124	0,00		36,77		0,00		36,77		0	0,00		0,23	
	LV 5/28	122	0,00		30,05		0,00		30,05		0	0,00		0,00	
	LV 5/26	120	0,00		27,53		0,00		27,53		0	0,00		0,00	
	LV 5/24	118	0,00		34,52		0,00		34,52		0	0,00		0,00	
	LV 5/22	116	0,00		31,74		0,00		31,74		0	0,00		0,00	
	LV 5/20	114	0,00		30,54		0,00		30,54		0	0,00		0,00	
	LV 5/19	113	0,00		28,79		0,00		28,79		0	0,00		0,00	
	LV 5/17	111	0,00		41,87		0,00		41,87		0	0,00		0,00	
	LV 5/15	109	0,00		27,33		0,00		27,33		0	0,00		0,00	
	LV 5/14	108	0,00		33,25		0,47		33,73		0	0,00		0,00	
	LV 5/12	106	0,00		30,79		0,54		31,34		0	0,00		0,00	
	LV 5/7	101	0,00		8,59		2,86		11,46		0	0,00		0,00	
	LV 5/5	99	0,00		1,56		12,84		14,40		0	0,00		0,00	
	LV 5/3	97	0,00		10,13		34,18		44,30		0	0,00		0,00	
	LV 5/1	95	0,00		57,79		1,92		59,71		0	0,00		0,00	
	LV 4/18	91	0,00		42,96		3,52		46,48		0	0,00		0,50	
	LV 4/6	79	0,00		3,52		1,76		5,28		0	0,00		2,11	
Tithonian	LV 3/66	56	0,00	0,00	8,05	56,23	16,67	9,62	24,71	65,85	0	0,00	2,68	0,00	0,89
	LV 3/63	53	0,00	0,00	67,53	22,54	2,27	4,65	69,81	21,05	1	0,32	2,59	0,97	1,29
	LV 3/58	48	0,00		45,60		5,21		50,81		0	0,00		0,00	
	LV 3/56,5	46,5	0,00		35,40		10,25		45,65		0	0,00		0,62	
	LV 3/55	45	0,00		74,67		9,00		83,67		13	4,33		0,00	
	LV 3/53	43	0,00		69,89		7,89		77,78		4	1,43		0,36	
	LV 3/52	42,6	0,00		45,19		15,93		61,11		5	1,85		0,00	
	LV 3/50	42,3	0,00		41,45		19,27		60,73		4	1,45		0,00	
	LV 3/48	42	0,00		60,75		9,81		70,56		8	3,74		2,80	
	LV 3/46	41,5	0,00		64,73		13,82		78,55		3	1,09		0,00	
	LV 3/44	41	0,00		67,79		10,65		78,44		2	0,52		0,00	
	LV 3/42	40,5	0,00		23,79		2,07		25,86		3	1,03		0,00	
	LV 3/40	40	0,00		62,19		14,13		76,33		12	4,24		0,00	

Lo Valdés

Age	Sample	Depth (m)	Inertinite A	%	Inertinite B	%	Inertinite total	%	Vitrinite A	%	Vitrinite B	%	Vitrinite total	%	Phytoclasts	%
Hauterivian	LV 9/149	539	27,78	30,31	24,44	27,07	52,22	57,38	6,67	2,86	24,89	11,52	31,56	14,37	84,00	72,25
	LV 9/143	533	37,70	12,60	35,60	13,47	73,30	18,45	6,56	2,14	14,29	9,74	20,84	10,95	94,15	18,03
	LV 9/129	519	35,87		40,76		76,63		4,89		7,88		12,77		89,95	
	LV 9/115	505	26,22		16,47		42,69		0,70		5,80		6,50		49,19	
	LV 9/102	492	26,10		36,95		63,05		1,04		1,88		2,92		65,97	
	LV 9/87	477	25,69		46,33		72,02		0,46		3,67		4,13		76,15	
	LV 9/69	459	23,29		45,88		69,18		1,41		7,29		8,71		77,88	
	LV 9/32	422	24,24		21,21		45,45		2,73		35,15		37,88		84,24	
	LV 9/24	414	33,24		21,31		54,55		1,42		5,68		7,10		61,65	
	LV 9/20	410	31,82		11,69		43,51		3,25		7,14		10,39		53,90	
	LV 9/12	402	62,70		16,67		79,37		2,38		8,73		11,11		90,74	
	LV 9/5	395	9,05		7,54		16,58		2,76		15,83		18,59		39,20	
Valanginian	LV 8/103	388	27,60	22,84	22,13	13,48	49,73	36,31	0,82	3,84	14,75	11,30	15,57	15,14	66,12	51,72
	LV 8/99	384	17,83	6,76	17,55	6,20	35,38	10,39	0,56	5,76	8,91	5,17	9,47	8,36	44,85	13,70
	LV 8/91	376	30,00		23,72		53,72		9,07		10,23		19,30		73,02	
	LV 8/83	368	29,04		9,57		38,61		1,32		5,94		7,26		45,87	
	LV 8/59	344	20,81		9,54		30,35		2,60		9,54		12,14		43,06	
	LV 8/54	339	25,99		4,46		30,45		1,73		11,14		12,87		43,32	
	LV 8/46	331	10,15		3,71		13,86		0,74		10,40		11,14		25,00	
	LV 8/41	326	16,83		16,19		33,02		1,90		24,76		26,67		60,63	
	LV 8/36	321	26,56		11,20		37,76		7,29		13,28		20,57		59,11	
	LV 8/20-36	310	19,74		14,47		34,21		19,74		13,16		32,89		67,11	
	LV 7/34	285	32,62		13,37		45,99		0,00		4,28		4,28		50,27	
	LV 7/28	279	16,89		15,80		32,70		0,27		9,26		9,54		42,23	
Berriasian	LV 7/25	276	9,40	25,13	7,69	31,75	17,09	56,88	0,00	1,32	2,56	6,33	2,56	7,66	19,66	64,69
	LV 7/16	267	19,30	8,37	8,77	11,32	28,07	16,86	1,46	3,53	11,70	7,70	13,16	11,09	41,81	15,14
	LV 6/65	258	18,37		25,40		43,76		0,23		10,43		10,66		54,42	
	LV 6/55	248	17,09		23,93		41,03		1,07		10,47		11,54		52,56	
	LV 6/50	243	13,89		32,36		46,25		1,46		9,14		10,60		57,04	
	LV 6/34	227	22,29		30,37		52,66		0,59		9,07		9,66		62,33	
	LV 6/29	222	16,41		26,56		42,97		0,78		4,17		4,95		47,92	
	LV 6/20	213	25,35		34,26		59,61		2,79		8,36		11,14		71,59	
	LV 6/10	203	26,79		27,03		53,83		2,39		7,42		9,81		63,64	
	LV 5/97	197	26,90		35,40		62,30		1,61		6,21		7,82		70,11	
	LV 5/75	169	28,63		47,51		76,14		0,43		1,74		2,17		78,31	
	LV 5/40	134	37,91		38,27		76,17		0,36		4,15		4,51		80,69	
	LV 5/35	129	35,98		34,35		70,33		0,23		5,37		5,61		75,93	
	LV 5/32	126	33,17		29,93		63,09		0,00		3,24		3,24		66,58	
	LV 5/30	124	30,44		27,87		58,31		0,70		3,98		4,68		63,23	
	LV 5/28	122	23,08		44,47		67,55		0,48		1,92		2,40		69,95	
	LV 5/26	120	27,53		41,19		68,72		0,00		3,74		3,74		72,47	
	LV 5/24	118	24,11		39,01		63,12		0,00		2,36		2,36		65,48	
	LV 5/22	116	33,26		29,35		62,61		0,65		5,00		5,65		68,26	
	LV 5/20	114	29,03		35,70		64,73		0,00		4,73		4,73		69,46	
	LV 5/19	113	37,01		27,92		64,94		0,65		5,63		6,28		71,21	
	LV 5/17	111	20,33		35,77		56,10		0,00		2,03		2,03		58,13	
	LV 5/15	109	29,11		42,89		72,00		0,00		0,67		0,67		72,67	
	LV 5/14	108	34,91		29,72		64,62		0,00		1,65		1,65		66,27	
	LV 5/12	106	36,24		27,79		64,03		0,00		4,63		4,63		68,66	
	LV 5/7	101	38,80		47,14		85,94		0,00		2,60		2,60		88,54	
	LV 5/5	99	23,54		60,70		84,24		0,00		1,36		1,36		85,60	
	LV 5/3	97	17,30		36,71		54,01		0,00		1,69		1,69		55,70	
	LV 5/1	95	11,99		12,47		24,46		2,64		11,75		14,39		38,85	
	LV 4/18	91	17,59		28,14		45,73		2,76		4,52		7,29		53,52	
	LV 4/6	79	13,38		15,49		28,87		19,72		44,01		63,73		94,72	
Tithonian	LV 3/66	56	29,89	2,99	35,63	16,01	65,52	19,00	2,30	0,50	7,47	6,69	9,77	7,19	75,29	27,08
	LV 3/63	53	4,55	6,50	12,34	11,67	16,88	14,43	0,65	1,47	11,36	15,73	12,01	16,06	29,87	20,10
	LV 3/58	48	13,68		3,26		16,94		7,49		17,59		25,08		42,02	
	LV 3/56,5	46,5	17,08		12,42		29,50		2,17		12,11		14,29		44,41	
	LV 3/55	45	0,67		9,67		10,33		0,00		1,00		1,00		11,33	
	LV 3/53	43	2,15		16,85		19,00		0,00		0,72		0,72		20,07	
	LV 3/52	42,6	1,48		32,22		33,70		0,00		0,37		0,37		34,07	
	LV 3/50	42,3	2,55		34,91		37,45		0,00		0,36		0,36		37,82	
	LV 3/48	42	0,93		18,22		19,16		0,00		2,34		2,34		24,30	
	LV 3/46	41,5	1,09		18,91		20,00		0,00		0,36		0,36		20,36	
	LV 3/44	41	0,00		20,00		20,00		0,00		0,26		0,26		20,26	
	LV 3/42	40,5	0,00		6,55		6,55		0,34		0,00		0,34		6,90	
	LV 3/40	40	2,47		14,49		16,96		0,00		0,00		0,00		16,96	

Lo Valdés

Age	Sample	Depth (m)	Filaments	%	marine OM	%	terrestrial OM	%	Palynomorphs %	OP/TR
Hauterivian	LV 9/149	539	0,00	1,56	0,00	0,11	100,00	99,84	0,00	3,99
	LV 9/143	533	0,00	3,50	0,00	0,29	100,00	0,33	0,23	
	LV 9/129	519	0,27		0,00		100,00		0,27	
	LV 9/115	505	0,00		0,00		100,00		0,00	
	LV 9/102	492	0,00		0,00		100,00		0,00	
	LV 9/87	477	0,00		0,00		100,00		0,00	
	LV 9/69	459	0,00		0,00		100,00		1,88	
	LV 9/32	422	0,91		0,00		100,00		0,91	
	LV 9/24	414	5,11		0,00		100,00		5,97	
	LV 9/20	410	11,69		0,00		99,35		12,34	
	LV 9/12	402	0,00		0,26		99,74		0,53	
	LV 9/5	395	0,75		1,01		98,99		7,79	
Valanginian	LV 8/103	388	0,00	1,15	0,00	0,03	100,00	99,97	1,37	2,40
	LV 8/99	384	0,00	3,26	0,00	0,10	100,00	0,10	1,11	
	LV 8/91	376	11,40		0,00		100,00		11,86	
	LV 8/83	368	0,00		0,33		99,67		0,66	
	LV 8/59	344	1,45		0,00		100,00		2,89	
	LV 8/54	339	0,00		0,00		100,00		0,50	
	LV 8/46	331	0,00		0,00		100,00		0,74	
	LV 8/41	326	0,95		0,00		100,00		9,21	
	LV 8/36	321	0,00		0,00		100,00		0,00	
	LV 8/20-36	310	0,00		0,00		100,00		0,44	
	LV 7/34	285	0,00		0,00		100,00		0,00	
	LV 7/28	279	0,00		0,00		100,00		0,27	
Berriasian	LV 7/25	276	0,00	0,05	0,00	0,00	100,00	100,00	0,00	7,43
	LV 7/16	267	0,00	0,26	0,00	0,00	100,00	0,00	1,17	
	LV 6/65	258	0,00		0,00		100,00		0,00	
	LV 6/55	248	0,00		0,00		100,00		0,00	
	LV 6/50	243	0,00		0,00		100,00		0,00	
	LV 6/34	227	0,00		0,00		100,00		0,00	
	LV 6/29	222	0,00		0,00		100,00		0,00	
	LV 6/20	213	0,00		0,00		100,00		0,00	
	LV 6/10	203	0,00		0,00		100,00		0,00	
	LV 5/97	197	0,00		0,00		100,00		0,00	
	LV 5/75	169	0,00		0,00		100,00		0,00	
	LV 5/40	134	0,00		0,00		100,00		0,00	
	LV 5/35	129	0,00		0,00		100,00		0,00	
	LV 5/32	126	0,00		0,00		100,00		0,00	
	LV 5/30	124	0,00		0,00		100,00		0,00	
	LV 5/28	122	0,00		0,00		100,00		0,00	
	LV 5/26	120	0,00		0,00		100,00		0,00	
	LV 5/24	118	0,00		0,00		100,00		0,00	
	LV 5/22	116	0,00		0,00		100,00		0,00	
	LV 5/20	114	0,00		0,00		100,00		0,00	
	LV 5/19	113	0,00		0,00		100,00		0,00	
	LV 5/17	111	0,00		0,00		100,00		0,00	
	LV 5/15	109	0,00		0,00		100,00		0,00	
	LV 5/14	108	0,00		0,00		100,00		0,00	
	LV 5/12	106	0,00		0,00		100,00		0,00	
	LV 5/7	101	0,00		0,00		100,00		0,00	
	LV 5/5	99	0,00		0,00		100,00		0,00	
	LV 5/3	97	0,00		0,00		100,00		0,00	
	LV 5/1	95	1,44		0,00		100,00		1,44	
	LV 4/18	91	0,00		0,00		100,00		0,00	
	LV 4/6	79	0,00		0,00		100,00		0,00	
Tithonian	LV 3/66	56	0,00	2,85	0,00	0,38	100,00	98,56	0,00	2,64
	LV 3/63	53	0,00	12,13	0,00	0,65	100,00	1,42	0,32	
	LV 3/58	48	2,28		0,00		95,11		2,28	
	LV 3/56,5	46,5	9,32		0,62		99,38		9,94	
	LV 3/55	45	0,00		0,67		99,33		5,00	
	LV 3/53	43	0,00		0,36		99,28		1,79	
	LV 3/52	42,6	0,00		0,00		97,04		1,85	
	LV 3/50	42,3	0,00		0,00		100,00		1,45	
	LV 3/48	42	0,00		0,00		98,60		3,74	
	LV 3/46	41,5	0,00		0,00		100,00		1,09	
	LV 3/44	41	0,00		0,00		99,22		0,52	
	LV 3/42	40,5	65,17		0,00		98,97		66,21	
	LV 3/40	37	0,00		1,06		97,88		5,30	

Lo Valdés			terrestrial																														AOM	
			parts of vascular plants												Pollen						Pollen	Spores													
			phytoclasts												Sporomorphs																				
			Inertinite				Vitrinite				Cutinite				nonsaccate	monosaccate					bisaccate	monosaccate	monolete				trilete				indet				terrestrial, translucent	terrestrial opaque
Age	Preservation		A	B	C	sum	A	B	C	sum	A	B	C	sum		A	B	C	sum			A	B	C	sum	A	B	C	sum	A	B	C	sum		
	Sample	Depth (m)																																		
Tithonian	LV 3/37	37	0	51	0	51	0	1	0	1	0	0	0	0	0	0	0	0	0	0	0	0	0	0	0	0	0	0	0	0	0	0	1	1	241	26
	LV 3/35	35	0	43	0	43	0	3	0	3	0	0	0	0	0	0	0	0	0	0	0	0	0	0	0	0	0	0	0	0	0	0	2	2	203	22
	LV 3/31	31	0	53	0	53	0	4	0	4	0	1	1	2	0	0	0	0	0	0	1	0	0	0	0	0	0	0	0	0	2	5	7	122	35
	LV 3/28	28	0	20	0	20	0	3	0	3	0	0	2	2	0	0	0	0	0	0	0	0	0	0	0	0	0	0	0	0	3	2	5	10	113	18
	LV 3/26	26	0	21	0	21	0	3	0	3	0	0	1	1	0	0	0	0	0	0	1	0	0	0	0	0	0	0	0	0	0	2	3	5	126	17
	LV 3/23	23	0	37	0	37	0	2	0	2	0	1	4	5	0	0	0	0	0	0	0	0	0	0	0	0	0	2	2	4	0	4	9	13	232	18
	LV 3/21	21	0	31	0	31	0	2	0	2	0	0	0	0	0	0	0	0	0	0	0	1	3	0	4	0	0	0	0	0	11	5	16	115	18
	LV 3/19	19	0	1	0	1	0	0	0	0	0	0	0	0	0	0	0	0	0	0	0	0	0	0	0	0	0	1	1	0	0	16	16	217	21
	LV 3/17	17	0	12	0	12	0	0	0	0	0	0	2	2	0	0	0	0	0	0	1	0	0	0	0	0	1	0	1	0	0	1	1	256	0
	LV 3/15	15	5	16	0	21	0	9	0	9	0	5	2	7	0	0	0	0	0	0	1	0	0	0	0	0	0	2	2	0	5	7	12	172	11
	LV 3/13	13	3	46	0	49	0	3	0	3	0	1	2	3	0	0	0	0	0	0	0	0	0	0	0	0	0	1	1	0	2	8	10	175	28
	LV 3/10	10	8	30	0	38	2	1	0	3	0	2	0	2	0	0	0	0	0	0	0	0	0	0	0	0	0	0	0	0	0	3	3	105	25
	LV 3/6	6	0	19	0	19	0	5	0	5	0	0	2	2	0	0	0	0	0	0	1	0	0	0	0	0	0	0	0	0	3	3	6	113	9
	LV 3/3	3	4	194	0	198	0	2	0	2	0	1	4	5	0	0	0	0	0	0	1	0	0	0	0	0	0	0	0	0	0	1	1	105	23
	LV 3/1-30	1	3	9	0	12	0	167	0	167	0	2	5	7	0	0	0	0	0	0	0	0	2	0	2	0	0	2	2	1	7	4	12	22	44
	LV 3/0,2	0,2	1	15	0	16	1	142	0	143	0	8	5	13	0	0	0	0	0	0	0	0	0	0	0	0	0	0	0	0	1	0	1	24	24

Lo Valdés

AOM	marine													diverse													
	rine phytoplankt				Zoomorphs				Zooclasts						mineral residues												
marine/sensu stricto	Dinocysts	Acritarchs	Prasinophytes	Leiospheres	foraminiferal test linings				Bivalves, Scolecodonts, Fungi					Filaments	Quartz	Pyrite	others	Glendonites									
					A	B	C	sum	A	B	C	sum							Totals	Dinocysts %		Acritarchs %		Foraminifera %		Leiospheres %	
0	0	0	0	0	0	0	0	0	0	0	0	0		0	0	9	2		320	0,00		0,00		0,00		0,00	
0	0	0	0	0	0	0	0	0	0	0	0	0		0	0	15	5	x	273	0,00		0,00		0,00		0,00	
0	0	0	0	0	0	0	1	1	0	3	2	5		0	0	33	25		230	0,00		0,00		0,43		0,00	
0	0	0	0	0	0	0	0	0	0	2	0	2		0	0	4	0		168	0,00		0,00		0,00		0,00	
0	0	0	0	0	0	0	0	0	0	1	0	1		0	0	13	0	x	175	0,00		0,00		0,00		0,00	
0	0	0	0	0	0	1	0	1	3	1	0	4		0	0	0	0		316	0,00		0,00		0,32		0,00	
0	0	0	0	0	0	1	1	2	2	0	0	2		0	0	0	0	x	190	0,00		0,00		1,05		0,00	
0	0	0	0	0	0	0	0	0	0	0	0	0		0	0	0	0		256	0,00		0,00		0,00		0,00	
0	0	0	0	0	0	0	0	0	0	0	4	4		0	0	0	0		277	0,00		0,00		0,00		0,00	
0	0	0	0	2	1	0	0	1	4	0	0	4		2	0	3	0		244	0,00		0,00		0,41		0,82	
0	0	0	0	5	2	0	0	2	8	0	0	8		0	0	9	1		284	0,00		0,00		0,70		1,76	
0	0	0	0	0	0	0	0	0	0	2	1	3		1	0	5	0		180	0,00		0,00		0,00		0,00	
0	0	0	0	0	0	1	0	1	0	2	1	3		0	0	0	0	x	159	0,00		0,00		0,63		0,00	
0	0	0	0	0	0	0	0	0	1	7	1	9		1	0	8	0	x	345	0,00		0,00		0,00		0,00	
0	0	0	0	0	1	3	2	6	0	0	0	0		12	5	7	0		286	0,00		0,00		2,10		0,00	
0	0	0	0	0	0	0	0	0	0	0	0	0		0	17	4	6		221	0,00		0,00		0,00		0,00	

Lo Valdés

Age	Sample	Depth (m)	marine AOM %	terrestrial AOM % translucent	terrestrial AOM % opaque	AOMT % total	Sporomorphs	Sporomorphs %	Cutinite %
Tithonian	LV 3/37	37	0,00	75,31	8,13	83,44	1	0,31	0,00
	LV 3/35	35	0,00	74,36	8,06	82,42	2	0,73	0,00
	LV 3/31	31	0,00	53,04	15,22	68,26	7	3,04	0,87
	LV 3/28	28	0,00	67,26	10,71	77,98	10	5,95	1,19
	LV 3/26	26	0,00	72,00	9,71	81,71	5	2,86	0,57
	LV 3/23	23	0,00	73,42	5,70	79,11	17	5,38	1,58
	LV 3/21	21	0,00	60,53	9,47	70,00	20	10,53	0,00
	LV 3/19	19	0,00	84,77	8,20	92,97	17	6,64	0,00
	LV 3/17	17	0,00	92,42	0,00	92,42	2	0,72	0,72
	LV 3/15	15	0,00	70,49	4,51	75,00	14	5,74	2,87
	LV 3/13	13	0,00	61,62	9,86	71,48	11	3,87	1,06
	LV 3/10	10	0,00	58,33	13,89	72,22	3	1,67	1,11
	LV 3/6	6	0,00	71,07	5,66	76,73	6	3,77	1,26
	LV 3/3	3	0,00	30,43	6,67	37,10	1	0,29	1,45
	LV 3/1-30	1	0,00	7,69	15,38	23,08	16	5,59	2,45
	LV 3/0,2	0,2	0,00	10,86	10,86	21,72	1	0,45	5,88

Lo Valdés

Age	Sample	Depth (m)	Inertinite A %	Inertinite B %	Inertinite % total	Vitrinite A %	Vitrinite B %	Vitrinite % total	Phytoclasts %
Tithonian	LV 3/37	37	0,00	15,94	15,94	0,00	0,31	0,31	16,25
	LV 3/35	35	0,00	15,75	15,75	0,00	1,10	1,10	16,85
	LV 3/31	31	0,00	23,04	23,04	0,00	1,74	1,74	25,65
	LV 3/28	28	0,00	11,90	11,90	0,00	1,79	1,79	14,88
	LV 3/26	26	0,00	12,00	12,00	0,00	1,71	1,71	14,29
	LV 3/23	23	0,00	11,71	11,71	0,00	0,63	0,63	13,92
	LV 3/21	21	0,00	16,32	16,32	0,00	1,05	1,05	17,37
	LV 3/19	19	0,00	0,39	0,39	0,00	0,00	0,00	0,39
	LV 3/17	17	0,00	4,33	4,33	0,00	0,00	0,00	5,05
	LV 3/15	15	2,05	6,56	8,61	0,00	3,69	3,69	15,16
	LV 3/13	13	1,06	16,20	17,25	0,00	1,06	1,06	19,37
	LV 3/10	10	4,44	16,67	21,11	1,11	0,56	1,67	23,89
	LV 3/6	6	0,00	11,95	11,95	0,00	3,14	3,14	16,35
	LV 3/3	3	1,16	56,23	57,39	0,00	0,58	0,58	59,42
	LV 3/1-30	1	1,05	3,15	4,20	0,00	58,39	58,39	65,03
	LV 3/0,2	0,2	0,45	6,79	7,24	0,45	64,25	64,71	77,83

Lo Valdés

Age	Sample	Depth (m)	Filaments %	marine OM %	terrestrial OM %	Palynomorphs %
Tithonian	LV 3/37	37	0,00	0,00	100,00	0,31
	LV 3/35	35	0,00	0,00	100,00	0,73
	LV 3/31	31	0,00	0,43	97,39	3,48
	LV 3/28	28	0,00	0,00	98,81	5,95
	LV 3/26	26	0,00	0,00	99,43	2,86
	LV 3/23	23	0,00	0,32	98,42	5,70
	LV 3/21	21	0,00	1,05	97,89	11,58
	LV 3/19	19	0,00	0,00	100,00	6,64
	LV 3/17	17	0,00	0,00	98,56	0,72
	LV 3/15	15	0,82	1,23	97,13	7,79
	LV 3/13	13	0,00	2,46	94,72	6,34
	LV 3/10	10	0,56	0,00	98,33	2,22
	LV 3/6	6	0,00	0,63	97,48	4,40
	LV 3/3	3	0,29	0,00	97,39	0,58
	LV 3/1-30	1	4,20	2,10	97,90	11,89
	LV 3/0,2	0,2	0,00	0,00	100,00	0,45

Nevenka 1

Age	Preservation		terrestrial																													
			parts of vascular plants												Pollen										Spores							
			phytoclasts																													
			Inertinite				Vitrinite				Cutinite				nonsaccate				monosaccate				bisaccate				monolete				trilete			
	Sample	Depth (m)	A	B	C	sum	A	B	C	sum	A	B	C	sum	A	B	C	sum	A	B	C	sum	A	B	C	sum	A	B	C	sum	A	B	C	sum
early Aptian	NEV 63	2102,5-2106	14	4	0	18	26	33	0	59	0	3	0	3	0	0	0	0	19	10	0	29	0	0	0	0	13	7	0	20	1	4	0	5
	NEV 62	2098-2102,5	45	6	0	51	26	24	0	50	2	0	0	2	0	0	0	0	3	4	0	7	0	0	0	0	5	1	0	6	2	1	0	3
	NEV 61	2107-2111,5	76	15	0	91	37	32	0	69	3	4	0	7	0	0	0	0	4	0	0	4	0	0	0	0	4	2	0	6	3	1	0	4
	NEV 60	2120,5-2125	41	16	0	57	13	16	0	29	4	2	0	6	1	0	0	1	5	1	0	6	0	0	0	0	4	1	0	5	1	3	0	4
late Barremian	NEV 59	2129,5-2134	32	23	0	55	10	11	0	21	1	4	0	5	0	0	0	0	5	3	0	8	0	0	0	0	5	3	0	8	0	1	0	1
	NEV 58	2138,5-2143	22	9	0	31	6	12	0	18	0	3	0	3	0	0	0	0	2	0	0	2	0	0	0	0	3	1	0	4	0	0	0	0
	NEV 57	2147,5-2152	12	23	0	35	18	29	0	47	0	0	0	0	0	1	0	1	0	0	0	0	0	0	0	0	6	1	0	7	0	2	0	2
	NEV 56	2156,5-2161	24	15	0	39	15	27	0	42	0	1	0	1	0	0	0	0	1	0	0	1	0	0	0	0	3	1	0	4	3	0	0	3
	NEV 55	2170-2174,5	25	26	0	51	11	8	0	19	0	2	0	2	0	0	0	0	8	0	0	8	0	0	0	0	10	5	0	15	2	1	0	3
	NEV 54	2179-2183,5	29	17	0	46	14	12	0	26	0	2	0	2	2	0	0	2	2	0	0	2	0	0	0	0	4	0	0	4	0	0	0	0
	NEV 53	2188-2192,5	60	16	0	76	19	6	0	25	1	4	0	5	2	0	0	2	2	1	0	3	0	0	0	0	5	1	0	6	1	0	0	1
	NEV 52	2197-2201,5	54	14	0	68	26	10	0	36	1	3	0	4	0	0	0	0	4	2	0	6	0	0	0	0	3	1	0	4	0	1	0	1
	NEV 51	2206-2210,5	60	25	0	85	17	21	0	38	0	2	1	3	0	0	0	0	4	0	0	4	0	0	0	0	2	0	0	2	1	1	0	2
	NEV 50	2219,5-2224	69	17	0	86	50	11	0	61	1	2	0	3	0	0	0	0	2	0	0	2	0	0	0	0	9	0	0	9	2	1	0	3
	NEV 49	2228,5-2232	60	34	0	94	34	10	0	44	3	3	0	6	0	0	0	0	3	1	0	4	0	0	0	0	11	1	0	12	2	2	0	4
	NEV 48	2237,5-2242	66	13	0	79	41	13	0	54	2	9	0	11	2	0	0	2	6	0	0	6	0	0	0	0	13	0	0	13	1	1	0	2
	NEV 47	2251-2252	69	13	0	82	28	12	0	40	0	4	0	4	4	0	0	4	7	2	0	9	0	0	0	0	16	0	0	16	10	4	0	14
	NEV 46	2258-2259	59	8	0	67	33	4	0	37	1	4	0	5	0	0	0	0	11	4	0	15	0	0	0	0	12	1	0	13	3	2	0	5
	NEV 45	2270-2271	20	15	0	35	17	8	0	25	0	3	0	3	0	0	0	0	8	3	0	11	0	0	0	0	6	1	0	7	1	2	0	3
	NEV 44	2280-2281	39	19	0	58	28	21	0	49	0	0	0	0	1	0	0	1	5	2	0	7	0	0	0	0	5	3	0	8	1	0	0	1
	NEV 43	2290	47	21	0	68	31	8	0	39	0	1	0	1	1	0	0	1	10	1	0	11	0	0	0	0	7	3	0	10	5	3	0	8
	NEV 42	2300	65	25	0	90	23	24	0	47	0	0	0	0	0	0	0	0	2	0	0	2	0	0	0	0	7	3	0	10	2	1	0	3
	NEV 41	2311	34	11	0	45	37	26	0	63	0	0	0	0	0	0	0	0	8	2	0	10	0	0	0	0	11	0	0	11	3	2	0	5
	NEV 40	2316	72	9	0	81	76	38	0	114	0	2	0	2	0	0	0	0	9	0	0	9	0	0	0	0	3	1	0	4	4	0	0	4
	NEV 39	2325	50	16	0	66	15	6	0	21	0	0	1	1	0	0	0	0	3	0	0	3	0	0	0	0	2	1	0	3	6	2	0	8
	NEV 38	2338	71	29	0	100	63	23	0	86	2	0	1	3	0	0	0	0	5	1	0	6	0	0	0	0	2	2	0	4	4	0	0	4
	NEV 37	2344	48	8	0	56	127	34	0	161	2	5	2	9	0	0	0	0	9	0	0	9	0	0	0	0	9	2	0	11	12	6	0	18
	NEV 36	2360	24	21	0	45	13	27	0	40	0	1	0	1	1	2	0	3	9	18	1	28	2	3	0	5	16	15	1	32	11	4	0	15
	NEV 35	2376	77	30	0	107	27	26	0	53	0	2	0	2	0	0	0	0	10	15	0	25	0	2	0	2	13	20	1	34	8	3	0	11
	NEV 34	2395	99	21	0	120	47	36	0	83	1	5	1	7	0	0	0	0	6	10	0	16	0	0	0	0	9	7	0	16	2	3	0	5
	NEV 33	2417	68	22	0	90	38	26	0	64	0	1	0	1	0	0	0	0	2	6	0	8	0	0	0	0	1	8	0	9	0	2	0	2
	NEV 32	2428	103	56	0	159	36	42	0	78	3	1	0	4	0	0	0	0	2	5	0	7	0	1	0	1	3	2	0	5	3	2	0	5
	NEV 31	2437-2438	48	54	0	102	71	33	0	104	3	5	0	8	0	0	0	0	1	3	0	4	0	0	0	0	5	5	0	10	5	4	0	9
	NEV 30	2448-2449	93	55	0	148	72	32	0	104	1	2	0	3	0	0	0	0	2	1	0	3	0	1	0	1	7	3	0	10	3	2	0	5
	NEV 29	2454-2455	92	31	0	123	44	28	0	72	1	5	0	6	0	0	0	0	6	7	0	13	0	0	0	0	3	3	0	6	5	16	1	22
	NEV 28	2461-2462	89	40	0	129	87	50	0	137	0	1	0	1	0	0	0	0	3	3	0	6	0	0	0	0	10	3	0	13	0	3	0	3
	NEV 27	2504	32	17	0	49	42	43	0	85	1	0	0	1	2	0	0	2	10	6	0	16	1	0	0	1	13	3	0	16	0	4	0	4
	NEV 26	2509-2509,5	108	14	0	122	45	16	0	61	0	2	0	2	1	0	0	1	6	1	0	7	0	0	0	0	13	4	0	17	3	1	1	5
	NEV 25	2516-2516,5	107	6	0	113	108	29	0	137	3	2	2	7	0	0	0	0	7	3	0	10	0	0	0	0	3	1	1	5	0	1	0	1
	NEV 24	2521-2521,5	115	10	0	125	79	51	0	130	0	5	3	8	0	0	0	0	1	0	0	1	0	0	0	0	4	3	1	8	1	0	0	1
	NEV 23	2536	62	15	0	77	42	18	0	60	0	0	0	0	4	0	0	4	25	8	0	33	0	1	0	1	25	5	0	30	3	2	0	5
	NEV 22	2541	74	22	0	96	30	28	0	58	0	0	0	0	0	0	0	0	7	3	0	10	0	0	0	0	7	1	0	8	0	2	1	3
	NEV 21	2546	178	31	0	209	58	26	0	84	0	0	2	2	0	0	0	0	6	4	0	10	0	0	0	0	0	1	0	1	1	1	0	2
	NEV 20	2556	79	4	0	83	55	19	0	74	0	0	0	0	0	0	0	0	1	1	1	3	0	0	0	0	0	0	0	0	0	0	0	0
	NEV 19	2593	137	19	0	156	42	26	0	68	0	0	0	0	0	0	0	0	2	9	0	11	0	0	0	0	0	8	1	9	3	4	3	10
	NEV 18	2607	133	6	0	139	62	40	1	103	0	0	0	0	0	0	0	0	1	4	1	6	0	0	0	0	1	7	1	9	0	1	0	1
	NEV 17	2616	114	14	0	128	69	30	0	99	0	0	0	0	0	0	0	0	5	2	0	7	0	1	0	1	2	3	0	5	0	0	2	2
	NEV 16	2625	110	30	0	140	36	35	0	71	0	6	0	6	1	0	0	1	11	1	0	12	0	0	0	0	2	0	0	2	0	0	0	0
	NEV 15	2632	133	9	0	142	65	44	0	109	0	1	0	1	1	0	0	1	12	3	0	15	0	0	0	0	7	0	0	7	1	3	0	4
	NEV 14	2644	100	7	0	107	88	15	0	103	2	13	3	18	2	0	0	2	13	27	1	41	1	1	0	2	17	3	0	20	1	1	1	3
	NEV 13	2649	103	10	0	113	62	31	0	93	2	3	3	8	4	0	0	4	5	4	0	9	0	0	0	0	2	0	0	2	0	3	0	3
	NEV 12	2655	71	4	0	75	40	18	0	58	0	1	0	1	1	0	0	1	8	7	0	15	0	0	0	0	8	3	0	11	3	0	0	3
	NEV 11	2659	124	3	0	127	47	24	0	71	0	1	0	1	2	0	0	2	12	7	1	20	1	0	0	1	4	2	1	7	2	1	0	3
	NEV 10	2662	113	16	0	129	60	24	0	84	6	2	0	8	6	0	0	6	26	9	4	39	1	0	0	1	19	4	0	23	8	0	2	10
	NEV 9	2665	122	33	0	155	67	37	0	104	3	0	0	3	1	0	0	1	7	10	7	24	1	1	0	2	3	2	0	5	4	0	0	4
	NEV 8	2671	92	20	0	112	60	20	0	80	0	0	0	0	1	1	0	2	10	7	3	20	1	0	0	1	10	2	0	12	4	1	0	5
	NEV 7	2688	192	40	0	232	86	48	0	134	0	0	2	2	0	0	0	0	13	8	0	21	0	1	0	1	9	3	1	13	11	3	0	14
	NEV 6	2699	160	84	0	244	45	29	0	74	0	0	0	0	0	0	0	0	5	3	0	8	0	0	0	0	8	4	0	12	3	0	0	3
	NEV 5	2798	135	24	0	159	81	32	0	113	0	1	2	3	0	0	0	0	4	1	0	5	1	0	0	1	4	1	0	5	1	0	0	1
	NEV 4	2800	169	115	0	284	44	34	0	78	0	0	0	0	0	0	0	0	3	2	0	5	0	0	0	0	2	1	0	3	1	0	0	1
	NEV 3	2804	177	104	0	281	38	21	0	59	0	2	0	2	0	0	0	0	2	3	0	5	0	0	0	0	4	0	0	4	3	2	0	5
	NEV 2	2808	154	66	0	220	51	25	0	76	1	3	0	4	0	1	0	1	2	3	0	5	0	0	0	0	5	1	0	6	1	0	1	2
	NEV 1	2812	177	74	0	251	41	33	0	74	0	0	0	0	0	0	0	0	1	2	0	3	0	0	0	0	0	0	0	0	2	0	0	2

terrestrial				AOM			marine																								diverse					
Spores							marine phytoplankton										Zoomorphs				Zooclasts										mineral residues					
indet				terrestrial, translucent	terrestrial opaque	marine/sensu stricto	Dinocysts				Acritarchs				Algae indet	Leiospheres	foraminiferal test linings				Bivalves, Scolecodonts, Fungi				Filaments		Quartz	Pyrite	others	Glendonites						
A	B	C	sum				A	B	C	sum	A	B	C	sum			A	B	C	sum	A	B	C	sum											Totals
10	52	0	62	107	0	62,1	0	0	0	0	0	0	0	0	0	0	0	0	0	0	0	0	0	0	0	18	0	83								365
2	9	0	11	40,1	0	76,9	4	6	4	14	1	0	0	1	13	0	0	0	0	0	0	0	0	0	0	349	44	136								275
12	8	2	22	69,2	0	76,8	6	3	5	14	1	1	1	3	0	0	0	0	0	0	1	0	0	1	0	364	43	5								367
7	8	0	15	105	2	154	2	0	2	4	3	0	0	3	4	0	0	0	0	0	0	0	0	0	0	141	34	60	x							395
8	8	2	18	64,9	2	242	2	3	2	7	0	0	0	0	0	0	0	0	0	0	2	0	0	2	0	30	19	95								434
4	8	1	13	102	0	207	0	2	0	2	1	0	0	1	4	0	0	0	0	0	2	0	0	2	0	33	16	0								389
2	8	0	10	214	1	98,8	0	0	0	0	0	0	0	0	0	0	0	0	0	0	0	0	0	0	0	17	4	0								416
8	4	0	12	118	0	216	0	0	0	0	0	1	0	1	5	0	0	0	0	0	1	0	0	1	0	33	13	0								443
14	9	2	25	60,1	0	167	5	7	4	16	9	5	1	15	0	0	0	0	0	0	2	0	0	2	0	99	43	0								383
3	0	0	3	97,3	0	195	0	0	1	1	1	0	0	1	13	0	0	0	0	0	1	0	0	1	0	116	15	0	x							393
9	2	0	11	87,3	0	122	3	1	2	6	3	1		4	9	0	0	0	0	0	1	0	0	1	0	186	22	0	x							358
14	11	0	25	51,8	1	175	3	2	4	9	4	0	1	5	13	0	0	0	0	0	0	0	0	0	0	141	49	0								399
11	11	1	23	54,5	0	140	4	2	3	9	2	1	0	3	14	0	0	0	0	0	1	0	0	1	0	214	54	0	x							379
6	2	0	8	120	0	81,2	3	3	2	8	2	1	0	3	11	0	0	0	0	0	0	0	0	0	0	147	15	0	x							395
11	5	0	16	30,8	1	104	5	5	3	13	6	1	0	7	0	0	0	0	0	0	1	0	0	1	0	188	51	0	x							337
10	12	0	22	55,2	0	120	11	10	2	23	4	0	0	4	15	0	1	0	0	1	1	0	0	1	3	94	79	0								411
22	4	0	26	58,3	0	98,7	18	12	5	35	4	0	0	4	0	1	0	0	1	1	3	0	0	3	3	28	91	0								399
13	22	0	35	31,9	0	145	5	3	5	13	3	1	0	4	12	2	0	0	0	0	3	0	0	3	0	276	104	0	x							388
9	10	4	23	112	0	171	3	4	2	9	0	0	0	0	0	0	0	0	0	0	0	0	0	0	0	142	31	3								399
4	7	2	13	68,4	0	187	1	2	0	3	0	0	0	0	4	0	0	0	0	0	0	0	0	0	0	155	63	0								399
14	7	1	22	93,1	0	139	1	1	0	2	1	0	0	1	5	0	0	0	0	0	0	0	0	0	1	208	82	0								401
10	0	0	10	99,8	0	163	3	3	1	7	0	0	0	0	0	0	0	0	0	0	2	0	0	2	3	204	89	0								437
12	0	0	12	87,5	0	179	1	0	0	1	1	0	0	1	9	1	0	0	0	0	0	0	0	0	7	34	43	0								431
7	4	0	11	69,7	0	62,3	4	3	2	9	2	0	0	2	12	2	0	0	0	0	1	0	0	1	3	60	8	0								386
0	4	0	4	54,2	0	219	2	1	0	3	0	0	0	0	0	0	0	0	0	0	0	0	0	0	0	79	16	0								382
6	8	0	14	91,4	0	72,6	5	1	0	6	0	1	0	1	0	4	0	0	0	0	0	0	0	0	0	109	16	0								392
2	4	0	6	84,3	0	53,7	0	1	0	1	1	0	0	1	11	3	0	0	0	0	4	0	0	4	4	138	13	1								432
0	43	0	43	143	0	59,9	1	1	0	2	0	0	0	0	7	1	0	0	0	0	0	0	0	0	3	85	4	0								428
4	42	0	46	47,8	0	58,2	4	1	0	5	0	0	0	0	0	0	0	0	0	0	1	0	0	1	0	124	3	0								392
3	11	0	14	61,6	0	60,4	2	5	3	10	1	1	0	2	0	0	0	0	0	0	1	0	0	1	8	224	15	0	x							404
2	19	0	21	49,5	0	92,5	3	1	5	9	0	0	0	0	10	3	0	0	0	0	1	0	0	1	7	167	10	0								367
4	14	1	19	75,6	0	26,4	0	0	1	1	0	0	0	0	6	0	0	0	0	0	0	0	0	0	12	39	2	0								399
0	6	0	6	74,6	0	25,4	0	0	1	1	0	0	0	0	4	0	0	0	0	0	0	0	0	0	4	111	2	0								352
2	5	0	7	64	0	17	0	2	0	2	0	0	0	0	4	0	0	0	0	0	2	0	0	2	0	94	5	0								370
1	32	1	34	55,3	0	37,7	1	0	0	1	0	0	0	0	0	1	0	0	0	0	0	0	0	0	0	160	0	0								371
0	12	0	12	94,7	0	24,3	0	0	0	0	0	0	0	0	4	0	0	0	0	0	6	0	0	6	2	104	0	0								432
8	34	1	43	158	0	44,4	0	0	0	0	0	0	0	0	3	0	0	0	0	0	7	1	0	8	1	48	1	0								431
3	22	1	26	141	0	52,7	1	1	1	3	1	0	0	1	10	0	0	0	0	0	0	0	0	0	2	138	8	0								451
3	4	0	7	50,1	1	39,9	11	4	2	17	0	0	0	0	0	6	0	0	0	0	0	0	0	0	0	361	15	0								394
5	3	0	8	28	2	36	9	7	6	22	0	0	0	0	0	0	0	0	0	0	6	0	0	6	0	450	10	0								375
7	57	5	69	71,3	2	45,7	0	1	1	2	0	0	0	0	0	4	0	0	0	0	0	0	0	0	0	160	7	2								404
1	36	9	46	93,6	0	75,4	4	2	1	7	0	0	0	0	6	0	1	0	0	1	0	0	0	0	0	187	7	0								404
1	13	17	31	64,6	0	15,4	1	1	1	3	0	0	0	0	4	0	0	0	0	0	0	0	0	0	1	65	2	0								427
0	7	46	53	135	0	62,1	1	1	0	2	1	0	0	1	3	1	0	0	0	0	0	0	0	0	2	81	1	0								419
0	24	8	32	98,4	0	13,6	2	0	1	3	0	0	0	0	0	1	0	0	0	0	0	0	0	0	0	107	5	0								402
2	14	12	28	71,9	0	39,1	5	4	0	9	1	0	0	1	3	6	0	0	0	0	0	0	0	0	0	173	4	0								416
7	11	12	30	69,7	2	37,3	3	1	1	5	2	0	0	2	15	0	0	1	0	1	0	0	0	0	2	223	14	0								406
1	8	12	21	66,9	0	46,1	2	3	2	7	0	0	0	0	0	4	0	0	0	0	1	0	0	1	0	350	33	6	x							378
1	5	3	9	48,1	0	41,9	5	3	0	8	2	0	0	2	15	0	0	0	0	0	2	0	0	2	0	430	21	2								405
1	42	17	60	49,4	0	26,6	1	0	1	2	0	0	0	0	0	0	0	0	0	0	2	5	1	8	0	63	4	0								442
3	10	1	14	28,3	0	67,7	6	4	3	13	2	1	0	3	22	0	0	0	0	0	4	0	0	4	0	309	43	3								384
1	9	0	10	28,5	0	137	1	1	0	2	3	0	0	3	8	0	0	0	0	0	3	0	0	3	0	550	19	2	x							356
4	8	3	15	64,4	0	49,6	8	6	3	17	0	0	0	0	0	0	0	0	0	0	0	0	0	0	6	236	31	4	x							384
1	9	11	21	46,7	0	30,3	3	1	1	5	0	0	0	0	0	0	0	0	0	0	2	0	0	2	0	91	6	0								405
0	13	7	20	59,6	0	21,4	0	0	1	1	2	0	0	2	8	0	0	0	0	0	3	0	0	3	0	63	9	0								413
2	10	10	22	58,5	0	30,5	1	0	1	2	0	0	0	0	12	0	0	0	0	0	0	0	0	0	0	109	8	0								357
1	2	0	3	38,8	0	11,2	0	1	0	1	0	0	0	0	0	0	0	0	0	0	1	1	0	2	0	74	1	0								473
0	6	2	8	48,7	0	5,3	0	1	0	1	1	1	0	2	7	0	0	0	0	0	0	0	0	0	0	30	3	0								413
3	11	3	17	50	1	20	1	1	0	2	3	0	0	3	17	0	0	0	0	0	1	0	0	1	0	92	5	3								398
1	2	0	3	28,8	0	3,17	1	1	0	2	3	0	0	3	12	0	0	0	0	0	1	0	0	1	0	27	2	0								424
0	5	0	5	45,7	0	21,3	0	1	0	1	3	0	0	3	16	0	0	0	0	0	0	0	0	0	0	162	5	0								448
0	2	2	4	54,1	1	15,9	1	1	0	2	1	0	0	1	0	0	0	0	0	0	2	0	0	2	0	116	7	4								394
0	5	1	6	71,5	3	8,5	1	0	0	1	0	0	0	0	5	0	0	0	0	0	0	0	0	0	0	207	8	0								425

Nevenka 1

Age	Sample	Depth (m)	Dino A	%	Dino B	%	Dino C	%	Dinocysts	%	Algae indet	%	Acritarchs	%	Foraminifera	%
early Aptian	NEV 63	2102,5-2106	0,00	0,90	0,00	0,75	0,00	0,83	0,00	2,48	0,00	1,43	0,00	0,49	0,00	0,00
	NEV 62	2098-2102,5	1,45	0,78	2,18	1,03	1,45	0,70	5,09	2,37	4,73	2,25	0,36	0,38	0,00	0,00
	NEV 61	2107-2111,5	1,63		0,82		1,36		3,81		0,00		0,82		0,00	
	NEV 60	2120,5-2125	0,51		0,00		0,51		1,01		1,01		0,76		0,00	
late Barremian	NEV 59	2129,5-2134	0,46	0,68	0,69	0,52	0,46	0,32	1,61	1,53	0,00	1,43	0,00	0,38	0,00	0,02
	NEV 58	2138,5-2143	0,00	0,85	0,51	0,62	0,00	0,41	0,51	1,72	1,03	1,47	0,26	0,63	0,00	0,06
	NEV 57	2147,5-2152	0,00		0,00		0,00		0,00		0,00		0,00		0,00	
	NEV 56	2156,5-2161	0,00		0,00		0,00		0,00		1,13		0,23		0,00	
	NEV 55	2170-2174,5	1,31		1,83		1,04		4,18		0,00		3,92		0,00	
	NEV 54	2179-2183,5	0,00		0,00		0,25		0,25		3,31		0,25		0,00	
	NEV 53	2188-2192,5	0,84		0,28		0,56		1,68		2,51		1,12		0,00	
	NEV 52	2197-2201,5	0,75		0,50		1,00		2,26		3,26		1,25		0,00	
	NEV 51	2206-2210,5	1,06		0,53		0,79		2,37		3,69		0,79		0,00	
	NEV 50	2219,5-2224	0,76		0,76		0,51		2,03		2,78		0,76		0,00	
	NEV 49	2228,5-2232	1,48		1,48		0,89		3,86		0,00		2,08		0,00	
	NEV 48	2237,5-2242	2,68		2,43		0,49		5,60		3,65		0,97		0,24	
	NEV 47	2251-2252	4,51		3,01		1,25		8,77		0,00		1,00		0,25	
	NEV 46	2258-2259	1,29		0,77		1,29		3,35		3,09		1,03		0,00	
	NEV 45	2270-2271	0,75		1,00		0,50		2,26		0,00		0,00		0,00	
	NEV 44	2280-2281	0,25		0,50		0,00		0,75		1,00		0,00		0,00	
	NEV 43	2290	0,25		0,25		0,00		0,50		1,25		0,25		0,00	
	NEV 42	2300	0,69		0,69		0,23		1,60		0,00		0,00		0,00	
	NEV 41	2311	0,23		0,00		0,00		0,23		2,09		0,23		0,00	
	NEV 40	2316	1,04		0,78		0,52		2,33		3,11		0,52		0,00	
	NEV 39	2325	0,52		0,26		0,00		0,79		0,00		0,00		0,00	
	NEV 38	2338	1,28		0,26		0,00		1,53		0,00		0,26		0,00	
	NEV 37	2344	0,00		0,23		0,00		0,23		2,55		0,23		0,00	
	NEV 36	2360	0,23		0,23		0,00		0,47		1,64		0,00		0,00	
	NEV 35	2376	1,02		0,26		0,00		1,28		0,00		0,00		0,00	
	NEV 34	2395	0,50		1,24		0,74		2,48		0,00		0,50		0,00	
	NEV 33	2417	0,82		0,27		1,36		2,45		2,72		0,00		0,00	
	NEV 32	2428	0,00		0,00		0,25		0,25		1,50		0,00		0,00	
	NEV 31	2437-2438	0,00		0,00		0,28		0,28		1,14		0,00		0,00	
	NEV 30	2448-2449	0,00		0,54		0,00		0,54		1,08		0,00		0,00	
	NEV 29	2454-2455	0,27		0,00		0,00		0,27		0,00		0,00		0,00	
	NEV 28	2461-2462	0,00		0,00		0,00		0,00		0,93		0,00		0,00	
	NEV 27	2504	0,00		0,00		0,00		0,00		0,70		0,00		0,00	
	NEV 26	2509-2509,5	0,22		0,22		0,22		0,67		2,22		0,22		0,00	
	NEV 25	2516-2516,5	2,79		1,02		0,51		4,31		0,00		0,00		0,00	
	NEV 24	2521-2521,5	2,40		1,87		1,60		5,87		0,00		0,00		0,00	
	NEV 23	2536	0,00		0,25		0,25		0,50		0,00		0,00		0,00	
	NEV 22	2541	0,99		0,50		0,25		1,73		1,49		0,00		0,25	
	NEV 21	2546	0,23		0,23		0,23		0,70		0,94		0,00		0,00	
	NEV 20	2556	0,24		0,24		0,00		0,48		0,72		0,24		0,00	
	NEV 19	2593	0,50		0,00		0,25		0,75		0,00		0,00		0,00	
	NEV 18	2607	1,20		0,96		0,00		2,16		0,72		0,24		0,00	
	NEV 17	2616	0,74		0,25		0,25		1,23		3,69		0,49		0,25	
	NEV 16	2625	0,53		0,79		0,53		1,85		0,00		0,00		0,00	
	NEV 15	2632	1,23		0,74		0,00		1,98		3,70		0,49		0,00	
	NEV 14	2644	0,23		0,00		0,23		0,45		0,00		0,00		0,00	
	NEV 13	2649	1,56		1,04		0,78		3,39		5,73		0,78		0,00	
	NEV 12	2655	0,28		0,28		0,00		0,56		2,25		0,84		0,00	
	NEV 11	2659	2,08		1,56		0,78		4,43		0,00		0,00		0,00	
	NEV 10	2662	0,74		0,25		0,25		1,23		0,00		0,00		0,00	
	NEV 9	2665	0,00		0,00		0,24		0,24		1,94		0,48		0,00	
	NEV 8	2671	0,28		0,00		0,28		0,56		3,36		0,00		0,00	
	NEV 7	2688	0,00		0,21		0,00		0,21		0,00		0,00		0,00	
	NEV 6	2699	0,00		0,24		0,00		0,24		1,69		0,48		0,00	
	NEV 5	2798	0,25		0,25		0,00		0,50		4,27		0,75		0,00	
	NEV 4	2800	0,24		0,24		0,00		0,47		2,83		0,71		0,00	
	NEV 3	2804	0,00		0,22		0,00		0,22		3,57		0,67		0,00	
	NEV 2	2808	0,25		0,25		0,00		0,51		0,00		0,25		0,00	
	NEV 1	2812	0,24		0,00		0,00		0,24		1,18		0,00		0,00	

Nevenka 1

Age	Sample	Depth (m)	Leiospheres	%	marine AOM	%	terrestrial AOM translucent	%	terrestrial AOM total	%	terrestrial AOM opaque	%	Sporo A	%
early Aptian	NEV 63	2102,5-2106	0,00	0,00	17,0	26,3	29,3	22,3	29,30	22,4	0,00	0,13	11,8	6,7
	NEV 62	2098-2102,5	0,00	0,00	28,0	9,7	14,6	6,8	14,57	6,9	0,00	0,25	4,4	3,5
	NEV 61	2107-2111,5	0,00		20,9		18,8		18,84		0,00		6,3	
	NEV 60	2120,5-2125	0,00		39,1		26,5		26,99		0,51		4,6	
late Barremian	NEV 59	2129,5-2134	0,00	0,17	55,8	20,2	15,0	18,2	15,42	18,3	0,46	0,07	4,1	5,2
	NEV 58	2138,5-2143	0,00	0,37	53,3	16,3	26,2	8,3	26,17	8,3	0,00	0,17	2,3	3,4
	NEV 57	2147,5-2152	0,00		23,8		51,5		51,72		0,24		1,9	
	NEV 56	2156,5-2161	0,00		48,7		26,6		26,65		0,00		3,4	
	NEV 55	2170-2174,5	0,00		43,6		15,7		15,69		0,00		8,9	
	NEV 54	2179-2183,5	0,00		49,5		24,8		24,77		0,00		2,8	
	NEV 53	2188-2192,5	0,00		34,0		24,4		24,38		0,00		5,3	
	NEV 52	2197-2201,5	0,00		43,9		13,0		13,24		0,25		5,3	
	NEV 51	2206-2210,5	0,00		37,1		14,4		14,39		0,00		4,7	
	NEV 50	2219,5-2224	0,00		20,6		30,3		30,33		0,00		4,8	
	NEV 49	2228,5-2232	0,00		30,9		9,1		9,45		0,30		8,0	
	NEV 48	2237,5-2242	0,00		29,1		13,4		13,43		0,00		7,8	
	NEV 47	2251-2252	0,25		24,7		14,6		14,60		0,00		14,8	
	NEV 46	2258-2259	0,52		37,4		8,2		8,23		0,00		10,1	
	NEV 45	2270-2271	0,00		42,8		28,1		28,12		0,00		6,0	
	NEV 44	2280-2281	0,00		46,8		17,1		17,14		0,00		4,0	
	NEV 43	2290	0,00		34,6		23,2		23,21		0,00		9,2	
	NEV 42	2300	0,00		37,3		22,8		22,84		0,00		4,81	
	NEV 41	2311	0,23		41,4		20,3		20,30		0,00		7,89	
	NEV 40	2316	0,52		16,1		18,0		18,05		0,00		5,96	
	NEV 39	2325	0,00		57,3		14,2		14,18		0,00		2,88	
	NEV 38	2338	1,02		18,5		23,3		23,31		0,00		4,34	
	NEV 37	2344	0,69		12,4		19,5		19,51		0,00		7,41	
	NEV 36	2360	0,23		14,0		33,4		33,42		0,00		9,11	
	NEV 35	2376	0,00		14,8		12,2		12,20		0,00		8,93	
	NEV 34	2395	0,00		15,0		15,2		15,24		0,00		4,95	
	NEV 33	2417	0,82		25,2		13,5		13,50		0,00		1,36	
	NEV 32	2428	0,00		6,6		18,9		18,94		0,00		3,01	
	NEV 31	2437-2438	0,00		7,2		21,2		21,20		0,00		3,13	
	NEV 30	2448-2449	0,00		4,6		17,3		17,30		0,00		3,78	
	NEV 29	2454-2455	0,27		10,2		14,9		14,91		0,00		4,04	
	NEV 28	2461-2462	0,00		5,6		21,9		21,91		0,00		3,01	
	NEV 27	2504	0,00		10,3		36,6		36,57		0,00		7,89	
	NEV 26	2509-2509,5	0,00		11,7		31,3		31,34		0,00		5,76	
	NEV 25	2516-2516,5	1,52		10,1		12,7		12,98		0,25		3,30	
	NEV 24	2521-2521,5	0,00		9,6		7,5		8,00		0,53		2,93	
	NEV 23	2536	0,99		11,3		17,7		18,15		0,50		15,84	
	NEV 22	2541	0,00		18,7		23,2		23,16		0,00		3,71	
	NEV 21	2546	0,00		3,6		15,1		15,14		0,00		1,87	
	NEV 20	2556	0,24		14,8		32,2		32,20		0,00		0,24	
	NEV 19	2593	0,25		3,4		24,5		24,47		0,00		1,24	
	NEV 18	2607	1,44		9,4		17,3		17,29		0,00		0,96	
	NEV 17	2616	0,00		9,2		17,2		17,66		0,49		3,45	
	NEV 16	2625	1,06		12,2		17,7		17,70		0,00		3,97	
	NEV 15	2632	0,00		10,3		11,9		11,88		0,00		5,43	
	NEV 14	2644	0,00		6,0		11,2		11,17		0,00		7,92	
	NEV 13	2649	0,00		17,6		7,4		7,37		0,00		3,65	
	NEV 12	2655	0,00		38,6		8,0		8,01		0,00		5,90	
	NEV 11	2659	0,00		12,9		16,8		16,78		0,00		6,51	
	NEV 10	2662	0,00		7,5		11,5		11,54		0,00		15,06	
	NEV 9	2665	0,00		5,2		14,4		14,42		0,00		3,87	
	NEV 8	2671	0,00		8,6		16,4		16,37		0,00		7,84	
	NEV 7	2688	0,00		2,4		8,2		8,19		0,00		7,19	
	NEV 6	2699	0,00		1,3		11,8		11,79		0,00		3,87	
	NEV 5	2798	0,00		5,0		12,6		12,81		0,25		3,27	
	NEV 4	2800	0,00		0,7		6,8		6,80		0,00		1,65	
	NEV 3	2804	0,00		4,7		10,2		10,21		0,00		2,01	
	NEV 2	2808	0,00		4,0		13,7		13,98		0,25		2,03	
	NEV 1	2812	0,00		2,0		16,8		17,53		0,71		0,71	

Nevenka 1

Age	Sample	Depth (m)	Sporo B	%	Sporo C	%	Sporomorphs total		Sporomorphs	%	Cutinites	%	Inertinite A	%	Inertinite B	%
early Aptian	NEV 63	2102,5-2106	20,0	7,94	0,0	0,14	116	52,5	31,8	14,81	0,82	1,24	3,8	12,8	1,1	2,9
	NEV 62	2098-2102,5	5,5	8,12	0,0	0,27	27	42,5	9,8	11,35	0,73	0,57	16,4	7,3	2,2	1,5
	NEV 61	2107-2111,5	3,0		0,5		36		9,8		1,91		20,7		4,1	
	NEV 60	2120,5-2125	3,3		0,0		31		7,8		1,52		10,4		4,1	
late Barremian	NEV 59	2129,5-2134	3,5	5,09	0,5	0,99	35	45,4	8,1	11,27	1,15	0,78	7,4	21,2	5,3	6,4
	NEV 58	2138,5-2143	2,3	4,77	0,3	1,87	19	29,1	4,9	7,05	0,77	0,84	5,7	10,8	2,3	5,6
	NEV 57	2147,5-2152	2,9		0,0		20		4,8		0,00		2,9		5,5	
	NEV 56	2156,5-2161	1,1		0,0		20		4,5		0,23		5,4		3,4	
	NEV 55	2170-2174,5	3,9		0,5		51		13,3		0,52		6,5		6,8	
	NEV 54	2179-2183,5	0,0		0,0		11		2,8		0,51		7,4		4,3	
	NEV 53	2188-2192,5	1,1		0,0		23		6,4		1,40		16,8		4,5	
	NEV 52	2197-2201,5	3,8		0,0		36		9,0		1,00		13,5		3,5	
	NEV 51	2206-2210,5	3,2		0,3		31		8,2		0,79		15,8		6,6	
	NEV 50	2219,5-2224	0,8		0,0		22		5,6		0,76		17,5		4,3	
	NEV 49	2228,5-2232	2,7		0,0		36		10,7		1,78		17,8		10,1	
	NEV 48	2237,5-2242	3,2		0,0		45		10,9		2,68		16,1		3,2	
	NEV 47	2251-2252	2,5		0,0		69		17,3		1,00		17,3		3,3	
	NEV 46	2258-2259	7,5		0,0		68		17,5		1,29		15,2		2,1	
	NEV 45	2270-2271	4,0		1,0		44		11,0		0,75		5,0		3,8	
	NEV 44	2280-2281	3,0		0,5		30		7,5		0,00		9,8		4,8	
	NEV 43	2290	3,5		0,2		52		13,0		0,25		11,7		5,2	
	NEV 42	2300	0,92		0,00		25		5,7		0,00		14,9		5,7	
	NEV 41	2311	0,93		0,00		38		8,8		0,00		7,9		2,6	
	NEV 40	2316	1,30		0,00		28		7,3		0,52		18,7		2,3	
	NEV 39	2325	1,83		0,00		18		4,7		0,26		13,1		4,2	
	NEV 38	2338	2,81		0,00		28		7,1		0,77		18,1		7,4	
	NEV 37	2344	2,78		0,00		44		10,2		2,08		11,1		1,9	
	NEV 36	2360	19,86		0,47		126		29,4		0,23		5,6		4,9	
	NEV 35	2376	20,92		0,26		118		30,1		0,51		19,6		7,7	
	NEV 34	2395	7,67		0,00		51		12,6		1,73		24,5		5,2	
	NEV 33	2417	9,54		0,00		40		10,9		0,27		18,5		6,0	
	NEV 32	2428	6,02		0,25		37		9,3		1,00		25,8		14,0	
	NEV 31	2437-2438	5,11		0,00		29		8,2		2,27		13,6		15,3	
	NEV 30	2448-2449	3,24		0,00		26		7,0		0,81		25,1		14,9	
	NEV 29	2454-2455	15,63		0,54		75		20,2		1,62		24,8		8,4	
	NEV 28	2461-2462	4,86		0,00		34		7,9		0,23		20,6		9,3	
	NEV 27	2504	10,90		0,23		82		19,0		0,23		7,4		3,9	
	NEV 26	2509-2509,5	6,21		0,44		56		12,4		0,44		23,9		3,1	
	NEV 25	2516-2516,5	2,28		0,25		23		5,8		1,78		27,2		1,5	
	NEV 24	2521-2521,5	1,60		0,27		18		4,8		2,13		30,7		2,7	
	NEV 23	2536	18,07		1,24		142		35,1		0,00		15,3		3,7	
	NEV 22	2541	10,40		2,48		67		16,6		0,00		18,3		5,4	
	NEV 21	2546	4,45		3,98		44		10,3		0,47		41,7		7,3	
	NEV 20	2556	1,91		11,22		56		13,4		0,00		18,9		1,0	
	NEV 19	2593	11,19		2,99		62		15,4		0,00		34,1		4,7	
	NEV 18	2607	6,25		3,37		44		10,6		0,00		32,0		1,4	
	NEV 17	2616	4,19		3,45		45		11,1		0,00		28,1		3,4	
	NEV 16	2625	2,38		3,17		36		9,5		1,59		29,1		7,9	
	NEV 15	2632	2,72		0,74		36		8,9		0,25		32,8		2,2	
	NEV 14	2644	16,74		4,30		128		29,0		4,07		22,6		1,6	
	NEV 13	2649	4,43		0,26		32		8,3		2,08		26,8		2,6	
	NEV 12	2655	5,34		0,00		40		11,2		0,28		19,9		1,1	
	NEV 11	2659	4,69		1,30		48		12,5		0,26		32,3		0,8	
	NEV 10	2662	5,43		4,20		100		24,7		1,98		27,9		4,0	
	NEV 9	2665	6,30		3,39		56		13,6		0,73		29,5		8,0	
	NEV 8	2671	5,88		3,64		62		17,4		0,00		25,8		5,6	
	NEV 7	2688	3,59		0,21		52		11,0		0,42		40,6		8,5	
	NEV 6	2699	3,15		0,48		31		7,5		0,00		38,7		20,3	
	NEV 5	2798	3,27		0,75		29		7,3		0,75		33,9		6,0	
	NEV 4	2800	1,18		0,00		12		2,8		0,00		39,9		27,1	
	NEV 3	2804	2,23		0,00		19		4,2		0,45		39,5		23,2	
	NEV 2	2808	1,78		0,76		18		4,6		1,02		39,1		16,8	
	NEV 1	2812	1,65		0,24		11		2,6		0,00		41,6		17,4	

Nevenka 1

Age	Sample	Depth (m)	Inertinite total	%	Vitrinite A	%	Vitrinite B	%	Vitrinite total	%	Phytoclasts	%	Filaments	%	marine OM	%
early Aptian	NEV 63	2102,5-2106	4,9	15,7	7,1	7,5	9,0	7,6	16,2	15,12	21,9	32,0	0,0	0,00	17,0	31
	NEV 62	2098-2102,5	18,5	8,3	9,5	3,1	8,7	2,4	18,2	5,31	37,5	11,4	0,0	0,00	38,2	11
	NEV 61	2107-2111,5	24,8		10,1		8,7		18,8		45,5		0,0		25,6	
	NEV 60	2120,5-2125	14,4		3,3		4,1		7,3		23,3		0,0		41,9	
late Barremian	NEV 59	2129,5-2134	12,7	27,6	2,3	11,5	2,5	6,2	4,8	17,64	18,7	46,1	0,0	0,31	57,4	24
	NEV 58	2138,5-2143	8,0	14,3	1,5	6,2	3,1	2,9	4,6	8,19	13,4	19,2	0,0	0,61	55,1	17
	NEV 57	2147,5-2152	8,4		4,3		7,0		11,3		19,7		0,0		23,8	
	NEV 56	2156,5-2161	8,8		3,4		6,1		9,5		18,5		0,0		50,1	
	NEV 55	2170-2174,5	13,3		2,9		2,1		5,0		18,8		0,0		51,7	
	NEV 54	2179-2183,5	11,7		3,6		3,1		6,6		18,8		0,0		53,4	
	NEV 53	2188-2192,5	21,2		5,3		1,7		7,0		29,6		0,0		39,3	
	NEV 52	2197-2201,5	17,0		6,5		2,5		9,0		27,1		0,0		50,7	
	NEV 51	2206-2210,5	22,4		4,5		5,5		10,0		33,2		0,0		43,9	
	NEV 50	2219,5-2224	21,8		12,7		2,8		15,4		38,0		0,0		26,1	
	NEV 49	2228,5-2232	27,9		10,1		3,0		13,1		42,7		0,0		36,8	
	NEV 48	2237,5-2242	19,2		10,0		3,2		13,1		35,0		0,73		39,6	
	NEV 47	2251-2252	20,6		7,0		3,0		10,0		31,6		0,75		35,0	
	NEV 46	2258-2259	17,3		8,5		1,0		9,5		28,1		0,00		45,4	
	NEV 45	2270-2271	8,8		4,3		2,0		6,3		15,8		0,0		45,1	
	NEV 44	2280-2281	14,5		7,0		5,3		12,3		26,8		0,0		48,5	
	NEV 43	2290	17,0		7,7		2,0		9,7		26,9		0,2		36,6	
	NEV 42	2300	20,6		5,3		5,5		10,8		31,4		0,7		38,9	
	NEV 41	2311	10,4		8,6		6,0		14,6		25,1		1,6		44,2	
	NEV 40	2316	21,0		19,7		9,8		29,5		51,0		0,8		22,6	
	NEV 39	2325	17,3		3,9		1,6		5,5		23,0		0,0		58,1	
	NEV 38	2338	25,5		16,1		5,9		21,9		48,2		0,0		21,3	
	NEV 37	2344	13,0		29,4		7,9		37,3		52,3		0,9		16,1	
	NEV 36	2360	10,5		3,0		6,3		9,3		20,1		0,7		16,3	
	NEV 35	2376	27,3		6,9		6,6		13,5		41,3		0,0		16,1	
	NEV 34	2395	29,7		11,6		8,9		20,5		52,0		2,0		17,9	
	NEV 33	2417	24,5		10,4		7,1		17,4		42,2		1,9		31,2	
	NEV 32	2428	39,8		9,0		10,5		19,5		60,4		3,0		8,4	
	NEV 31	2437-2438	29,0		20,2		9,4		29,5		60,8		1,1		8,6	
	NEV 30	2448-2449	40,0		19,5		8,6		28,1		68,9		0,0		6,2	
	NEV 29	2454-2455	33,2		11,9		7,5		19,4		54,2		0,0		10,7	
	NEV 28	2461-2462	29,9		20,1		11,6		31,7		61,8		0,5		6,6	
	NEV 27	2504	11,4		9,7		10,0		19,7		31,3		0,2		11,0	
	NEV 26	2509-2509,5	27,1		10,0		3,5		13,5		41,0		0,4		14,8	
	NEV 25	2516-2516,5	28,7		27,4		7,4		34,8		65,2		0,0		16,0	
	NEV 24	2521-2521,5	33,3		21,1		13,6		34,7		70,1		0,0		15,5	
	NEV 23	2536	19,1		10,4		4,5		14,9		33,9		0,0		12,8	
	NEV 22	2541	23,8		7,4		6,9		14,4		38,1		0,0		22,1	
	NEV 21	2546	48,9		13,6		6,1		19,7		69,1		0,2		5,2	
	NEV 20	2556	19,8		13,1		4,5		17,7		37,5		0,5		16,5	
	NEV 19	2593	38,8		10,4		6,5		16,9		55,7		0,0		4,4	
	NEV 18	2607	33,4		14,9		9,6		24,8		58,2		0,0		14,0	
	NEV 17	2616	31,5		17,0		7,4		24,4		55,9		0,5		14,9	
	NEV 16	2625	37,0		9,5		9,3		18,8		57,4		0,0		15,1	
	NEV 15	2632	35,1		16,0		10,9		26,9		62,2		0,0		16,5	
	NEV 14	2644	24,2		19,9		3,4		23,3		51,6		0,0		6,5	
	NEV 13	2649	29,4		16,1		8,1		24,2		55,7		0,0		27,5	
	NEV 12	2655	21,1		11,2		5,1		16,3		37,6		0,0		42,3	
	NEV 11	2659	33,1		12,2		6,3		18,5		51,8		1,6		17,3	
	NEV 10	2662	31,9		14,8		5,9		20,7		54,6		0,0		8,7	
	NEV 9	2665	37,5		16,2		9,0		25,2		63,4		0,0		7,9	
	NEV 8	2671	31,4		16,8		5,6		22,4		53,8		0,0		12,5	
	NEV 7	2688	49,0		18,2		10,1		28,3		77,8		0,0		2,6	
	NEV 6	2699	59,1		10,9		7,0		17,9		77,0		0,0		3,7	
	NEV 5	2798	39,9		20,4		8,0		28,4		69,1		0,0		10,6	
	NEV 4	2800	67,0		10,4		8,0		18,4		85,4		0,0		4,8	
	NEV 3	2804	62,7		8,5		4,7		13,2		76,3		0,0		9,2	
	NEV 2	2808	55,8		12,9		6,3		19,3		76,1		0,0		4,8	
	NEV 1	2812	59,1		9,6		7,8		17,4		76,5		0,0		3,4	

Nevenka 1

Age	Sample	Depth (m)	terrestrial OM %		Palynomorphs %	OP/TR
early Aptian	NEV 63	2102,5-2106	83,0	69	31,8	1,04
	NEV 62	2098-2102,5	61,8	12	20,0	
	NEV 61	2107-2111,5	74,2		14,4	
	NEV 60	2120,5-2125	57,6		10,6	
late Barremian	NEV 59	2129,5-2134	41,7	76	9,7	1,57
	NEV 58	2138,5-2143	44,4	17	6,7	
	NEV 57	2147,5-2152	76,0		4,8	
	NEV 56	2156,5-2161	49,7		5,9	
	NEV 55	2170-2174,5	47,8		21,4	
	NEV 54	2179-2183,5	46,4		6,6	
	NEV 53	2188-2192,5	60,4		11,7	
	NEV 52	2197-2201,5	49,1		15,8	
	NEV 51	2206-2210,5	55,8		15,0	
	NEV 50	2219,5-2224	73,9		11,1	
	NEV 49	2228,5-2232	62,6		16,6	
	NEV 48	2237,5-2242	60,1		22,1	
	NEV 47	2251-2252	64,2		28,3	
	NEV 46	2258-2259	53,8		25,5	
	NEV 45	2270-2271	54,9		13,3	
	NEV 44	2280-2281	51,5		9,3	
	NEV 43	2290	63,4		15,2	
	NEV 42	2300	60,6		8,0	
	NEV 41	2311	55,8		13,2	
	NEV 40	2316	77,1		14,5	
	NEV 39	2325	41,9		5,5	
	NEV 38	2338	78,7		9,9	
	NEV 37	2344	82,9		14,8	
	NEV 36	2360	83,7		32,5	
	NEV 35	2376	83,6		31,4	
	NEV 34	2395	81,8		17,6	
	NEV 33	2417	68,5		18,8	
	NEV 32	2428	91,6		14,0	
	NEV 31	2437-2438	91,4		10,8	
	NEV 30	2448-2449	93,2		8,6	
	NEV 29	2454-2455	89,3		20,8	
	NEV 28	2461-2462	92,1		9,3	
	NEV 27	2504	87,2		20,0	
	NEV 26	2509-2509,5	85,2		16,0	
	NEV 25	2516-2516,5	83,8		11,7	
	NEV 24	2521-2521,5	82,4		10,7	
	NEV 23	2536	86,7		36,6	
	NEV 22	2541	77,9		20,0	
	NEV 21	2546	94,8		12,2	
	NEV 20	2556	83,5		15,5	
	NEV 19	2593	95,6		16,4	
	NEV 18	2607	86,0		15,1	
	NEV 17	2616	84,7		17,2	
	NEV 16	2625	84,6		12,4	
	NEV 15	2632	83,0		15,1	
	NEV 14	2644	91,7		29,4	
	NEV 13	2649	71,4		18,2	
	NEV 12	2655	56,9		14,9	
	NEV 11	2659	82,7		18,5	
	NEV 10	2662	90,8		25,9	
	NEV 9	2665	91,4		16,2	
	NEV 8	2671	87,5		21,3	
	NEV 7	2688	97,0		11,2	
	NEV 6	2699	96,3		9,9	
	NEV 5	2798	88,9		12,8	
	NEV 4	2800	95,0		6,8	
	NEV 3	2804	90,8		8,7	
	NEV 2	2808	94,4		5,3	
	NEV 1	2812	95,9		4,0	

Sofia 1			terrestrial																													
			parts of vascular plants												Pollen											Spores							
			phytoclasts																													
			Inertinite				Vitrinite				Cutinite				nonsaccate				monosaccate				bisaccate				monolete				trilete			
Age	Preservation		A	B	C	sum	A	B	C	sum	A	B	C	sum	A	B	C	sum	A	B	C	sum	A	B	C	sum	A	B	C	sum	A	B	C	sum
	Sample	Depth (m)																																
middle Zapata - Hauterivian to Aptian	SOF 60	1999-2002	103	67	0	170	1	10	0	11	0	0	0	0	0	0	0	0	0	0	0	0	0	0	0	0	0	0	1	1	0	0	0	0
	SOF 59	2008-2011	111	116	0	227	5	20	0	25	0	0	0	0	0	0	0	0	0	0	0	0	0	0	0	0	0	5	0	5	0	2	0	2
	SOF 58	2020-2023	77	69	0	146	3	12	0	15	0	4	0	4	0	0	0	0	0	0	0	0	0	0	0	0	0	1	0	1	0	0	0	0
	SOF 57	2029-2032	125	116	0	241	0	9	0	9	0	2	0	2	0	0	0	0	0	0	0	0	0	0	0	0	0	0	0	0	0	2	0	2
	SOF 56	2038-2041	150	115	0	265	5	8	0	13	0	0	0	0	0	0	0	0	0	0	0	0	0	0	0	0	0	1	0	1	0	0	0	0
	SOF 55	2050-2053	134	68	0	202	3	10	0	13	0	0	0	0	0	0	0	0	0	0	0	0	0	0	0	0	0	0	0	0	0	0	0	0
	SOF 54	2059-2062	82	116	0	198	4	9	0	13	0	0	0	0	0	0	0	0	0	0	0	0	0	0	0	0	0	1	0	1	0	0	0	0
	SOF 53	2068-2071	91	155	0	246	4	19	0	23	0	0	0	0	0	0	0	0	0	0	0	0	0	0	0	0	1	0	0	1	0	1	1	2
	SOF 52	2080-2083	89	155	0	244	1	7	0	8	0	0	0	0	0	0	0	0	0	0	0	0	0	0	0	0	0	1	0	1	0	1	0	1
	SOF 51	2089-2092	119	195	0	314	1	0	0	1	0	0	0	0	0	0	0	0	0	0	0	0	0	0	0	0	0	1	0	1	0	0	0	0
	SOF 50	2098-2101	77	125	0	202	3	25	0	28	0	0	0	0	0	0	0	0	0	0	0	0	0	0	0	0	2	1	0	3	1	1	0	2
	SOF 49	2107-2110	107	95	0	202	3	17	0	20	0	0	0	0	0	0	0	0	0	0	0	0	0	0	0	0	0	0	0	0	0	0	0	0
	SOF 48	2119-2122	61	135	0	196	5	15	0	20	0	3	0	3	0	0	0	0	0	0	0	0	0	0	0	0	0	0	0	0	0	0	0	0
	SOF 47	2128-2131	78	180	0	258	3	10	0	13	0	0	0	0	0	0	0	0	0	0	0	0	0	0	0	0	0	0	0	0	0	0	0	0
	SOF 46	2137-2142	94	161	0	255	15	5	0	20	0	0	0	0	0	0	0	0	0	0	0	0	0	0	0	0	0	1	0	1	0	1	0	1
	SOF 45	2149-2152	101	161	0	262	2	1	0	3	0	0	0	0	0	0	0	0	0	0	0	0	0	0	0	0	0	0	0	0	0	0	0	0
	SOF 44	2161-2164	69	195	0	264	1	0	0	1	0	0	0	0	0	0	0	0	0	0	0	0	0	0	0	0	0	0	0	0	0	0	0	0
	SOF 43	2170-2173	64	195	0	259	0	0	0	0	0	0	0	0	0	0	0	0	0	0	0	0	0	0	0	0	0	0	0	0	0	0	0	0
	SOF 42	2179-2182	46	195	0	241	4	0	0	4	0	0	0	0	0	0	0	0	0	0	0	0	0	0	0	0	0	0	0	0	0	0	0	0
	SOF 41	2188-2191	62	180	0	242	2	1	0	3	0	0	0	0	0	0	0	0	0	0	0	0	0	0	0	0	0	0	0	0	0	0	0	0
	SOF 40	2197-2200	58	195	0	253	0	2	0	2	0	0	0	0	0	0	0	0	0	0	0	0	0	0	0	0	0	0	0	0	0	0	0	0
	SOF 39	2209-2212	82	195	0	277	3	0	0	3	0	0	0	0	0	0	0	0	0	0	0	0	0	0	0	0	0	0	0	0	0	0	0	0
	SOF 38	2218-2221	39	195	0	234	1	5	0	6	0	0	0	0	0	0	0	0	0	0	0	0	0	0	0	0	0	0	0	0	0	0	0	0
	SOF 37	2227-2230	64	180	0	244	0	1	0	1	0	0	0	0	0	0	0	0	0	0	0	0	0	0	0	0	0	0	0	0	0	0	0	0
	SOF 36	2239-2242	57	177	0	234	1	3	0	4	0	2	0	2	0	0	0	0	0	0	0	0	0	0	0	0	0	0	0	0	0	0	0	0
	SOF 35	2248-2251	66	195	0	261	4	0	0	4	0	0	0	0	0	0	0	0	0	0	0	0	0	0	0	0	0	0	0	0	0	0	0	0
	SOF 34	2257-2260	77	120	0	197	3	2	0	5	0	0	0	0	0	0	0	0	0	0	0	0	0	0	0	0	0	0	0	0	0	0	0	0
	SOF 33	2269-2272	76	157	0	233	3	1	0	4	0	0	0	0	0	0	0	0	0	0	0	0	0	0	0	0	0	0	0	0	0	0	0	0
	SOF 32	2281-2284	45	178	0	223	1	1	0	2	0	0	0	0	0	0	0	0	0	0	0	0	0	0	0	0	0	0	0	0	0	0	0	0
	SOF 31	2290-2292	23	147	0	170	4	3	0	7	0	0	0	0	0	0	0	0	0	0	0	0	0	0	0	0	0	0	0	0	0	0	0	0
	SOF 30	2299-2302	50	161	0	211	4	8	0	12	0	0	0	0	0	0	0	0	0	0	0	0	0	0	0	0	0	0	0	0	0	1	0	1
	SOF 29	2308-2311	56	144	0	200	9	11	0	20	0	0	0	0	0	0	0	0	0	0	0	0	0	0	0	0	0	0	0	0	0	0	0	0
	SOF 28	2320-2323	76	143	0	219	7	7	0	14	0	0	0	0	0	0	0	0	0	0	0	0	0	0	0	0	0	0	0	0	0	0	0	0
	SOF 27	2326-2329	59	132	0	191	3	6	0	9	0	0	0	0	0	0	0	0	0	0	0	0	0	0	0	0	0	0	0	0	0	0	0	0
	SOF 26	2335-2338	76	135	0	211	7	7	0	14	0	0	0	0	0	0	0	0	0	0	0	0	0	0	0	0	0	1	0	1	0	3	0	3
	SOF 25	2341-2344	88	112	0	200	13	19	0	32	0	0	0	0	0	0	0	0	0	0	0	0	0	0	0	0	0	1	0	1	0	0	0	0
	SOF 24	2350-2353	89	160	0	249	9	4	0	13	0	0	0	0	0	0	0	0	0	0	0	0	0	0	0	0	0	0	0	0	0	0	0	0
	SOF 23	2359-2362	104	151	0	255	4	5	0	9	0	0	0	0	0	0	0	0	0	0	0	0	0	0	0	0	0	0	0	0	0	0	0	0
lower Zapata - Valanginian	SOF 22	2368-2371	97	136	0	233	2	1	0	3	0	0	0	0	0	0	0	0	0	0	0	0	0	0	0	0	0	0	0	0	0	1	0	1
	SOF 21	2377-2380	73	178	0	251	32	5	0	37	0	0	0	0	0	0	0	0	0	0	0	0	0	0	0	0	0	0	0	0	0	0	0	0
	SOF 20	2389-2390	84	147	0	231	11	5	0	16	0	0	0	0	0	0	0	0	0	0	0	0	0	0	0	0	0	0	0	0	0	0	0	0
	SOF 19	2396-2399	130	119	0	249	6	0	0	6	0	0	0	0	0	0	0	0	0	0	0	0	0	0	0	0	0	0	0	0	0	0	0	0
	SOF 18	2408-2411	144	104	0	248	0	0	0	0	0	0	0	0	0	0	0	0	0	0	0	0	0	0	0	0	0	0	0	0	0	0	0	0
	SOF 17	2420-2421	134	107	0	241	5	4	0	9	0	0	0	0	0	0	0	0	0	0	0	0	0	0	0	0	0	0	0	0	0	0	0	0
	SOF 16	2429-2430	131	182	0	313	0	0	0	0	0	0	0	0	0	0	0	0	0	0	0	0	0	0	0	0	0	0	0	0	0	0	0	0
	SOF 15	2439-2440	117	165	0	282	4	1	0	5	0	0	0	0	0	0	0	0	0	0	0	0	0	0	0	0	0	0	0	0	0	0	0	0
	SOF 14	2450-2451	130	110	0	240	3	4	0	7	0	0	0	0	0	0	0	0	0	0	0	0	0	0	0	0	0	0	0	0	0	0	0	0
	SOF 13	2459-2460	78	195	0	273	1	0	0	1	0	0	0	0	0	0	0	0	0	0	0	0	0	0	0	0	0	0	0	0	0	0	0	0
low. Zap. - Berrias	SOF 12	2469-2470	105	195	0	300	1	0	0	1	0	0	0	0	0	0	0	0	0	0	0	0	0	0	0	0	0	0	0	0	0	0	0	0
	SOF 11	2475-2476	129	172	0	301	2	1	0	3	0	0	0	0	0	0	0	0	0	0	0	0	0	0	0	0	0	0	0	0	0	0	0	0
	SOF 10	2478-2479	150	154	0	304	3	1	0	4	0	0	0	0	0	0	0	0	0	0	0	0	0	0	0	0	0	0	0	0	0	0	0	0
Tithonian	SOF 9	2482,5-2483,0	124	201	0	325	8	1	0	9	0	0	0	0	0	0	0	0	0	0	0	0	0	0	0	0	0	0	0	0	0	0	0	0
	SOF 8	2486,0-2486,5	144	167	0	311	4	2	0	6	0	0	0	0	0	0	0	0	0	0	0	0	0	0	0	0	0	0	0	0	0	0	0	0
	SOF 7	2488-2489	134	196	0	330	6	0	0	6	0	1	0	1	0	0	0	0	0	0	0	0	0	0	0	0	0	0	0	0	0	0	0	0
	SOF 6	2512-2513	113	160	0	273	0	2	0	2	0	0	0	0	0	0	0	0	0	0	0	0	0	0	0	0	0	0	0	0	0	0	0	0
	SOF 5	2520-2521	121	106	0	227	5	5	0	10	0	0	0	0	0	0	0	0	0	0	0	0	0	0	0	0	0	0	0	0	0	0	0	0
	SOF 4	2525-2526	134	121	0	255	15	10	0	25	0	0	0	0	0	0	0	0	0	0	0	0	0	0	0	0	0	0	0	0	0	0	0	0
	SOF 3	2530-2531	154	131	0	285	17	21	0	38	0	0	0	0	0	0	0	0	0	0	0	0	0	0	0	0	0	0	0	0	0	0	0	0
	SOF 2	2535-2536	152	129	0	281	12	6	0	18	0	0	0	0	0	0	0	0	0	0	0	0	0	0	0	0	0	1	0	1	0	0	0	0
	SOF 1	2539-2540	133	119	0	252	7	7	0	14	0	0	0	0	0	0	0	0	0	0	0	0	0	0	0	0	0	0	0	0	0	1	0	1

terrestrial				AOM			marine																				diverse					
Spores																																
							marine phytoplankton											Zoomorphs				Zooclasts						mineral residues				
indet				terrestrial, translucent	terrestrial opaque	marine/sensu stricto	Dinocysts				Acritarchs				Algae indet	Leiospheres	foraminiferal test linings				Bivalves, Scolecodonts, Fungi				Filaments	Quartz	Pyrite	others	Glendonites				
A	B	C	sum				A	B	C	sum	A	B	C	sum			A	B	C	sum	A	B	C	sum							Totals
0	1	7	8	116	6	0	0	0	0	0	0	0	0	0	0	0	0	0	0	0	1	0	0	1	0	225	55		x	313
0	6	7	13	72	0	0	0	1	0	1	0	0	0	0	0	0	0	0	0	0	2	0	0	2	0	236	44			347
0	8	3	11	138	11	0	0	0	0	0	0	0	0	0	0	0	0	0	0	0	0	0	0	0	0	345	49			326
1	6	9	16	70	4	0	0	0	0	0	0	0	0	0	0	0	0	0	0	0	0	0	0	0	0	294	54		x	344
0	3	5	8	53	4	0	0	1	0	1	0	0	0	0	0	0	0	0	0	0	0	0	0	0	0	380	64	51	x	345
1	5	12	18	26	0	0	0	0	0	0	0	0	0	0	0	0	0	0	0	0	0	0	0	0	0	430	29	42		259
1	8	18	27	48	0	0	0	0	0	0	0	0	0	0	0	0	0	0	0	0	0	0	0	0	0	314	29	8	x	287
1	14	10	25	26	0	0	0	1	0	1	0	0	0	0	0	0	0	0	0	0	0	0	0	0	0	252	49	69	x	324
0	4	11	15	44	0	0	0	0	0	0	0	0	0	0	0	0	0	0	0	0	0	0	0	0	0	320	48	32	x	313
0	1	5	6	22	0	0	0	0	0	0	0	0	0	0	0	0	0	0	0	0	0	0	0	0	0	232	38	7	x	344
1	9	9	19	46	1	0	0	0	0	0	0	0	1	1	0	0	0	0	0	0	0	0	0	0	0	420	25	17		302
2	4	5	11	14	1	0	0	1	0	1	0	0	0	0	0	0	0	0	0	0	0	0	0	0	0	467	56	20	x	249
1	4	2	7	43	0	0	0	0	0	0	0	0	0	0	0	0	0	0	0	0	0	0	0	0	0	470	50	93		269
0	3	5	8	37	0	0	0	0	0	0	0	0	0	0	0	0	0	0	0	0	0	0	0	0	0	235	39	7	x	316
0	1	4	5	16	2	0	0	0	0	0	0	0	0	0	0	0	0	0	0	0	0	0	0	0	0	384	54	0		300
0	1	0	1	25	1	0	0	0	0	0	0	0	0	0	0	0	0	0	0	0	0	0	0	0	0	282	61	0	x	292
0	0	1	1	7	0	0	0	0	0	0	0	0	0	0	0	0	0	0	0	0	0	0	0	0	0	210	75	28		273
0	0	0	0	5	6	0	0	0	0	0	0	0	0	0	0	0	0	0	0	0	0	0	0	0	0	125	51	0	x	270
0	0	0	0	8	0	0	0	0	0	0	0	0	0	0	0	0	0	0	0	0	0	0	0	0	0	140	63	62	x	253
0	0	0	0	4	9	0	0	0	0	0	0	0	0	0	0	0	0	0	0	0	0	0	0	0	0	167	73	71	x	258
0	1	0	1	5	4	0	0	0	0	0	0	0	0	0	0	0	0	0	0	0	0	0	0	0	0	112	57	63		265
0	0	0	0	11	11	0	0	0	0	0	0	0	0	0	0	0	0	0	0	0	2	0	0	2	0	158	50	47	x	304
0	0	0	0	3	5	0	0	0	0	0	0	0	0	0	0	0	0	0	0	0	0	0	0	0	0	129	70	91		248
0	0	0	0	3	11	0	0	0	0	0	0	0	0	0	0	0	0	0	0	0	0	0	0	0	0	140	52	39	x	259
0	0	0	0	6	9	0	0	0	0	0	0	0	0	0	0	0	0	0	0	0	0	0	0	0	0	205	124	58	x	255
0	2	3	5	7	9	0	0	0	0	0	0	0	0	0	0	0	0	0	0	0	2	0	0	2	0	189	123	74		288
0	2	0	2	39	6	0	0	0	0	0	0	0	0	0	0	0	0	0	0	0	2	0	0	2	0	252	99	37		251
0	0	2	2	20	3	0	0	0	0	0	0	0	0	0	0	0	0	0	0	0	0	0	0	0	0	192	88	20	x	262
0	0	1	1	5	3	0	0	0	0	0	0	0	0	0	0	0	0	0	0	0	0	0	0	0	0	272	73	7		234
0	0	1	1	15	1	0	0	0	0	0	0	0	0	0	0	0	0	0	0	0	0	0	0	0	0	388	45	0		194
0	0	2	2	7	4	0	0	0	0	0	0	0	0	0	0	0	0	0	0	0	6	0	0	6	0	223	93	0		243
0	4	4	8	3	0	0	0	0	0	0	0	0	0	0	0	0	0	0	0	0	3	0	0	3	0	218	66	0		234
0	0	3	3	7	2	0	0	1	0	1	0	0	0	0	0	0	0	0	0	0	0	0	0	0	0	496	80	0		246
0	1	0	1	4	2	0	0	0	0	0	0	0	0	0	0	0	0	0	0	0	0	0	0	0	0	432	85	0		207
0	5	9	14	11	2	0	0	1	0	1	0	0	0	0	0	0	0	0	0	0	0	0	0	0	0	437	132	0		257
1	13	9	23	14	2	0	0	0	0	0	0	0	0	0	0	0	0	0	0	0	0	0	0	0	0	408	155	0		272
0	0	2	2	3	0	0	0	0	0	0	0	0	0	0	0	0	0	0	0	0	0	0	0	0	0	280	75	0		267
0	1	0	1	30	0	0	0	0	0	0	0	0	0	0	0	0	0	0	0	0	2	0	0	2	0	185	46	0		297
0	0	0	0	81	0	0	0	0	0	0	0	0	0	0	0	0	0	0	0	0	0	0	0	0	0	84	46	0		318
0	1	0	1	53	0	0	0	1	0	1	0	1	0	1	0	0	0	0	0	0	0	0	0	0	0	65	83	0		344
0	1	0	1	40	6	0	0	0	0	0	0	0	0	0	0	0	0	0	0	0	0	0	0	0	0	273	111	0		294
0	0	0	0	49	2	0	0	0	0	0	0	0	0	0	0	0	0	0	0	0	0	0	0	0	0	173	73	0		306
0	0	0	0	51	0	0	0	0	0	0	0	0	0	0	0	0	0	0	0	0	0	0	0	0	0	107	79	0		299
0	0	1	1	50	0	0	0	0	0	0	0	0	0	0	0	0	0	0	0	0	0	0	0	0	0	146	42	0		301
0	0	0	0	4	0	0	0	0	0	0	0	0	0	0	0	0	0	0	0	0	0	0	0	0	0	55	37	0		317
0	0	0	0	29	0	0	0	0	0	0	0	0	0	0	0	0	0	0	0	0	0	0	0	0	0	75	40	0		316
0	0	3	3	50	0	0	0	0	0	0	0	0	0	0	0	0	0	0	0	0	0	0	0	0	0	114	29	0		300
0	0	0	0	10	0	0	0	0	0	0	0	0	0	0	0	0	0	0	0	0	0	0	0	0	0	31	25	0		284
0	0	0	0	3	0	0	0	0	0	0	0	0	0	0	0	0	0	0	0	0	0	0	0	0	0	17	16	0		304
0	0	0	0	15	0	0	0	0	0	0	0	0	0	0	0	0	0	0	0	0	0	0	0	0	0	44	19	0		319
0	0	0	0	12	0	0	0	0	0	0	0	0	0	0	0	0	0	0	0	0	0	0	0	0	0	70	9	0		320
0	0	0	0	4	2	0	0	0	0	0	0	0	1	1	0	0	0	0	0	0	0	0	0	0	0	82	20	0		341
0	1	0	1	17	0	0	0	0	0	0	0	0	0	0	0	0	0	0	0	0	0	0	0	0	0	193	69	0		335
0	0	0	0	22	0	0	0	0	0	0	0	0	0	0	0	0	0	0	0	0	0	0	0	0	0	150	33	0		359
0	0	1	1	12	0	0	0	0	0	0	0	0	0	0	0	0	0	0	0	0	0	0	0	0	0	238	37	0		288
0	0	1	1	54	0	0	0	0	0	0	0	0	0	0	0	0	0	0	0	0	0	0	0	0	0	325	83	0		292
0	1	3	4	46	0	0	0	0	0	0	0	0	0	0	0	0	0	0	0	0	0	0	0	0	0	283	77	0		330
0	0	1	1	38	0	0	0	0	0	0	0	0	0	0	0	0	0	0	0	0	0	0	0	0	0	247	72	2		362
0	2	4	6	27	0	0	0	0	0	0	0	0	0	0	0	0	0	0	0	0	0	0	0	0	0	49	66	3		333
0	1	6	7	40	0	0	0	0	0	0	0	0	0	0	0	0	0	0	0	0	0	0	0	0	0	255	87	0		314

Sofia 1

Age	Sample	Depth (m)	Dino A	%	Dino B	%	Dino C	%	Dinocysts total	%	Acritarchs	%	Foraminifera	%	Leiospheres	%	marine AOM	%
middle Zapata - Hauterivian to Aptian	SOF 60	1999-2002	0,00	0,0	0,00	0,05	0,00	0,0	0,00	0,05	0,00	0,01	0,00	0,00	0,00	0,0	0,00	0,0
	SOF 59	2008-2011	0,00	0,0	0,29	0,13	0,00	0,0	0,29	0,13	0,00	0,05	0,00	0,00	0,00	0,0	0,00	0,0
	SOF 58	2020-2023	0,00		0,00		0,00		0,00		0,00		0,00		0,00		0,00	
	SOF 57	2029-2032	0,00		0,00		0,00		0,00		0,00		0,00		0,00		0,00	
	SOF 56	2038-2041	0,00		0,29		0,00		0,29		0,00		0,00		0,00		0,00	
	SOF 55	2050-2053	0,00		0,00		0,00		0,00		0,00		0,00		0,00		0,00	
	SOF 54	2059-2062	0,00		0,00		0,00		0,00		0,00		0,00		0,00		0,00	
	SOF 53	2068-2071	0,00		0,31		0,00		0,31		0,00		0,00		0,00		0,00	
	SOF 52	2080-2083	0,00		0,00		0,00		0,00		0,00		0,00		0,00		0,00	
	SOF 51	2089-2092	0,00		0,00		0,00		0,00		0,00		0,00		0,00		0,00	
	SOF 50	2098-2101	0,00		0,00		0,00		0,00		0,33		0,00		0,00		0,00	
	SOF 49	2107-2110	0,00		0,40		0,00		0,40		0,00		0,00		0,00		0,00	
	SOF 48	2119-2122	0,00		0,00		0,00		0,00		0,00		0,00		0,00		0,00	
	SOF 47	2128-2131	0,00		0,00		0,00		0,00		0,00		0,00		0,00		0,00	
	SOF 46	2137-2142	0,00		0,00		0,00		0,00		0,00		0,00		0,00		0,00	
	SOF 45	2149-2152	0,00		0,00		0,00		0,00		0,00		0,00		0,00		0,00	
	SOF 44	2161-2164	0,00		0,00		0,00		0,00		0,00		0,00		0,00		0,00	
	SOF 43	2170-2173	0,00		0,00		0,00		0,00		0,00		0,00		0,00		0,00	
	SOF 42	2179-2182	0,00		0,00		0,00		0,00		0,00		0,00		0,00		0,00	
	SOF 41	2188-2191	0,00		0,00		0,00		0,00		0,00		0,00		0,00		0,00	
	SOF 40	2197-2200	0,00		0,00		0,00		0,00		0,00		0,00		0,00		0,00	
	SOF 39	2209-2212	0,00		0,00		0,00		0,00		0,00		0,00		0,00		0,00	
	SOF 38	2218-2221	0,00		0,00		0,00		0,00		0,00		0,00		0,00		0,00	
	SOF 37	2227-2230	0,00		0,00		0,00		0,00		0,00		0,00		0,00		0,00	
	SOF 36	2239-2242	0,00		0,00		0,00		0,00		0,00		0,00		0,00		0,00	
	SOF 35	2248-2251	0,00		0,00		0,00		0,00		0,00		0,00		0,00		0,00	
	SOF 34	2257-2260	0,00		0,00		0,00		0,00		0,00		0,00		0,00		0,00	
	SOF 33	2269-2272	0,00		0,00		0,00		0,00		0,00		0,00		0,00		0,00	
	SOF 32	2281-2284	0,00		0,00		0,00		0,00		0,00		0,00		0,00		0,00	
	SOF 31	2290-2292	0,00		0,00		0,00		0,00		0,00		0,00		0,00		0,00	
	SOF 30	2299-2302	0,00		0,00		0,00		0,00		0,00		0,00		0,00		0,00	
	SOF 29	2308-2311	0,00		0,00		0,00		0,00		0,00		0,00		0,00		0,00	
	SOF 28	2320-2323	0,00		0,41		0,00		0,41		0,00		0,00		0,00		0,00	
	SOF 27	2326-2329	0,00		0,00		0,00		0,00		0,00		0,00		0,00		0,00	
	SOF 26	2335-2338	0,00		0,39		0,00		0,39		0,00		0,00		0,00		0,00	
	SOF 25	2341-2344	0,00		0,00		0,00		0,00		0,00		0,00		0,00		0,00	
	SOF 24	2350-2353	0,00		0,00		0,00		0,00		0,00		0,00		0,00		0,00	
	SOF 23	2359-2362	0,00		0,00		0,00		0,00		0,00		0,00		0,00		0,00	
lower Zapata - Berriasian to Valanginian	SOF 22	2368-2371	0,00	0,0	0,00	0,02	0,00	0,0	0,00	0,02	0,00	0,02	0,00	0,00	0,00	0,0	0,00	0,0
	SOF 21	2377-2380	0,00	0,0	0,29	0,08	0,00	0,0	0,29	0,08	0,29	0,08	0,00	0,00	0,00	0,0	0,00	0,0
	SOF 20	2389-2390	0,00		0,00		0,00		0,00		0,00		0,00		0,00		0,00	
	SOF 19	2396-2399	0,00		0,00		0,00		0,00		0,00		0,00		0,00		0,00	
	SOF 18	2408-2411	0,00		0,00		0,00		0,00		0,00		0,00		0,00		0,00	
	SOF 17	2420-2421	0,00		0,00		0,00		0,00		0,00		0,00		0,00		0,00	
	SOF 16	2429-2430	0,00		0,00		0,00		0,00		0,00		0,00		0,00		0,00	
	SOF 15	2439-2440	0,00		0,00		0,00		0,00		0,00		0,00		0,00		0,00	
	SOF 14	2450-2451	0,00		0,00		0,00		0,00		0,00		0,00		0,00		0,00	
	SOF 13	2459-2460	0,00		0,00		0,00		0,00		0,00		0,00		0,00		0,00	
	SOF 12	2469-2470	0,00		0,00		0,00		0,00		0,00		0,00		0,00		0,00	
	SOF 11	2475-2476	0,00		0,00		0,00		0,00		0,00		0,00		0,00		0,00	
	SOF 10	2478-2479	0,00		0,00		0,00		0,00		0,00		0,00		0,00		0,00	
Tithonian	SOF 9	2482,5-2483,0	0,00	0,0	0,00	0,00	0,00	0,0	0,00	0,00	0,29	0,03	0,00	0,00	0,00	0,0	0,00	0,0
	SOF 8	2486,0-2486,5	0,00	0,0	0,00	0,00	0,00	0,0	0,00	0,00	0,00	0,10	0,00	0,00	0,00	0,0	0,00	0,0
	SOF 7	2488-2489	0,00		0,00		0,00		0,00		0,00		0,00		0,00		0,00	
	SOF 6	2512-2513	0,00		0,00		0,00		0,00		0,00		0,00		0,00		0,00	
	SOF 5	2520-2521	0,00		0,00		0,00		0,00		0,00		0,00		0,00		0,00	
	SOF 4	2525-2526	0,00		0,00		0,00		0,00		0,00		0,00		0,00		0,00	
	SOF 3	2530-2531	0,00		0,00		0,00		0,00		0,00		0,00		0,00		0,00	
	SOF 2	2535-2536	0,00		0,00		0,00		0,00		0,00		0,00		0,00		0,00	
	SOF 1	2539-2540	0,00		0,00		0,00		0,00		0,00		0,00		0,00		0,00	

Sofia 1

Age	Sample	Depth (m)	terrestrial AOM translucent	%	terrestrial AOM opaque	%	AOMT % total	Sporo A	%	Sporo B	%	Sporo C	%	Sporomorphs total	
middle Zapata - Hauterivian to Aptian	SOF 60	1999-2002	37,1	8,89	1,92	1,14	39,0	0,00	0,12	0,32	1,18	2,56	1,37	9	7,82
	SOF 59	2008-2011	20,7	9,40	0,00	1,28	20,7	0,00	0,28	3,75	1,45	2,02	1,52	20	8,74
	SOF 58	2020-2023	42,3		3,37		45,7	0,00		2,76		0,92		12	
	SOF 57	2029-2032	20,3		1,16		21,5	0,29		2,33		2,62		18	
	SOF 56	2038-2041	15,4		1,16		16,5	0,00		1,16		1,45		9	
	SOF 55	2050-2053	10,0		0,00		10,0	0,39		1,93		4,63		18	
	SOF 54	2059-2062	16,7		0,00		16,7	0,35		3,14		6,27		28	
	SOF 53	2068-2071	8,0		0,00		8,0	0,62		4,63		3,40		28	
	SOF 52	2080-2083	14,1		0,00		14,1	0,00		1,92		3,51		17	
	SOF 51	2089-2092	6,4		0,00		6,4	0,00		0,58		1,45		7	
	SOF 50	2098-2101	15,2		0,33		15,6	1,32		3,64		2,98		24	
	SOF 49	2107-2110	5,6		0,40		6,0	0,80		1,61		2,01		11	
	SOF 48	2119-2122	16,0		0,00		16,0	0,37		1,49		0,74		7	
	SOF 47	2128-2131	11,7		0,00		11,7	0,00		0,95		1,58		8	
	SOF 46	2137-2142	5,3		0,67		6,0	0,00		1,00		1,33		7	
	SOF 45	2149-2152	8,6		0,34		8,9	0,00		0,34		0,00		1	
	SOF 44	2161-2164	2,6		0,00		2,6	0,00		0,00		0,37		1	
	SOF 43	2170-2173	1,9		2,22		4,1	0,00		0,00		0,00		0	
	SOF 42	2179-2182	3,2		0,00		3,2	0,00		0,00		0,00		0	
	SOF 41	2188-2191	1,6		3,49		5,0	0,00		0,00		0,00		0	
	SOF 40	2197-2200	1,9		1,51		3,4	0,00		0,38		0,00		1	
	SOF 39	2209-2212	3,6		3,62		7,2	0,00		0,00		0,00		0	
	SOF 38	2218-2221	1,2		2,02		3,2	0,00		0,00		0,00		0	
	SOF 37	2227-2230	1,2		4,25		5,4	0,00		0,00		0,00		0	
	SOF 36	2239-2242	2,4		3,53		5,9	0,00		0,00		0,00		0	
	SOF 35	2248-2251	2,4		3,13		5,6	0,00		0,69		1,04		5	
	SOF 34	2257-2260	15,5		2,39		17,9	0,00		0,80		0,00		2	
	SOF 33	2269-2272	7,6		1,15		8,8	0,00		0,00		0,76		2	
	SOF 32	2281-2284	2,1		1,28		3,4	0,00		0,00		0,43		1	
	SOF 31	2290-2292	7,7		0,52		8,2	0,00		0,00		0,52		1	
	SOF 30	2299-2302	2,9		1,65		4,5	0,00		0,41		0,82		3	
	SOF 29	2308-2311	1,3		0,00		1,3	0,00		1,71		1,71		8	
	SOF 28	2320-2323	2,8		0,81		3,7	0,00		0,00		1,22		3	
	SOF 27	2326-2329	1,9		0,97		2,9	0,00		0,48		0,00		1	
	SOF 26	2335-2338	4,3		0,78		5,1	0,00		3,50		3,50		18	
	SOF 25	2341-2344	5,1		0,74		5,9	0,37		5,15		3,31		24	
	SOF 24	2350-2353	1,1		0,00		1,1	0,00		0,00		0,75		2	
	SOF 23	2359-2362	10,1		0,00		10,1	0,00		0,34		0,00		1	
lower Zapata - Berriasian to Valanginian	SOF 22	2368-2371	25,47	11,09	0,00	0,21	25,5	0,00	0,00	0,31	0,07	0,00	0,10	1	0,54
	SOF 21	2377-2380	15,41	7,68	0,00	0,58	15,4	0,00	0,00	0,29	0,14	0,00	0,28	1	0,88
	SOF 20	2389-2390	13,61		2,04		15,6	0,00		0,34		0,00		1	
	SOF 19	2396-2399	16,01		0,65		16,7	0,00		0,00		0,00		0	
	SOF 18	2408-2411	17,06		0,00		17,1	0,00		0,00		0,00		0	
	SOF 17	2420-2421	16,61		0,00		16,6	0,00		0,00		0,33		1	
	SOF 16	2429-2430	1,26		0,00		1,3	0,00		0,00		0,00		0	
	SOF 15	2439-2440	9,18		0,00		9,2	0,00		0,00		0,00		0	
	SOF 14	2450-2451	16,67		0,00		16,7	0,00		0,00		1,00		3	
	SOF 13	2459-2460	3,52		0,00		3,5	0,00		0,00		0,00		0	
	SOF 12	2469-2470	0,99		0,00		1,0	0,00		0,00		0,00		0	
	SOF 11	2475-2476	4,70		0,00		4,7	0,00		0,00		0,00		0	
	SOF 10	2478-2479	3,75		0,00		3,8	0,00		0,00		0,00		0,0	
Tithonian	SOF 9	2482,5-2483,0	1,17	8,92	0,59	0,07	1,8	0,00	0,00	0,00	0,24	0,00	0,55	0,0	2,56
	SOF 8	2486,0-2486,5	5,07	5,47	0,00	0,20	5,1	0,00	0,00	0,30	0,33	0,00	0,66	1,0	3,05
	SOF 7	2488-2489	6,13		0,00		6,1	0,00		0,00		0,00		0,0	
	SOF 6	2512-2513	4,17		0,00		4,2	0,00		0,00		0,35		1,0	
	SOF 5	2520-2521	18,49		0,00		18,5	0,00		0,00		0,34		1,0	
	SOF 4	2525-2526	13,94		0,00		13,9	0,00		0,30		0,91		4,0	
	SOF 3	2530-2531	10,50		0,00		10,5	0,00		0,00		0,28		1,0	
	SOF 2	2535-2536	8,11		0,00		8,1	0,00		0,90		1,20		7,0	
	SOF 1	2539-2540	12,74		0,00		12,7	0,00		0,64		1,91		8,0	

Sofia 1

Age	Sample	Depth (m)	Sporomorphs %		Inertinite A	%	Inertinite B	%	Inertinite total	%	Vitrinite A	%	Vitrinite B	%	Vitrinite total	%	
middle Zapata - Hauterivian to Aptian	SOF 60	1999-2002	2,9	2,67	32,9	28,2	21,4	54,91	54,3	83,12	0,3	1,37	3,2	2,45	3,5	3,82	
	SOF 59	2008-2011	5,8	2,94	32,0	7,7	33,4	16,08	65,4	12,07	1,4	1,23	5,8	2,24	7,2	2,89	
	SOF 58	2020-2023	3,7		23,6		21,2		44,8		0,9		3,7		4,6		
	SOF 57	2029-2032	5,2		36,3		33,7		70,1		0,0		2,6		2,6		
	SOF 56	2038-2041	2,6		43,5		33,3		76,8		1,4		2,3		3,8		
	SOF 55	2050-2053	6,9		51,7		26,3		78,0		1,2		3,9		5,0		
	SOF 54	2059-2062	9,8		28,6		40,4		69,0		1,4		3,1		4,5		
	SOF 53	2068-2071	8,6		28,1		47,8		75,9		1,2		5,9		7,1		
	SOF 52	2080-2083	5,4		28,4		49,5		78,0		0,3		2,2		2,6		
	SOF 51	2089-2092	2,0		34,6		56,7		91,3		0,3		0,0		0,3		
	SOF 50	2098-2101	7,9		25,5		41,4		66,9		1,0		8,3		9,3		
	SOF 49	2107-2110	4,4		43,0		38,2		81,1		1,2		6,8		8,0		
	SOF 48	2119-2122	2,6		22,7		50,2		72,9		1,9		5,6		7,4		
	SOF 47	2128-2131	2,5		24,7		57,0		81,6		0,9		3,2		4,1		
	SOF 46	2137-2142	2,3		31,3		53,7		85,0		5,0		1,7		6,7		
	SOF 45	2149-2152	0,3		34,6		55,1		89,7		0,7		0,3		1,0		
	SOF 44	2161-2164	0,4		25,3		71,4		96,7		0,4		0,0		0,4		
	SOF 43	2170-2173	0,0		23,7		72,2		95,9		0,0		0,0		0,0		
	SOF 42	2179-2182	0,0		18,2		77,1		95,3		1,6		0,0		1,6		
	SOF 41	2188-2191	0,0		24,0		69,8		93,8		0,8		0,4		1,2		
	SOF 40	2197-2200	0,4		21,9		73,6		95,5		0,0		0,8		0,8		
	SOF 39	2209-2212	0,0		27,0		64,1		91,1		1,0		0,0		1,0		
	SOF 38	2218-2221	0,0		15,7		78,6		94,4		0,4		2,0		2,4		
	SOF 37	2227-2230	0,0		24,7		69,5		94,2		0,0		0,4		0,4		
	SOF 36	2239-2242	0,0		22,4		69,4		91,8		0,4		1,2		1,6		
	SOF 35	2248-2251	1,7		22,9		67,7		90,6		1,4		0,0		1,4		
	SOF 34	2257-2260	0,8		30,7		47,8		78,5		1,2		0,8		2,0		
	SOF 33	2269-2272	0,8		29,0		59,9		88,9		1,1		0,4		1,5		
	SOF 32	2281-2284	0,4		19,2		76,1		95,3		0,4		0,4		0,9		
	SOF 31	2290-2292	0,5		11,9		75,8		87,6		2,1		1,5		3,6		
	SOF 30	2299-2302	1,2		20,6		66,3		86,8		1,6		3,3		4,9		
	SOF 29	2308-2311	3,4		23,9		61,5		85,5		3,8		4,7		8,5		
	SOF 28	2320-2323	1,2		30,9		58,1		89,0		2,8		2,8		5,7		
	SOF 27	2326-2329	0,5		28,5		63,8		92,3		1,4		2,9		4,3		
	SOF 26	2335-2338	7,0		29,6		52,5		82,1		2,7		2,7		5,4		
	SOF 25	2341-2344	8,8		32,4		41,2		73,5		4,8		7,0		11,8		
	SOF 24	2350-2353	0,7		33,3		59,9		93,3		3,4		1,5		4,9		
	SOF 23	2359-2362	0,3		35,0		50,8		85,9		1,3		1,7		3,0		
lower Zapata - Berriasian to Valanginian	SOF 22	2368-2371	0,3	0,18	30,5	37,4	42,8	48,84	73,3	86,26	0,6	1,68	0,3	0,54	0,9	2,22	
	SOF 21	2377-2380	0,3	0,29	21,2	8,3	51,7	10,83	73,0	9,47	9,3	2,50	1,5	0,65	10,8	2,96	
	SOF 20	2389-2390	0,3		28,6		50,0		78,6		3,7		1,7		5,4		
	SOF 19	2396-2399	0,0		42,5		38,9		81,4		2,0		0,0		2,0		
	SOF 18	2408-2411	0,0		48,2		34,8		82,9		0,0		0,0		0,0		
	SOF 17	2420-2421	0,3		44,5		35,5		80,1		1,7		1,3		3,0		
	SOF 16	2429-2430	0,0		41,3		57,4		98,7		0,0		0,0		0,0		
	SOF 15	2439-2440	0,0		37,0		52,2		89,2		1,3		0,3		1,6		
	SOF 14	2450-2451	1,0		43,3		36,7		80,0		1,0		1,3		2,3		
	SOF 13	2459-2460	0,0		27,5		68,7		96,1		0,4		0,0		0,4		
	SOF 12	2469-2470	0,0		34,5		64,1		98,7		0,3		0,0		0,3		
	SOF 11	2475-2476	0,0		40,4		53,9		94,4		0,6		0,3		0,9		
	SOF 10	2478-2479	0,0		46,9		48,1		95,0		0,9		0,3		1,3		
Tithonian	SOF 9	2482,5-2483,0	0,0	0,79	36,4	40,9	58,9	44,97	95,3	85,92	2,3	2,44	0,3	1,80	2,6	4,24	
	SOF 8	2486,0-2486,5	0,3	0,94	43,0	2,9	49,9	9,58	92,8	7,73	1,2	1,56	0,6	1,80	1,8	3,16	
	SOF 7	2488-2489	0,0		37,3		54,6		91,9		1,7		0,0		1,7		
	SOF 6	2512-2513	0,3		39,2		55,6		94,8		0,0		0,7		0,7		
	SOF 5	2520-2521	0,3		41,4		36,3		77,7		1,7		1,7		3,4		
	SOF 4	2525-2526	1,2		40,6		36,7		77,3		4,5		3,0		7,6		
	SOF 3	2530-2531	0,3		42,5		36,2		78,7		4,7		5,8		10,5		
	SOF 2	2535-2536	2,1		45,6		38,7		84,4		3,6		1,8		5,4		
	SOF 1	2539-2540	2,5		42,4		37,9		80,3		2,2		2,2		4,5		

Sofia 1

Age	Sample	Depth (m)	Phytoclasts	%	Filaments	%	marine OM	%	terrestrial OM	%	Palynomorphs %	OP/TR
middle Zapata - Hauterivian to Aptian	SOF 60	1999-2002	57,8	86,94	0,0	0,00	0,0	0,06	97,8	98,60	2,9	21,79
	SOF 59	2008-2011	72,6	10,88	0,0	0,00	0,3	0,14	99,1	1,39	6,1	
	SOF 58	2020-2023	49,4		0,0		0,0		96,6		3,7	
	SOF 57	2029-2032	72,7		0,0		0,0		98,8		5,2	
	SOF 56	2038-2041	80,6		0,0		0,3		98,6		2,9	
	SOF 55	2050-2053	83,0		0,0		0,0		100,0		6,9	
	SOF 54	2059-2062	73,5		0,0		0,0		100,0		9,8	
	SOF 53	2068-2071	83,0		0,0		0,3		99,7		9,0	
	SOF 52	2080-2083	80,5		0,0		0,0		100,0		5,4	
	SOF 51	2089-2092	91,6		0,0		0,0		100,0		2,0	
	SOF 50	2098-2101	76,2		0,0		0,3		99,3		8,3	
	SOF 49	2107-2110	89,2		0,0		0,4		99,2		4,8	
	SOF 48	2119-2122	80,3		0,0		0,0		100,0		2,6	
	SOF 47	2128-2131	85,8		0,0		0,0		100,0		2,5	
	SOF 46	2137-2142	91,7		0,0		0,0		99,3		2,3	
	SOF 45	2149-2152	90,8		0,0		0,0		99,7		0,3	
	SOF 44	2161-2164	97,1		0,0		0,0		100,0		0,4	
	SOF 43	2170-2173	95,9		0,0		0,0		97,8		0,0	
	SOF 42	2179-2182	96,8		0,0		0,0		100,0		0,0	
	SOF 41	2188-2191	95,0		0,0		0,0		96,5		0,0	
	SOF 40	2197-2200	96,2		0,0		0,0		98,5		0,4	
	SOF 39	2209-2212	92,1		0,0		0,0		95,7		0,0	
	SOF 38	2218-2221	96,8		0,0		0,0		98,0		0,0	
	SOF 37	2227-2230	94,6		0,0		0,0		95,8		0,0	
	SOF 36	2239-2242	93,3		0,0		0,0		96,5		0,0	
	SOF 35	2248-2251	92,0		0,0		0,0		96,2		1,7	
	SOF 34	2257-2260	80,5		0,0		0,0		96,8		0,8	
	SOF 33	2269-2272	90,5		0,0		0,0		98,9		0,8	
	SOF 32	2281-2284	96,2		0,0		0,0		98,7		0,4	
	SOF 31	2290-2292	91,2		0,0		0,0		99,5		0,5	
	SOF 30	2299-2302	91,8		0,0		0,0		95,9		1,2	
	SOF 29	2308-2311	94,0		0,0		0,0		98,7		3,4	
	SOF 28	2320-2323	94,7		0,0		0,4		98,8		1,6	
	SOF 27	2326-2329	96,6		0,0		0,0		99,0		0,5	
	SOF 26	2335-2338	87,5		0,0		0,4		98,8		7,4	
	SOF 25	2341-2344	85,3		0,0		0,0		99,3		8,8	
	SOF 24	2350-2353	98,1		0,0		0,0		100,0		0,7	
	SOF 23	2359-2362	88,9		0,0		0,0		99,3		0,3	
lower Zapata - Berriasian to Valanginian	SOF 22	2368-2371	74,2	88,48	0,0	0,00	0,0	0,04	100,0	99,75	0,3	38,83
	SOF 21	2377-2380	83,7	7,97	0,0	0,00	0,6	0,16	99,4	0,58	0,9	
	SOF 20	2389-2390	84,0		0,0		0,0		98,0		0,3	
	SOF 19	2396-2399	83,3		0,0		0,0		99,3		0,0	
	SOF 18	2408-2411	82,9		0,0		0,0		100,0		0,0	
	SOF 17	2420-2421	83,1		0,0		0,0		100,0		0,3	
	SOF 16	2429-2430	98,7		0,0		0,0		100,0		0,0	
	SOF 15	2439-2440	90,8		0,0		0,0		100,0		0,0	
	SOF 14	2450-2451	82,3		0,0		0,0		100,0		1,0	
	SOF 13	2459-2460	96,5		0,0		0,0		100,0		0,0	
	SOF 12	2469-2470	99,0		0,0		0,0		100,0		0,0	
	SOF 11	2475-2476	95,3		0,0		0,0		100,0		0,0	
	SOF 10	2478-2479	96,3		0,0		0,0		100,0		0,0	
Tithonian	SOF 9	2482,5-2483,0	97,9	90,16	0,0	0,00	0,3	0,03	99,1	99,90	0,3	20,26
	SOF 8	2486,0-2486,5	94,6	5,71	0,0	0,00	0,0	0,10	100,0	0,29	0,3	
	SOF 7	2488-2489	93,6		0,0		0,0		100,0		0,0	
	SOF 6	2512-2513	95,5		0,0		0,0		100,0		0,3	
	SOF 5	2520-2521	81,2		0,0		0,0		100,0		0,3	
	SOF 4	2525-2526	84,8		0,0		0,0		100,0		1,2	
	SOF 3	2530-2531	89,2		0,0		0,0		100,0		0,3	
	SOF 2	2535-2536	89,8		0,0		0,0		100,0		2,1	
	SOF 1	2539-2540	84,7		0,0		0,0		100,0		2,5	

Byers Group

Age	Preservation		terrestrial																													
			parts of vascular plants												Pollen												Spores					
			phytoclasts																													
			Inertinite				Vitrinite				Cutinite				nonsaccate				monosaccate				bisaccate				monolete				trilete			
	Sample	Formation	A	B	C	sum	A	B	C	sum	A	B	C	sum	A	B	C	sum	A	B	C	sum	A	B	C	sum	A	B	C	sum	A	B	C	sum
lower Valanginian - middle Valanginian	P.2186.22	CCF - SHM	11	3	0	14	31	48	0	79	0	0	0	0	1	0	0	1	8	3	0	11	0	0	0	0	9	10	0	19	12	2	0	14
	P.2186.21	CCF - SHM	42	1	0	43	83	10	0	93	0	2	0	2	5	0	0	5	8	5	1	14	1	0	0	1	30	19	2	51	17	5	1	23
	P.2186.20	CCF - SHM	75	4	0	79	40	62	0	102	5	#	3	22	3	0	0	3	4	0	0	4	0	0	0	0	12	0	0	12	21	0	0	21
	P.2186.19	CCF - SHM	50	5	0	55	75	14	0	89	0	3	0	3	2	0	0	2	14	1	0	15	0	1	0	1	26	20	0	46	20	3	0	23
	P.2186.18	CCF - SHM	103	73	0	176	30	12	0	42	0	2	2	4	0	0	0	0	3	3	0	6	0	0	0	0	6	13	1	20	6	5	0	11
	P.2186.17	CCF - SHM	17	0	0	17	61	46	0	107	4	4	5	13	4	0	0	4	4	0	0	4	0	0	0	0	21	0	0	21	22	3	0	25
	P.2186.16	CCF - SHM	25	0	0	25	72	57	0	129	2	1	0	3	0	0	0	0	15	5	1	21	0	0	0	0	16	11	1	28	8	6	0	14
	P.2186.15	CCF - SHM	70	7	0	77	78	17	0	95	0	4	1	5	2	0	0	2	13	5	0	18	0	0	0	0	10	10	0	20	8	2	0	10
	P.2186.14	CCF - SHM	9	0	0	9	90	45	0	135	0	3	0	3	2	0	0	2	14	0	0	14	0	1	0	1	23	2	0	25	18	1	0	19
	P.2186.13	CCF - SHM	18	2	0	20	62	44	0	106	#	#	4	30	6	0	0	6	12	0	0	12	0	0	0	0	13	3	0	16	24	3	0	27
	P.2186.12	CCF - SHM	32	8	0	40	29	41	0	70	4	8	7	19	0	1	0	1	5	10	0	15	0	0	0	0	3	3	0	6	5	4	0	9
	P.2186.11	CCF - SHM	10	0	0	10	77	47	0	124	0	2	0	2	0	0	0	0	10	4	0	14	0	0	0	0	13	4	0	17	7	3	0	10
	P.2186.10	CCF - SHM	32	17	0	49	45	73	0	118	3	4	10	17	2	4	0	6	3	5	0	8	0	0	0	0	5	16	0	21	10	6	0	16
	P.2186.9 A	CCF - SHM	52	4	0	56	64	15	0	79	2	3	0	5	0	0	0	0	22	3	0	25	0	0	0	0	9	11	0	20	17	3	1	21
	P.2186.9 B	CCF - SHM	13	2	0	15	83	26	0	109	6	2	0	8	0	0	0	0	13	1	0	14	1	0	0	1	15	3	0	18	21	1	0	22
	P.2186.8	CCF - SHM	29	0	0	29	54	42	0	96	0	0	0	0	0	0	0	0	19	11	0	30	0	0	0	0	18	15	0	33	21	8	0	29
	P.2186.7	CCF - SHM	23	2	0	25	57	40	0	97	4	#	0	14	0	0	0	0	4	5	0	9	2	0	0	2	11	17	0	28	7	4	0	11
	P.2186.6	CCF - SHM	79	13	0	92	51	20	0	71	2	1	2	5	0	0	0	0	8	2	0	10	0	0	0	0	11	13	0	24	12	1	0	13
	P.2186.5	CCF - SHM	56	6	0	62	76	25	0	101	1	5	0	6	1	0	0	1	24	2	0	26	0	0	0	0	17	5	0	22	14	7	0	21
	P.2186.4	CCF - SHM	89	1	0	90	105	6	0	111	0	0	0	0	2	1	0	3	11	5	1	17	1	0	0	1	17	24	2	43	23	11	2	36
	P.2186.3	CCF - SHM	140	80	0	220	2	9	0	11	0	0	1	1	0	0	0	0	0	0	0	0	0	0	0	0	0	0	0	0	1	0	0	1
	P.2186.2	CCF - SHM	75	21	0	96	70	32	0	102	0	4	3	7	0	0	0	0	6	1	0	7	1	0	0	1	12	20	0	32	25	3	0	28
	P.2186.1	CCF - SHM	20	2	0	22	90	89	0	179	0	0	0	0	0	0	0	0	31	8	0	39	1	0	0	1	25	7	0	32	13	2	0	15
late Berriasian - early Valanginian	P.2175.7	CCF -DPM	167	90	0	257	0	1	0	1	0	0	0	0	0	0	0	0	0	0	0	0	0	0	0	0	0	0	0	0	0	0	0	0
	P.2175.1	CCF -DPM	54	9	0	63	6	7	0	13	0	0	0	0	0	0	0	0	0	0	0	0	0	0	0	0	0	0	0	0	0	1	0	1
	P.2174.37	CCF -DPM	103	40	0	143	0	6	0	6	0	0	0	0	0	0	0	0	0	0	0	0	0	0	0	0	0	0	0	0	0	0	0	0
	P.2174.31	CCF -DPM	144	46	0	190	4	12	0	16	0	0	0	0	0	0	0	0	0	1	0	1	0	0	0	0	0	0	0	0	0	0	0	0
	P.2174.30	CCF -DPM	132	45	0	177	6	10	0	16	0	0	0	0	0	0	0	0	0	0	0	0	0	0	0	0	0	0	0	0	0	0	1	1
	P.2174.28 B	CCF -DPM	163	108	0	271	1	7	0	8	0	0	0	0	0	0	0	0	0	0	0	0	0	0	0	0	0	0	0	0	0	0	0	0
	P.2174.28 A	CCF -DPM	131	69	0	200	8	24	0	32	0	0	0	0	0	0	0	0	0	0	0	0	0	0	0	0	0	0	0	0	0	0	0	0
	P.2174.26	CCF -DPM	110	101	0	211	6	23	0	29	0	0	0	0	0	0	0	0	0	0	0	0	0	0	0	0	0	0	0	0	0	1	0	1
	P.2172.9	CCF -DPM	89	115	0	204	5	22	0	27	0	1	0	1	0	0	0	0	0	0	0	0	0	0	0	0	0	0	0	0	0	1	0	1
	P.2172.8	CCF -DPM	74	153	0	227	1	9	0	10	0	0	0	0	0	0	0	0	0	0	0	0	0	0	0	0	0	0	0	0	0	0	0	0
	P.2172.7	CCF -DPM	44	164	0	208	4	5	0	9	0	0	0	0	0	0	0	0	0	0	0	0	0	0	0	0	0	0	0	0	0	0	0	0
	P.2172.6	CCF -DPM	123	108	0	231	10	15	0	25	0	0	0	0	0	0	0	0	0	0	0	0	0	0	0	0	0	0	1	1	1	0	0	1
	P.2173.3	CCF -DPM	119	111	0	230	1	1	0	2	0	0	0	0	0	0	0	0	0	0	0	0	0	0	0	0	0	0	0	0	0	1	0	1
	P.2173.2 B	CCF -DPM	94	56	0	150	2	4	0	6	0	1	0	1	0	0	0	0	0	0	0	0	0	0	0	0	1	0	0	1	2	0	0	2
	P.2173.2 A	CCF -DPM	25	16	0	41	0	6	0	6	0	0	0	0	0	0	0	0	0	0	0	0	0	0	0	0	0	0	0	0	0	0	0	0
	P.2171.6	CCF -DPM	41	8	0	49	118	41	0	159	5	2	0	7	0	0	0	0	8	5	0	13	0	0	0	0	12	8	0	20	22	7	0	29
	P.2171.3	CCF -DPM	18	2	0	20	109	41	0	150	#	#	2	33	0	0	0	0	10	2	0	12	0	0	0	0	11	3	0	14	20	8	0	28
	P.2171.2	CCF -DPM	37	7	0	44	103	49	0	152	#	#	1	25	1	0	0	1	12	5	0	17	2	0	0	2	20	2	0	22	21	5	0	26
	P.2171.1	CCF -DPM	14	1	0	15	91	44	0	135	0	0	3	3	0	0	0	0	12	8	0	20	0	0	0	0	34	6	0	40	24	5	0	29
early Berriasian - middle Berriasian	P.2224.7	PBF	71	10	0	81	40	87	0	127	1	0	0	1	0	0	0	0	2	0	0	2	0	0	0	0	4	0	0	4	4	1	0	5
	P.2224.1	PBF	51	37	0	88	19	45	0	64	0	6	8	14	1	0	0	1	8	5	0	13	0	0	0	0	12	1	0	13	10	3	0	13
	P.2220.20	PBF	70	41	0	111	32	81	0	113	0	0	0	0	0	0	0	0	0	0	0	0	0	0	0	0	0	2	0	2	4	3	1	8
	P.2220.11	PBF	62	19	0	81	54	88	0	142	0	0	0	0	0	0	0	0	0	0	0	0	0	0	0	0	0	2	0	2	1	3	0	4
	P.2220.4	PBF	97	22	0	119	30	58	0	88	0	2	0	2	0	0	0	0	0	0	0	0	0	0	0	0	1	7	0	8	1	3	0	4
	P.2222.3	PBF	59	14	0	73	44	43	0	87	0	0	0	0	0	0	0	0	0	0	0	0	0	0	0	0	0	3	1	4	0	2	1	3
	P.2176.38	PBF	148	72	0	220	2	5	0	7	0	0	0	0	0	0	0	0	0	1	0	1	0	0	0	0	0	1	0	1	0	0	0	0
	P.2176.37	PBF	104	110	0	214	2	5	0	7	0	0	0	0	0	0	0	0	0	0	0	0	0	0	0	0	0	0	0	0	0	0	0	0
	P.2176.35	PBF	74	71	0	145	5	25	0	30	0	0	0	0	0	0	0	0	0	0	0	0	0	0	0	0	0	0	0	0	0	0	0	0
	P.2176.34	PBF	95	97	0	192	0	16	0	16	0	0	2	2	0	0	0	0	0	0	0	0	0	0	0	0	0	0	0	0	0	0	0	0
	P.2176.32	PBF	107	164	0	271	0	19	0	19	0	0	0	0	0	0	0	0	0	0	0	0	0	0	0	0	0	0	0	0	0	0	0	0
	P.2176.31	PBF	128	92	0	220	0	9	0	9	0	0	1	1	0	0	0	0	0	0	0	0	0	0	0	0	0	0	0	0	0	0	0	0
	P.2176.30	PBF	125	83	0	208	4	21	0	25	0	0	0	0	0	0	0	0	0	0	0	0	0	0	0	0	0	0	0	0	0	0	0	0
	P.2176.27	PBF	13	5	0	18	46	58	0	104	0	0	1	1	0	0	0	0	10	6	1	17	0	1	0	1	10	4	0	14	8	5	0	13
	P.2176.18	PBF	34	6	0	40	24	90	0	114	0	1	0	1	0	0	0	0	0	1	1	2	0	0	0	0	1	2	0	3	5	1	1	7
	P.2176.17 C	PBF	26	2	0	28	81	55	0	136	0	2	0	2	0	0	0	0	0	3	0	3	0	0	0	0	6	11	0	17	7	5	0	12
	P.2176.15	PBF	13	5	0	18	90	57	0	147	2	8	0	10	5	0	0	5	30	3	0	33	2	0	0	2	16	3	0	19	31	8	1	40
	P.2176.14	PBF	19	1	0	20	61	53	0	114	8	6	3	17	1	0	0	1	13	7	0	20	4	0	0	4	46	5	0	51	43	8	1	52
	P.2176.9	PBF	78	42	0	120	25	28	0	53	0	5	21	26	0	0	0	0	6	1	1	8	0	0	0	0	5	0	0	5	1	1	0	2
	P.2176.2	PBF	103	22	0	125	3	41	0	44	0	0	22	22	0	0	0	0	1	0	0	1	0	0	0	0	1	2	0	3	5	2	0	7
	P.2176.24	PBF	118	106	0	224	6	11	0	17	0	0	0	0	0	0	0	0	0	0	0	0	0	0	0	0	0	0	0	0	1	0	0	1
	P.2176.23	PBF	45	21	0	66	13	22	0	35	0	1	25	26	1	0	0	1	1	0	0	1	0	0	0	0	2	4	0	6	1	0	0	1
	P.2183.12	PBF	25	7	0	32	35	40	0	75	2	9	0	11	0	2	0	2	2	7	0	9	0	0	0	0	0	5	0	5	3	7	0	10
	P.2183.11	PBF	77	5	0	82	58	11	0	69	0	0	0	0	0	0	0	0	16	12	1	29	0	0	0	0	15	4	0	19	25	4	0	29
	P.2183.10	PBF	9	0	0	9	41	38	0	79	0	0	0	0	1	1	0	2	13	7	0	20	0	0	0	0	17	9	0	26	10	4	0	14
	P.2183.8	PBF	31	51	0	82	13	52	0	65	0	0	0	0	0	0	0	0	1	1	0	2	0	0	0	0	0	0	0	0	0	5	0	5
	P.2183.7	PBF	31	7	0	38	75	63	0	138	0	0	0	0	0	0	0	0	1	5	0	6	0	0	0	0	2	5	2	9	6	2	0	8

terrestrial				AOM			marine																					diverse					
Spores							marine phytoplankton											Zoomorphs				Zooclasts						mineral residues					
indet				terrestrial, translucent	terrestrial opaque	marine/sensu stricto	Dinocysts				Acritarchs				Algae indet	Leiospheres	foraminiferal test linings				Bivalves, Scolecodonts, Fungi				Filaments	Quartz	Pyrite	others	Glendonites					
A	B	C	sum				A	B	C	sum	A	B	C	sum			A	B	C	sum	A	B	C	sum						Totals			
7	7	5	19	85,0	0	68,0	0	1	0	1	0	0	0	0	0	0	0	0	0	0	0	0	0	0	0	58	3	21	x	311			
2	25	5	32	94,0	0	26,0	0	0	0	0	0	0	0	0	5	0	0	0	0	0	0	0	0	0	0	110	0	0	x	389			
50	0	0	50	104,0	0	32,0	2	0	0	2	0	0	0	0	6	3	0	0	0	0	0	0	0	0	0	78	9	0		440			
5	23	1	29	82,0	0	31,0	3	2	0	5	0	0	0	0	9	0	0	0	0	0	0	2	1	3	2	60	3	0		395			
1	5	0	6	73,0	0	21,0	0	1	0	1	0	0	0	0	5	0	0	0	0	0	0	2	0	2	0	133	120	2		367			
44	1	0	45	68,0	0	50,0	1	0	0	1	0	0	0	0	10	3	1	0	0	1	0	0	0	0	0	19	3	0		369			
3	4	0	7	49,0	0	33,0	0	1	0	1	0	0	0	0	0	0	0	0	0	0	1	0	0	1	1	90	3	0		312			
0	13	2	15	87,0	0	34,0	0	0	0	0	0	0	0	0	0	0	0	0	0	0	0	1	0	1	0	67	3	0		364			
3	4	0	7	51,0	0	40,0	0	1	0	1	0	1	0	1	0	0	0	0	0	0	1	0	0	1	0	94	3	0	x	309			
40	5	0	45	127,0	0	53,0	5	2	0	7	0	0	0	0	5	1	0	0	0	0	3	0	0	3	0	8	12	1		458			
2	20	5	27	97,0	0	52,0	0	0	0	0	0	0	0	0	6	1	0	0	0	0	8	0	0	8	2	31	3	0		353			
4	12	1	17	74,0	0	46,0	2	3	0	5	0	0	0	0	3	0	0	0	0	0	4	0	0	4	2	50	2	0	x	328			
0	26	5	31	50,0	0	51,0	0	0	0	0	0	0	0	0	0	0	0	0	0	0	8	0	0	8	4	88	1	0		379			
4	8	0	12	89,0	0	40,0	0	3	0	3	0	0	0	0	2	0	0	0	0	0	5	0	0	5	0	120	7	0		357			
8	19	2	29	83,0	0	43,0	0	1	0	1	0	0	0	0	2	0	0	0	0	0	4	0	0	4	0	21	3	16		349			
4	12	0	16	57,0	0	54,0	0	0	0	0	0	0	0	0	0	0	0	0	0	0	1	0	0	1	0	218	5	0	x	345			
7	1	0	8	61,0	0	43,0	0	0	0	0	0	1	0	1	4	0	0	1	0	1	8	1	0	9	0	33	5	0		313			
3	16	1	20	117,0	0	25,0	2	0	0	2	0	1	0	1	7	3	0	0	0	0	1	3	0	4	0	112	2	0		394			
10	18	0	28	60,0	1	19,0	2	0	1	3	0	0	0	0	7	0	0	0	0	0	0	0	0	0	0	101	2	2	x	357			
0	8	0	8	44,0	0	28,0	1	1	0	1	1	0	0	1	6	0	1	0	0	1	0	1	0	1	0	95	2	0		391			
0	1	2	3	50,0	2	45,0	0	0	0	0	0	0	0	0	0	0	0	0	0	0	0	0	0	0	3	243	285	20		336			
2	25	2	29	98,0	0	26,0	1	0	0	1	0	0	0	0	5	0	0	0	0	0	0	3	0	3	5	20	2	0		440			
0	7	0	7	50,0	0	28,0	0	2	1	3	0	0	0	0	4	0	1	0	0	1	0	0	0	0	0	111	10	0	x	381			
0	0	0	0	48,7	0	9,3	0	0	0	0	0	0	0	0	0	0	0	0	0	0	0	0	0	0	0	140	71	0		316			
0	0	0	0	31,5	0	8,5	0	0	0	0	0	0	0	0	0	0	0	0	0	0	2	0	0	2	0	228	19	3	x	119			
0	0	1	1	18,3	0	2,7	0	0	0	0	0	0	0	0	0	0	0	0	0	0	0	0	0	0	0	66	153	57		171			
0	0	1	1	60,0	0	15,0	0	0	0	0	0	0	0	0	0	0	0	0	0	0	0	0	0	0	0	194	53	0		283			
0	1	5	6	78,6	0	23,4	0	0	0	0	0	0	0	0	0	0	0	0	0	0	0	0	0	0	0	173	4	0		302			
0	0	0	0	13,0	0	0,0	0	0	0	0	0	0	0	0	0	0	0	0	0	0	0	0	0	0	0	10	138	0		292			
0	0	0	0	29,0	1	0,0	0	0	0	0	0	0	0	0	0	0	0	0	0	0	0	0	0	0	0	11	1	0		262			
1	1	0	2	40,4	2	12,6	0	0	0	0	0	0	0	0	2	0	0	0	0	0	2	0	0	2	0	46	32	100	x	302			
0	0	19	19	49,5	0	21,5	0	0	0	0	0	0	0	0	0	0	0	0	0	0	4	0	0	4	25	164	20	0		352			
0	0	13	13	87,0	2	1,0	0	0	0	0	0	0	0	0	0	0	0	0	0	0	1	0	0	1	0	127	10	24		341			
1	4	0	5	106,4	0	1,6	0	0	0	0	0	0	0	0	0	0	0	0	0	0	0	0	0	0	0	190	2	0	x	330			
1	1	23	25	63,8	0	11,2	0	0	0	0	0	0	0	0	0	0	0	0	0	0	2	0	0	2	0	81	49	28	x	360			
0	0	0	0	14,9	12	1,1	0	0	0	0	0	0	0	0	0	0	0	0	0	0	0	0	0	0	10	176	6	1		271			
0	0	0	0	49,5	1	31,5	0	0	0	0	0	0	0	0	0	0	0	0	0	0	0	0	0	0	44	286	11	12	x	286			
1	2	0	3	115,9	0	42,1	0	0	0	0	0	0	0	0	0	0	0	0	0	0	0	0	0	0	86	190	3	11	x	294			
2	8	1	11	58,4	0	17,6	0	0	0	0	0	0	1	0	1	2	0	0	0	0	2	0	0	2	2	66	28	0	x	371			
1	3	0	4	75,2	0	29,8	1	1	2	4	0	0	0	0	6	0	0	0	0	0	#	0	0	11	0	12	4	56		387			
2	4	0	6	84,3	0	28,7	3	1	0	4	0	0	0	0	6	0	0	0	0	0	5	0	0	5	0	9	7	19		423			
3	3	0	6	75,2	0	26,8	0	0	0	0	1	0	0	1	11	0	0	0	0	0	9	0	0	9	5	76	3	87		376			
4	1	0	5	49,0	4	59,3	0	0	0	0	0	0	0	0	0	0	0	0	0	0	0	0	0	0	0	174	18	0		337			
0	6	1	7	72,4	0	37,6	0	0	0	0	0	0	0	0	25	0	0	0	0	0	6	0	0	6	0	41	64	15	x	354			
4	24	15	43	34,4	0	24,6	0	0	0	0	0	0	0	0	3	0	0	1	0	1	0	0	0	0	0	105	4	20	x	340			
24	17	3	44	10,0	0	26,0	0	0	0	0	0	0	0	0	22	2	0	0	0	0	0	0	0	0	0	68	3	0		333			
4	26	6	36	59,8	0	22,2	0	0	0	0	0	0	0	0	2	0	0	0	0	0	0	0	0	0	0	159	27	1		341			
0	15	13	28	98,6	0	47,4	0	0	0	0	0	0	0	0	0	0	0	0	0	0	0	0	0	0	0	160	10	0		341			
0	3	1	4	84,8	2	41,2	0	0	0	0	0	0	0	0	0	0	0	0	0	0	0	0	0	0	0	321	55	0		361			
0	0	0	0	84,8	0	75,2	0	0	0	0	0	0	0	0	0	0	0	0	0	0	0	0	0	0	0	174	11	0		381			
0	1	0	1	64,0	1	36,0	0	0	0	0	0	0	0	0	0	0	0	0	0	0	1	0	0	1	3	305	47	39		281			
1	2	4	7	36,8	0	9,2	0	0	0	0	0	0	0	0	0	0	0	0	0	0	2	0	0	2	0	114	19	43		265			
0	2	2	4	50,1	0	12,9	0	0	0	0	0	0	0	0	0	0	0	0	0	0	0	0	0	0	0	141	8	2		357			
0	1	0	1	19,7	1	1,3	0	0	0	0	0	0	0	0	0	0	0	0	0	0	0	0	0	0	0	141	30	58		253			
0	0	4	4	20,6	0	0,4	0	0	0	0	0	0	0	0	0	0	0	0	0	0	0	0	0	0	0	37	59	36		258			
3	10	0	13	99,3	0	36,7	0	0	2	2	0	0	0	0	2	0	0	0	0	0	3	0	0	3	1	26	1	70		325			
2	19	5	26	29,5	1	76,5	0	0	0	0	0	0	0	0	0	0	0	0	0	0	0	0	0	0	6	182	40	0	x	306			
0	13	1	14	120,8	0	24,2	1	1	0	2	0	0	0	0	5	0	0	0	0	0	1	0	0	1	3	2	0	0		368			
9	10	1	20	46,6	0	17,4	2	2	0	4	0	0	0	0	5	0	0	0	0	0	0	0	0	0	0	22	11	0	x	367			
4	9	0	13	65,0	0	15,0	3	2	1	6	0	0	0	0	10	0	1	1	0	2	2	0	0	2	5	4	28	44		397			
2	1	0	3	27,9	7	15,1	0	0	0	0	0	0	0	0	7	0	0	0	0	0	#	0	0	27	6	84	38	65		307			
2	2	0	4	47,7	1	64,3	0	0	0	0	0	0	0	0	5	0	0	0	0	0	3	0	0	3	0	243	34	70		327			
0	4	1	5	11,4	0	18,6	0	0	0	0	0	0	0	0	3	0	0	0	0	0	1	#	5	23	0	409	24	3		303			
0	0	0	0	50,7	0	45,3	0	0	0	0	0	0	0	0	0	0	0	0	0	0	0	0	0	0	0	247	28	10		232			
1	10	2	13	94,0	0	44,0	0	1	0	1	0	1	0	1	4	0	0	0	0	0	3	0	0	3	2	32	0	0		306			
7	16	0	23	43,0	0	47,0	2	1	0	3	1	0	0	1	8	0	1	0	0	1	3	1	0	4	0	136	23	0		358			
1	11	2	14	73,0	0	98,0	0	0	0	0	0	0	0	0	5	0	0	0	0	0	0	0	0	0	1	88	0	28	x	341			
1	14	11	26	68,0	2	11,0	0	0	0	0	0	0	0	0	0	0	0	0	0	0	0	0	0	0	0	43	1	35	x	261			
9	21	4	34	101,0	0	12,0	1	2	1	4	0	0	0	0	3	0	1	0	0	1	1	0	0	1	5	95	19	15	x	360			

Byers Group

Age	Sample	Formation	Dino A	%	Dino B	%	Dino C	%	Dinocysts total	%	Acritarchs	%	Algae indet	%	Foraminifera	%
lower Valanginian - middle Valanginian	P.2186.22	CCF - SHM	0,00	0,21	0,32	0,21	0,00	0,02	0,32	0,44	0,00	0,05	0,00	0,98	0,00	0,05
	P.2186.21	CCF - SHM	0,00	0,31	0,00	0,28	0,00	0,08	0,00	0,48	0,00	0,11	1,29	0,82	0,00	0,11
	P.2186.20	CCF - SHM	0,45		0,00		0,00		0,45		0,00		1,36		0,00	
	P.2186.19	CCF - SHM	0,76		0,51		0,00		1,27		0,00		2,28		0,00	
	P.2186.18	CCF - SHM	0,00		0,27		0,00		0,27		0,00		1,36		0,00	
	P.2186.17	CCF - SHM	0,27		0,00		0,00		0,27		0,00		2,71		0,27	
	P.2186.16	CCF - SHM	0,00		0,32		0,00		0,32		0,00		0,00		0,00	
	P.2186.15	CCF - SHM	0,00		0,00		0,00		0,00		0,00		0,00		0,00	
	P.2186.14	CCF - SHM	0,00		0,32		0,00		0,32		0,32		0,00		0,00	
	P.2186.13	CCF - SHM	1,09		0,44		0,00		1,53		0,00		1,09		0,00	
	P.2186.12	CCF - SHM	0,00		0,00		0,00		0,00		0,00		1,70		0,00	
	P.2186.11	CCF - SHM	0,61		0,91		0,00		1,52		0,00		0,91		0,00	
	P.2186.10	CCF - SHM	0,00		0,00		0,00		0,00		0,00		0,00		0,00	
	P.2186.9 A	CCF - SHM	0,00		0,84		0,00		0,84		0,00		0,56		0,00	
	P.2186.9 B	CCF - SHM	0,00		0,29		0,00		0,29		0,00		0,57		0,00	
	P.2186.8	CCF - SHM	0,00		0,00		0,00		0,00		0,00		0,00		0,00	
	P.2186.7	CCF - SHM	0,00		0,00		0,00		0,00		0,32		1,28		0,32	
	P.2186.6	CCF - SHM	0,51		0,00		0,00		0,51		0,25		1,78		0,00	
	P.2186.5	CCF - SHM	0,56		0,00		0,28		0,84		0,00		1,96		0,00	
	P.2186.4	CCF - SHM	0,26		0,00		0,00		0,26		0,26		1,53		0,26	
	P.2186.3	CCF - SHM	0,00		0,00		0,00		0,00		0,00		0,00		0,00	
	P.2186.2	CCF - SHM	0,23		0,00		0,00		0,23		0,00		1,14		0,00	
	P.2186.1	CCF - SHM	0,00		0,52		0,26		0,79		0,00		1,05		0,26	
late Berriasian - early Valanginian	P.2175.7	CCF -DPM	0,00	0,05	0,00	0,03	0,00	0,03	0,00	0,10	0,00	0,03	0,00	0,37	0,00	0,00
	P.2175.1	CCF -DPM	0,00	0,17	0,00	0,08	0,00	0,12	0,00	0,31	0,00	0,08	0,00	0,78	0,00	0,00
	P.2174.37	CCF -DPM	0,00		0,00		0,00		0,00		0,00		0,00		0,00	
	P.2174.31	CCF -DPM	0,00		0,00		0,00		0,00		0,00		0,00		0,00	
	P.2174.30	CCF -DPM	0,00		0,00		0,00		0,00		0,00		0,00		0,00	
	P.2174.28 B	CCF -DPM	0,00		0,00		0,00		0,00		0,00		0,00		0,00	
	P.2174.28 A	CCF -DPM	0,00		0,00		0,00		0,00		0,00		0,00		0,00	
	P.2174.26	CCF -DPM	0,00		0,00		0,00		0,00		0,00		0,66		0,00	
	P.2172.9	CCF -DPM	0,00		0,00		0,00		0,00		0,00		0,00		0,00	
	P.2172.8	CCF -DPM	0,00		0,00		0,00		0,00		0,00		0,00		0,00	
	P.2172.7	CCF -DPM	0,00		0,00		0,00		0,00		0,00		0,00		0,00	
	P.2172.6	CCF -DPM	0,00		0,00		0,00		0,00		0,00		0,00		0,00	
	P.2173.3	CCF -DPM	0,00		0,00		0,00		0,00		0,00		0,00		0,00	
	P.2173.2 B	CCF -DPM	0,00		0,00		0,00		0,00		0,00		0,00		0,00	
	P.2173.2 A	CCF -DPM	0,00		0,00		0,00		0,00		0,00		0,00		0,00	
	P.2171.6	CCF -DPM	0,00		0,00		0,00		0,00		0,27		0,54		0,00	
	P.2171.3	CCF -DPM	0,26		0,26		0,52		1,03		0,00		1,55		0,00	
	P.2171.2	CCF -DPM	0,71		0,24		0,00		0,95		0,00		1,42		0,00	
	P.2171.1	CCF -DPM	0,00		0,00		0,00		0,00		0,27		2,93		0,00	
early Berriasian - middle Berriasian	P.2224.7	PBF	0,00	0,08	0,00	0,08	0,00	0,03	0,00	0,20	0,00	0,03	0,00	1,15	0,00	0,04
	P.2224.1	PBF	0,00	0,19	0,00	0,17	0,00	0,12	0,00	0,40	0,00	0,08	7,06	1,67	0,00	0,12
	P.2220.20	PBF	0,00		0,00		0,00		0,00		0,00		0,88		0,29	
	P.2220.11	PBF	0,00		0,00		0,00		0,00		0,00		6,61		0,00	
	P.2220.4	PBF	0,00		0,00		0,00		0,00		0,00		0,59		0,00	
	P.2222.3	PBF	0,00		0,00		0,00		0,00		0,00		0,00		0,00	
	P.2176.38	PBF	0,00		0,00		0,00		0,00		0,00		0,00		0,00	
	P.2176.37	PBF	0,00		0,00		0,00		0,00		0,00		0,00		0,00	
	P.2176.35	PBF	0,00		0,00		0,00		0,00		0,00		0,00		0,00	
	P.2176.34	PBF	0,00		0,00		0,00		0,00		0,00		0,00		0,00	
	P.2176.32	PBF	0,00		0,00		0,00		0,00		0,00		0,00		0,00	
	P.2176.31	PBF	0,00		0,00		0,00		0,00		0,00		0,00		0,00	
	P.2176.30	PBF	0,00		0,00		0,00		0,00		0,00		0,00		0,00	
	P.2176.27	PBF	0,00		0,00		0,62		0,62		0,00		0,62		0,00	
	P.2176.18	PBF	0,00		0,00		0,00		0,00		0,00		0,00		0,00	
	P.2176.17 C	PBF	0,27		0,27		0,00		0,54		0,00		1,36		0,00	
	P.2176.15	PBF	0,54		0,54		0,00		1,09		0,00		1,36		0,00	
	P.2176.14	PBF	0,76		0,50		0,25		1,51		0,00		2,52		0,50	
	P.2176.9	PBF	0,00		0,00		0,00		0,00		0,00		2,28		0,00	
	P.2176.2	PBF	0,00		0,00		0,00		0,00		0,00		1,53		0,00	
	P.2176.24	PBF	0,00		0,00		0,00		0,00		0,00		0,99		0,00	
	P.2176.23	PBF	0,00		0,00		0,00		0,00		0,00		0,00		0,00	
	P.2183.12	PBF	0,00		0,33		0,00		0,33		0,33		1,31		0,00	
	P.2183.11	PBF	0,56		0,28		0,00		0,84		0,28		2,23		0,28	
	P.2183.10	PBF	0,00		0,00		0,00		0,00		0,00		1,47		0,00	
	P.2183.8	PBF	0,00		0,00		0,00		0,00		0,00		0,00		0,00	
	P.2183.7	PBF	0,28		0,56		0,28		1,11		0		0,83		0,28	

Byers Group

Age	Sample	Formation	Leiospheres	%	marine AOM	%	terrestrial AOM translucent	%	terrestrial AOM opaque	%	AOMT total	%	Sporo A	%
lower Valanginian - middle Valanginian	P.2186.22	CCF - SHM	0,00	0,12	21,9	10,8	27,3	20,6	0,00	0,04	27,33	20,6	11,9	13,4
	P.2186.21	CCF - SHM	0,00	0,26	6,7	4,1	24,2	5,2	0,00	0,13	24,16	5,2	16,2	6,3
	P.2186.20	CCF - SHM	0,68		7,3		23,6		0,00		23,64		20,5	
	P.2186.19	CCF - SHM	0,00		7,8		20,8		0,00		20,76		17,0	
	P.2186.18	CCF - SHM	0,00		5,7		19,9		0,00		19,89		4,4	
	P.2186.17	CCF - SHM	0,81		13,6		18,4		0,00		18,43		25,7	
	P.2186.16	CCF - SHM	0,00		10,6		15,7		0,00		15,71		13,5	
	P.2186.15	CCF - SHM	0,00		9,3		23,9		0,00		23,90		9,1	
	P.2186.14	CCF - SHM	0,00		12,9		16,5		0,00		16,50		19,4	
	P.2186.13	CCF - SHM	0,22		11,6		27,7		0,00		27,73		20,7	
	P.2186.12	CCF - SHM	0,28		14,7		27,5		0,00		27,48		4,2	
	P.2186.11	CCF - SHM	0,00		14,0		22,6		0,00		22,56		10,4	
	P.2186.10	CCF - SHM	0,00		13,5		13,2		0,00		13,19		5,3	
	P.2186.9 A	CCF - SHM	0,00		11,2		24,9		0,00		24,93		14,6	
	P.2186.9 B	CCF - SHM	0,00		12,3		23,8		0,00		23,78		16,6	
	P.2186.8	CCF - SHM	0,00		15,7		16,5		0,00		16,52		18,0	
	P.2186.7	CCF - SHM	0,00		13,7		19,5		0,00		19,49		9,9	
	P.2186.6	CCF - SHM	0,76		6,3		29,7		0,00		29,70		8,6	
	P.2186.5	CCF - SHM	0,00		5,3		16,8		0,28		17,09		18,5	
	P.2186.4	CCF - SHM	0,00		7,2		11,3		0,00		11,25		13,8	
	P.2186.3	CCF - SHM	0,00		13,4		14,9		0,60		15,48		0,3	
	P.2186.2	CCF - SHM	0,00		5,9		22,3		0,00		22,27		10,5	
	P.2186.1	CCF - SHM	0,00		7,3		13,1		0,00		13,12		18,4	
late Berriasian - early Valanginian	P.2175.7	CCF -DPM	0,00	0,00	2,9	4,79	15,4	18,72	0,00	0,34	15,42	19,05	0,00	3,07
	P.2175.1	CCF -DPM	0,00	0,00	7,1	3,98	26,5	8,68	0,00	1,01	26,50	8,33	0,00	5,99
	P.2174.37	CCF -DPM	0,00		1,6		10,7		0,00		10,72		0,00	
	P.2174.31	CCF -DPM	0,00		5,3		21,2		0,00		21,20		0,00	
	P.2174.30	CCF -DPM	0,00		7,8		26,0		0,00		26,02		0,00	
	P.2174.28 B	CCF -DPM	0,00		0,0		4,5		0,00		4,45		0,00	
	P.2174.28 A	CCF -DPM	0,00		0,0		11,1		0,38		11,45		0,00	
	P.2174.26	CCF -DPM	0,00		4,2		13,4		0,66		14,03		0,33	
	P.2172.9	CCF -DPM	0,00		6,1		14,1		0,00		14,06		0,00	
	P.2172.8	CCF -DPM	0,00		0,3		25,5		0,59		26,10		0,00	
	P.2172.7	CCF -DPM	0,00		0,5		32,2		0,00		32,25		0,30	
	P.2172.6	CCF -DPM	0,00		3,1		17,7		0,00		17,72		0,56	
	P.2173.3	CCF -DPM	0,00		0,4		5,5		4,43		9,92		0,00	
	P.2173.2 B	CCF -DPM	0,00		11,0		17,3		0,35		17,66		1,05	
	P.2173.2 A	CCF -DPM	0,00		14,3		39,4		0,00		39,41		0,34	
	P.2171.6	CCF -DPM	0,00		4,8		15,7		0,00		15,73		11,86	
	P.2171.3	CCF -DPM	0,00		7,7		19,4		0,00		19,44		10,85	
	P.2171.2	CCF -DPM	0,00		6,8		19,9		0,00		19,94		13,71	
	P.2171.1	CCF -DPM	0,00		7,1		20,0		0,00		19,99		19,41	
early Berriasian - middle Berriasian	P.2224.7	PBF	0,00	0,02	17,6	9,57	14,5	19,30	1,2	0,19	15,71	19,49	4,2	4,93
	P.2224.1	PBF	0,00	0,10	10,6	7,16	20,5	9,27	0,0	0,46	20,46	9,18	8,8	6,93
	P.2220.20	PBF	0,00		7,2		10,1		0,0		10,10		2,4	
	P.2220.11	PBF	0,60		7,8		3,0		0,0		3,00		7,5	
	P.2220.4	PBF	0,00		6,5		17,5		0,0		17,55		1,8	
	P.2222.3	PBF	0,00		13,9		28,9		0,0		28,93		0,0	
	P.2176.38	PBF	0,00		11,4		23,5		0,55		24,04		0,00	
	P.2176.37	PBF	0,00		19,7		22,3		0,00		22,26		0,00	
	P.2176.35	PBF	0,00		12,8		22,8		0,36		23,13		0,00	
	P.2176.34	PBF	0,00		3,5		13,9		0,00		13,89		0,38	
	P.2176.32	PBF	0,00		3,6		14,0		0,00		14,03		0,00	
	P.2176.31	PBF	0,00		0,5		7,8		0,40		8,20		0,00	
	P.2176.30	PBF	0,00		0,2		8,0		0,00		7,97		0,00	
	P.2176.27	PBF	0,00		11,3		30,5		0,00		30,54		9,54	
	P.2176.18	PBF	0,00		25,0		9,6		0,33		9,97		2,61	
	P.2176.17 C	PBF	0,00		6,6		32,8		0,00		32,84		3,53	
	P.2176.15	PBF	0,00		4,7		12,7		0,00		12,71		25,34	
	P.2176.14	PBF	0,00		3,8		16,4		0,00		16,38		27,96	
	P.2176.9	PBF	0,00		4,9		9,1		2,28		11,35		4,56	
	P.2176.2	PBF	0,00		19,7		14,6		0,31		14,89		2,75	
	P.2176.24	PBF	0,00		6,2		3,7		0,00		3,75		0,33	
	P.2176.23	PBF	0,00		19,5		21,8		0,00		21,84		2,16	
	P.2183.12	PBF	0,00		14,4		30,7		0,00		30,72		1,96	
	P.2183.11	PBF	0,00		13,1		12,0		0,00		12,01		17,60	
	P.2183.10	PBF	0,00		28,7		21,4		0,00		21,41		12,32	
	P.2183.8	PBF	0,00		4,2		26,1		0,77		26,82		0,77	
	P.2183.7	PBF	0,00		3,3		28,1		0,00		28,06		5,00	

Byers Group

Age	Sample	Formation	Sporo B	%	Sporo C	%	Sporomorphs total	Sporomorphs total	%	Cutinite total	%	Inertinite A	%	Inertinite B	%
lower Valanginian - middle Valanginian	P.2186.22	CCF - SHM	7,1	7,8	1,6	0,53	64	20,6	21,7	0,00	1,9	3,5	12,5	1,0	3,0
	P.2186.21	CCF - SHM	13,9	4,3	2,31	0,64	126	32,4	6,71	0,51	1,96	10,8	9,5	0,3	6,13
	P.2186.20	CCF - SHM	0,00		0,00		90	20,5		5,00		17,0		0,9	
	P.2186.19	CCF - SHM	12,2		0,3		116	29,4		0,76		12,7		1,3	
	P.2186.18	CCF - SHM	7,1		0,27		43	11,7		1,09		28,1		19,9	
	P.2186.17	CCF - SHM	1,1		0,00		99	26,8		3,52		4,6		0,0	
	P.2186.16	CCF - SHM	8,3		0,64		70	22,4		0,96		8,0		0,0	
	P.2186.15	CCF - SHM	8,2		0,55		65	17,9		1,37		19,2		1,9	
	P.2186.14	CCF - SHM	2,6		0,00		68	22,0		0,97		2,9		0,0	
	P.2186.13	CCF - SHM	2,4		0,0		106	23,1		6,55		3,9		0,4	
	P.2186.12	CCF - SHM	10,8		1,4		58	16,4		5,38		9,1		2,3	
	P.2186.11	CCF - SHM	7,0		0,30		58	17,7		0,61		3,0		0,0	
	P.2186.10	CCF - SHM	15,0		1,32		82	21,6		4,49		8,4		4,5	
	P.2186.9 A	CCF - SHM	7,0		0,28		78	21,8		1,40		14,6		1,1	
	P.2186.9 B	CCF - SHM	6,9		0,57		84	24,1		2,29		3,7		0,6	
	P.2186.8	CCF - SHM	13,3		0,00		108	31,3		0,00		8,4		0,0	
	P.2186.7	CCF - SHM	8,6		0,00		58	18,5		4,47		7,3		0,6	
	P.2186.6	CCF - SHM	8,1		0,25		67	17,0		1,27		20,1		3,3	
	P.2186.5	CCF - SHM	9,0		0,00		98	27,5		1,68		15,7		1,7	
	P.2186.4	CCF - SHM	12,5		1,28		108	27,6		0,00		22,8		0,3	
	P.2186.3	CCF - SHM	0,30		0,60		4	1,2		0,30		41,7		23,8	
	P.2186.2	CCF - SHM	11,1		0,5		97	22,0		1,59		17,0		4,8	
	P.2186.1	CCF - SHM	6,3		0,00		94	24,7		0,00		5,2		0,5	
late Berriasian - early Valanginian	P.2175.7	CCF -DPM	0,00	1,39	0,00	1,00	0	0,00	5,46	0,00	0,93	52,8	31,75	28,5	21,85
	P.2175.1	CCF -DPM	0,84	2,23	0,00	2,02	1	0,84	7,83	0,00	2,30	45,4	19,06	7,6	15,91
	P.2174.37	CCF -DPM	0,00		0,58		1	0,58		0,00		60,2		23,4	
	P.2174.31	CCF -DPM	0,35		0,35		2	0,71		0,00		50,9		16,3	
	P.2174.30	CCF -DPM	0,33		1,99		7	2,32		0,00		43,7		14,9	
	P.2174.28 B	CCF -DPM	0,00		0,00		0	0,00		0,00		55,8		37,0	
	P.2174.28 A	CCF -DPM	0,00		0,00		0	0,00		0,00		50,0		26,3	
	P.2174.26	CCF -DPM	0,66		0,00		3	0,99		0,00		36,4		33,4	
	P.2172.9	CCF -DPM	0,28		5,40		20	5,68		0,28		25,3		32,7	
	P.2172.8	CCF -DPM	0,00		3,81		13	3,81		0,00		21,7		44,9	
	P.2172.7	CCF -DPM	1,21		0,00		5	1,52		0,00		13,3		49,7	
	P.2172.6	CCF -DPM	0,28		6,67		27	7,50		0,00		34,2		30,0	
	P.2173.3	CCF -DPM	0,37		0,00		1	0,37		0,00		43,9		41,0	
	P.2173.2 B	CCF -DPM	0,00		0,00		3	1,05		0,35		32,9		19,6	
	P.2173.2 A	CCF -DPM	0,68		0,00		3	1,02		0,00		8,5		5,4	
	P.2171.6	CCF -DPM	7,55		0,27		73	19,68		1,89		11,1		2,2	
	P.2171.3	CCF -DPM	4,13		0,00		58	14,99		8,53		4,7		0,5	
	P.2171.2	CCF -DPM	3,78		0,00		74	17,49		5,91		8,7		1,7	
	P.2171.1	CCF -DPM	5,85		0,00		95	25,27		0,80		3,7		0,3	
early Berriasian - middle Berriasian	P.2224.7	PBF	0,6	5,46	0,0	1,24	16	4,7	11,62	0,3	1,45	21,1	20,80	3,0	12,30
	P.2224.1	PBF	4,2	4,26	0,3	1,46	47	13,3	9,54	4,0	2,72	14,4	12,46	10,5	12,97
	P.2220.20	PBF	8,5		4,7		53	15,6		0,0		20,6		12,1	
	P.2220.11	PBF	6,6		0,9		50	15,0		0,0		18,6		5,7	
	P.2220.4	PBF	10,6		1,8		48	14,1		0,6		28,4		6,5	
	P.2222.3	PBF	5,9		4,4		35	10,3		0,0		17,3		4,1	
	P.2176.38	PBF	1,39		0,28		6	1,66		0,00		41,0		19,9	
	P.2176.37	PBF	0,00		0,00		0	0,00		0,00		27,3		28,9	
	P.2176.35	PBF	0,36		0,00		1	0,36		0,00		26,3		25,3	
	P.2176.34	PBF	0,75		1,51		7	2,64		0,75		35,8		36,6	
	P.2176.32	PBF	0,56		0,56		4	1,12		0,00		30,0		45,9	
	P.2176.31	PBF	0,40		0,00		1	0,40		0,40		50,6		36,4	
	P.2176.30	PBF	0,00		1,55		4	1,55		0,00		48,4		32,2	
	P.2176.27	PBF	8,00		0,31		58	17,85		0,31		4,0		1,5	
	P.2176.18	PBF	7,52		2,29		38	12,42		0,33		11,1		2,0	
	P.2176.17 C	PBF	8,70		0,27		46	12,50		0,54		7,1		0,54	
	P.2176.15	PBF	6,54		0,54		119	32,43		2,72		3,5		1,4	
	P.2176.14	PBF	7,30		0,25		141	35,52		4,28		4,8		0,25	
	P.2176.9	PBF	0,98		0,33		18	5,86		8,47		25,4		13,7	
	P.2176.2	PBF	1,83		0,00		15	4,59		6,73		31,5		6,7	
	P.2176.24	PBF	1,32		0,33		6	1,98		0,00		38,9		35,0	
	P.2176.23	PBF	1,72		0,00		9	3,88		11,21		19,4		9,1	
	P.2183.12	PBF	10,13		0,65		39	12,7		3,59		8,2		2,3	
	P.2183.11	PBF	10,06		0,28		100	27,9		0,00		21,5		1,4	
	P.2183.10	PBF	9,38		0,59		76	22,3		0,00		2,6		0,0	
	P.2183.8	PBF	7,66		4,21		33	12,6		0,00		11,9		19,5	
	P.2183.7	PBF	9,17		1,67		57	15,8		0,00		8,6		1,9	

Byers Group

Age	Sample	Formation	Inertinite total	%	Vitrinite A	%	Vitrinite B	%	Vitrinite total	%	Phytoclasts	%	Filaments	%	marine OM	%
lower Valanginian - middle Valanginian	P.2186.22	CCF - SHM	4,5	15,5	10,0	17,0	15,4	9,9	25,4	26,9	29,9	44,3	0,0	0,22	22,2	12,4
	P.2186.21	CCF - SHM	11,1	14,9	21,3	7,0	2,6	6,1	23,9	9,8	35,5	9,0	0,0	0,38	8,0	3,8
	P.2186.20	CCF - SHM	18,0		9,1		14,1		23,2		46,1		0,0		9,8	
	P.2186.19	CCF - SHM	13,9		19,0		3,5		22,5		37,2		0,5		11,4	
	P.2186.18	CCF - SHM	48,0		8,2		3,3		11,4		60,5		0,0		7,4	
	P.2186.17	CCF - SHM	4,6		16,5		12,5		29,0		37,1		0,0		17,6	
	P.2186.16	CCF - SHM	8,0		23,1		18,3		41,3		50,3		0,3		10,9	
	P.2186.15	CCF - SHM	21,2		21,4		4,7		26,1		48,6		0,0		9,3	
	P.2186.14	CCF - SHM	2,9		29,1		14,6		43,7		47,6		0,0		13,6	
	P.2186.13	CCF - SHM	4,4		13,5		9,6		23,1		34,1		0,0		14,4	
	P.2186.12	CCF - SHM	11,3		8,2		11,6		19,8		36,5		0,6		16,7	
	P.2186.11	CCF - SHM	3,0		23,5		14,3		37,8		41,5		0,6		16,5	
	P.2186.10	CCF - SHM	12,9		11,9		19,3		31,1		48,5		1,1		13,5	
	P.2186.9 A	CCF - SHM	15,7		17,9		4,2		22,1		39,2		0,0		12,6	
	P.2186.9 B	CCF - SHM	4,3		23,8		7,4		31,2		37,8		0,0		13,2	
	P.2186.8	CCF - SHM	8,4		15,7		12,2		27,8		36,2		0,0		15,7	
	P.2186.7	CCF - SHM	8,0		18,2		12,8		31,0		43,5		0,0		15,7	
	P.2186.6	CCF - SHM	23,4		12,9		5,1		18,0		42,6		0,0		9,6	
	P.2186.5	CCF - SHM	17,4		21,3		7,0		28,3		47,3		0,0		8,1	
	P.2186.4	CCF - SHM	23,0		26,9		1,5		28,4		51,4		0,0		9,5	
	P.2186.3	CCF - SHM	65,5		0,6		2,7		3,3		69,0		0,9		13,4	
	P.2186.2	CCF - SHM	21,8		15,9		7,3		23,2		46,6		1,1		7,3	
	P.2186.1	CCF - SHM	5,8		23,6		23,4		47,0		52,8		0,0		9,4	
late Berriasian - early Valanginian	P.2175.7	CCF -DPM	81,3	53,60	0,0	6,80	0,32	5,25	0,32	12,0	81,6	66,58	0,0	3,02	2,9	5,29
	P.2175.1	CCF -DPM	52,9	29,29	5,0	10,96	5,9	3,93	10,92	14,4	63,9	18,90	0,0	7,40	7,1	4,36
	P.2174.37	CCF -DPM	83,6		0,0		3,5		3,51		87,1		0,0		1,6	
	P.2174.31	CCF -DPM	67,1		1,4		4,2		5,65		72,8		0,0		5,3	
	P.2174.30	CCF -DPM	58,6		2,0		3,3		5,30	4,4	63,9		0,0		7,8	
	P.2174.28 B	CCF -DPM	92,8		0,3		2,4		2,74		95,5		0,0		0,0	
	P.2174.28 A	CCF -DPM	76,3		3,1		9,2		12,21		88,5		0,0		0,0	
	P.2174.26	CCF -DPM	69,9		2,0		7,6		9,60		79,5		0,0		4,8	
	P.2172.9	CCF -DPM	58,0		1,4		6,3		7,67		65,9		7,1		6,1	
	P.2172.8	CCF -DPM	66,6		0,3		2,6		2,93		69,5		0,0		0,3	
	P.2172.7	CCF -DPM	63,0		1,2		1,5		2,73		65,8		0,0		0,5	
	P.2172.6	CCF -DPM	64,2		2,8		4,2		6,94		71,1		0,0		3,1	
	P.2173.3	CCF -DPM	84,9		0,4		0,4		0,74		85,6		3,7		0,4	
	P.2173.2 B	CCF -DPM	52,4		0,7		1,4		2,10		54,9		15,4		11,0	
	P.2173.2 A	CCF -DPM	13,9		0,0		2,0		2,04		16,0		29,3		14,3	
	P.2171.6	CCF -DPM	13,2		31,8		11,1		42,86		58,0		0,5		5,6	
	P.2171.3	CCF -DPM	5,2		28,2		10,6		38,76		52,5		0,0		10,3	
	P.2171.2	CCF -DPM	10,4		24,3		11,6		35,93		52,2		0,0		9,1	
	P.2171.1	CCF -DPM	4,0		24,2		11,7		35,90		40,7		1,3		10,3	
early Berriasian - middle Berriasian	P.2224.7	PBF	24,0	33,10	11,9	8,99	25,8	13,25	37,7	22,2	62,0	56,78	0,0	0,33	17,6	11,00
	P.2224.1	PBF	24,9	23,93	5,4	7,04	12,7	7,68	18,1	12,5	46,9	15,35	0,0	0,58	17,7	7,25
	P.2220.20	PBF	32,6		9,4		23,8		33,2		65,9		0,0		8,4	
	P.2220.11	PBF	24,3		16,2		26,4		42,6		67,0		0,0		15,0	
	P.2220.4	PBF	34,9		8,8		17,0		25,8		61,3		0,0		7,1	
	P.2222.3	PBF	21,4		12,9		12,6		25,5		46,9		0,0		13,9	
	P.2176.38	PBF	60,9		0,55		1,4		1,94		62,9		0,00		11,4	
	P.2176.37	PBF	56,2		0,52		1,3		1,84		58,0		0,00		19,7	
	P.2176.35	PBF	51,6		1,78		8,9		10,68		62,3		1,07		12,8	
	P.2176.34	PBF	72,5		0,00		6,0		6,04		79,2		0,00		3,5	
	P.2176.32	PBF	75,9		0,00		5,3		5,32		81,2		0,00		3,6	
	P.2176.31	PBF	87,0		0,00		3,6		3,56		90,9		0,00		0,5	
	P.2176.30	PBF	80,6		1,55		8,1		9,69		90,3		0,00		0,2	
	P.2176.27	PBF	5,5		14,15		17,8		32,00		37,8		0,31		12,5	
	P.2176.18	PBF	13,1		7,84		29,4		37,25		50,7		1,96		25,0	
	P.2176.17 C	PBF	7,6		22,01		14,9		36,96		45,1		0,82		8,5	
	P.2176.15	PBF	4,9		24,52		15,5		40,05		47,7		0,00		7,2	
	P.2176.14	PBF	5,0		15,37		13,4		28,72		38,0		1,26		8,3	
	P.2176.9	PBF	39,1		8,14		9,1		17,26		64,8		1,95		7,2	
	P.2176.2	PBF	38,2		0,92		12,5		13,46		58,4		0,00		21,2	
	P.2176.24	PBF	73,9		1,98		3,6		5,61		79,5		0,00		7,1	
	P.2176.23	PBF	28,4		5,60		9,5		15,09		54,7		0,00		19,5	
	P.2183.12	PBF	10,5		11,4		13,1		24,5		38,6		0,7		16,3	
	P.2183.11	PBF	22,9		16,2		3,1		19,3		42,2		0,0		16,8	
	P.2183.10	PBF	2,6		12,0		11,1		23,2		25,8		0,3		30,2	
	P.2183.8	PBF	31,4		5,0		19,9		24,9		56,3		0,0		4,2	
	P.2183.7	PBF	10,6		20,8		17,5		38,3		48,9		1,4		5,6	

Byers Group

Age	Sample	Formation	terrestrial C%		Palynomorphs %		OP/TR
lower Valanginian - middle Valanginian	P.2186.22	CCF - SHM	77,8	86,8	20,90	23,5	1,5
	P.2186.21	CCF - SHM	92,0	4,1	33,68	7,0	
	P.2186.20	CCF - SHM	90,2		22,95		
	P.2186.19	CCF - SHM	87,8		33,42		
	P.2186.18	CCF - SHM	92,1		13,35		
	P.2186.17	CCF - SHM	82,4		30,89		
	P.2186.16	CCF - SHM	88,8		23,08		
	P.2186.15	CCF - SHM	90,4		17,86		
	P.2186.14	CCF - SHM	86,1		22,65		
	P.2186.13	CCF - SHM	84,9		25,98		
	P.2186.12	CCF - SHM	81,0		18,98		
	P.2186.11	CCF - SHM	82,3		20,73		
	P.2186.10	CCF - SHM	84,4		22,69		
	P.2186.9 A	CCF - SHM	86,0		23,25		
	P.2186.9 B	CCF - SHM	85,7		24,93		
	P.2186.8	CCF - SHM	84,1		31,30		
	P.2186.7	CCF - SHM	81,5		20,45		
	P.2186.6	CCF - SHM	89,3		20,30		
	P.2186.5	CCF - SHM	91,6		30,25		
	P.2186.4	CCF - SHM	90,3		29,92		
	P.2186.3	CCF - SHM	86,0		2,08		
	P.2186.2	CCF - SHM	92,0		24,55		
	P.2186.1	CCF - SHM	90,6		26,77		
late Berriasian - early Valanginian	P.2175.7	CCF -DPM	97,1	94,11	0,00	8,99	29,8
	P.2175.1	CCF -DPM	91,2	4,83	0,84	10,40	
	P.2174.37	CCF -DPM	98,4		0,58		
	P.2174.31	CCF -DPM	94,7		0,71		
	P.2174.30	CCF -DPM	92,2		2,32		
	P.2174.28 B	CCF -DPM	100,0		0,00		
	P.2174.28 A	CCF -DPM	100,0		0,00		
	P.2174.26	CCF -DPM	94,5		1,66		
	P.2172.9	CCF -DPM	92,8		12,78		
	P.2172.8	CCF -DPM	99,4		3,81		
	P.2172.7	CCF -DPM	99,5		1,52		
	P.2172.6	CCF -DPM	96,3		7,50		
	P.2173.3	CCF -DPM	99,6		4,06		
	P.2173.2 B	CCF -DPM	89,0		16,43		
	P.2173.2 A	CCF -DPM	85,7		30,27		
	P.2171.6	CCF -DPM	93,9		21,02		
	P.2171.3	CCF -DPM	86,9		17,57		
	P.2171.2	CCF -DPM	89,7		19,86		
	P.2171.1	CCF -DPM	87,3		29,79		
early Berriasian - middle Berriasian	P.2224.7	PBF	82,4	88,23	4,74	13,38	4,9
	P.2224.1	PBF	80,6	7,30	20,34	10,75	
	P.2220.20	PBF	91,6		16,76		
	P.2220.11	PBF	85,0		22,22		
	P.2220.4	PBF	92,9		14,66		
	P.2222.3	PBF	86,1		10,26		
	P.2176.38	PBF	88,6		1,66		
	P.2176.37	PBF	80,3		0,00		
	P.2176.35	PBF	86,8		1,42		
	P.2176.34	PBF	95,8		2,64		
	P.2176.32	PBF	96,4		1,12		
	P.2176.31	PBF	99,5		0,40		
	P.2176.30	PBF	99,8		1,55		
	P.2176.27	PBF	86,5		19,38		
	P.2176.18	PBF	75,0		14,38		
	P.2176.17 C	PBF	91,3		15,22		
	P.2176.15	PBF	92,8		34,88		
	P.2176.14	PBF	91,2		41,31		
	P.2176.9	PBF	84,0		10,10		
	P.2176.2	PBF	77,9		6,12		
	P.2176.24	PBF	85,3		2,97		
	P.2176.23	PBF	80,5		3,88		
	P.2183.12	PBF	82,7		15,36		
	P.2183.11	PBF	82,1		31,56		
	P.2183.10	PBF	69,8		24,05		
	P.2183.8	PBF	95,8		12,64		
	P.2183.7	PBF	94,2		19,44		

Byers Group			terrestrial																															
			parts of vascular plants												Pollen												Spores							
			phytoclasts																															
			Inertinite				Vitrinite				Cutinite				nonsaccate				monosaccate				bisaccate				monolete				trilete			
Age	Preservation		A	B	C	sum	A	B	C	sum	A	B	C	sum	A	B	C	sum	A	B	C	sum	A	B	C	sum	A	B	C	sum	A	B	C	sum
	Sample	Formation																																
early Berriasian - middle Berriasian	P.2183.6	PBF	76	10	0	86	32	60	0	92	0	3	8	11	0	0	0	0	11	11	1	23	0	0	0	0	1	5	0	6	14	10	1	25
	P.2183.5	PBF	45	6	0	51	49	79	0	128	0	1	0	1	0	0	0	0	6	2	0	8	0	0	0	0	3	1	0	4	2	3	0	5
	P.2183.4	PBF	72	30	0	102	47	21	0	68	0	0	0	0	0	0	0	0	1	7	1	9	0	0	0	0	0	0	0	0	3	5	1	9
	P.2183.3	PBF	85	34	0	119	8	79	0	87	0	0	0	0	0	0	0	0	0	0	0	0	0	0	0	0	0	0	0	0	0	0	0	0
	P.2183.2	PBF	61	38	0	99	25	32	0	57	0	3	0	3	0	0	0	0	5	2	0	7	0	0	0	0	5	6	0	11	10	8	1	19
	P.2183.1	PBF	55	38	0	93	57	64	0	121	0	0	0	0	0	0	0	0	0	2	1	3	0	0	0	0	1	8	0	9	1	2	2	5
middle Tithonian	P.2223.72	AF	73	39	0	112	1	3	0	4	0	0	0	0	0	0	0	0	0	0	0	0	0	0	0	0	0	0	0	0	0	0	0	0
	P.2223.63	AF	150	53	0	203	2	5	0	7	0	2	8	10	0	0	0	0	0	0	0	0	0	0	0	0	0	0	0	0	0	0	0	0
	P.2223.62	AF	97	69	0	166	2	3	0	5	0	0	1	1	0	0	0	0	0	0	0	0	0	0	0	0	0	0	0	0	0	0	0	0
	P.2223.60	AF	72	91	0	163	0	7	0	7	0	0	1	1	0	0	0	0	0	0	0	0	0	0	0	0	0	0	0	0	0	0	0	0
	P.2223.56	AF	109	85	0	194	0	3	0	3	0	0	0	0	0	0	0	0	0	0	0	0	0	0	0	0	0	0	0	0	0	0	0	0
	P.2223.51	AF	93	45	0	138	0	0	0	0	0	0	0	0	0	0	0	0	0	0	0	0	0	0	0	0	0	0	0	0	0	0	0	0
	P.2223.49 A	AF	85	90	0	175	1	0	0	1	0	0	0	0	0	0	0	0	0	0	0	0	0	0	0	0	0	0	0	0	0	0	0	0
	P.2223.49 B	AF	149	62	0	211	2	24	0	26	0	0	0	0	0	0	0	0	0	0	0	0	0	0	0	0	0	0	0	0	0	0	0	0
	P.2223.47	AF																																
	P.2223.46	AF	113	54	0	167	0	1	0	1	0	0	0	0	0	0	0	0	0	0	0	0	0	0	0	0	0	0	0	0	0	0	0	0
	P.2223.45	AF	102	73	0	175	0	16	0	16	0	1	8	9	0	0	0	0	0	0	0	0	0	0	0	0	0	0	0	0	0	0	0	0
	P.2223.45 A	AF	99	49	0	148	1	2	0	3	0	0	0	0	0	0	0	0	0	0	0	0	0	0	0	0	0	0	0	0	0	0	0	0
	P.2223.44	AF	64	20	0	84	0	13	0	13	0	0	0	0	0	0	0	0	0	0	0	0	0	0	0	0	0	0	0	0	0	0	0	0
	P.2223.30	AF	108	131	0	239	2	14	0	16	0	0	0	0	0	0	0	0	0	0	0	0	0	0	0	0	0	0	0	0	0	0	0	0
	P.2223.26	AF	88	140	0	228	1	22	0	23	0	0	0	0	0	0	0	0	0	0	0	0	0	0	0	0	0	0	0	0	0	0	0	0
	P.2223.25 B	AF																																
	P.2223.25 A	AF	85	19	0	104	0	1	0	1	0	0	0	0	0	0	0	0	0	0	0	0	0	0	0	0	0	0	0	0	0	0	0	0
	P.2223.23	AF	95	94	0	189	0	6	0	6	0	0	11	11	0	0	0	0	0	0	0	0	0	0	0	0	0	0	0	0	0	0	0	0
	P.2223.20	AF	95	69	0	164	16	95	0	111	0	0	0	0	0	0	0	0	0	0	0	0	0	0	0	0	0	0	0	0	0	0	0	0
	P.2225.3 A	AF	115	103	0	218	0	2	0	2	0	0	0	0	0	0	0	0	0	0	0	0	0	0	0	0	0	0	0	0	0	0	0	0
	P.2225.3 B	AF	81	71	0	152	1	3	0	4	0	0	0	0	0	0	0	0	0	0	0	0	0	0	0	0	0	0	0	0	0	0	0	0

terrestrial				AOM			marine																	diverse					
Spores							marine phytoplankton										Zoomorphs				Zooclasts					mineral residues				
indet				terrestrial, translucent	terrestrial opaque	marine/sensu stricto	Dinocysts				Acritarchs				Algae indet	Leiospheres	foraminiferal test linings				Bivalves, Scolecodonts, Fungi				Filaments	Quartz	Pyrite	others	Glendonites	
A	B	C	sum				A	B	C	sum	A	B	C	sum			A	B	C	sum	A	B	C	sum						Totals
1	30	9	40	103,0	0	41,0	1	1	0	2	1	0	0	1	8	0	0	0	0	0	0	0	0	0	3	91	25			441
4	12	10	26	66,0	0	32,0	0	0	0	0	0	0	0	0	5	0	0	0	0	0	0	0	0	0	0	76	9	0		326
0	8	5	13	144,0	0	17,0	0	0	0	0	0	0	0	0	2	0	0	0	0	0	0	0	0	0	0	157	1	0		364
0	3	1	4	117,0	0	32,0	0	0	0	0	0	0	0	0	0	0	0	0	0	0	0	0	0	0	2	61	3	0		361
8	32	2	42	114,0	0	3,0	0	0	0	0	0	0	0	0	2	0	0	0	0	0	0	4	1	5	0	3	10	0		362
4	28	12	44	45,0	0	5,0	0	0	0	0	0	0	0	0	6	0	0	0	0	0	0	0	0	0	0	63	4	3	x	331
0	0	0	0	20,0	4	0,0	0	0	0	0	0	0	0	0	0	0	0	0	0	0	0	0	0	0	0	306	23	47		140
0	4	2	6	82,3	5	19,7	0	0	1	1	0	0	0	0	0	0	0	0	0	0	0	0	0	0	0	233	36	2		334
0	0	0	0	130,0	9	6,0	0	0	0	0	0	0	0	0	0	0	0	0	0	0	0	0	0	0	0	203	96	53	x	317
0	0	0	0	13,5	5	0,5	0	0	0	0	0	0	0	0	0	0	0	0	0	0	0	0	0	0	0	116	45	20	x	190
1	2	2	5	54,8	0	23,2	0	0	0	0	0	0	0	0	0	0	0	0	0	0	0	0	0	0	0	128	87	3		280
0	1	0	1	49,5	4	1,5	0	0	0	0	0	0	0	0	0	0	0	0	0	0	0	0	0	0	0	272	50	57	x	194
23	2	1	26	3,0	0	0,0	1	0	0	1	6	0	0	6	85	0	0	0	0	0	0	0	0	0	0	202	21	40		297
5	0	0	5	67,0	0	20,0	0	0	0	0	0	0	0	0	0	0	0	0	0	0	0	0	0	0	0	200	28	0		329
0	1	0	1	35,5	2	7,5	0	0	0	0	0	0	0	0	0	0	0	0	0	0	0	0	0	0	0	183	111	9	x	214
0	0	0	0	69,1	7	6,9	0	0	0	0	0	0	0	0	0	0	0	0	0	0	0	0	0	0	0	161	56	25		283
0	0	0	0	14,0	0	1,4	0	0	0	0	0	0	0	0	0	0	0	0	0	0	0	0	0	0	0	247	58	103	x	166
0	0	0	0	78,0	3	0,0	0	0	0	0	0	0	0	0	0	0	0	0	0	0	0	0	0	0	0	289	21	176		178
0	0	0	0	22,0	0	0,0	0	0	0	0	0	0	0	0	0	0	0	0	0	0	0	0	0	0	0	215	23	0		277
0	3	0	3	36,0	0	0,0	0	0	0	0	0	0	0	0	0	0	0	0	0	0	0	0	0	0	0	204	56	19	x	290
0	0	0	0	108,0	1	0,0	0	0	0	0	0	0	0	0	0	0	0	0	0	0	0	0	0	0	0	1323	36	2	x	214
0	0	0	0	44,0	0	0,0	0	0	0	0	0	0	0	0	0	0	0	0	0	0	1	0	0	1	0	196	51	94	x	251
33	22	6	61	22,0	0	3,0	0	0	0	0	0	0	0	0	0	0	0	0	0	0	0	0	0	0	9	82	10	0		370
0	0	1	1	8,9	22	0,1	0	0	0	0	0	0	0	0	0	0	0	0	0	0	0	0	0	0	0	108	161	0	x	252
0	0	0	0	117,0	3	2,0	0	0	0	0	0	0	0	0	0	0	0	0	0	0	0	0	0	0	0	228	87	0		278

Byers Group

Age	Sample	Formation	Dino A	%	Dino B	%	Dino C	%	Dinocysts total	%	Acritarchs	%	Algae indet	%	Foraminifera	%
early Berriasian - middle Berriasian	P.2183.6	PBF	0,23		0,23		0,00		0,45		0,23		1,81		0,00	
	P.2183.5	PBF	0,00		0,00		0,00		0,00		0,00		1,53		0,00	
	P.2183.4	PBF	0,00		0,00		0,00		0,00		0,00		0,55		0,00	
	P.2183.3	PBF	0,00		0,00		0,00		0,00		0,00		0,00		0,00	
	P.2183.2	PBF	0,00		0,00		0,00		0,00		0,00		0,55		0,00	
	P.2183.1	PBF	0,00		0,00		0,00		0,00		0,00		1,81		0,00	
middle Tithonian	P.2223.72	AF	0,00	0,02	0,00	0,00	0,00	0,02	0,00	0,03	0,00	0,11	0,00	1,51	0,00	0,00
	P.2223.63	AF	0,00	0,08	0,00	0,00	0,30	0,07	0,30	0,10	0,00	0,46	0,00	6,57	0,00	0,00
	P.2223.62	AF	0,00		0,00		0,00		0,00		0,00		0,00		0,00	
	P.2223.60	AF	0,00		0,00		0,00		0,00		0,00		0,00		0,00	
	P.2223.56	AF	0,00		0,00		0,00		0,00		0,00		0,00		0,00	
	P.2223.51	AF	0,00		0,00		0,00		0,00		0,00		0,00		0,00	
	P.2223.49 A	AF	0,34		0,00		0,00		0,34		2,02		28,62		0,00	
	P.2223.49 B	AF	0,00		0,00		0,00		0,00		0,00		0,00		0,00	
	P.2223.47	AF														
	P.2223.46	AF	0,00		0,00		0,00		0,00		0,00		0,00		0,00	
	P.2223.45	AF	0,00		0,00		0,00		0,00		0,00		0,00		0,00	
	P.2223.45 A	AF	0,00		0,00		0,00		0,00		0,00		0,00		0,00	
	P.2223.44	AF	0,00		0,00		0,00		0,00		0,00		0,00		0,00	
	P.2223.30	AF	0,00		0,00		0,00		0,00		0,00		0,00		0,00	
	P.2223.26	AF	0,00		0,00		0,00		0,00		0,00		0,00		0,00	
	P.2223.25 B	AF														
	P.2223.25 A	AF	0,00		0,00		0,00		0,00		0,00		0,00		0,00	
	P.2223.23	AF	0,00		0,00		0,00		0,00		0,00		0,00		0,00	
	P.2223.20	AF	0,00		0,00		0,00		0,00		0,00		0,00		0,00	
	P.2225.3 A	AF	0,00		0,00		0,00		0,00		0,00		0,00		0,00	
	P.2225.3 B	AF	0,00		0,00		0,00		0,00		0,00		0,00		0,00	

Byers Group

Age	Sample	Formation	Leiospheres %		marine AOM %		terrestrial AOM % translucent		terrestrial AOM % opaque		AOMT % total		Sporo A %	
early Berriasian - middle Berriasian	P.2183.6	PBF	0,00		9,30		23,36		0,00		23,36		6,12	
	P.2183.5	PBF	0,00		9,82		20,25		0,00		20,25		4,60	
	P.2183.4	PBF	0,00		4,67		39,56		0,00		39,56		1,10	
	P.2183.3	PBF	0,00		8,86		32,41		0,00		32,41		0,00	
	P.2183.2	PBF	0,00		0,83		31,49		0,00		31,49		7,73	
	P.2183.1	PBF	0,00		1,51		13,60		0,00		13,60		1,81	
middle Tithonian	P.2223.72	AF	0,00	0,00	0,00	1,66	14,29	20,35	2,86	1,43	17,14	21,78	0,00	0,98
	P.2223.63	AF	0,00	0,00	5,89	2,50	24,65	14,68	1,50	2,08	26,15	14,67	0,00	2,62
	P.2223.62	AF	0,00		1,89		41,01		2,84		43,85		0,00	
	P.2223.60	AF	0,00		0,24		7,13		2,63		9,76		0,00	
	P.2223.56	AF	0,00		8,29		19,57		0,00		19,57		0,36	
	P.2223.51	AF	0,00		0,80		25,49		2,06		27,55		0,00	
	P.2223.49 A	AF	0,00		0,00		1,01		0,00		1,01		7,74	
	P.2223.49 B	AF	0,00		6,08		20,36		0,00		20,36		1,52	
	P.2223.47	AF												
	P.2223.46	AF	0,00		3,52		16,58		0,93		17,51		0,00	
	P.2223.45	AF	0,00		2,44		24,41		2,47		26,89		0,00	
	P.2223.45 A	AF	0,00		0,84		8,41		0,00		8,41		0,00	
	P.2223.44	AF	0,00		0,00		43,82		1,69		45,51		0,00	
	P.2223.30	AF	0,00		0,00		7,94		0,00		7,94		0,00	
	P.2223.26	AF	0,00		0,00		12,41		0,00		12,41		0,00	
	P.2223.25 B	AF												
	P.2223.25 A	AF	0,00		0,00		50,47		0,47		50,93		0,00	
	P.2223.23	AF	0,00		0,00		17,53		0,00		17,53		0,00	
	P.2223.20	AF	0,00		0,81		5,95		0,00		5,95		8,92	
	P.2225.3 A	AF	0,00		0,05		3,53		8,73		12,26		0,00	
	P.2225.3 B	AF	0,00		0,71		42,09		1,08		43,17		0,00	

Byers Group

Age	Sample	Formation	Sporo B	%	Sporo C	%	Sporomorphs total	Sporomorphs total	%	Cutinite total	%	Inertinite A	%	Inertinite B	%
early Berriasian - middle Berriasian	P.2183.6	PBF	12,70		2,49		94	21,3		2,49		17,2		2,3	
	P.2183.5	PBF	5,52		3,07		43	13,2		0,31		13,8		1,8	
	P.2183.4	PBF	5,49		1,92		31	8,5		0,00		19,8		8,2	
	P.2183.3	PBF	0,83		0,28		4	1,1		0,00		23,5		9,4	
	P.2183.2	PBF	13,26		0,83		79	21,8		0,83		16,9		10,5	
	P.2183.1	PBF	12,08		4,53		61	18,4		0,00		16,6		11,5	
middle Tithonian	P.2223.72	AF	0,00	0,56	0,00	0,19	0	0,0	1,7	0,0	0,6	52,1	39,9	27,9	28,1
	P.2223.63	AF	1,20	1,36	0,60	0,41	6	1,8	4,10	3,0	1,33	44,9	9,18	15,9	11,77
	P.2223.62	AF	0,00		0,00		0	0,0		0,3		30,6		21,8	
	P.2223.60	AF	0,00		0,00		0	0,0		0,5		37,9		47,9	
	P.2223.56	AF	0,71		0,71		5	1,8		0,0		38,9		30,4	
	P.2223.51	AF	0,52		0,00		1	0,5		0,0		47,9		23,2	
	P.2223.49 A	AF	0,67		0,34		26	8,8		0,0		28,6		30,3	
	P.2223.49 B	AF	0,00		0,00		5	1,5		0,0		45,3		18,8	
	P.2223.47	AF													
	P.2223.46	AF	0,47		0,00		1	0,5		0,0		52,8		25,2	
	P.2223.45	AF	0,00		0,00		0	0,0		3,2		36,0		25,8	
	P.2223.45 A	AF	0,00		0,00		0	0,0		0,0		59,5		29,4	
	P.2223.44	AF	0,00		0,00		0	0,0		0,0		36,0		11,2	
	P.2223.30	AF	0,00		0,00		0	0,0		0,0		39,0		47,3	
	P.2223.26	AF	1,03		0,00		3	1,0		0,0		30,3		48,3	
	P.2223.25 B	AF													
	P.2223.25 A	AF	0,00		0,00		0	0,0		0,0		39,7		8,9	
	P.2223.23	AF	0,00		0,00		0	0,0		4,4		37,8		37,5	
	P.2223.20	AF	5,95		1,62		61	16,5		0,0		25,7		18,6	
	P.2225.3 A	AF	0,00		0,40		1	0,4		0,0		45,6		40,9	
	P.2225.3 B	AF	0,00		0,00		0	0,0		0,0		29,1		25,5	

Byers Group

Age	Sample	Formation	Inertinite total	%	Vitrinite A	%	Vitrinite B	%	Vitrinite total	%	Phytoclasts	%	Filaments	%	marine OM	%
early Berriasian - middle Berriasian	P.2183.6	PBF	19,5		7,3		13,6		20,9		42,9		0,7		11,8	
	P.2183.5	PBF	15,6		15,0		24,2		39,3		55,2		0,0		11,3	
	P.2183.4	PBF	28,0		12,9		5,8		18,7		46,7		0,0		5,2	
	P.2183.3	PBF	33,0		2,2		21,9		24,1		57,1		0,6		8,9	
	P.2183.2	PBF	27,3		6,9		8,8		15,7		43,9		0,0		1,4	
	P.2183.1	PBF	28,1		17,2		19,3		36,6		64,7		0,0		3,3	
middle Tithonian	P.2223.72	AF	80,0	68,0	0,71	0,5	2,1	3,9	2,9	4,4	82,9	73,0	0,0	0,1	0,0	3,3
	P.2223.63	AF	60,8	14,59	0,6	0,97	1,5	5,88	2,1	6,7	65,9	13,69	0,0	0,56	6,2	7,15
	P.2223.62	AF	52,4		0,6		0,9		1,6		54,3		0,0		1,9	
	P.2223.60	AF	85,8		0,0		3,7		3,7		90,0		0,0		0,2	
	P.2223.56	AF	69,3		0,0		1,1		1,1		70,4		0,0		8,3	
	P.2223.51	AF	71,1		0,0		0,0		0,0		71,1		0,0		0,8	
	P.2223.49 A	AF	58,9		0,3		0,0		0,3		59,3		0,0		31,0	
	P.2223.49 B	AF	64,1		0,6		7,3		7,9		72,0		0,0		6,1	
	P.2223.47	AF														
	P.2223.46	AF	78,0		0,0		0,5		0,47		78,5		0,0		3,5	
	P.2223.45	AF	61,8		0,0		5,7		5,7		70,7		0,0		2,4	
	P.2223.45 A	AF	88,9		0,6		1,2		1,8		90,7		0,0		0,8	
	P.2223.44	AF	47,2		0,0		7,3		7,3		54,5		0,0		0,0	
	P.2223.30	AF	86,3		0,72		5,1		5,8		92,1		0,0		0,0	
	P.2223.26	AF	78,6		0,3		7,6		7,9		86,6		0,0		0,0	
	P.2223.25 B	AF														
	P.2223.25 A	AF	48,6		0,0		0,5		0,5		49,1		0,0		0,0	
	P.2223.23	AF	75,3		0,0		2,4		2,4		82,1		0,0		0,0	
	P.2223.20	AF	44,3		4,3		25,7		30,0		74,3		2,4		0,8	
	P.2225.3 A	AF	86,5		0,0		0,8		0,8		87,3		0,0		0,0	
	P.2225.3 B	AF	54,7		0,4		1,1		1,4		56,1		0,0		0,7	

Byers Group

Age	Sample	Formation	terrestrial C%		Palynomorphs %		OP/TR
early Berriasian - middle Berriasian	P.2183.6	PBF	88,2		24,49		
	P.2183.5	PBF	88,7		14,72		
	P.2183.4	PBF	94,8		9,07		
	P.2183.3	PBF	91,1		1,66		
	P.2183.2	PBF	97,2		22,38		
	P.2183.1	PBF	96,7		20,24		
middle Tithonian	P.2223.72	AF	100,0	96,7	0,00	3,2	50,20
	P.2223.63	AF	93,8	7,14	2,10	9,32	
	P.2223.62	AF	98,1		0,00		
	P.2223.60	AF	99,8		0,00		
	P.2223.56	AF	91,7		1,79		
	P.2223.51	AF	99,2		0,52		
	P.2223.49 A	AF	69,0		39,73		
	P.2223.49 B	AF	93,9		1,52		
	P.2223.47	AF			0,00		
	P.2223.46	AF	96,5		0,47		
	P.2223.45	AF	97,6		0,00		
	P.2223.45 A	AF	99,2		0,00		
	P.2223.44	AF	100,0		0,00		
	P.2223.30	AF	100,0		0,00		
	P.2223.26	AF	100,0		1,03		
	P.2223.25 B	AF			0,00		
	P.2223.25 A	AF	100,0		0,00		
	P.2223.23	AF	99,6		0,00		
	P.2223.20	AF	99,2		18,92		
	P.2225.3 A	AF	100,0		0,40		
	P.2225.3 B	AF	99,3		0,00		

D = Nordenskjöld & Kotick Point Formation | **KG = Fossil Bluff Group**

			terrestrial																											
			parts of vascular plants												Pollen												Spores			
			phytoclasts																											
			Inertinite				Vitrinite				Cutinite				nonsaccate				monosaccate				bisaccate				monolete			
Age	Preservation		A	B	C	sum	A	B	C	sum	A	B	C	sum	A	B	C	sum	A	B	C	sum	A	B	C	sum	A	B	C	sum
	Sample	Formation																												
early Albian	D.8403.30	Kotick Point Fm	99	27	0	126	36	77	0	113	1	3	6	10	0	0	0	0	4	6	0	10	0	0	0	0	2	3	0	5
	D.8403.65	Kotick Point Fm	76	7	0	83	113	44	0	157	0	2	0	2	0	0	0	0	4	0	0	4	0	1	0	1	5	0	0	5
late Aptian	D.8406.6	Kotick Point Fm	54	5	0	59	117	75	0	192	0	0	0	0	0	0	0	0	5	0	0	5	0	0	0	0	4	0	0	4
	D.8406.18	Kotick Point Fm	40	12	0	52	103	78	0	181	4	0	0	4	0	0	0	0	7	1	0	8	0	0	0	0	5	2	0	7
	D.8406.4	Kotick Point Fm	27	4	0	31	89	55	0	144	7	14	4	25	3	0	0	3	17	4	0	21	0	0	0	0	11	1	0	12
	D.8633.10	Kotick Point Fm	79	1	0	80	98	74	0	172	2	3	0	5	0	0	0	0	10	1	0	11	1	0	0	1	11	7	0	18
middle Tithonian	D.8751.4	Nordenskjöld Fm	52	13	0	65	24	25	0	49	4	3	0	7	2	0	0	2	4	3	0	7	0	0	0	0	13	2	0	15
	D.8751.3	Nordenskjöld Fm	127	15	0	142	49	41	0	90	2	0	0	2	0	0	0	0	5	0	0	5	0	0	0	0	15	1	0	16
	D.8751.2	Nordenskjöld Fm	88	10	0	98	28	49	0	77	1	4	0	5	0	0	0	0	8	1	0	9	0	0	0	0	11	2	0	13
	D.8751.1	Nordenskjöld Fm	112	8	0	120	30	48	0	78	2	3	0	5	0	0	0	0	9	2	0	11	1	0	0	1	18	10	0	28
upper Aptian	KG.3403.213	Pluto Glacier Fm	114	24	0	138	28	89	0	117	0	0	0	0	0	0	0	0	0	0	0	0	0	0	0	0	0	0	0	0
middle Aptian	KG.3403.70	Pluto Glacier Fm	27	7	0	34	6	47	0	53	0	0	0	0	0	0	0	0	0	0	0	0	0	0	0	0	0	0	0	0
lower Aptian	KG.3402.286	Pluto Glacier Fm	49	13	0	62	5	21	0	26	0	0	0	0	0	0	0	0	0	0	0	0	0	0	0	0	0	0	0	0
	KG.3403.4	Pluto Glacier Fm	34	36	0	70	7	45	0	52	0	0	0	0	0	0	0	0	0	0	0	0	0	0	0	0	0	1	0	1
	KG.3402.105	Pluto Glacier Fm	18	5	0	23	2	5	0	7	0	0	0	0	0	0	0	0	1	1	0	2	0	0	0	0	0	0	0	0
	KG.3402.16	Pluto Glacier Fm	46	12	0	58	14	17	0	31	0	0	0	0	0	0	0	0	0	0	0	0	0	0	0	0	0	0	0	0
Valanginian ?-Barremian	KG.3457.54	Spartan Glacier Fm	87	41	0	128	13	31	0	44	0	0	0	0	0	0	0	0	0	0	0	0	0	0	0	0	0	0	0	0
	KG.3401.608	Spartan Glacier Fm	42	17	0	59	3	11	0	14	0	0	0	0	0	0	0	0	0	0	0	0	0	0	0	0	0	0	0	0
	KG.3456.65	Spartan Glacier Fm	113	57	0	170	4	41	0	45	0	2	0	0	0	0	0	0	0	0	0	0	0	0	0	0	0	0	0	0
	KG.3455.170	Spartan Glacier Fm	116	41	0	157	7	45	0	52	0	0	0	0	0	0	0	0	0	0	0	0	0	0	0	0	0	0	0	0
	KG.3455.24	Spartan Glacier Fm	80	18	0	98	8	44	0	52	0	0	0	0	0	0	0	0	0	0	0	0	0	0	0	0	0	0	0	0
Valanginian ?	KG.3461.26	Spartan Glacier Fm	18	57	0	75	0	21	0	21	0	0	0	0	0	0	0	0	0	0	0	0	0	0	0	0	0	0	0	0
late Berr.-early Val.	KG.2942.10	Himalia Ridge Fm	28	40	0	68	6	17	0	23	0	0	0	0	0	0	0	0	0	0	0	0	0	0	0	0	0	0	0	0
Berriasian	KG.3401.2	Himalia Ridge Fm	101	63	0	164	5	21	0	26	0	0	0	0	0	0	0	0	0	0	0	0	0	0	0	0	0	0	0	0
	KG.3404.283	Himalia Ridge Fm	135	26	0	161	5	16	0	21	0	0	0	0	0	0	0	0	0	0	0	0	0	0	0	0	0	0	0	0
upper Tithonian	KG.3404.34	Himalia Ridge Fm	56	115	0	171	5	64	0	69	0	0	0	0	0	0	0	0	0	0	0	0	0	0	0	0	0	0	0	0
	KG.2802.662	Himalia Ridge Fm	50	73	0	123	4	20	0	24	0	0	0	0	0	0	0	0	0	0	0	0	0	0	0	0	0	0	0	0
	KG.2929.1	Himalia Ridge Fm	34	30	0	64	14	46	0	60	0	0	0	0	0	0	0	0	0	0	0	0	0	0	0	0	0	0	0	0
	KG.2802.332	Himalia Ridge Fm			0				0																					
middle Tithonian	KG.2802.98	Himalia Ridge Fm	83	162	0	245	3	11	0	14	0	0	0	0	0	0	0	0	0	0	0	0	0	0	0	0	0	0	0	0
	KG.2940.10	Himalia Ridge Fm	49	30	0	79	4	5	0	9	0	0	0	0	0	0	0	0	0	0	0	0	0	0	0	0	0	0	0	0

terrestrial								AOM			marine																						diverse					
Spores																																					
											marine phytoplankton												Zoomorphs				Zooclasts						mineral residues				
trilete				indet				terrestrial, translucent	terrestrial opaque	marine/sensu stricto	Dinocysts				Acritarchs				Algae indet	Leiospheres	foraminiferal test linings				Bivalves, Scolecodonts, Fungi				Filaments	Quartz	Pyrite	others	Glendonites					
A	B	C	sum	A	B	C	sum				A	B	C	sum	A	B	C	sum			A	B	C	sum	A	B	C	sum						Totals				
5	3	0	8	0	4	5	9	61,5	0	20,5	0	3	3	6	0	2	0	2	15	0	0	0	0	0	1	0	0	1	0	52	12	2			387		
4	3	0	7	2	3	0	5	6,58	0	1,42	3	3	1	7	0	0	0	0	0	177	1	0	0	1	2	0	0	2	0	0	9	23	x		459		
7	0	0	7	6	15	5	26	30	0	39	2	1	0	3	2	1	1	4	0	178	3	2	0	5	2	0	0	2	0	6	5	0			554		
9	0	0	9	7	4	4	15	10	0	13	0	1	0	1	3	1	0	4	0	168	1	2	0	3	0	0	0	0	5	3	7	0			480		
18	6	0	24	2	4	0	6	60,2	0	45,8	4	5	0	9	1	2	0	3	20	0	1	0	0	1	0	0	0	0	0	8	19	0			405		
12	7	2	21	10	8	1	19	17	0	11	0	0	0	0	1	1	0	2	6	1	0	2	0	2	2	0	0	2	0	1	11	1			368		
8	4	0	12	1	2	0	3	16,2	2	23,8	0	7	0	7	70	26	0	96	0	0	0	0	0	0	5	0	0	5	0	35	37	7			310		
15	3	0	18	5	14	3	22	23	0	30	5	2	1	8	7	2	0	9	5	0	0	0	0	0	2	0	0	2	0	107	21	2			372		
2	2	2	6	5	9	7	21	3	0	20	6	2	0	8	82	1	0	83	0	16	0	1	0	1	1	0	0	1	0	185	30	2			361		
7	0	0	7	0	7	7	14	5	0	30	7	4	0	11	90	12	0	102	21	24	0	1	0	1	5	0	0	5	5	190	29	4			468		
0	0	0	0	1	0	0	1	65	0	8	0	0	0	0	0	2	0	2	11	0	0	0	0	0	0	0	0	0	0	275	1	0			342		
0	0	0	0	0	0	0	0	207	0	20	0	0	0	0	0	0	0	0	5	0	0	0	0	0	0	0	0	0	0	186	13	0	x		319		
0	0	0	0	0	1	5	6	187	0	16	0	0	0	0	0	0	0	0	14	0	0	0	0	0	0	0	0	0	0	380	10	3			311		
2	0	0	2	3	6	2	11	105	2	11	0	0	0	0	0	0	0	0	4	0	0	0	0	0	0	0	0	0	0	225	4	0			258		
0	0	0	0	0	1	0	1	33	0	0	0	0	0	0	0	0	0	0	0	0	0	0	0	0	0	0	0	0	0	318	13	12			66		
0	0	0	0	2	0	0	2	170	0	13	0	0	0	0	0	0	0	0	2	0	0	0	0	0	0	0	0	0	0	285	21	0	x		276		
0	0	0	0	0	0	1	1	101	0	0	0	0	0	0	0	0	0	0	0	0	0	0	0	0	0	0	0	0	0	260	15	0	x		274		
0	0	0	0	0	0	0	0	77	0	0	0	0	0	0	0	0	0	0	0	0	0	0	0	0	0	0	0	0	0	234	33	12			150		
0	0	0	0	0	0	1	1	39,6	0	1,44	0	0	0	0	0	0	0	0	0	0	0	0	0	0	0	0	0	0	0	209	29	6	x		257		
0	0	0	0	0	0	2	2	78,1	0	4,94	0	0	0	0	0	0	0	0	0	0	0	0	0	0	0	0	0	0	0	223	19	0	x		294		
0	0	0	0	0	1	8	9	190	0	15	0	0	0	0	0	0	0	0	9	0	0	0	0	0	0	0	0	0	0	215	15	0	x		373		
0	0	0	0	0	0	0	0	5	0	0	0	0	0	0	0	0	0	0	0	0	0	0	0	0	0	0	0	0	0	320	5	11	x		101		
0	0	0	0	0	2	3	5	152	2	4,49	0	0	0	0	0	0	0	0	0	0	0	0	0	0	0	0	0	0	0	340	22	6			254		
0	0	0	0	0	0	0	0	28	1	0	0	0	0	0	0	0	0	0	0	0	0	0	0	0	0	0	0	0	0	477	48	0	x		219		
0	0	0	0	0	1	0	1	63,4	0	2,64	0	0	0	0	0	0	0	0	0	0	0	0	0	0	0	0	0	0	0	788	80	5	x		249		
0	0	0	0	0	0	0	0	9,9	0	0,1	0	0	0	0	0	0	0	0	0	0	0	0	0	0	0	0	0	0	0	211	3	17			250		
0	0	0	0	0	2	1	3	64,8	0	7,2	0	0	0	0	0	0	0	0	0	0	0	0	0	0	0	0	0	0	0	350	20	5			222		
0	0	0	0	0	0	2	2	35,6	0	1,42	0	0	0	0	0	0	0	0	0	0	0	0	0	0	0	0	0	0	0	561	5	4			163		
								0		0																							x		0		
0	0	0	0	0	0	0	0	12,3	0	0,71	0	0	0	0	0	0	0	0	0	0	0	0	0	0	0	0	0	0	0	278	18	0			272		
0	0	0	0	0	0	4	4	183	0	5,42	0	0	0	0	0	0	0	0	0	0	0	0	0	0	0	0	0	0	0	167	39	5			280		

D = Nordenskjöld & Kotick Point Formation

KG = Fossil Bluff Group

Age	Sample	Formation	Dino A	%	Dino B	%	Dino C	%	Dinocysts total	%	Acritarchs	%	Algae indet	%
early Albian	D.8403.30	Kotick Point Fm	0,00	0,33	0,78	0,51	0,78	0,17	1,55	1,01	0,52	0,56	3,88	1,74
	D.8403.65	Kotick Point Fm	0,65	0,42	0,65	0,46	0,22	0,31	1,53	0,88	0,00	0,30	0,00	2,19
late Aptian	D.8406.6	Kotick Point Fm	0,36	0,34	0,18	0,41	0,00	0,00	0,54	0,74	0,72	0,71	0,00	1,64
	D.8406.18	Kotick Point Fm	0,00	0,47	0,21	0,56	0,00	0,00	0,21	1,01	0,83	0,12	0,00	2,33
	D.8406.4	Kotick Point Fm	0,99		1,23		0,00		2,22		0,74		4,94	
	D.8633.10	Kotick Point Fm	0,00		0,00		0,00		0,00		0,54		1,63	
middle Tithonian	D.8751.4	Nordenskjöld Fm	0,00	1,13	2,26	1,05	0,00	0,07	2,26	2,24	30,97	19,54	0,00	1,46
	D.8751.3	Nordenskjöld Fm	1,34	0,76	0,54	0,82	0,27	0,13	2,15	0,08	2,42	12,12	1,34	2,12
	D.8751.2	Nordenskjöld Fm	1,66		0,55		0,00		2,22		22,99		0,00	
	D.8751.1	Nordenskjöld Fm	1,50		0,85		0,00		2,35		21,79		4,49	
upper Aptian	KG.3403.213	Pluto Glacier Fm	0,00	0,00	0,00	0,00	0,00	0,00	0,00	0,00	0,58	0,10	3,22	1,93
middle Aptian	KG.3403.70	Pluto Glacier Fm	0,00	0,00	0,00	0,00	0,00	0,00	0,00	0,00	0,00	0,24	1,57	1,66
lower Aptian	KG.3402.286	Pluto Glacier Fm	0,00		0,00		0,00		0,00	0,00	0,00		4,50	
	KG.3403.4	Pluto Glacier Fm	0,00		0,00		0,00		0,00		0,00		1,55	
	KG.3402.105	Pluto Glacier Fm	0,00		0,00		0,00		0,00	0,00	0,00		0,00	
	KG.3402.16	Pluto Glacier Fm	0,00		0,00		0,00		0,00		0,00		0,72	
Valanginian ?-Barremian	KG.3457.54	Spartan Glacier Fm	0,00	0,0	0,00	0,0	0,00	0,0	0,00	0,0	0,00	0,00	0,00	0,40
	KG.3401.608	Spartan Glacier Fm	0,00	0,0	0,00	0,0	0,00	0,0	0,00	0,0	0,00	0,00	0,00	0,99
	KG.3456.65	Spartan Glacier Fm	0,00		0,00		0,00		0,00		0,00		0,00	
	KG.3455.170	Spartan Glacier Fm	0,00		0,00		0,00		0,00		0,00		0,00	
	KG.3455.24	Spartan Glacier Fm	0,00		0,00		0,00		0,00		0,00		2,41	
Valanginian ?	KG.3461.26	Spartan Glacier Fm	0,00		0,00		0,00		0,00		0,00		0,00	
late Berr.-early Val.	KG.2942.10	Himalia Ridge Fm	0,00	0,0	0,00	0,0	0,00	0,0	0,00	0,0	0,00	0,00	0,00	0,0
Berriasian	KG.3401.2	Himalia Ridge Fm	0,00	0,0	0,00	0,0	0,00	0,0	0,00	0,0	0,00	0,00	0,00	0,0
	KG.3404.283	Himalia Ridge Fm	0,00		0,00		0,00		0,00		0,00		0,00	
upper Tithonian	KG.3404.34	Himalia Ridge Fm	0,00	0,00	0,00	0,00	0,00	0,00	0,00	0,00	0,00	0,00	0,00	0,00
	KG.2802.662	Himalia Ridge Fm	0,00	0,0	0,00	0,0	0,00	0,0	0,00	0,0	0,00	0,00	0,00	0,0
	KG.2929.1	Himalia Ridge Fm	0,00		0,00		0,00		0,00		0,00		0,00	
	KG.2802.332	Himalia Ridge Fm												
middle Tithonian	KG.2802.98	Himalia Ridge Fm	0,00	0,00	0,00	0,00	0,00	0,00	0,00	0,00	0,00	0,00	0,00	0,00
	KG.2940.10	Himalia Ridge Fm	0,00	0,00	0,00	0,00	0,00	0,00	0,00	0,00	0,00	0,00	0,00	0,00

D = Nordenskjöld & Kotick Point Formation

KG = Fossil Bluff Group

Age	Sample	Formation	Foraminifera	%	Leiospheres	%	marine AOM	%	terrestrial AOM translucent	%	terrestrial AOM opaque	%
early Albian	D.8403.30	Kotick Point Fm	0,00	0,42	0,00	17,66	5,30	4,94	15,9	7,39	0,00	0,00
	D.8403.65	Kotick Point Fm	0,22	0,33	38,56	19,35	0,31	3,88	1,4	6,38	0,00	0,00
late Aptian	D.8406.6	Kotick Point Fm	0,90	0,58	32,13	16,85	7,04	6,01	5,4	6,75	0,00	0,00
	D.8406.18	Kotick Point Fm	0,63	0,27	35,00	19,34	2,71	4,05	2,1	5,60	0,00	0,00
	D.8406.4	Kotick Point Fm	0,25		0,00		11,30		14,9		0,00	
	D.8633.10	Kotick Point Fm	0,54		0,27		2,99		4,6		0,00	
middle Tithonian	D.8751.4	Nordenskjöld Fm	0,00	0,12	0,00	2,39	7,69	6,93	5,2	3,32	0,65	0,16
	D.8751.3	Nordenskjöld Fm	0,00	0,14	0,00	2,77	8,06	1,16	6,2	2,77	0,00	0,32
	D.8751.2	Nordenskjöld Fm	0,28		4,43		5,54		0,83		0,00	
	D.8751.1	Nordenskjöld Fm	0,21		5,13		6,41		1,1		0,00	
upper Aptian	KG.3403.213	Pluto Glacier Fm	0,00	0,00	0,00	0,00	2,34	3,79	19,0	49,39	0,00	0,13
middle Aptian	KG.3403.70	Pluto Glacier Fm	0,00	0,00	0,00	0,00	6,27	2,26	64,9	17,34	0,00	0,32
lower Aptian	KG.3402.286	Pluto Glacier Fm	0,00		0,00		5,14		60,1		0,00	
	KG.3403.4	Pluto Glacier Fm	0,00		0,00		4,26		40,7		0,78	
	KG.3402.105	Pluto Glacier Fm	0,00		0,00		0,00		50,0		0,00	
	KG.3402.16	Pluto Glacier Fm	0,00		0,00		4,71		61,6		0,00	
Valanginian ?-Barremian	KG.3457.54	Spartan Glacier Fm	0,00	0,0	0,00	0,0	0,00	1,0	36,9	31,0	0,00	0,0
	KG.3401.608	Spartan Glacier Fm	0,00	0,0	0,00	0,0	0,00	1,6	51,3	18,9	0,00	0,0
	KG.3456.65	Spartan Glacier Fm	0,00		0,00		0,56		15,4		0,00	
	KG.3455.170	Spartan Glacier Fm	0,00		0,00		1,68		26,6		0,00	
	KG.3455.24	Spartan Glacier Fm	0,00		0,00		4,02		50,9		0,00	
Valanginian ?	KG.3461.26	Spartan Glacier Fm	0,00		0,00		0,00		5,0		0,00	
late Berr.-early Val.	KG.2942.10	Himalia Ridge Fm	0,00	0,0	0,00	0,0	1,77	0,9	59,6	32,6	0,79	0,4
Berriasian	KG.3401.2	Himalia Ridge Fm	0,00	0,0	0,00	0,0	0,00	0,9	12,8	24,2	0,46	0,4
	KG.3404.283	Himalia Ridge Fm	0,00		0,00		1,06		25,4		0,00	
upper Tithonian	KG.3404.34	Himalia Ridge Fm	0,00	0,00	0,00	0,00	0,04	1,39	4,0	18,33	0,00	0,00
	KG.2802.662	Himalia Ridge Fm	0,00	0,0	0,00	0,0	3,24	1,7	29,2	13,0	0,00	0,0
	KG.2929.1	Himalia Ridge Fm	0,00		0,00		0,87		21,8		0,00	
	KG.2802.332	Himalia Ridge Fm										
middle Tithonian	KG.2802.98	Himalia Ridge Fm	0,00	0,00	0,00	0,00	0,26	1,10	4,5	34,86	0,00	0,00
	KG.2940.10	Himalia Ridge Fm	0,00	0,00	0,00	0,00	1,93	1,18	65,2	42,92	0,00	0,00

D = Nordenskjöld & Kotick Point Formation

KG = Fossil Bluff Group

Age	Sample	Formation	AOMT % total		Sporo A	%	Sporo B	%	Sporo C	%	Sporomorphs total	Sporomorphs % total		Cutinite total	%
early Albian	D.8403.30	Kotick Point Fm	15,89	7,39	2,84	6,74	4,13	3,30	1,29	0,64	32	8,3	10,68	2,58	1,90
	D.8403.65	Kotick Point Fm	1,43	6,38	3,27	4,41	1,53	1,81	0,00	0,53	22	4,8	5,62	0,44	2,28
late Aptian	D.8406.6	Kotick Point Fm	5,42	6,75	3,97	8,59	2,71	3,53	0,90	0,64	42	7,6	12,76	0,00	2,09
	D.8406.18	Kotick Point Fm	2,08	5,60	5,83	4,33	1,46	2,03	0,83	0,43	39	8,1	5,77	0,83	2,78
	D.8406.4	Kotick Point Fm	14,87		12,59		3,70		0,00		66	16,3		6,17	
	D.8633.10	Kotick Point Fm	4,62		11,96		6,25		0,82		70	19,0		1,36	
middle Tithonian	D.8751.4	Nordenskjöld Fm	5,86	3,48	9,03	8,62	3,55	4,08	0,00	1,20	39	12,6	13,90	2,26	1,31
	D.8751.3	Nordenskjöld Fm	6,18	2,93	10,75	1,64	4,84	0,55	0,81	1,06	61	16,4	1,72	0,54	0,72
	D.8751.2	Nordenskjöld Fm	0,83		7,20		3,88		2,49		49	13,6		1,39	
	D.8751.1	Nordenskjöld Fm	1,07		7,48		4,06		1,50		61	13,0		1,07	
upper Aptian	KG.3403.213	Pluto Glacier Fm	19,01	49,52	0,29	0,75	0,00	1,01	0,00	0,40	1	0,3	2,15	0,00	0,00
middle Aptian	KG.3403.70	Pluto Glacier Fm	64,89	17,27	0,00	0,82	0,00	1,45	0,00	0,67	0	0,0	2,31	0,00	0,00
lower Aptian	KG.3402.286	Pluto Glacier Fm	60,13		0,00		0,32		1,61		6	1,9		0,00	
	KG.3403.4	Pluto Glacier Fm	41,47		1,94		2,71		0,78		14	5,4		0,00	
	KG.3402.105	Pluto Glacier Fm	50,00		1,52		3,03		0,00		3	4,5		0,00	
	KG.3402.16	Pluto Glacier Fm	61,59		0,72		0,00		0,00		2	0,7		0,00	
Valanginian ?-Barremian	KG.3457.54	Spartan Glacier Fm	36,86	31,0	0,00	0,0	0,00	0,0	0,36	0,6	1	0,4	0,64	0,00	0,00
	KG.3401.608	Spartan Glacier Fm	51,33	18,9	0,00	0,0	0,00	0,1	0,00	0,8	0	0,0	0,91	0,00	0,00
	KG.3456.65	Spartan Glacier Fm	15,39		0,00		0,00		0,39		1	0,4		0,00	
	KG.3455.170	Spartan Glacier Fm	26,55		0,00		0,00		0,68		2	0,7		0,00	
	KG.3455.24	Spartan Glacier Fm	50,94		0,00		0,27		2,14		9	2,4		0,00	
Valanginian ?	KG.3461.26	Spartan Glacier Fm	4,95		0,00		0,00		0,00		0	0,0		0,00	
late Berr.-early Val.	KG.2942.10	Himalia Ridge Fm	60,44	33,0	0,00	0,0	0,79	0,4	1,18	0,4	5	2,0	0,8	0,00	0,0
Berriasian	KG.3401.2	Himalia Ridge Fm	13,24	24,5	0,00	0,0	0,00	0,4	0,00	0,7	0	0,0	1,0	0,00	0,0
	KG.3404.283	Himalia Ridge Fm	25,45		0,00		0,40		0,00		1	0,4		0,00	
upper Tithonian	KG.3404.34	Himalia Ridge Fm	3,96	13,74	0,00	0,00	0,00	0,30	0,00	0,56	0	0,0	0,86	0,00	0,00
	KG.2802.662	Himalia Ridge Fm	29,19	14,0	0,00	0,0	0,90	0,5	0,45	0,6	3	1,4	0,7	0,00	0,0
	KG.2929.1	Himalia Ridge Fm	21,83		0,00		0,00		1,23		2	1,2		0,00	
	KG.2802.332	Himalia Ridge Fm	0,00												
middle Tithonian	KG.2802.98	Himalia Ridge Fm	4,52	34,86	0,00	0,00	0,00	0,00	0,00	0,71	0	0,0	0,71	0,00	0,00
	KG.2940.10	Himalia Ridge Fm	65,21	42,92	0,00	0,00	0,00	0,00	1,43	1,01	4	1,4	1,01	0,00	0,00

D = Nordenskjöld & Kotick Point Formation

KG = Fossil Bluff Group

Age	Sample	Formation	Inertinite A	%	Inertinite B	%	Inertinite total	%	Vitrinite A	%	Vitrinite B	%	Vitrinite total	%
early Albian	D.8403.30	Kotick Point Fm	25,6	14,73	7,0	2,19	32,6	16,92	9,3	20,85	19,9	15,49	29,2	36,34
	D.8403.65	Kotick Point Fm	16,6	7,71	1,5	2,46	18,1	9,29	24,6	6,04	9,6	4,09	34,2	5,81
late Aptian	D.8406.6	Kotick Point Fm	9,7	11,55	0,9	1,17	10,6	12,72	21,1	22,80	13,5	15,87	34,7	38,67
	D.8406.18	Kotick Point Fm	8,3	6,73	2,5	0,95	10,8	6,19	21,5	2,58	16,3	3,10	37,7	5,53
	D.8406.4	Kotick Point Fm	6,7		1,0		7,7		22,0		13,6		35,6	
	D.8633.10	Kotick Point Fm	21,5		0,3		21,7		26,6		20,1		46,7	
middle Tithonian	D.8751.4	Nordenskjöld Fm	16,8	24,81	4,2	3,18	21,0	27,98	7,7	8,77	8,1	10,73	15,8	19,50
	D.8751.3	Nordenskjöld Fm	34,1	7,13	4,0	1,17	38,2	7,29	13,2	3,00	11,0	2,27	24,2	3,96
	D.8751.2	Nordenskjöld Fm	24,4		2,8		27,1		7,8		13,6		21,3	
	D.8751.1	Nordenskjöld Fm	23,9		1,7		25,6		6,4		10,3		16,7	
upper Aptian	KG.3403.213	Pluto Glacier Fm	33,3	19,11	7,0	6,54	40,4	25,66	8,2	3,75	26,0	13,11	34,2	16,86
middle Aptian	KG.3403.70	Pluto Glacier Fm	8,5	9,32	2,2	4,14	10,7	10,79	1,9	2,49	14,7	7,84	16,6	9,54
lower Aptian	KG.3402.286	Pluto Glacier Fm	15,8		4,2		19,9		1,6		6,8		8,4	
	KG.3403.4	Pluto Glacier Fm	13,2		14,0		27,1		2,7		17,4		20,2	
	KG.3402.105	Pluto Glacier Fm	27,3		7,6		34,8		3,0		7,6		10,6	
	KG.3402.16	Pluto Glacier Fm	16,7		4,3		21,0		5,1		6,2		11,2	
Valanginian ?-Barremian	KG.3457.54	Spartan Glacier Fm	31,8	30,4	15,0	20,6	46,7	51,0	4,7	2,1	11,3	13,7	16,1	15,9
	KG.3401.608	Spartan Glacier Fm	28,0	10,1	11,3	18,4	39,3	17,6	2,0	1,5	7,3	4,6	9,3	3,9
	KG.3456.65	Spartan Glacier Fm	44,0		22,2		66,1		1,6		16,0		17,5	
	KG.3455.170	Spartan Glacier Fm	39,5		13,9		53,4		2,4		15,3		17,7	
	KG.3455.24	Spartan Glacier Fm	21,4		4,8		26,3		2,1		11,8		13,9	
Valanginian ?	KG.3461.26	Spartan Glacier Fm	17,8		56,4		74,3		0,0		20,8		20,8	
late Berr.-early Val.	KG.2942.10	Himalia Ridge Fm	11,0	37,1	15,7	18,3	26,8	55,4	2,4	2,2	6,7	7,6	9,1	9,8
Berriasian	KG.3401.2	Himalia Ridge Fm	46,1	23,0	28,8	9,4	74,9	25,3	2,3	0,2	9,6	1,8	11,9	1,8
	KG.3404.283	Himalia Ridge Fm	54,2		10,4		64,7		2,0		6,4		8,4	
upper Tithonian	KG.3404.34	Himalia Ridge Fm	22,4	21,93	46,0	32,43	68,4	54,36	2,0	4,13	25,6	20,94	27,6	25,07
	KG.2802.662	Himalia Ridge Fm	22,5	0,9	32,9	13,8	55,4	14,6	1,8	3,9	9,0	10,4	10,8	13,2
	KG.2929.1	Himalia Ridge Fm	20,9		18,4		39,3		8,6		28,2		36,8	
	KG.2802.332	Himalia Ridge Fm												
middle Tithonian	KG.2802.98	Himalia Ridge Fm	30,5	24,01	59,6	35,14	90,1	59,14	1,1	1,27	4,0	2,91	5,1	4,18
	KG.2940.10	Himalia Ridge Fm	17,5	9,20	10,7	34,54	28,2	43,74	1,4	0,23	1,8	1,60	3,2	1,37

D = Nordenskjöld & Kotick Point Formation

KG = Fossil Bluff Group

Age	Sample	Formation	Phytoclasts	%	Filaments	%	marine OM	%	terrestrial OM	%	Palynomorphs %	OP/TR
early Albian	D.8403.30	Kotick Point Fm	64,3	55,16	0,0	0,17	11,2	26,33	88,5	73,40	14,21	0,5
	D.8403.65	Kotick Point Fm	52,7	9,69	0,0	0,43	40,6	16,05	58,9	16,01	45,10	
late Aptian	D.8406.6	Kotick Point Fm	45,3	53,48	0,0	0,26	41,3	26,53	58,3	73,24	41,88	0,3
	D.8406.18	Kotick Point Fm	49,4	11,08	1,0	0,52	39,4	16,90	60,6	16,79	45,83	
	D.8406.4	Kotick Point Fm	49,4		0,0		19,5		80,5		24,44	
	D.8633.10	Kotick Point Fm	69,8		0,0		6,0		93,5		22,01	
middle Tithonian	D.8751.4	Nordenskjöld Fm	39,0	48,79	0,0	0,27	40,9	32,68	57,5	66,44	45,81	1,4
	D.8751.3	Nordenskjöld Fm	62,9	10,41	0,0	0,53	14,0	12,71	85,5	13,04	22,31	
	D.8751.2	Nordenskjöld Fm	49,9		0,0		35,5		64,3		43,49	
	D.8751.1	Nordenskjöld Fm	43,4		1,1		40,4		58,5		48,08	
upper Aptian	KG.3403.213	Pluto Glacier Fm	74,6	42,52	0,0	0,00	6,1	5,81	93,9	94,19	4,09	1,8
middle Aptian	KG.3403.70	Pluto Glacier Fm	27,3	17,88	0,0	0,00	7,8	3,25	92,2	3,25	1,57	
lower Aptian	KG.3402.286	Pluto Glacier Fm	28,3		0,0		9,6		90,4		6,43	
	KG.3403.4	Pluto Glacier Fm	47,3		0,0		5,8		94,2		6,98	
	KG.3402.105	Pluto Glacier Fm	45,5		0,0		0,0		100,0		4,55	
	KG.3402.16	Pluto Glacier Fm	32,2		0,0		5,4		94,6		1,45	
Valanginian ?-Barremian	KG.3457.54	Spartan Glacier Fm	62,8	66,9	0,0	0,0	0,0	1,4	100,0	98,6	0,36	3,2
	KG.3401.608	Spartan Glacier Fm	48,7	20,7	0,0	0,0	0,0	2,5	100,0	2,5	0,00	
	KG.3456.65	Spartan Glacier Fm	83,7		0,0		0,6		99,4		0,39	
	KG.3455.170	Spartan Glacier Fm	71,1		0,0		1,7		98,3		0,68	
	KG.3455.24	Spartan Glacier Fm	40,2		0,0		6,4		93,6		4,83	
Valanginian ?	KG.3461.26	Spartan Glacier Fm	95,0		0,0		0,0		100,0		0,00	
late Berr.-early Val.	KG.2942.10	Himalia Ridge Fm	35,8	65,2	0,0	0,0	1,8	0,9	98,2	99,1	1,97	5,6
Berriasian	KG.3401.2	Himalia Ridge Fm	86,8	26,4	0,0	0,0	0,0	0,9	100,0	0,9	0,00	
	KG.3404.283	Himalia Ridge Fm	73,1		0,0		1,1		98,9		0,40	
upper Tithonian	KG.3404.34	Himalia Ridge Fm	96,0	79,43	0,0	0,00	0,0	1,39	100,0	98,61	0,00	2,9
	KG.2802.662	Himalia Ridge Fm	66,2	15,2	0,0	0,0	3,2	1,7	96,8	1,7	1,35	
	KG.2929.1	Himalia Ridge Fm	76,1		0,0		0,9		99,1		1,23	
	KG.2802.332	Himalia Ridge Fm										
middle Tithonian	KG.2802.98	Himalia Ridge Fm	95,2	63,32	0,0	0,00	0,3	1,10	99,7	98,90	0,00	13,1
	KG.2940.10	Himalia Ridge Fm	31,4	45,11	0,0	0,00	1,9	1,18	98,1	1,18	1,43	

Microfacies Analysis

LXVIII–LXXVII

Microfacies Analysis CM section

Sample	remarks/content	remarks	rmf-type		Stage
CM 13/2,74	peloids	moderately sorted subrounded Bioclastic Packstone packed Biomicrite	9 Mid-ramp to Outer ramp	1	
CM 13/18	peloids	moderately sorted subangular Bioclastic Grainstone poorly washed Biosparite	14 inner ramp - open marine	2	
CM 14/3	peloids burrows	poorly sorted rounded packstone packed Biomicrite	8 Mid-ramp	3	
CM 14/15	peloids shells burrows	poorly sorted subangular packstone packed Biomicrite	8 Mid-ramp	4	
CM 15/4	peloids burrows	well sorted/very well sorted subrounded, packstone packed biomicrite poorly washed biosparite	8 Mid-ramp	5	
CM 16/7	peloids shells burrows	moderately sorted subangular/subrounded Packstone packed biomicrite	4/9 Mid-ramp to outer ramp	6	
CM 16/16	peloids shells	poorly sorted subrounded Grainstone poorly washed biosparite	14 inner ramp - open marine	7	
CM 16/24	peloids skeletal grains	poorly sorted rounded Grainstone unsorted biosparite	14 inner ramp - open marine	8	Tithonian
CM 16/36	peloids skeletal grains	poorly sorted subrounded Packstone poorly washed biosparite	4/9 Mid ramp to outer ramp	9	
CM 16/44	peloids skeletal grains	poorly sorted subrounded Packstone poorly washed biosparite	4/9 Mid ramp to outer ramp	10	
CM 16/70	peloids ooids, cortoids burrows skeletal grains	moderately sorted rounded Grainstone rounded biosparite	8 Mid-ramp	11	
CM 16/80	extremely fine grained	well sorted agular mud-wackestone/calcisiltite micrite	5 Mid ramp, outer ramp, basin	12	
CM 16/100	peloids, shells cortoids, burrows clasts up to 1 mm size	poorly sorted rounded Grainstone unsorted biosparite	8 Mid-ramp	13	
CM 16/112	peloids, shells burrows clasts up to 0.5 mm size	poorly sorted subangular Packstone/Grainstone poorly washed biosparite	8 Mid-ramp	14	
CM 17/23	some rounded bioclasts some unfilled veins	poorly sorted rounded mud-wackestone micrite	5 Mid ramp, outer ramp, basin	15	Berr.

Sample	remarks/content	remarks	rmf-type		Stage
CM 17/28	few bioclasts unfilled veins	poorly sorted rounded mud-wackestone fossiliferous micrite	5 Mid ramp, outer ramp, basin	16	
CM 17/32	abundant bioclasts unfilled veins well preserved shells	moderately sorted rounded wackestone fossiliferous micrite	5 Mid ramp, outer ramp, basin	17	
CM 17/35,5	few bioclasts plenty filled and unfilled veins	poorly sorted rounded mudstone/calcisiltite micrite/fossiliferous micrite	1 Outer ramp, basin	18	
CM 17/40	few bioclasts some filled and unfilled veins	poorly sorted subrounded mudstone/calcisiltite micrite/fossiliferous micrite	1 Outer ramp, basin	19	
CM 17/44	well preserved cinoids and foraminifers some unfilled veins	poorly sorted angular wackestone fossiliferous micrite	7 Inner ramp - restricted/open marine; Mid-ramp	20	
CM 17/48	plenty rounded bioclasts some unfilled veins	moderately sorted subangular mud-wackestone micrite/fossiliferous micrite	1 Outer ramp, basin (9 Lagoon?)	21	
CM 17/54	plenty rounded bioclasts some filled and unfilled veins	poorly sorted subangular wackestone/calcisiltite micrite/fossiliferous micrite	1 Outer ramp, basin	22	
CM 17/57	plenty rounded bioclasts some filled and unfilled veins	moderately sorted subrounded mud-wackestone fossiliferous micrite	5 Mid ramp, outer ramp, basin	23	Berriasian
CM 17/62	plenty rounded bioclasts some filled and unfilled veins	poorly sorted subrounded mud-wackestone fossiliferous micrite	1 Outer ramp, basin (9 Lagoon?)	24	
CM 17/65	few rounded bioclasts filled veins	moderately sorted angular mudstone micrite	1 Outer ramp, basin (9 Lagoon?)	25	
CM 17/71	abundant bioclasts unrounded larger bioclasts unfilled veins	poorly sorted subangular mud-wackestone fossiliferous micrite	1 Outer ramp, basin 5 Mid ramp, outer ramp, basin	26	
CM 17/73	some large bioclasts laminated	poorly sorted angular mud-wackestone fossiliferous micrite	1 Outer ramp, basin 5 Mid ramp, outer ramp, basin	27	
CM 17/75	few rounded bioclasts abundant unfilled veins laminated	poorly sorted angular mud-wackestone fossiliferous micrite	1 Outer ramp, basin	28	
CM 17/80	abundant small bioclasts abundant unfilled veins	moderately sorted subrounded mudstone micrite	1 Outer ramp, basin	29	
CM 17/83	abundant small bioclasts few larger shell fragments	moderately sorted subangular mudstone micrite	1 Outer ramp, basin	30	
CM 17/85	some larger shell fragments larger unfilled veins	moderately sorted subangular mud-wackestone fossiliferous micrite	5 Mid ramp, outer ramp, basin	31	

Sample	remarks/content	remarks	rmf-type		
CM 17/88	abundant small bioclasts plenty filled and unfilled veins	moderately sorted subrounded mudstone micrite	1 Outer ramp, basin	32	Berriasian
CM 17/94	abundant small reounded bioclasts few larger shell fragments	well sorted angular mud-wackestone fossiliferous micrite	5 Mid ramp, outer ramp, basin	33	
CM 17/97	few larger shell fragments filled veins bioclasts	moderately sorted subangular mud-wackestone fossiliferous micrite	5 Mid ramp, outer ramp, basin	34	
CM 17/102	abundan bioclasts filled veins laminated	well sorted angular mud-wackestone fossiliferous micrite	5 Mid ramp, outer ramp, basin	35	
CM 17/114	few larger shell fragments few filled and unfilled veins	well sorted angular mud-wackestone fossiliferous micrite	1 Outer ramp, basin	36	
CM 18/1,5	shell fragments in various sizes some unfilled veins	moderately sorted subangular floatstone sparse biomicrite	3 Mid ramp, outer ramp	37	
CM 18/3	abundant shell fragments in various sizes micritic matrix (burrows?)	moderately sorted subrounded rudstone packed biomicrite	28 Mid-ramp shoal 3 Mid ramp, outer ramp	38	
CM 18/15	recrystallised shells, rounded bioclasts plenty unfilled v eins micritic matrix	poorly sorted subrounded mudstone/calcisiltite fossiliferous micrite	1 Outer ramp, basin 5 Mid ramp, outer ramp, basin	39	
CM 18/19	recrystallised shells, rounded bioclasts unfilled veins micritic matrix	well sorted subrounded mudstone/calcisiltite fossiliferous micrite	1 Outer ramp, basin 5 Mid ramp, outer ramp, basin	40	
CM 18/22	recrystallised shells, rounded bioclasts unfilled veins micritic matrix	moderately sorted rounded mudstone/calcisiltite fossiliferous micrite	1 Outer ramp, basin 5 Mid ramp, outer ramp, basin	41	
CM 18/27	some large recrystallised shells some filled veins dark lithoclasts burrows	poorly sorted rounded mud-wackestone fossiliferous micrite	3 Mid-ramp to outer ramp 8 Mid-ramp	42	Valanginian
CM 18/37	some large recrystallised shells some filled veins dark lithoclasts burrows	poorly sorted rounded mud-wackestone fossiliferous micrite	3 Mid-ramp to outer ramp 8 Mid-ramp	43	
CM 18/46	some large recrystallised shells some filled veins	well sorted subrounded wackestone sparce biomicrite	9 Mid-ramp to outer ramp	44	
CM 18/57	large shell fragment plenty small shell fragments fine grained matrix, burrows dark lithoclasts	poorly sorted rounded rudstone packed biomicrite	28 Mid-ramp shoal 3 Mid-ramp to outer ramp	45	
CM 18/67	abundant shell fragments some filled veins dark lithoclasts echinoderms	poorly sorted subangular wackestone fossiliferous micrite	3 Mid-ramp to outer ramp 8 Mid-ramp	46	
CM 19/1	plenty recrystallised shells abundant rounded bioclasts some unfilled veins	well sorted subrounded packstone packed biomicrite	9 Mid-ramp to outer ramp 14 inner ramp - open marine	47	

Sample	remarks/content	remarks	rmf-type		Stage
CM 19/8	abundant large shell fragments shells partly recrystallised dark lithoclasts, fine grained matrix dark filled veins	well sorted subrounded packstone packed biomicrite	9 Mid-ramp to outer ramp 14 inner ramp - open marine	48	
CM 19/10	abundant large shell fragments shells partly recrystallised some unfilled veins	poorly sorted subangular wackestone sparse biomicrite	9 Mid-ramp to outer ramp 14 inner ramp - open marine	49	
CM 19/17	fes bioclasts dark filled veins	poorly sorted subangular mudstone micrite	19 Peritidal/Lagoon 24 Peritidal zone	50	
CM 19/26	abudnant peloids plenty recrystallised shells dark bioclasts dark filled veins	poorly sorted subangular wackestone sparse biomicrite	9 Mid-ramp to outer ramp 14 inner ramp - open marine 7 Inner ramp - restricted/open marine; Mid-ramp	51	
CM 19/28	plenty shell fragmenty and bioclasts plenty well preserved shell fragments dark filled veins echinoderms	poorly sorted subangular packstone packed biomicrite	3 Mid-ramp to outer ramp 7 Inner ramp - restricted/open marine; Mid-ramp	52	
CM 20/0,1	abundant large shell fragments, majorly r dark bioclasts, echinoderms fine grained matrix dark filled veins	poorly sorted subrounded wackestone packed biomicrite	9 Mid-ramp to outer ramp 7 Inner ramp - restricted/open marine; Mid-ramp	53	
CM 20/8	abundant shell fragments filled veins echinoderms	moderately sorted rounded wackestone biomicrite	8 Mid-ramp 7 Inner ramp - restricted/open marine; Mid-ramp 21 Peritidal/Lagoon	54	
CM 20/12	some well preserved shell fragments filled veins echinoderms	poorly sorted subrounded wackestone sparse biomicrite	7 Inner ramp - restricted/open marine; Mid-ramp 9 Mid-ramp to outer ramp	55	
CM 20/20	abundant well preserved bioclasts in vari few unfilled veins	poorly sorted angular wackestone sparse biomicrite	9 Mid-ramp to outer ramp	56	
CM 20/30	abundant well preserved bioclasts in various shapes and sizes some filled and unfilled veins laminated	poorly sorted subangular mud-wackestone fossiliferous micrite	9 Mid-ramp to outer ramp 14 inner ramp - open marine	57	
CM 20/36	abundant well preserved bioclasts in various shapes and sizes filled and unfilled veins echinoderms	poorly sorted subrounded mud-wackestone fossiliferous micrite	9 Mid-ramp to outer ramp 7 Inner ramp - restricted/open marine; Mid-ramp	58	
CM 21/1-8	abundant well preserved bioclasts unfilled and filled veins (sparitic) micritic matrix	poorly sorted subrounded mud-wackestone fossiliferous micrite	9 Mid-ramp to outer ramp	59	
CM 21/8-15	abundant well preserved bioclasts few grain aggregates echinoderms sparitic filled pores	poorly sorted subangular packstone unsorted biosparite	7 Inner ramp - restricted/open marine; Mid-ramp	60	Valanginian
CM 22/5-9	abundant and well preserved calcareous algae and echinoderms some unfilled veins sparitic filled pores	poorly sorted subrounded grainstone unsorted biosparite	26/27 Inner ramp shoal/ Mid ramp shoal	61	
CM 22/18	abundant and well preserved echinoderm some grain aggregates sparitic filled pores	poorly sorted subrounded grainstone unsorted biosparite	26/27 Inner ramp shoal/ Mid ramp shoal	62	
CM 22/24	abundant and well preserved calcareous algae and echinoderms wenige grain aggeregates sparitic filled pores	moderately sorted subrounded grainstone unsorted biosparite	26 Inner ramp shoal/ Mid ramp shoal	63	Hauterivian

Sample	remarks/content	remarks	rmf-type		Stage
CM 22/44	abundant and well preserved calcareous algae and echinoderms sparitic filled pores	moderately sorted subrounded grainstone unsorted biosparite	26 Inner ramp shoal/ Mid ramp shoal	64	
CM 22/52	abundant and well preserved calcareous algae and echinoderms micritic matrix	well sorted subrounded packstone packed biomicrite	20 Inner ramp - Lagoon 26 Inner ramp shoal/ Mid ramp shoal	65	
CM 22/60	abundant and well presevred echinoderms, skeletal grains micritic/sparitic matrix	moderately sorted subrounded packstone/grainstone poorly washed biosparite	20 Inner ramp - Lagoon 26 Inner ramp shoal/ Mid ramp shoal	66	
CM 22/70	abundant and well presevred echinoderm abundant bioclasts some filled veins micritic/sparitic matrix	moderately sorted subrounded packstone/grainstone packed biomicrite	20 Inner ramp - Lagoon 26 Inner ramp shoal/ Mid ramp shoal	67	
CM 23/4	some peloids filled and unfilled veins micritic matrix laminated	moderately sorted subangular mud-wackestone fossiliferous micrite	19 Peritidal Zone/Inner ramp lagoon	68	
CM 23/10	few small bioclasts filled veins micritic matrix	moderately sorted rounded mud-wackestone fossiliferous micrite	19 Peritidal Zone/Inner ramp lagoon	69	
CM 23/18	few small bioclasts filled and unfilled veins micritic matrix	moderately sorted subrounded mud-wackestone fossiliferous micrite	19 Peritidal Zone/Inner ramp lagoon	70	
CM 23/27	few bioclasts, few skeletal grains filled and unfilled veins micritic matrix	well sorted rounded mud-wackestone fossiliferous micrite	19 Peritidal Zone/Inner ramp lagoon	71	
CM 23/34	abundant bioclasts unfilled veins micritic matrix	well sorted rounded mud-wackestone fossiliferous micrite	19 Peritidal Zone/Inner ramp lagoon	72	
CM 23/40	abundant echinoderms, skeletal grains abundant bio-/lithoclasts filled veins micritic/sparitic matrix	poorly sorted subrounded packstone packed biomicrite	27 Inner ramp shoal/ Mid ramp shoal	73	
CM 23/49	abundant echinoderms, skeletal grains, calcareous algae abundant bio-/lithoclasts micritic/sparitic matrix	poorly sorted subangular packstone poorly washed biosparite	20 Inner ramp - Lagoon 26/27 Inner ramp shoal/ Mid ramp shoal	74	
CM 23/60	some bioclasts, abundant skeletal grains calcite filled veins micritic matrix	moderately sorted subrounded mudstone fossiliferous micrite	19 Peritidal Zone/Inner ramp lagoon	75	
CM 23/69	fine grained matrix filled veins	well sorted subrounded mudstone micrite	19 Peritidal Zone/Inner ramp lagoon	76	

Hauterivian

Microfacies Analysis LV section

Sample	remarks/content	remarks	rmf-type		Stage
LV 3/1-30	some bioclasts skeletal grains	poorly sorted subangular wackestone fossiliferous micrite	24 peritidal zone	1	Tithonian
LV 3/3	abundant bioclasts burrows (?)	moderately sorted subrounded packstone sparse biomicrite	26 Inner ramp - mid-ramp shoal	2	
LV 3/10	skeletal grains bioclasts	moderately sorted rounded packstone poorly washed biosparite	26 Inner ramp - mid-ramp shoal	3	
LV 3/15	baioclasts laminated few skeletal grains	poorly sorted subangular mudstone micrite	22 peritidal	4	
LV 3/28	shells, bioclasts skeletal grains coated grains (?)	poorly sorted rounded packstone packed Biomicrite	26 Inner ramp - mid-ramp shoal	5	
LV 3/40	coated grains bioclasts skeletal grains peloids	moderately sorted rounded packstone packed biomicrite	26 Inner ramp - mid-ramp shoal	6	
LV 3/53	coated grains bioclasts skeletal grains peloids	poorly sorted subrounded grainstone unsorted biosparite	26 Inner ramp - mid-ramp shoal	7	
LV 3/63	encrusted grains skeletal grains	poorly sorted subangular/subrounded packstone poorly washed biosparite	14 inner ramp open marine	8	
LV 3/66-73	Andesit			9	Berriasian
LV 4/6	Andesit			10	
LV 5/3	rounded bioclasts laminated	poorly sorted subangular mudstone micrite	5 mid-ramp, outer ramp, basin	11	
LV 5/20	echinoderms few skeletal grains	poorly sorted subrounded mudstone micrite	2 mid-ramp, outer ramp, basin	12	
LV 5/24	some skeletal grains few echinoderms	poorly sorted subrounded mudstone micrite	2 mid-ramp, outer ramp, basin	13	
LV 5/30	abundant bioclasts some skeletal grains	poorly sorted rounded wackestone sparse biomicrite	9 mid-ramp, outer ramp	14	
LV 5/35	abundant echinoderms abundant bioklasten	moderately sorted rounded mud-wackestone	5 mid-ramp, outer ramp, basin	15	

Sample	remarks/content	remarks	rmf-type		Stage
LV 5/47	abundant bioclasts echinoderms +/- laminated	poorly sorted subrounded mudstone fossiliferous micrite	5 mid-ramp, outer ramp, basin	16	Berriasian
LV 5/58	few bioclasts evtl echinoderms laminated	moderately sorted rounded mudstone fossiliferous micrite	22 peritidal 5 mid-ramp, outer ramp, basin 19 peritidal - inner ramp lagoon	17	
LV 5/65	few bioclasts calcite filled veins	moderately rounded mudstone micrite	22 peritidal 5 mid-ramp, outer ramp, basin 19 peritidal - inner ramp lagoon	18	
LV 5/69	abundant bioclasts skeletal grains	poorly sorted subrounded mud-wackestone fossiliferous micrite	5 mid-ramp, outer ramp, basin	19	
LV 5/74	abundant skeletal grains few echinoderms	poorly sorted subangular mudstone fossiliferous micrite	5 mid-ramp, outer ramp, basin	20	
LV 5/82	abundant skeletal grains	poorly sorted subangular mud-wackestone fossiliferous micrite	5 mid-ramp, outer ramp, basin	21	
LV 5/86	abundant bioclasts laminated few skeletal grains	moderately sorted subrounded mudstone fossiliferous micrite	19 peritidal - inner ramp lagoon 3 mid-ramp, outer ramp (no burrows!)	22	
LV 5/94	few skeletal grains laminated micritic intraclasts	poorly sorted subrounded mudstone fossiliferous micrite	19 peritidal - inner ramp lagoon 2 mid-ramp, outer ramp, basin	23	
LV 5/99	some skeletal grains +/- laminated calcite filled veins	poorly sorted subrounded mudstone fossiliferous micrite	19 peritidal - inner ramp lagoon	24	
LV 6/1	abundant skeletal grains abundant bioclasts micritic intraclasts	poorly sorted subangular packstone packed biomicrite	9 mid-ramp, outer ramp	25	
LV 6/10	few bioclasts few skeletal grains foraminifers	well sorted rounded mud-wackestone fossiliferous micrite	5 mid-ramp, outer ramp, basin 9 mid-ramp, outer ramp	26	
LV 6/14	few bioclasts micritic intraclasts laminated burrows (?)	well sorted rounded mudstone micrite	22 peritidal 19 peritidal - inner ramp lagoon	27	
LV 6/20	abundant skeletal grains burrows some echinoderms	poorly sorted subrounded packstone packed biomicrite	3 mid-ramp, outer ramp	28	
LV 6/29	abundant echinoderms few skeletal grains foraminifers	moderately sorted rounded mud-wackestone fossilieferous micrite	5 mid-ramp, outer ramp, basin	29	
LV 6/35	abundant peloids/bioclasts few skeletal grains	moderately sorted rounded mud-wackestone fossiliferous micrite	4 outer ramp	30	
LV 6/41	abundant skeletal grains micritic intraclasts abundant echinoderms	poorly sorted subangular wackestone sparse biomicrite	9 mid-ramp, outer ramp	31	

Sample	remarks/content	remarks	rmf-type		Stage
LV 6/47	very few skeletal grains micritic intraclasts very few forams burrows (?)	well sorted rounded mudstone micrite	2 mid-ramp, outer ramp, basin	32	
LV 6/53	abundant peloids skeletal grains micritic intraclasts	moderately sorted rounded mud-wackestone fossiliferous micrite	4 outer ramp	33	
LV 6/58	burrows very few skeletal grains few peloids	moderately sorted subangular mud-wackestone fossiliferous micrite	2 mid-ramp, outer ramp, basin 5 mid-ramp, outer ramp, basin	34	
LV 7/2	abundant foraminifers abundant skeletal grains very few echinoderms few burrows	poorly sorted subangular packsteone sparse biomicrite	3 mid-ramp, outer ramp 13 inner ramp - restricted, open marine	35	Berriasian
LV 7/11	abundant skeletal grains some echinoderms very few micritic intarclasts borings (?)	poorly sorted subangular packstone packed biomicrite	7 inner ramp - restricted, open marine, mid-ramp 13 inner ramp - restricted, open marine	36	
LV 7/20	few foraminifera, some echinoderms abundant skeletal grains some micritic intraclasts burrows (?)	poorly sorted subangular wackestone-packstone sparse-packed biomicrite	3 mid-ramp, outer ramp 7 inner ramp - restricted, open marine, mid-ramp	37	
LV 7/25	abundant peloids abundant echinoderms some micritic intraclasts, burrows few skeletal grains	moderately sorted subrounded wacksetone sparse biomicrite	3 mid-ramp, outer ramp 4 outer ramp	38	
LV 7/29	abundant echinoderms some skeletal grains some micritic intraclasts abundant peloids	moderately sorted subrounded wacksetone sparse biomicrite	4 outer ramp 9 mid-ramp, outer ramp	39	
LV 7/34	abundant echinoderms abundant skeletal grains abundant peloids/skeletal grain debirs some micritic intraclasts, burrows (?)	poorly sorted angular wackestone-packstone sparse-packed biomicrite	8 mid-ramp 9 mid-ramp, outer ramp	40	
LV 8/2	abundant echinoderms abundant skeletal grains some peloids some micritic intraclasts, foraminifera (?)	poorly sorted subangular wackestone-packstone sparse-packed biomicrite	9 mid-ramp, outer ramp 7 inner ramp - restricted, open marine, mid-ramp	41	
LV 8/20	barely any matrix abundant echinoderms/debris	poorly sorted subangular grainstone unsorted biosparite	27 Inner ramp - mid-ramp shoal 10 mid-ramp, outer ramp	42	Valanginian
LV 8/36	abundant echinoderms abundant micritic intraclasts some large skeletal grains (with borings) some peloids	poorly sorted subangular floatstone packed biomicrite	28 Inner ramp - mid-ramp shoal 15 Inner ramp - open marine 9 mid-ramp, outer ramp	43	
LV 8/43	abundant carbonate debris few echinoderms abundant burrows	well sorted subrounded grainstone sorted biosparite	8 mid-ramp 9 mid-ramp, outer ramp	44	
LV 8/50	abundant echinoderms abundant carbonate debris some micritic intraclasts	well sorted angular packstone-grainstone packed biomicrite	7 inner ramp - restricted, open marine, mid-ramp 9 mid-ramp, outer ramp 14 inner ramp - open marine	45	
LV 8/59	dominated by echinoderms/debris abundant carbonate debris some micritic intraclasts	poorly sorted subangular grainstone unsorted biosparite	27 Inner ramp - mid-ramp shoal 10 mid-ramp, outer ramp	46	
LV 8/87	abundant echinoderms abundant carbonate debris some micritic intraclasts some skeletal grains	moderately sorted rounded packstone-grainstone poorly washed biosparite	9 mid-ramp, outer ramp 27 Inner ramp - mid-ramp shoal	47	

Sample	remarks/content	remarks	rmf-type		Stage
LV 8/91	abundant echinoderms/debris	moderately sorted	27 Inner ramp - mid-ramp shoal	48	Valanginian
	abundant carbonate debris/peloids	rounded	9 mid-ramp, outer ramp		
	some skeletal grains	packstone-grainstone			
	some micritic intraclasts	poorly washed biosparite			
LV 8/95	abundant echinoderms/debris	poorly sorted	26 Inner ramp - mid-ramp shoal	49	
	abundant carbonate debris	subangular	10 mid-ramp, outer ramp		
	abundant skeletal grains	packstone			
	some lithoclasts	packed biomicrite			
LV 8/103	abundant skeletal grains	poorly sorted	9 mid-ramp, outer ramp	50	
	abundant echinoderms/debris	subrounded	10 mid-ramp, outer ramp		
	few lithoclasts	packstone-grainstone			
	abundant carbonate debris, stromatoporid (?	unsorted biosparite			
LV 9/5	abundant skeletal grains	moderately sorted	26 Inner ramp - mid-ramp shoal	51	Hauterivian
	abundant echinoderms/debris	subrounded	27 Inner ramp - mid-ramp shoal		
	abundant carbonate debris	grainstone	14 inner ramp - open marine (no ooids!)		
	few lithoclasts, stromatoporid (?)	unsorted biosparite			
LV 9/16	abundant skeletal grains (same kind)	moderately sorted	26 Inner ramp - mid-ramp shoal	52	
	abundant echinoderms/debris	rounded	27 Inner ramp - mid-ramp shoal		
	abundant carbonate debris	grainstone	14 inner ramp - open marine (no ooids!)		
	few micritic intraclasts/multigrain-clasts	unsorted biosparite			
LV 9/24	abundant skeletal grains	well sorted	26 Inner ramp - mid-ramp shoal	53	
	abundant echinoderms/debris	rounded	27 Inner ramp - mid-ramp shoal		
	abundant carbonate debris	grainstone	14 inner ramp - open marine (no ooids!)		
	few micritic intraclasts/multigrain-clasts	sorted biosparite			
LV 9/32	abundant skeletal grains	moderately sorted	26 Inner ramp - mid-ramp shoal	54	
	abundant echinoderms/debris	subrounded	27 Inner ramp - mid-ramp shoal		
	abundant carbonate debris	grainstone	14 inner ramp - open marine (no ooids!)		
	few micritic intraclasts, stromatoporid (?)	unsorted biosparite			
LV 9/69	abundant peloids	moderately sorted	4 outer ramp	55	
	some foraminifera	rounded			
	some skeletal grains	wackestone			
	few echinoderms	packed biomicrite			
LV 9/79	abundant peloids/carbonate debris	moderately sorted	4 outer ramp	56	
	some foraminifera (?)	subrounded			
	some skeletal grains (very well preserved - t	wackestone			
	few echinoderms	sparse biomicrite			
LV 9/87	abundant peloids/carbonate debris	well sorted	4 outer ramp	57	
	some skeletal grains	rounded			
	some echinoderms	mud-wackestone			
	foraminifera (?)	sparse biomicrite			
LV 9/102	abundant peloids/carbonate debris	well sorted	4 outer ramp	58	
	some skeletal grains (foraminifera ?)	rounded			
	some echinoderms	mud-wackestone			
	some micritic intraclasts	sparse biomicrite			
LV 9/129	abundant peloids/carbonate debris	well sorted	2 mid-ramp, outer ramp, basin	59	
	some skeletal grains	rounded	4 outer ramp		
	some echinoderms	mud-wackestone			
	few micritic intraclasts, some burrows	fossiliferous micrite			
LV 9/143	abundant foraminfera	moderately sorted	5 mid-ramp, outer ramp, basin	60	
	abundant skeletal grains	subangular			
	some micritic intraclasts	wackestone			
		sparse biomicrite			
LV 9/149	laminated	well sorted	5 mid-ramp, outer ramp, basin	61	
	very few echinoderms	rounded			
	very few skeletal grains	mudstone			
	few carbonate debris	fossiliferous micrite			

Stable Isotope Analysis

LXXVIII–XC

C & O Isotope Analysis shell material	Identifier 1	Identifier 2	d13C Mean V-PDB	d18O Mean V-PDB	Age
	CM 15-18	Heidelberg	-0,31	-8,64	
	CM 16-22	Heidelberg	0,52	-10,20	
	CM 16-44	Heidelberg	-0,33	-5,49	
	CM 16-52	Heidelberg	-0,12	-10,01	Tithonian
	CM 16-54	Heidelberg	0,11	-10,08	
	CM 16-100	Heidelberg	-7,64	-6,47	
	CM 16-102	Heidelberg	-14,35	-6,33	
	CM 17-2	Heidelberg	-0,63	-8,31	
	CM 17-46	Heidelberg	-4,40	-7,84	
	CM 17-6	Heidelberg	-2,66	-8,22	
	CM 17-73	Heidelberg	-1,30	-7,99	
	CM 17-99	Heidelberg	0,26	-6,44	
	CM 17-102	Heidelberg	0,62	-6,03	
	CM 17-108	Heidelberg	0,45	-7,41	Berriasian
	CM 17-111	Heidelberg	0,30	-7,44	
	CM 18-1.5	Heidelberg	0,62	-7,90	
	CM 18-3	Heidelberg	1,96	-2,98	
	CM 18-17	Heidelberg	1,43	-6,93	
	CM 18-19	Heidelberg	-0,01	-7,12	
	CM 18-24	Heidelberg	0,06	-3,65	
	CM 18-32	Heidelberg	0,25	-4,16	
	CM 18-37	Heidelberg	-1,20	-4,53	
	CM 18-42	Heidelberg	-5,99	-2,68	
	CM 18-50	Heidelberg	-1,07	-6,07	
	CM 18-52	Heidelberg	-0,12	-5,27	
	CM 18-54	Heidelberg	-0,25	-5,59	
	CM 18-57	Heidelberg	0,22	-5,57	
	CM 18-60	Heidelberg	0,16	-4,93	
	CM 18-62	Heidelberg	1,60	-7,07	
	CM 18-67	Heidelberg	0,46	-6,17	
	CM 18-70	Heidelberg	-0,10	-6,35	Valanginian
	CM 19-1	Heidelberg	0,64	-2,83	
	CM 19-19	Heidelberg	-0,44	-6,36	
	CM 19-21	Heidelberg	1,08	-7,43	
	CM 19-24	Heidelberg	1,07	-7,44	
	CM 19-28	Heidelberg	-0,31	-5,23	
	CM 19-4	Heidelberg	0,31	-5,28	
	CM 20-0.1	Heidelberg	-0,86	-5,00	
	CM 20-12	Heidelberg	-1,91	-4,45	
	CM 20-22	Heidelberg	-1,13	-6,71	
	CM 20-26	Heidelberg	0,40	-8,07	
	CM 20-34	Heidelberg	-0,21	-7,82	
	CM 23-40	Heidelberg	1,03	-4,16	Hauterivian
	CM 23-66	Heidelberg	-1,71	-7,36	

C & O Isotope Analysis shell material	Identifier 1	Identifier 2	d13C Mean V-PDB	d18O Mean V-PDB	Age
	LV 3-6	Heidelberg	-0,28	-11,78	
	LV 3-6-c	Heidelberg	0,18	-11,74	
	LV 3-10	Heidelberg	-0,02	-14,10	
	LV 3-13	Heidelberg	-0,05	-10,14	
	LV 3-13-b	Heidelberg	0,40	-12,52	
	LV 3-15	Heidelberg	0,17	-12,73	
	LV 3-28	Heidelberg	-0,09	-12,81	
	LV 3-29	Heidelberg	0,42	-11,32	
	LV 3-40	Heidelberg	0,14	-10,51	
	LV 3-40-b	Heidelberg	-0,31	-12,23	
	LV 3-42	Heidelberg	0,00	-10,47	Tithonian
	LV 3-43	Heidelberg	-0,85	-6,39	
	LV 3-44	Heidelberg	0,41	-10,59	
	LV 3-44-b	Heidelberg	0,13	-11,68	
	LV 3-46	Heidelberg	-0,29	-9,75	
	LV 3-48	Heidelberg	0,18	-9,37	
	LV 3-48-b	Heidelberg	-0,33	0,42	
	LV 3-49	Heidelberg	-0,65	-8,07	
	LV 3-50	Heidelberg	-0,29	-7,17	
	LV 3-51	Heidelberg	-3,56	-7,29	
	LV 3-51-b	Heidelberg	-0,12	-10,93	
	LV 5-7	Heidelberg	-3,72	-10,83	
	LV 5-82	Heidelberg	1,28	-5,85	
	LV 5-89	Heidelberg	1,66	-8,95	
	LV 5-98	Heidelberg	0,70	-3,93	
	LV 6-1	Heidelberg	0,86	-8,33	
	LV 6-2	Heidelberg	0,26	-4,47	
	LV 6-16	Heidelberg	-0,27	-8,16	
	LV 6-20	Heidelberg	-0,42	-7,05	Berriasian
	LV 6-21	Heidelberg	-0,53	-7,95	
	LV 6-33	Heidelberg	0,13	-8,22	
	LV 6-41	Heidelberg	-1,50	-7,27	
	LV 6-53	Heidelberg	0,49	-3,39	
	LV 7-11	Heidelberg	-1,25	-7,62	
	LV 7-11-b	Heidelberg	-0,33	0,42	
	LV 7-12	Heidelberg	-4,42	-7,38	
	LV 7-26	Heidelberg	0,07	-8,18	
	LV 7-4	Heidelberg	-1,71	-4,67	
	LV 7-6	Heidelberg	-0,10	-7,59	
	LV 7-8	Heidelberg	-1,55	-7,67	Valanginian
	LV 8-2	Heidelberg	-0,44	-6,49	
	LV 8-3	Heidelberg	-0,54	-6,25	
	LV 8-36	Heidelberg	-0,10	-9,10	
	LV 9-16	Heidelberg	1,70	-6,68	Hauterivian
	LV 9-9	Heidelberg	1,89	-6,26	

Standards	C & O Isotope Analysis shell material			
10/17/15	Sol 2	Heidelberg	0,12	-5,81
10/16/15	Sol 2	Heidelberg	0,23	-5,80
10/16/15	Sol 2	Heidelberg	0,11	-5,92
10/17/15	Sol 2	Heidelberg	0,19	-5,70
10/15/15	Sol 2	Heidelberg	0,17	-5,76
10/14/15	Sol 2	Heidelberg	0,12	-5,71
10/14/15	Sol 2	Heidelberg	0,17	-5,73
10/14/15	Sol 2	Heidelberg	0,15	-5,86
10/14/15	Sol 2	Heidelberg	0,05	-5,86
10/14/15	Sol 2	Heidelberg	0,16	-5,72
10/13/15	Sol 2	Heidelberg	0,17	-5,80
10/13/15	Sol 2	Heidelberg	0,15	-5,89
10/13/15	Sol 2	Heidelberg	0,11	-5,77
10/14/15	Sol 2	Heidelberg	0,07	-5,74
10/17/15	Sol 2	Heidelberg	-0,02	-5,67
		mean	0,13	-5,78
		1 std.dev.	0,06	0,07
		spec	0,13	-5,78
10/16/15	Erl 5	Heidelberg	-49,10	-16,66
10/16/15	Erl 5	Heidelberg	-49,07	-16,79
10/17/15	Erl 5	Heidelberg	-49,28	-16,55
10/14/15	Erl 5	Heidelberg	-49,15	-16,61
10/14/15	Erl 5	Heidelberg	-49,22	-16,71
10/15/15	Erl 5	Heidelberg	-49,25	-16,69
10/13/15	Erl 5	Heidelberg	-49,19	-16,66
10/13/15	Erl 5	Heidelberg	-49,21	-16,75
10/13/15	Erl 5	Heidelberg	-49,14	-16,64
10/14/15	Erl 5	Heidelberg	-49,27	-16,63
10/17/15	Erl 5	Heidelberg	-49,20	-16,66
		mean	-49,19	-16,67
		1 std.dev.	0,07	0,06
		spec	-49,2	-16,67

C Isotope Analysis isolated organic matter	Identifier 1	Identifier 2	d13C permil V-PDB	Age
	CM 14-5	Brysch	-25,30	
	CM 15-6.5	Brysch	-27,09	Tithonian
	CM 15-8.4	Brysch	-27,68	
	CM 17-8	Brysch	-26,81	
	CM 17-14	Brysch	-27,80	
	CM 17-16	Brysch	-25,37	
	CM 17-19	Brysch	-26,75	
	CM 17-20	Brysch	-27,12	
	CM 17-23	Brysch	-28,20	
	CM 17-24	Brysch	-25,00	
	CM 17-25	Brysch	-26,66	
	CM 17-28	Brysch	-25,75	
	CM 17-34	Brysch	-26,32	
	CM 17-35.5	Brysch	-27,57	
	CM 17-38	Brysch	-26,21	
	CM 17-44	Brysch	-27,19	
	CM 17-46	Brysch	-27,15	
	CM 17-48	Brysch	-27,74	
	CM 17-49	Brysch	-25,79	
	CM 17-51	Brysch	-26,76	
	CM 17-54	Brysch	-25,81	
	CM 17-57	Brysch	-27,14	
	CM 17-58	Brysch	-26,52	
	CM 17-60	Brysch	-26,63	
	CM 17-62	Brysch	-27,12	
	CM 17-64	Brysch	-26,30	
	CM 17-65	Brysch	-27,02	
	CM 17-68	Brysch	-27,61	
	CM 17-71	Brysch	-27,38	Berriasian
	CM 17-73	Brysch	-26,57	
	CM 17-75	Brysch	-27,34	
	CM 17-77	Brysch	-24,99	
	CM 17-80	Brysch	-26,80	
	CM 17-81	Brysch	-25,44	
	CM 17-83	Brysch	-25,10	
	CM 17-86	Brysch	-25,27	
	CM 17-88	Brysch	-25,07	
	CM 17-91	Brysch	-26,15	
	CM 17-94	Brysch	-25,75	
	CM 17-97	Brysch	-25,82	
	CM 17-99	Brysch	-26,90	
	CM 17-102	Brysch	-26,28	
	CM 17-104	Brysch	-25,74	
	CM 17-108	Brysch	-26,29	
	CM 17-111	Brysch	-25,92	
	CM 17-114	Brysch	-24,54	
	CM 18-1.5	Brysch	-25,87	
	CM 18-09	Brysch	-25,34	
	CM 18-12	Brysch	-26,09	
	CM 18-15	Brysch	-25,79	
	CM 18-17	Brysch	-26,55	
	CM 18-19	Brysch	-25,78	
	CM 18-22	Brysch	-26,51	
	CM 18-24	Brysch	-25,86	

C Isotope Analysis isolated organic matter	Identifier 1	Identifier 2	d13C permil V-PDB	Age
	CM 18-30	Brysch	-26,98	
	CM 18-62	Brysch	-26,10	
	CM 18-67	Brysch	-25,37	
	CM 18-9	Brysch	-25,34	
	CM 19-1	Brysch	-25,49	
	CM 19-4	Brysch	-24,22	
	CM 20-8	Brysch	-27,26	Valanginian
	CM 20-16	Brysch	-27,85	
	CM 20-20	Brysch	-26,55	
	CM 20-30	Brysch	-27,96	
	CM 20-34	Brysch	-27,76	
	CM 21-1-8	Brysch	-28,55	
	CM 21-15	Brysch	-29,62	
	CM 21-15-29	Brysch	-28,07	
	CM 22-12	Brysch	-27,03	
	CM 22-70	Brysch	-26,20	
	CM 23-0.1	Brysch	-25,59	
	CM 23-4	Brysch	-26,38	
	CM 23-10	Brysch	-25,83	Hauterivian
	CM 23-18	Brysch	-26,30	
	CM 23-27	Brysch	-25,54	
	CM 23-34	Brysch	-26,63	
	CM 23-60	Brysch	-26,66	
	CM 23-69	Brysch	-27,82	

Standards	C Isotope Analysis isolated organic matter		
	urea	Brysch	-28,25
	urea	Brysch	-27,99
	urea	Brysch	-27,96
	urea	Brysch	-28,13
	urea	Brysch	-27,95
	urea	Brysch	-28,14
	urea	Brysch	-28,16
	urea	Brysch	-28,15
	urea	Brysch	-28,22
	urea	Brysch	-28,11
	urea	Brysch	-28,10
	urea	Brysch	-28,19
	urea	Brysch	-28,06
	urea	Brysch	-28,11
	urea	Brysch	-28,03
	urea	Brysch	-28,07
	urea	Brysch	-28,04
	urea	Brysch	-28,08
	urea	Brysch	-28,07
		avg	-28,09
		1 std.dev.	0,08
		spec	-28,10

C & O Isotope Analysis bulk rock CM section	Identifier 1	Identifier 2	d13C Mean V-PDB	d18O Mean V-PDB	Age
	CM 13-10.8	Brysch	1,26	-9,89	
	CM 13-18	Brysch	1,30	-8,68	
	CM 14-08	Brysch	0,02	-9,80	
	CM 14-08-3	Brysch	-0,17	-9,75	
	CM 14-13	Brysch	0,42	-9,72	
	CM 15-4	Brysch	-3,13	-9,31	
	CM 15-8.4	Brysch	-0,81	-10,06	
	CM 16-5	Brysch	0,48	-9,97	
	CM 16-7	Brysch	0,28	-9,74	
	CM 16-9	Brysch	0,65	-9,44	
	CM 16-11	Brysch	0,93	-9,07	
	CM 16-13	Brysch	0,48	-9,44	
	CM 16-16	Brysch	0,77	-9,40	
	CM 16-22	Brysch	0,98	-9,51	
	CM 16-24	Brysch	0,88	-9,20	
	CM 16-26	Brysch	0,81	-9,58	
	CM 16-28	Brysch	0,58	-9,82	
	CM 16-30	Brysch	0,67	-9,75	Tithonian
	CM 16-32	Brysch	0,41	-9,34	
	CM 16-36	Brysch	0,86	-9,76	
	CM 16-38	Brysch	0,78	-9,07	
	CM 16-44	Brysch	0,75	-9,11	
	CM 16-46	Brysch	0,50	-9,58	
	CM 16-48	Brysch	0,41	-9,28	
	CM 16-52	Brysch	0,41	-9,57	
	CM 16-54	Brysch	0,56	-9,53	
	CM 16-70	Brysch	0,52	-9,35	
	CM 16-74	Brysch	0,50	-9,32	
	CM 16-80	Brysch	0,01	-9,80	
	CM 16-86	Brysch	0,08	-9,23	
	CM 16-90	Brysch	0,18	-8,96	
	CM 16-96	Brysch	-0,13	-8,81	
	CM 16-98	Brysch	-0,32	-8,40	
	CM 16-100	Brysch	-0,57	-8,30	
	CM 16-102	Brysch	-0,70	-8,40	
	CM 17-0.15	Brysch	-2,09	-8,25	
	CM 17-1	Brysch	-2,73	-8,55	
	CM 17-2	Brysch	-1,48	-8,32	
	CM 17-4	Brysch	-1,39	-7,98	
	CM 17-5	Brysch	-0,97	-8,09	
	CM 17-7	Brysch	-1,44	-8,04	
	CM 17-8	Brysch	-1,96	-10,23	
	CM 17-14	Brysch	-1,46	-8,00	
	CM 17-15	Brysch	-1,79	-8,14	
	CM 17-16	Brysch	0,44	-5,64	
	CM 17-19	Brysch	-2,54	-8,20	
	CM 17-20	Brysch	-0,79	-8,30	
	CM 17-23	Brysch	-1,61	-8,60	
	CM 17-24	Brysch	-1,53	-8,30	
	CM 17-25	Brysch	-1,32	-8,38	Berriasian
	CM 17-28	Brysch	-2,77	-8,85	
	CM 17-30	Brysch	-2,95	-8,41	
	CM 17-34	Brysch	-1,20	-8,49	
	CM 17-35.5	Brysch	-2,06	-8,42	
	CM 17-38	Brysch	-0,80	-8,60	
	CM 17-40	Brysch	-2,80	-8,53	
	CM 17-42	Brysch	-1,14	-7,78	
	CM 17-44	Brysch	-1,34	-7,58	
	CM 17-46	Brysch	-1,82	-8,10	
	CM 17-48	Brysch	-3,32	-8,41	
	CM 17-49	Brysch	-0,89	-9,01	
	CM 17-51	Brysch	-3,06	-8,15	
	CM 17-54	Brysch	-0,54	-8,30	
	CM 17-57	Brysch	-1,44	-7,87	
	CM 17-58	Brysch	-0,51	-8,40	

C & O Isotope Analysis bulk rock CM section	Identifier 1	Identifier 2	d13C Mean V-PDB	d18O Mean V-PDB	Age
	CM 17-60	Brysch	-0,30	-7,98	
	CM 17-62	Brysch	-1,68	-7,86	
	CM 17-64	Brysch	-0,89	-8,19	
	CM 17-65	Brysch	-0,55	-9,04	
	CM 17-68	Brysch	-0,82	-8,02	
	CM 17-71	Brysch	-0,61	-7,84	
	CM 17-73	Brysch	-0,55	-8,38	
	CM 17-75	Brysch	-0,17	-8,16	
	CM 17-77	Brysch	0,43	-8,37	
	CM 17-80	Brysch	-0,09	-8,15	
	CM 17-81	Brysch	0,23	-8,47	
	CM 17-83	Brysch	0,39	-8,43	
	CM 17-86	Brysch	0,29	-8,57	
	CM 17-88	Brysch	-0,03	-8,12	
	CM 17-91	Brysch	0,36	-7,92	
	CM 17-94	Brysch	0,26	-8,53	
	CM 17-97	Brysch	0,18	-8,03	
	CM 17-99	Brysch	0,27	-7,05	Berriasian
	CM 17-102	Brysch	0,29	-7,86	
	CM 17-104	Brysch	0,42	-8,14	
	CM 17-106	Brysch	0,46	-7,78	
	CM 17-108	Brysch	0,34	-7,51	
	CM 17-111	Brysch	0,49	-7,50	
	CM 17-114	Brysch	0,10	-7,35	
	CM 18-1.5	Brysch	0,42	-7,37	
	CM 18-3	Brysch	0,52	-7,66	
	CM 18-7	Brysch	0,36	-7,06	
	CM 18-9	Brysch	0,20	-7,18	
	CM 18-12	Brysch	0,33	-7,27	
	CM 18-15	Brysch	0,20	-7,50	
	CM 18-17	Brysch	0,36	-7,38	
	CM 18-19	Brysch	-0,07	-7,27	
	CM 18-22	Brysch	-3,28	-7,23	
	CM 18-24	Brysch	-1,50	-7,20	
	CM 18-27	Brysch	-2,35	-7,15	
	CM 18-29	Brysch	-1,28	-7,05	
	CM 18-30	Brysch	-1,56	-7,03	
	CM 18-31	Brysch	-1,78	-6,97	
	CM 18-32	Brysch	-1,67	-7,15	
	CM 18-37	Brysch	-2,30	-7,18	
	CM 18-39	Brysch	-2,79	-6,94	
	CM 18-42	Brysch	-1,94	-6,96	
	CM 18-45	Brysch	-0,85	-7,21	
	CM 18-50	Brysch	-0,67	-7,00	
	CM 18-52	Brysch	0,06	-6,92	
	CM 18-54	Brysch	-0,08	-6,98	
	CM 18-60	Brysch	0,19	-7,02	
	CM 18-62	Brysch	0,40	-7,14	
	CM 18-67	Brysch	0,79	-7,44	
	CM 18-70	Brysch	0,08	-7,00	Valanginian
	CM 19-1	Brysch	-0,03	-6,43	
	CM 19-4	Brysch	-0,35	-6,96	
	CM 19-8	Brysch	0,23	-6,91	
	CM 19-10	Brysch	0,30	-6,98	
	CM 19-13	Brysch	0,28	-6,94	
	CM 19-17	Brysch	-0,20	-7,40	
	CM 19-19	Brysch	-0,37	-7,16	
	CM 19-21	Brysch	-0,22	-7,40	
	CM 19-24	Brysch	-0,50	-7,64	
	CM 19-28	Brysch	-0,31	-7,62	
	CM 20-0.1	Brysch	-1,15	-7,88	
	CM 20-8	Brysch	-2,01	-8,06	
	CM 20-12	Brysch	-1,43	-7,76	
	CM 20-16	Brysch	-3,00	-8,00	
	CM 20-18	Brysch	-2,57	-8,04	

C & O Isotope Analysis bulk rock CM section	Identifier 1	Identifier 2	d13C Mean V-PDB	d18O Mean V-PDB	Age
	CM 20-22	Brysch	-1,74	-7,71	
	CM 20-26	Brysch	-1,79	-7,95	
	CM 20-30	Brysch	-2,16	-8,14	
	CM 20-34	Brysch	-0,93	-7,55	Valanginian
	CM 21-1-8	Brysch	-0,98	-7,54	
	CM 21-8-15	Brysch	2,02	-4,86	
	CM 21-15-29	Brysch	-1,51	-7,48	
	CM 22-12	Brysch	1,44	-5,92	
	CM 22-15	Brysch	1,52	-5,71	
	CM 22-18	Brysch	1,71	-5,48	
	CM 22-21	Brysch	1,96	-5,06	
	CM 22-24	Brysch	2,07	-5,10	
	CM 22-44	Brysch	2,18	-4,81	
	CM 22-49	Brysch	1,91	-4,84	
	CM 22-52	Brysch	1,58	-5,24	
	CM 22-55	Brysch	2,16	-5,03	
	CM 22-59	Brysch	2,12	-4,94	
	CM 22-60	Brysch	1,57	-5,73	
	CM 22-64	Brysch	1,66	-5,77	
	CM 22-67	Brysch	1,42	-5,91	Hauterivian
	CM 22-70	Brysch	-0,32	-5,81	
	CM 23-0.1	Brysch	0,22	-5,71	
	CM 23-4	Brysch	-0,05	-6,01	
	CM 23-10	Brysch	0,15	-6,07	
	CM 23-15	Brysch	0,59	-5,81	
	CM 23-18	Brysch	0,07	-5,73	
	CM 23-27	Brysch	0,40	-5,80	
	CM 23-34	Brysch	0,80	-5,83	
	CM 23-40	Brysch	0,69	-5,38	
	CM 23-46	Brysch	0,79	-5,77	
	CM 23-60	Brysch	0,09	-5,74	
	CM 23-66	Brysch	0,34	-5,93	
	CM 23-69	Brysch	0,35	-6,09	

Standards	C & O Isotope Analysis bulk rock CM section			
	Erl 5	Brysch	-49,07	-16,73
	Erl 5	Brysch	-49,27	-16,72
	Erl 5	Brysch	-49,20	-16,60
	Erl 5	Brysch	-49,24	-16,64
	Erl 5	Brysch	-49,22	-16,70
	Erl 5	Brysch	-49,18	-16,69
	Erl 5	Brysch	-49,20	-16,63
	Erl 5	Brysch	-49,04	-16,68
	Erl 5	Brysch	-49,29	-16,70
	Erl 5	Brysch	-49,20	-16,67
	Erl 5	Brysch	-49,28	-16,61
	Erl 5	Brysch	-49,09	-16,70
	Erl 5	Brysch	-49,20	-16,71
	Erl 5	Brysch	-49,28	-16,59
	Erl 5	Brysch	-49,18	-16,72
	Erl 5	Brysch	-49,20	-16,68
	Erl 5	Brysch	-49,23	-16,61
	Erl 5	Brysch	-49,25	-16,68
		mean	-49,20	-16,67
		1 std.dev.	0,07	0,04
		spec	-49,20	-16,67
	Sol 2	Brysch	0,16	-5,69
	Sol 2	Brysch	0,15	-5,72
	Sol 2	Brysch	0,11	-5,81
	Sol 2	Brysch	0,11	-5,84
	Sol 2	Brysch	0,14	-5,75
	Sol 2	Brysch	0,18	-5,79
	Sol 2	Brysch	0,16	-5,81
	Sol 2	Brysch	0,10	-5,77
	Sol 2	Brysch	0,15	-5,76
	Sol 2	Brysch	0,15	-5,78
	Sol 2	Brysch	0,21	-5,70
	Sol 2	Brysch	0,15	-5,80
	Sol 2	Brysch	0,12	-5,74
	Sol 2	Brysch	0,08	-5,88
	Sol 2	Brysch	0,11	-5,79
	Sol 2	Brysch	0,18	-5,72
	Sol 2	Brysch	0,16	-5,74
	Sol 2	Brysch	0,16	-5,72
	Sol 2	Brysch	0,09	-5,86
	Sol 2	Brysch	0,19	-5,75
	Sol 2	Brysch	0,11	-5,72
	Sol 2	Brysch	0,11	-5,83
	Sol 2	Brysch	0,08	-5,82
	Sol 2	Brysch	0,17	-5,79
	Sol 2	Brysch	0,05	-5,87
		mean	0,13	-5,78
		1 std.dev.	0,04	0,05
		spec	0,13	-5,78

C & O Isotope Analysis bulk rock LV section	Identifier 1	Identifier 2	d13C Mean V-PDB	d18O Mean V-PDB	Age
	LV 3-0.2	Brysch	0,34	-13,24	
	LV 3-1-30	Brysch	0,29	-10,85	
	LV 3-3	Brysch	-0,13	-11,39	
	LV 3-6	Brysch	-0,09	-12,65	
	LV 3-10	Brysch	-2,36	-14,55	
	LV 3-15	Brysch	0,35	-13,11	
	LV 3-17	Brysch	-0,06	-12,54	
	LV 3-19	Brysch	-0,03	-12,62	
	LV 3-21	Brysch	0,67	-12,16	
	LV 3-23	Brysch	-0,59	-12,40	
	LV 3-26	Brysch	-0,54	-11,74	
	LV 3-28	Brysch	-0,12	-11,92	
	LV 3-31	Brysch	-0,54	-12,39	
	LV 3-33	Brysch	-0,36	-12,69	Tithonian
	LV 3-35	Brysch	-0,15	-12,62	
	LV 3-37	Brysch	-0,01	-12,54	
	LV 3-40	Brysch	0,24	-12,13	
	LV 3-42	Brysch	0,09	-11,69	
	LV 3-44	Brysch	-0,16	-11,15	
	LV 3-46	Brysch	0,06	-11,04	
	LV 3-48	Brysch	-0,23	-11,19	
	LV 3-50	Brysch	0,07	-10,65	
	LV 3-52	Brysch	-0,73	-10,73	
	LV 3-53	Brysch	-0,42	-10,86	
	LV 3-55	Brysch	-0,21	-12,63	
	LV 3-56.5	Brysch	-1,49	-10,09	
	LV 3-58	Brysch	0,51	-10,50	
	LV 3-63	Brysch	0,40	-11,16	
	LV 4-6	Brysch	-6,44	-13,98	
	LV 5-1	Brysch	-4,40	-14,14	
	LV 5-3	Brysch	-3,44	-11,26	
	LV 5-5	Brysch	-3,76	-12,59	
	LV 5-7	Brysch	-3,19	-11,05	
	LV 5-12	Brysch	-2,96	-10,77	
	LV 5-14	Brysch	-3,72	-9,45	
	LV 5-15	Brysch	-3,47	-10,99	
	LV 5-17	Brysch	-4,16	-10,72	
	LV 5-19	Brysch	-2,73	-10,78	
	LV 5-20	Brysch	-2,88	-10,83	
	LV 5-22	Brysch	-3,18	-10,70	
	LV 5-24	Brysch	-2,42	-10,57	
	LV 5-26	Brysch	-1,75	-10,73	
	LV 5-28	Brysch	-6,45	-10,33	
	LV 5-29	Brysch	-0,10	-9,66	
	LV 5-30	Brysch	-2,35	-9,62	Berriasian
	LV 5-32	Brysch	-1,72	-10,39	
	LV 5-35	Brysch	-1,61	-10,17	
	LV 5-37	Brysch	-2,01	-9,60	
	LV 5-39	Brysch	-1,80	-9,54	
	LV 5-40	Brysch	-2,48	-9,70	
	LV 5-41	Brysch	-1,99	-10,24	
	LV 5-43	Brysch	-4,37	-9,62	
	LV 5-44	Brysch	-1,36	-10,94	
	LV 5-45	Brysch	-1,54	-9,95	
	LV 5-47	Brysch	-1,45	-10,01	
	LV 5-50	Brysch	-1,43	-9,67	
	LV 5-51	Brysch	-1,62	-9,56	
	LV 5-55	Brysch	-1,88	-9,60	
	LV 5-58	Brysch	-0,34	-9,64	
	LV 5-60	Brysch	-0,60	-9,67	
	LV 5-62	Brysch	1,84	-11,25	

C & O Isotope Analysis bulk rock LV section	Identifier 1	Identifier 2	d13C Mean V-PDB	d18O Mean V-PDB	Age
	LV 5-63	Brysch	-1,44	-10,27	
	LV 5-64	Brysch	-0,94	-9,38	
	LV 5-67	Brysch	-0,53	-10,11	
	LV 5-68	Brysch	-0,49	-8,72	
	LV 5-69	Brysch	-0,53	-9,36	
	LV 5-71	Brysch	-0,73	-9,29	
	LV 5-73	Brysch	-0,87	-9,49	
	LV 5-74	Brysch	-0,53	-9,25	
	LV 5-75	Brysch	-0,48	-9,45	
	LV 5-76	Brysch	-0,03	-9,24	
	LV 5-77	Brysch	-1,22	-8,67	
	LV 5-80	Brysch	-0,66	-8,70	
	LV 5-84	Brysch	-0,26	-9,35	
	LV 5-86	Brysch	-0,30	-9,06	
	LV 5-88	Brysch	0,10	-9,14	
	LV 5-89	Brysch	0,00	-9,71	
	LV 5-90	Brysch	-0,03	-9,01	
	LV 5-92	Brysch	0,01	-8,96	Berriasian
	LV 5-94	Brysch	0,14	-8,93	
	LV 5-97	Brysch	0,34	-8,42	
	LV 6-4	Brysch	-0,52	-8,50	
	LV 6-10	Brysch	-0,04	-8,34	
	LV 6-15	Brysch	-0,85	-8,13	
	LV 6-20	Brysch	-0,84	-7,59	
	LV 6-25	Brysch	-0,27	-8,23	
	LV 6-29	Brysch	-0,10	-8,14	
	LV 6-34	Brysch	-0,42	-7,91	
	LV 6-45	Brysch	-0,21	-8,79	
	LV 6-50	Brysch	0,23	-8,14	
	LV 6-55	Brysch	-0,06	-7,89	
	LV 6-65	Brysch	-0,10	-7,83	
	LV 7-3	Brysch	-2,06	-7,67	
	LV 7-16	Brysch	-0,79	-7,92	
	LV 7-25	Brysch	-1,18	-7,97	
	LV 7-28	Brysch	-1,19	-8,11	
	LV 7-34	Brysch	-1,28	-8,12	
	LV 8-20-36	Brysch	-1,30	-7,67	
	LV 8-36	Brysch	-1,50	-8,71	
	LV 8-41	Brysch	-1,47	-7,14	
	LV 8-46	Brysch	-1,11	-7,46	
	LV 8-54	Brysch	-0,85	-6,94	Valanginian
	LV 8-59	Brysch	-0,76	-6,50	
	LV 8-83	Brysch	1,10	-7,12	
	LV 8-87	Brysch	0,94	-7,36	
	LV 8-91	Brysch	0,74	-7,50	
	LV 8-99	Brysch	0,51	-5,92	
	LV 8-103	Brysch	0,93	-7,20	
	LV 9-5	Brysch	1,65	-7,13	
	LV 9-12	Brysch	1,70	-6,98	
	LV 9-20	Brysch	1,85	-6,54	
	LV 9-24	Brysch	2,12	-5,86	
	LV 9-32	Brysch	2,29	-5,57	
	LV 9-69	Brysch	0,24	-6,03	
	LV 9-71	Brysch	0,34	-6,12	Hauterivian
	LV 9-87	Brysch	0,29	-8,51	
	LV 9-102	Brysch	-0,12	-6,38	
	LV 9-115	Brysch	0,37	-6,57	
	LV 9-129	Brysch	0,42	-6,49	
	LV 9-143	Brysch	0,29	-7,20	

Standards	C & O Isotope Analysis bulk rock LV section			
	Sol 2	Brysch	0,21	-5,72
	Sol 2	Brysch	0,15	-5,73
	Sol 2	Brysch	0,08	-5,84
	Sol 2	Brysch	0,06	-5,90
	Sol 2	Brysch	0,19	-5,71
	Sol 2	Brysch	0,12	-5,85
	Sol 2	Brysch	0,12	-5,76
	Sol 2	Brysch	0,10	-5,80
	Sol 2	Brysch	0,12	-5,68
	Sol 2	Brysch	0,13	-5,83
	Sol 2	Brysch	0,10	-5,83
	Sol 2	Brysch	0,19	-5,75
	Sol 2	Brysch	0,08	-5,83
	Sol 2	Brysch	0,18	-5,71
	Sol 2	Brysch	0,10	-5,78
	Sol 2	Brysch	0,10	-5,80
	Sol 2	Brysch	0,11	-5,79
	Sol 2	Brysch	0,19	-5,80
	Sol 2	Brysch	0,13	-5,71
	Sol 2	Brysch	0,12	-5,80
	Sol 2	Brysch	0,16	-5,76
	Sol 2	Brysch	0,08	-5,84
	Sol 2	Brysch	0,18	-5,77
	Sol 2	Brysch	0,12	-5,70
		avg	0,13	-5,78
		1 std.dev.	0,04	0,06
		spec	0,13	-5,78
	Erl-5	Brysch	-49,26	-16,75
	Erl-5	Brysch	-49,23	-16,68
	Erl-5	Brysch	-49,15	-16,69
	Erl-5	Brysch	-49,23	-16,71
	Erl-5	Brysch	-49,20	-16,61
	Erl-5	Brysch	-49,22	-16,71
	Erl-5	Brysch	-49,19	-16,64
	Erl-5	Brysch	-49,24	-16,69
	Erl-5	Brysch	-49,17	-16,62
	Erl-5	Brysch	-49,08	-16,61
	Erl-5	Brysch	-49,23	-16,67
	Erl-5	Brysch	-49,25	-16,69
	Erl-5	Brysch	-49,24	-16,69
	Erl-5	Brysch	-49,13	-16,68
	Erl-5	Brysch	-49,24	-16,72
	Erl-5	Brysch	-49,18	-16,66
	Erl-5	Brysch	-49,23	-16,63
	Erl-5	Brysch	-49,09	-16,59
		avg	-49,20	-16,67
		1 std.dev.	0,05	0,04
		spec	-49,2	-16,67

TOC/TIC, Carbon/Nitrogen/Sulphur
XCI–XCVII

TOC/TIC CM section	Nr.	Sample	N [%]		C_{total} [%]		S [%]		C_{org} [%]		TIC [%]		$CaCO_3$ [%]		Corg/N	
	140	CM 23/69	0,027	0,010	8,72	10,26	0,011	0,03	0,41	0,37	8,31	9,89	69,20	82,36	15	37,58
	139	CM 23/66	0,004	0,011	10,90	1,27	0,022	0,01	0,17	0,21	10,73	1,38	89,40	11,51	40	62,05
	138	CM 23/60	0,019		8,00		0,040		0,44		7,56		62,97		23	
	137	CM 23/46	0,016		9,25		0,026		0,32		8,93		74,36		20	
	136	CM 23/40	0,004		10,87		0,023		0,29		10,58		88,17		69	
	135	CM 23/34	0,031		8,48		0,035		0,56		7,92		65,95		18	
	134	CM 23/27	0,022		8,10		0,047		0,50		7,60		63,33		23	
	133	CM 23/18	0,004		8,85		0,021		0,28		8,57		71,43		62	
	132	CM 23/15	0,019		8,88		0,025		0,38		8,50		70,79		21	
	131	CM 23/10	0,005		10,84		0,026		0,40		10,44		86,96		82	
	130	CM 23/4	0,033		7,80		0,057		0,94		6,86		57,16		29	
	129	CM 23/0.1	0,033		10,38		0,052		0,98		9,40		78,31		29	
Hauterivian	128	CM 22/70	0,005		11,13		0,032		0,29		10,84		90,31		58	
	127	CM 22/67	0,003		10,81		0,027		0,27		10,54		87,80		81	
	126	CM 22/64	0,003		10,43		0,013		0,36		10,07		83,85		114	
	125	CM 22/60	0,002		11,23		0,016		0,47		10,76		89,61		224	
	124	CM 22/59	0,002		11,65		0,009		0,41		11,24		93,62		190	
	123	CM 22/55	0,002		11,51		0,015		0,31		11,21		93,35		138	
	122	CM 22/52	0,002		11,09		0,021		0,19		10,90		90,78		99	
	121	CM 22/49	0,002		11,49		0,031		0,38		11,11		92,51		222	
	120	CM 22/44	0,002		11,65		0,015		0,07		11,58		96,47		45	
	119	CM 22/24	0,003		11,33		0,010		0,24		11,09		92,42		93	
	118	CM 22/21	0,002		11,18		0,016		0,16		11,02		91,79		87	
	117	CM 22/18	0,002		11,19		0,022		0,19		11,01		91,68		88	
	116	CM 22/15	0,003		10,73		0,036		0,43		10,30		85,77		166	
	115	CM 22/12	0,003		10,20		0,033		0,18		10,02		83,46		67	
	114	CM 21/15-29	0,011	0,006	5,01	7,66	0,187	0,10	0,40	0,29	4,61	7,37	38,38	61,43	38	72,77
	113	CM 21/15	0,008	0,007	9,39	2,02	0,044	0,27	0,31	0,17	9,08	2,03	75,64	16,88	40	61,98
	112	CM 21/8-15	0,003		11,21		0,027		0,06		11,15		92,89		19	
	111	CM 21/1-8	0,002		9,13		0,036		0,19		8,94		74,46		86	
	110	CM 20/34	0,002		8,71		0,136		0,29		8,42		70,14		131	
	109	CM 20/30	0,036		1,86		1,652		0,50		1,36		11,31		14	
	108	CM 20/26	0,005		6,08		0,032		0,21		5,87		48,90		43	
	107	CM 20/22	0,004		6,78		0,040		0,20		6,58		54,81		48	
	106	CM 20/18	0,005		3,24		0,119		0,25		3,00		24,96		53	
	105	CM 20/16	0,032		3,41		0,498		0,35		3,06		25,45		11	
	104	CM 20/12	0,003		7,75		0,166		0,15		7,59		63,27		48	
	103	CM 20/8	0,014		3,62		0,278		0,24		3,38		28,19		17	
	102	CM 20/0.1	0,004		9,04		0,025		0,14		8,90		74,14		35	
	101	CM 19/28	0,003		7,83		0,025		0,15		7,68		63,99		45	
	100	CM 19/24	0,004		8,19		0,020		0,14		8,05		67,08		37	
	99	CM 19/21	0,003		8,00		0,038		0,18		7,82		65,13		56	
	98	CM 19/19	0,003		7,96		0,040		0,17		7,79		64,87		65	
	97	CM 19/17	0,008		6,90		0,041		0,15		6,75		56,24		19	
	96	CM 19/13	0,005		7,02		0,011		0,16		6,87		57,19		30	
Valanginian	95	CM 19/10	0,003		8,86		0,010		0,47		8,39		69,89		141	
	94	CM 19/8	0,004		8,55		0,020		0,19		8,36		69,62		50	
	93	CM 19/4	0,003		9,29		0,032		0,47		8,82		73,47		155	
	92	CM 19/1	0,005		9,31		0,038		0,58		8,73		72,74		126	
	91	CM 18/70	0,003		10,07		0,013		0,32		9,75		81,19		102	
	90	CM 18/67	0,003		9,63		0,023		0,54		9,09		75,69		170	
	89	CM 18/62	0,003		9,11		0,034		0,91		8,20		68,30		319	
	88	CM 18/60	0,003		8,16		0,030		0,13		8,03		66,87		42	
	87	CM 18/57	0,004		8,26		0,010		0,22		8,04		66,97		54	
	86	CM 18/54	0,002		9,95		0,011		0,20		9,74		81,16		82	
	85	CM 18/52	0,003		9,23		0,011		0,58		8,64		71,99		219	
	84	CM 18/50	0,004		7,12		0,014		0,18		6,94		57,79		42	
	83	CM 18/45	0,004		7,92		0,037		0,40		7,52		62,60		105	
	82	CM 18/42	0,004		8,30		0,067		0,35		7,95		66,22		90	
	81	CM 18/39	0,004		7,13		0,097		0,21		6,91		57,60		57	
	80	CM 18/37	0,003		7,81		0,048		0,21		7,60		63,27		77	
	79	CM 18/32	0,018		6,06		0,041		0,34		5,72		47,64		19	
	78	CM 18/30	0,004		6,49		0,024		0,20		6,29		52,40		45	
	77	CM 18/29	0,006		7,22		0,016		0,24		6,98		58,16		43	
	76	CM 18/27	0,003		9,21		0,028		0,18		9,03		75,19		65	
	75	CM 18/24	0,004	0,058	8,79	8,78	0,045	0,04	0,30	1,30	8,49	7,48	70,72	62,31	77	41,94
	74	CM 18/22	0,004	0,042	8,64	1,34	0,035	0,02	0,37	0,77	8,27	1,43	68,87	11,88	99	61,79
	73	CM 18/19	0,006		9,58		0,024		0,72		8,87		73,87		110	
	72	CM 18/17	0,008		8,96		0,019		0,49		8,47		70,52		63	
	71	CM 18/15	0,018		8,62		0,022		0,89		7,73		64,36		51	
	70	CM 18/12	0,017		8,35		0,023		0,59		7,76		64,63		35	
	69	CM 18/9	0,006		9,42		0,023		0,86		8,56		71,32		136	
	68	CM 18/7	0,004		8,98		0,028		0,30		8,68		72,26		77	
	67	CM 18/3	0,003		10,41		0,022		0,26		10,15		84,57		83	
	66	CM 18/1.5	0,003		10,68		0,033		1,12		9,56		79,66		439	
	65	CM 17/114	0,020		6,72		0,109		0,68		6,05		50,36		33	
	64	CM 17/111	0,020		8,22		0,042		0,60		7,62		63,50		31	
Berriasian	63	CM 17/108	0,041		8,01		0,057		0,80		7,21		60,04		19	
	62	CM 17/106	0,058		8,81		0,038		1,25		7,56		62,94		22	
	61	CM 17/104	0,072		9,64		0,032		1,59		8,05		67,06		22	
	60	CM 17/102	0,059		9,15		0,043		1,43		7,72		64,30		24	
	59	CM 17/99	0,014		9,44		0,030		0,54		8,90		74,16		38	
	58	CM 17/97	0,132		8,83		0,030		2,57		6,26		52,13		20	
	57	CM 17/94	0,125		9,22		0,021		1,80		7,42		61,81		14	
	56	CM 17/91	0,078		9,48		0,028		2,16		7,32		60,98		28	
	55	CM 17/88	0,102		10,26		0,026		2,21		8,05		67,05		22	
	54	CM 17/86	0,160		10,01		0,032		4,40		5,61		46,70		27	
	53	CM 17/83	0,147		8,87		0,025		2,75		6,12		51,02		19	
	52	CM 17/81	0,126		8,26		0,023		1,69		6,56		54,67		13	
	51	CM 17/80	0,027		8,95		0,041		1,09		7,86		65,50		40	
	50	CM 17/77	0,035		10,97		0,037		1,86		9,11		75,90		53	

TOC/TIC CM section	Nr.	Sample	N [%]		C_{total} [%]		S [%]		C_{org} [%]		TIC [%]		$CaCO_3$ [%]		Corg/N	
	49	CM 17/75	0,112		9,47		0,055		2,16		7,31		60,92		19	
	48	CM 17/73	0,110		9,60		0,023		2,07		7,53		62,73		19	
	47	CM 17/71	0,09		9,37		0,044		1,88		7,49		62,38		22	
	46	CM 17/65	0,087		7,63		0,036		1,67		5,96		49,67		19	
	45	CM 17/64	0,105		6,45		0,036		0,93		5,52		46,02		9	
	44	CM 17/58	0,111		7,93		0,062		1,27		6,67		55,55		11	
	43	CM 17/57	0,055		10,67		0,039		1,57		9,10		75,81		28	
	42	CM 17/54	0,107		8,55		0,018		1,99		6,56		54,67		19	
	41	CM 17/51	0,056		8,90		0,024		0,78		8,12		67,64		14	
	40	CM 17/49	0,107		6,61		0,020		1,24		5,38		44,80		12	
	39	CM 17/46	0,057		9,12		0,021		0,92		8,20		68,31		16	
	38	CM 17/44	0,079		8,36		0,017		0,92		7,45		62,04		12	
	37	CM 17/42	0,082		7,94		0,024		0,77		7,16		59,68		9	
	36	CM 17/40	0,068		6,65		0,013		0,84		5,81		48,42		12	
Berriasian	35	CM 17/38	0,053		11,88		0,022		1,38		10,51		87,51		26	
	34	CM 17/35.5	0,079		5,24		0,024		0,87		4,38		36,46		11	
	33	CM 17/34	0,052		10,93		0,025		1,24		9,69		80,73		24	
	32	CM 17/25	0,067		6,19		0,035		1,19		5,00		41,64		18	
	31	CM 17/23	0,025		9,83		0,033		0,63		9,20		76,62		25	
	30	CM 17/19	0,054		10,54		0,028		0,41		10,13		84,39		8	
	29	CM 17/16	0,049		8,25		0,030		2,04		6,20		51,68		42	
	28	CM 17/8	0,019		7,36		0,061		2,31		5,05		42,03		121	
	27	CM 17/7	0,072		8,07		0,056		1,50		6,57		54,71		21	
	26	CM17/6	0,063		8,76		0,045		2,10		6,66		55,46		33	
	25	CM 17/5	0,037		9,91		0,047		1,78		8,13		67,76		48	
	24	CM 17/4	0,042		9,80		0,033		0,70		9,10		75,84		17	
	23	CM 17/2	0,043		7,40		0,100		1,34		6,07		50,52		31	
	22	CM 17/1	0,032		7,32		0,089		1,45		5,87		48,86		45	
	21	CM 17/0.15	0,015		6,98		0,029		0,33		6,65		55,43		22	
	20	CM 16/102	0,011	0,011	5,68	5,65	0,029	0,033	0,34	0,26	5,34	5,40	44,47	44,95	30	28,25
	19	CM 16/100	0,009	0,005	6,55	1,55	0,027	0,033	0,26	0,19	6,29	1,44	52,43	11,97	30	32,73
	18	CM 16/96	0,010		5,53		0,027		0,16		5,37		44,73		16	
	17	CM 16/86	0,013		6,23		0,016		0,37		5,86		48,81		28	
	16	CM 16/80	0,019		3,25		0,014		0,18		3,07		25,59		10	
	15	CM 16/74	0,006		8,36		0,017		0,82		7,54		62,85		148	
	14	CM 16/70	0,010		5,63		0,011		0,26		5,37		44,72		27	
	13	CM 16/48	0,007		5,45		0,013		0,11		5,34		44,47		15	
	12	CM 16/44	0,008		4,88		0,019		0,17		4,71		39,20		20	
Tithonian	11	CM 16/32	0,009		4,94		0,022		0,11		4,83		40,25		11	
	10	CM 16/28	0,019		2,84		0,007		0,07		2,77		23,06		4	
	9	CM 16/26	0,014		5,34		0,011		0,12		5,22		43,51		8	
	8	CM 16/25	0,007		5,16		0,013		0,17		4,99		41,59		23	
	7	CM 16/22	0,011		6,87		0,017		0,19		6,68		55,68		18	
	6	CM 16/13	0,014		5,13		0,017		0,10		5,03		41,92		7	
	5	CM 16/9	0,006		6,07		0,027		0,19		5,87		48,93		35	
	4	CM 16/5	0,010		6,17		0,059		0,14		6,02		50,19		14	
	3	CM 15/8.4	0,019		3,64		0,109		0,50		3,15		26,20		26	
	2	CM 15/4	0,019		5,69		0,116		0,22		5,48		45,61		12	
	1	CM 14/13	0,008		9,62		0,088		0,64		8,97		74,76		83	

TOC/TIC LV section	Nr.	Sample	N [%]		C_{total} [%]		S [%]		C_{org} [%]		TIC [%]		$CaCO_3$ [%]		Corg/N	
	76	LV9/143	0,010	0,021	11,12	9,08	0,01	0,08	0,53	0,65	10,6	8,43	88,1	70,20	56	36,59
Hauterivian	75	LV9/102	0,011	0,012	8,27	1,36	0,05	0,07	0,44	0,24	7,8	1,44	65,2	12,02	39	14,94
	74	LV9/87	0,033		8,50		0,18		1,00		7,5		62,5		30	
	73	LV9/71	0,030		8,43		0,09		0,64		7,8		64,9		21	
	72	LV8/87	0,023	0,01	10,17	8,62	0,01	0,02	0,14	0,21	10,0	8,41	83,6	70,04	6	50,16
Valanginian	71	LV8/46	0,004	0,01	7,43	1,41	0,01	0,01	0,24	0,06	7,2	1,47	59,9	12,22	54	42,23
	70	LV7/28	0,003		8,25		0,03		0,25		8,0		66,6		90	
	69	LV7/16	0,004	0,08	8,52	7,53	0,03	0,76	0,19	1,87	8,3	5,66	69,4	47,16	53	35,18
	68	LV7/3	0,024	0,09	7,95	2,27	0,06	1,10	0,75	0,97	7,2	2,22	59,9	18,49	31	19,38
	67	LV6/65	0,011		10,57		0,07		0,89		9,7		80,7		79	
	66	LV6/55	0,014		8,66		0,12		0,66		8,0		66,6		46	
	65	LV6/50	0,030		9,48		0,42		1,37		8,1		67,5		45	
	64	LV6/45	0,024		8,00		0,03		0,57		7,4		61,9		24	
	63	LV6/34	0,020		7,90		0,42		0,91		7,0		58,2		45	
	62	LV6/29	0,032		6,78		0,94		1,46		5,3		44,3		46	
	61	LV6/25	0,067		3,35		0,55		1,41		1,9		16,2		21	
	60	LV6/20	0,008		7,88		0,06		0,48		7,4		61,7		57	
	59	LV6/15	0,041		5,81		0,29		0,88		4,9		41,0		22	
	58	LV6/10	0,039		7,97		0,18		0,81		7,2		59,6		21	
	57	LV6/4	0,036		8,11		0,23		1,25		6,9		57,1		35	
	56	LV5/94	0,038		7,07		0,07		0,78		6,3		52,4		21	
	55	LV5/92	0,105		8,92		0,24		1,89		7,0		58,6		18	
	54	LV5/90	0,102		9,00		0,48		1,92		7,1		59,0		19	
	53	LV5/88	0,116		7,90		1,15		1,96		5,9		49,4		17	
	52	LV5/86	0,108		9,17		0,21		2,95		6,2		51,8		27	
	51	LV5/84	0,110		9,40		0,10		2,65		6,7		56,2		24	
	50	LV5/83	0,103		8,35		0,15		2,10		6,2		52,0		21	
	49	LV5/80	0,082		8,78		0,51		2,47		6,3		52,6		30	
	48	LV5/77	0,047		8,74		0,65		1,60		7,1		59,4		34	
	47	LV5/76	0,025		11,31		0,29		1,46		9,9		82,1		59	
	46	LV5/75	0,099		7,31		0,86		2,50		4,8		40,0		25	
	45	LV5/74	0,108		8,45		2,32		4,39		4,1		33,8		41	
	44	LV5/73	0,091		7,71		0,61		1,53		6,2		51,5		17	
	43	LV5/71	0,103		5,97		1,30		1,34		4,6		38,6		13	
	42	LV5/69	0,063		8,66		0,25		1,17		7,5		62,3		19	
	41	LV5/68	0,051		7,67		0,34		1,11		6,6		54,6		21	
	40	LV5/67	0,158		7,34		0,14		2,35		5,0		41,5		15	
	39	LV5/64	0,119		9,61		0,48		3,51		6,1		50,8		29	
	38	LV5/63	0,091		9,16		0,24		2,60		6,6		54,7		29	
Berriaisan	37	LV5/62	0,122		3,15		7,97		2,20		1,0		8,0		18	
	36	LV5/60	0,114		10,12		0,25		3,35		6,8		56,4		29	
	35	LV5/58	0,771		11,59		0,25		4,70		6,9		57,5		6	
	34	LV5/55	0,075		9,30		0,10		0,99		8,3		69,2		13	
	33	LV5/54	0,135		1,47		0,06		1,10		0,4		3,1		8	
	32	LV5/51	0,064		5,41		2,41		2,29		3,1		26,1		36	
	31	LV5/50	0,070		7,79		0,91		2,00		5,8		48,3		28	
	30	LV5/47	0,087		6,71		0,97		2,18		4,5		37,8		25	
	29	LV5/45	0,106		8,70		0,61		3,10		5,6		46,6		29	
	28	LV5/44	0,100		4,65		1,75		2,37		2,3		19,0		24	
	27	LV5/43	0,040		8,87		0,29		1,89		7,0		58,1		48	
	26	LV5/41	0,080		5,45		2,31		3,58		1,9		15,6		45	
	25	LV5/40	0,066		8,52		1,08		2,40		6,1		50,9		36	
	24	LV5/39	0,053		9,17		0,99		2,45		6,7		56,0		46	
	23	LV5/37	0,038		7,94		0,82		2,00		5,9		49,5		52	
	22	LV5/35	0,120		8,45		1,00		2,05		6,4		53,4		17	
	21	LV5/32	0,063		8,62		0,39		1,99		6,6		55,2		32	
	20	LV5/30	0,068		7,76		2,04		2,45		5,3		44,2		36	
	19	LV5/28	0,018		10,73		0,17		1,17		9,6		79,6		66	
	18	LV5/26	0,072		8,32		0,78		2,37		6,0		49,6		33	
	17	LV5/24	0,052		9,36		0,79		1,83		7,5		62,7		36	
	16	LV5/22	0,071		7,20		1,20		2,11		5,1		42,4		30	
	15	LV5/20	0,089		7,02		1,69		2,74		4,3		35,6		31	
	14	LV5/19	0,085		7,16		1,10		2,82		4,3		36,1		33	
	13	LV5/17	0,053		6,55		1,45		2,12		4,4		36,9		40	
	12	LV5/15	0,093		7,06		1,98		4,03		3,0		25,3		43	
	11	LV5/14	0,023		7,02		0,96		1,13		5,9		49,0		50	
	10	LV5/12	0,025		9,86		0,41		1,16		8,7		72,5		47	
	9	LV5/7	0,019		5,79		1,50		2,10		3,7		30,7		110	
	8	LV5/5	0,034		4,90		0,03		1,62		3,3		27,3		48	
	7	LV5/3	0,034		6,05		0,04		1,30		4,8		39,6		38	
	6	LV5/1	0,034		3,89		0,02		0,91		3,0		24,8		26	
	5	LV4/18	0,004		0,40		0,00		0,41		0,0		-0,1		107	
	4	LV4/6	0,008		0,39		0,00		0,39		0,0		0,0		50	
	3	LV3/63	0,006	0,004	6,73	6,12	0,005	0,007	0,25	0,22	6,5	5,90	54,0	49,15	40	58,48
Tithonian	2	LV3/40	0,003	0,002	5,49	0,62	0,005	0,003	0,25	0,04	5,2	0,62	43,7	5,19	75	17,23
	1	LV3/15	0,003		6,15		0,010		0,17		6,0		49,8		60	

TOC/TIC Nevenka 1	Nr.	Sample	N [%]		C_{total} [%]		S [%]		C_{org} [%]		TIC [%]		$CaCO_3$ [%]		Corg/N	
	63	Nev 63	0,058	0,03	3,41	1,89	0,168	0,32	2,70	0,98	0,7	0,92	5,8	7,64	46	22,73
Early Aptian	62	Nev 62	0,020	0,02	1,70	1,05	0,231	0,17	0,26	1,17	1,4	0,35	12,0	2,93	13	16,19
	61	Nev 61	0,022		0,98		0,322		0,25		0,7		6,1		11	
	60	Nev 60	0,034		1,49		0,564		0,70		0,8		6,6		20	
	59	Nev 59	0,054	0,05	2,12	2,88	1,312	0,49	1,56	1,76	0,6	1,12	4,7	9,36	29	31,51
	58	Nev 58	0,042	0,03	2,46	1,90	1,027	0,45	1,12	1,84	1,3	0,62	11,2	5,16	27	16,04
	57	Nev 57	0,104		4,64		1,298		3,79		0,9		7,1		36	
	56	Nev 56	0,077		3,16		1,533		2,25		0,9		7,6		29	
	55	Nev 55	0,032		1,26		1,004		0,59		0,7		5,6		19	
	54	Nev 54	0,050		2,20		1,189		1,13		1,1		8,9		22	
	53	Nev 53	0,041		1,29		0,708		0,64		0,7		5,5		15	
	52	Nev 52	0,041		2,92		0,733		0,61		2,3		19,3		15	
	51	Nev 51	0,039		1,74		1,225		0,92		0,8		6,8		23	
	50	Nev 50	0,033		1,02		1,048		0,59		0,4		3,6		18	
	49	Nev 49	0,042		1,95		1,304		0,61		1,3		11,1		15	
	48	Nev 48	0,027		4,33		0,235		0,44		3,9		32,5		16	
	47	Nev 47	0,032		1,65		1,268		0,48		1,2		9,8		15	
	46	Nev 46	0,039		1,73		0,851		0,64		1,1		9,1		16	
	45	Nev 45	0,037		3,04		0,668		1,33		1,7		14,3		36	
	44	Nev 44	0,029		4,14		0,517		1,15		3,0		24,9		40	
	43	Nev 43	0,024		2,79		0,853		0,84		2,0		16,3		34	
	42	Nev 42	0,023		2,56		1,100		0,76		1,8		15,0		33	
	41	Nev 41	0,021		1,79		1,029		0,97		0,8		6,8		47	
	40	Nev 40	0,066		3,43		0,594		2,84		0,6		4,9		43	
	39	Nev 39	0,031		2,56		1,524		1,25		1,3		11,0		41	
	38	Nev 38	0,042		1,41		0,539		0,88		0,5		4,4		21	
	37	Nev 37	0,021		1,26		0,213		0,97		0,3		2,4		46	
	36	Nev 36	0,016		1,59		0,059		0,94		0,7		5,5		58	
	35	Nev 35	0,018		1,47		0,048		0,61		0,9		7,2		33	
	34	Nev 34	0,021		1,16		0,156		0,52		0,6		5,3		24	
	33	Nev 33	0,021		1,89		0,071		0,86		1,0		8,6		41	
	32	Nev 32	0,081		7,26		0,189		6,83		0,4		3,6		84	
	31	Nev 31	0,033		2,96		0,100		1,84		1,1		9,4		55	
Late Barremian	30	Nev 30	0,060		4,81		0,134		3,52		1,3		10,8		59	
	29	Nev 29	0,030		2,43		0,048		1,58		0,9		7,1		53	
	28	Nev 28	0,073		5,62		0,130		4,48		1,1		9,5		61	
	27	Nev 27	0,060		4,53		0,170		2,74		1,8		14,9		46	
	26	Nev 26	0,036		2,52		0,220		1,04		1,5		12,3		29	
	25	Nev 25	0,045		1,58		0,586		0,75		0,8		6,9		17	
	24	Nev 24	0,039		1,09		0,378		0,43		0,7		5,5		11	
	23	Nev 23	0,041		2,20		0,121		0,90		1,3		10,8		22	
	22	Nev 22	0,035		1,57		0,181		0,54		1,0		8,5		16	
	21	Nev 21	0,078		5,89		0,160		4,18		1,7		14,2		54	
	20	Nev 20	0,038		2,11		0,078		1,36		0,8		6,3		36	
	19	Nev 19	0,045		2,41		0,201		1,38		1,0		8,6		31	
	18	Nev 18	0,042		1,65		0,269		0,64		1,0		8,4		15	
	17	Nev 17	0,038		1,21		0,183		0,53		0,7		5,7		14	
	16	Nev 16	0,028		1,33		0,332		0,29		1,0		8,7		10	
	15	Nev 15	0,032		1,42		0,113		0,30		1,1		9,3		9	
	14	Nev 14	0,046		3,55		0,093		1,70		1,9		15,5		37	
	13	Nev 13	0,041		1,20		0,356		0,44		0,8		6,3		11	
	12	Nev 12	0,045		1,48		0,250		0,67		0,8		6,8		15	
	11	Nev 11	0,045		1,22		0,322		0,55		0,7		5,6		12	
	10	Nev 10	0,061		4,05		0,112		2,33		1,7		14,3		38	
	9	Nev 9	0,079		4,27		0,248		2,54		1,7		14,4		32	
	8	Nev 8	0,052		2,33		0,131		1,36		1,0		8,1		26	
	7	Nev 7	0,162		8,05		0,802		7,09		1,0		8,1		44	
	6	Nev 6	0,169		10,17		0,147		9,24		0,9		7,7		55	
	5	Nev 5	0,042		1,83		0,213		1,03		0,8		6,7		25	
	4	Nev 4	0,119		7,19		0,138		6,03		1,2		9,7		51	
	3	Nev 3	0,087		4,34		0,147		3,68		0,7		5,5		42	
	2	Nev 2	0,064		2,80		0,216		2,29		0,5		4,3		36	
	1	Nev 1	0,102		3,26		0,055		2,12		1,1		9,4		21	

TOC/TIC Sofia 1	Nr.	Sample	N [%]		C_{total} [%]		S [%]		C_{org} [%]		TIC [%]		$CaCO_3$ [%]		Corg/N	
Hauterivian to Aptian	60	SOF 60	0,003	0,02	0,86	1,58	0,18	0,50	0,42	0,27	0,45	1,32	3,71	10,97	121,84	18,55
	59	SOF 59	0,017	0,01	1,39	0,90	0,17	0,47	0,24	0,12	1,15	0,82	9,60	6,86	14,22	21,42
	58	SOF 58	0,026		0,66		0,33		0,18		0,48		3,98		7,06	
	57	SOF 57	0,015		1,73		0,14		0,30		1,42		11,85		19,66	
	56	SOF 56	0,019		1,18		0,30		0,20		0,98		8,19		10,55	
	55	SOF 55	0,017		1,10		0,09		0,20		0,90		7,50		11,23	
	54	SOF 54	0,023		1,02		0,12		0,17		0,84		7,04		7,47	
	53	SOF 53	0,013		1,06		0,17		0,18		0,88		7,32		14,01	
	52	SOF 52	0,024		1,24		0,31		0,28		0,96		7,96		11,62	
	51	SOF 51	0,026		1,21		0,31		0,23		0,99		8,22		8,71	
	50	SOF 50	0,023		0,84		0,11		0,18		0,66		5,48		7,69	
	49	SOF 49	0,020		0,49		0,07		0,14		0,35		2,88		6,98	
	48	SOF 48	0,010		0,51		0,23		0,17		0,34		2,80		16,84	
	47	SOF 47	0,019		0,73		0,30		0,20		0,52		4,35		10,93	
	46	SOF 46	0,024		0,75		0,25		0,18		0,57		4,79		7,47	
	45	SOF 45	0,026		0,69		0,49		0,26		0,43		3,62		9,84	
	44	SOF 44	0,017		2,18		1,18		0,40		1,78		14,81		24,26	
	43	SOF 43	0,012		3,37		0,78		0,47		2,90		24,16		39,00	
	42	SOF 42	0,011		1,97		1,07		0,36		1,61		13,41		33,73	
	41	SOF 41	0,005		2,34		1,30		0,35		1,98		16,52		75,68	
	40	SOF 40	0,023		2,48		1,32		0,41		2,07		17,23		18,35	
	39	SOF 39	0,014		2,07		1,03		0,34		1,73		14,42		23,24	
	38	SOF 38	0,022		2,63		1,46		0,46		2,17		18,06		21,21	
	37	SOF 37	0,021		2,86		1,26		0,45		2,42		20,12		21,66	
	36	SOF 36	0,018		1,72		1,30		0,27		1,45		12,07		15,67	
	35	SOF 35	0,020		4,74		0,09		0,65		4,09		34,10		31,91	
	34	SOF 34	0,025		0,57		0,47		0,13		0,44		3,63		5,33	
	33	SOF 33	0,031		1,55		1,47		0,36		1,19		9,91		11,58	
	32	SOF 32	0,022		0,76		0,73		0,21		0,55		4,56		9,80	
	31	SOF 31	0,022		1,53		0,20		0,15		1,38		11,46		6,90	
	30	SOF 30	0,020		1,47		0,34		0,24		1,22		10,19		11,86	
	29	SOF 29	0,017		1,69		0,53		0,22		1,47		12,26		12,38	
	28	SOF 28	0,016		1,91		0,11		0,17		1,74		14,46		11,09	
	27	SOF 27	0,020		2,49		0,05		0,14		2,35		19,59		7,10	
	26	SOF 26	0,011		2,49		0,07		0,16		2,33		19,37		14,49	
	25	SOF 25	0,022		2,01		0,09		0,17		1,84		15,33		7,55	
	24	SOF 24	0,031		1,07		0,24		0,20		0,87		7,27		6,48	
	23	SOF 23	0,032		0,86		0,31		0,30		0,56		4,66		9,31	
Valanginian	22	SOF 22	0,028	0,033	0,67	1,09	0,65	0,84	0,41	0,55	0,26	0,54	2,15	4,48	14,48	16,46
	21	SOF 21	0,031	0,007	1,00	0,47	0,78	0,19	0,24	0,30	0,76	0,27	6,34	2,21	7,58	6,84
	20	SOF 20	0,028		1,10		0,69		0,30		0,81		6,72		10,41	
	19	SOF 19	0,038		0,81		0,64		0,39		0,42		3,50		10,08	
	18	SOF 18	0,030		0,64		0,68		0,48		0,16		1,32		15,95	
	17	SOF 17	0,033		1,21		0,90		0,62		0,59		4,87		18,72	
	16	SOF 16	0,043		2,06		1,16		1,07		0,99		8,25		24,64	
	15	SOF 15	0,035		0,72		0,79		0,40		0,32		2,68		11,60	
	14	SOF 14	0,021		0,97		0,94		0,53		0,44		3,65		25,76	
	13	SOF 13	0,044		1,75		1,14		1,11		0,64		5,36		25,34	
Berriasian	12	SOF 12	0,045	0,017	2,93	0,78	1,34	1,10	1,87	0,25	1,06	0,53	8,83	4,44	41,64	15,20
	11	SOF 11	0,024	0,008	3,08	0,32	0,62	1,00	0,61	0,11	2,46	0,23	20,52	1,90	25,47	1,62
	10	SOF 10	0,029		0,90		1,01		0,41		0,49		4,10		14,17	
Tithonian	9	SOF 9	0,028	0,018	1,15	1,00	1,11	0,85	0,37	0,25	0,78	0,74	6,52	6,17	13,06	14,54
	8	SOF 8	0,017	0,006	0,72	0,66	0,69	0,57	0,28	0,07	0,44	0,64	3,68	5,37	16,84	1,78
	7	SOF 7	0,025		1,13		2,24		0,34		0,79		6,60		13,61	
	6	SOF 6	0,009		0,49		0,38		0,13		0,36		3,03		15,14	
	5	SOF 5	0,014		1,43		0,66		0,24		1,19		9,88		17,80	
	4	SOF 4	0,018		2,47		0,33		0,25		2,22		18,53		13,57	
	3	SOF 3	0,020		0,78		0,79		0,26		0,53		4,38		12,56	
	2	SOF 2	0,014		0,39		0,67		0,21		0,18		1,49		14,80	
	1	SOF 1	0,017		0,39		0,83		0,22		0,17		1,40		13,51	

TOC/TIC Antarctica	Nr.	Sample	N [%]		C_{total} [%]		S [%]		C_{org} [%]		TIC [%]		$CaCO_3$ [%]		Corg/N	
early Albian	1	D.8403.30	0,027	0,028	0,44	6,18	0,146	0,206	0,35	0,60	0,08	5,58	0,69	46,47	13	28,52
	2	D.8403.65	0,012	0,015	8,87	3,40	0,023	0,284	0,76	0,16	8,11	3,25	67,59	27,05	64	21,01
late Aptian	3	D.8406.6	0,052		5,91		0,706		0,60		5,31		44,24		12	
	4	D.8406.18	0,022		7,41		0,042		0,58		6,83		56,89		27	
	5	D.8633.10	0,027		8,28		0,114		0,72		7,56		62,94		27	
middle Tithonian	6	D.8751.3	0,018	0,018	6,03	6,00	0,086	0,041	0,39	0,51	5,63	5,49	46,94	45,76	22	29,58
	7	D.8751.2	0,020	0,002	5,95	0,05	0,029	0,040	0,48	0,14	5,47	0,13	45,57	1,10	23	11,85
	8	D.8751.1	0,015		6,04		0,008		0,66		5,37		44,76		43	
late Aptian	1	KG.3403.213	0,013	0,024	0,20	0,30	0,008	0,098	0,21	0,23	0,00	0,07	-0,03	0,58	16	10,94
middle Aptian	2	KG.3403.70	0,021	0,009	0,43	0,09	0,134	0,096	0,31	0,05	0,13	0,05	1,05	0,42	15	4,32
	3	KG.3402.286	0,028		0,34		0,246		0,27		0,08		0,66		9	
early Aptian	4	KG.3403.4	0,019		0,24		0,065		0,20		0,04		0,37		10	
	5	KG.3402.16	0,036		0,28		0,035		0,18		0,10		0,83		5	
Valanginian-?Barremian	6	KG.3401.608	0,028	0,029	1,05	0,69	0,397	0,219	0,24	0,28	0,80	0,42	6,71	3,46	9	9,79
	7	KG.3455.170	0,026	0,004	0,53	0,31	0,060	0,169	0,33	0,04	0,20	0,34	1,66	2,81	13	2,45
	8	KG.3455.24	0,033		0,51		0,201		0,26		0,24		2,01		8	
early Valanginian - middle Valanginian	1	P.2186.22	0,062	0,074	0,80	1,11	0,01	0,042	0,68	0,80	0,11	0,32	0,94	2,63	11	10,75
	2	P.2186.21	0,085	0,025	0,99	0,72	0,00	0,088	0,98	0,28	0,01	0,84	0,04	6,99	12	0,98
	3	P.2186.20	0,068		0,82		0,03		0,77		0,06		0,48		11	
	4	P.2186.19	0,076		0,92		0,09		0,92		0,00		0,01		12	
	5	P.2186.18	0,014		0,89		0,38		0,15		0,74		6,12		11	
	6	P.2186.17	0,080		1,04		0,16		1,03		0,02		0,14		13	
	7	P.2186.16	0,074		0,87		0,00		0,81		0,05		0,43		11	
	8	P.2186.15	0,072		0,79		0,01		0,76		0,04		0,30		10	
	9	P.2186.14	0,057		0,58		0,00		0,48		0,10		0,86		8	
	10	P.2186.13	0,066		0,78		0,01		0,72		0,06		0,51		11	
	11	P.2186.12	0,085		0,97		0,01		0,96		0,01		0,09		11	
	12	P.2186.11	0,084		1,00		0,00		0,96		0,04		0,31		11	
	13	P.2186.10	0,079		0,92		0,01		0,88		0,04		0,30		11	
	14	P.2186.8	0,055		0,56		0,01		0,52		0,04		0,34		9	
	15	P.2186.7	0,102		1,07		0,00		0,98		0,10		0,80		10	
	16	P.2186.6	0,102		1,12		0,00		1,09		0,03		0,27		11	
	17	P.2186.5	0,095		1,00		0,00		0,94		0,06		0,50		10	
	18	P.2186.4	0,103		1,05		0,00		1,01		0,04		0,32		10	
	19	P.2186.3	0,011		3,82		0,06		0,10		3,71		30,94		10	
	20	P.2186.2	0,099		2,42		0,01		1,09		1,33		11,11		11	
	21	P.2186.1	0,086		1,00		0,07		0,95		0,04		0,37		11	
late Berriasian - early Valanginian	22	P.2175.7	0,176	0,112	0,80	0,92	0,40	0,324	0,61	0,46	0,19	0,46	1,58	3,86	3	5,92
	23	P.2175.1	0,253	0,067	0,31	1,33	0,38	0,504	0,31	0,17	0,01	1,19	0,06	9,94	1	4,09
	24	P.2174.31	0,165		0,52		1,52		0,41		0,12		0,97		2	
	25	P.2174.28	0,128		0,37		1,04		0,35		0,02		0,18		3	
	26	P.2174.26	0,117		0,36		0,05		0,30		0,06		0,52		3	
	27	P.2172.9	0,064		0,75		0,02		0,62		0,13		1,09		10	
	28	P.2172.7	0,065		0,42		0,07		0,39		0,02		0,20		6	
	29	P.2173.3	0,053		0,51		0,01		0,43		0,08		0,66		8	
	30	P.2173.2	0,024		0,35		0,06		0,31		0,03		0,28		13	
	31	P.2171.6	0,119		0,88		0,01		0,49		0,39		3,24		4	
	32	P.2171.1	0,072		4,89		0,02		0,84		4,05		33,70		12	
early Berriasian - middle Berriasian	33	P.2220.20	0,048	0,084	5,57	1,52	0,05	0,094	0,58	0,69	4,99	0,83	41,53	6,93	12	8,73
	34	P.2220.11	0,086	0,027	1,70	1,21	0,41	0,176	0,78	0,31	0,92	1,30	7,69	10,87	9	4,55
	35	P.2222.3	0,057		1,41		0,14		1,12		0,29		2,39		20	
	36	P.2176.35	0,046		3,70		0,01		0,29		3,41		28,45		6	
	37	P.2176.32	0,074		1,12		0,00		0,36		0,76		6,35		5	
	38	P.2176.31	0,088		1,23		0,00		0,50		0,73		6,12		6	
	39	P.2176.30	0,115		1,98		0,00		0,97		1,01		8,42		8	
	40	P.2176.27	0,057		1,14		0,02		1,00		0,14		1,20		18	
	41	P.2176.24	0,081		2,00		0,01		0,10		1,90		15,86		1	
	42	P.2176.18	0,036		0,91		0,62		0,27		0,63		5,29		8	
	43	P.2176.17	0,098		1,02		0,01		0,94		0,09		0,72		10	
	44	P.2183.13	0,131		0,55		0,00		0,42		0,12		1,01		3	
	45	P.2183.12	0,122		1,09		0,00		0,98		0,11		0,90		8	
	46	P.2183.11	0,080		0,87		0,38		0,76		0,10		0,85		10	
	47	P.2183.10	0,089		1,15		0,01		1,08		0,07		0,55		12	
	48	P.2183.9	0,119		0,73		0,01		0,51		0,23		1,90		4	
	49	P.2183.8	0,099		0,79		0,01		0,67		0,12		1,00		7	
	50	P.2183.6	0,092		0,91		0,10		0,84		0,07		0,58		9	
	51	P.2183.4	0,084		0,97		0,01		0,87		0,10		0,81		10	
middle Tithonian	52	P.2223.63	0,058	0,022	0,67	1,67	0,398	0,587	0,33	0,32	0,34	1,35	2,86	11,27	6	25,32
	53	P.2223.62	0,046	0,015	1,01	2,31	1,023	0,708	0,45	0,42	0,56	1,95	4,67	16,27	10	57,37
	54	P.2223.60	0,020		0,55		1,383		0,23		0,32		2,66		11	
	55	P.2223.56	0,024		0,67		0,802		0,28		0,39		3,27		12	
	56	P.2223.51	0,019		0,47		0,292		0,18		0,29		2,40		9	
	57	P.2223.49 B	0,025		0,85		0,435		0,24		0,61		5,10		9	
	58	P.2223.49 A	0,007		3,47		0,096		0,15		3,32		27,67		22	
	59	P.2223.47	0,022		1,35		2,224		0,14		1,21		10,06		6	
	60	P.2223.46	0,031		0,62		0,271		0,22		0,40		3,32		7	
	61	P.2223.44	0,029		0,77		0,207		0,28		0,49		4,10		10	
	62	P.2223.30	0,039		1,46		2,162		0,27		1,19		9,90		7	
	63	P.2223.26	0,014		0,56		0,141		0,20		0,37		3,06		14	
	64	P.2223.25 B	0,007		0,68		0,075		0,09		0,59		4,92		13	
	65	P.2223.25 A	0,006		0,52		0,140		0,08		0,44		3,66		15	
	66	P.2223.23	0,014		0,71		0,219		0,08		0,63		5,23		6	
	67	P.2223.20	0,008		9,49		0,037		1,92		7,57		63,04		247	
	68	P.2225.3	0,011		4,59		0,079		0,30		4,29		35,73		27	

Thin Section Analysis

XCVIII–CIII

Thin sections Byers Group

Age	Nr.	Sample	Observations/Remarks	Sediment type
late Berriasian-early Valanginian	1.	**P.2171.1**	main component very fine dark shale coarse bands layers of quartz grains mono- and plycrystalline, boundaries sutured but also straight Quartz grains mostly well rounded with varying sphericity, sorting very poor Feldspars of different size and shape (mostly low sphericity and angular to subrounded) veins filled with plagioklase and clay in layers few other rock fragments small-scale sedimentary structures (layers), fining/coarsening trends	Shale Argillaceous rock SILTY MUDSTONE
	2.	**P.2171.3**	main component very fine dark shale coarse bands layers of quartz grains mono- and plycrystalline, boundaries sutured but also straight Feldspars of different size and shape (mostly low sphericity and angular to subrounded) in coarse bands Layers have fine grained (clay) matrix few other rock fragments small-scale sedimentary structures (layers), fining/coarsening trends	Shale Argillaceous rock SILTSTONE
	3.	**P.2172.8**	dark fine grained material (dark shale) several bands of coarser minerals are present, minerals are small quartz, matrix dark clay, well sorted quartz grains in bands are angular to subangular few shell fragments few other rock fragments lamination and fining/coarsening trends	Shale Argillaceous rock MUDSTONE and thin SANDSTONE laminae
	4.	**P.2172.9**	four layers of dark fine grained shales (or claystone) (2x) and 2 layers of coarser material (still small particles - siltstone) layered conatcts partly sharp, partly progressive few shell fragments in rock types coarser layers contain fine grained shale matrix and coarser fragments of shales and slates, also quartz and other rock fragments, sorting moderate to poor fine grained shale layers with small-sclae sedimentary structures no sedimentary structures in coarser silty layers	shale-siltstone alternating sequence MUDSTONE
	5.	**P.2173.2**	two phases: fine (clay) - coarse (rock frgament mix) - fine (clay) coarse grained layer with various rock fragments and fine grained matrix/cement, sorting poor pyrite clasts fine grained layers contain small opaque particles layered conatcts partly sharp, partly progressive small-scale sedimentary structures in fine grained layers, fining/coarsening trends	shale-fine conglomerate alternation MEDIUM TO VERY FINE SANDSTONE
	6.	**P.2173.3**	brown claystone/shale pores filled with dark material (organic matter? oil stained?) fine grained layers contain small opaque particles dark stains in layers otherwise no sedimentary structures CHONDRITES	claystone/shale Argillaceous rock MEDIUM SILTSTONE
	7.	**P.2174.26**	alteration of dark brown fine grained chale/clay and coarse (feinsand) sized conglomerate (clay matrix) few shell fragments in shale layers shale layers with small-sized sedimentary structures shale layers with signs of bioturbation coarser grained layers with various rock fragments, i.e. quartz, feldspar, shales/slates, opake minerals, all with varying sphericity, poorly sorted layered conatcts partly sharp, partly progressive	shale-fine conglomerate alternation INTERLAMINATED MUDSTONE/SANDSTONE
	8.	**P.2174.28**	one layer each of fine grained clay sized brown material and fine sand sized brighter conglomerate very few shell fragments in the clay layer shale layers with small-sized sedimentary structures (few grain size changes) shale layers with few signs of bioturbation coarser grained layers with various rock fragments, i.e. quartz, feldspar, shales/slates, opake minerals, others, all with varying sphericity, sorting very poor layered conatcts partly sharp, partly progressive	shale-fine conglomerate alternation INTERLAMINATED MUDSTONE/SANDSTONE
	9.	**P.2174.31**	high frequence layers of fine grained shale material several bands of coarser silt sized material, various rock fragments, various sphericities bioturbation in clay layers high frequence fining and coarsenig trends, planar bedding in the clay layers several thin bands of very dark material are present. Parallel to the bedding, probably organic origin few shell fragments/skeletal grains in the fine grained material silty areas with fine grained (clay) matrix, pore space partly with opake (organic?) material	claystone/shale Argillaceous rock alteration INTERLAMINATED MUDSTONE/SANDSTONE

Age	Nr.	Sample	Observations/Remarks	Sediment type
late Berriasian-early Valanginian	10.	**P.2174.37**	fine sand layer, various rock fragments, fine grained matrix, plenty opake minerals (pyrite?) silt-sized layer, with few coarse bands, few shell fragments/skeletal grains black fine organic bands/intercalations in the fine sand sized layers, fine sand layers with rock fragments of various sphericity , well sorted silty layer with high frequence fining and coarsenig trends, planar bedding	silt-fine conglomerate alternation INTERBEDDED MUDSTONE/SANDSTONE
	11.	**P.2175.1**	One half micro breccia, shale matrix, low sphericity, angular to subangular, few ell rounded, very poorly sorted, various rock fragments one half silt/fine sand sized material, with clay intercalations relatively sharp conatct between the two rock types small scale sedimentary structrures in silty material i.e. cross bedding and varioations in grain size coarse grained material feldspar, quarzt, shale/slates, various other rock fragments, few volcanic rock fragments	alteration silt/fine sand to micro breccia SILTY MUDSTONE THIN VERY FINE SANDSTONE LAYERS CURRENT RIPPLE CROSS LAMINATED
	12.	**P.2175.7**	silt/fine sand layer dark brown clay/shale layer with darker inclusions/intercalations multi directional --> probably bioturbation in fine layer small band of coarser material (silt sized) coarseing upward trend from clay layer over silty to fine sand at the top Silt/fine sand part with small sclae sedimentary structures - planar bedding with intercalations of clay sized material some opaque bands in silt/fine sand layer acting as matrix --> organic origin?, other matrix mostly clay silt/fine sand layer with opaque rock fragents (pyrite?) plenty of quarzt in silt/fine sand layer, moderately sorted, subangular and low sphericity	fine sand/silt and clay INTERLAMINATED MUDSTONE/SANDSTONE
early-middle Berriasian	13.	**P.2220.11**	brown very fine material - clay bright intercalations filled with small quartz grains and calcite cement small scale sedimentary structures - planar bedding in clay some layers filled with very fine dark brown to black material (organic matter?), pore space/voids filled with opaque material (organic matter) few grain size trends, bright layers with poorly sorted sphericity varies single calcite grains interbedded in clay (shells/skeletal grains?)	claystone MUDSTONE CONCRETION
	14.	**P.2222.3**	brown very fine grained claystone plenty of rock fragments interbedded in claystone layers - calcite, quartz, clay slates several grain size trends sedimentary structures - planar bedding some layers filled with very fine dark brown to black material (organic matter?), pore space/voids filled with opaque material (organic matter)	claystone MUDSTONE PLANAR LAMINATED/CONCRETIONARY
	15.	**P.2176.34**	continuos transition from dark brown fine sand/silt sized to clay sized material - fining trend mostly dark brown clay matrix sedimentary structures - planar bedding moderate to well sorted, sphericities vary few bright intercalations in silty part of the sample	claystone to very fine conglomerate (silt) MUDSTONE VERY FINE SANDSTONE LAMINAE
	16.	**P.2176.31 A**	mostly fine sand sized conglomerate, matrix fine grained (dark brown clay), quartz cements in bright parts of the sample one thin layer with finer material (clay) planar bedding sorting moderate to well, varying sphericity (high and low) fine sand layers with few dark brown to black bands and pore/fracture filling with black (organic) material coarser material with opaque rock fragments (pyrite?) and some feldspars keine wesentlichen Unterschiede zu P.2176.30 B	fine sand conglomerate FINE TO MEDIUM SANDSTONE
	17.	**P.2176.31 B**	mostly fine sand sized conglomerate, matrix fine grained (dark brown clay), quartz cements in bright parts of the sample lower part of the sample with silt sized dark brown material transitioning in an coarsing upward trend towards bright fine sand material planar bedding, one small lens of coarse (fine sand) bright material sorting moderate to well, varying sphericity (high and low) fine sand layers with plenty dark brown to black bands and pore/fracture filling with black (organic) material coarser material with opaque rock fragments (pyrite?) and some feldspars only minor differences to samples P.2176.30 B and P.2176.31 A	fine sand conglomerate FINE TO MEDIUM SANDSTONE
	18.	**P.2176.30 A**	one big coarsening/fining upward trend, dark clay to bright fine sand sized material matrix in coarser material clay sized coarser part with various rock fragments, well to very well sorted rock fragments quartz, opaque minerals (pyrite?), others, all with low sphericity, mostly subangular small scale sedimentary structures, filling direction, lamination, fining/coarsening trend coarse part of the sample with two dark broen/black bands - organic matter, probably oil? Also in clay part but in finer layers	claystone to fine conglomerate VERY FINE TO MEDIUM SANDSTONE

Age	Nr.	Sample	Observations/Remarks	Sediment type
early-middle Berriasian	19.	**P.2176.30 B**	mostly fine sand sized conglomerate, matrix fine grained (clay), some quartz cements few layers with finer material (silt sized and clay) planar, wavy bedding sorting moderate to well, varying sphericity (high and low) fine sand layers with few dark brown/black bands and pore/fracture filling with black (organic) material coarser material with opaque rock fragments (pyrite?) and some feldspars	fine sand conglomerate VERY FINE TO MEDIUM SANDSTONE
	20.	**P.2176.27**	very fine (clay) dark brown material band of bright fine material - cemented fracture? Durchgehende Auslöschung bei gekreuztem Polarisator small scale sedimentary structures, cross bedding, lamination, fining/coarsening trends laminations in clay dark brown/black - oil filled ?	claystone MUDSTONE
	21.	**P.2176.17c**	dark brown clay planar bedding (sedimentary structures), several fining and coarsening trends very few shell fragments one thinning bright band some thin intercalations oil stained ? coarser intercalations (silt sized grains) with very small black/opaque minerals	claystone SILTY CLAYSTONE
	22.	**P.2176.14**	dark brown clay few intercalations with silt sized grains signs for bioturbation in the coarser part (maybe only round shale fragments) small scale sedimentary structures --> grain size variatins/trends	claystone MUDSTONE
	23.	**P.2176.9**	fine to medium sand sized conglomerate quartz, feldapr, shale or slate fragments and various other rock fragments (some volcanic rock fragments), few opaque rock fragments clay matrix moderately sorted, mostly low sphericity, angular to subrounded	fine conglomerate/sandstone MEDIUM SANDSTONE
	24.	**P.2176.2**	fine to medium sand sized conglomerate quarz, feldapr, shale or slate fragments and various other rock fragments (few volcanic rock fragments) clay matrix moderately sorted, mostly high sphericity, subangular to subrounded	fine conglomerate/sandstone MEDIUM TO FINE SANDSTONE
	25.	**P.2176.23**	fine to medium sand sized conglomerate quartz, feldapr, shale or slate fragments and various other rock fragments (some volcanic rock fragments), few opaque rock fragments clay matrix moderately sorted, mostly low sphericity, angular to subrounded fractures quartz filled, clacite cements	fine conglomerate/sandstone COARSE SANDSTONE
middle Tithonian	26.	**P.2223.72**	brown clay to siltstone many intraclasts, various rock fragments made of bioclasts and clay no bedding planes, few small scale grainzise variations fractures filled with opaque material several borings/bioturbation few patches of fine sand sized material	clay to siltstone MUDSTONE
	27.	**P.2223.63**	brown clay to siltstone with several intercalationsof clay and micro breccia claystone has so many intraclasts aligned with the bedding that it appears as a siltstone intraclasts are transluscent and rounded - bioclasts one large fracture ist filled with quartz some small fractures within the siltstone are opaque (pyrite/organic matter filled); alsofine dark bands within and parallel to the bedding breccia layers are poorly sorted and with various sphericities, dark grey clay matrix, clasts mainly quartz	clay to siltstone MUDSTONE/SANDSTONE INTERLAMINATED
	28.	**P.2223.60 A**	succession of siltstone with claystone bands/intercalations and coarser material on top and bottom (conglomerate) siltstones with plenty of bioclasts mostly rounded and elongated aligned with the bedding a total of four dark grey interbeds some coarse intercalataion within the silt layer, silt layer often with thin dark brown to black bands conglomerate with various unsorted rock fragments, clay matrix, quartz cements no large quartz grains in conglomerate	clay to siltstone MUDSTONE/SANDSTONE INTERLAMINATED
	29.	**P.2223.60 B**	brown silt to grey fine sand silt layer with few intraclasts ubt plenty dark/black bands as in P.2223.60 A sharp contact to the sandstone layer, two claystone intercalations within the fine sandstone sandstone layer well sorted and well rounded, various rock fragments (also pyrite), clay matrix siltstone layer with few sand interlayers/intercalations	silt to fine sandstone MUDSTONE/SANDSTONE INTERLAMINATED

Age	Nr.	Sample	Observations/Remarks	Sediment type
middle Tithonian	30.	**P.2223.56**	bipartite sample - silt-conglomerate alternating sequence and fine sandstone siltstone layers dark brown, with plenty of intraclasts - rounded clay and quartz, also skeletal grains/shell fragments - bioclasts are poorly sorted sandstone with multi couloured clay matrix (light brown and grey) sandstone grains with low sphericity, subangular to rounded in coarse grained layers opaque minerals are present (pyrite?)	alternating sequence of silt to sand MEDIUM SANDSTONE/MUDSTONE
	31.	**P.2223.51**	brown siltstone with plenty of white round clasts (skeletal grains/intraclasts - bioclasts are poorly sorted) fractures fileld with quartz and pyrite grey/brown patches without intraclasts --> borings weakly developed small scale sedimentary structures planar bedding noticeable due intraclasts in layers	siltstone MUDSTONE BIOTURBATED
	32.	**P.2223.47**	tripartite sample - micro conglomerate, micro breccia with fining trend to claystone between the clay and conglomerate a clay layer is interbedded with large phenocrysts (Epidot?) which sunk into the clay conglomerate and braccia with pyrite crystals light brown clay layer with few dark brown patches fine dispersed grey clay intraclasts throughout the sample coarse - fine - fine with intraclasts - coarse	micro conglomerate and micro breccia divided by claystone MEDIUM SANDSTONE TO SILTSTONE NORMALLY GRADED ?ASH
	33.	**P.2223.46**	tripartite sequence - micro breccia fining to silt sized, clay sized layer with intrusion (?) phenocryst/interbed interspersed and bordered with prite crystals, filled with clay matrix, large cyrstals and other rock fragments breccia with clay matrix, and sharp contact to the fine clay/silt part clay/silt part with opaque filled fractures (pyrite/oranic matter?) clay/silt part with opaque with dark brown bands (borings?) phenocryst/interbed with sharp contact to all surrounding rocks	claystone to silt to fine conglomerate MUDSTONE/SANDSTONE INTERLAMINATED
	34.	**P.2223.45 A**	brown clay/siltstone plenty of intracalsts - most are skeletal grains/shell fragments (different size and shape) but also clay, few quartz and pyrite voids/pores filled with dark grey clay in various forms and sizes small fractures filled with opaque material (pyrite/organic matter?) few grain size changes but no distinct trends some darker brown clay bands with fewer/no intraclasts - borings?	clay to siltstone MUDSTONE/SANDSTONE NORMALLY GRADED SANDSTONE
	35.	**P.2223.45 B**	brown clay/silt to micro gonglomerate - continuous grain size trend clay layers with bioturbatoin/borings micro conglomerate moderate to well sorted, rock fragments i.a. quartz, angular to subrounded, mostly low sphericity, no calcitic intraclasts/skeletal grains calcitic grains/skeletal grains within clay/silt layer common, also rock fragments of clay and quartz present between silty layer and microconglomerat one layer of clay one fine conglomerate band within the clay layer	clay/silt to micro conglomerate MUDSTONE/SANDSTONE NORMALLY GRADED SANDSTONE
	36.	**P.2223.44**	sample tripartite one large transition from clay to silt to fine conglomerate/micro breccia dark brown clay with plenty of intraclasts of different shapes and sizes, also skeletal grains/shell fragments, pore filling also with grey clay, borings/bioturbation clay part with dark brown patches - probably borings, plenty of dark grey skeletal grains silty transitional zone with various intraclasts/rock fragments - also opaque minerals (pyrite?) and skeletal grains, non-uniform grain size distribution conglomerate/breccia sorting moderate to poor, various rock fragments - i.a. quartz and shale slates, mostly low shpericity and angular, matrix clay fractures fileld with opaque material (pyrite?) and few with quartz	claystone to silt to fine conglomerate BIOTURBATED MUDSTONE THIN SANDSTONE LAMINAE
	37.	**P.2223.25 A**	light grey clay/siltstonewith various intraclsts without any clear orientation dark brown to black flakey intercalations/void fills made of organic matter (?) plenty of dark grey patches no clear sedimentary sequences	clay to siltstone SILTSTONE/CLAYSTONE ALTERED ASH ?
	38.	**P.2223.25 B**	light grey to light brown bipartite sample, claystone, micro breccia claystone with few intraclasts and few grain size trends; few sedimentary structures - dark brown filled bedding planes micro breccia band/intercalation, poorly sorted, mostly high sphericity, brown clay matrix, various intraclasts also plenty of volcanic origin in contrast to P.2223.25 A no flakey brown void fills and no patches micro breccia is thinning --> intrusion? Contact to one side sharp, transitional on the other side despite the colour and grain size relatively different to P.2223.25 A	claystone to microbreccia SILTSTONE/CLAYSTONE ALTERED ASH ?

Age	Nr.	Sample	Observations/Remarks	Sediment type
middle Tithonian	40.	**P.2223.23**	sample tripartite - dark brown fine silt/clay, fine conglomerate and fine breccia silt/clay with plenty of intraclasts/rock fragments, few shell fragments/skeletal grains, no clear grainsize trend, few brighter bands/intercalations conglomerate with bright clay matrix, various rock fragments, moderately to well sorted, mostly well rounded, varying sphericity breccia with dark brown clay matrix, light brown flakey clay minerals, various frock fragments, poorly sorted, subangular to subrounded, varying spherecitiy few pores/voids/fractures filled with drak brown to black matter (organic?)	claystone to silt to fine conglomerate MUDSTONE/SANDSTONE NORMALLY GRADED SANDSTONE
	41.	**P.2225.3**	twopartite sample - clay/silt stone with smooth transition to breccia with calcite and quarzt fragments and a clay matrix breccia-free brown claystone with lamination/planar bedding and plenty of aligned intraclasts (shell fragments/skeletal grains), grey clay interlayer intermediate zone of grey/brown claystone with no intraclats and no lamination but slight coaresning grainsize trend towards the breccia breccia layer with large clacite & quartz clasts, silty matrix with very small opaque (pyrite?) minerals; poorly sorted structures suppose that the breccia is up fractures filled with calcite and quartz	claystone to breccia MUDSTONE NORMALLY GRADED

Glendonite

CIV–CXV

Glendonites

Section	Sample	diametre µm	Mean diameter	Age
Cajón del Morado	CM 22/60	80	86,8	Hauterivian
		76	11,2	
		90		
		101		
	CM 21/8-15	89	78,5	Valanginian
		90	12,8	
		69		
		66		
	CM 19/21	65	62,1	
		86	18,8	
		87		
		55		
		40		
		43		
		59		
	CM 19/19	133	69,0	
		71	45,8	
		38		
		34		
	CM 19/13	72	88,5	
		105	23,3	
	CM 18/70	55	40,6	
		45	12,0	
		39		
		42		
		22		
	CM 18/67	26	48,2	
		40	29,2	
		48		
		29		
		98		
	CM 18/62	69	70,0	
		80	7,0	
		64		
		67		
	CM 18/57	86	81,5	
		77	6,4	
	CM 18/50	67	45,2	
		77	22,2	
		24		
		33		
		44		
		26		
	CM 18/42	63	52,3	
		60	15,9	
		34		
	CM 18/37	162	162,0	
	CM 17/2	38	37,0	Berriasian
		20	12,1	
		42		
		48		
	CM 16/48	19	44,9	Tithonian
		64	15,5	
		64		
		49		
		38		
		53		
		35		
		37		
	CM 16/38	54	52,5	
		51	2,1	
	CM 16/32	36	35,3	
		29	6,0	
		41		

Section	Sample	diametre µm	Mean diameter	Age
Cajón del Morado	CM 16/22	54	54,0	Tithonian
	CM 16/13	91	91,0	
	CM 16/11	37	58,4	
		77	17,5	
		39		
		45		
		65		
		70		
		76		
	CM 16/9	59	45,8	
		51	12,7	
		44		
		29		
	CM 14/3,5	28	58,8	
		24	28,3	
		44		
		59		
		47		
		69		
		48		
		77		
		70		
		122		
	CM 13/10,8	26	50,8	
		48	18,5	
		68		
		61		
Lo Valdés	LV 8/91	32	35,9	Valanginian
		40	13,2	
		38		
	LV 8/83	40		
		48		
		32		
	LV 8/41	37		
		70		
		27		
		27		
		24		
		30		
	LV 8/20-36	24		
		26		
		26		
		26		
		64		
		35		
	LV 5/3	26	41,6	Berriasian
		26	19,8	
		14		
		26		
		33		
		18		
		25		
	LV 4/6	52		
		51		
		72		
		53		
		73		
		57		
		57		
	LV 3/66	72	37,2	Tithonian
		44	25,3	
		28		
		172		
		90		
		120		
		102		

Section	Sample	diametre µm	Mean diameter	Age
Lo Valdés	LV 3/66	101		Tithonian
		63		
		110		
		66		
		50		
		112		
	LV 3/58	75	59,8	
		74	17,2	
		48		
		42		
	LV 3/56,5	29	51,3	
		25	43,4	
		35		
		116		
		26		
		30		
		39		
		113		
		68		
		31		
		32		
		26		
	LV 3/55	37	28,8	
		35	8,5	
		23		
		20		
		15		
		33		
		34		
		49		
		27		
		33		
		32		
		28		
		29		
	LV 3/52	19	19,5	
		15	3,4	
		23		
		21		
		50		
		25		
		24		
		26		
		23		
		30		
		35		
		26		
		19		
		24		
		18		
		26		
		26		
		25		
		26		
		19		
		28		
		34		
		38		
		33		
		20		
		26		
		26		
		21		
		45		
		27		
		23		
		19		

Section	Sample	diametre µm	Mean diameter	Age
Lo Valdés	LV 3/52	21		Tithonian
		22		
		25		
		26		
	LV 3/50	13		
		16		
		18		
		23		
		36		
		21		
		24		
		54		
		48		
		37		
		75		
		67		
		26		
	LV 3/48	27		
		15		
		26		
		37		
		26		
		26		
		33		
	LV 3/44	28		
		26		
		18		
		31		
		28		
		34		
		29		
	LV 3/40	20		
		26		
		16		
		19		
		24		
	LV 3/35	34		
		27		
		24		
		16		
		30		
		29		
		25		
		36		
		33		
		32		
		28		
		33		
		24		
		50		
		34		
		31		
		31		
		37		
		84		
		47		
	LV 3/26	29		
	LV 3/21	31		
		38		
		20		
		50		
		79		
		18		
		23		
		18		
		17		
		26		

Section	Sample	diametre µm	Mean diameter	Age
Lo Valdés	LV 3/6	30		Tithonian
		54		
		39		
		41		
		18		
		48		
		76		
		45		
		38		
	LV 3/3	65		
		35		
		40		
		76		
		65		
		64		
Kotick Point	D.8403.65	49	66,2	early Albian
		85	19,0	
		62		
		72		
		41		
		88		
Pluto Glacier	KG.3403.70	89	32,1	middle Aptian
		43	28,5	
		57		
	KG.3402.16	13		early Aptian
		16		
		13		
		14		
		12		
Spartan Glacier	K.G3457.54	68	84,6	Valanginian - ?Barremian
		74	34,2	
	KG.3456.65	132		
	KG.3455.170	141		
	KG.3455.24	83		
		38		
		44		
	KG.3461.26	85		Valanginian?
		68		
		81		
		77		
		64		
		145		
Himalia Ridge	KG.3401.2	103	52,3	late Berrias - early valangin
		49	21,7	
		52		
		53		
	KG.3404.283	32		Berriasian
		39		
		43		
		47		
	KG.2802.332	107	97,8	late Tithonian
		117	17,1	
		81		
		86		
Chester Cone - Sealer Hill	P.2186.22	50	64,8	early - middle Valanginian
		40	25,5	
		70		
	P.2186.21	30		
	P.2186.14	64		
		35		
		38		
		67		
		61		

Section	Sample	diametre µm	Mean diameter	Age
Chester Cone - Sealer Hill	P.2186.14	42		early - middle Valanginian
	P.2186.14	55		
	P.2186.11	71		
		47		
		65		
	P.2186.8	54		
		53		
		89		
	P.2186.5	63		
		69		
		140		
		43		
	P.2186.1	91		
		116		
		81		
		85		
Chester Cone - Devils Point	P.2175.1	66	65,2	late Berriasian - early Valanginian
		62	40,9	
	P.2174.26	87		
		39		
		42		
		90		
	P.2172.6	111		
		59		
	P.2172.7	36		
		39		
		43		
		76		
		33		
		46		
		46		
	P.2173.2A	56		
		47		
		238		
		49		
		26		
		86		
		76		
		151		
		135		
	P.2173.2B	34		
		59		
		72		
		28		
		55		
		95		
		70		
		49		
		100		
		50		
	P.2171.6	50		
		26		
		26		
		21		
		69		
President Beaches	P.2224.1	79	64,8	early - middle Berriaisan
		72	45,2	
		126		
		216		
		183		
	P.2220.20	37		
		38		
	P.2176.18	140		
		161		
	P.2176.15	41		
		30		

Section	Sample	diametre µm	Mean diameter	Age
President Beaches	P.2176.15	32		early - middle Berriaisan
	P.2176.15	47		
		42		
		73		
		61		
	P.2183.13	38		
		46		
	P.2183.10	39		
		32		
		62		
		42		
	P.2183.8	55		
		25		
		55		
		38		
	P.2183.7	60		
		39		
	P.2183.1	99		
		44		
		96		
		42		
		41		
		43		
		41		
		47		
		35		
Anchorage	P2223_62	131	80,0	middle Tithonian
		62	32,0	
		87		
		85		
	P2223_60	48		
		83		
	P2223_51	82		
		61		
		62		
		89		
	P2223_46	101		
		68		
		50		
		67		
		123		
		76		
	P2223_45A	57		
		54		
	P2223_26	139		
		49		
		118		
	P2223_25A	84		
		65		
		78		
		172		
		108		
		101		
	P2223_23	113		
		47		
	P2225_3A	31		
		58		
		52		
		40		

Nevenka 1	NEV 60	65	68,0	early Aptian
		58	15,8	
		101		
		66		
		47		
		54		

Section	Sample	diametre µm	Mean diameter	Age
Nevenka 1	NEV 60	69		early Aptian
		80		
		72		
	NEV 54	34	38,1	Late Barremian
		12	15,8	
	NEV 53	48		
		36		
		35		
		64		
		23		
		60		
	NEV 51	30		
		39		
		10		
		11		
		10		
		11		
		30		
	NEV 50	39		
		51		
		62		
		47		
		58		
		29		
		73		
	NEV 49	24		
		27		
		33		
		37		
		32		
		24		
		35		
		39		
		54		
		32		
		34		
		45		
		55		
		50		
		27		
		14		
		26		
	NEV 46	21		
		47		
		33		
		45		
	NEV 34	53		
		36		
		31		
		28		
	NEV 16	18		
		16		
		19		
	NEV 12	10		
		17		
		12		
		9		
		7		
		10		
		48		
		10		
		8		
		26		
		13		
	NEV 11	27		
		30		
		15		

Section	Sample	diametre µm	Mean diameter	Age
Nevenka 1	NEV 11	28		Late Barremian
		25		
Sofia 1	SOF 60	44	60,1	Hauterivian - Aptian
		54	27,2	
		87		
		64		
		72		
		101		
		29		
		15		
		58		
		54		
		160		
		82		
	SOF 57	50		
		36		
		44		
		43		
		76		
	SOF 56	55		
		46		
		56		
		65		
		45		
		42		
		41		
		104		
	SOF 54	78		
		79		
		89		
		153		
		63		
	SOF 53	92		
		76		
		112		
		80		
		165		
		55		
		48		
	SOF 52	95		
		56		
		80		
		58		
		38		
		45		
		54		
	SOF 51	89		
		46		
		50		
		58		
		54		
		53		
		64		
		42		
		52		
		54		
		44		
		51		
		73		
		74		
		34		
		49		
		80		
	SOF 49	59		
		77		
		31		

Section	Sample	diametre µm	Mean diameter	Age
Sofia 1		44		Hauterivian - Aptian
		49		
		47		
		49		
		48		
		34		
		35		
	SOF 47	139		
		45		
		64		
		90		
		52		
		86		
		113		
		109		
		62		
		66		
		39		
		70		
	SOF 45	70		
		50		
		50		
		59		
		162		
		62		
		136		
		104		
		139		
	SOF 43	100		
		42		
		103		
		38		
		62		
	SOF 42	47		
		42		
		26		
		85		
		63		
		106		
		53		
		101		
		70		
		81		
		49		
		46		
		22		
		24		
		31		
		26		
		28		
		32		
		47		
		42		
		29		
		29		
		22		
		35		
		45		
		47		
		44		
		44		
		78		
		61		
		32		
		37		
		40		
		45		

Section	Sample	diametre µm	Mean diameter	Age
Sofia 1	SOF 42	29		Hauterivian - Aptian
		54		
		5		
	SOF 41	57		
		36		
		46		
		64		
		71		
		50		
		48		
		30		
		72		
		63		
		37		
		66		
		53		
		41		
		43		
		39		
		39		
		45		
		30		
	SOF 39	103		
		64		
		36		
		37		
		51		
		56		
		39		
		53		
		79		
	SOF 37	65		
		48		
		51		
		54		
		55		
		53		
		55		
		45		
		41		
		90		
		54		
		36		
		76		
		65		
		69		
	SOF 36	77		
		88		
		82		
		74		
		82		
		67		
		60		
	SOF 33	80		
		65		
		81		
		79		
		56		
		42		
		32		
		30		
		64		
		29		
		35		